

University of Nottingham

**Discovery of Highly Potent and Selective
Phosphatidylinositol 3-kinase- δ
Inhibitors for the Treatment of Blood
Cancers and Autoimmune Diseases**

By Anas Buzrieda, BSc, MSc

Thesis submitted to the University of Nottingham
for the degree of Doctor of Philosophy

Abstract

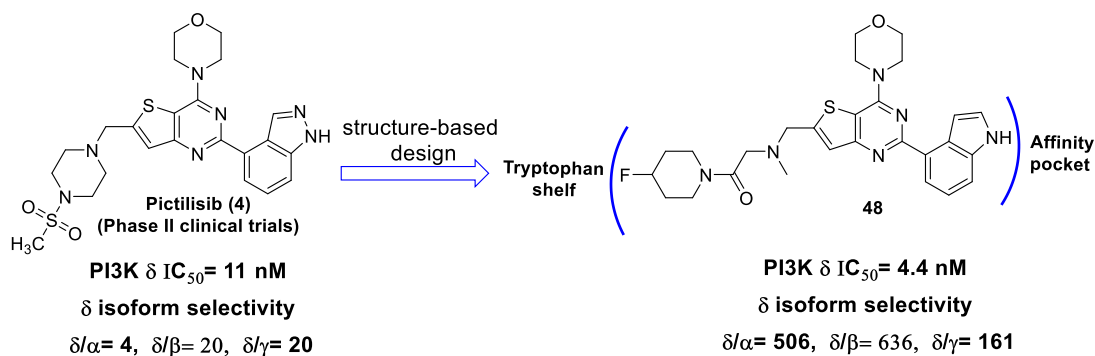
Phosphatidylinositol-3-kinase (PI3K) are a group of the lipid kinases superfamily, that play a crucial role in signalling pathways involved in the regulation of numerous cellular processes such as survival, growth, proliferation and differentiation. PI3K δ belongs to the class-IA subset of PI3Ks and is mainly present in leukocytes, where it regulates the development and function of adaptive immune cells (the B and T lymphocytes). However, PI3K δ dysregulation is implicated in human diseases, including blood cancers such as leukaemia and autoimmune diseases such as rheumatoid arthritis. The selective inhibition of PI3K δ may therefore provide an exciting therapeutic opportunity to treat different types of haematological malignancies and autoimmune disorders.

Idelalisib (**8**) is the only selective PI3K δ inhibitor approved by the Food and Drug Administration (FDA) for the treatment of chronic lymphocytic leukaemia, small lymphocytic lymphoma and follicular lymphoma. However when dosed, idelalisib (**8**) has been shown to have several side effects such as chronic diarrhoea, colitis and hepatotoxicity, which often lead to the discontinuation of treatment. Therefore, this medicinal chemistry research was undertaken with the aim to discover alternative PI3K δ inhibitors that can display comparable or greater potency and selectivity than idelalisib (**8**), but without adverse effects.

The first chapter describes how the non-selective PI3K inhibitor pictilisib (**4**) was used as the starting point for the design and synthesis of novel, flat-shaped PI3K δ selective inhibitors containing the thienopyrimidine scaffold.

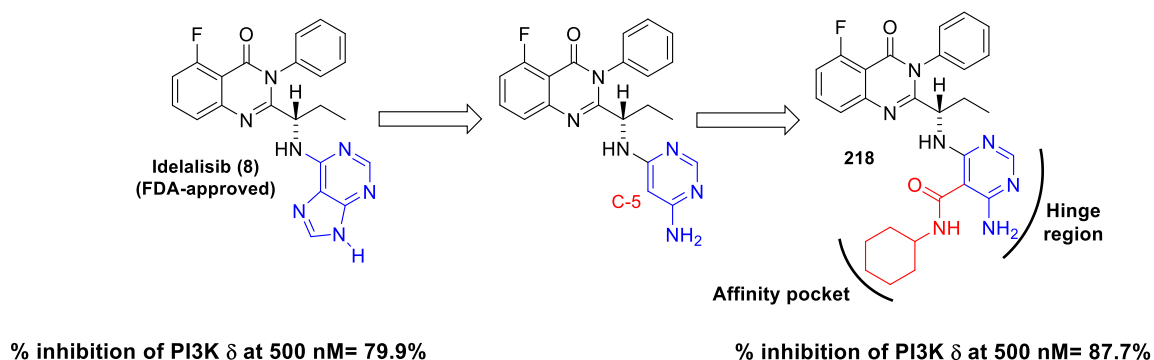
Abstract

Herein, structural modifications were performed on pictilisib (**4**) based on its key reported interactions seen in the ligand co-crystal structure with PI3K δ . The aim of the research presented in this chapter was to optimize the interactions in the conserved affinity pocket and to occupy the unexploited tryptophan shelf, the space between Trp⁷⁶⁰ and Thr⁷⁵⁰, that is exclusively found in the PI3K δ isoform and not in the other three isoforms (α , β and γ). This optimization strategy led to the synthesis of 38 thienopyrimidine derivatives as new PI3K δ inhibitors. Among them, indole analogue **48**, bearing a fluoropiperidine group was identified as the best compound, due to its combination of low nanomolar potency for PI3K δ inhibition and excellent selectivity for PI3K δ over the other isoforms. In addition, it possesses favourable predicted physicochemical properties for oral administration. Based on the docking studies from ligand crystal structure studies from other research groups, it was hypothesized that aliphatic heterocycles such as fluoropiperidine may form a favourable C-H/pi interaction with the tryptophan shelf, which may explain the improved PI3K δ potency and selectivity of compound **48**. On the other hand, occupancy of the affinity pocket by the indole ring of compound **48** may aid in increasing the PI3K δ selectivity through the formation of a distal hydrogen bond network that can be accommodated only in PI3K δ .



Abstract

Chapter 3, 4 and 5 focused on propeller-shaped PI3K δ inhibitors. The crystal structure of the FDA-approved idelalisib (**8**) bound to PI3K δ showed that the affinity pocket is not occupied in this class of inhibitor. Therefore, the goal of the work in chapters 2 and 3 was to extend the structure **8** ($IC_{50} = 11$ nM) into the unoccupied affinity pocket so as to further improve the PI3K δ potency. However, this structure-based approach proved unsuccessful with all 18 extended idelalisib analogues exhibiting weak or no activity against PI3K δ , suggesting that chemical modification of the core structure of **8** was needed. Consequently, chapter 5 reports, bioisosteric replacement of the purine group of idelalisib (**8**) with a 4-aminopyrimidine ring, followed by addition of a new affinity pocket-binding substituent at the C-5 position of this ring. The resulting 11 aminopyrimidine analogues displayed excellent inhibitory activity against PI3K δ at a single concentration of 500 nM. For example, the cyclohexyl analogue **218**, showed 87.7% of PI3K δ inhibitory activity. Unfortunately, full determination of the IC_{50} values of the 4-aminopyrimidine derivatives against PI3K δ has been delayed due to the COVID-19 pandemic. However, these results will be obtained from our collaborator in Monash, and if successful will hopefully form the basis of a publication.



Acknowledgements

Acknowledgements

I would like to thank my supervisors Prof. Michael Stocks and Dr. Shailesh Mistry to their valuable suggestions, continued support and encouragement during my Ph.D. study, and for their important advice throughout the writing of the dissertation. I am also very grateful to Dr. Christophe Fromont, Dr. Fadi Soukarieh, Dr. Nicholas Kindon, Dr. Sarah Mistry, Dr. Divneet Kaur and Dr. Aimie Graces for providing me with their assistance throughout the duration of my three-year research project.

Many thanks to Simon Macdonald (GlaxoSmithKline) for supplying the chemical starting point for my first project and for their help in assaying of the compounds covered in Chapter 2, 3 and 4. My gratitude also goes to Prof. Philip Thompson (Monash University) for screening the compounds covered in Chapter 5. I would like to express my sincere appreciation to James Awford and Ana Tellechea Lopez (University of Nottingham) for assistance in setting up the PI3K assay. I also thank Jia Ong for providing biological data for 13 compounds derived from his project.

I am also glad to have worked with wonderful labmates in C30: Alaa Mashabi, Jack Ayre, Matthew Allison, Rui Liu and Scott Grossman, who were always so helpful and made the lab environment more friendly and enjoyable. I also greatly value the friendship and support received from my colleagues in C22, C25 and C35 labs.

This thesis would not have been possible without funding from the Libyan Ministry of Higher Education and Scientific Research.

Finally, I especially thank my mom, dad, brothers and sister, for their continued support and unconditional love. I could not have made it this far without you. I love you all dearly.

Abbreviations

Abbreviations

ADME	Absorption, distribution, metabolism and excretion
ADP	Adenosin diphosphate
ALT	Alanine transaminase
APC	Allophycocyanin
APDS	Activated PI3K kinase delta syndrome
ARDS	Acute respiratory distress syndrome
AST	Aspartate transaminase
ATP	Adenosine triphosphate
BCR	B-cell receptors
BEP	2-Bromo-1-ethylpyridinium tetrafluoroborate
BTK	Bruton tyrosine kinase
CAK	CDK-activating kinase
CAN	Ceric ammonium nitrate
CLL	Chronic lymphocytic leukemia
cLog P	Calculated Log P
CML	Chronic myeloid leukemia
COVID-19	Coronavirus
DNA-PK	DNA-dependent protein kinase
EDTA	Ethylenediaminetetraacetic acid
EIF4E	Eukaryotic translation initiation factor 4E
FDA	Food and Drug Administration
FL	Follicular lymphoma
Fsp3	Fraction of sp ³ hybridized carbons
Glu	Glutamate
GLUT4	Glucose transporter 4
GPCR	G protein-coupled receptors
GSK	GlaxoSmithKline
H.B	Hydrogen bonding
HATU	(1-[Bis(dimethylamino)methylene]-1H-1,2,3-triazolo[4,5-b]- Pyridinium 3-oxide hexafluorophosphate
HBA	Hydrogen bond acceptor
HBD	Hydrogen bond donor
HER2	Human epidermal growth factor receptor 2
HMDS	Hexamethyldisilazane
HR-positive	Hormone receptor-positive breast cancer
HTRF	Homogeneous time-resolved fluorescence
IBCF	Isobutyl chloroformate
IFN	Interferon
ILs	Interleukins
IRS	Insulin receptor substrate
LUMO	Lowest unoccupied molecular orbital
mTOR	Mammalian target of rapamycin
NF-kB	Nuclear factor kappa-light-chain-enhancer
NMM	N-methylmorpholine

Abbreviations

PDB	Protein data bank
PDK1	3-Phosphoinositide-dependent kinase 1
PI(3,4,5)P3	Phosphatidyl 3,4,5-trisphosphate
PI3K	Phosphoinositide 3-kinase
PIKK	Phosphatidylinositol 3-kinase-related kinase
PMB	para-methoxybenzyl protecting group
PTEN	Phosphatase and tensin homolog
PyBOP	Benzotriazole-1-yl-oxytrypyrrolidinophosphonium-hexafluorophosphate
PyBroP	Bromotripyrrolidinophosphonium hexafluorophosphate
RASA3	Ras GTPase-activating protein 3
RTKs	Receptor tyrosine kinases
S6K1	Ribosomal protein S6 kinase beta-1
SAR	Structure-activity relationship
SLL	Small lymphocytic lymphoma
S _N 2	Bimolecular nucleophilic substitution reaction
S _N Ar	Aromatic nucleophilic substitution reaction
SS	Sjörgen syndrome
ssRNA	Single-stranded RNA
T1D	Type 1 diabetes
Th cells	Helper T cells
TLC	Thin-layer chromatography
TLRs	Toll-like receptors
TNF	Tissue necrosis factor
tPSA	Topological polar surface area
Treg	Regulatory T cells
VEGF	Vascular endothelial growth factor
Vps34	Vacuolar protein sorting 34

Table of Contents

Chapter 1	Introduction	1
1.1	Phosphoinositide 3-kinase (PI3K).....	1
1.2	PI3K/Akt/mTOR pathway.....	2
1.3	Classes of PI3K.....	4
1.3.1	Class I PI3K.....	4
1.3.2	Class II PI3K.....	5
1.3.3	Class III PI3K.....	6
1.4	Isoforms of class I	7
1.4.1	PI3K α	7
1.4.2	PI3K β	9
1.4.3	PI3K γ	11
1.4.4	PI3K δ	12
1.5	ATP substrate-binding sites of class I PI3Ks.....	17
1.6	Regions of the PI3K δ binding site.....	18
1.6.1	Hinge region	19
1.6.2	Hydrophobic region II.....	20
1.6.3	Affinity pocket (hydrophobic region I).....	22
1.6.4	Specificity pocket.....	22
1.6.5	Tryptophan shelf.....	23
1.7	PI3K δ isoform selectivity.....	23
1.7.1	Isoform selective PI3K δ inhibitors compared to pan-PI3K inhibitors....	23
1.7.2	Approaches achieve PI3K δ isoform selectivity.....	24
1.8	Types of PI3K inhibitors based on their isoform selectivity.....	30
1.8.1	Pan-PI3K inhibitor: pictilisib (4)	31
1.8.2	Dual-selective PI3K inhibitor	32
1.8.3	PI3K δ isoform-specific inhibitors	38
1.9	Aim and objectives	44

Table of Contents

1.9.1 Flat-shaped inhibitors (chapter 2)	45
1.9.2 Propeller-shaped inhibitors (Chapters 3, 4 and 5):	47
Chapter 2 Design, Synthesis and Pharmacological Characterization of Novel Thienopyrimidine-based PI3K δ selective Inhibitors (Flat-Shaped Inhibitors).....	50
2.1 Aim.....	50
2.2 Binding Interactions of the lead compound (pictilisib, 4)	52
2.3 Structural Modifications on pictilisib (4).....	52
2.3.1 Thienopyrimidine scaffold	52
2.3.2 Morpholine (hinge binder)	53
2.3.3 N-sulfonylpiperazine side chain (tryptophan shelf binder)	54
2.3.4 Indazole ring (Affinity pocket binder)	55
2.4 Discussion.....	56
2.4.1 Chemistry Section.....	56
2.5 Biology Section.....	59
2.5.1 Matched molecular pair analysis of the functional groups that occupy the affinity pocket.	61
2.5.2 Matched molecular pair analysis of the functional groups that occupy the tryptophan shelf.....	72
2.5.3 Conclusion derived from the first SAR study (Table 9).....	78
2.6 Conclusion	91
Chapter 3 Design, Synthesis and Pharmacological Characterization of Novel Quinazolinone-based PI3K δ selective Inhibitors (Propeller-shaped inhibitors)	93
3.1 Aim.....	93
3.2 Binding interaction of the lead compound: idelalisib (8)	95
3.2.1 Quinazolinone scaffold (Specificity pocket).....	95
3.2.2 Purine group (Hinge binder).....	95
3.2.3 Phenyl group (hydrophobic region II)	96
3.2.4 Affinity pocket (unoccupied).....	98
3.3 Aims	99

Table of Contents

3.3.1 Medicinal chemistry strategy.....	Error! Bookmark not defined.
3.4 Medicinal chemistry strategy	101
3.4.1 Variation of Linker length	101
3.4.2 Types of binding groups	101
3.4.3 Site of extension	102
3.5 Discussion.....	103
3.5.1 Chemistry Section.....	103
3.6 Biological section.....	129
3.6.1 Conclusion derived from the initial SAR study (Table 22).....	133
3.6.2 The linking strategy to make the final compounds	134
3.6.3 Screening of the final compounds (Single concentration compound screening) (Table 23)	135
3.6.4 Gatekeeper.....	138
3.6.5 Determination of IC ₅₀ (Table 25)	139
3.6.6 Conclusion derived from the second structure activity relationship (Table 23 and Table 25)	142
3.6.7 Effect of the ethyl side chain (R ₃) on PI3K δ activity.....	143
3.7 Conclusion	144
Chapter 4 Design, Synthesis and Pharmacological Characterization of Novel N- 7-substituted purine derivatives as PI3K δ selective Inhibitors (Propeller-shaped inhibitors).	146
4.1 Aim.....	146
4.2 Drawback associated with the extension of binding group from N-7 of purine	149
4.3 Medicinal chemistry strategy	152
4.3.1 Length of the linker	152
4.3.2 Affinity pocket-binding group (binding group).....	153
4.3.3 Modification of Hinge-binding moiety	158
4.4 Discussion.....	161

Table of Contents

4.4.1 Chemistry Section.....	161
4.4.2 Regiospecific N-7 alkylation of 6-chloropurine derivatives.....	168
4.4.3 Biology Section.....	172
4.5 Conclusion	183
Chapter 5 Design, Synthesis, biological evaluation and docking studies of pyrimidine derivatives as highly potent and selective PI3K δ inhibitors (propeller-shaped inhibitor).....	185
5.1 Aim.....	185
5.2 Types of the linker used in the previously reported PI3K δ inhibitors	186
5.2.1 Planar aryl linker.....	186
5.2.2 Linear acetylene linker.....	186
5.3 Reasons for selection of planar aryl and linear ethynyl linkers in PI3K δ inhibitors.....	188
5.4 Medicinal chemistry strategy	189
5.4.1 Modification of the hinge-binding scaffold	190
5.4.2 Linker.....	191
5.4.3 Types of functional groups.....	193
5.5 Discussion.....	206
5.5.1 Chemistry Section.....	206
5.5.2 Synthesis of aldehyde analogue 220 (reference)	214
5.5.3 Synthesis of des-aminated analogues 226 and 227.....	214
5.5.4 Biology Section.....	215
Chapter 6 General conclusion and recommendations for future work.....	224
6.1 General conclusion.....	224
6.2 Recommendations for future work	231
6.2.1 Flat-shaped PI3K δ inhibitors (Chapter 2).....	231
6.2.2 Propeller-shaped PI3K δ inhibitors (Chapter 5).....	239
6.2.3 A novel potential role of PI3K δ inhibitors in the treatment of COVID-19 induced acute respiratory distress syndrome (ARDS).....	245

Table of Contents

Chapter 7	Experimental.....	248
7.1	Molecular Docking.....	248
7.1.1	Preparation of protein.....	248
7.1.2	Receptor grid generation.....	248
7.1.3	Ligand preparation.....	248
7.1.4	Ligand virtual screening.....	249
7.2	Analysis of drug-likeness.....	249
7.3	Chemistry.....	249
7.3.1	Materials and instrumentation.....	249
7.3.2	Experimental for Chapter 2.....	250
7.3.3	Experimental for Chapter 3.....	262
7.3.4	Experimental for Chapter 4.....	286
7.3.5	Experimental for Chapter 5.....	296
7.4	Pharmacology.....	314
7.4.1	ADP-Glo assay.....	315
7.4.2	Homogenous Time Resolved Fluorescence assay (HTRF).....	317
7.5	References.....	319

Chapter 1 Introduction

1.1 Phosphoinositide 3-kinase (PI3K)

Kinases are enzymes that catalyse the transfer of the terminal phosphate group from adenosine triphosphate (ATP) to free hydroxyl groups on a specific substrate¹. The introduction of the bulky negatively charged phosphate group leads to a significant effect on the properties of the substrates, such as activity, subcellular localization and the ability to bind to other molecules². Kinases are classified into three types based on the nature of their substrates: protein kinases, lipid kinases and sugar kinases^{3,4}. PI3Ks are a family of lipid kinase enzymes that can selectively introduce a phosphate group to the 3-hydroxyl group of the inositol ring in phosphoinositide such as phosphatidylinositol-4,5-bisphosphate (PI(4,5)P₂) to form phospholipids such as phosphatidylinositol-3,4,5-trisphosphate (PI(3,4,5)P₃), which acts as a second messenger (Figure 1)^{5,6}, activating specific protein kinases, which in turn, phosphorylate transcription factors, to produce a particular cellular response⁷⁻¹¹. Thus, PI3Ks play a major part in controlling various cellular process including cell survival, cell growth and cell proliferation¹².

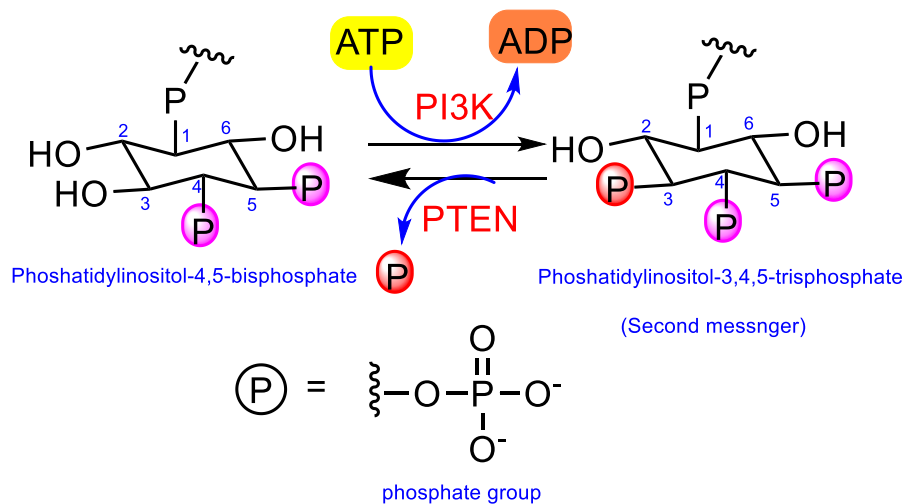


Figure 1. PI3K catalyses the transfer of phosphate group from ATP to the 3 position hydroxyl group of the inositol ring of PI(4,5)P₂ to generate the second messenger PI(3,4,5)P₃, which, activates intracellular enzymes.

1.2 PI3K/Akt/mTOR pathway

PI3K/Akt/mTOR represents a major pathway downstream of growth factor tyrosine kinase receptors (RTKs) that is involved in cell growth and metabolism^{13,14}. The activation of protein tyrosine kinases by growth factors¹⁵, induces the recruitment of PI3K to the plasma membrane¹⁶. The phosphotyrosine residues on RTKs bind to PI3K through a Src homology domain-2 (SH2), leading to activation of PI3K. Once activated, PI3K converts PI(4,5)P₂ to the second messenger PI(3,4,5)P₃ (Figure 2)¹⁵⁻¹⁸. Akt is then activated by the binding of its PH domain to PI(3,4,5)P₃ enriched sites at the plasma membrane. Activated Akt, in turn, phosphorylates mTOR at Ser²⁴⁴⁸ in the kinase activation loop, causing partial activation of mTOR^{19,20}. Once activated, mTOR phosphorylates and activates two ribosomal proteins P70S6 kinase (S6K1) and elf4E Binding Protein (4EBP) (Figure 2)^{10,21,22}, which then translocate to the nucleus where they promote various biological processes, including transcription, translation, protein and lipid synthesis, cell growth/size and cell metabolism^{11,23,24}.

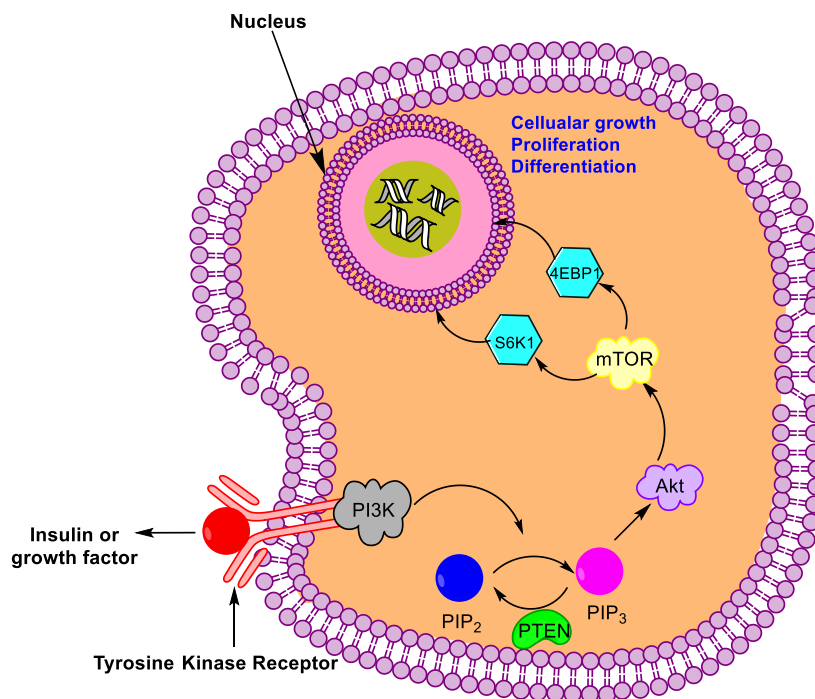


Figure 2. Graphical representation illustrating the role of PI3K/Akt/mTOR pathway in promoting cellular growth, survival, proliferation, metabolism and differentiation. Binding of ligands to receptor tyrosine kinase RTK (or GPCRs) activates PI3K (in grey) at the plasma membrane. Then, PI3K phosphorylates PI(4,5)P₂ (in blue) into PI(3,4,5)P₃ (in magenta), which in turn, activates the serine/threonine kinases AKT (in violet) that phosphorylates mTOR (in yellow). The activation of mTOR leads to the stimulation of ribosomal protein S6K1 (in cyan) and inactivation of 4E-BP1 (a repressor of translation initiation) (in cyan), which in turn, stimulate gene expression and protein synthesis in the nucleus. The lipid phosphatase PTEN (in green) reverses the effect of PI3K by dephosphorylating PI(3,4,5)P₃ (in magenta) into PI(4,5)P₂ (blue)²⁵⁻²⁷.

Over activation of the PI3K/Akt/mTOR pathway has the potential to cause significant dysregulation of a variety of cellular process such as protein synthesis, cell proliferation, cell survival and apoptosis (Figure 2). For instance, somatic mutations in the PI3K signalling pathway are among the most common genetic abnormalities detected in cancer^{28,29}. Moreover, hyperactivation of the PI3K/Akt/mTOR signalling pathway is also associated with autoimmune disorders, cardiovascular diseases and diabetes^{30,31}. Therefore, these findings suggest that PI3K/Akt/mTOR axis is an attractive target for intervention in a wide range of diseases³².

1.3 Classes of PI3K

The PI3K family is divided into three classes based on the lipid substrate structure, sequence homology and function³³. There are eight isoforms of PI3K in humans, four isoforms of class I, three isoforms of class II and one isoform of class III^{34–36}. The four isoforms of class I have long been considered promising therapeutic targets for the many drug discovery programs, whereas the isoforms of class II and class III have been largely neglected as potential therapeutic targets³⁵.

1.3.1 Class I PI3K

Class I PI3Ks are 110-130 kDa heterodimeric enzymes, composed of catalytic and regulatory subunits^{37–39}. The catalytic subunit p110 is linked to the upstream signalling proteins (RTKs or G-protein-coupled receptors (GPCRs)) by regulatory subunits (Figure 3)^{38,40}. Class I PI3Ks are normally kept in an inactive state by association of the catalytic subunit (p110) with its regulatory subunits^{41,42}. However, binding of regulatory subunits to the cell surface receptor (RTKs or GPCRs) results in the activation of the PI3K pathway⁴¹.

Class I PI3Ks are subdivided into two classes, which differ in upstream signalling and regulatory subunits⁴²: Class IA includes α , β and δ isoforms which are activated by RTK, the p110 catalytic subunits of class IA PI3Ks interact with the same regulatory subunit p85 (Figure 3)^{33,43}. The α and β isoforms are ubiquitously expressed while δ isoform is mainly expressed in leukocytes³⁷. Class IB contains only a single isoform (PI3K γ) which is activated by GPCRs (Figure 3), the p110 catalytic subunit of PI3K γ is associated with the regulatory subunit p101³³. PI3K γ is mainly found in

hematopoietic cells and in negligible number in smooth muscles, endothelia and cardiomyocyte⁴⁴.

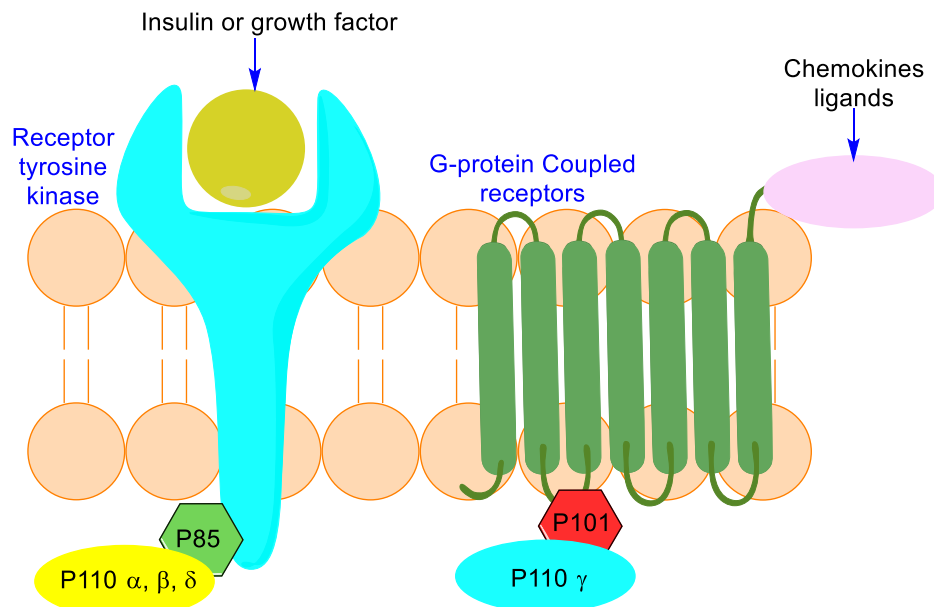


Figure 3. Class IA PI3Ks (PI3K α , β and δ) are heterodimers composed of the catalytic subunit p110 (in yellow) and regulatory subunit p85 (in green). Class IA isoforms are activated by extracellular signals through tyrosine kinase receptor (RTKs), whereas in Class IB PI3K (PI3K γ), the catalytic subunit p110 (in cyan) associates with the regulatory subunit p101 or p87 (in red). PI3K γ is activated by extracellular signals through GPCRs.

Class I PI3Ks catalyse the conversion of phosphatidylinositol (PI) into phosphatidylinositol-3-phosphate (PI(3)P), phosphatidylinositol 4-phosphate (PI(4)P) into phosphatidylinositol (3,4)-bisphosphate (PI(4)P) and phosphatidylinositol (4,5)-bisphosphate into phosphatidylinositol (3,4,5)-trisphosphate (PI(3,4,5)P₃)⁴⁵, where the class I PI3Ks have the unique ability to produce (PI(3,4,5)P₃)^{44,45}, which is necessary for PI3K-mediated tumour development, explaining the fact that class II and class III PI3Ks have not associated with cancer⁴⁵.

1.3.2 Class II PI3K

Class II PI3Ks are monomeric enzymes with a high molecular weight⁴⁶, there are three isoforms of class II PI3K : PI3K-C2 α , PI3K-C2 β and PI3K-C2 γ . Class II PI3Ks prefer to phosphorylate PI, with some activity at PI(4)P^{46,47}.

Class II PI3Ks differ from class I PI3Ks for being unable to generate PI(3,4,5)P₃^{36,48}. PI3K-C2 α is ubiquitously expressed in all cells and tissues, with particularly high levels in the pancreatic β -cells⁴⁹. Leibiger *et al*⁵⁰ showed that knockdown of PI3K-C2 α impaired glucose-stimulated insulin secretion from the β -cells of the pancreas. This finding revealed that PI3K-C2 α pathway may constitute a potential druggable target for treatment of type 2 diabetes⁵⁰. PI3K-C2 β is ubiquitously expressed, with particularly high levels in T-cells, where PI3K-C2 β -mediated PtdIns (3)P production leads to the activation of the voltage-gated K⁺ channel involved in T-cell proliferation^{51,52}, thus PI3K-C2 β may represent a novel therapeutic target for treatment of blood cancers (lymphoma and leukaemia)³⁴. Finally, PI3K-C2 γ is only expressed in hepatocytes, whereas its physiological role is presently unknown⁵³.

1.3.3 Class III PI3K

Class III is the only class of PI3K which is conserved in yeasts, plants and mammals⁵⁴. There is a single isoform in this class, which is known as vacuolar protein sorting 34 (Vps34)⁵⁵. Vps34 is only able to phosphorylate phosphatidylinositol to produce PI(3)P⁵⁶. Vps34 plays an important role in the stimulation of autophagy in different cell types⁵⁷. Autophagy is the process that delivers long-lived proteins and damaged cellular organelles to lysosomes for degradation⁵⁸. Disruption of Vps34 function is associated with abnormalities in autophagy, which leads to accumulation of aggregated proteins in neurons and generation of neurodegenerative disorders such as Alzheimer's disease⁵⁹.

1.4 Isoforms of class I

As previously mentioned, class I PI3K is further subdivided into two classes: class IA which includes three isoforms (PI3K α , PI3K β and PI3K δ). Class IB is composed of only one isoform - PI3K γ . In this chapter, the four isoforms of class I PI3K will be reviewed, with a particular focus on the PI3K δ isoform, as the main aim of this project is to design and develop novel selective inhibitors for PI3K δ .

1.4.1 PI3K α

1.4.1.1 Physiological role of PI3K α

PI3K α is ubiquitously expressed in all cells in the body⁶⁰, where receptor tyrosine kinase (RTKs) functions upstream of PI3K α signalling⁶¹. PI3K α plays a key role in mediating the metabolic effects of insulin, where it involves in insulin-mediating glucose uptake in adipose tissue via glucose transporter protein type-4 (GLUT4) (Figure 4)^{62,63}. In the hepatic cells, PI3K α transmits the insulin signal downstream from insulin receptor substrate-1 (IRS-1) to Akt and other downstream signalling molecules⁶⁴. Insulin signalling in the liver maintains normal glucose and lipid homeostasis^{63,65}, by inhibiting gluconeogenesis and promoting the conversion of excess glucose into glycogen for storage and later use^{64,66}.

1.4.1.2 Pathological role of PI3K α

Dysregulation of the PI3K α signalling pathway in the liver results in the development of insulin resistance and type 2 diabetes mellitus that cannot be recovered by metformin^{63,67}. Additionally, it was found that PI3K α is the second most commonly mutated protein in human cancer after p53^{30,68}. The

Chapter 1

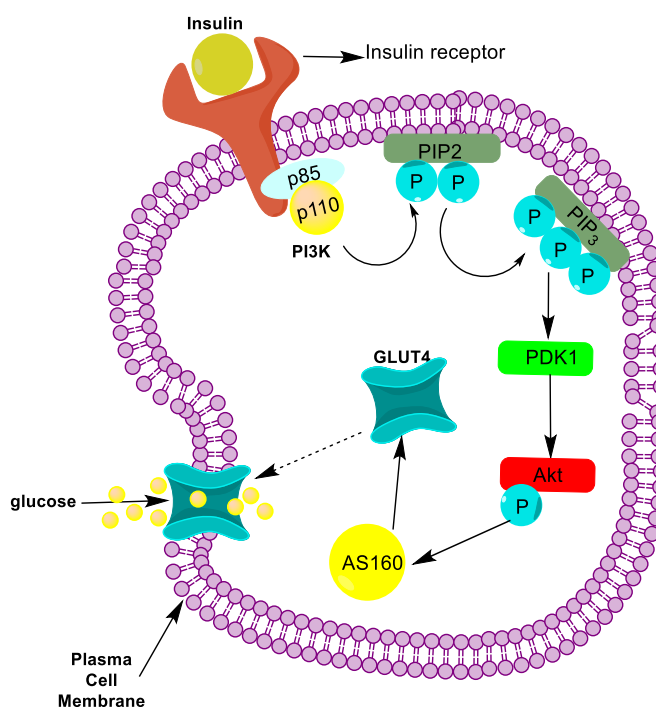


Figure 4. PI3K α pathway mediates glucose uptake by peripheral tissues. Binding of insulin to the insulin receptor inducing its activation via autophosphorylation. When activated, insulin receptor triggers activation of PI3K that converts PI(4,5)P₂ into PI(3,4,5)P₃, resulted in 3-phosphoinositoid-depentent kinase 1 (PDK1) activation, which in turn, stimulates Akt phosphorylation. Activated Akt catalyses the phosphorylation of AS160 (Akt substrate of 160kDa) which is necessary for translocation of glucose transporter (Glut4) from the cytoplasm to the plasma membrane, leading to increased glucose uptake into the cell⁶⁹.

tumorigenesis associated with over activation of the PI3K α pathway results from mutation in *PI3KCA*, the gene that encodes PI3K α , or from hyperactivation of upstream RTK signalling⁶¹. Mutations in *PI3KCA* lead to the development of different types of cancers such as breast, prostate and colon cancers⁴⁰. Therefore, PI3K α inhibition provides an attractive target for therapeutic intervention in different types of solid tumours and metastasis⁷⁰. For instance, the selective PI3K α inhibitor alpelisib (1) (Figure 5) has recently been approved by the US FDA for the treatment of hormone receptor HR-positive, human epidermal growth factor 2 negative (HER2-) advanced or metastatic breast cancer in combination with endocrine therapy fulvestrant^{71,72}.

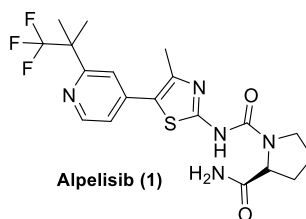


Figure 5. The selective PI3K α inhibitor alpelisib (1), which was approved by the FDA in 2019 for treatment of metastatic HR-positive, HER2-negative metastatic breast cancer⁷³.

1.4.2 PI3K β

1.4.2.1 Physiological role of PI3K β

PI3K β is similar to PI3K α , being ubiquitously expressed⁶¹. However, the lipid phosphorylation activity of PI3K β is notably less compared to PI3K α ⁷⁴. In addition, PI3K β is unique among the PI3Ks in its ability to be activated by both RTK and GPCRs (Figure 6)^{75,76}, whereas the PI3K α pathway can only be activated by RTKs⁷⁷. Among the four isoforms of class I PI3K, PI3K β serves the most important role in platelet activation and platelet procoagulant activity⁷⁸. The mechanism by which PI3K β regulates platelet function remains undefined, but it is thought to integrate signalling proteins regulated downstream of PI(3,4,5)P₃ (Figure 6), where the platelets, unlike many other body cells, have Ras GTPase-activating protein 3 (RASA3) as a major PI(3,4,5)P₃-binding protein instead of Akt.

1.4.2.2 Pathological role of PI3K β

PI3K β is the predominant isoform expressed in phosphatase and tensin homolog PTEN-deficient tumours, which indicates that PTEN-null tumours appear to be highly dependent on PI3K β signaling⁷⁹. Thus, PI3K β inhibitors may be useful for treating PTEN-null tumors^{61,68,79}. On the other hand, PI3K β plays a major role in thrombus formation by promoting vascular collagen-induced platelet aggregation through the stimulation of the intracellular Ca²⁺

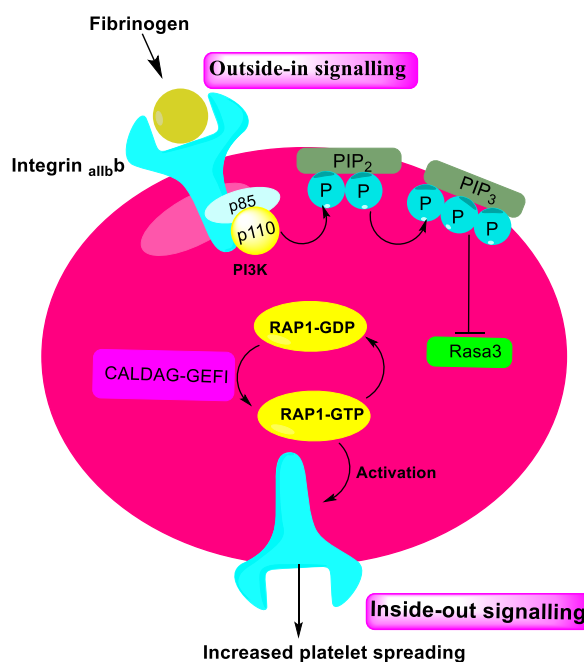


Figure 6. Physiological role of PI3K β in regulating platelet migration, proliferation and differentiation. Fibrinogen binds to its platelet receptor, integrin $_{\alpha IIb\beta 3}$, resulted in outside-in signalling, which triggers the activation of PI3K β leads to the generation of the second messenger PI(3,4,5)P $_3$. This, in turn, binds and inhibits RASA3. Inactivation of RASA3 permits CALDAG-GEFI-mediated activation of RAP1-GTP to process unreversed. Activated GTP-bound Rap1 induces the stimulation of integrin $_{\alpha IIb\beta 3}$ and inside-out signalling process resulting eventually in platelet spreading and granule secretion⁸⁰.

secretion and mobilization⁸¹. This finding was confirmed by the study showing that blocking of PI3K β delays initial thrombus formation and prevents platelets aggregation without increasing the bleeding⁸². Therefore, the PI3K β isoform could be a new therapeutic target for antithrombotic drugs⁸³. For instance, the selective PI3K β inhibitor AZD 6482 (**2**) (Figure 7), developed by AstraZeneca, has passed phase I clinical trials as an antithrombotic drug. AZD 6482 (**2**) prevents platelet aggregation by blocking PI3K β signalling pathway⁸⁴ and is associated with a lower risk of major bleeding compared with warfarin and other anticoagulants.

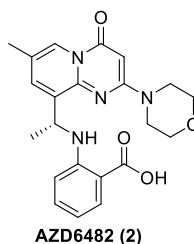


Figure 7. The selective PI3K β inhibitor AZD6482 (**2**), which is currently undergoing phase I clinical trials for the treatment of thrombosis⁸³.

1.4.3 PI3K γ

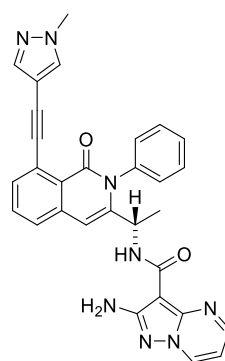
1.4.3.1 Physiological role of PI3K γ

PI3K γ is the only PI3K isoform within the class IB subfamily⁸⁵. In different types of immune cells, Binding of an extracellular ligand to GPCRs leads to the activation of PI3K γ and rapid synthesis of the second messenger PI(3,4,5)P₃⁸⁶. The most common extracellular ligands activating PI3K γ signalling via GPCRs include chemokines and cytokines, which are involved in inflammatory and immune responses to infection and tissue injury⁸⁷. PI3K γ is primarily expressed in haematopoietic cells and it plays a critical physiological role in promoting the innate immune response^{88,89}, by controlling many neutrophil activities, including chemotactic migration to the site of infection, endothelial adhesion, and subsequent pathogen killing^{90–93}.

1.4.3.2 Pathological role of PI3K γ

PI3K γ takes part in the pathogenic mechanism of several acute and chronic inflammatory conditions and autoimmune diseases such as rheumatoid arthritis, systemic lupus erythematosus and asthma⁹⁴. It is widely believed that over activation of PI3K γ signalling in neutrophils and T-cells (both involved in the physiological immune response), causes these cells to release excessive amounts of pro-inflammatory cytokines such as tissue necrosis factor α (TNF- α) and interleukin-1 β , -6 and -8 (IL-1 β , IL-6 and IL-8), therefore, disrupting immune homeostasis, eventually leading to the development of a plethora of chronic inflammatory and autoimmune diseases⁹². Camps *et al*⁹⁵ and Banham-Hall *et al*⁹² showed that the pharmacological inhibition of PI3K γ is a useful therapeutic strategy in the treatment of various inflammatory diseases⁹⁵.

Furthermore, PI3K γ can increase tumour growth and metastasis by promoting the trafficking and infiltration of inflammatory cells into tumours⁹⁶. Schmid *et al*⁹⁶ reported that blocking the PI3K γ signalling pathway stops tumour growth by inhibiting tumour inflammation and angiogenesis without directly affecting cancer cells⁹⁶. Hence, the inhibition of PI3K γ with a pharmacological inhibitor represents an attractive strategy for treatment of different types of solid tumours and haematological malignancies⁹⁷. For example, selective PI3K γ inhibitor eganelisib (**3**) (Figure 8) has passed phase I clinical trials for the treatment of advanced solid tumours⁹⁸.



Eganelisib (**3**)

Figure 8. The selective PI3K γ inhibitor eganelisib (**3**), which is in phase II clinical studies for treatment of different types of advanced solid tumours such as breast cancer⁹⁹.

1.4.4 PI3K δ

1.4.4.1 Physiological role of PI3K δ

PI3K δ is mainly expressed in haematopoietic cells¹⁰⁰, where it plays an important physiological role in the activation, proliferation and survival of adaptive immune cells (B- and T-cells) (Figure 10a). B-cells have a central role in the body's immune response, by secreting antibodies and by serving as antigen-presenting cells (APCs) for T-cells. PI3K δ has a major role in transducing antigen-dependent signals from B-cell receptors (BCR) to the downstream signalling proteins (Figure 10a). Antigen-dependent BCR signals

Chapter 1

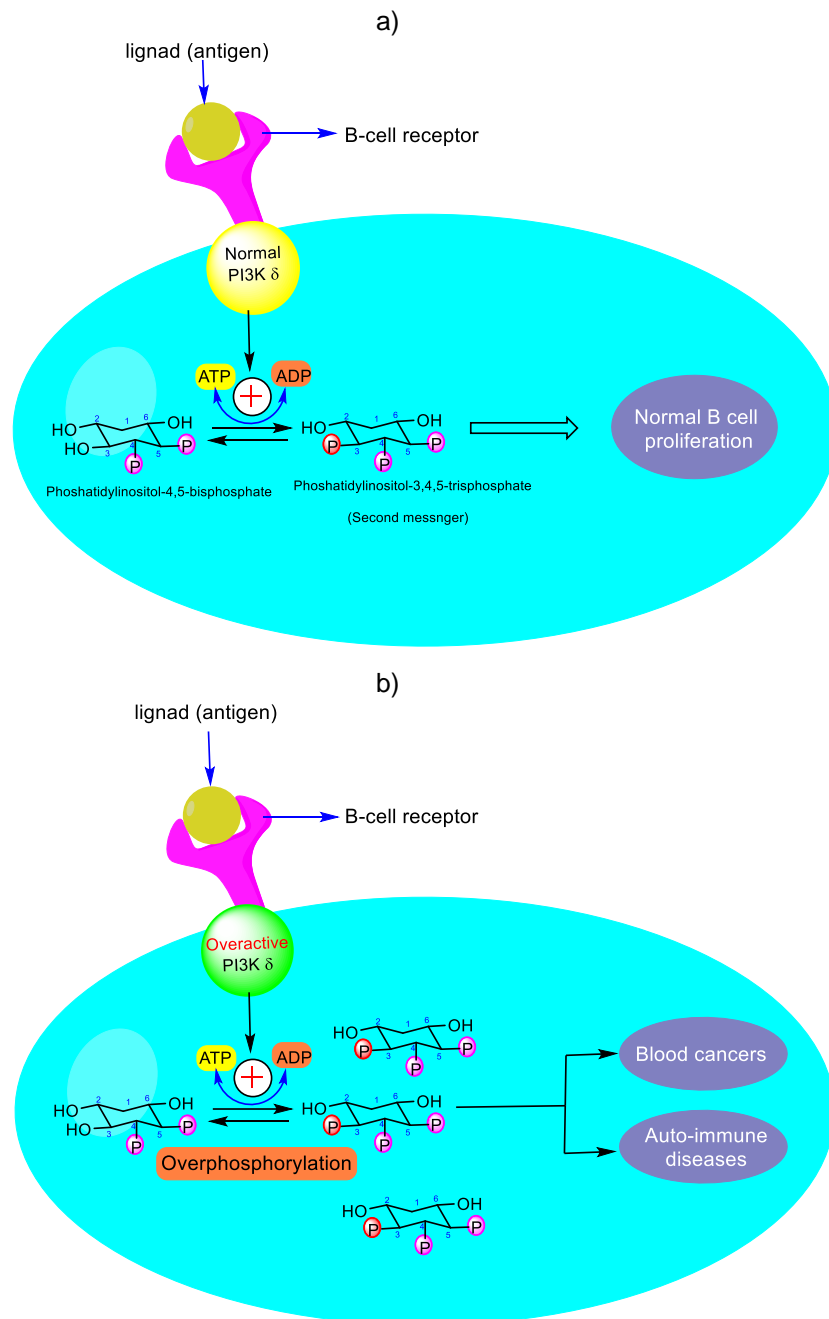


Figure 10. Blood B-cells in normal and cancerous state. a) In normal B-cells, PI3K δ is normally physiologically active (in yellow), thus it leads to the controlled proliferation of B-cells. b) In cancerous B-cells, the PI3K δ isoform is overactive (in green), resulting in overphosphorylation of PIP₂ and overproduction of the second messenger PI(3,4,5)P₃, which finally leads to the development of 2 types of diseases: haematological cancers and autoimmune diseases.

regulate the survival, proliferation and activation of B-cells¹⁰¹. Therefore, PI3K δ signalling is required for B cell development and antibody secretion^{102,103}. In T-cells, PI3K δ acts as a key component in the CD20-evoked signalling pathway for naïve T helper cells differentiation into Th1 and Th2 cells, where

Th1 cells secrete the cytokines interferon- γ (IFN- γ) and tumour necrosis factor- β (TNF- β)¹⁰⁴, which have the ability to defend the body against infectious diseases caused by viruses and intracellular bacteria that grow in the macrophages as well as killing cancerous cells¹⁰⁵. Whereas Th2 cells secrete IL-4, -5, -10 and 13 which induce antibody production from B-cells to fight against parasitic organisms^{104,106,107}.

Furthermore, PI3K δ regulates the development and function of Treg cells that are responsible for establishing tolerance to self-antigens and innocuous antigens such as intestinal flora¹⁰⁸. Additionally, Tregs cells have the capacity to prevent autoimmune diseases and inflammations by suppressing other cells in the immune system such as helper T-cells and B-cells^{109,110}.

1.4.4.2 Pathological role of PI3K δ

The dysregulation of PI3K δ signaling in B-cells leads to two types of diseases: (i) blood cancers such as lymphoma and leukemia; (ii) autoimmune diseases such as rheumatoid arthritis and systemic lupus erythematosus (Figure 10b)^{100,111–113}.

1.4.4.2.1 PI3K δ and blood cancers

PI3K δ plays a role in the development of several types of haematological malignancies such as chronic lymphocytic leukaemia (CLL), follicular lymphoma (FL) and small lymphocytic lymphoma (SLL)^{100,111}. CLL is the most common type of leukaemia in adults, it is characterized by progressive accumulation of mature-appearing neoplastic B lymphocytes in the blood, bone marrow, lymph nodes and spleen¹¹⁴. As the number of cancerous lymphocytes gradually increase, they crowd out normal blood cells, resulting

Chapter 1

in a decreased number of normal lymphocytes in blood, which causes a decrease in the amount of antibodies produced and weakens the immune system¹¹⁵. It was found that PI3K δ is over activated and/or overexpressed in CLL cells compared to normal B-cells (Figure 10b), suggesting that hyperactive PI3K δ signalling contributes to the pathogenesis of CLL^{116,117}. This is supported by the fact that disruption of PI3K δ signalling promotes CLL cells death through one of two pathways (intrinsic and extrinsic)^{116,118}. In the intrinsic mitochondrial pathway, inhibition of PI3K δ results in the upregulation of pro-apoptotic proteins (Bim, Bad, Bax and Bak), which increases the mitochondrial membrane permeability¹¹⁹, followed by subsequent release of cytochrome c from mitochondria to the cytosol, resulting in B-cell death^{116,118,120}. In the extrinsic pathway, PI3K δ inhibition blocks the external pro-survival signal provided by microenvironmental cytokines, leading to B cell death¹²¹.

SLL is also a type of non-Hodgkin lymphoma, which shares many similarities with CLL, both diseases affect B lymphocytes and tend to grow slowly over time¹²². The only difference between SLL and CLL is the part of the body where the cancer primarily occurs. In SLL most of the cancer cells are located in the lymph nodes, whereas in CLL, they are mainly in the bloodstream and bone marrow¹²³. As in CLL, PI3K δ has been found to be overexpressed in SLL cells, where it enhances tumour cell survival and proliferation^{124,125}. Thus, PI3K δ offers a new treatment target for SLL¹²⁶.

FL is a blood cancer that arises from B lymphocytes, and is characterized by uncontrolled proliferation of abnormal B-cells in the lymph nodes, the cancer cells tend to aggregate into well-defined follicles within lymph nodes¹²⁷. The

growth and proliferation of follicular B-cells are dependent on the crosstalk between these cells and the follicular helper T-cells, in which the latter cells secrete tumour necrosis factor- α (TNF- α), lymphotoxin α and IL-4, which bind to BCRs resulting in activation of follicular cells¹²⁸. In FL tumour cells, PI3K δ acts as an exclusive transducer of BCR downstream signalling in follicular B-cells¹²⁸, therefore, PI3K δ plays a fundamental role in the pathogenesis of FL¹²⁹.

1.4.4.2.2 PI3K δ in autoimmune diseases and inflammation

Autoimmune disease is a condition in which the immune system, designed to only attack cancer cells or foreign cells such as viruses and bacteria, mistakenly attacks and destroys healthy body cells and tissues⁹². There are over 80 different types of autoimmune diseases, the most common include: rheumatoid arthritis, colitis, systemic lupus erythematosus and type I diabetes (T1D)^{112,113}. B-cells contribute to the pathogenesis of a plethora of autoimmune diseases through their secretion of autoantibodies and presentation of antigen to T-cells¹³⁰. Autoantibodies can bind to different receptors or receptor ligands leading to activation or inhibition of receptor functions¹³¹. For example, autoantibodies secreted by auto-reactive B-cells are necessary for the initiation of rheumatoid arthritis by binding to cartilage proteoglycan, subsequently triggering chemokine and cytokine secretion from activated macrophages in synovial fluid¹³², which results in cartilage degradation and bone erosion¹³³. A large number of studies have found that autoreactive B cell activation and proliferation are highly regulated by PI3K δ signalling¹³¹. Hence, inhibition of PI3K δ leads to greatly decreased

autoantibodies directed against cartilage proteoglycan which in turn prevents irreversible joint damage¹³⁴.

On the other hand, T helper cells are also known to play a role in the pathophysiology of multiple autoimmune diseases. For example, in T1D, β -cell destruction is mediated through pro-inflammatory cytokine secretion by helper T-cells within pancreatic islets¹³⁵. PI3K δ takes part in the releasing of pro-inflammatory cytokines from pancreatic T lymphocytes in T1D^{136,137}, where it was found that T-cells in T1D patients expressed higher levels of PI3K δ compared to healthy T-cells, suggesting that PI3K δ over activation plays an essential role in the development of T1D⁹². Taken together, these results demonstrate that PI3K δ inhibitors could prove to be effective in the treatment of different types of autoimmune diseases¹³⁸.

1.5 ATP substrate-binding sites of class I PI3Ks

ATP substrate-PI3K γ (PDB code 1E8X) (Figure 11) was the first reported crystal structure of the class I PI3Ks¹³⁹. ATP binds in the cleft between the smaller *N*-terminal lobe and larger *C*-terminal lobe of the catalytic domain of PI3K^{139,140}. The ATP binding site is similar in all 4 isoforms of class I PI3K¹⁴¹, where the active site of PI3K α , β , γ and δ contain twenty fully conserved residues¹³⁹. The crystal structure of the ATP-PI3K γ complex (Figure 11b) reveals that ATP binds to PI3K γ in three regions: the adenine-binding region (hinge region), the ribose region (hydrophobic region II), and the phosphate region^{142,143}.

In the hinge region, the nitrogen-1 (N-1) atom of the adenine ring engages in a hydrogen bond with the backbone amide of Val⁸⁸² (Figure 11b)¹⁴⁰, this hinge

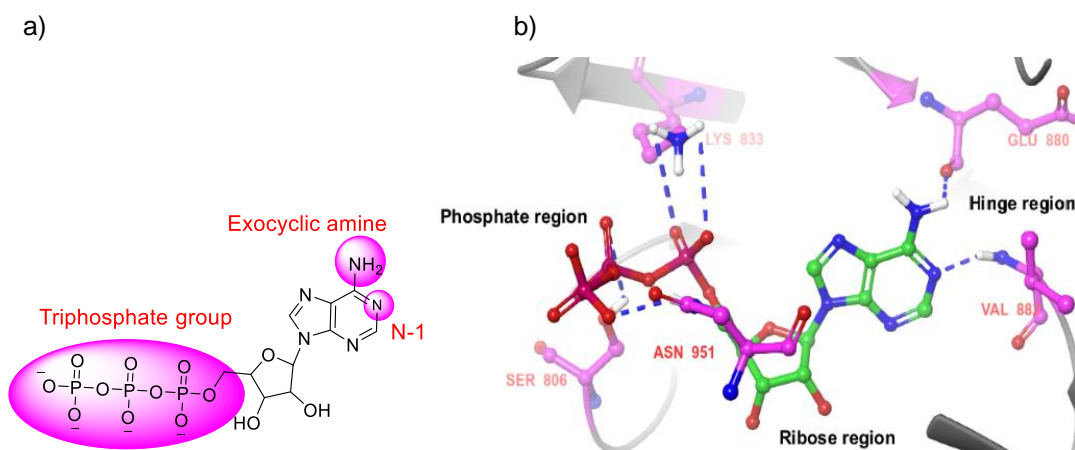


Figure 11. Molecular structure of ATP, highlighting the three binding motifs (exocyclic amine, nitrogen-1 and triphosphate group)¹⁴⁰. b) Crystal structure of porcine PI3K γ (PDB code 1E8X) with ATP bound, highlights the three regions of the PI3K γ binding site. Blue dashed lines represent the proposed hydrogen interactions¹⁴⁰.

interaction is preserved in all PI3K-inhibitor complexes where all of the inhibitors possess a hydrogen bond acceptor occupying the identical position to nitrogen-1 of ATP^{140,141}. Moreover, the backbone carbonyl of hinge Glu⁸⁸⁰ makes a hydrogen bond with the exocyclic amino group of adenine¹⁴⁰. In the phosphate region, ATP makes three additional hydrogen bonds to PI3K (Figure 11b). These hydrogen bonds involve the three phosphate groups attached to the ribose ring: the α -phosphate group interacts with Lys⁸³³, β -phosphate interacts with Ser⁸⁰⁶ and γ -phosphate interacts with Asn⁹⁵¹^{140,144}. None of the PI3K inhibitors binds in the position occupied by the β and γ phosphates of ATP. The ribose group extends toward hydrophobic region II (ribose region), where it does not participate in hydrogen bond interaction with PI3K (Figure 11b)¹⁴⁴.

1.6 Regions of the PI3K δ binding site

All four isoforms of class I PI3K possess three common binding regions, two of them occupied by ATP which are hinge region and hydrophobic region II (Table 1)^{144–146}, whereas the third region, called the affinity pocket, is not occupied by ATP. However, the binding site of PI3K δ has two more binding

regions which are not present in the other three isoforms: the specificity pocket and tryptophan shelf (hydrophobic dimple) (Table 1).

Table 1. Different Regions of the PI3K binding site. The region that presents in PI3K isoforms is highlighted in blue, whereas the isoform-lacking region is highlighted in red. It also highlights the binding regions that can be exploited to achieve PI3K δ selectivity^{144,145}.

Regions of binding site	no. of residues	PI3K δ	PI3K α	PI3K β	PI3K γ	Regions contribute to PI3K δ selectivity
Hinge region	4	Present	Present	Present	Present	Not contributing
Affinity pocket	8	Present	Present	Present	Present	Not contributing
Hydrophobic region II	8	Present	Present	Present	Present	Not contributing
Tryptophan shelf	1	present	Not present	Not present	Not present	Contributing
Specificity pocket	2	present	Not present	Not present	Not present	Contributing

1.6.1 Hinge region

As mentioned, all four class I PI3K isoforms are composed of a smaller *N*-terminal lobe and larger *C*-terminal lobe (Figure 12)^{139,147}. The short linker of four residues (826- 829 in PI3K δ) that connects between the two lobes is known as hinge region (Figure 12)¹⁴⁷⁻¹⁴⁹. All four of these residues (δ Glu⁸²⁶, δ Val⁸²⁷, δ Val⁸²⁸ and δ Leu⁸²⁹) are conserved across all isoforms of class I PI3K (Figure 13b), so interaction at the hinge region cannot modulate isoform selectivity¹⁴⁴. All PI3K inhibitors make a key hydrogen bond with the backbone amide of hinge δ Val⁸²⁸ (Figure 13b), which is essential for activity¹⁴⁴, thus, all PI3K δ inhibitors possess a hydrogen acceptor (primarily nitrogen) which points towards the hinge region¹⁵⁰. In addition, the backbone carbonyl of Glu⁸²⁶ at the hinge region is usually involved in inhibitor-enzyme interaction by serving as a hydrogen bond acceptor (Figure 13b), thus making possible

the formation of double hydrogen bonds with PI3K δ inhibitors¹⁵⁰. As a result, many PI3K δ inhibitors have a hydrogen bond donor and acceptor separated by one atom in *syn*-like arrangement¹⁵⁰.

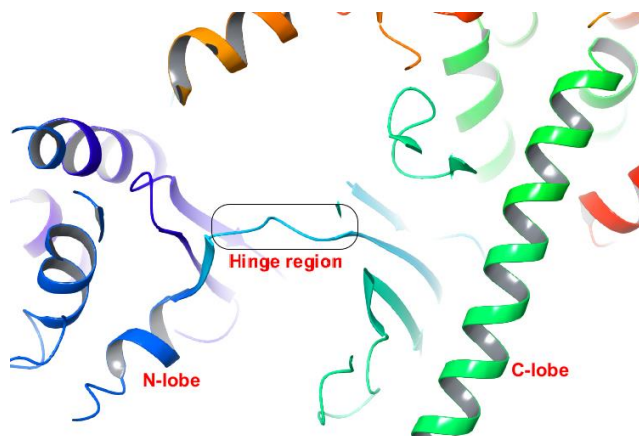


Figure 12. Crystal structure of murine PI3K δ (PDB code 4XE0). Highlights the Hinge region in the black square. This region connects the larger C-lobe to the smaller N-lobe and is thus known as the hinge region.

1.6.2 Hydrophobic region II

Hydrophobic region II (also known as the ribose-binding region) is located at the entrance of the ATP-binding site (Figure 13a)^{145,146}, where it is occupied by the ribose moiety of ATP. Hydrophobic region II does not appear to play an important role in inhibitor binding. However, it can be exploited to increase the aqueous solubility of PI3K δ inhibitors, by introducing a polar substituent to this region^{145,146}. There are 8 residues (δ Leu⁸²⁹, δ His⁸³⁰, δ Ser⁸³¹, δ Asp⁸³², δ Thr⁸³³, δ Ile⁸³⁴, δ Ala⁸³⁵ and δ Asn⁸³⁶) in the hydrophobic region II, four of them are variable across the four isoforms (Figure 13c)¹⁴⁴. Among the 8 residues, only Asn⁸³⁶ has been reported to have the ability to modulate inhibitor selectivity¹⁵¹ (discussed in more detail in Chapter 3, Section 3.2.3).

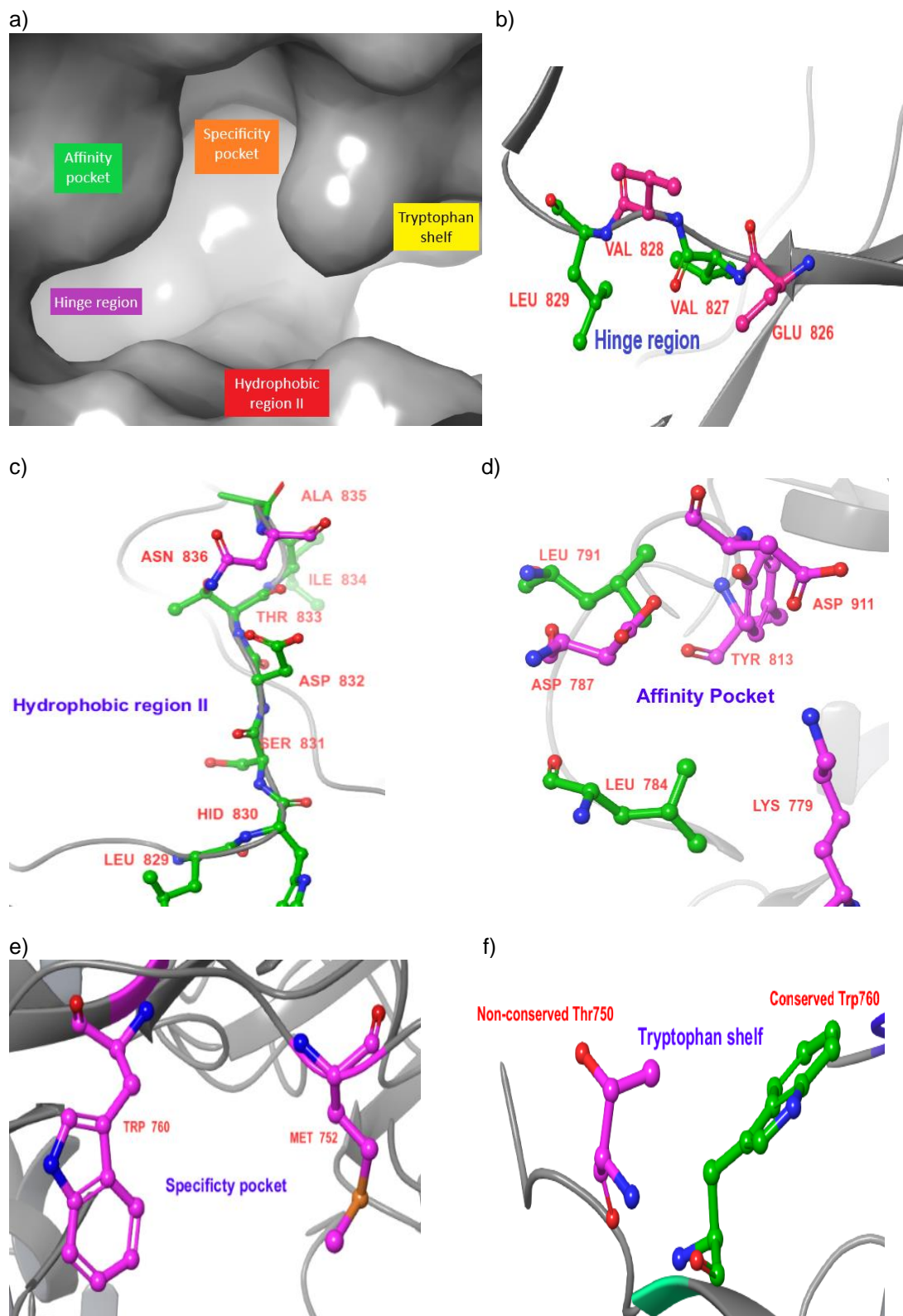


Figure 13. a) The binding site of PI3K δ (PDB code 4XE0), highlighting the binding regions with colored squares. It should be noted that the affinity pocket cannot be shown in this two-dimensional structure, as it is located behind the bulge. b) The hinge region consists of 4 residues, two of them Glu⁸²⁶ and Val⁸²⁸ (highlighted in magenta) are typically engaged in key hydrogen bond interactions with PI3K δ inhibitors. c) The hydrophobic region II is composed of 8 residues, among them, only Asn⁸³⁶ (highlighted in magenta) was identified as a key residue for selectivity¹⁵¹. d) The affinity pocket is comprised of 6 residues, four of them Lys⁷⁷⁹, Asp⁷⁸⁷, Asp⁹¹¹ and Tyr⁸¹³ (highlighted in magenta) participate in hydrogen bond with

PI3K δ inhibitors. e) The specificity pocket is formed upon inhibitor binding by reorientation Met⁷⁵² and Trp⁷⁶⁰ residues (highlighted in magenta). f) The tryptophan shelf is the space located between conserved δ Trp⁷⁶⁰ (green) and non-conserved Thr750 (magenta), this region is not accessible in the other three isoforms.

1.6.3 Affinity pocket (hydrophobic region I)

The affinity pocket lies outside of the ATP binding site (Figure 13a)^{140,152}. The six residues that line the affinity pocket are strictly conserved across the class I isoforms^{151,158}. These 6 residues include δ Lys⁷⁷⁹, δ Leu⁷⁸⁴, δ Asp⁷⁸⁷, δ Leu⁷⁹¹, δ Tyr⁸¹⁵ and δ Asp⁹¹¹ (Figure 13d)^{160,162}. The affinity pocket is not directly involved in ATP binding, whereas many PI3K inhibitors make hydrogen bond interactions with this pocket, resulting in increased binding affinity (discussed in more details in Section 0)¹⁴⁹.

1.6.4 Specificity pocket

The specificity pocket is not present in the PI3K δ apoenzyme¹⁴⁶. The specificity pocket is created between Trp⁷⁶⁰ and Met⁷⁵², that are normally packed against each other in the apoenzyme, on binding a PI3K δ inhibitor the residues are displaced by ~ 6.5 Å (Figure 13e)¹⁵³, forming a pocket in which the inhibitor is sandwiched between the indole ring of Trp⁷⁶⁰ and the side chain of Met⁷⁵², suggesting that this pocket is created by an induced-fit mechanism^{146,154}. The induced Met⁷⁵²/Trp⁷⁶⁰ specificity pocket exists in PI3K δ and is believed to be the main factor of the PI3K δ isoform selectivity of propeller-shaped PI3K δ inhibitors (discussed in more details in Section 0)^{154–156}, while the formation of this pocket in the other isoforms (α and β) is less favourable compared to PI3K δ .

1.6.5 Tryptophan shelf

The tryptophan shelf (hydrophobic dimple) is the region of space located between Trp⁷⁶⁰ and the non-conserved residue Thr750 (Figure 13f)^{157,158}. The tryptophan shelf is exclusively found in the PI3K δ isoform, as the equivalent residues to δ Thr750 are Arg⁷⁷⁰ in PI3K α , Lys⁸⁰² in PI3K β and Lys⁷⁷¹ in PI3K γ (Figure 14)^{159,160}. These amino acid side chains make cation-pi interactions with the corresponding tryptophan residue and occlude access to the tryptophan shelf^{159,160} (see Section 1.7.2.1 for more details)^{160,161}.

	Non-conserved residues opposed to the key tryptophan											The key conserved Trp that makes the tryptophan shelf
PI3K α	Arg 770	Ile 771	Met 772	Ser 773	Ser 774	Ala 775	Lys 776	Arg 777	Pro 778	Leu 779	Trp 780	
PI3K β	Lys 771	Tyr 772	Met 773	Asp 774	Ser 775	Lys 776	Met 777	Lys 778	Pro 779	Leu 780	Trp 781	
PI3K γ	Lys 802	Val 803	Met 804	Ala 805	Ser 806	Lys 807	Lys 808	Lys 809	Pro 810	Leu 811	Trp 812	
PI3K δ	Thr 750	Phe 751	Met 752	Asp 753	Ser 754	Lys 755	Met 756	Lys 757	Pro 758	Leu 759	Trp 760	

Figure 14. Sequence of the residues at the periphery of the tryptophan shelf in the four isoforms of class I PI3K. The key tryptophan (orange) is conserved between the four isoforms. However, in PI3K δ , the residue opposed to the key tryptophan is threonine (red), while in the other three isoforms is Arg (yellow) or Lys (blue), which forms a cation/pi interaction with Trp, blocking access to the tryptophan shelf.

1.7 PI3K δ isoform selectivity

1.7.1 Isoform selective PI3K δ inhibitors compared to pan-PI3K inhibitors

Pharmacological inhibition of the four isoforms of class I PI3K (pan-class I PI3K inhibition) for the treatment of blood cancers and autoimmune diseases

is not tolerated due to the generation of off-target side effects^{162–167}, including: (i) hyperglycaemia (likely resulting from inhibition of the α isoform, because intracellular PI3K α signalling mediates insulin action downstream of insulin receptor substrate-1 (IRS-1)^{168,169}); (ii) colitis (likely secondary to inhibition of PI3K γ ^{162–167}); (iii) neutropenia a blood disorder characterized by a decrease in the number of neutrophils in the blood stream and associated with increased susceptibility to infection¹⁷⁰ (the inhibition of PI3K γ signaling pathway in neutrophils by pan PI3K inhibitors may be associated with the incidence of neutropenia^{166,171}). Based on these findings, it was suggested that the severe side effects associated with pan PI3K inhibitors are the major challenge to obtain the drug exposure needed to achieve the optimal treatment effectiveness³². Hence, selective inhibition of a single PI3K isoform over the other isoforms will be necessary.

1.7.2 Approaches achieve PI3K δ isoform selectivity

The four class I isoforms PI3K bind to the same substrates which are ATP and PI(4,5)P₂. Thus, the active sites of the four isoforms have a high degree of amino acid conservation combined with high structural similarity^{139,161}, which explains the difficulty in achieving PI3K δ isoform selectivity⁸⁵. However, there are 3 unique regions of the PI3K δ binding site that can be exploited to achieve PI3K δ selectivity over the other three isoforms^{144,149}. The 3 binding regions include: 1) the tryptophan shelf, 2) the specificity pocket and 3) the affinity pocket. Although the residues occupying the above-mentioned regions are conserved, there are subtle variations in the non-binding amino acid residues that are positioned around the periphery of these regions, which can be targeted to achieve δ isoform selectivity¹⁶¹.

1.7.2.1 Tryptophan shelf

The tryptophan shelf defines the region of space located between δTrp^{760} and δThr^{750} . δTrp^{760} is located within PI3K δ binding site and it is conserved across all isoforms (Trp^{780} in α , Trp^{812} in β and Trp^{781} in γ) (Figure 15), whereas δThr^{750} located at the periphery of the PI3K δ binding site. In the

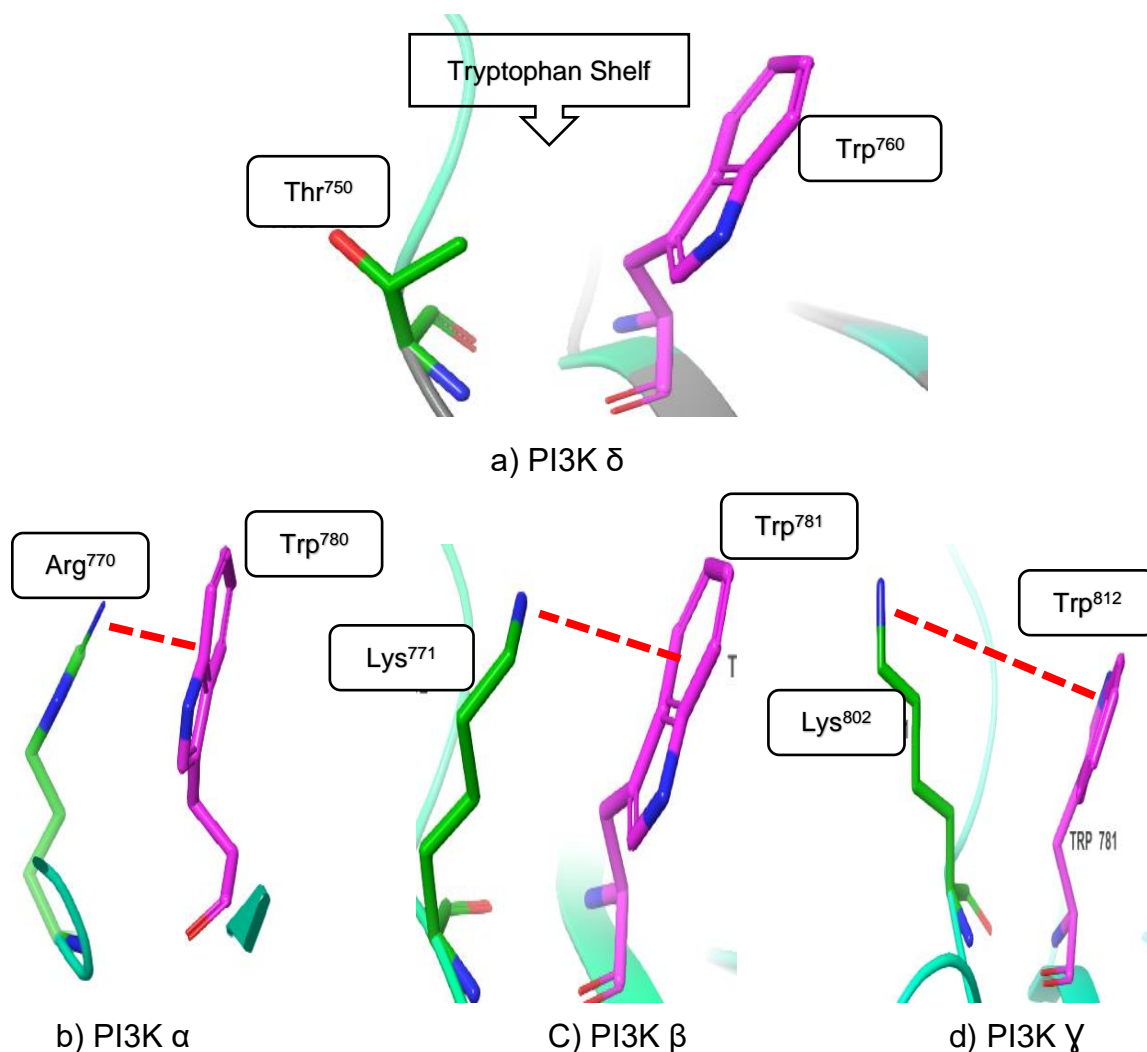


Figure 15. Comparison of the tryptophan region of PI3K δ , PI3K α , PI3K β and PI3K γ . a) Crystal structure of murine PI3K δ (PDB4XE0) demonstrates a big gap between the key Trp^{760} (magenta) and the opposed Thr^{750} (green), which is called the tryptophan shelf. b) Crystal structure of human PI3K α (PDB code 3HHM) demonstrates a cation-pi interaction between the key Trp^{780} (magenta) and the opposed Arg^{770} (green). c) Crystal structure of human PI3K β (PDB code 3Y3A) demonstrates a cation-pi interaction between the key Trp^{781} (magenta) and the opposed Lys^{771} (green). d) Crystal structure of human PI3K γ (PDB code 3ENE) demonstrates a cation-pi interaction between the key Trp^{812} (magenta) and the opposed Lys^{802} (green).

other three isoforms, the position equivalent to δ Thr750 is occupied by a basic amino acid (arginine or lysine) (Figure 15)^{159,160}, which forms a cation-pi interaction with Trp⁷⁶⁰, resulting in the blocking of the tryptophan shelf. Thus, this subtle difference in δ Thr⁷⁵⁰ residue peripheral to the ATP binding site can be exploited to improve PI3K δ selectivity, where PI3K δ inhibitors can make pi-pi or C-H/pi interactions with Trp⁷⁶⁰ (more details in chapter 2)^{159,172}.

1.7.2.2 Specificity pocket

As mentioned in Section 1.6.4, the specificity pocket is an induced hydrophobic pocket, which is not found in the PI3K δ apoenzyme and only created upon contact of an inhibitor with PI3K δ , it is worth noting that this hypothesis is based on observation of the crystal structure of PI3K δ and it is not necessary a reflection of what actually happens. The specificity pocket comprises of the side chains of Trp⁷⁶⁰ and Ile⁷⁷⁷ on one side and Met⁷⁵² and Pro⁷⁵⁸, on the other side¹⁷³. These four residues are conserved in the four isoforms of class I PI3K. However, there are slight differences in the amino acid residues surrounding the specificity pocket (Figure 16)¹⁴⁹. In PI3K δ , the specificity pocket is created due the movement of Trp⁷⁶⁰ side chain away from Met⁷⁵², forming a wide deep pocket which can be filled by an inhibitor scaffold such as the quinazolinone ring (Figure 17a). The ability of the Trp⁷⁶⁰ residue to move is due to the high degree of flexibility of its side chain, which is not involved in any hydrogen bond with the neighbouring Met⁷⁶² residue (Figure 17a)¹⁴⁹. Whereas in the other three isoforms (α , β and γ) the movement of Trp residues (equivalent to Trp⁷⁶⁰ of PI3K δ) is partially or completely restricted, thus the opening of the specificity pocket in these isoforms is less

Chapter 1

	The two conserved residues that form the specificity pocket		The non-conserved residue at the periphery of the specificity pocket
PI3K α	Trp780	Met772	Glu798
PI3K β	Trp781	Met773	Glu858
PI3K γ	Trp812	Met804	Glu814
PI3K δ	Trp760	Met752	Met762

Figure 16. Amino acid sequence alignment of the specificity pocket of PI3K δ with other three isoforms of class I PI3K. PI3K α , β and γ contains polar residue glutamate (highlighted in blue) located adjacent to the specificity pocket, which makes a hydrogen bond with the key tryptophan, thereby restricting its movement and disfavours the opening of the specificity pocket. Whereas in PI3K δ , the equivalent residue to glutamate is the non-polar methionine (highlighted in red) which cannot form a hydrogen bond with the key tryptophan, the flexibility of tryptophan allows the opening of the specificity pocket in PI3K δ .

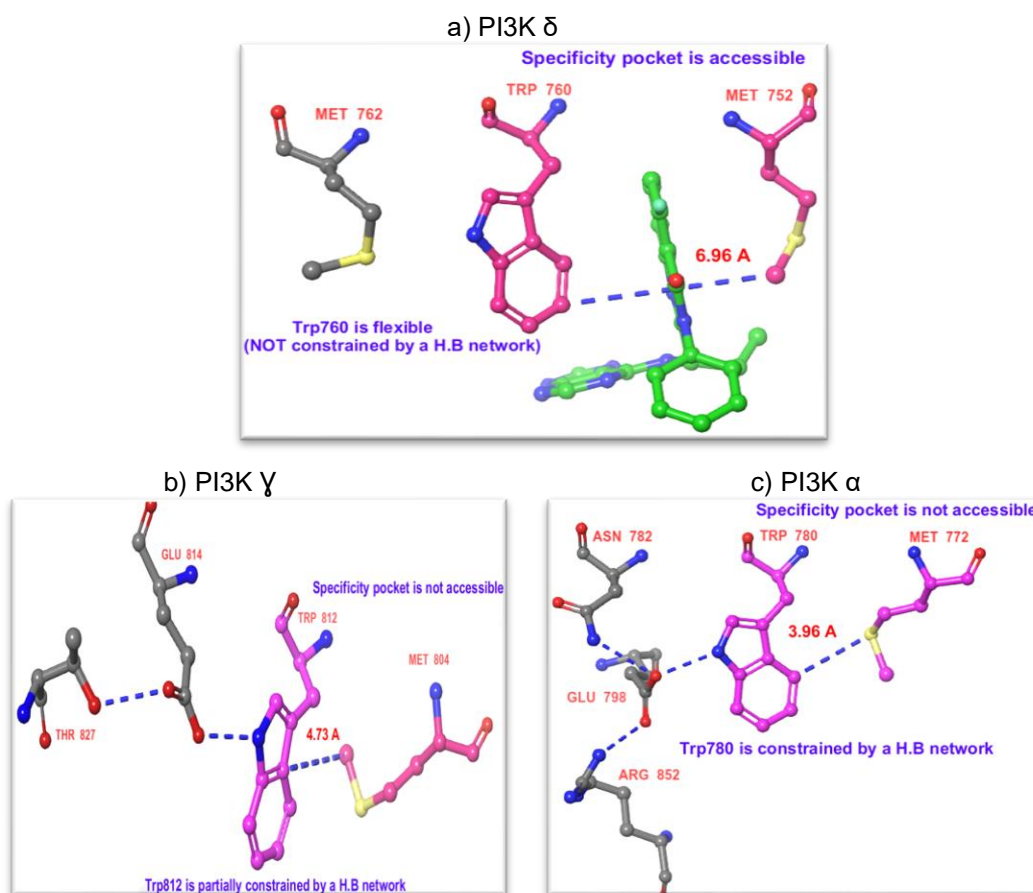


Figure 17. The specificity pocket. (a) The specificity pocket in PI3K δ (PDB code 4XE0) is opened by the synchronized movement between Trp⁷⁶⁰ (magenta) and Met⁷⁵² (magenta), Trp⁷⁶⁰ is flexible because it does not make an interaction with the surrounding residue Met⁷⁶². (b) The specificity pocket in PI3K γ (PDB 3ENE) is difficult to access because the movement of Trp⁸¹² (magenta) is partially restricted by the hydrogen bond network (blue dashed line) with the surrounding residues Glu⁸¹⁴ (grey) and Thr⁸²⁷ (grey). (c) The specificity pocket in PI3K α (PDB 4JPS) cannot be accessed because the movement of Trp⁸¹² (magenta) is tightly restricted by the hydrogen bond network (blue dashed line) with the surrounding residues Glu⁷⁹⁸ (grey), Asn⁷⁸² (grey) and Arg⁸⁵² (grey). The distances between Trp (magenta) and Met (magenta) in the specificity pocket are marked with red dashed lines.

energetically favoured compared to PI3K δ ^{144,173,174}. In PI3K γ , the movement of Trp⁸¹² (corresponding to Trp⁷⁶⁰ in PI3K δ) is partially restricted by the hydrogen bond network with the neighbouring residue Glu⁸¹⁴ (equivalent to Met⁷⁶² in PI3K δ) (Figure 17b). In contrast to the relatively hydrophobic residue δ Met762, γ Glu⁸¹⁴ has a polar, charged side chain, which is able to form a hydrogen bond with γ Trp⁸¹², causing restriction of its movement (Figure 17b)¹⁷⁵, thus, the specificity pocket in PI3K γ needs more energy to open^{144,173,174}. Whereas in the PI3K α isoform, the movement of Trp⁷⁸⁰ (corresponding to Trp⁷⁶⁰ in PI3K δ) is tightly restricted (Figure 17c), as it makes a hydrogen bond with the surrounding residue Glu⁷⁹⁸ (corresponding to Met⁷⁶² in PI3K δ). Glu⁷⁹⁸ in turn forms two hydrogen bond interactions with Asn⁷⁸² and Arg⁸⁵², leads to the formation of an extended hydrogen bond network (Figure 17c), consequently, the opening of the specificity pocket in PI3K α requires overcoming a high energy barrier for the breaking of the hydrogen network^{144,173,174}.

1.7.2.3 The affinity pocket

This pocket is lined with polar and hydrophobic residues (two aspartates, lysine, tyrosine and two leucines). All of these 6 residues are conserved across the four isoforms of class I PI3K^{144,145}. Interestingly, Sutherlin *et al*¹⁶⁰, Schwehm *et al*¹⁵⁹ and Berndt *et al*¹⁴⁵ reported that the affinity pocket can be exploited to achieve selectivity for PI3K δ , which can be attributed to differences in the hydrogen bond network, caused by non-conserved residues beyond the affinity pocket^{140,149,172}. In PI3K α , β and γ , the tyrosine residue (α Tyr⁸³⁶, β Tyr⁸³³ and γ Tyr⁸⁶⁷), which lines the affinity pocket and always participates in a key hydrogen bonding with inhibitors, is constrained

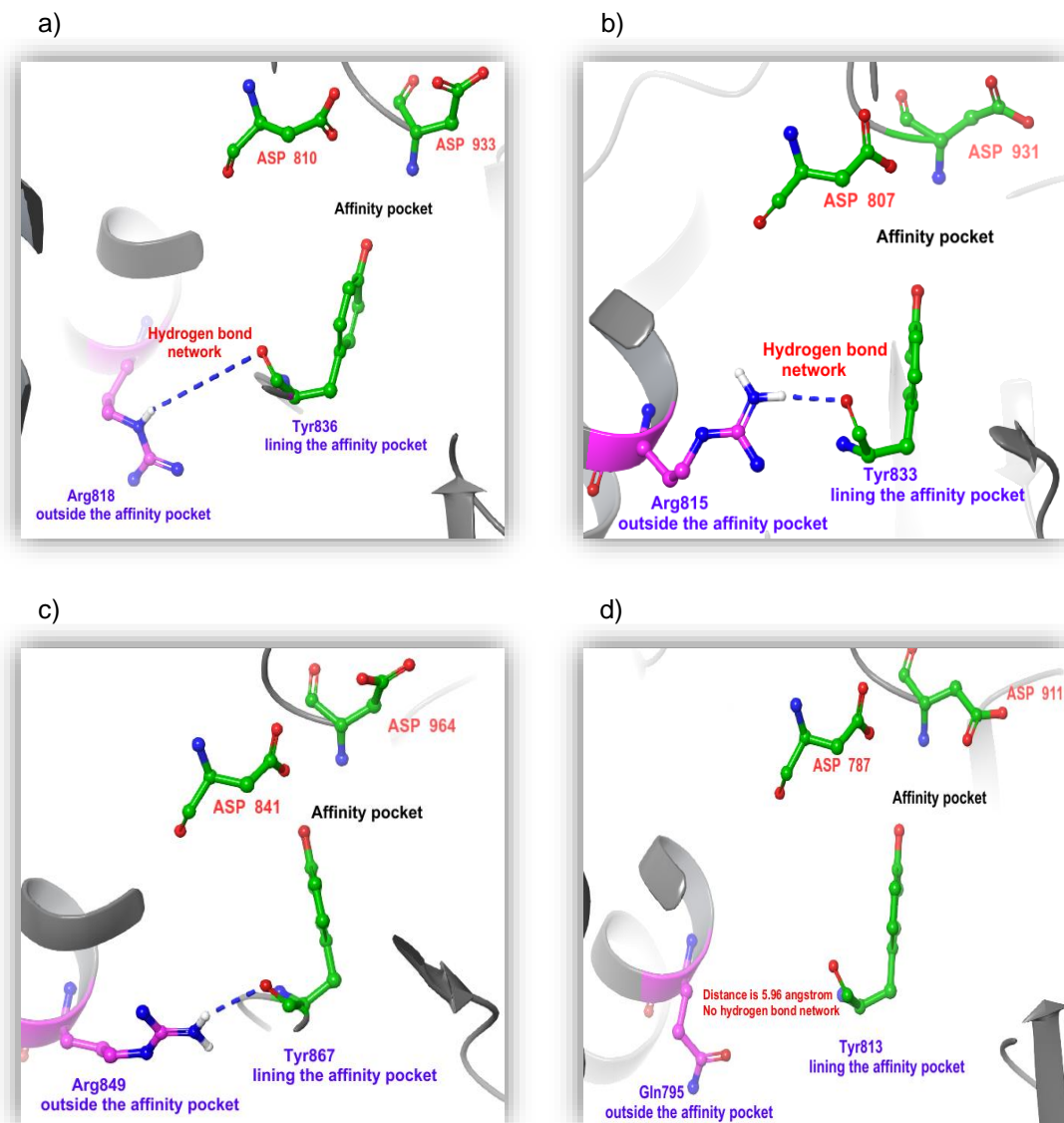


Figure 18. The Affinity pocket (a) Affinity pocket in PI3K α (PDB code 4JPS), highlights the key α Tyr⁸³⁶, which is conformationally restrained by a hydrogen bond to α Arg⁸¹⁸ (magenta), located outside the affinity pocket. (b) Affinity pocket in PI3K β (PDB code 2Y3A), highlights the key tyrosine residue (β Tyr⁸³³), which is conformationally restrained by a hydrogen bond to β Arg⁸¹⁵ (magenta), located outside the affinity pocket. (c) Affinity pocket in PI3K γ (PDB code 3ENE), highlights the key tyrosine residue (γ Tyr⁸⁶⁷), which is conformationally restrained by a hydrogen bond to γ Arg⁸⁴⁹ (magenta), located outside the affinity pocket. (d) Affinity pocket in PI3K δ (PDB code 4XE0), highlights the key tyrosine residue (δ Tyr⁸¹³), which is NOT conformationally restrained by a hydrogen bond, as the equivalent residue to arginine is Glutamine (δ Gln⁷⁹⁵) that has a shorter side chain. The lack of hydrogen bond interaction is explained by 5.96 Å separation distance between the carbonyl backbone of δ Tyr⁸¹³ and the side chain of δ Gln⁷⁹⁵.

because it is involved in a hydrogen bond network with the nearby arginine (α Arg⁸¹⁸, β Arg⁸¹⁵ and γ Arg⁸⁴⁹) (Figure 18a, 18b and 18c). However, the corresponding residue to arginine is a glutamine (Gln⁷⁹⁵) in PI3K δ . Glutamine has a shorter side chain than arginine, therefore it would not be able to form

a hydrogen bond with δTyr^{813} (Figure 18d). Accordingly, δTyr^{813} has greater rotational freedom when compared to its equivalents in other three isoforms (discussed in chapter 2 in more detail)¹⁴⁴.

1.8 Types of PI3K inhibitors based on their isoform selectivity

Class-I PI3K inhibitors are subdivided into three categories based on their isoform selectivity profile: non-selective (pan) inhibitors (inhibit the four isoforms), dual inhibitors (inhibit two isoforms) and isoform-selective PI3K inhibitors (inhibit a single isoform)^{176,177}. The following section reviews selected examples of each class (Table 2).

Table 2. List of PI3K inhibitors that are approved for use or undergoing clinical development. This list also includes the therapeutic use of these inhibitors and their biochemical activities against class-I PI3K isoforms^{178–180}.

Compd	Status in 2020	Selectivity	Clinical use	Isoform potency IC ₅₀ (nM)			
				PI3K δ	PI3K α	PI3K β	PI3K γ
Pictilisib (4)	Phase II	Pan PI3K	Locally advanced and metastatic solid tumours	3	3	33	75
Duvelisib (5)	Approved	Dual PI3K δ/γ	CLL, SLL and FL	2.5	1602	85.0	27.4
Copanilisib (6)	Approved	Dual PI3K α/δ	Relapsed FL and non-Hodgkin lymphoma	0.7	0.5	3.7	6.4
Leniolisib (7)	Phase III	Selective PI3K δ	Activated PI3K kinase delta syndrome (APDS)	27	792	1710	>9100
Idelalisib (8)	Approved	Selective PI3K δ	CLL, SLL and FL	11	14000	2800	56

1.8.1 Pan-PI3K inhibitor: pictilisib (4)

Pictilisib (4) (Figure 19) is a potent, orally available, highly selective class-I PI3K inhibitor with a good margin of selectivity against other members of the PI3K-related kinases (PIKK) family such as mTOR and DNA-dependent protein kinase (DNA-PK)^{181,182}. Pictilisib (4) possesses equal activities against PI3K α and δ with $IC_{50} = 3$ nM, but shows comparatively less activity against PI3K β and γ with IC_{50} values of 33 nM and 75 nM, respectively (Table 2)^{181,182}. In vitro and preclinical studies have displayed that 4 was effective against tumours driven by *PI3KCA* or PTEN mutations^{181,183,184}. Pictilisib (4) is currently undergoing phase II clinical trials in combination with other anticancer drugs such as paclitaxel and anastrozole, for treatment of locally advanced and metastatic solid tumours that harbour PI3KCA mutations such as breast cancer^{185–187}.

However, the efficacy of 4 was likely limited by the development of serious, often intolerable adverse effects especially neutropenia, haemolytic anaemia, decreased appetite and diarrhoea, which appear to be attributable to the non-isoform selective inhibition of PI3K. Diarrhoea was found to be the major cause for discontinuation of pictilisib (4) treatment in the clinical studies¹⁸⁷. Based on these findings, Genentech stopped the clinical development of 4 in 2018¹⁸⁶.

1.8.1.1 Binding Interactions of pictilisib (4) with PI3K δ

Pictilisib (4) has a thienopyrimidine core that bears three binding arms (Figure 19). The morpholine ring forms a critical hydrogen bond to the amide backbone of Val⁸²⁸ (conserved) in the hinge region of the kinase (Figure 19b). On the other hand, the indazole ring fits deeply into the affinity pocket where

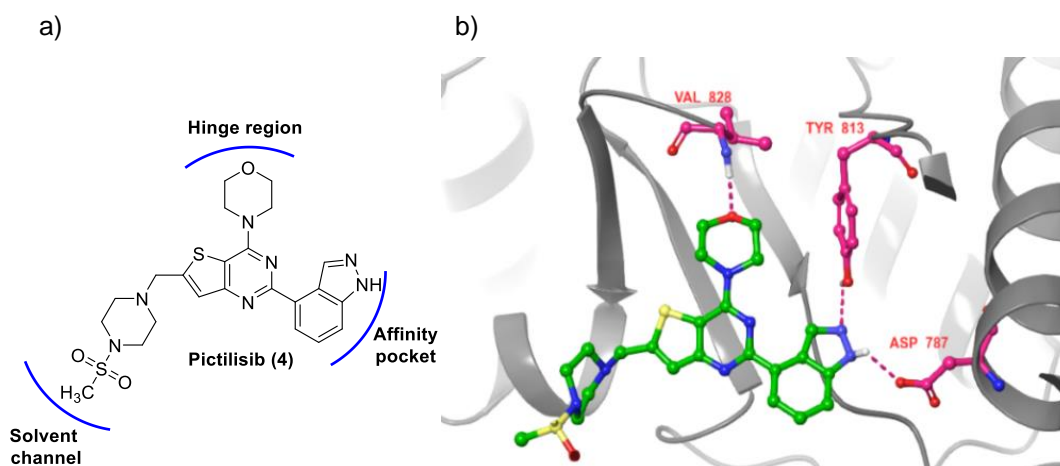


Figure 19. a) The non-selective PI3K inhibitor pictilisib (**4**) and its binding points at PI3K δ ¹⁸². b) Crystal structure of murine PI3K δ (PDB code 2WXP) with pictilisib (**4**) bound. Dashed pink lines represent the proposed hydrogen bonds¹⁴⁹.

the indazole N-1 forms a hydrogen bond with the side chain of Asp⁷⁸⁷ and N-2 makes a hydrogen bond with the phenolic side chain of Tyr⁸¹³ (Figure 19b). The 4-methanesulfonyl-piperazine-ylmethyl group fits into a channel pointing towards solvent, leading to the improvement the solubility (Figure 19b)¹⁸². All the residues (Val⁸²⁸, Tyr⁸¹³ and Asp⁷⁸⁷) that **4** binds to are conserved among the four isoforms of class I PI3K, thus **4** is considered a non-selective class I PI3K inhibitor^{182,188}.

1.8.2 Dual-selective PI3K inhibitor

The term 'dual-selective PI3K inhibitors' refers to the compounds with a predominant activity against only two PI3K isoforms and little or no activity against the other two isoforms¹⁸⁹. The main idea behind developing dual inhibitors is that they can offer an improvement in safety versus pan PI3K inhibitors¹⁹⁰. Moreover, dual PI3K inhibitors show superior efficacy when compared with isoform-specific inhibitors for treating different types of blood cancers and autoimmune diseases^{190,191}.

1.8.2.1 PI3K δ and γ dual inhibitor: duvelisib (5)

Duvelisib (5) (Figure 20) was developed by Verastem Oncology as an orally bioavailable dual PI3K δ / γ inhibitors (Table 2)¹⁹². δ and γ isoforms are both preferentially expressed in immune cells, where they exert complementary non-overlapping roles in the pathogenesis of blood cancers and inflammation¹⁹³. In CLL disease, PI3K δ is expressed in malignant B-cells^{96,194}, where it regulates CLL cell survival, migration and proliferation^{96,194,195}, whereas PI3K γ is mainly expressed in macrophages within tumour microenvironment, where it mediates the release of cytokines that induce immune suppression and promotes CLL proliferation (cross-talk mechanism)^{196–198}. Thus, dual blockade of isoforms PI3K δ and γ provides an effective therapeutic strategy for patients with CLL and other blood cancers¹⁹⁹. Accordingly, duvelisib (5) (Copiktra, developed by Verastem) has been approved by the FDA in 2018 for treatment of CLL, SLL and follicular non-Hodgkin's lymphoma (FL) (Table 2)^{189,200}.

However, 5 treatment was associated with severe adverse events including colitis, pneumonitis, hepatotoxicity and diarrhoea^{201,202}. Duvelisib-induced colitis and pneumonitis are thought to be immune-related, caused by the suppression of the PI3K δ signalling in the Treg cells, which play a key role in the prevention of autoimmune response by maintaining self-tolerance^{202–204}. The mechanism responsible for duvelisib-induced liver injury is not known, but it can be a consequence of inhibition of PI3K δ and/or PI3K γ in hepatocytes (direct toxicity) or due to immune-mediated liver injury (indirect toxicity)^{202,205}. Hepatotoxicity of 5 explains why it has not been commonly used since its approval in 2018²⁰⁵.

1.8.2.2 Binding Interactions of duvelisib (**5**) with PI3K δ

The PI3K δ and γ isoforms have unique structural differences from the α and β isoforms, that could be exploited for their selective targeting¹⁴⁵. It was widely suggested that **5** achieved a high degree of selectivity for PI3K δ and γ isoforms versus α and β by exploiting the induced specificity pocket that can be easily accessed in PI3K δ and PI3K γ ¹⁸⁹, while the opening of this pocket in α and β isoforms was less easy (see Section 0 and Figure 17c for more details).

To date, a crystal structure of PI3K δ in complex with **5** is not available¹⁸⁹. However, owing to the structural similarity between **5** and idelalisib (**8**) (will be covered in Section 1.8.3.2.2), it was hypothesized that the binding mechanisms of the two compounds to the active site of PI3K δ are similar¹⁸⁹. (Figure 23 in Section 1.8.3.2.2 shows the crystal structure of PI3K δ with idelalisib (**8**) bound. To support this hypothesis, molecular docking of **5** to the PI3K δ binding site was carried out (Figure 20b). The docking results were consistent with the above hypothesis, revealing that the 8-chloroisoquinolinone ring of **5** was sandwiched between the side chains of Met⁷⁵⁰ and Trp⁷⁶⁰ in the newly created specificity pocket. The occupation of this pocket forces **5** to adopt a propeller-shaped conformation in the PI3K δ binding site, where the 8-chloroisoquinolinone scaffold lies perpendicular to the purine and phenyl rings (Figure 20b). The purine ring makes two hydrogen bonds with the hinge region, one formed between the hydrogen bond acceptor purine N-3 and the amide backbone of Val⁸²⁸. The second between the hydrogen bond donor NH-9 of the purine and the carbonyl backbone of Glu⁸²⁶ (Figure 20b). Finally, the phenyl ring of **5** is extended into the

hydrophobic region II where it makes hydrophobic interactions with the side chains of Asp⁸³², Thr⁸³³ and Asn⁸³⁶ (Figure 20b).

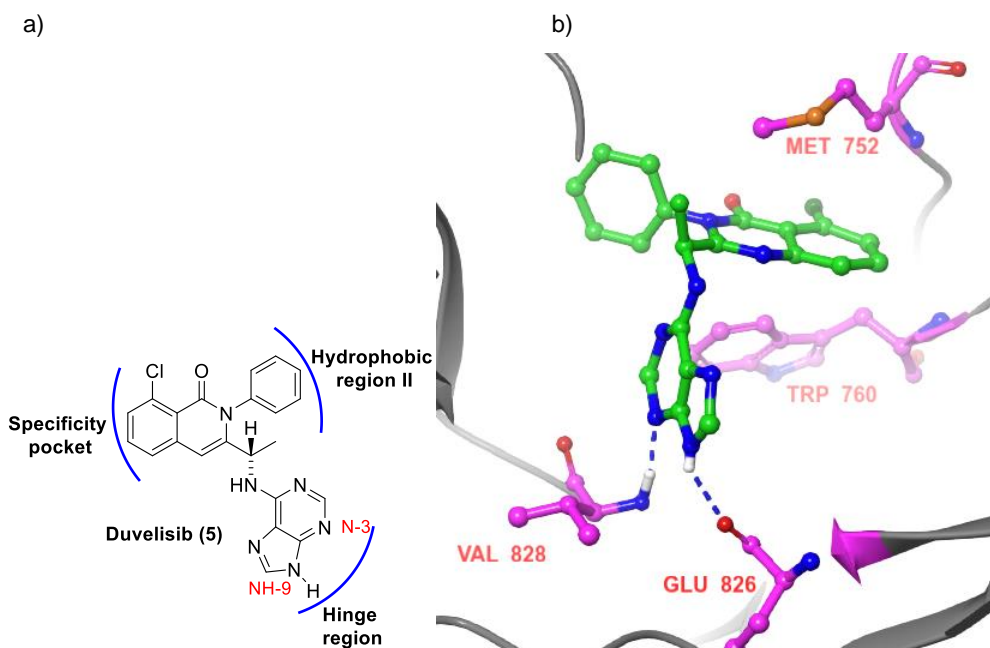


Figure 20. The dual PI3K δ / γ inhibitor duvelisib (**5**) and its binding points at PI3K δ ¹⁷⁸. b) Duvelisib (**5**) docked into the PI3K δ model (generated from PDB code 4XE0), It can be noticed that duvelisib (**5**) adopts a perpendicular conformation in the binding site of PI3K δ . Dashed blue lines represent the proposed hydrogen bonds.

1.8.2.3 PI3K δ and α dual inhibitor: copanilisib (**6**)

Copanilisib (**6**) (Figure 21) is an intravenous dual PI3K inhibitor, mainly targeting PI3K α and δ isoforms^{206,207}. Copanilisib (**6**) displayed sub-nanomolar potency against PI3K δ and α isoforms (IC₅₀ values of 0.7 and 0.3 nM, respectively) with more than 10-fold selectivity over PI3K β and PI3K γ (Table 2)^{179,208,209}. Copanilisib (**6**) is the only approved PI3K inhibitor, that is given intravenously²⁰⁹, this might be because **6** has a highly reactive amide group (Figure 21), which is prone to hydrolysis by intestinal digestive enzymes²¹⁰.

Copanilisib (**6**) can be used for the treatment of solid tumours as well as haematological cancers (Table 2)^{179,211}. In solid tumours, **6** is capable of inhibiting tumour cells proliferation, by blocking the signalling pathway of PI3K

α (encoded by the *PIK3CA* gene)²⁰⁸, which is considered to be among the most frequently mutated oncogenes in solid tumours such as breast cancer^{208,212}. Whereas in haematological cancers, **6** exerts antitumor activity by inducing apoptosis of cancerous B-cells through the inhibition of the PI3K δ pathway^{208,209}. For instance, **6** was found to be around 10-fold more active than **5** in inhibiting survival of CLL cells¹⁹², suggesting that dual inhibition of PI3K δ and α is more effective treatment for CLL than dual PI3K δ and γ inhibition¹⁹². Accordingly, on September, 2017, the FDA granted accelerated approval for **6** (Aliqopa, developed by Bayern) to treat patients with relapsed FL who have received at least two prior systemic therapies, based on the results of phase II clinical trials (Table 2)²⁰⁷.

The most common adverse effects of **6** include hyperglycaemia, neutropenia, infections, hypertension and diarrhoea^{209,213}. Hyperglycaemia is attributable to the on-target effect of PI3K α inhibition that results in disruption of insulin-receptor signalling and decreased glucose uptake in peripheral tissue^{207,209,214}. Copanilisib-induced hyperglycaemia could be managed with short-acting insulin and/or oral anti-diabetic drugs following intravenous treatment with copanilisib (**6**)²¹⁵. Hypertension is an uncommon adverse effect of PI3K inhibitors, and is only noticed with **6**, it is likely attributable to the infusion-related inhibition of the PI3K α isoform^{209,213,216}. However, copanilisib-related hypertension is reversible and temporary in nature and can be relieved by stopping the taking of the drug²¹⁵. In comparison to other class I PI3K inhibitors, **6** is associated with less gastrointestinal toxic effects^{209,213}, which is not surprising, given the fact that **6** is only administered via intravenous infusion²⁰⁹.

1.8.2.4 Binding Interactions of copanilisib (6) with PI3K δ

There is no available crystal structure of PI3K δ bound to **6**. However, Bayern published the only crystal structure of **6** bound to human PI3K γ (PDB code 5G2N) (Figure 21b)^{179,209}. The structure reveals that nitrogen N-1 on the imidazoline ring makes a hydrogen bond with Val⁸⁸² (equivalent to δ Val⁸²⁸) in the hinge region (Figure 21b)^{179,209}. The aminopyrimidine ring extends to the affinity pocket, where the exocyclic amino group N-2 is involved in two hydrogen bonds with Asp⁸³⁶ and Asp⁸⁴¹ (equivalent to δ Asp⁹¹¹ and δ Asp⁷⁸⁷, respectively), whereas the pyrimidine nitrogen N-3 acts as a hydrogen bond acceptor for Lys⁸³³ (equivalent to δ Lys⁷⁷⁹) (Figure 21b)^{179,209}. The methoxy group projects toward the ribose-binding pocket, the introduction of the methoxy group or other substituents to this pocket did not lead to an increase in potency, which could explain the fact that the ribose pocket is not frequently exploited in the discovery of PI3K inhibitors²¹⁷. Finally, the morpholine group

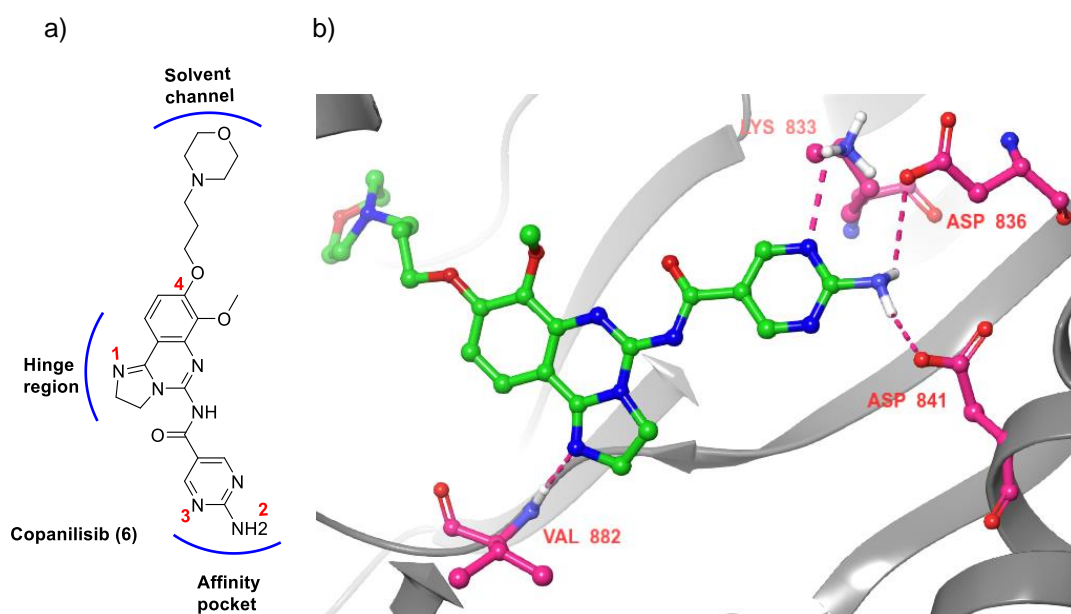


Figure 21. a) The dual PI3K α/δ inhibitor copanilisib (**6**), and its binding points at PI3K γ , highlights the atoms and groups (in red) involved in interactions with PI3K γ b) Crystal structure of human PI3K γ (PDB code 5G2N) with copanilisib (**6**) bound, pink dashed lines indicate the proposed hydrogen bond with Lys⁸³³ (Lys⁷⁷⁹ in PI3K δ), Asp⁸⁴¹ (Asp⁹¹¹ in PI3K δ) and Asp⁸³⁶ (Asp⁷⁸⁷ in PI3K δ) at the affinity pocket and with Val⁸⁸² (Val⁸²⁸ in PI3K δ) at the hinge region¹⁷⁹.

was added to position 4 of the central scaffold via a propoxy linker, where it extends towards the solvent channel at the entrance of the binding pocket (Figure 21b). The main role of the morpholine group is to increase the water solubility and oral bioavailability of **6**^{179,209}.

1.8.3 PI3K δ isoform-specific inhibitors

Single isoform inhibitors represent the newest generation of PI3K inhibitors that maximize on-target and minimize off-target binding events. Yang *et al*²⁰⁶ and Wang *et al*¹⁷⁷ have reported that isoform-selective PI3K δ inhibitors have superior safety than dual and pan PI3K inhibitors. Moreover, the functional non-redundancy between the four isoforms of PI3K expressed in solid and haematological malignancies has encouraged the development of isoform-specific inhibitors¹⁷⁷. Selective PI3K δ inhibitors are sub classified into two categories, based on their binding modes within the active site of PI3K δ : relatively flat-shaped inhibitors and propeller-shaped inhibitors^{144,145}.

1.8.3.1 Relatively flat-shaped PI3K δ inhibitors: leniolisib (7)

The flat-shaped inhibitors adopt a flat (extended) conformation in the ATP binding site when bound to PI3K δ ^{146,159}. Flat-shaped inhibitors bind to PI3K δ by interacting with three binding regions: 1) The affinity pocket is typically filled by either an aryl or heteroaryl group, where it forms two hydrogen bonds, one with the carboxylate side chain of δ Asp⁷⁸⁷ and the other with the phenolic side chain of δ Tyr^{813/157}. 2) The hinge region is usually occupied by either a saturated or unsaturated heterocycle, where it engages in a single hydrogen bond with the side chain of δ Val^{828/157,159,160}. 3) Tryptophan shelf is usually

occupied by a linear or saturated heterocyclic group, where it makes C-H/ π interactions with the δ Trp⁷⁶⁰ 218–220, (more details in chapter 2).

There are currently no FDA-approved flat-shaped PI3K δ inhibitors, however leniolisib (**7**) has been developed by Novartis and is currently is being tested in phase III clinical trials for the treatment of activated PI3K δ syndrome (APDS) (Table 2)²²¹, which is a genetic disorder caused by mutations in PI3K3D gene encoding the PI3K δ enzyme, resulting in hyperactivation of PI3K δ signalling in B and T lymphocytes²²². APDS leads to immunodeficiency associated with increased susceptibility to bacterial and viral infections²²³. Moreover, **7** is currently in phase II clinical trials for treatment of Sjögren syndrome (SS) (Table 2)^{219,221}, an autoimmune disease characterized by two hallmark symptoms dry eyes and dry mouth²²⁴, it results from lymphocytes attacking salivary and lacrimal glands, leading to their dysfunction and destruction²²⁵. Novartis reported that in Phase II/III, **7** did not cause hyperglycaemia, neutropenia and diarrhoea, which are known class effects of PI3K inhibitors^{226–228}. Leniolisib (**7**) displayed excellent potency against PI3K δ (IC₅₀ value of 9 nM) with 29, 183 and 514-fold selectivity over PI3K α , β and γ respectively (Table 2)²²⁹.

1.8.3.1.1 Binding Interactions of leniolisib (**7**) with PI3K δ

Crystal structure of PI3K δ in complex with Leniolisib (**7**) (PDB code 5O83) was determined. The structure revealed that **7** adopts a relatively extended conformation (Figure 22b)²²⁹, where the propionamide group is directed towards the tryptophan shelf, stacking with the indole ring of δ Trp⁷⁶⁰, resulting in a C-H/ π interaction. The methoxypyridine moiety inserts deeply into the affinity pocket, where the methoxy group engages in a charge-enhanced

hydrogen bond with δ Lys⁷⁷⁹ (Figure 22b). Lastly, the nitrogen atom N-1 of the central piperido-pyrimidine scaffold forms a single hydrogen bond interaction with δ Val⁸²⁸ of the hinge region (Figure 22b)^{219,229}.

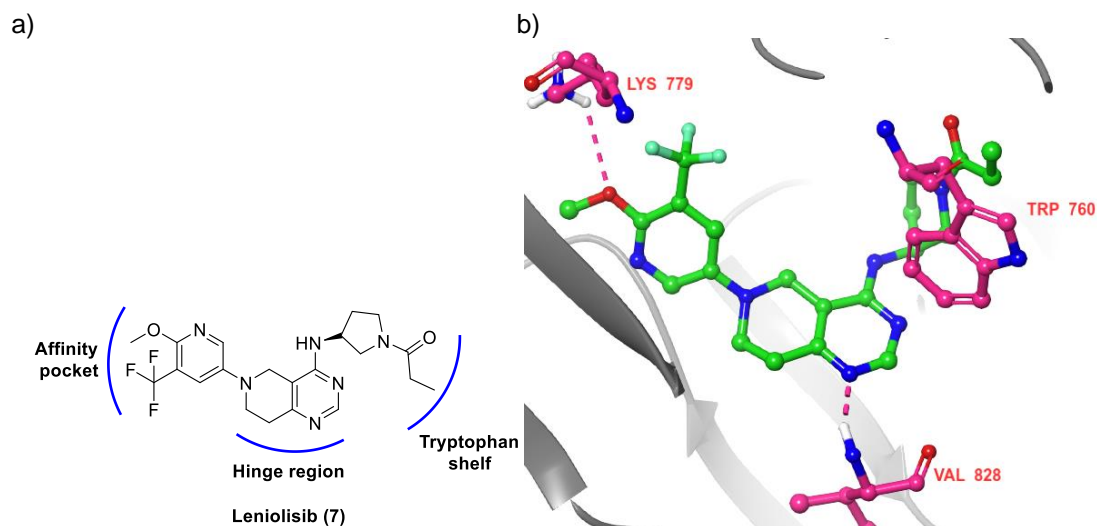


Figure 22. a) The flat-shaped selective PI3K δ inhibitor leniolisib (**7**), and its binding points at PI3K δ . b) Crystal structure of leniolisib (**7**) complexed with murine PI3K δ (PDB code 5O83) showed that **7** adopts a relatively flat conformation at the PI3K δ binding site. The propionamide group folds to fit the tryptophan shelf and make C-H/pi interactions with Trp⁷⁶⁰. Dashed pink lines represent the proposed C-H/pi interactions.

1.8.3.2 Propeller-shaped PI3K δ inhibitor: idelalisib (**8**)

In contrast to flat-shaped PI3K δ inhibitors, all propeller-shaped PI3K inhibitors adopt orthogonal conformations when they bind to PI3K δ ^{146,149}, where the three substituents (blades) are twisted almost perpendicularly^{146,149}. It is also important to note that propeller-shaped inhibitor interaction regions on PI3K δ are different from flat-shaped inhibitor binding regions, the former inhibitors bind to PI3K δ at the hinge region, specificity pocket and hydrophobic region II (Table 3), while the latter interact with PI3K δ in the hinge region, affinity pocket and tryptophan shelf^{145,146,152}. The specificity pocket is generally occupied by a hetero-bicyclic ring system, which is usually quinazolinone ring¹⁴⁵. Hydrophobic region II is usually filled by an aryl ring such as phenyl group and tolyl groups, where it makes Van der Waals

interactions with the residues lining this region. Lastly, in the hinge region, propeller-shaped inhibitors engage in dual hydrogen bond interactions with the backbones of Glu⁸²⁶ and Val⁸²⁸. Therefore, the hinge binder of propeller-shaped inhibitors is typically a heterocyclic ring, which contains both a hydrogen bond acceptor and donor such as a purine and aminopyrimidine ring¹⁸⁰. A classic example of a propeller-shaped PI3K δ inhibitor is idelalisib (**8**) (Figure 23a)^{154,230,231}, which is the only FDA-approved single isoform selective PI3K δ inhibitor. Thus, in this thesis, **8** will be used as a starting point to develop more potent and selective PI3K δ inhibitors.

Table 3. The difference between the binding regions of flat-shaped inhibitors and propeller-shaped inhibitors in the PI3K δ binding site^{145,146,152}.

Binding regions	Flat-shaped inhibitors	Propeller-shaped inhibitors
Specificity pocket	Not bound	Bound
Hydrophobic region II	Not bound	Bound
Hinge region	Bound (1 H.B interaction)	Bound (2 H.B interactions)
Affinity pocket	Bound	Not bound
Tryptophan shelf	Bound	Not bound

1.8.3.2.1 Uses and biological activity of idelalisib (**8**)

Idelalisib (**8**) (Zydelig, developed by Gilead) was approved in 2014 for the treatment of three types of B-malignancies^{126,180}. Idelalisib (**8**) is used in combination with rituximab (monoclonal antibody) to treat patients with relapsed or refractory CLL (Table 2)^{232,233}. Moreover, it can be used alone in the treatment of patients with relapsed FL and relapsed SLL, who have received two lines of treatment, including rituximab and alkylating agents as first or second line therapy^{126,180}. Idelalisib (**8**) demonstrated low nanomolar

potency against PI3K δ ($IC_{50} = 11$ nM) while having 1273, 255 and 5-fold selectivity over PI3K α , β and γ , respectively (Table 2)¹⁸⁰. To understand the mechanism underlying PI3K δ selectivity of **8**, the crystal structure of the idelalisib-PI3K δ complex was studied.

1.8.3.2.2 Binding interactions of idelalisib (**8**) to PI3K δ

Somoza *et al*¹⁵³ disclosed the crystal structure of **8** in complex with PI3K δ . The structure showed that **8** adopts a propeller-shaped (T-shaped) conformation in the binding site of PI3K δ (Figure 23b)²³⁴. Idelalisib (**8**) occupies the induced specificity pocket with the quinazolinone ring, where Trp⁷⁶⁰ and Met⁷⁵² that are normally packed against each other in the apoenzyme, when they come in contact with **8** they move away from each other by ~ 6.5 Å, to create the pocket for the fluoro quinazolinone core to fit (Figure 23)¹⁵³. The phenyl group is oriented perpendicular to the quinazolinone scaffold and points toward the hydrophobic region II, where it

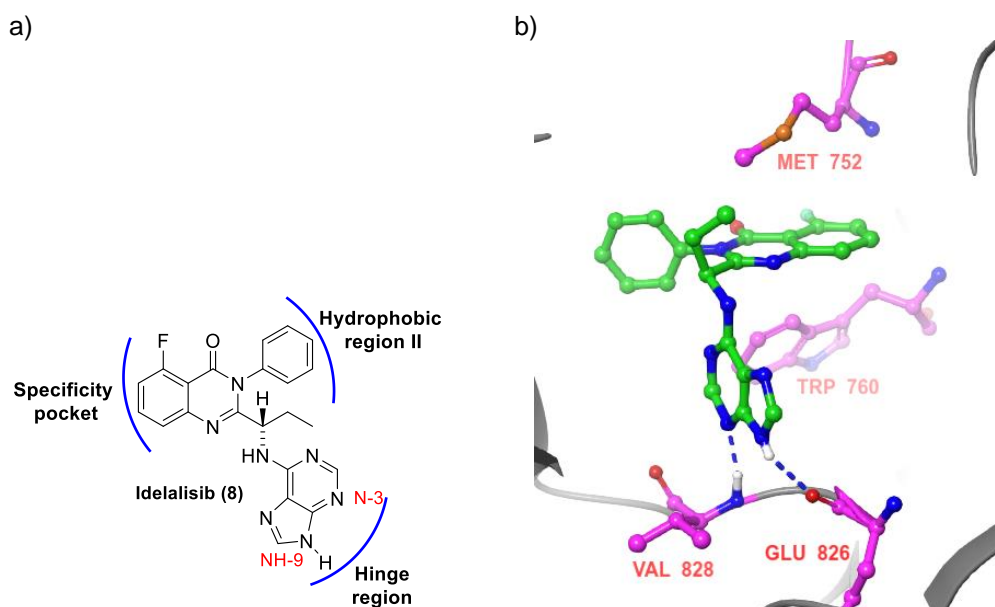


Figure 23. a) The propeller-shaped selective PI3K δ inhibitor idelalisib (**8**). b) Crystal structure of murine PI3K δ (PDB code 4XE0) with **8** bound. It can be noticed that **8** adopts a perpendicular conformation in the binding site of PI3K δ . Dashed blue lines represent the proposed hydrogen bonds.

forms Van der Waals interactions with the side chains of Asp⁸³², Thr⁸³³ and Asn⁸³⁶ (Figure 23b)^{140,145,153}. Idelalisib (**8**) occupies the hinge region with the purine ring, which comprises the third arm of the inhibitor and adopts a binding conformation perpendicular to the quinazolinone ring²³⁵. The N-3 of the purine ring serves as a hydrogen bond acceptor to the amide backbone of Val⁸²⁸, whereas the NH-9 acts as a hydrogen bond donor to the carbonyl backbone of Glu⁸²⁶ (Figure 23b)²³⁴. The number of hydrogen bond interactions at the hinge region is one of the most striking differences between the propeller-shaped inhibitors such as **8** and flat-shaped inhibitors such as **7**, the former make two hydrogen bonds (Figure 23b), while the latter only form one hydrogen bond (Figure 22b)^{159,218,229}.

1.8.3.2.3 Side effects of idelalisib (**8**)

Unfortunately, **8** has a black box warning on its product label for causing serious and fatal side effects which can include diarrhoea, serious hepatotoxicity, colitis, serious pneumonitis and neutropenia^{154,230,231}. One or more of these adverse events were observed in 68% of patients treated with **8**^{236,237}, where they are the main cause of dose reduction and treatment discontinuation of **8**²³⁸.

1.8.3.3 A new hypothesis about the nature of idelalisib-induced side effects

As outlined in Section 1.8.3.1, Rao *et al*²²⁶ reported that the selective oral PI3K δ inhibitor, **7**, does not cause serious adverse effects such as diarrhoea, colitis, neutropenia and liver toxicity, that are observed with **8** (Table 4). Moreover, a recent study by Shin *et al*²³⁹ reported that idelalisib-related hepatotoxicity may result from an off-target effect derived from its chemical

structure. These findings contradict the traditional hypothesis that idelalisib-associated adverse effects produced as a result of inhibition of PI3K δ (on-target effect). Thus, based on the literature information mentioned above, a new hypothesis could be proposed, which states that serious toxicities observed with **8** are chemical-based and not mechanism-related, providing a great opportunity for the development of safer and more effective PI3K δ inhibitors, by using classic medicinal chemistry structure-activity relationship (SAR) approach.

Table 4. Comparison of side effects of **8** (number of patients= 110)²³⁷ and **7** (number of patients= 6)²²⁶.

Adverse effects		Idelalisib (8)	Leniolisib (7)
Diarrhoea and colitis		35 / 110 patients	0 / 6 patients
Neutropenia		71 / 110 patients	2 / 6 patients
Liver toxicity	ALT increased	43 / 110 patients	0 / 6 patients
	AST increased	31 / 110 patients	0 / 6 patients
Skin rash		31 / 110 patients	0 / 6 patients

1.9 Aim and objectives

Currently, **8** is the only selective PI3K δ inhibitor approved in the market¹⁵⁵. However, the efficacy of **8** is limited for its frequent therapy-related adverse events (described above), which might cause patients to permanently stop **8** treatment²⁴⁰, thus **8** has a black box warning in its package insert given by FDA¹⁵⁴. Accordingly, the main aim of this work was to discover and develop potent and highly selective PI3K δ inhibitors as potential anticancer and anti-inflammatory drugs, which may represent better alternatives to **8**. The novel inhibitors should show equal or even higher activity and selectivity than **8**,

with an improved tolerability and safety profile. In turn, these research efforts were centred in the development of novel compounds belong to two classes of PI3K δ inhibitors (flat-shaped and propeller-shaped inhibitors). The distinctions between the flat-shaped and propeller-shaped PI3K δ inhibitors are shown in Figure 24.

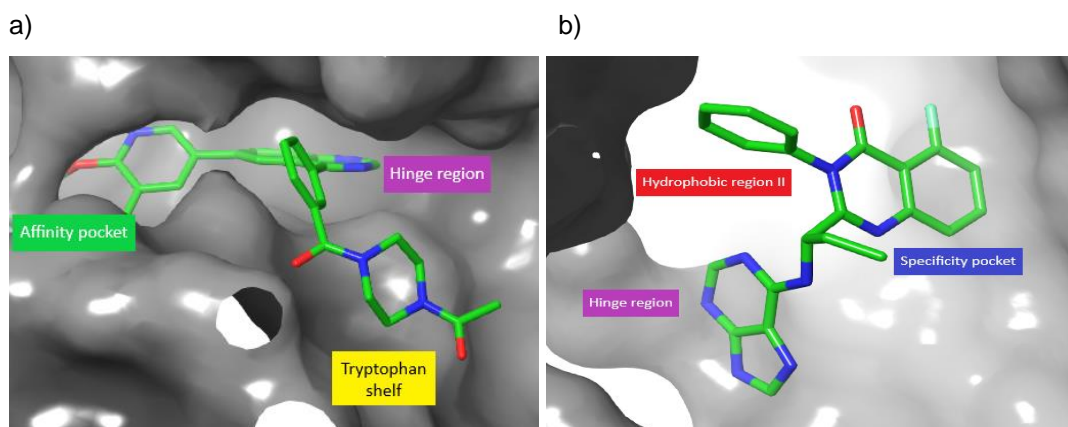


Figure 24. Differences between the flat-shaped inhibitor **7** and propeller-shaped inhibitor **8**. a) Crystal structure of murine PI3K δ (PDB code 5O83) with **7** bound, displays that **7** adopts a relatively flat conformation in the binding site of PI3K δ , where it interacts with three binding regions: affinity pocket (in green), tryptophan shelf (in yellow) and hinge region (in violet). b) Crystal structure of murine PI3K δ (PDB code 4XE0) with **8** bound displays that **8** adopts a perpendicular conformation in the binding site of PI3K δ , where it interacts with three binding regions: specificity pocket (in blue), hydrophobic region II (in red) and hinge region (in violet).

1.9.1 Flat-shaped inhibitors (chapter 2)

The non-selective PI3K inhibitor pictilisib (**4**) serves as a lead compound for extensive structural modification with an aim to explore novel and selective PI3K δ inhibitors. In this research, a novel series of thienopyrimidine derivatives were designed, synthesised and evaluated for their PI3K δ activity and selectivity.

Based on the crystal structure of murine PI3K δ with **4** (PDB code 2WXP), two directions were explored to improve the PI3K δ activity and selectivity of **4**. First, PI3K δ , in contrast to the other three isoforms, exclusively contains a tryptophan shelf, which could be exploited to achieve selective inhibition of PI3K δ . Pictilisib (**4**) does not bind to the tryptophan shelf, thus it does not

display selective activity against PI3K δ . This could be attributed to the conformational rigidity of the cyclic side chain (4-methanesulfonyl-piperazine-ylmethyl group), which makes **4** unable to fold and interact with Trp⁷⁶⁰ at the tryptophan shelf (Figure 25). Driven by this hypothesis, a bioisosteric replacement of the cyclic piperazine with an open side chain (Figure 25), which can fold to fit the tryptophan shelf due to its increased conformational flexibility, was conducted. Meanwhile, a terminal binding group (R) was introduced onto the flexible side chain to interact with Trp⁷⁶⁰ at the tryptophan shelf.

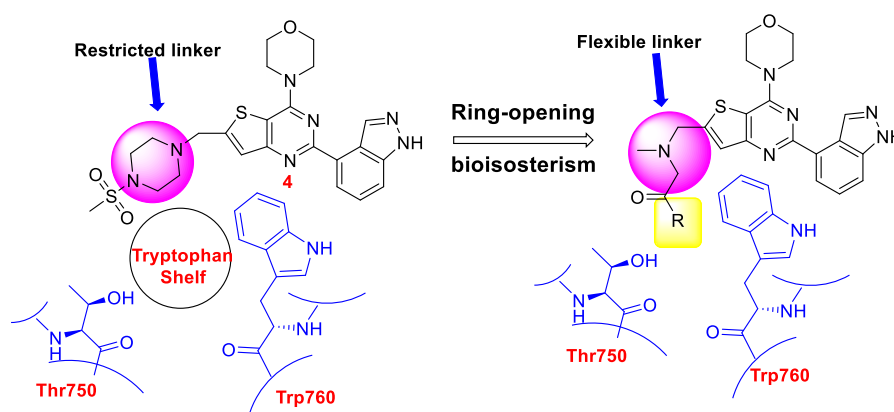


Figure 25. The replacement of the piperazine ring of **4** with acyclic analogues could improve the flexibility of the side chain and potentially allow it to fit in the tryptophan shelf region. Thus, the binding group R (in yellow) would be able to make an interaction with Trp⁷⁶⁰ at the tryptophan shelf.

The second direction was to utilize the affinity pocket to confer PI3K δ selectivity. It is widely believed that selective PI3K δ inhibition at the affinity pocket is the most difficult to achieve because the residues lining this pocket are conserved across all isoforms. However, Sutherland *et al*¹⁶⁰, Schwehm *et al*¹⁵⁹ and Berndt *et al*¹⁴⁵ reported that substitutions at the affinity pocket could modulate PI3K δ potency and selectivity, which is most likely due to the presence of non-conserved residues outside this pocket (in the surrounding) which influence isoform selectivity. The crystal structure of **4** bound to murine

PI3K δ (PDB code 2WXP) shows that the indazole moiety resides within the affinity pocket where it engages in two hydrogen bonds with Asp⁷⁸⁷ and Tyr⁸¹³. Thus, similar motifs to indazole which would be able to form similar interactions with the affinity pocket were sought out. Bioisosteric groups such as indole and phenol groups were explored (Figure 26), in order to mimic the spatial arrangement of indazole such that interactions with the affinity pocket were retained or enhanced. To test this hypothesis, in this research, two series of compounds would be designed and synthesized by replacing the indazole ring with an indole and phenol groups to test their potential as selective PI3K δ inhibitors.

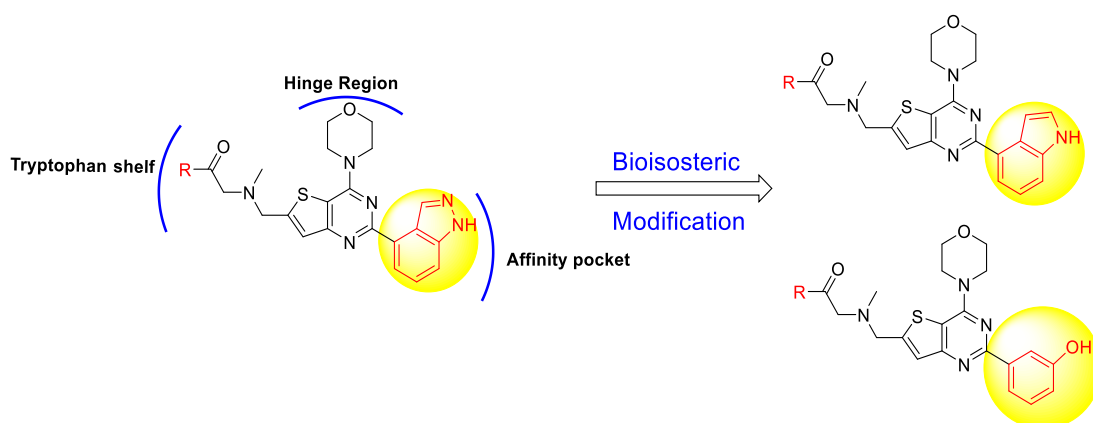


Figure 26. The proposed two series of compounds resulting from bioisosteric replacement of indazole moiety in **4**. One series will have an indole group as an affinity pocket binder while the second series will have a phenol group as an affinity pocket binder.

1.9.2 Propeller-shaped inhibitors (Chapters 3, 4 and 5):

The majority of propeller-shaped inhibitors including **8** have been designed to interact with PI3K δ at the three binding points (specificity pocket, hinge region and hydrophobic region II), while leaving the fourth region (affinity pocket) unoccupied (Figure 27). Figure 24a has shown that the affinity pocket is normally occupied by the flat-shaped PI3K δ inhibitors which accounts for their high PI3K δ activity. This finding suggests that the affinity pocket is druggable and can also be targeted by propeller-shaped PI3K δ inhibitors to

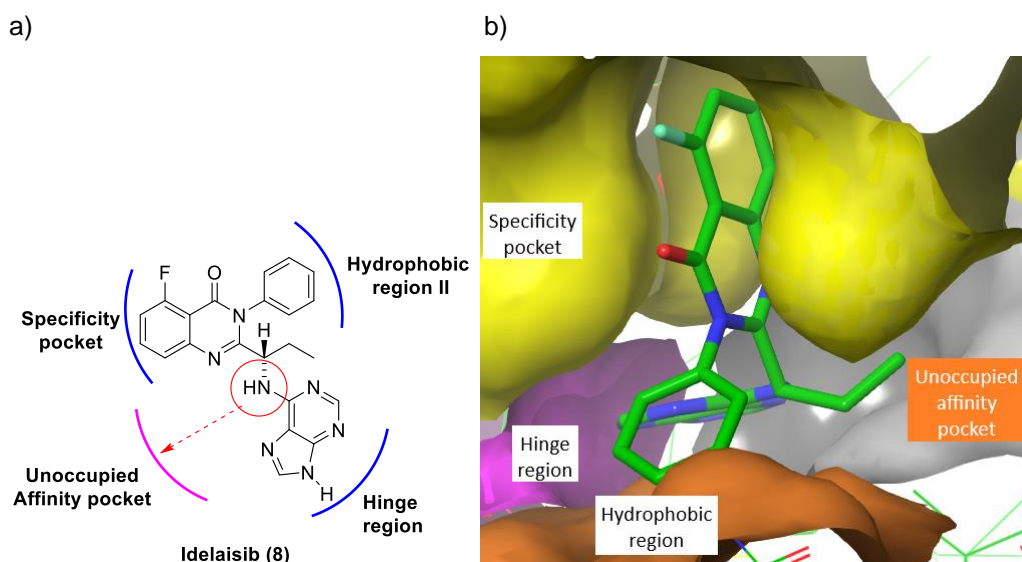


Figure 27. a) The typical propeller-shaped PI3K δ inhibitor idelalisib (**8**) and its binding points at PI3K δ , highlights the unoccupied affinity pocket¹⁵³. b) Crystal structure of murine PI3K δ (PDB code 4XE0) with **8** bound, shows that **8** adopts a propeller-shaped conformation. The hinge region is shown in violet, the open specificity pocket in yellow, the hydrophobic region II in orange, and the unoccupied affinity pocket in grey¹⁸⁰.

increase the number of binding interactions from 3 to 4, leading to a positive impact on the potency of the inhibitors. In support of this hypothesis, Berndt *et al*¹⁷³ and Williams *et al*¹⁹³ reported that additional gains of activity for propeller-shaped inhibitors **9** can be obtained when substituents bearing hydrogen bond donor and/or acceptor added to the lead compound that extended to the affinity pocket and involved in hydrogen bonding with polar residues that lined the affinity pocket²⁴¹. For instance, 3-fluorophenol in SW13 (**10**) and butynol in SW30 (**11**) (Table 5) projects from the central pyrazolopyrimidinineamine core to the affinity pocket where they engage in hydrogen bonding with Asp⁷⁸⁷ (in **10** and **11**) and Lys⁷⁷⁹ (in **10**). These interactions result in improved affinity at the δ isoform in comparison to the parent compound **9** (Table 5)²⁴². However, this extension strategy has never been tried on FDA-approved **8**, thus, pioneering research would be carried out, in which the structure of **8** ($IC_{50} = 11$ nM) is modified by extending the molecule toward the affinity pocket (Figure 27), where it could make new

Chapter 1

hydrogen bond interactions with the residues lining this pocket. This approach is known as drug extension and it may increase the potency of **8** by 10 to 100-fold.

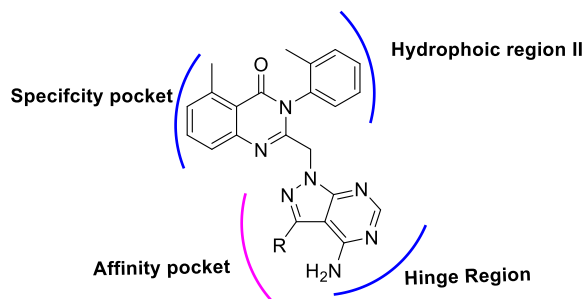


Table 5. Biological evaluation and isoform selectivity for PI3K δ for compounds **9-11** reported by Berndt *et al*¹⁷³, Compound **10** and **11** have a substituent (R) that extends towards the affinity pocket, resulting in a significant improvement of PI3K δ potency, compared to the parent compound **9**.

compd	R	PI3K δ IC ₅₀ (nM)	Isoform selectivity		
			δ/α	δ/β	δ/γ
9 ¹⁷³	-H	130	1538	123	469
10 ¹⁷³		0.7	1857	314	47
11 ¹⁷³		7	12142	107	186

Chapter 2 Design, Synthesis and Pharmacological Characterization of Novel Thienopyrimidine-based PI3K δ selective Inhibitors (Flat-Shaped Inhibitors)

2.1 Aim

As mentioned in the introduction, selective PI3K δ inhibitors are segregated into two classes: flat-shaped inhibitors and propeller-shaped inhibitors, this chapter will cover the former class. They are called flat-shaped inhibitors because they adopt a flat conformation in the ATP binding site when they bound to class I PI3Ks (see Figure 24a in Chapter 1), in contrast to propeller-shape inhibitors that adopt orthogonal conformation (see Figure 24b in Chapter 1). In this medicinal chemistry research, pictilisib (**4**) (Figure 28) (Table 6), a non-selective PI3K inhibitor (IC_{50} values of 44, 220, 220 and 11 nM for isoforms PI3K α , β and γ and δ , respectively), was chosen as the starting point for chemical modification in order to improve PI3K δ potency and selectivity. Therefore, the co-crystal structure of PI3K δ and pictilisib (**4**) is crucial for structure-based design of isoform selective PI3K δ inhibitors (Figure 28b).

Table 6. Biological evaluation and isoform selectivity for PI3K δ for non-selective PI3K inhibitor (pictilisib, **4**).

Isoform potency ^{a,b} IC_{50} (nM)	Isoform selectivity		
	PI3K δ	δ/α	δ/β
11	4	20	20

^aPotency against the different PI3K isoforms is given as IC_{50} values ($n = 7$). ^bThe potency threshold for the PI3K δ assay is $\sim IC_{50}$ 1 nM due to substrate concentration. The standard errors were not provided by GlaxoSmithKline (GSK).

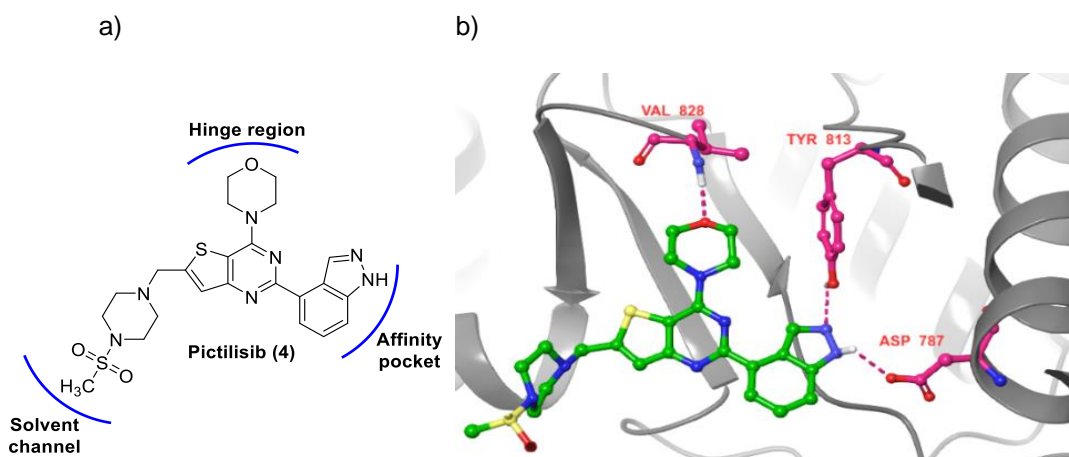


Figure 28. a) The non-selective PI3K inhibitor pictilisib (**4**) and its binding points at PI3K δ ¹⁸². b) Crystal structure of murine PI3K δ (PDB code 2WXP) with pictilisib (**4**) bound. Dashed pink lines represent the proposed hydrogen bonds.

PI3K δ selectivity can be achieved by taking advantage of the difference in the peripheral residues contained within the ATP binding sites of the PI3K class 1 isoforms. One of these sites is called the “tryptophan shelf” that is exclusively found in the PI3K δ isoform and not in other three isoforms (α , β and γ)¹⁶⁰. The tryptophan shelf in PI3K δ is the region in space located between Trp⁷⁶⁰ and Thr⁷⁵⁰ (see Figure 15 in Chapter 1), where π -stacking groups can bind. PI3K α , β and γ lack this tryptophan shelf, as the equivalent residues to Thr (PI3K δ) are Arg in PI3K α and Lys in PI3K β and γ . These amino acid side chains make cation- π interactions with the corresponding Trp residue and occlude access to the tryptophan shelf (see Figure 15 in Chapter 1).

There is currently no clinically-approved drug from this class of PI3K δ inhibitors. The most advanced compound (leniolisib, **7**) (see Section 1.8.3.1 and Figure 22 in Chapter 1) is in phase II clinical studies for treatment of Sjogren syndrome²²⁹. The aim of this medicinal chemistry program is the discovery of a novel series of highly potent and selective thienopyrimidine-based PI3K δ inhibitors as anticancer and anti-inflammatory agents which

maintain the desirable PI3K δ activity in pictilisib (**4**) (Table 6), while improving the selectivity against the other three isoforms (PI3K α , β and γ).

2.2 Binding Interactions of the lead compound (pictilisib, **4**)

Pictilisib (**4**) has a thienopyrimidine core that bears three binding arms (Figure 28). The morpholine ring forms a critical hydrogen bond to the amide backbone of Val⁸²⁸ (conserved) in the hinge region of the kinase. On the other hand, the indazole ring fits deeply into the affinity pocket where the indazole N-1 forms a hydrogen bond with the side chain of Asp⁷⁸⁷ and N-2 makes a hydrogen bond with the phenolic side chain of Tyr⁸¹³. The 4-(methanesulfonyl)piperazine-ylmethyl group fits into a channel pointing towards solvent, leading to the improvement of solubility (Figure 28b)¹⁸². All the residues (Val⁸²⁸, Tyr⁸¹³ and Asp⁷⁸⁷) that pictilisib (**4**) binds to are conserved among the four isoforms of class I PI3K, thus pictilisib (**4**) is considered to be a non-selective class I PI3K inhibitor (PI3K δ = 11 nM, PI3K α = 44 nM, PI3K β = 220 nM and PI3K γ = 220 nM)^{182,188}.

2.3 Structural Modifications on pictilisib (**4**)

2.3.1 Thienopyrimidine scaffold

The thienopyrimidine nucleus serves as the scaffold for many PI3K δ inhibitors^{159,243}, Schwem *et al*¹⁵⁹, Sutherlin *et al*¹⁶⁰ and Safina *et al*¹⁶¹ reported series of thienopyrimidine-based selective PI3K δ inhibitors (Table 7)^{159,243}, where it was found that the thienopyrimidine scaffold can retain the original binding groups of the molecule in a good binding orientation^{182,243}, proposing that subtype selectivity for PI3K δ could be achieved within the thienopyrimidine class of PI3K inhibitors. Thus, thienopyrimidine is considered a privileged scaffold for PI3K δ inhibition and therefore the

suggested compounds in this chapter would be thienopyrimidine-based derivatives.

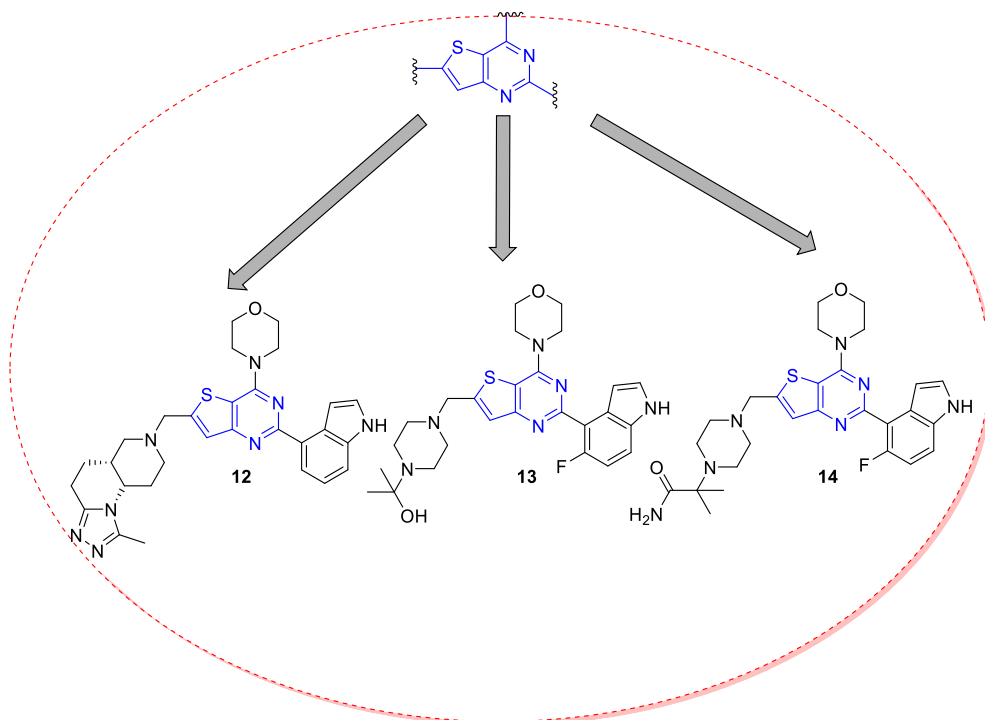


Table 7. Biological evaluation and isoform selectivity for PI3K δ for thienopyrimidine-based selective PI3K δ inhibitors.

compd	PI3K δ potency IC_{50} (nM)	Isoform fold-selectivity		
		δ/α	δ/β	δ/γ
12 ¹⁴⁴	0.7	4000	400	2000
13 ¹⁶⁰	3.8	340	200	410
14 ¹⁶¹	1.8	129	104	1444

2.3.2 Morpholine (hinge binder)

The morpholine ring has been reported in many selective PI3K δ inhibitors^{159,182,243}. The crucial characteristic of these inhibitors is the critical interaction between the morpholino oxygen and the backbone amide of Val⁸²⁸ in the hinge region (Figure 28b). Replacement of oxygen of the morpholine moiety by sulfur, nitrogen, hydroxymethyl or methylene led to a major loss in the PI3K δ activity (Table 8)^{244,245}. This showed that the desirable PI3K δ inhibitory activity was attainable with a morpholine group binding to the hinge

region²⁴⁴. Moreover, morpholine proved to have better physiochemical properties than its analogues where the weak basicity (pKa= 8.4) of morpholine allows an increase in solubility without affecting permeability²⁴⁶. According to this, the morpholine is the best group combining potency and physiochemical properties.

Table 8. Biological evaluation and isoform selectivity for PI3K δ for compounds **15** and **16** reported by Andrs *et al*²⁴⁵.

Compd	R ₁	Isoform Potency IC ₅₀ (nM)			
		PI3K δ	PI3K α	PI3K β	PI3K γ
15 ²⁴⁵		100	500	5	> 10000
16 ²⁴⁵		1000	-	-	20000

2.3.3 N-sulfonylpiperazine side chain (tryptophan shelf binder)

Pictilisib (**4**) will undergo structural modifications to increase its PI3K δ selectivity. This can be achieved by increasing the flexibility of the side chain (4-(methanesulfonyl)piperazine-ylmethyl group) that points towards the solvent channel, where it does not play a significant role in the binding¹⁸². The increase in the side chain flexibility might allow it to access the face of Trp⁷⁶⁰ (tryptophan shelf), that can be only accessed in PI3K δ (see Figure 15 in Chapter 1), affording improved PI3K δ potency and selectivity. A ring opening strategy would be applied to the piperazine ring to generate a flexible and linear acyclic side chain (Figure 29), with a higher degree of conformational freedom. This side chain will act as a flexible linker to bridge between a thienopyrimidine scaffold and the functional group R that could target the tryptophan shelf.

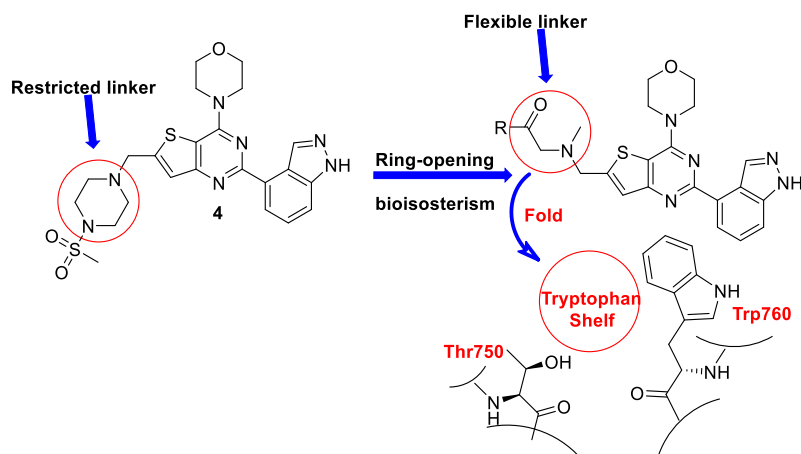


Figure 29. The replacement of the piperazine ring of pictilisib (**4**) with acyclic analogues could improve the flexibility of the side chain and potentially allow it to fit in the tryptophan shelf region.

2.3.4 Indazole ring (Affinity pocket binder)

Additionally, the second functional group in the pictilisib (**4**) chemical structure which will undergo structural modification is the indazole moiety that fits deep into the affinity pocket (Figure 30), where indoles and phenols will be used as bioisosteres for the indazole ring. Although the affinity pocket contains conserved residues across the class 1 isoforms, it was found that replacement of the indazole with an indole group offers higher PI3K δ selectivity, while PI3K δ potency was improved by replacement of indazole with a phenol group^{159,182,243}. The variation in the PI3K δ activity and selectivity between the bioisosteric analogues is due to differences in the hydrogen bond network, caused by non-conserved residues that surrounding the affinity pocket (see Section 2.5.1, Figure 34 and Figure 35 for more details)^{140,149,172}.

In conclusion, the thienopyrimidine scaffold and the morpholine hinge binder would be retained in the proposed compounds. The indazole ring that fits into the affinity pocket would be replaced by the bioisosteric indole and phenol moieties, while a ring-opening strategy would be used to increase the

flexibility of the sulfonylpiperazine side chain to allow access to the tryptophan shelf.

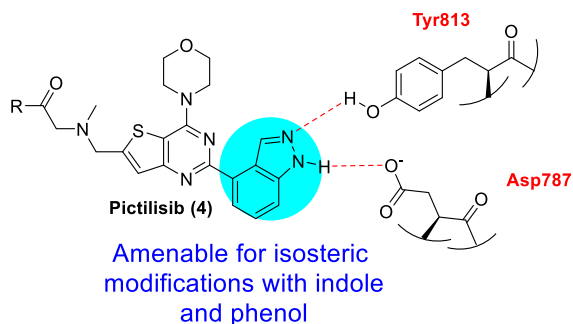


Figure 30. The non-selective PI3K inhibitor pictilisib (4), highlighting the indazole group in the affinity pocket that will undergo bioisosteric replacement.

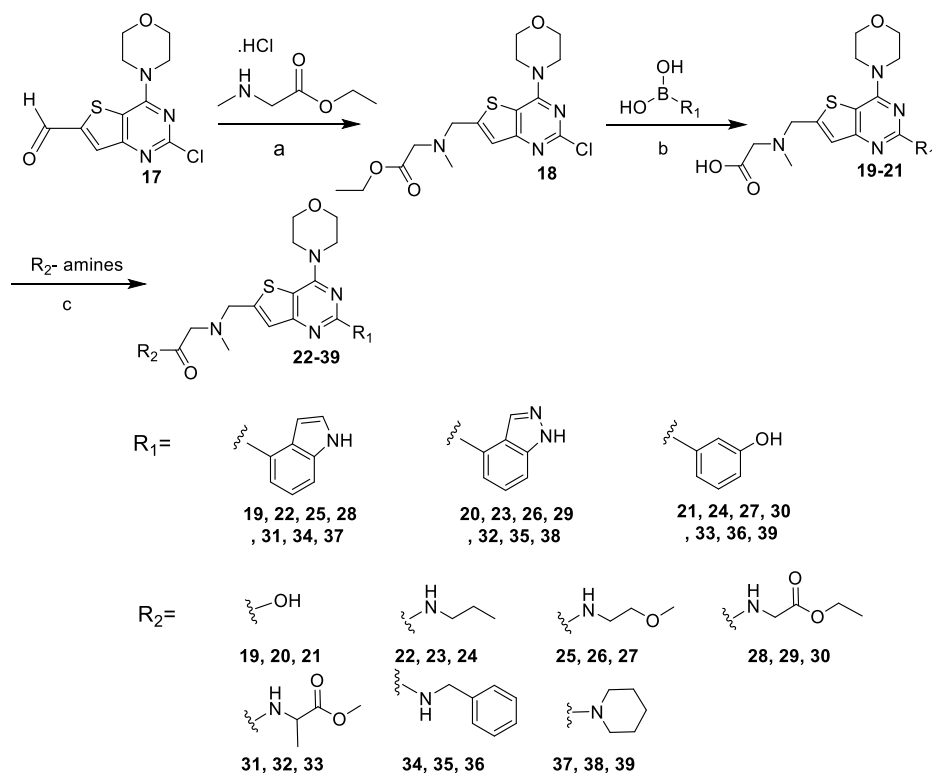
2.4 Discussion

2.4.1 Chemistry Section

Compound **17** (supplied by GSK) was reacted with sarcosine ethyl ester hydrochloride under reductive amination conditions to give intermediate **18** (Scheme 1), the relatively low yield of the compound **18** was due to some of the aldehyde being reduced to the corresponding alcohol before reacting with amine. Compound **18** underwent a Pd-catalysed Suzuki coupling with arylboronic acids (4-indazole, 4-indole and 3-phenol), yielding the biaryl compounds (**19-21**) using microwave irradiation. Generally, aryl chlorides are less reactive towards Suzuki cross coupling reactions as compared to aryl bromides and iodides^{247,248}. However, in compound **18**, the electron withdrawing pyrimidine ring facilitated the reaction by weakening the C-Cl bond and accelerated S_N2 oxidative addition to the palladium centre²⁴⁷. In addition to aryl-aryl coupling, ester hydrolysis took place to yield the free carboxylic acids (**19-21**). with various aliphatic amines in the presence of HATU afforded the corresponding amides (**22-39**) in moderate to good yields (26- 87%).

Chapter 2

Scheme 1. Synthesis of compounds (17-39)



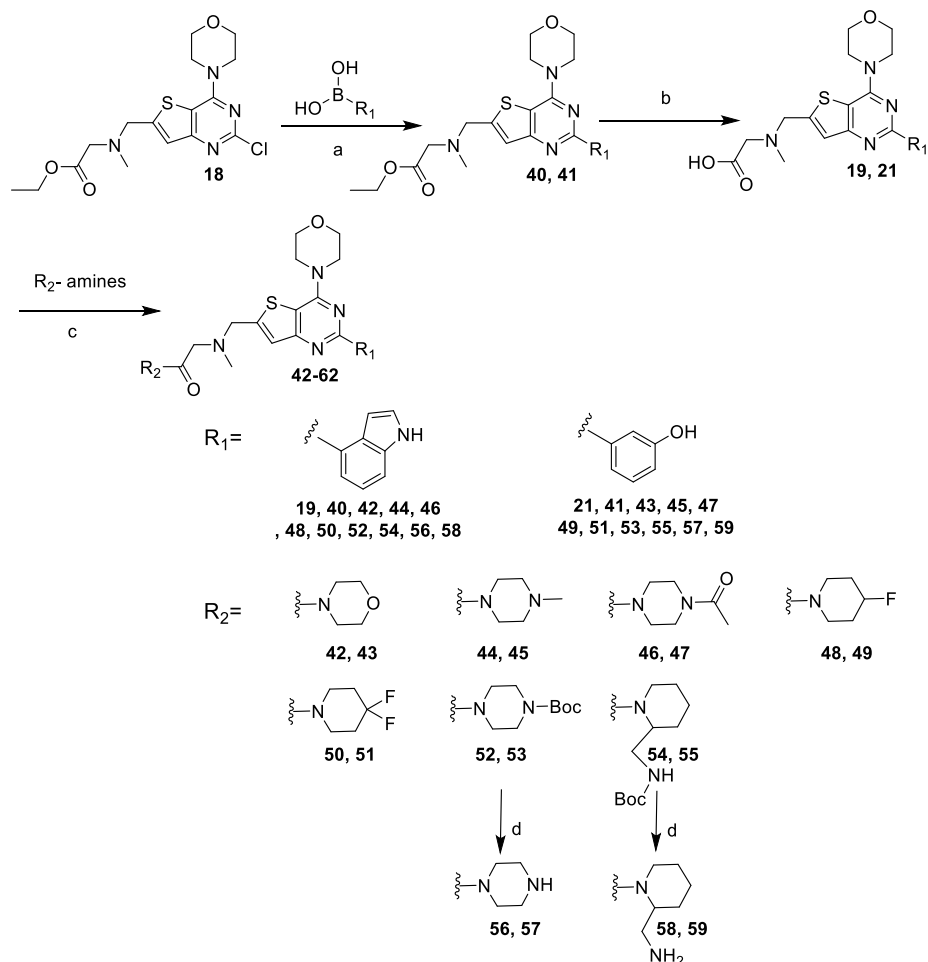
^aReagents and conditions: (a) triethylamine, picoline borane, 10% AcOH in ethanol, rt, 20 h, yield 42%; (b) Na₂CO₃, ethanol (EtOH), boronic acid, *bis*(triphenylphosphine) palladium (II) chloride, microwave 125 °C, 3 h, yield 68-71%; (c) (1-[Bis(dimethylamino)methylene]-1H-1,2,3-triazolo[4,5-b]pyridinium 3-oxide hexafluorophosphate (HATU), N,N-Diisopropylethylamine (DIPEA), rt, 24 h, yields 26-87%.

In the first reaction to synthesise the second set of the compounds (Scheme 2), Suzuki couplings were used to introduce 3-phenol and 4-indole rings, derived from commercially available 3-phenolboronic acid and 4-indole pinacol ester respectively, into a compound **18**. Somewhat surprisingly, the use of THF as a solvent in this Suzuki coupling reaction did not result in the formation zwitterionic compounds **19** and **21** as it was observed with ethanol (step b in Scheme 1), this may be due to the fact that the resulting biaryl products (**31** and **32**) were insoluble in THF, and thus they did not undergo in situ hydrolysis of ester. In the second step, KOH was used to hydrolyse the ester. The resulting carboxylic acids **19** and **21** were then coupled with several aliphatic cyclic amines using HATU as a coupling reagent affording

Chapter 2

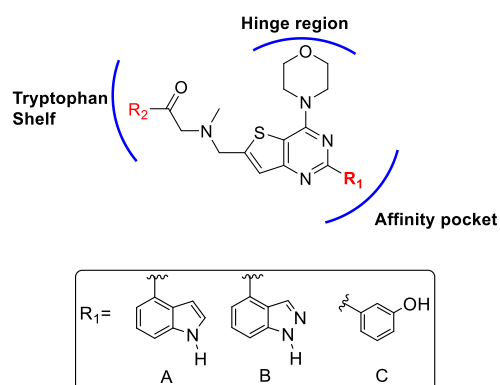
the desired analogues (**42-55**). Finally, deprotection of the *N*-*tert*-butoxycarbonyl (*N*-Boc) protected amines (**52, 53, 54, 55**) led to the amine hydrochloride salts (**56, 57, 58** and **59**, respectively).

Scheme 2. Synthesis of compounds (**42- 59**)



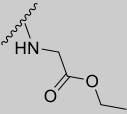
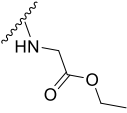
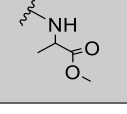
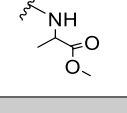
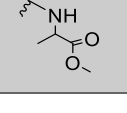
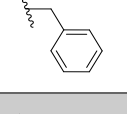
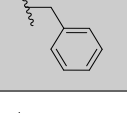
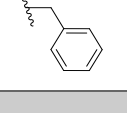
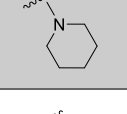
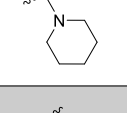
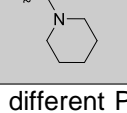
^aReagents and conditions: (a) Na_2CO_3 , bis(triphenylphosphine) palladium (II) chloride, tetrahydrofuran (THF), microwave 125 °C, 3 h, yield 81-82%; (b) KOH, methanol, 35 °C, 20 h, yield 75-82%; (c) HATU, DIPEA, rt, 24 hr, yields 34-97%. (d) 4 N HCl, dioxane; rt, 2 h, yields 90-96%.

2.5 Biology Section

Table 9. Biological evaluation and isoform selectivity for PI3K δ for compounds 19-39.

Compd	R ₁	R ₂	Isoform potency ^{a,b} IC ₅₀ (nM)				Isoform selectivity		
			PI3K δ	PI3K α	PI3K β	PI3K γ	δ/α	δ/β	δ/γ
19	A	OH	175	1400	710	555	8	4	3
20	B	OH	1000	441	1400	1400	0.4	1.4	1.4
21	C	OH	110	100	710	140	1	6	1.3
22	A		28	2800	2800	1400	100	100	50
23	B		44	280	2800	710	6	63	14
24	C		14	70	1000	175	4	63	14
25	A		35	2225	2800	1750	64	80	50
26	B		44	280	3500	555	6	80	13
27	C		14	56	555	175	4	40	13
28	A		14	1000	1750	710	71	125	51

Chapter 2

Compd	R ₁	R ₂	Isoform potency ^{a,b} IC ₅₀ (nM)				Isoform selectivity		
			PI3K δ	PI3K α	PI3K β	PI3K γ	δ/α	δ/β	δ/γ
29	B		22	140	1750	220	6	80	10
30	C		7	28	280	140	4	40	20
31	A		35	2800	3500	1100	79	100	32
32	B		44	280	4400	1750	6	100	40
33	C		10	44	555	140	5	63	16
34	A		70	220	5500	1000	3	79	14
35	B		28	1400	1400	1400	50	50	50
36	C		*	*	*	*	*	*	*
37	A		11	1100	2800	280	100	255	25
38	B		10	140	2800	110	14	280	11
39	C		2	35	44	35	18	220	18

^aPotency against the different PI3K isoforms is given as IC₅₀ values (n = 1). ^bThe potency threshold for the PI3K δ assay is ~ IC₅₀ 1 nM due to substrate concentration. Compounds **20**, **22**, **23**, **25**, **26**, **28**, **31**, **32**, **34**, **35**, **36**, **37** and **38** were prepared by Jia Ong. * Compound **33** has not been tested.

2.5.1 Matched molecular pair analysis of the functional groups that occupy the affinity pocket.

The compounds (**19**, **20** and **21**), (**22**, **23** and **24**), (**25**, **26** and **27**), (**28**, **29** and **30**), (**31**, **32** and **33**), (**34**, **35** and **36**) and (**37**, **38** and **39**) were all matched molecular pairs, they differ only by the aryl group in the right hand of the molecule which occupies the affinity pocket. Matched molecular pair analysis was used to identify any change in PI3K δ activity and selectivity following bioisosteric replacement of indazole with indole and phenol. Table 9 showed that the 4-indole analogues (**22**, **25**, **28**, **31**, **34** and **37**) exhibited high PI3K δ selectivity compared to their 4-indazole (**23**, **26**, **29**, **32**, **35** and **38**) and 3-phenol counterparts (**24**, **27**, **30**, **33**, **36** and **39**). This is very apparent when looking at a matched pair analysis between compounds containing the 4-indole ring and the 4-indazole containing compounds, where the PI3K δ activity of these compounds were plotted against their δ/α selectivity (Figure 32), based on the assumption suggested by Safina *et al*¹⁶¹, which states that the selectivity against PI3K α could be an acceptable predictor for overall isoform selectivity^{159,161}. This analysis showed that the matched-pairs commonly had comparable potency against PI3K δ , however 4-indole analogues demonstrated less potent activity against PI3K α and thus have high δ/α selectivity. For example, 4-indole analogue **22** inhibited PI3K δ with IC_{50} of 28 nM with 100-fold PI3K δ/α selectivity in contrast to the non-selective 4-indazole **23** and 3-phenol **24** analogues (only 6 and 4-fold, PI3K δ/α selectivity respectively) (Table 9). In comparison, 4-indole analogue **37** was 10-times more PI3K δ selective than its 4-indazole **38** and 3-phenol **39** counterparts. The high PI3K δ selectivity of 4-indole analogues over PI3K α

was due to the loss of activity against the latter rather than increased potency against the former. For instance, 4-indazole **23** and 3-phenol **24** analogues displayed sub-micromolar potency against PI3K α with IC_{50} of 280 and 70 nM, respectively, while the 4-indole counterpart **22** inhibited PI3K α in the micromolar range with IC_{50} of 2500 nM.

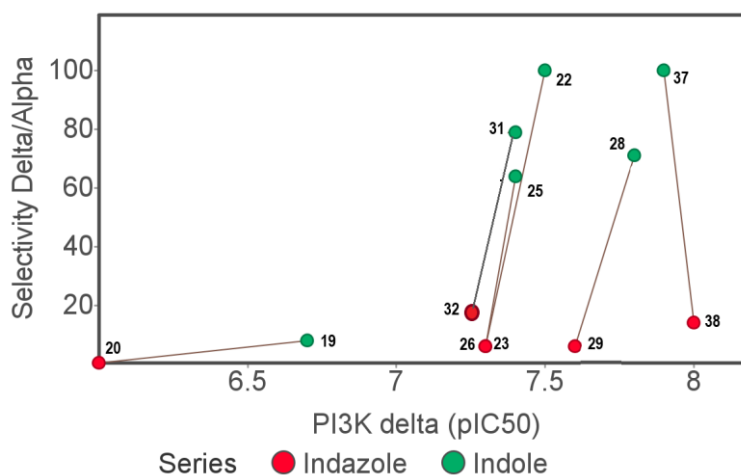
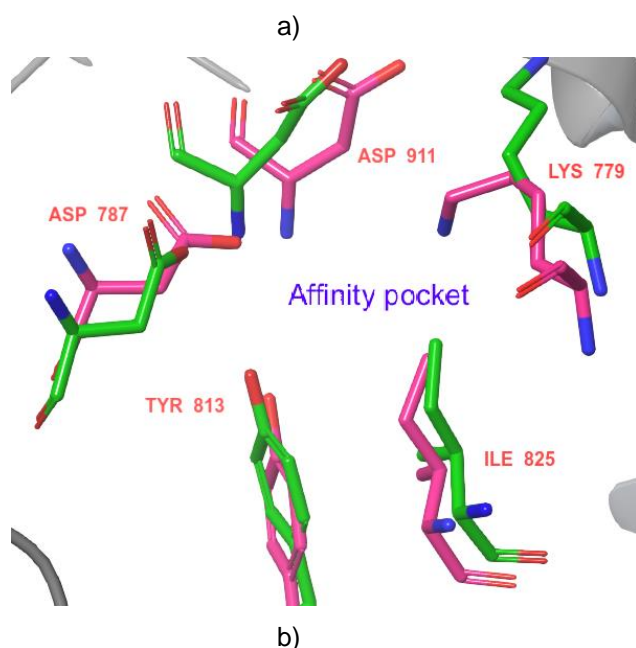


Figure 32. Plot of PI3K δ activity (pIC_{50}) as a function of PI3K δ isoform selectivity (vs PI3K α), Matched-pair analysis for the 4-indole-containing compounds (green), and 4-indazole-containing compounds (red) showing a general trend that indole compounds are more PI3K δ selective than their corresponding matched pair 4-indazole.

Generally, replacement of 4-indole with 4-indazole and 3-phenol can cause 2- to 4-fold drop in δ over γ selectivity (compare matched-pairs **22**, **23** and **24** and matched-pairs **37**, **38** and **39** for PI3K δ/γ), whereas PI3K β/δ selectivity of the three series was greater than selectivity for PI3K δ over α or δ over γ isoforms, it is noteworthy that 4-indole and 4-indazole compounds had similar level of selectivity for PI3K δ over PI3K β (compare matched-pairs **25** and **28** and matched-pairs **31** and **32** for PI3K β/δ selectivity). These high levels of PI3K δ isoform selectivity achieved at the affinity pocket by the indole analogues was somewhat surprising, given the fact that the affinity pockets are conserved between the four isoforms of class I PI3K and consists of only identical residues (Figure 33)^{149,152,220}.

Chapter 2



All residues that line the affinity pocket are conserved

PI3K δ	Lys ⁷⁷⁹	Leu ⁷⁸⁴	Asp ⁷⁸⁷	Ile ⁸²⁵	Tyr ⁸¹³	Asp ⁹¹¹
PI3K α	Lys ⁸⁰²	Leu ⁸⁰⁷	Asp ⁸¹⁰	Ile ⁸⁴⁸	Tyr ⁸³⁶	Asp ⁹³³
PI3K β	Lys ⁷⁹⁹	Leu ⁸⁰⁴	Asp ⁸⁰⁷	Ile ⁸⁴⁵	Tyr ⁸³³	Asp ⁹³¹
PI3K γ	Lys ⁸³³	Leu ⁸³⁸	Asp ⁸⁴¹	Ile ⁸⁷⁹	Tyr ⁸⁶⁷	Asp ⁹⁶⁴

Figure 33. a) Crystal structure of murine PI3K δ (PDB code 2WXP) and human PI3K γ (PDB code 3DBS). Superposition of residues lining the affinity pocket of the PI3K δ and γ isoforms shows that this pocket is highly conserved in both isoforms. PI3K δ residues are colored pink, whereas PI3K γ residues are colored green. b) Sequences of the residues lining the affinity pocket in the four isoforms of class I PI3K. In total, 6 residues that line the affinity pocket are conserved in the four isoforms of class I PI3K.

This variation in PI3K δ selectivity between the three series can be attributed to the distal hydrogen bond network to residues beyond the affinity pocket which is able to influence isoform selectivity. The hydrogen bond networks made by the indole group in the affinity pocket cannot be formed by the less selective indazole and phenol containing series. Sutherland *et al*²⁴³ explained

the high δ selectivity of their 4-indole-containing compounds over their 4-indazole counterparts (Table 10) by hypothesizing that the hydrogen bond networks formed with Tyr⁸¹³ and the indole ring C-H in the affinity pocket is different from that formed by the isosteric indazole ring²⁴³. This can be seen in the crystal structure of human K802T-mutant PI3K γ bound to the indole-based compound **60** (PDB code 4EZJ) (Figure 34) and indazole-based compound **61** (PDB code 4EZK) (Figure 35) which have great structural similarity to the final compounds presented in this chapter. The change of an indole **60** for an indazole moiety **61** significantly decreases the δ/α selectivity by 10-fold (Table 10).

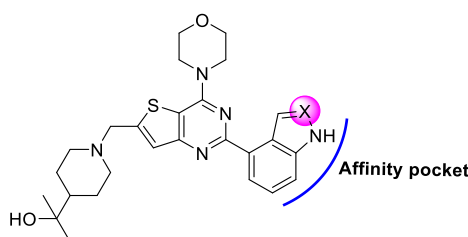


Table 10. Biological evaluation and isoform selectivity for PI3K δ for compounds **60** and **61** reported by Sutherlin *et al*²⁴³.

compd	X	PI3K δ IC ₅₀ (nM)	Isoform selectivity		
			δ/α	δ/β	δ/γ
60 ²⁴³	-CH-	3.8	1292	760	1558
61 ²⁴³	-N-	6.3	139	491	1638

In compound **60**, C-H (C-2) of the indole ring makes a hydrogen bonding interaction with the phenolic oxygen of Tyr⁸⁶⁷ (Tyr⁸¹³ in PI3K δ) (Figure 34), while the phenolic hydrogen makes a new interaction with the carbonyl backbone of His⁹⁶² (His⁹⁰⁹ in PI3K δ), establishing a new hydrogen bonding network that can be accommodated only in PI3K δ (Figure 34), while the other three isoforms cannot adapt this new network of hydrogen bonds. This leads to high δ selectivity within the 4-indole series.

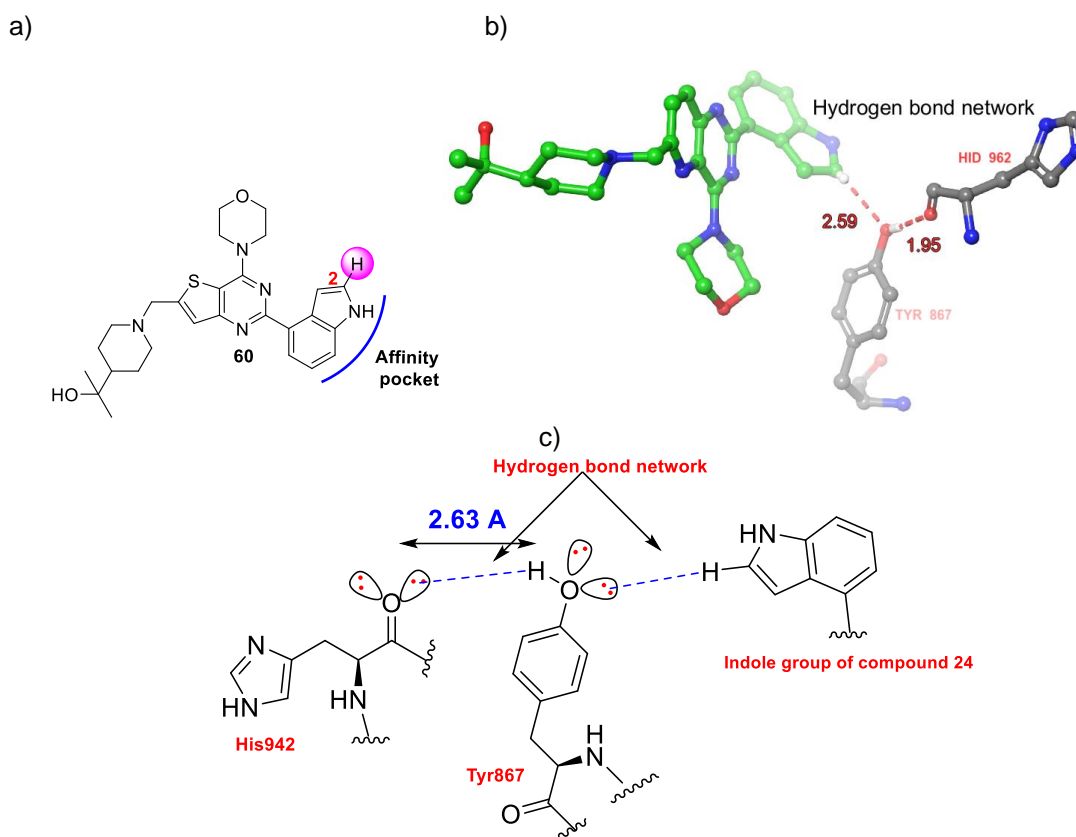


Figure 34. a) The selective PI3K δ inhibitor compound **60**. b) Crystal structure of human K802T-mutant PI3K γ (PDB code 4EZJ) with compound **60** bound, pink dashed lines indicate the proposed hydrogen bond network that is suggested to be responsible for PI3K δ selectivity of compound **60**. c) Simplified diagram depicts the hydrogen bond network (dashed blue line) between compound **60**, Tyr⁸⁶⁷ (Tyr⁸¹³ in PI3K δ) and His⁹⁶² (His⁹⁰⁹ in PI3K δ) in the affinity pocket.

In contrast, in 4-indazole-containing compound **61** (Table 10), the N-2 of the indazole acts as a hydrogen bond acceptor and makes a hydrogen bond to the phenolic hydrogen of Tyr⁸⁶⁷ (Tyr⁸¹³ in PI3K δ) (Figure 35), while the phenolic oxygen with its lone pair becomes free and results in electrostatic repulsion (lone pair-lone pair repulsion) with the carbonyl backbone of His⁹⁶² (His⁹⁰⁹ in PI3K δ). This can be seen by the increase in the distance between the two residues to 3.79 Å (Figure 35), thus indazole compounds cannot form the hydrogen bond network, which translates into reduced isoform selectivity. However, there is uncertainty about the Sutherland's hypothesis¹⁶⁰, which will be discussed in more detail in Chapter 6 (see compound **62** versus **63** in Table 64).

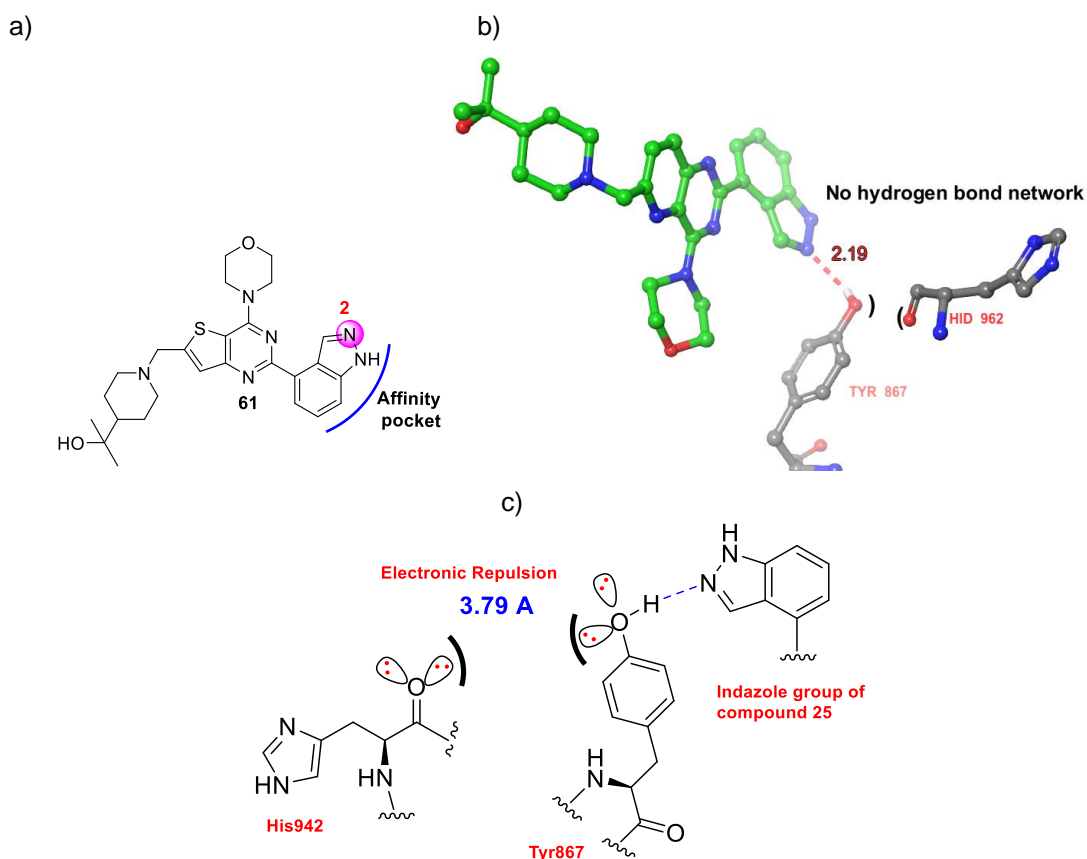


Figure 35. a) The selective PI3K δ inhibitor compound **61**. b) Crystal structure of human K802T-mutant PI3K γ (PDB code 4EZK) with compound **61** bound, pink dashed lines indicate the proposed hydrogen bond between compound **61** and Tyr⁸⁶⁷ (Tyr⁸¹³ in PI3K δ), it also displays the electrostatic repulsion between the Tyr⁸⁶⁷ (Tyr⁸¹³ in PI3K δ) and His⁹⁶² (His⁹⁰⁹ in PI3K δ), as the distance between them increases up to 3.79 Å. c) Simplified diagram shows the electrostatic repulsion between Tyr⁸⁶⁷ (Tyr⁸¹³ in PI3K δ) and His⁹⁶² (His⁹⁰⁹ in PI3K δ) with distance between them increased up to 3.79 Å, which excludes the possibility of forming the hydrogen bond network.

In terms of PI3K δ activity, the 3-phenol analogues (**24**, **27**, **30**, **33**, **39**) exhibited the best inhibitory activity against PI3K δ amongst the three series. This can be seen clearly in Figure 36, which describes the matched pair analysis between the phenol-containing compounds and indazole containing compounds, where the PI3K δ activity of these compounds was plotted against their δ/α selectivity, it showed that 3-phenol containing compounds were more potent than the corresponding 4-indazoles. For example, the phenol derivative **39** was 5-fold more potent against PI3K δ with IC₅₀ value of 2 nM than the corresponding indole **37** and indazole **38** analogues (IC₅₀ values of 11 and 10 nM, respectively) while compound **33** has IC₅₀ value of

Chapter 2

10 nM was 3-fold more active than indole **31** and indazole **32** derivatives (IC₅₀ values of 35 and 44 nM, respectively) (Table 9). However, the 3-phenol-containing analogues had less selectivity for PI3K δ over PI3K α , compared to the indoles and indazoles, whereas all phenol derivatives (**24**, **27**, **30**, **33** and **39**) were more selective for PI3K δ over PI3K α by factors of only 1-18-fold. For example, compound **24** was only 4-fold more selective against PI3K δ over PI3K α , in contrast to its indole analogue **22** which was 100-fold selective. The selectivity of phenol-containing compound **33** was only 5-fold higher for PI3K δ than PI3K α , while its indole counterpart **31** was 79-fold selective (Table 9). On the other hand, replacing the 4-indole group with 3-phenol displayed a smaller decrease in the selectivity against PI3K β and γ . In general, 3-phenol analogues generally showed a range of 2- to 3-fold reduction in the selectivity against PI3K β and γ comparing to their 4-indole counterparts.

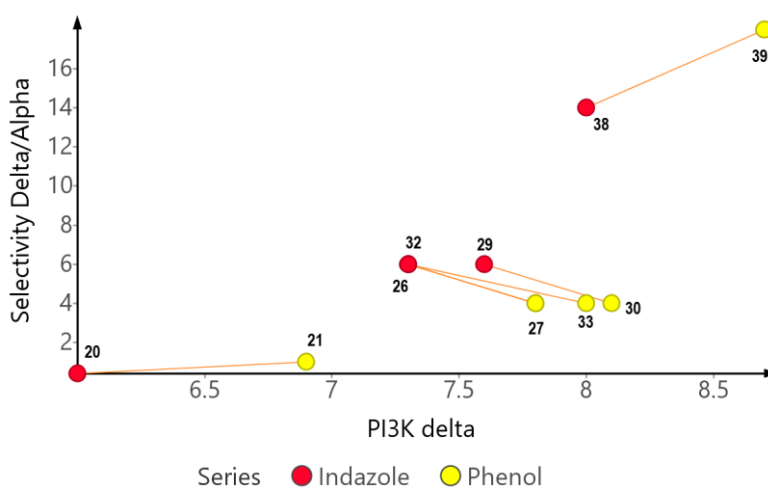


Figure 36. Plot of PI3K δ activity (pIC₅₀) as a function of PI3K δ isoform selectivity (vs PI3K α), Matched-pair analysis for the phenol-containing compounds (yellow), and indazole-containing compounds (red) showing a general trend that phenol compounds are more PI3K δ potent than their corresponding matched pair indazoles. However, they show similar selectivity profile.

The binding modes of the phenol-containing compound **39** with PI3K δ were predicted by molecular docking analysis to explain the high PI3K δ inhibitory

activity and low selectivity of the phenol series, where compound **39** was docked into the crystal structure of human K802T-mutant PI3K γ (generated from PDB code 4EZJ) (Figure 37). The proposed binding mode of compound **39** revealed that the 3-phenol ring bound to the affinity pocket in a different orientation to that of the indole and indazole groups contained in compounds **37** and **38**, respectively, (Figure 37b). The 3-phenol group was oriented in such a manner that this group was in close proximity to the Lys⁸³³ (Lys⁷⁷⁹ in PI3K δ) and Asp⁹⁶⁴ (Asp⁹¹¹ in PI3K δ) residues (Figure 38) instead of Tyr⁸⁶⁷ (Tyr⁸¹³ in PI3K δ) and Asp⁸⁴¹ (Asp⁷⁸⁷ in PI3K δ) which indole and indazole bound to (Figure 34b and 35b), thus the 3-phenol makes two charge-enhanced hydrogen bonding interactions with Lys⁸³³ (Lys⁷⁷⁹ in PI3K δ) and Asp⁹⁶⁴ (Asp⁹¹¹ in PI3K δ) (Figure 38), while the indole and indazole isosteres only make one conventional hydrogen bonding interaction with Tyr⁸⁶⁷ (Tyr⁸¹³ in PI3K δ) and one charge-enhanced hydrogen bond with Asp⁸⁴¹ (Asp⁷⁸⁷ in PI3K δ) (Figure 34b) (Figure 35b). This substantial change in the residue interactions could suggest the high potency observed with phenol-containing series.

The second possible reason for the high PI3K δ activity of phenol analogues may be explained by the strength of the hydrogen bond that they formed with the polar residues in the affinity pocket, in contrast to their indole and indazole analogues. The strength of hydrogen bonds relies on the proton donor ability, the stronger the proton donor the stronger the hydrogen bond²⁴⁹, Abraham *et al*²⁵⁰ and Bauer *et al*²⁵¹ mentioned that the hydroxy group (-OH) is generally greater hydrogen bond donor than amine (-NH), thus it could make a stronger hydrogen bond with Asp⁹⁶⁴. Thus, phenol analogues would create a stronger

Chapter 2

hydrogen bond than their indole counterparts, resulting in higher PI3K δ activity. A future study will be performed to enhance the hydrogen bond donor character of phenol by increasing the acidity of the phenolic proton in the presence of an electron withdrawing group at the para position (this will be discussed in more detail in Chapter 6, Section 6.2.1.2.2).

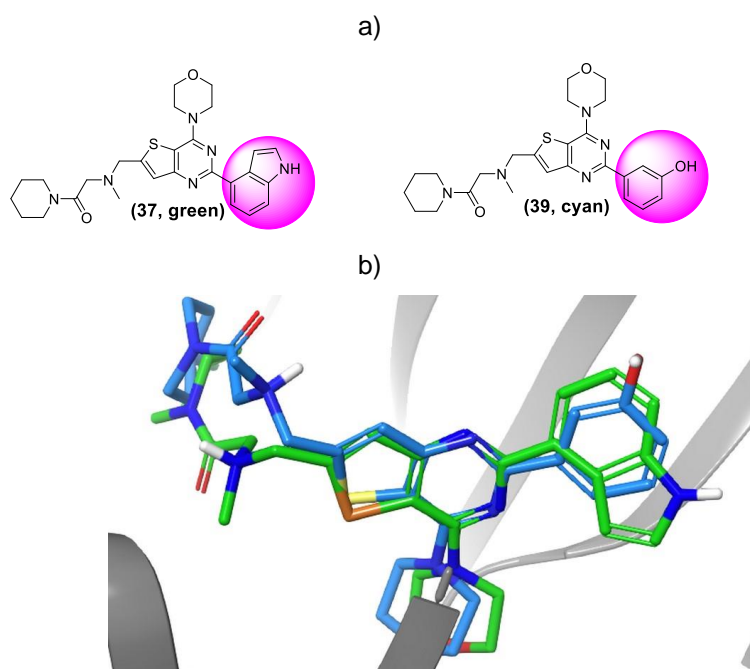


Figure 37. a) Compounds **37** and **39**, highlight the indole and phenol groups that bind to the affinity pocket b) Compounds **37** and **39** docked into K802T-mutant PI3K γ receptor model (generated from PDB code 4EZJ). Illustrates that indole group in compound **37** (blue) and phenol group in compound **39** (green) bind in two different orientations into the affinity pocket.

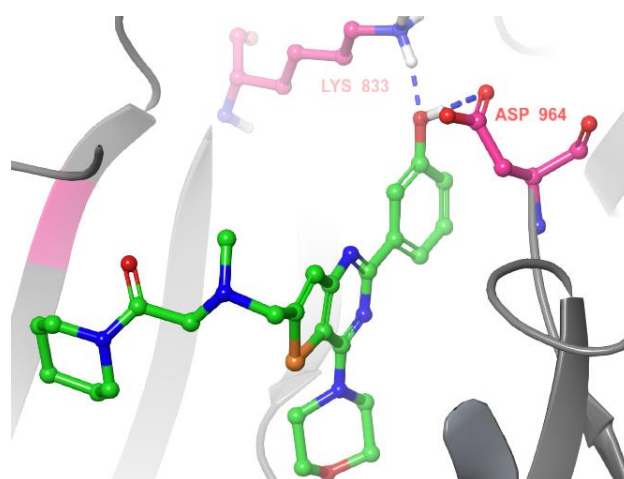


Figure 38. Compound **39** docked into K802T-mutant PI3K γ receptor model (generated from PDB code 4EZJ). Dashed pink lines represent the proposed charge-enhanced hydrogen bonds.

Chapter 2

Meanwhile, modelling studies did not explain the poor selectivity of the phenolic series in contrast to the indole-containing compounds particularly against PI3K α , where phenolic analogues were 5- to 25-fold less selective versus PI3K α than their indole counterparts. A docking study of compound **39** (Figure 38) did not reveal any hydrogen bonding networks between compound **39** and the protein such as that found in the indole-containing series, which Sutherlin *et al*¹⁶⁰ believed was responsible for the observed high PI3K δ selectivity of indole analogues. Since there is no crystal structure available for phenol-containing compounds bound to PI3K δ , the mechanism underlying their poor PI3K δ selectivity cannot be revealed. It was hypothesized that the predicted interaction with Lys⁷⁷⁹, could be behind the drop in PI3K δ selectivity of the phenol series. Hoegenauer *et al*²¹⁸ in his paper described the quinazoline-based analogue **64** with 2-methoxyphenyl inserted into the affinity pocket possessed a PI3K δ/α selectivity of 13-fold (Table 11), while the introduction of trifluoromethyl group into the 3-position of the pyridine resulted in compound **65** with reduced PI3K δ selectivity, especially for PI3K α isoforms (δ/α = 9-fold) (Table 11)²¹⁸. The authors theorised that the decrease in the PI3K δ selectivity in compound **65** was

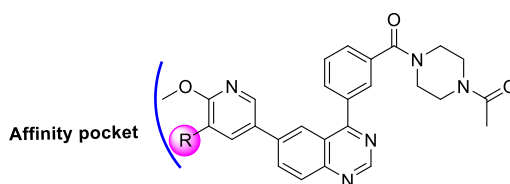


Table 11. Biological evaluation and isoform selectivity for PI3K δ for compounds **64** and **65** reported by Hoegenauer *et al*²¹⁸, highlights the drop in the selectivity against PI3K α , after the addition of trifluoromethyl group that potentially binds to Lys⁷⁷⁹.

compd	R	PI3K δ IC ₅₀ (nM)	Isoform selectivity		
			δ/α	δ/β	δ/γ
64 ²¹⁸	H	20	14	208	395
65 ²¹⁸	CF ₃	9	9	44	1033

due to the charge-enhanced hydrogen bond between Lys⁷⁹⁹ and one of fluorine atoms of the newly added trifluoromethyl group²¹⁸, which is consistent with the hypothesis stated above.

Additionally, it was noticed that this lack of PI3K δ selectivity was also observed in the FDA-approved drug (copanilisib **6**) which exhibited potency against isoforms PI3K δ and α with IC₅₀ values of 0.7 and 0.5 nM, respectively, and almost 10-fold selectivity over the other class I isoforms¹⁷⁹. The crystal structure of the copanilisib-PI3K γ complex (see Figure 21b in Chapter 1) showed that the nitrogen of pyrimidine forms a key hydrogen bond with Lys⁸³³ (Lys⁷⁷⁹ in PI3K δ) in the affinity pocket. This interaction significantly improves activity against PI3K δ and α ¹⁷⁹. According to this, one could hypothesize that the hydrogen bonding with Lys⁷⁷⁹ could be the reason for the diminished PI3K δ selectivity of the 3-phenol containing series.

In the light of the findings, in the three different series of compounds, the indole-containing compounds showed the highest selectivity for PI3K δ against the remaining three class I PI3K isoforms (Figure 39), while the phenol analogues turned out to possess the best inhibitory activity against PI3K δ isoform (Figure 39). Finally, the indazole analogues exhibited moderate PI3K δ selectivity in contrast to their indole counterparts and 3- to 5-fold decrease in potency compared to their phenol counterparts (Figure 39). Thus, the indazole series was considered unsuitable for a focused optimisation effort. Based on this potency and selectivity profile, two series of indole compounds (most PI3K δ selective) and phenol compounds (most PI3K δ active) were suggested for the next SAR study.

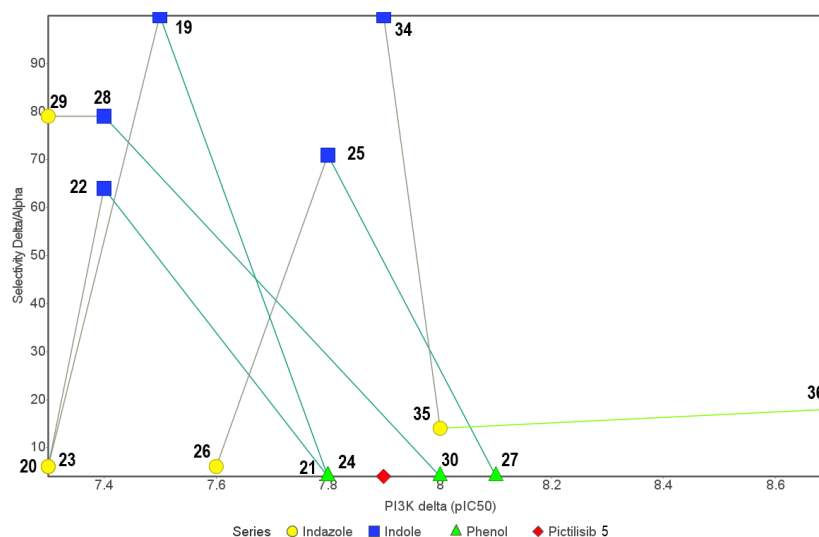


Figure 39. Plot of PI3K δ isoform activity (pIC_{50}) as a function of PI3K δ isoform selectivity (vs PI3K α). Matched-pair analysis for the indole-containing compounds (blue), phenol-containing compounds (green) and indazole-containing compounds (yellow). The indole series is the most PI3K δ selective and phenol series is the most PI3K δ active.

2.5.2 Matched molecular pair analysis of the functional groups that occupy the tryptophan shelf

In the tryptophan shelf region (R_2), all carboxylic acids (**19**, **20** and **21**) exhibited poor PI3K δ inhibitory activity with IC_{50} values in low-micromolar to mid-nanomolar range (IC_{50} values of 175, 1000 and 110 nM, respectively) with complete loss of PI3K δ selectivity over the other three isoforms of class I PI3K. Introduction of propylamine by amide coupling resulted in compounds **22**, **23** and **24** which exhibited superior improvement in PI3K δ potency and selectivity with IC_{50} values of 28, 44 and 14 nM against PI3K δ , respectively. This modification was also accompanied by improving in δ isoform selectivity, for example, compound **22** exhibited 100-fold selectivity over PI3K α and β and 50-fold against PI3K γ .

It was hypothesized that the reason behind the high PI3K δ activity and selectivity of the propyl-containing compounds was possibly due to the ability of the propyl group to make a favourable C-H/ π interaction with the tryptophan shelf. C-H/ π interaction is a dispersion interaction taking place

between aliphatic C-H donors (soft acid, propyl group) and aromatic π -acceptors (soft base, Trp⁷⁶⁰)^{252,253}. These findings are consistent to that published by *Hoegenaur. K et al*^{18,229} who confirmed that the propionamide group of leniolisib (**7**) (Figure 40) and acetyl-piperazine group of compound **66** (Figure 41) (Table 12) were directed towards the tryptophan shelf, stacked to the indole ring of Trp⁷⁶⁰, resulting in attractive dispersion forces. This interaction could only take place in PI3K δ , as the residue that opposed to Trp⁷⁶⁰ was Thr⁷⁵⁰ (Figure 40b), whereas in PI3K α , β and γ was the larger side chain of Arg or Lys, which also forms a strong cation/ π interaction with Trp, blocking access to the tryptophan shelf, as this would need to be disrupted for any interaction to take place with the ligand. This could be seen clearly in the crystal structure of compound **66** in human PI3K α (PDB code 5ITD) (Figure 41c), where the compound **66** adopted an extended conformation in PI3K α because the acetyl piperazine cannot access the tryptophan shelf, that was occluded by the large and cationic residue (Arg⁷⁷⁰), whereas in PI3K δ , compound **66** adopted a folded conformation because the acetyl piperazine group was able to fold and make a C-H/ π interaction with the tryptophan shelf (Figure 41b). This contributes to the enhanced PI3K δ potency leading to increased PI3K δ selectivity of leniolisib (**7**) and compound **66** versus the other three isoforms of class I PI3K (Table 12)^{218,229}.

Table 1. Biological evaluation and isoform selectivity for PI3K δ for leniolisib (**7**) and compound **66** reported by *Hoegenaur. K et al*^{218,229}.

compd	PI3K δ IC50 (nM)	Isoform selectivity		
		δ/α	δ/β	δ/γ
Leniolisib (7) ²³⁹	28	25	63	357
66 ²²⁷	9	29	183	514

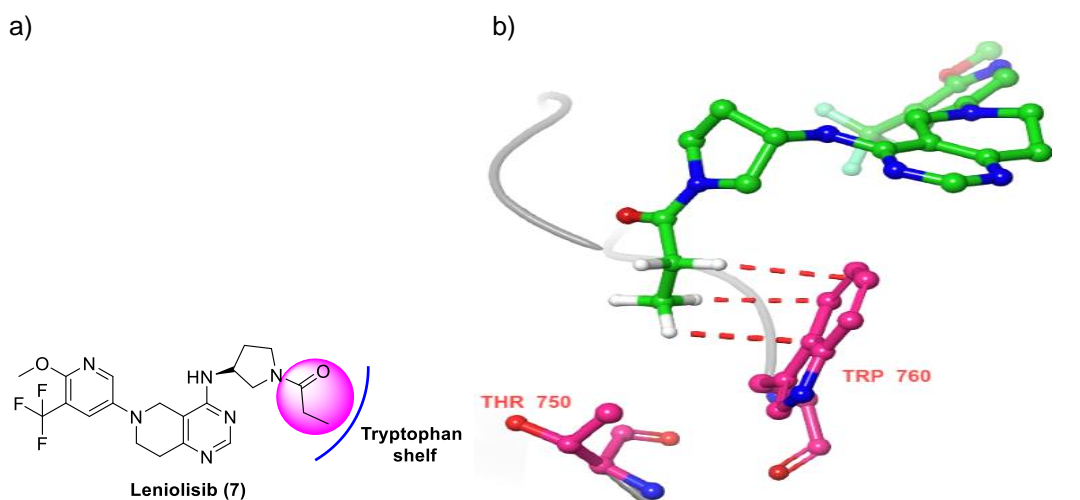


Figure 40. a) The selective PI3K δ inhibitor leniolisib (**7**), highlighted the propionamide side chain that forms key C-H/pi interactions with tryptophan shelf. b) Crystal structure of leniolisib (**7**) complexed with murine PI3K δ (PDB code 5O83) indicated that the propionamide group folds to fit the tryptophan shelf and make C-H/pi interactions with Trp⁷⁶⁰. Dashed pink lines represent the proposed C-H/pi interactions.

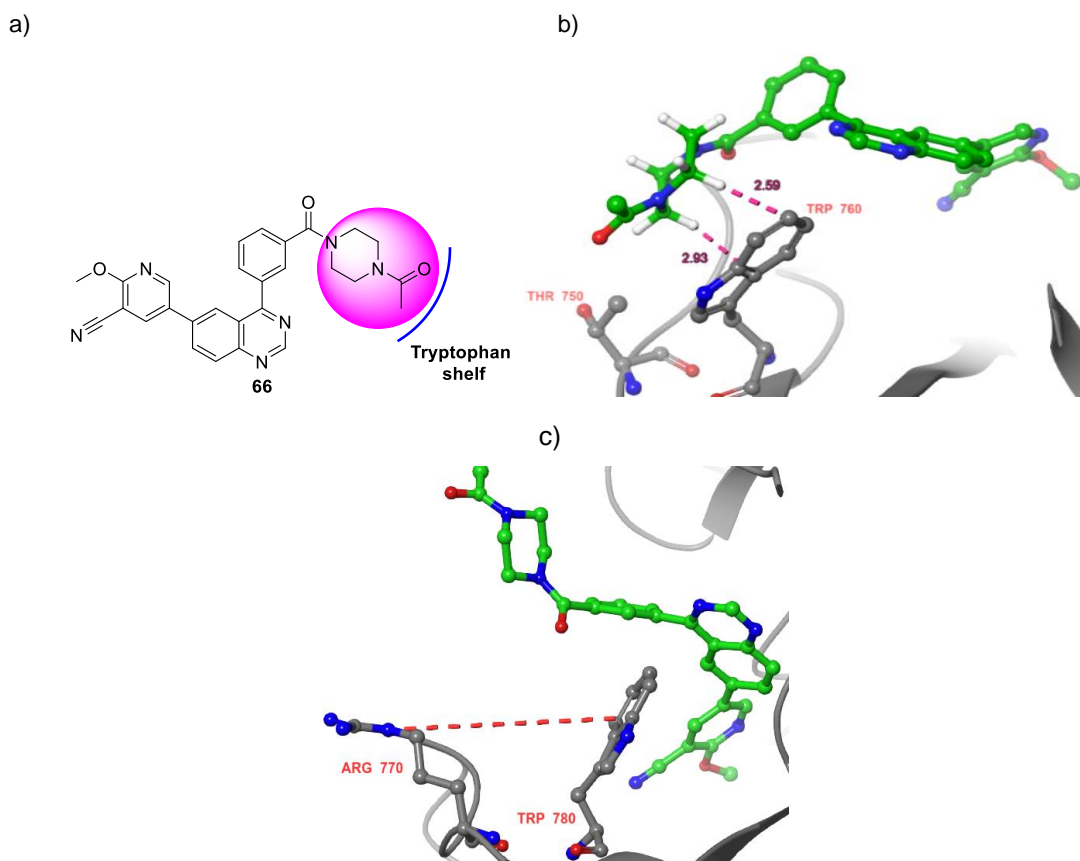


Figure 41. a) The selective PI3K δ inhibitor compound **66**, highlighted the *N*-acetylpiperazine that forms a key C-H/pi interaction with tryptophan shelf²¹⁸. b) Crystal structure of murine PI3K δ (PDB code 5IS5) with compound **66** bound, pink dashed lines indicate the proposed C-H/pi interaction that takes place between the piperazine ring and Trp⁷⁶⁰ at the tryptophan shelf²¹⁸. c) Crystal structure of human PI3K α (PDB code 5ITD) bound to the compound **66**. The tryptophan shelf is blocked by a cation/pi interaction (represented by a red dashed line) between Arg⁷⁷⁰ and Trp⁷⁸⁰ makes the compound **66** to adopt an extended conformation, preventing acetylpiperazine from accessing the tryptophan shelf²¹⁸.

Chapter 2

The importance of the propylamide was probed by replacing it with ethoxy ethylamide resulted in compounds **19,20** and **21** which displayed equipotent activity against PI3K δ compared with their propyl analogues with similar selectivity profile. Amidation of the parent carboxylic acids with glycine ethyl ester resulted in compounds (**28-30**) which demonstrated comparable PI3K δ inhibitory activity as their propyl counterparts but lower selectivity over PI3K α and β by almost 2-fold. Compounds (**31-33**) with a racemic alanine methyl ester showed a pronounced increase in the selectivity against PI3K β (approximately 2-fold) compared to the propyl analogues (**22-24**), while maintaining similar potency against PI3K δ .

Replacing the *N*-alkyl amide with the corresponding *N*-benzylamide group was explored, to direct the phenyl-substituent towards the tryptophan shelf to probe a potential pi-pi stacking interaction. The resulting *N*-benzyl compounds (**34** and **35**) showed equipotent inhibition compared with their propyl analogues (**22** and **23**), while demonstrating less selectivity for PI3K δ over PI3K α , β and γ with only 50-fold selectivity over the other class I PI3K isoforms. This was somewhat a surprising finding, given the ability of benzyl moiety to make a pi-pi interaction with Trp⁷⁶⁰ in the tryptophan shelf and thus benzyl analogues were expected to exhibit greater PI3K δ potency and selectivity compared to their alkyl analogues which were only able to make hydrophobic interactions. These results were compatible with Terstiege *et al*²⁰ findings, which showed that the replacement of the phenyl group of compound **67** with morpholine (compound **68**) and tetrahydropyran (compound **69**) did not lead to a decrease in the PI3K δ activity and selectivity over the other three isoforms of class I PI3K (Table 13), which further

Chapter 2

confirmed that the non-covalent interaction that took place between the R₂ substituent and Trp⁷⁶⁰ in the tryptophan shelf was a C-H/pi interaction and not a pi-pi stacking.

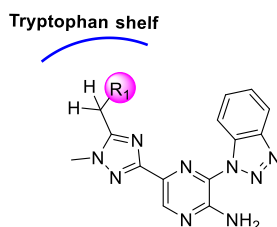


Table 13. Biological evaluation and isoform selectivity for PI3K δ for compounds (**67-69** reported by Terstiege *et al*²²⁰).

compd	R ₁	PI3K δ IC ₅₀ (nM)	Isoform selectivity		
			δ/α	δ/β	δ/γ
67 ²²⁰		22	6	25	13
68 ²²⁰		22	6	32	13
69 ²²⁰		56	3	10	6

Finally, amidation of the carboxylic acids **19**, **20** and **21** with piperidine resulted in compounds **37**, **38** and **39**, which showed improved PI3K δ activity (IC₅₀ values of 11, 10 and 2 nM, respectively) compared to their acyclic analogues (**22** to **33**). As examples, the piperidine derivatives **37**, **38** and **39** showed 3-, 4- and 7-fold increase of potency comparing to their propyl counterparts **22**, **23** and **24**, respectively. Additionally, the piperidine ring imparts improved selectivity (220- to 280-fold) for PI3K δ relative to PI3K β . This led us to the exciting possibility that saturated heterocycles, such as piperidine, might be able to make stronger attractive dispersion force (C-H/pi) interaction with the tryptophan shelf than linear alkyl derivatives²⁵⁴. Kozmon, *et al*²⁵⁵ and Ran J, *et al*²⁵⁴ in their studies proved that stronger CH/pi interactions exist for cyclic against linear alkanes. This can be attributed to two possible factors. First, Aliphatic heterocycles have more polar character

than their linear counterparts, as the strength of the dispersion energy depends on polarizability^{254,256}, thus, the CH donor ability of aliphatic heterocycles is stronger than their acyclic counterparts. A second reason is that the piperidine ring is able to make multiple C-H/ π interactions with Trp⁷⁶⁰, Chen Zhao *et al* and Ciunik Z, *et al*^{257,258} reported that the strength of C-H/ π interaction was correlated with the number of C-H/ π contacts, as they could work in a cooperative manner (Figure 42). It was proved that the saturated hydrocarbon-aromatic system complex gave the most stable conformation when they contact each other by multiple (2-4) CH/ π interactions (Figure 42)^{253,254}. The piperidine group could position a greater number of carbon atoms (5 carbons) over the aromatic ring of tryptophan, this allowed it to establish 3 CH/ π contacts using the 3 axial hydrogens that were located on the same face of the piperidine ring (Figure 43), made an attractive complementary surface for the planar indole ring of Trp⁷⁶⁰²⁵⁹.

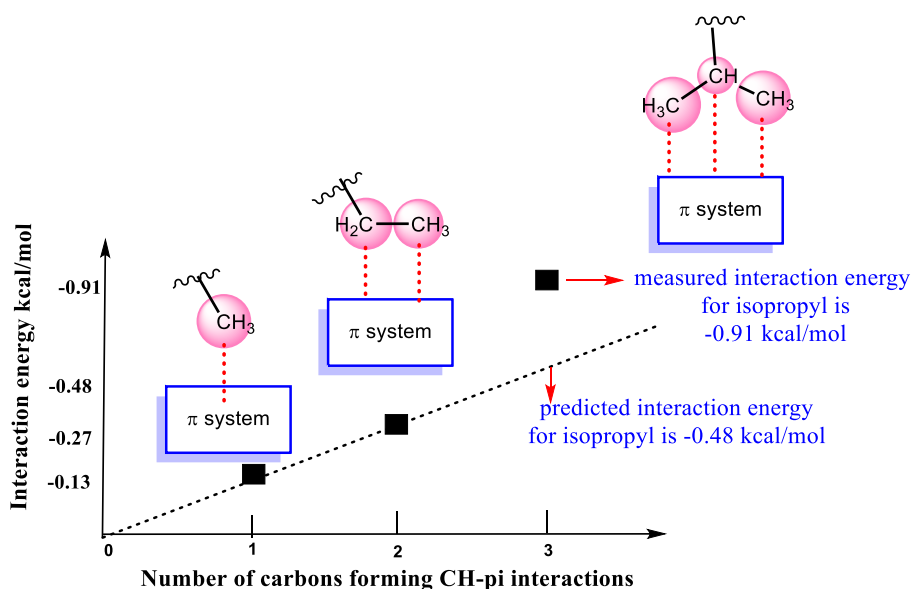


Figure 42. Graph taken from Zhao *et al*²⁵⁷: correlation between the number of carbons forming CH/ π contacts and the interaction energy. The C-H/ π interaction exhibits additivity for linear alkyl groups (methyl and ethyl), as the ethyl/ π interaction energy is nearly twice that for the methyl/ π complex, whereas the C-H groups of the branched chain (isopropyl group) interact with the π system in a cooperative manner, which results in a C-H/ π interaction energy larger than expected. According to Kozmon *et al*²⁵⁵, the positive cooperativity of C-H/ π interactions is also observed in alicyclic rings included in the current study.

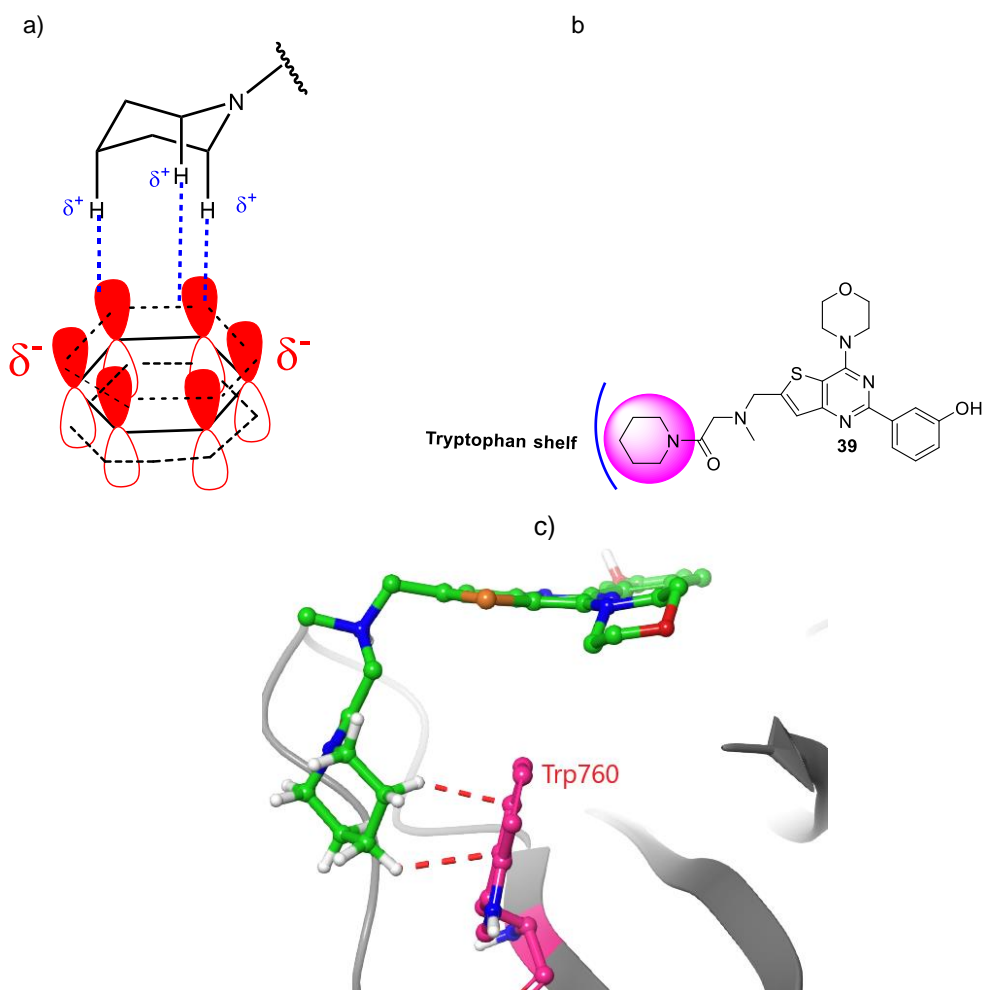


Figure 43. a) The suggested C-H/ π interactions between three electropositive hydrogens in the piperidine ring and indole ring of Trp⁷⁶⁰, which could contribute to high PI3K δ activity and selectivity of piperidine derivatives (**37-39**). b) Compound **39**, highlights the piperidine ring that might form a key C-H/ π interaction with tryptophan shelf. c) Compound **39** docked into the PI3K δ model (generated from PDB code 5IS5). Dashed pink lines represent the proposed C-H/ π interaction.

2.5.3 Conclusion derived from the first SAR study (Table 9)

First SAR study (Table 9) revealed that high PI3K δ activity and selectivity could be obtained through three structural modifications on the lead compound (pictilisib, **4**).

First, the ring opening strategy by substituting the piperazine group with a flexible linker resulted in better PI3K δ inhibitory activity and isoform selectivity than the lead compound (pictilisib, **4**). This could be because the flexible linker has the capability to insert the R₂ group into the tryptophan shelf. This can be shown in the molecular docking study (Figure 44) of the compound **39** with

pictilisib (**4**) into PI3K δ (PDB code 2WXP) where compound **39** adopted a folded conformation due to the flexibility of the linear linker connecting the thienopyrimidine scaffold to the tryptophan shelf binder (piperidine) which inserted deep into the tryptophan shelf (Figure 44c). In contrast, the rigid piperazine linker retained the extended conformation of pictilisib (**4**), preventing it from folding and accessing the tryptophan shelf.

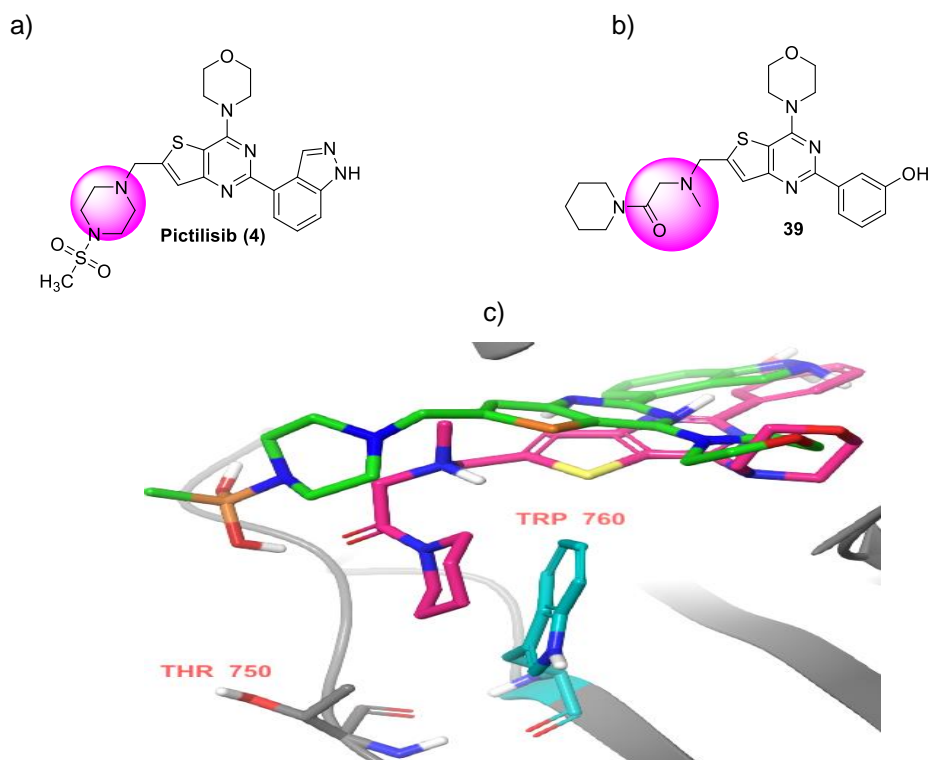


Figure 44. a) The non-selective PI3K inhibitor pictilisib (**4**), highlighted the restricted linker (piperazine ring). b) Compound **39**, highlighted the flexible open-chain linker. c) Compound **39** (pink) docked into the PI3K δ model (generated from PDB code 2WXP), overlaid on pictilisib (**4**) (green), showing pictilisib (**4**) adopts an extended conformation, while compound **39** adopts a folded conformation.

Second, the isosteric replacement of the 4-indazole moiety in the affinity pocket with a 4-indole group could achieve the highest level of PI3K δ selectivity, whereas substitution of the 4-indazole group with a 3-phenol ring achieved the highest degree of PI3K δ inhibitory activity. Thus, two series were suggested for the next SAR study, where one series will have an indole

Chapter 2

group as an affinity pocket binder while the second series will have a phenol group as an affinity pocket binder.

Third, high PI3K δ potency and selectivity could be obtained by targeting the tryptophan shelf with saturated nitrogen containing heterocycles. It was thought that C-H/ π interaction with the tryptophan shelf could be improved by enhancing the proton donor ability of the piperidine ring. Several studies have reported that an increase in the acidity of the donor protons results in an increase in the strength of the C-H/ π interaction^{252,253,259}. This can be achieved by implementing two strategies, firstly, replacement of piperidine with more electron deficient saturated rings, such as morpholine or piperazine, in which the carbon atom in the 4-position of the piperidine ring was replaced by a more electronegative heteroatom (oxygen in morpholine and nitrogen in piperazine). These replacements induce an electron withdrawing inductive effect (Figure 45c and 45d), resulted in increasing the acidity (proton-donor ability) of C-Hs leading to the stronger C-H/ π interaction with tryptophan shelf. Secondly, incorporation of one or two strongly electronegative fluorine atoms at the 4-position of a piperidine ring could increase the acidity of hydrogens of the piperidine ring (Figure 45e and 45f), resulting in a strengthening of the C-H/ π interaction and thus in an enhancement of biological activity²⁶⁰. These two approaches could optimize the C-H/ π interaction at the tryptophan shelf and hence might improve PI3K δ activity and selectivity even more.

Chapter 2

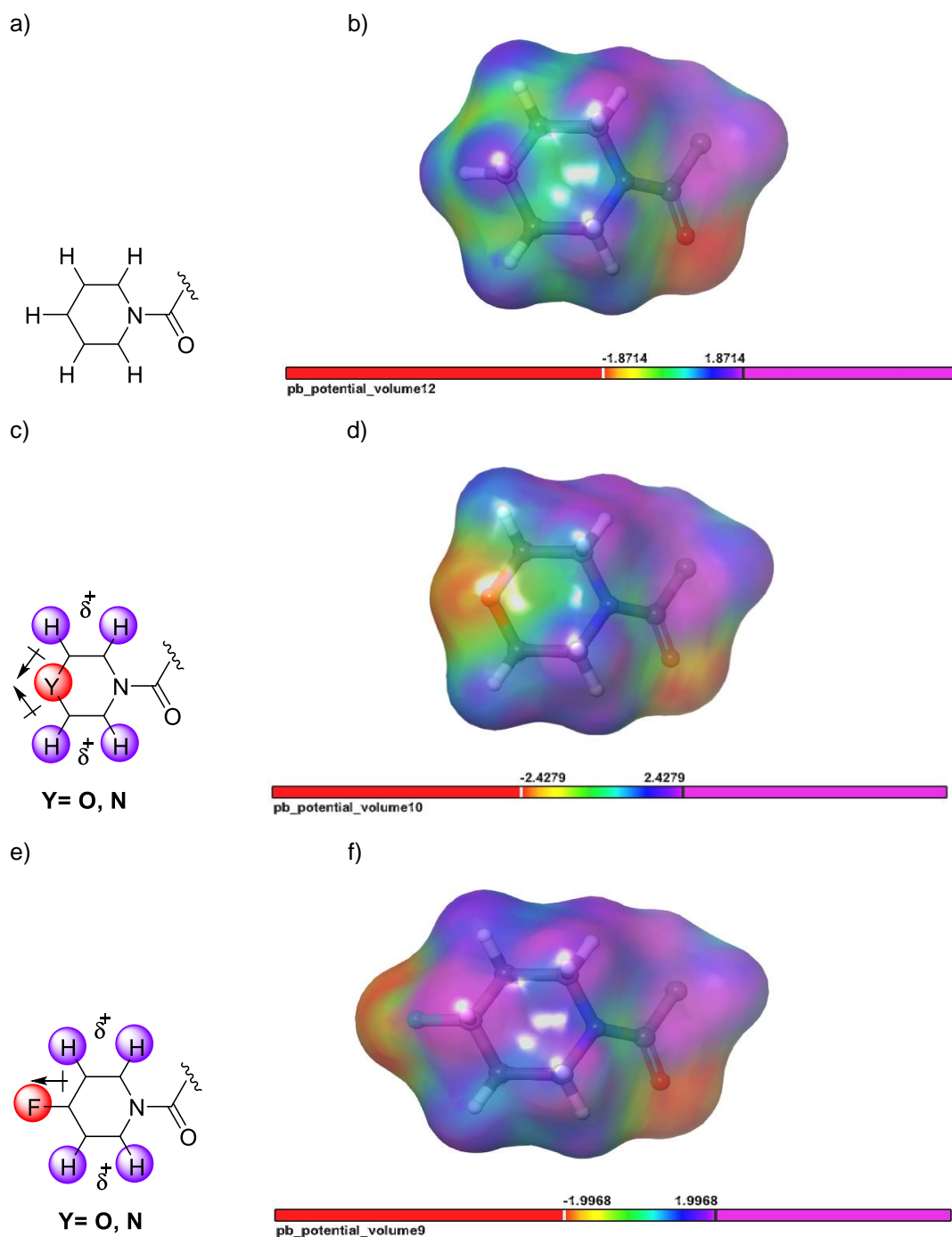


Figure 45. Two approaches suggested to increase the proton donor ability of the piperidine ring and enhance the CH/ π interaction with tryptophan shelf: a) Chemical structure of the piperidine ring. b) Electrostatic potential map of piperidine ring c) One carbon atom of piperidine is replaced by one of the heteroatoms oxygen or nitrogen, which makes the ring more electron deficient and thus better C-H donor than piperidine. d) Electrostatic potential map of morpholine. e) Introduction of the strong electronegative fluorine atom at the 4-position of piperidine ring makes the ring more electropositive than piperidine and thus increases the C-H donating ability of the ring. f) Electrostatic potential map of 4-fluoropiperidine.

Chapter 2

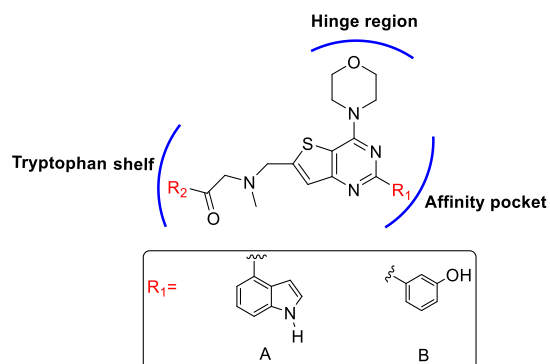


Table 14. Biological evaluation and isoform selectivity for PI3K δ for compounds (37, 39 and 42- 59).

Compd	R ₂	R ₁	Isoform potency ^{a,b} IC ₅₀ (nM)				Isoform selectivity		
			PI3K δ	PI3K α	PI3K β	PI3K γ	δ/α	δ/β	δ/γ
37		A	11	1100	2800	280	100	255	25
39		B	2	35	44	35	18	220	18
42		A	11	2800	2800	1400	255	255	127
43		B	2.2	110	1750	220	50	795	100
56		A	11	1100	555	1750	100	50	159
57		B	5.5	28	140	220	5	25	40
44		A	17.5	1750	1750	4400	100	100	251
45		B	5.5	70	555	110	6	101	20
52		A	5.5	7000	5500	17.5	1273	1000	3
53		B	1.4	70	2800	441	50	2000	315

Compd	R ₂	R ₁	Isoform potency ^{a,b} IC ₅₀ (nM)				Isoform selectivity		
			PI3K δ	PI3K α	PI3K β	PI3K γ	δ/α	δ/β	δ/γ
46		A	100	28000	22000	350	280	220	3.5
47		B	22	11000	7000	7000	500	318	318
58		A	11	5500	1400	7000	500	127	636
59		B	2.2	17.5	175	350	8	79	159
54		A	11	2800	2800	710	255	255	65
55		B	4.4	100	2800	110	23	506	25
48		A	4.4	2225	2800	710	506	636	161
49		B	1.1	17.5	555	35	16	505	32
50		A	4.4	1400	1400	710	318	318	161
51		B	2.2	35	555	56	16	500	25

^aPotency against the different PI3K isoforms is given as IC₅₀ values (n = 1). ^bThe potency threshold for the PI3K δ assay is ~ IC₅₀ 1 nM due to substrate concentration.

The two piperidine compounds (**37** and **39**) would be used as parent compounds in this SAR study (Table 14) to evaluate any enhancement in PI3K δ activity or selectivity. The morpholine analogues (**42** and **43**) demonstrated comparable PI3K δ inhibitory potency (IC₅₀ value of 11 and 2.2 nM, respectively) to their piperidine counterparts (**37** and **39**). However, they displayed higher selectivity over PI3K α and γ. Morpholine-containing compounds **42** and **43** were 2.5- and 5-fold more selective over PI3K α and

γ , respectively than their corresponding piperidine analogues **37** and **39**. This increase in the selectivity is due to loss of activity against PI3K α and γ . These consistent results are interesting, because they showed PI3K α/δ and PI3K γ/δ selectivity advantage of morpholine analogues over their piperidine analogues.

Piperazine derivatives **56** and **57** exhibited similar potency to the parent piperidines **37** and **39** with slightly higher isoform selectivity versus PI3K γ (159 and 40-fold, respectively) compared to their piperidine analogues. However, they were far less selective against PI3K β where β/δ selectivity ratio reduced by 5- and 9-fold for compounds **56** and **57**, respectively (Table 14). *N*-methylation of piperazine ring in compounds **44** and **45** had little impact on PI3K δ potency and isoform selectivity against PI3K α and γ . However, it enhanced the selectivity against β isoform by 2 and 4-fold, respectively, in comparison with their non-methylated analogues **56** and **57**.

N-Boc-protected piperazine analogues **52** and **53** exhibited high PI3K δ potency profile (IC_{50} values of 5.5 and 1.4 nM, respectively) with 2- and 4-fold improvement than their unprotected analogues **56** and **57** (Table 14). Strikingly, bulky group (Boc group) at *N*-4 of piperazine could be tolerated in the tryptophan shelf without loss of activity, which suggested that tryptophan shelf of the PI3K δ was not spatially constrained and a wide range of groups could be tolerated in this position. Thus, replacement of acid-labile group Boc with similar size bioisosteres such as urea and sulfonamide will lead to the development of the physiologically stable analogues which can be useful tool for medicinal chemistry and drug discovery (Figure 46). Furthermore, compounds **52** and **53** displayed remarkable improvement in the selectivity

(10-fold) against PI3K α , while their δ/β selectivity increased by 12- to 80-fold comparing to their unprotected analogues **56** and **57**. However, compound **52** showed an unexpected diminish in the selectivity against PI3K γ ($\gamma/\delta=3$) which was due to its high activity against PI3K γ ($IC_{50}=17.5$ nM).

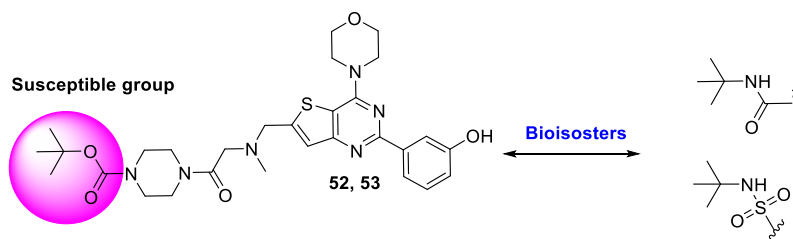


Figure 46. Bioisosteric replacement of metabolically labile Boc group of compounds **52** and **53** with stable urea and sulphonamide groups.

N-acetylation of piperazine **56** resulted in compound **46** which was the least active compound in this series with an IC_{50} of 100 nM. This finding was unexpected, because it was known that the acetyl group was an electron withdrawing group by inductive effect, which made the piperazine ring more electron deficient and possibly enhanced C-H/ π interaction²⁶¹. Thus, it was expected to be more active than the deacetylated analogue **56**. Moreover, it showed almost no inhibitory activity on PI3K α and β , while displaying poor selectivity against γ isoform ($\gamma/\delta=3.5$) (Table 14). The matched pair phenol **47** was about 5-fold more potent as PI3K δ inhibitor compared to its indole counterpart **46**. Additionally, it was found to be 100-fold more selective for PI3K δ against PI3K γ .

Introduction of aminomethyl group at the 2-position of piperidine in compounds **37** and **39** resulted in analogues **58** and **59** which exhibited similar potency (IC_{50} values of 11 and 2 nM, respectively) to their unsubstituted counterparts (Table 14). The compound **58** possessed excellent PI3K δ selectivity over the other three isoforms (500, 136 and 636-

fold against PI3K α , β and γ , respectively). Interestingly, Boc-protected 2-(aminomethyl) piperidine derivatives **54** and **55** showed equipotent inhibition of PI3K δ compared with non-protected counterparts. These findings proved that substitution at the 2-position of piperidine group even with a bulky group did not have a detrimental impact on PI3K δ inhibitory activity and selectivity. However, PI3K γ/δ selectivity had reduced by 10- and 6-fold in compounds **54** and **55**, respectively.

Introduction of fluorine atom at the 4-position of piperidine in compounds **37** and **39** affording monofluorinated analogues **48** and **49** resulted in a 2-fold increase of potency against PI3K δ (IC_{50} of 4.4 and 1.1 nM, respectively) as well as accompanied enhancement in the selectivity versus the other three class I isoforms (5, 2.5 and 6.5-fold against PI3K α , β and γ , respectively) (Table 14). It was hypothesized that the favorable PI3K δ activity and selectivity profile of monofluoropiperidine derivatives **48** and **49** might be due to the strong electronegative fluorine atom pulling electron density away from the piperidine ring by the inductive effect (Figure 45e and 45f) which would make the hydrogens of the ring more acidic than the des-fluoro analogues **37** and **39** and thus increased the strength of C-H/ π interaction with Trp⁷⁶⁰ in the tryptophan shelf^{252,262}. The increase in the acidity of piperidine protons can be observed using nuclear magnetic resonance (NMR) technique by assessing the deshielding of protons on piperidine caused purely by the inductive effect of the fluorine atoms. This can be done through comparing the ¹H NMR spectra of monofluorinated analogue **48** with its desfluorinated counterpart **37** (Table 15). The fluorine atom caused a strong deshielding of 2.16 ppm at geminal hydrogen H-4, however the deshielding effect

Chapter 2

decreased with the distance to fluorine atom increased, whereas H-3 and H-2 experienced downfield shifts of 0.26 and 0.04, respectively (Table 15). It was hypothesized that despite the substitution of a fluorine atom for a hydrogen, monofluorinated analogues **48** and **49** were still able to form 3 C-H/ π interactions with Trp⁷⁶⁰, which was equal to the number of C-H/ π interactions that non-fluorinated analogues made (Figure 47), because the newly introduced fluorine atom preferred to be in the equatorial position because it avoided the steric interaction with the axial hydrogen atoms (Figure 47), thus there would be 3 axial hydrogens on the α -face of piperidine that could make 3 C-H/ π interactions with Trp⁷⁶⁰ in the tryptophan shelf (Figure 47).

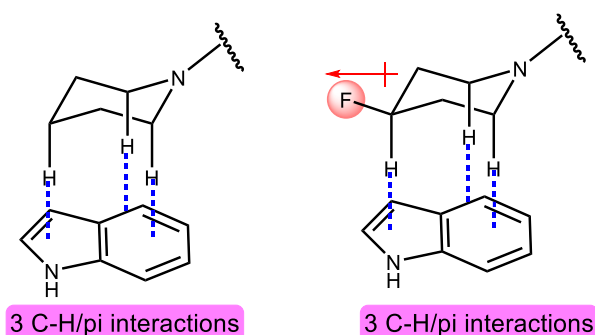
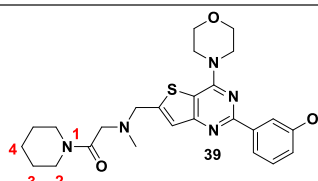
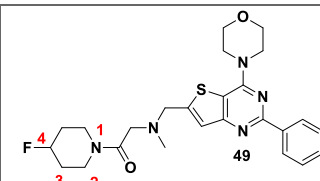


Figure 47. Depicts the possible number of potential C-H/ π interactions that could be made by desfluorinated (**37** and **39**) and monofluorinated analogues (**48** and **49**) with the tryptophan shelf.

Table 15. Assessing the deshielding of the piperidine protons caused purely by the inductive effect of one fluorine atom.

Protons			Change in the chemical shift (ppm)
H-4	1.45 ppm	3.61 ppm	+ 2.16
H-3	1.57 ppm	1.83 ppm	+ 0.26
H-2	3.42 ppm	3.46 ppm	+ 0.04

Chapter 2

An additional fluorine atom was introduced at the C-4 position of piperidine ring in compounds **48** and **49** resulted in the generation of gem-difluoro analogues **50** and **51**, respectively. The newly added fluorine atom could make the piperidine hydrogens more acidic and thus formed a stronger C-H/ π interaction with Trp⁷⁶⁰ than that of monofluorinated analogues **48** and **49**. Comparison of ¹H NMR spectra of compound **49** with **51** (Table 16) showed that the two fluorine atoms resulted in a further deshielding of H-3 by 0.16 and H-2 by 0.15 comparing to the monofluoro analogues. Surprisingly, Compounds **50** and **51** showed no improvement in PI3K δ activity (IC₅₀ values of 4.4 and 2.2 nM, respectively) over their monofluorinated counterparts **48** and **49**, respectively. Additionally, no change in PI3K δ selectivity was observed. It was hypothesized that in spite of the slight increase in the acidity of the H-3 and H-2, the C-H/ π interaction was not reinforced due to the loss of the geminal and the most acidic proton (H-4) by the ipso substitution of the second fluorine atom (Figure 48), thus, no further gain in PI3K δ activity and selectivity was achieved.

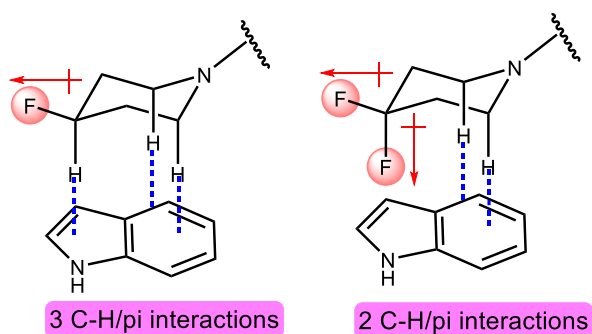
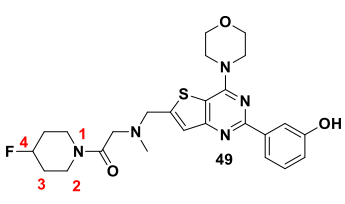
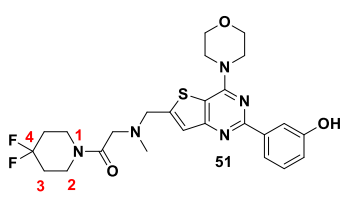


Figure 48. Depicts the possible number of potential C-H/ π interactions that could be made by the monofluorinated (**48** and **49**) and geminal difluorinated analogues (**50** and **51**) with the tryptophan shelf.

Table 16. Assessing the deshielding of piperidine protons in compound **51**, caused purely by the inductive effect of the second fluorine atom.

Proton			Change in the chemical shift
H-4	3.61 ppm	Not exist	-
H-3	1.83 ppm	1.99 ppm	+ 0.16
H-2	3.46 ppm	3.61 ppm	+ 0.15

Based on these findings, 4-fluoropiperidyl analogue **48** showed the best balance between PI3K δ potency (IC_{50} value of 4.4 nM) and selectivity over other class I isoforms (Figure 49) with more than 500-fold over PI3K α and β and 160-fold against PI3K γ . In addition to high PI3K δ activity and selectivity, compound **48** was more likely to have more optimal physicochemical and absorption, distribution, metabolism and excretion (ADME) properties for oral drugs, than the other analogues and the lead compound pictilisib (**4**), where it has calculated log P (clog P) value of 2.79 (calculated by DataWarrior, using principal component analysis), which lies in the optimum range of lipophilicity (log P= 2- 3) (Figure 50) that gives a good balance between solubility and permeability^{263,264}, whereas the lead compound pictilisib (**4**) has a clog P value of 1.33 (calculated by DataWarrior) (Figure 50). Moreover, compound **48** possesses a topological polar surface area (tPSA) of 105.83 Å² that is lower than that of pictilisib (**4**) (Figure 51), which has a tPSA of 144.17 Å² (exceeding 140 Å²) and is thus more likely to show poor membrane permeability^{265–267}. The matched pair phenol **49** displayed the highest degree of PI3K δ inhibitory activity in this series with IC_{50} value of 1.1 nM, however, it had moderate selectivity with only 16 and 35-fold more selective against PI3K α and β ,

Chapter 2

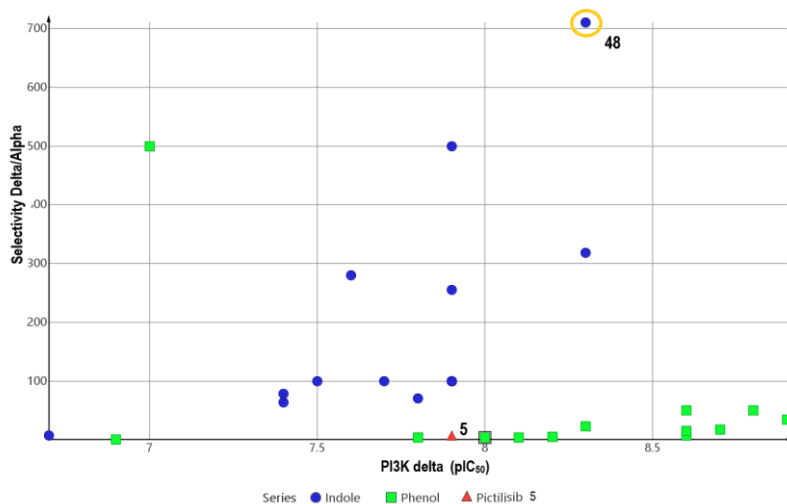


Figure 49. Plot of PI3K δ activity as a function of PI3K δ isoform selectivity (vs PI3K α). Highlighted is the compound **48** that shows the most favourable PI3K δ isoform selectivity.

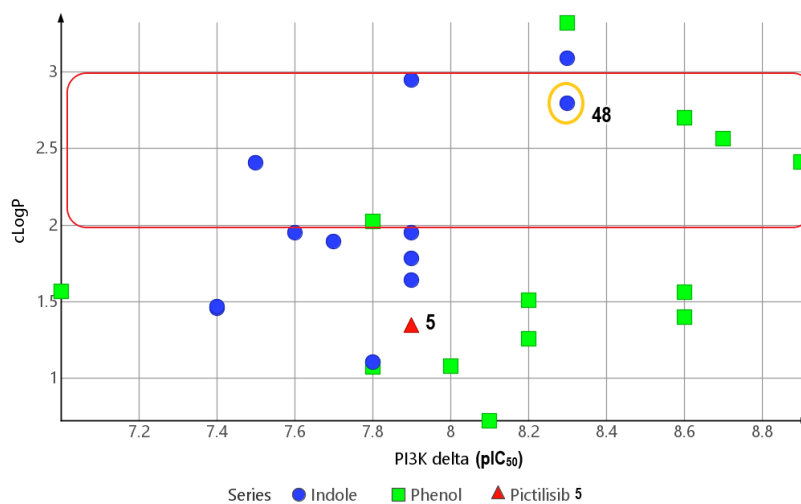


Figure 50. Plot of PI3K δ activity (pIC_{50}) as a function of calculated log P, highlighted is the compound **48** that lies in the optimum region of lipophilicity for oral drugs ($clog P = 2 - 3$, highlighted in the red box).

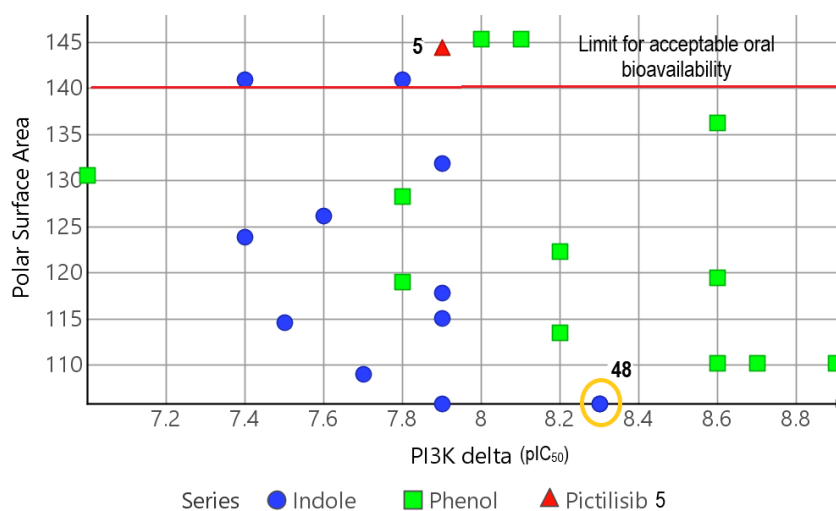


Figure 51. Plot of PI3K δ activity (pIC_{50}) as a function of tPSA, highlighted is the compound **48** with tPSA less than 140 Å ($=105.83$ Å), which is in the favourable range for oral administration.

respectively. Thus, only compound **48** had fulfilled the optimal expectations for ideal selective PI3K δ inhibitors (excellent PI3K δ potency, selectivity and predicted physicochemical properties).

2.6 Conclusion

This chapter has shown how the thienopyrimidine based inhibitors, originating from non-selective PI3K inhibitor (pictilisib, **4**), could be converted into a series of highly potent and selective PI3K δ inhibitors. Compound **48** had emerged to be the best compound in the whole series, having excellent PI3K δ inhibitory activity with great selectivity (161- 636-fold) over other PI3K isoforms, it was noteworthy that the compound **48** had more favorable PI3K δ selectivity profile than the developmental candidate (Leniolisib, **7**) (Table 17). Furthermore, this research led to the discovery of compound **49**, which was 10-fold more potent than pictilisib (**4**) and idelalisib (**8**) at inhibiting PI3K δ (Table 17), but did have moderate selectivity against PI3K α and γ . High PI3K δ activity and selectivity have been achieved by using a flexible linker which could increase the accessibility of R₂ group to the tryptophan shelf that was exposed only in δ isoform, where it was found that targeting the tryptophan shelf with saturated heterocycles was an efficient strategy for the future design of highly selective PI3K δ inhibitors. Furthermore, modulation in the affinity pocket could enhance the PI3K δ inhibitory activity as well as the selectivity against the other three isoforms. The use of indole was required to provide PI3K δ selectivity, whereas phenols moiety exhibited the highest PI3K δ activity, when inserted deeply into the affinity pocket.

Chapter 2

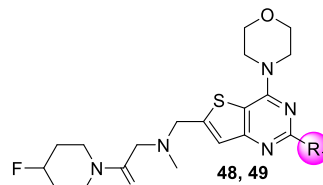
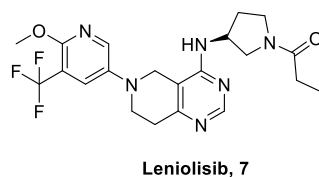
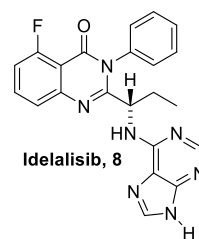
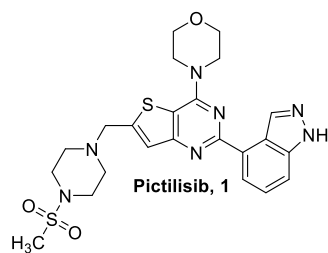


Table 17. Biological evaluation and isoform selectivity for PI3K δ for compounds pictilisib (4), idelalisib (8), leniolisib (7), 48 and 49.

		Isoform Potency ^{a,b} IC ₅₀ (nM)	Isoform selectivity		
Compd	R ₁	PI3K δ	δ/α	δ/β	δ/γ
Pictilisib (4)	-	11	4	20	20
Idelalisib (8)	-	11	14000	56	56
Leniolisib (7) ²³⁹	-	28	25	63	357
48		4.4	506	636	161
49		1.1	16	505	32

^aPotency against the different PI3K isoforms is given as IC₅₀ values (n = 1). ^bThe potency threshold for the PI3K δ assay is ~ IC₅₀ 1 nM due to substrate concentration.

Chapter 3 Design, Synthesis and Pharmacological Characterization of Novel Quinazolinone-based PI3K δ selective Inhibitors (Propeller-shaped inhibitors)

3.1 Aim

This chapter covered the second class of PI3K δ inhibitors which were called “the propeller-shaped” PI3K δ inhibitors which adopted a orthogonal conformation when bound to PI3K δ , where the three substituents (blades) are twisted almost perpendicularly (Figure 52)^{146,149}, this is distinct from the flat-shaped inhibitors, which adopt a flat conformation (discussed in the previous chapter). It is important to note that propeller-shaped inhibitors interact with several pockets in PI3K δ different from the flat-shaped inhibitors binding regions (see Table 3 in Chapter 1), the former inhibitors bound to PI3K δ at the hinge region, specificity pocket and hydrophobic region II, while the latter interacted with PI3K δ in the hinge region, affinity pocket and the tryptophan shelf^{145,146,152}. One example of the propeller-shaped inhibitors is idelalisib (**8**) (Figure 52), which was the first FDA-approved selective PI3K δ inhibitor to treat three types of hematological malignancies including CLL, relapsed follicular B-cell non-Hodgkin lymphoma and relapsed SLL. However, **8** was associated with a significant number of side effects include long-term diarrhoea, hepatotoxicity, colitis and pneumonitis^{154,230,231}.

In this research, Idelalisib (**8**) was synthesized and tested against the four isoforms of class I PI3K. As reported in the literature, it displays good potency for PI3K δ with an IC₅₀ of 11 nM and very good selectivity over the other isoforms (α/δ = 1400, β/δ = 56 and γ/δ = 56). However, it was believed that the

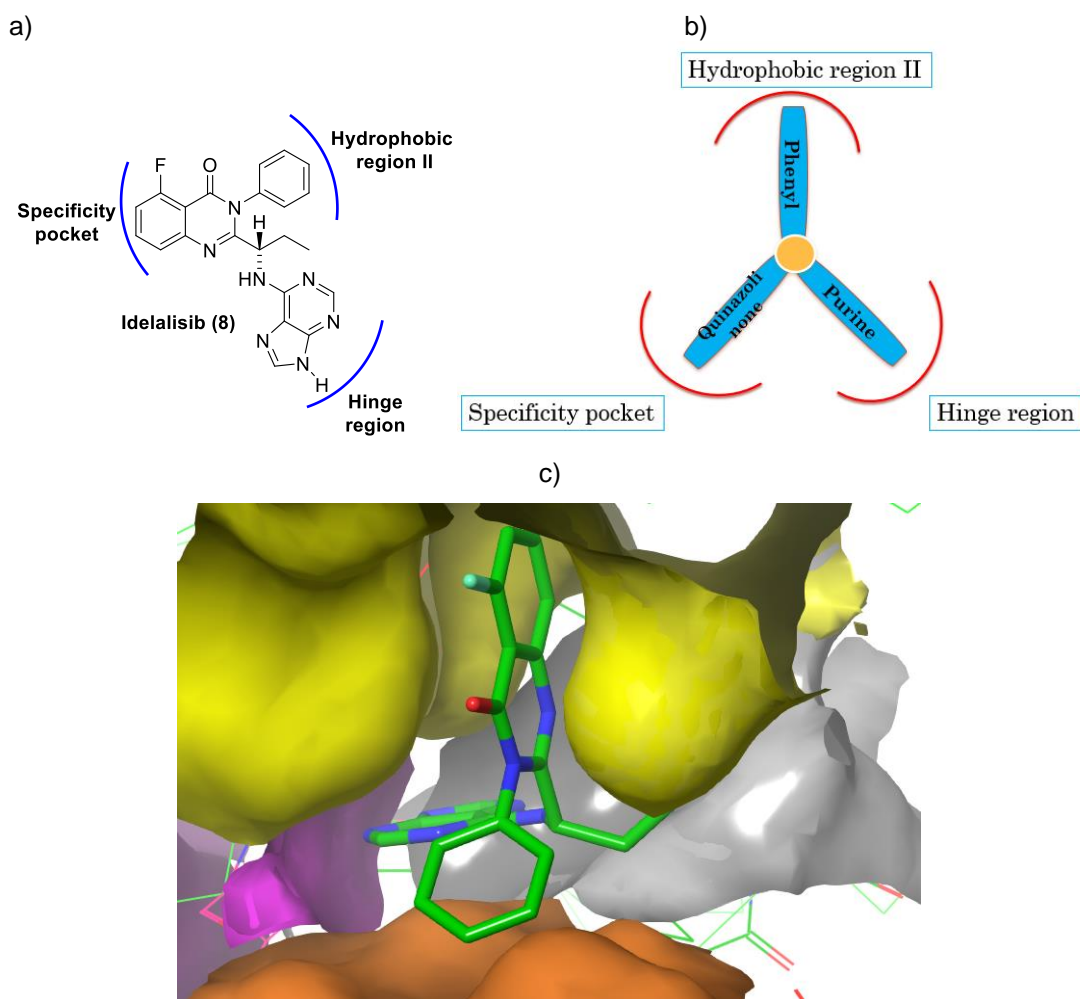


Figure 52. a) The typical propeller-shaped selective PI3K δ inhibitor idelalisib (**8**)¹⁵³. b) Diagram shows the three-bladed propeller-like structure of **8** and its interactions in the three regions of PI3K δ binding site. c) Crystal structure of murine PI3K δ (PDB code 4XE0) with idelalisib (**8**) bound, showing that **8** adopts a propeller-shaped conformation. The hinge region is shown in violet, the open specificity pocket in yellow, the hydrophobic region II in orange¹⁸⁰.

potency of **8** could be further improved, given the fact that there was a plethora of published PI3K δ inhibitors that were 10- to 100-fold more potent than **8**, some of these compounds were developed in the previous chapter (compounds **48**, **49**, **50**, **51** and **59**). It was hypothesized that gains in idelalisib (**8**) potency could be obtained by exploiting the unoccupied affinity pocket, which is lined with polar residues. First, the co-crystal structure of PI3K δ with **8** needed to be explored.

3.2 Binding interaction of the lead compound: idelalisib (**8**)

3.2.1 Quinazolinone scaffold (Specificity pocket)

The propeller shape of **8** induces structural changes in the conformation of the binding site of the PI3K δ enzyme¹⁷⁴. It was seen that Trp⁷⁶⁰ and Met⁷⁵² that are normally packed against each other in the apoenzyme distance away from each other by ~ 6.5 Å when **8** binds (see Figure 17a in Chapter 1). This creates a new pocket (termed specificity pocket) in which the fluoroquinazolinone ring fits¹⁵³, sandwiched between Trp⁷⁶⁰ and Ile⁷⁷⁷ on one side and Met⁷⁵² and Pro⁷⁵⁸ on the other side (see Figure 17a in Chapter 1)¹⁵³. The induced specificity pocket is believed to be the main factor of the PI3K δ isoform selectivity of idelalisib (**8**) and other propeller-shaped PI3K δ inhibitors^{154–156}, as discussed earlier in Section 0.

3.2.2 Purine group (Hinge binder)

The purine ring interacts with the hinge region of PI3K δ , the N3 of purine makes a critical hydrogen bond with the amide backbone of Val⁸²⁸, whereas the NH-9 of purine also bound to the Glu⁸²⁶'s carbonyl oxygen (Figure 53b). Thus, **8** and all propeller-shaped inhibitors engage in dual hydrogen bond interactions with the hinge region. In contrast, all flat-shaped inhibitors make only one hinge interaction *via* hydrogen bonding between the oxygen of morpholine and the amide backbone of Val⁸²⁸ (see Figure 28b in Chapter 2), as it was already mentioned in the previous chapter. This is another difference between the two classes of PI3K δ inhibitors.

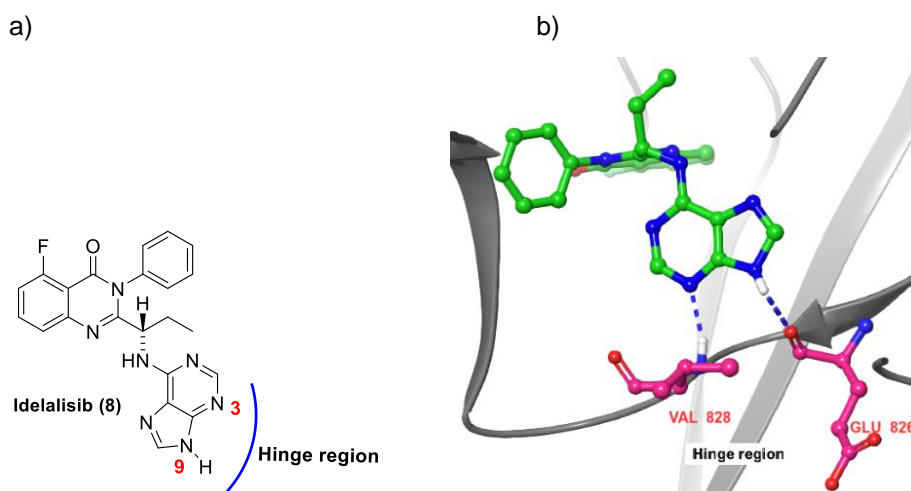


Figure 53. a) The propeller-shaped selective PI3K δ inhibitor idelalisib (**8**), highlighted the nitrogen atoms N3 and NH-9 of the purine that make two critical hydrogen bonds to the hinge region. b) Crystal structure of murine PI3K δ (PDB code 4XE0) with idelalisib (**8**) bound, blue dashed lines indicate the proposed dual hydrogen bonds to the hinge region¹⁸⁰.

3.2.3 Phenyl group (hydrophobic region II)

The phenyl group occupies the hydrophobic region II (ribose binding pocket), where the crystal structure of murine PI3K δ in complex with **8** (PDB code 4XE0) revealed that the phenyl group interacts through hydrophobic interactions with the side chains of Asp⁸³², Thr⁸³³ and Asn⁸³⁶ (Figure 54). Hydrophobic region II is composed of 8 residues, four of them are variable across the four isoforms.

The hydrophobic region II has been exploited to provide PI3K δ selectivity. Perry *et al*¹⁵¹ has reported the design of thiazolidinopyridone-based compound **70**, which showed poor PI3K δ selectivity, particularly against PI3K γ . The introduction of basic centres at the *meta*-position of the phenyl group resulting in the discovery of a new generation of PI3K δ inhibitors. For example, compound **71** with a dimethylamino methyl group was selected as a representative of this series (Table 18)¹⁵¹. Compound **71** showed 3- and 28-fold improvement in PI3K δ selectivity over PI3K α and γ , respectively, compared to the unsubstituted parent analogue **70** (Table 18).

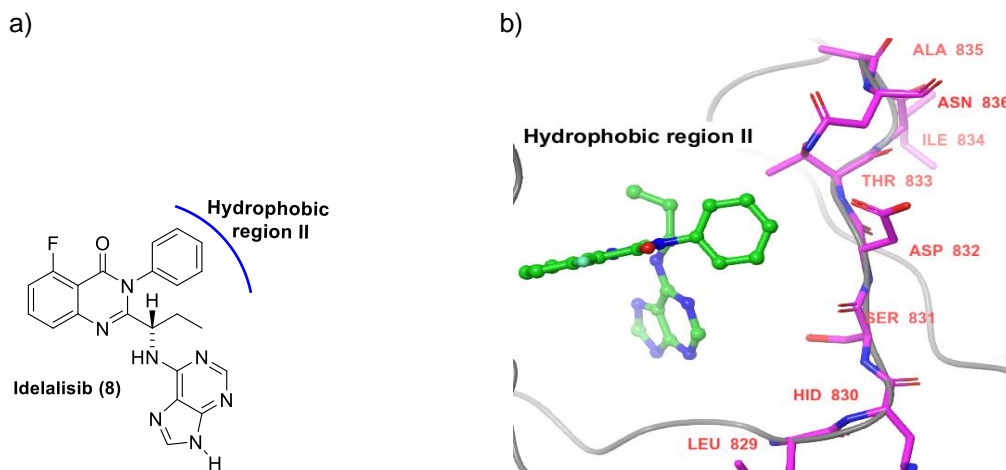


Figure 54. a) The selective PI3K δ inhibitor idelalisib (**8**), highlights the phenyl ring that fills the hydrophobic region II. b) Crystal structure of murine PI3K δ (PDB code 4XE0) with idelalisib (**8**) bound, highlights the eight amino acid residues that line the hydrophobic region II that make hydrophobic interactions with the phenyl moiety of idelalisib (**8**).

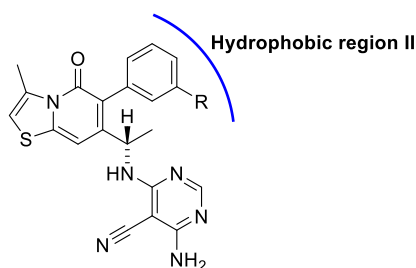


Table 18. Biological evaluation and isoform selectivity for PI3K δ for compounds **70** and **71** reported by Perry *et al*¹⁵¹.

compd	R	PI3K δ IC ₅₀ (nM)	Isoform selectivity		
			δ/α	δ/β	δ/γ
70 ¹⁵¹	H	0.4	1388	110	28
71 ¹⁵¹	CH ₂ NMe ₂	0.7	4000	80	793

The crystal structure of murine PI3K δ in complex with **71** (PDB code 5NCY) revealed that the dimethylamino methyl group pointed toward δ Asn⁸³⁶ (Figure 55), where the side chain of δ Asn⁸³⁶ shifted slightly in order to accommodate the inhibitor. However, in PI3K γ , the corresponding residues of δ Asn⁸³⁶ was the cationic residue γ Lys⁸⁹⁰, which made an unfavourable electrostatic interaction with the dimethylamino group, resulted in a large decrease in PI3K γ potency (Table 18). Whereas in the PI3K α isoform, the equivalent residue to δ Asn⁸³⁶ was α Gln⁸⁵⁹, which had a longer side chain, leading to a steric

clash with the dimethylamino methyl group. As a consequence, compound **71** displayed a 5-fold drop in PI3K α potency compared with its unsubstituted analogue **70** (Table 18). On the contrary, the introduction of the dimethylamino methyl group was associated with a slight decrease in δ/β selectivity (Table 18). This could be because, in PI3K β , δ Asn⁸³² was substituted by the negatively charged residue β Asp⁸⁵⁶, which formed a salt bridge with the dimethylamino methyl group of **71**. Taken together, these findings suggested that the hydrophobic region II contributed to the isoform selectivity of PI3K δ inhibitors over other class-I PI3K members. However, in this research, the hydrophobic region II would not be explored, thus the phenyl group of **8** was kept unchanged.

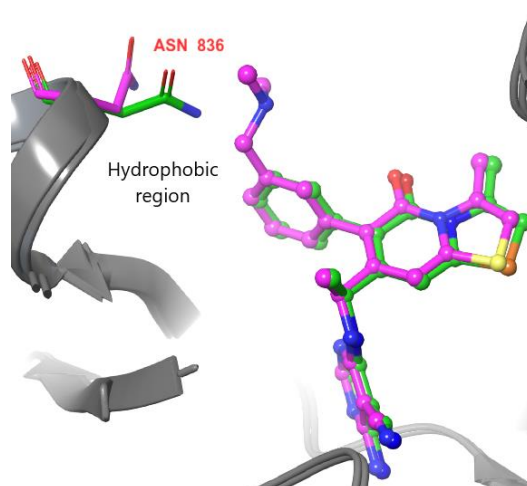


Figure 55. Overlay of crystal structures of **70** (PDB code 5NCZ) (green) and **71** (PDB code 5NCY) (magenta) bound to PI3K δ . It reveals that Asn836 (magenta) in the case of compound **71** changes its side chain position to allow the dimethylamino methyl group to fit. In contrast, the corresponding Gln⁸⁵⁶ in PI3K α and Lys⁸⁹⁰ in PI3K γ does not undergo a conformational change to accommodate compound **71**, which might explain the superior selectivity of compound **71** for PI3K δ versus α and γ isoforms.

3.2.4 Affinity pocket (unoccupied)

This pocket is lined with polar and hydrophobic residues (two aspartates, lysine, tyrosine and two leucines). All these residues are conserved among the four isoforms of class I PI3Ks. Idelalisib (**8**) does not extend towards the

affinity pocket leaving it unoccupied (Figure 56). Whereas, flat-shaped inhibitors bind within this pocket making two hydrogen bond interactions with Tyr⁸¹³ and Asp⁷⁸⁷, as stated previously in Chapter 2.

3.3 Aims

As it was already mentioned, **8** binds to PI3K δ at the three interaction points (specificity pocket, hinge region and hydrophobic region II) leaving the fourth region (affinity pocket) unused. Therefore, targeting of this pocket would increase the number of binding pockets engaged from 3 to 4 (Figure 56). It was believed that the current inhibitor potency ($IC_{50} = 11$ nM) of **8** could be further increased by exploring interactions with the polar residues lining the unoccupied affinity pocket (Figure 56b). The design strategy was to increase the size of idelalisib (**8**) by adding a new substituent to access the affinity pocket. The additional substituent should bear polar binding groups in order to make hydrogen bonding with the polar residues (Asp⁷⁸⁷, Asp⁹¹¹, Tyr⁸¹³ and Lys⁷⁷⁹) surrounding the affinity pocket (Figure 56b). This appeared to be an

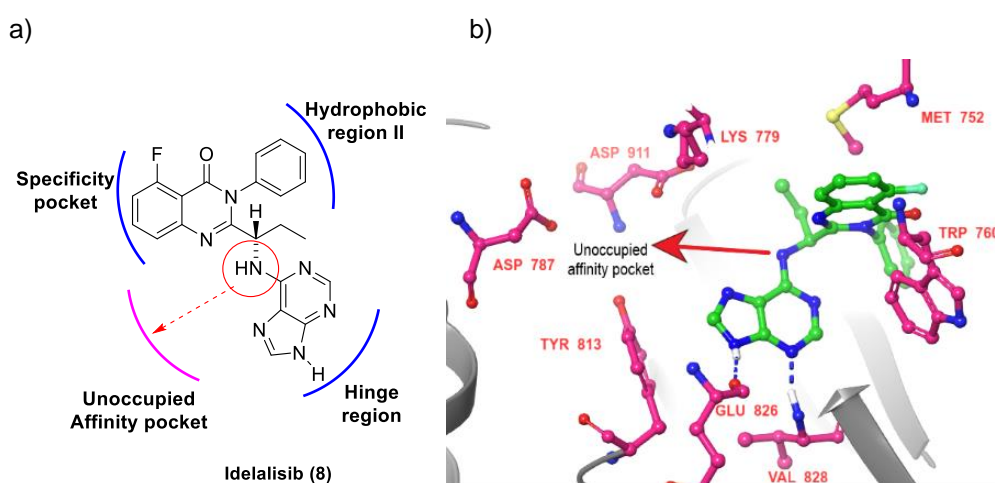


Figure 56. a) The selective PI3K δ inhibitor idelalisib (**8**) and its binding points at PI3K δ . b) Crystal structure of murine PI3K δ (PDB code 4XE0) with idelalisib (**8**) bound, highlights the addition of extra functional group to idelalisib (**8**) in order to probe the binding interactions with the affinity pocket. Blue dashed lines represent the proposed hydrogen bonds.

attractive strategy to develop a new series of propeller-shaped PI3K δ inhibitors which could be 10-100 times more potent than **8**. This approach is known as drug extension or tree growing branches.

The strategy of extension was not novel and has been used to increase the activity of many published propeller-shaped PI3K δ inhibitors, but to the best of this author's knowledge, has never been tried on FDA-approved idelalisib (**8**). Berndt *et al*¹⁷³ and Williams *et al*¹⁹³ concluded that additional gains of activity for propeller-shaped inhibitors **9** can be obtained when substituents bearing hydrogen bond donor and/or acceptor motifs added to the lead compound that extended to the affinity pocket and involved in hydrogen bonding with polar residues that lined the affinity pocket²⁴¹. For instance, 3-fluorophenol in SW13 (**10**) (Table 19) (Figure 57a) projected from the central pyrazolopyrimidineamine core to the affinity pocket where it engaged in hydrogen bonding with Asp⁷⁸⁷ and Lys⁷⁷⁹ (Figure 57b). These interactions resulted in improving the affinity at δ isoform in comparison to the parent compound **9** (Table 19)²⁴².

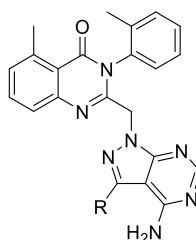
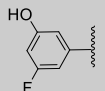


Table 19. Biological evaluation and isoform selectivity for PI3K δ for compounds **9** and **10** reported by Berndt *et al*¹⁷³, highlighted the improvement in PI3K δ potency in compound **10**¹⁷³.

compd	R	PI3K δ IC ₅₀ (nM)	Isoform selectivity		
			δ/α	δ/β	δ/γ
9 ¹⁷³	H	130	1538	123	469
10 ¹⁷³		0.7	1857	314	47

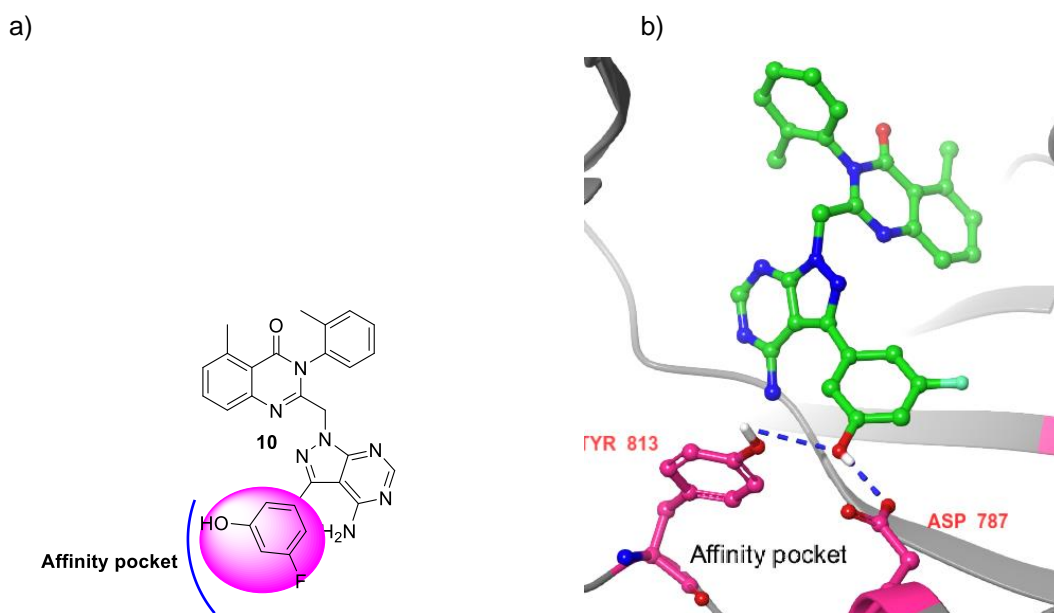


Figure 57. a) The selective PI3K δ inhibitor compound **10**, highlights the meta-fluorophenol group that forms hydrogen bond interactions with the affinity pocket. b) Crystal structure of murine PI3K δ (PDB code 2WXG) with compound **10** bound. Blue dashed lines represent the proposed hydrogen bonds that take place between the phenol group in compound **10** with Asp⁷⁸⁷ and Tyr⁸¹³ in the affinity pocket.

3.4 Medicinal chemistry strategy

3.4.1 Variation of Linker length

The first task in this medicinal chemistry project was to identify the optimal length of the linker that could connect between **8** and the newly added functional group (hydrogen bond donor and/or acceptor) that would be targeting the affinity pocket. The strategy used in the current study was to link the new binding group (hydroxy, amido and cyano) with **8** through a linker of variable length (2-4 carbon atoms) (Figure 58), this would help to identify the most appropriate linker length for PI3K δ inhibition. It was believed that increases in the linker length past 4 carbons may reduce PI3K δ activity.

3.4.2 Types of binding groups

The second task was to determine the terminal polar functional groups that would interact with the unoccupied affinity pocket. There are four polar residues (Asp⁷⁸⁷, Asp⁹¹¹, Tyr⁸¹³ and Lys⁷⁷⁹) that line the affinity pocket. Thus,

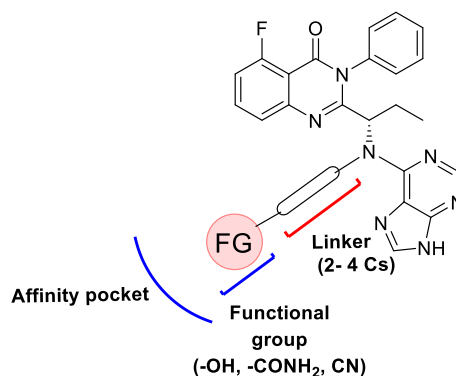


Figure 58. Idelalisib (**8**) connected by variable length linkers to the terminal functional group (hydroxyl, amide or cyano) in order to explore the affinity pocket.

a key point to be considered when selecting the binding group, is the ability to participate in hydrogen bonding interactions with these polar residues. Based on this, the hydroxyl group, amido group and cyano group were chosen (Figure 58). The hydroxyl and amido groups could serve as hydrogen bond acceptors and donors, whereas the cyano group can only act as an acceptor.²⁶⁸ The absence of a hydrogen bond donating ability in cyano group could be useful in the identification of the specific binding residues in the affinity pocket. If nitrile-containing compounds exhibited PI3K δ potency comparable with that of alcohol and amide analogues, then it is likely that Lys⁷⁷⁹ or Tyr⁸¹³ are involved in ligand binding. On the other hand, if nitrile analogues are much less active than the corresponding alcohols and amides, then Asp⁷⁸⁷ or Asp⁹¹¹ residues may directly interact with the ligands.

3.4.3 Site of extension

The last task was to identify the best site on **8** from which to build the additional substituent that could extend directly into the affinity pocket. Based on the crystal structure of murine PI3K δ in complex with **8** (PDB code 4XE0) (Figure 59b), there are three potential points of attachment on **8** to introduce the new functionality (R_1), namely the exocyclic amine, N-7 and C-8 of purine.

It was believed that the exocyclic amine was the best site to place the new functional group in order to access the affinity pocket. Moreover, the introduction of a new functional group to the exocyclic amine is synthetically accessible and convenient than functionalisation of N-7 and C-8 of purine positions.

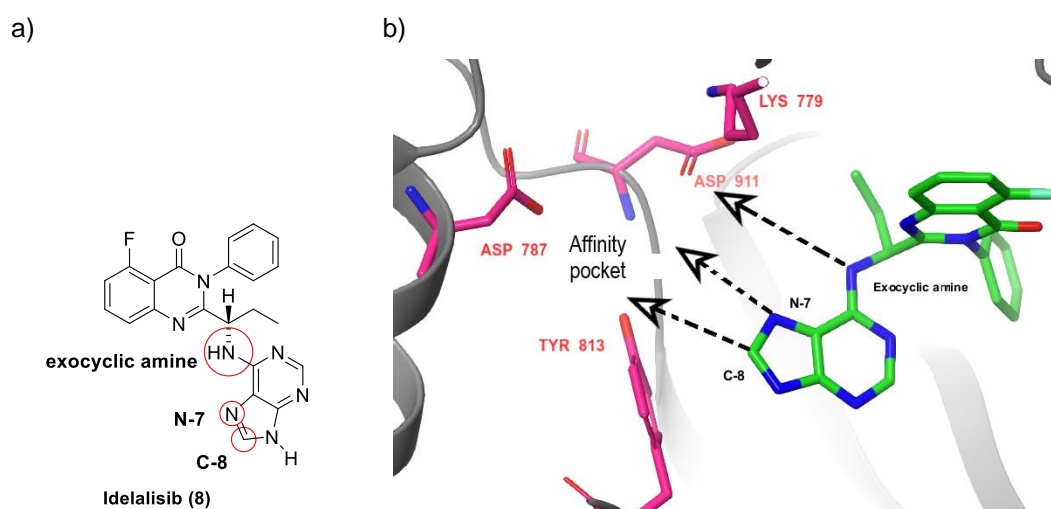


Figure 59. a) The selective PI3K δ inhibitor idelalisib (**8**). b) Crystal structure of murine PI3K δ (PDB code 4XE0) with **8** bound, highlights the three possible sites (exocyclic amine, N-7 and C-8 of purine) in idelalisib structure to add the extra substituents which may extend to the unoccupied affinity pocket.

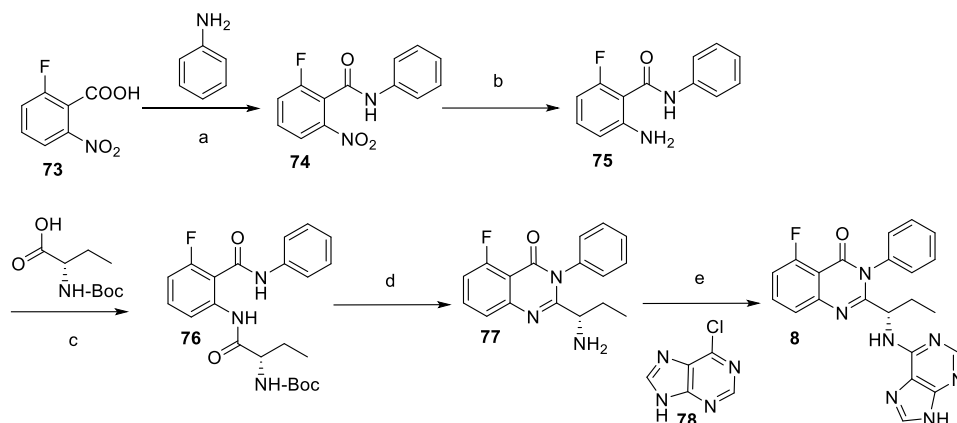
3.5 Discussion

3.5.1 Chemistry Section

A general synthetic strategy was developed, through which **8** would be synthesised first (Scheme 3), followed by the addition of the new substituent (affinity pocket binder) onto the exocyclic amine by an alkylation reaction.

3.5.1.1 Synthesis of idelalisib **8** (step a-e)

The route (Scheme 3) began by following the procedure mentioned by Liu, J *et al*⁶⁹. The benzamide derivative **74** was prepared in high yield by reacting 2-fluoro-6-nitrobenzoic acid (**73**) with aniline using HATU as a coupling reagent and DIPEA as a base. Then, **74** was subjected to catalytic hydrogenation using 10% palladium on carbon in methanol and the resulting

Scheme 3. Synthesis of idelalisib (**8**)

^aReagents and conditions: (a) HATU (2.5 equiv), DIPEA (3 equiv), dimethylformamide (DMF), rt, 24 h, yield 98%; (b) H₂, 10%Pd/C (0.05 equiv), methanol, rt, 12 h, yield 100%; (c) isobutyl chloroformate (IBCF) (3.5 equiv), N-methylmorpholine (3.5 equiv), THF, 60 °C, 24 hr, yield 61%; (d) hexamethyldisilazane (HMDS) (9 equiv), I₂ (3 equiv), dichloromethane (DCM), rt, 24 h, 56%; (e) DIPEA (10 equiv), *tert*-butanol, microwave 130 °C, 10 h, yield 75%.

amine **75**. In a first attempt to synthesize the diamide derivative **76**, compound **75** underwent amidation with *N*-Boc-L- α -aminobutyric acid following the same conditions outlined in step **a**, however this reaction went extremely slowly with very low yield (5%), this could be attributed to the steric effect exerted by the bulky group (*N*-acetylaniline) at the *ortho*-position of amine in compound **75**. Steric hindrance is a common issue that negatively impacts the reactivity of amide coupling^{270,271}, resulting in increases in the duration of reaction and reduction in yield. As a result, an alternative coupling reagent IBCF was investigated. Thus, *N*-Boc-L- α -aminobutyric acid was treated with 3.5 equiv. of N-methylmorpholine (NMM) followed by the addition of 3.5 equiv of IBCF in THF at -10 °C for 2h. Then aniline derivative **75** was added gradually to the reaction mixture, and the reaction was heated at 60 °C for 12 h, to provide the diamide **76** in 60% yield, which was relatively high comparing to HATU-coupling method.

The most challenging step in this synthesis is the cyclisation and formation of quinolizinone derivative **77**. There were only few general methods reported in

the literature to synthesise the compound **77**^{272,273}. However, the drawback of these methods was that they were carried out in two steps. Fortunately, a novel and convenient one-step synthesis of quinolizinone-based compound **77** with simultaneous deprotection of boc group was described by Xialong. W. *et al*²⁷⁴. In which HMDS-iodine induced the intramolecular dehydrative cyclisation of diamide **76** affording the quinazolinone derivative **77** (Scheme 3). However, the mechanism of simultaneous deprotection of the Boc group in this reaction is still not understood.

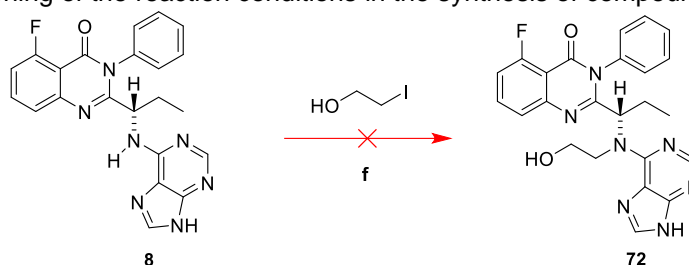
In the next step, the primary amine **77** was reacted with 6-chloropurine **78** in *tert*-butanol with DIPEA. The reaction was carried out either by reflux for conventional synthesis or by microwave irradiation (130°C). The microwave assisted reaction was completed within 8-10 h and gave idelalisib (**8**) in good yield (75%). In contrast, conventional heating needed longer reaction time (48 h) to achieve its maximum yield (53%). These findings are in agreement with the previous studies^{275,276}, which reported that the optimum conditions for nucleophilic displacement of 6-chloropurine **78** were to be carried out in microwave (130°C) in alcohol solvent (isopropanol, *n*-butanol and *tert*-butanol) with DIPEA used as a base.

3.5.1.2 Introduction of the new functional group (step f)

The final step involved the addition of the new functionalities which were simple chain haloalcohol derivatives (β -chloroethanol, γ -chloropropanol and δ -chlorobutanol) into the exocyclic amine of idelalisib (**8**). The reaction was carried out under two conditions; the conventional reflux and the microwave irradiation with a screening of the temperature (25, 60 and 120°C), solvents (DMF, dimethylsulfoxide DMSO and N-methyl-2-pyrrolidone NMP) and base

(DIPEA, triethylamine TEA and K_2CO_3) (Table 20). Unfortunately, *N*-alkylation did not take place with any of the reaction conditions tried.

Table 20. Screening of the reaction conditions in the synthesis of compound **72**.



Solvent	Temp ^a (°C)	Base ^b	Conv ^c (%)
DMF	RT	DIPEA	0
DMF	60°C	DIPEA	0
DMF	60°C	TEA	0
DMF	60°C	K_2CO_3	0
DMF	120°C	DIPEA	0
DMF	120°C	K_2CO_3	0
DMSO	60°C	DIPEA	0
DMSO	60°C	TEA	0
DMSO	60°C	K_2CO_3	0
DMSO	120°C	DIPEA	0
DMSO	120°C	K_2CO_3	0
NMP	120°C	DIPEA	0
NMP	120°C	K_2CO_3	0

^aHeating at 120°C was carried out under microwave irradiation. ^bThe reactions were carried out in the presence of 3 equiv of base. ^cConversion was based on liquid chromatography-mass spectrometry (LC-MS) analysis.

It was suggested that the combined steric and electronic effects were responsible for the failure of the final *N*-alkylation step. The steric effect could be exerted by the three surrounding substituents (purine ring, quinazolinone ring and/or ethyl side chain) (Figure 60a). The steric hindrance has been known for being a main factor in the failure of S_N2 reactions^{277,278}. The electronic effect caused by the electron-withdrawing purine ring, reduces the

nucleophilicity of the exocyclic amine by resonance delocalisation (Figure 60b). Thus, reversing the steps was proposed, where one of the three bulky groups would be introduced at the final step of the synthesis after the introduction of the required substituent at the exocyclic amine.

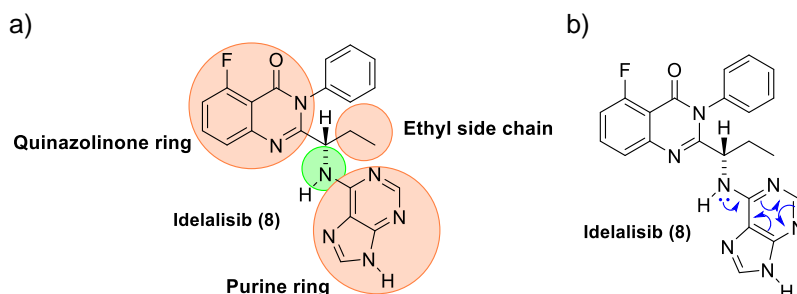


Figure 60. a) The selective PI3K δ inhibitor idelalisib (**8**), displays the three substituents (highlighted in orange) that could exert steric hindrance on the exocyclic amine (highlighted in green). b) The lone pair of electrons on exocyclic amine delocalises into the purine ring, resulting in reduced nucleophilicity.

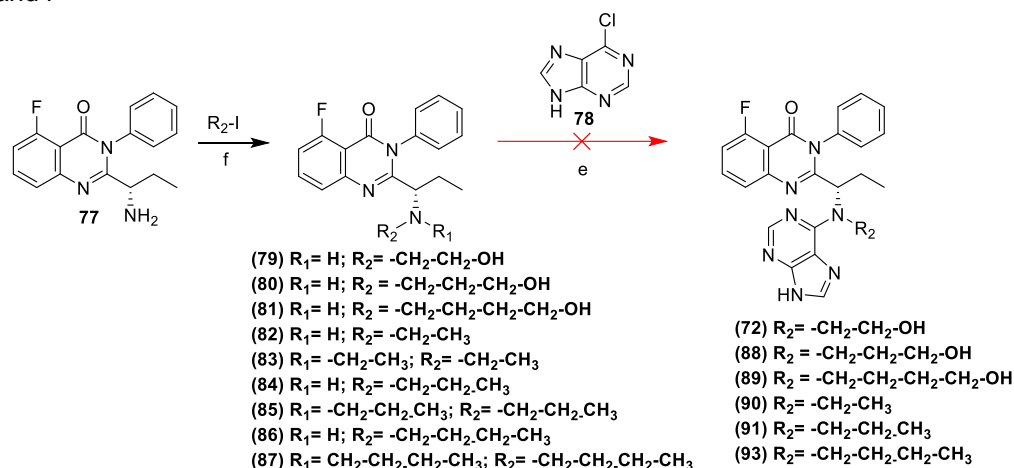
3.5.1.2.1 Purine group

The purine ring could reduce the nucleophilicity of the exocyclic amine by steric hindrance and electronic effect by conjugation. Thus, it was hypothesised that the *N*-alkylation could take place when the exocyclic amine is not attached to the purine ring. Hence, reversing the steps (e and f) was considered (Scheme 4), it was speculated that alkylation of exocyclic amine (step f) with the new functionality prior to the introduction of the purine ring (step e) (reordering of steps) might overcome the problem of the low nucleophilicity of exocyclic amine.

Thus, monoalkylation of primary amine **77** using iodoalkyl alcohols of different chain length (C2 to C4) in acetonitrile in the presence of alkali carbonate (K_2CO_3) has been carried out resulted in the generation of secondary amines (**79-81**) (Scheme 4). The yield obtained for alcohol derivatives **79**, **80** and **81**

Chapter 3

Scheme 4. Failed attempt to synthesize the final products **72** and **79-93**, by reversing steps e and f



^aReagents and conditions: f) K_2CO_3 (3 equiv), CH_3CN , 80 °C, 12 h, yield 30- 51%. e) DIPEA (10 equiv), *tert*-Bu OH, microwave 130 °C, 16 h, (unsuccessful).

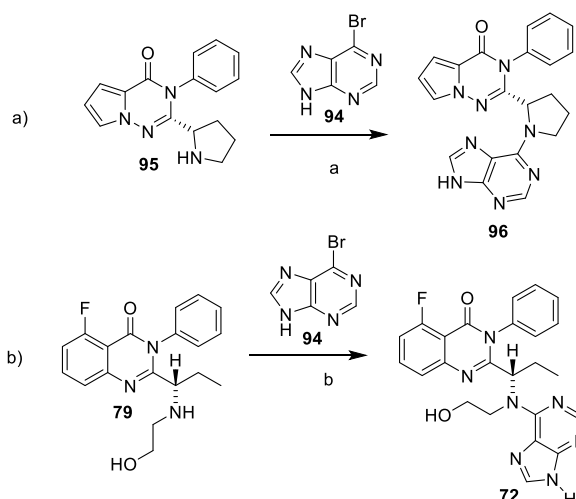
was (30-51%), the reaction did not go to the completion with 50% of starting amine recovered. However, no overalkylation products were detected, suggesting the reaction had good chemoselectivity. Whereas, *N*-alkylation of primary amine **77** by the corresponding alkyl iodides resulted in a mixture of the desired secondary amines (**82**, **84**, **86**) and the undesired tertiary amines (**83**, **85**, **87**). Unfortunately, the reaction of the resulting secondary amines (**79-81**, **82**, **84** and **86**) with 6-chloropurine **78** failed to give the desired products (**72** and **88-93**), although the reaction was conducted under the optimum conditions for nucleophilic displacement of 6-chloropurine **78** (Hünig base, *n*-butanol, 130°C) that was reported by Kolarski, D *et al*⁷⁵ and Chang, Y *et al*⁷⁶.

After the displacement of 6-chloropurine **78** proved to be difficult, a new strategy to replace the 6-chloro purine **78** with more reactive 6-substituted purine was conducted. Liu, J *et al*⁷⁹ and Legraverend, M *et al*⁸⁰ reported that the order of the reactivity of 6-halopurine for aromatic nucleophilic displacement was (F > Br > Cl > I), which suggested that fluorine and bromine

Chapter 3

were displaced more rapidly in nucleophilic aromatic substitution reactions. Thus, 6-bromopurine **94** was employed as an alkylating reagent in the alkylation of the secondary amines (**79- 81, 82, 84** and **86**), the reaction followed the appropriate conditions that was reported by Bernal Anchuela F J *et al*²⁸¹ for displacement of 6-bromopurine **94** (scheme 5a), where the reaction of secondary amine **79** with 6-bromopurine **94** was carried out in *tert*-butanol at 80 °C ²⁸¹. However, the reaction was unsuccessful and both the starting materials were recovered (Scheme 5b).

Scheme 5. a) Reaction reported by Anchuela *et al*²⁸¹ representing an example of nucleophilic displacement of 6-bromopurine **94** with a secondary amine **95**. b) Failed attempt to displace the 6-bromopurine with a secondary amine **79** using Anchuela conditions

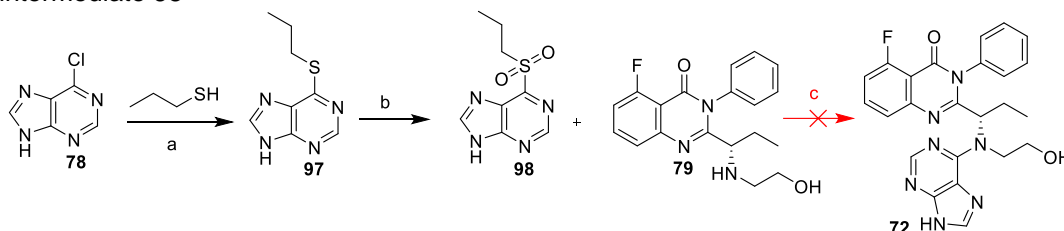


^aReagents and conditions: a) DIPEA (1.1 equiv), *tert*-Bu OH, 80 °C, 16 h, yields 80%²⁸¹. b) Employing the same reaction conditions reported for step a, (unsuccessful).

Alternatively, Liu, J *et al*²⁷⁹ and Xiaoyu lin *et al*²⁸² mentioned that 6-(alkylsulfonyl) purine was found to be more reactive than all 6-halopurine derivatives. Thus, 6-(propylsulfonyl) purine **98** (Scheme 6) was prepared from 6-chloropurine **78** starting material, which was coupled with 1-propanethiol at ambient temperature, to afford 6-(propylthio) purine **97**. The reaction of compound **97** with oxone in DCM provided the corresponding sulfone **98** in moderate yield 36%. Unfortunately, treatment of **98** with the secondary amine

79 in *n*-butanol at 100°C to afford the final products **72**, only resulted in unreacted starting materials.

Scheme 6. Failed attempt to Synthesize the final product **72** via 6-(propylsulfonyl) purine intermediate **98**



^aReagents and conditions: a) DBU (3 equiv), DMF, rt, 16 h, yield 13%; b) oxone (9.5 equiv), DCM, rt, 15 h, yield 36%. c) *n*-butanol, 100 °C, 15 h, (unsuccessful).

Despite reordering of the last two steps, by adding the purine group after the introduction of the new functional group, the synthesis of final idelalisib analogues (**72** and **88- 93**) still remained a highly challenging task. Thus, a number of alternative approaches would be considered.

3.5.1.2.2 Quinazolinone ring

It was assumed that the steric hindrance could be exerted by the bicyclic quinazolinone ring on the exocyclic amine. Additionally, intramolecular hydrogen bonding could take place between the N1 of quinazolinone and the proton on the exocyclic amino group forming a five-membered ring (Figure 61), which could hamper the reactivity of the exocyclic amine against the nucleophilic substitution reaction.

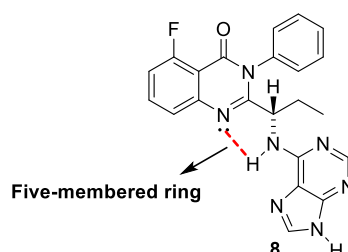
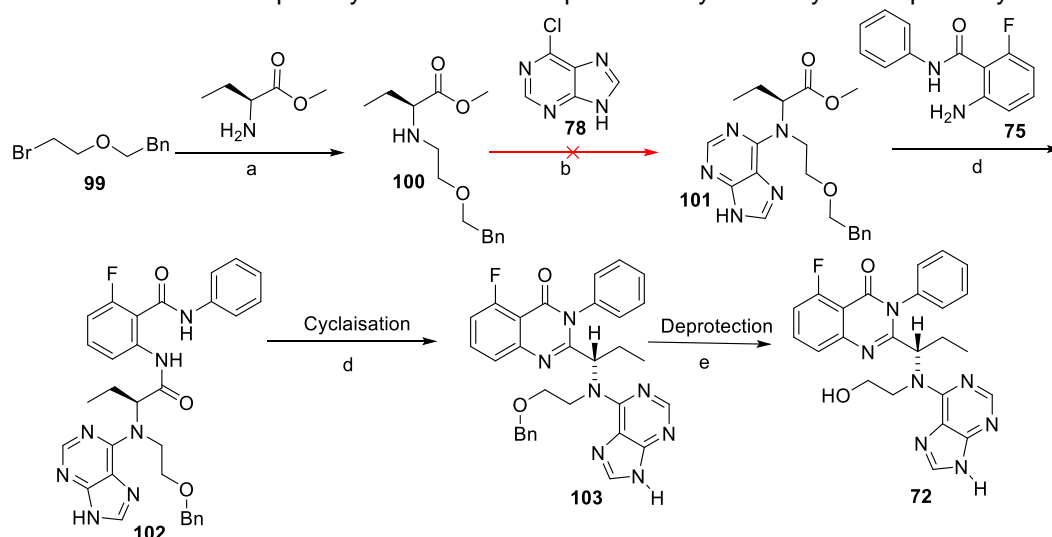


Figure 61. The suggested five-membered hydrogen-bonded ring, which might reduce the reactivity of exocyclic amine against nucleophilic substitution reaction.

Thus, a new synthetic pathway of the final compounds (**72** and **88-93**) was developed (Scheme 7). In this case, the steps would be reordered such that the exocyclic amine alkylation preceded quinazolinone formation. The introduction of the affinity pocket functional group would take place in the beginning of the reaction sequence, to form intermediate **102** which would later undergo cyclisation to quinazolinone **103** followed by *O*-debenzylation to generate the final product **72**. The alkylation of the amino group of 2-aminobutyric methyl ester **99** took place in refluxing acetonitrile overnight, resulted in secondary amine intermediate **100**. However, displacement of chlorine from 6-chloropurine did not take place and no traces of product **101** could be detected, although the reaction took place under the optimum conditions needed for the displacement of 6-chloropurine (*n*-butanol, DIPEA and 120 °C)²⁷⁶.

Scheme 7. Failed attempt to synthesize the compound **72** by a new synthetic pathway



^aReagents and conditions: (a) K_2CO_3 (6 equiv), CH_3CN , reflux, yield 28%; (b) DIPEA (3 equiv), *n*-butanol, reflux, 15 h, (unsuccessful).

These findings revealed that the synthesis of tertiary amine **101** bearing a purine ring was a very challenging task, even if the other two substituents

were relatively small and proved that bicyclic quinazolinone ring was not responsible for the very low nucleophilicity of the exocyclic amine.

3.5.1.2.3 Ethyl side chain

Another approach to diminish the steric effect was the removal of the ethyl side chain alpha to the exocyclic amino moiety (Figure 60). Cushing, T. *et al*¹⁵⁶ pointed out in his series of propeller-shaped inhibitors that were structurally related to idelalisib (**8**) (Figure 62), that the presence of a methyl group located α to the exocyclic amine made it more sterically hindered.

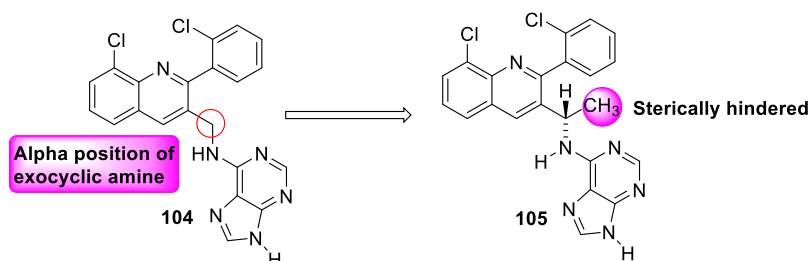


Figure 62. Structure of PI3K δ selective inhibitors **104** and **105** described by Cushing *et al*¹⁵⁶, which have very close structural similarity to idelalisib (**8**). Cushing proposed that the addition of the methyl group at α -position of the exocyclic amine leads to more sterically congested exocyclic amine.

Thus, idelalisib (**8**) would undergo structural simplification then structural extension to afford synthetically more tractable exocyclic *N*-substituted analogues (Figure 63). As might be expected, the removal of the ethyl group could lead to a reduction in the PI3K δ activity (the role of the ethyl group in ligand-protein interaction will be discussed later in Section 3.6.7). However, because the main purpose of this research was to examine the increase in inhibitor potency that could be obtained by exploring interactions within the affinity pocket. Thus, comparison of the biological activity between des-ethylated idelalisib **106** and its extended analogue **107** could also be useful (Figure 63).

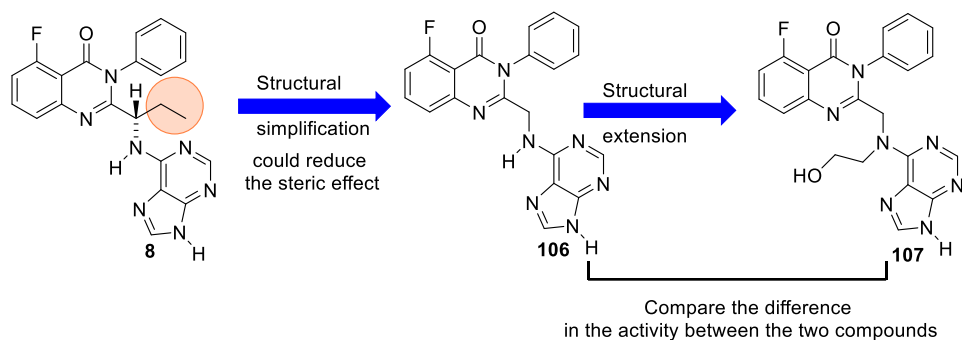
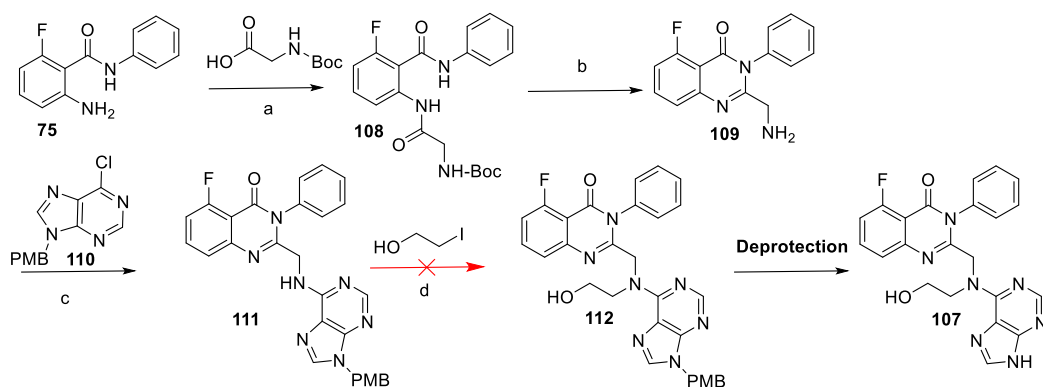


Figure 63. Structural simplification of idelalisib (**8**) by removal of the ethyl side chain followed by structural extension with a new binding group added to the exocyclic amine.

Des-ethyl idelalisib analogue **106** was obtained by the same synthetic procedure as idelalisib (**8**), but in this synthetic methodology (Scheme 8), aniline intermediate **75** was acylated with *N*-*boc*-glycine instead of *N*-*boc*-2-aminobutyric acid to afford the amide intermediate **108** in yield 30%, followed by cyclisation to give quinazolinone derivative **109** in low yield (20%), which then further reacted with 9-*paramethoxybenzyl*-6-chloropurine **110** to form des-ethyl idelalisib **111** in 39% yield.

Scheme 8. Synthesis of the des-ethylated idelalisib analogue **107**



^aReagents and conditions. (a) IBCF (3.5 equiv), NMM (3.5 equiv), dry THF, 60 °C, 24 h, 25%; (b) HMDS (9 equiv), I₂ (3 equiv), DCM, rt, 24 h, 20%; (c) DIPEA (9 equiv), *tert*-butanol, reflux, 15 h, 39%; (d) K₂CO₃ (3.5 equiv), KI (0.5 equiv), DMF, 55 °C, 22 h (unsuccessful, fragmentation of **111** to the two side products).

With **111** in hand, the final alkylation step was attempted to generate the tertiary amine product **112**. Unfortunately, it was found that treatment of **111** with alkylating reagent (benzyl-2-bromoethylether) in the presence of

potassium carbonate in DMF at 55 °C (Scheme 8), gave rise to the formation of two side products with no traces of product **112** detected. By combination of LC-MS and ^1H NMR, one of the side products was identified as being 9-*para*-methoxybenzyl-6-aminopurine **113** (Figure 64). Which indicated that considerable amount of the starting amine **111** was decomposed, such decomposition could occur through the aliphatic C-N bond cleavage¹⁵⁶, which suggested that des-ethyl idelalisib **111** was chemically unstable, owing to the absence of the steric hindrance exerted by the ethyl group, that would enhance the susceptibility to *N*-dealkylation. This was supported by the fact that such decomposition was not seen in the parent compound (idelalisib **8**).

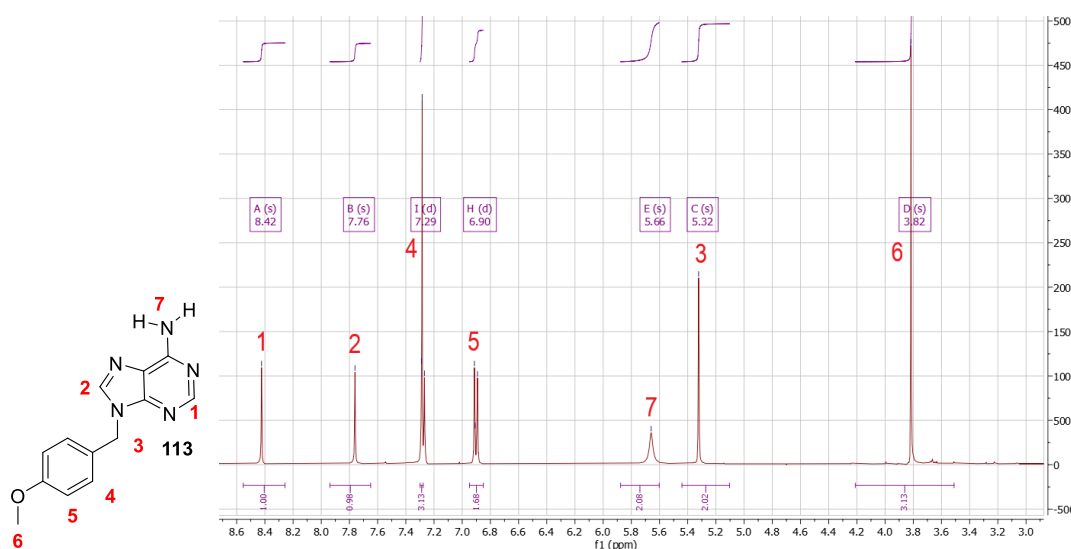


Figure 64. The 9-PMB-6-aminopurine **113** fragment produced by decomposition of the compound **111** with its ^1H NMR spectrum.

3.5.1.2.4 Test the feasibility of the exocyclic amine alkylation

It is well known that $\text{S}_{\text{N}}2$ reactions are accelerated by adjacent multiple bonds at C_α position of the leaving group, for example, the rate of the $\text{S}_{\text{N}}2$ reaction of benzyl halides is 800 times faster than that of the alkyl bromide²⁸³, while the allyl halide undergoes $\text{S}_{\text{N}}2$ reaction 40 times faster than *n*-propyl halide^{284–286}, this effect is named benzylic and allylic effect²⁸⁴, which is attributed to the two factors. First, because the benzylic (allylic) carbon is connected to the

electron-pulling sp² hybridized carbon atom, this makes it more electrophilic and more susceptible to nucleophilic attack²⁸⁷. The second is that the hyperconjugation between the pi-system of the adjacent double bond and the orbital of nucleophile would stabilize the bimolecular transition state (Figure 65)^{288,289}. It has been reported that allylic and benzylic substrates are the optimum model system to study the effect of steric hindrance on the reactivity trend²⁹⁰. To test this hypothesis, allyl and benzyl halides would be used as alkylating reagents to investigate the possibility of alkylation on the sterically crowded amine overcoming the observed steric resistance.

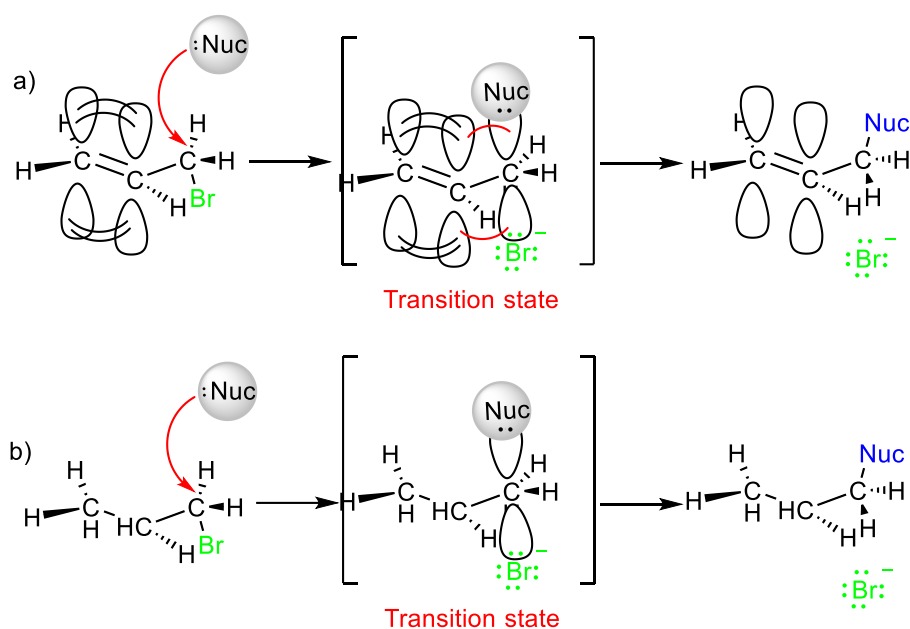
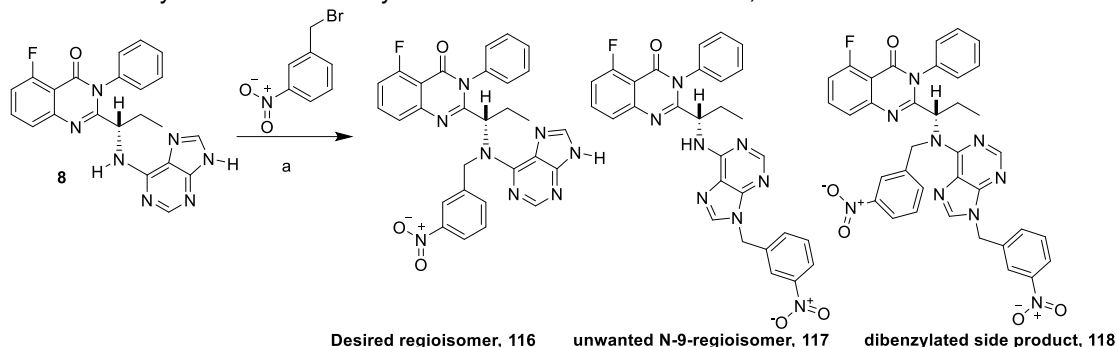


Figure 65. a) The p-orbital on the allylic carbon aligns with the pi-system of the alkene, resulting in the extra stabilization of the transition state, which improves the rate of S_N2 reaction. b) In propylbromide, there is no extra stabilisation of the transition state of S_N2 reaction.

When benzyl halide derivative (3-nitrobenzylbromide) was used as an alkylating agent in isopropanol with DIPEA, exocyclic N-alkylation took place for the first time, however N-9 of purine was benzylated as well, resulted in the formation of 3 compounds (Scheme 9): two regioisomers **116** and **117** and the dialkylated side product **118**. The desired regioisomer **116** was the major product with a yield of 40%, while the N-9 regioisomer **117** was isolated

in a yield of 7% (Scheme 9). Heteronuclear multiple bond correlation (2D ^1H - ^{13}C HMBC NMR) technique was used to distinguish between the two regioisomeric structures **116** and **117** (Figure 66 and 67, respectively).

Scheme 9. Synthesis of N-benzylated idelalisib derivatives **116**, **117** and **118**



^aReagents and conditions. (a) DIPEA (3 equiv), isopropanol, microwave 130°C, 4 h, yield of **116** is 40%, yield of **117** is 7%.

Under the same reaction conditions, allylation of the exocyclic amine of idelalisib (**8**) with allyl bromide was achieved, to give a mixture of two regioisomers **119** and **120** in isolated yields of 53 and 12%, respectively, in addition to the diallylated side product **121** (Figure 68), which was the same regioselectivity observed in the alkylation with benzylbromide derivative. 2D ^1H - ^{13}C HMBC NMR technique was used again to distinguish between the two synthetic regioisomers **119** and **120**.

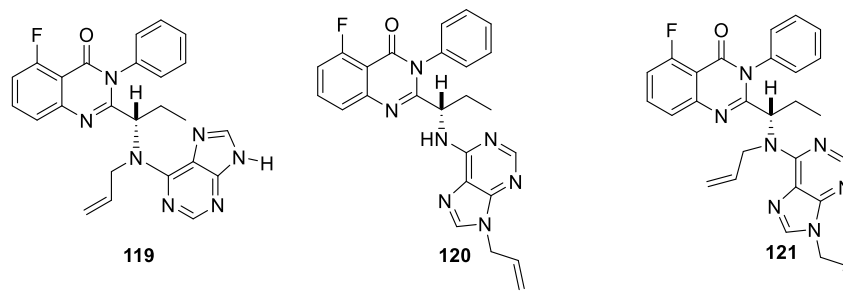


Figure 68. N-allyl idelalisib derivatives **119**, **120** and **121**.

Chapter 3

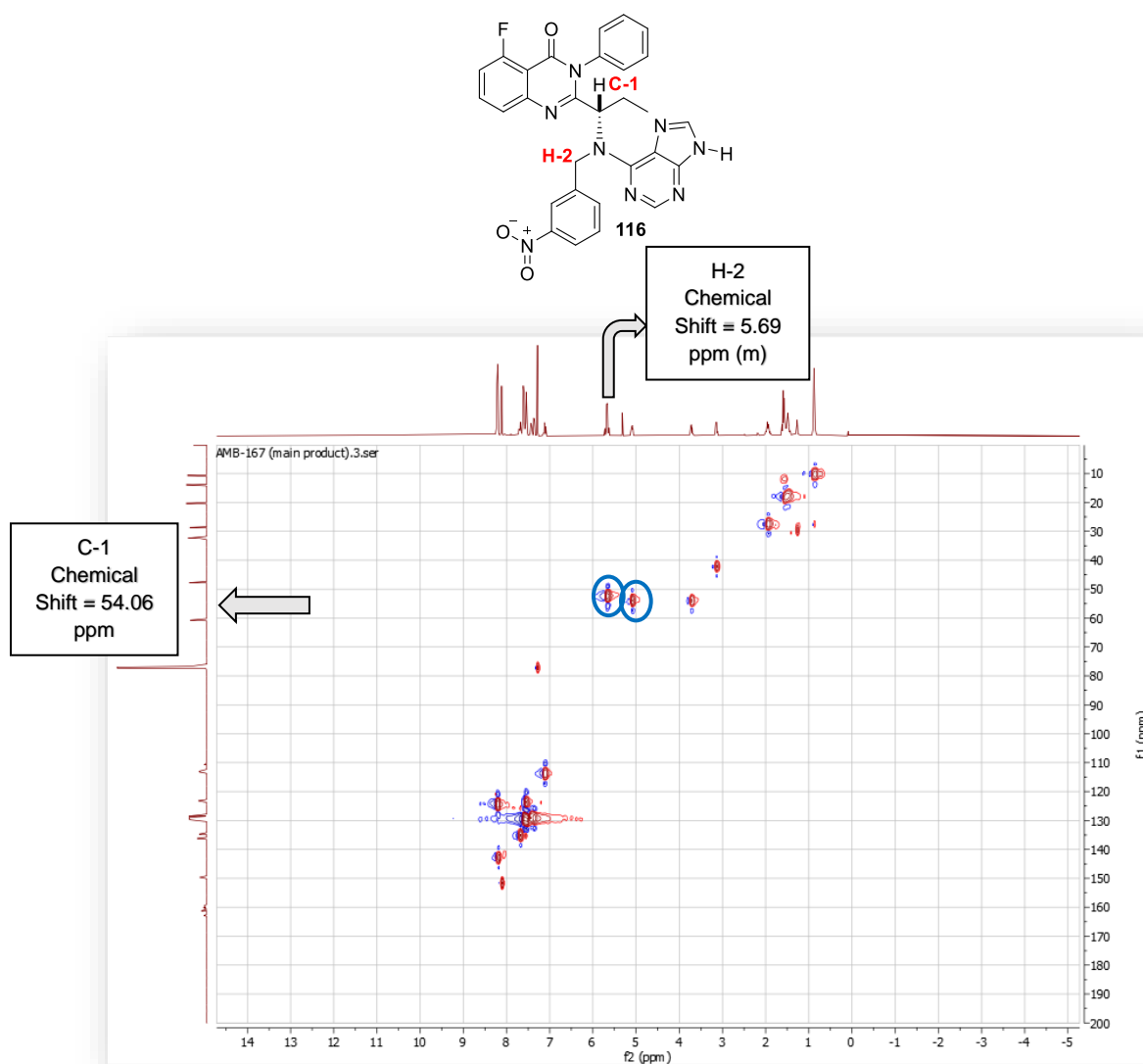


Figure 66. HMBC spectra of regioisomers **116**. The peaks outlined in blue showed the three-bond correlation between C-1 and H-2, which indicates that the correlation between C-1 and H-2 are three bonds apart.

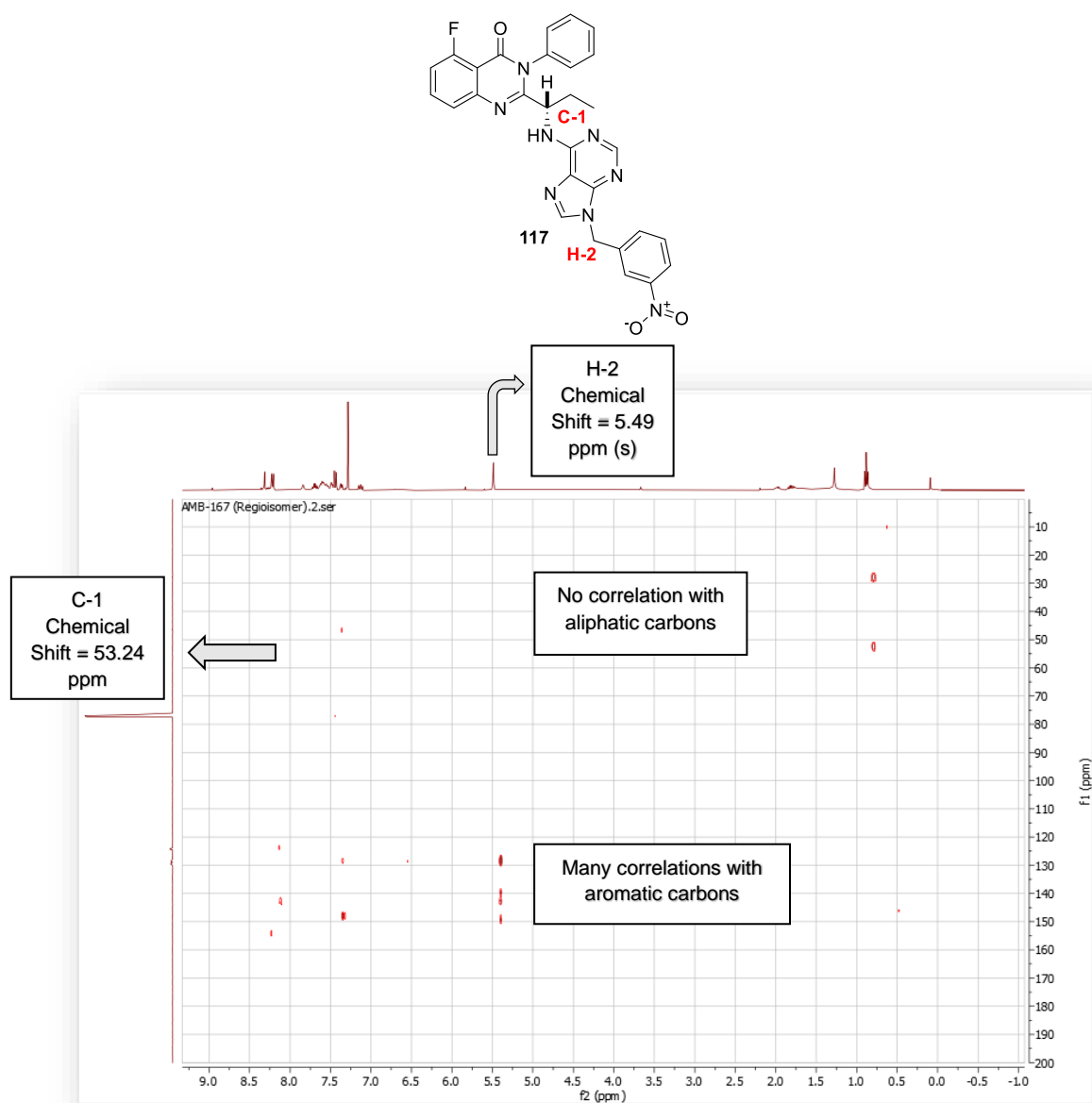


Figure 67. HMBC spectra of regioisomer **117** demonstrates that there is no correlation between H-2 and C-1 or any other aliphatic carbons, while it displays a lot of correlations (peaks) with many aromatic carbons, which indicates that benzylation took place at N-9 of the purine.

It was suggested that the success of the alkylation of the exocyclic amine with benzyl and allyl halides in contrast to the alkyl halides was due to the improved rate of bimolecular nucleophilic substitution at a saturated carbon adjacent to a double bond²⁸³. Two classes of electrophile that have adjacent unsaturated functionality similar to allylic and benzylic halide are the α -halocarbonyl compounds (esters and amides) and α -halonitriles. Thus, they

could be used for introducing substituents containing the desired functional groups (hydroxyl, amido and cyano) at the sterically hindered exocyclic amine. But before going further in the synthesis, it was essential to protect the N-9 of the purine.

3.5.1.2.5 Protection of N-9 of purine

The formation of regioisomeric side products in the previous two reactions suggested the need for the protection of N-9 of purine with a suitable protecting group (Figure 70). Tetrahydropyran (THP) was effectively used as a protecting group of N-9 of purine during the synthesis of idelalisib (**8**) by Liu *et al*⁶⁹ and Vinayak *et al*⁹¹. THP can be installed easily and it is stable under the basic conditions used for the alkylation of the exocyclic amine²⁹². Moreover, it can be removed by mildly acidic aqueous conditions. For instance, Liu, J *et al*⁶⁹ reported the deprotection of THP from N-9 purine of idelalisib (**8**) with 99% yield using aqueous hydrochloric acid (1 M) in ethanol, at room temperature (RT). The formation of 9-(tetrahydropyran-2-yl)-6-chloropurine **122** was conducted by reacting 6-chloropurine **78** with 3, 4-dihydro-2H-pyran in the presence of *p*-toluenesulfonic acid in ethyl acetate, providing N-9-THP-protected 6-chloropurine **123** in 99% yield.

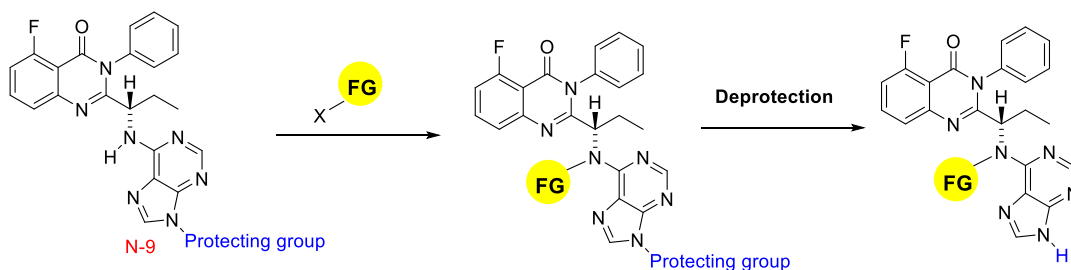


Figure 70. Installation and removal of the protecting group on the N-9 of purine ring, to prevent the formation of the undesired N-9-regioisomer.

3.5.1.2.6 Reaction with α -halo carbonyl and nitrile

The success of introducing of benzyl and allyl to the exocyclic amine and formation of tertiary amines **116** and **119** showed the necessity of using very reactive electrophiles to overcome the steric effect. However, in contrast to allylic and benzylic halides, which could follow both unimolecular (S_N1) or bimolecular (S_N2) nucleophilic substitution mechanism²⁹³, α -halo carbonyl compounds have been known to react only via S_N2 mechanism²⁸⁴. Clayden *et al*²⁹⁴ mentioned that α -halocarbonyl compounds are 500 and 1260 times more reactive towards S_N2 reaction than benzyl and allyl halides, respectively²⁹⁴. Where the adjacent carbonyl group accelerates the S_N2 reaction by making C-Br more reactive, because (C=O) has low-energy empty orbital (π^*) and also (C-Br) has low-energy empty orbital (σ^*), where these two orbitals combine to form a new lowest unoccupied molecular orbital (LUMO) ($\pi^* + \sigma^*$) (Figure 71), this makes the two neighbouring carbons very strong electrophile²⁹³. Hence, a practical method for β -functionalisation of the exocyclic amine via substitution reaction with α -halo carbonyl (α -haloacetamide and ester) and α -halonitrile was suggested.

According to this, protected idelalisib analogue **123** was treated with α -bromoacetamide in DMF in the presence of K_2CO_3 as a base (Scheme 10). This reaction afforded a complex mixture of three compounds: the protected **124** and deprotected **125** products and the starting material **123**. This composition of protected **124** and deprotected **125** products was surprising, as the THP protecting group was expected to be relatively stable under the strong basic conditions²⁹⁵. Fortunately, however, the final product **125** was isolated in 12% yield and confirmed by 2D 1H - ^{13}C HMBC NMR. Under the

Chapter 3

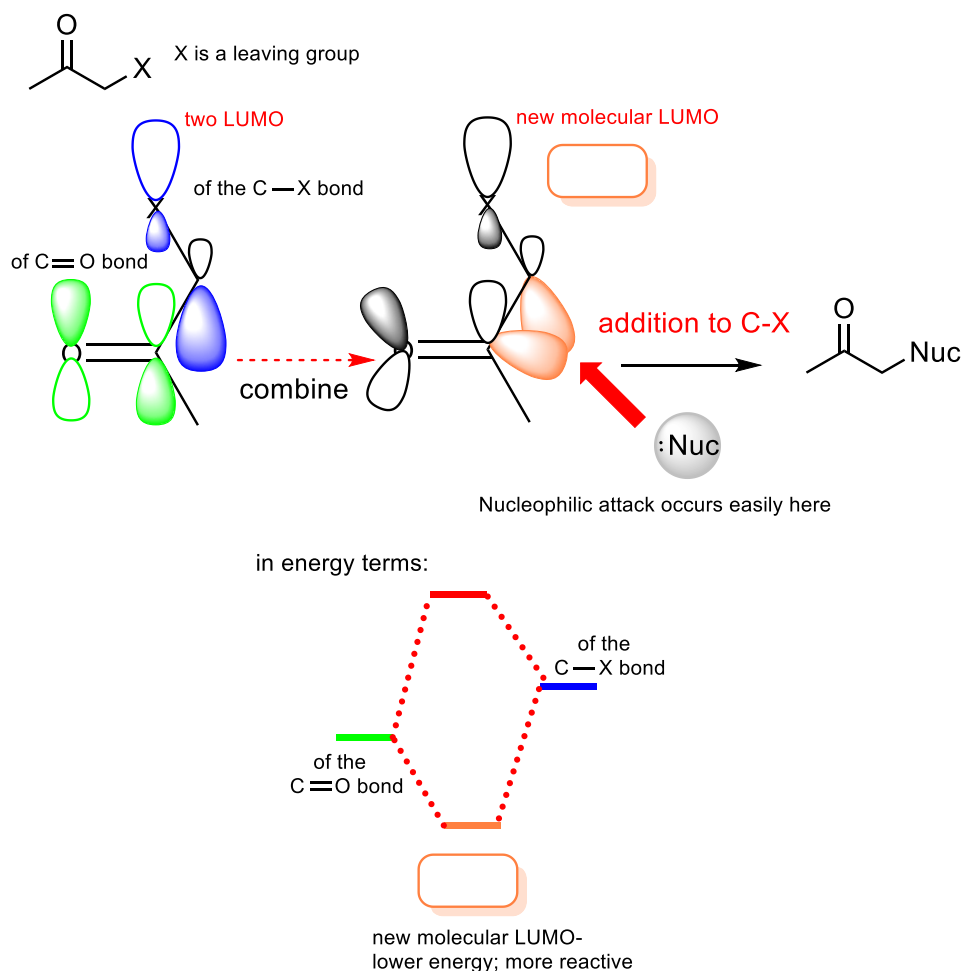
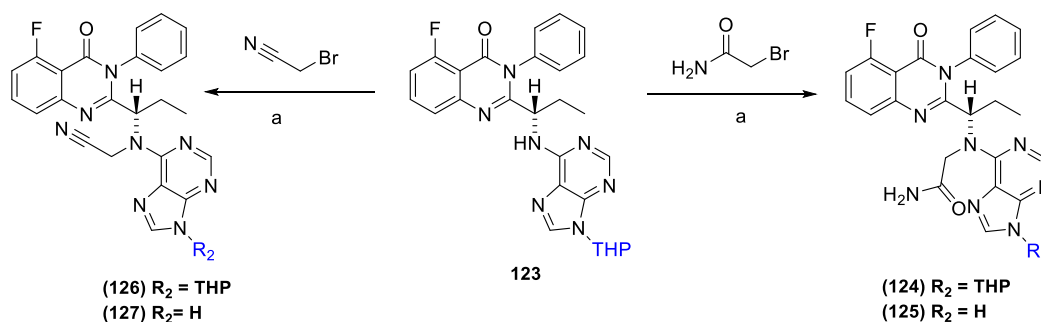


Figure 71. The low-energy empty orbital of C=O (π^*) and the low-energy empty orbital C-Br (σ^*) align together, to generate LUMO ($\pi^*+\sigma^*$), making the two adjacent carbons highly electrophilic, which explains the high reactivity of α -halocarbonyl compound for S_N2 reaction.

Scheme 10. Synthesis of the final amide **125** and nitrile **127** products



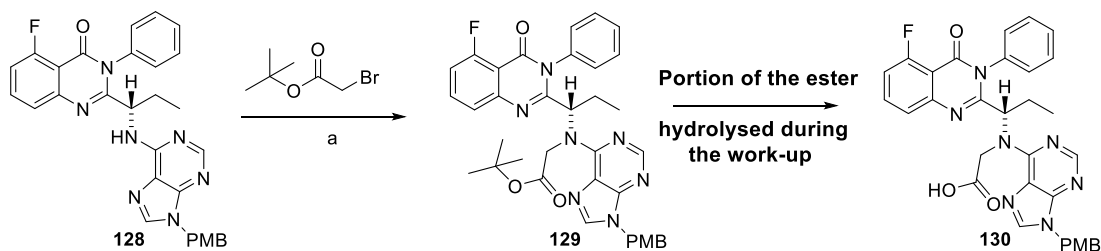
^aReagents and conditions: (a) K_2CO_3 (3 equiv), DMF, 50 °C, 16 h, yield of **125** is 12%, yield of **127** is 15%.

strong basic conditions²⁹⁵. Fortunately, however, the final product **125** was isolated in 12% yield and confirmed by 2D ^1H - ^{13}C HMBC NMR. Under the same condition (Scheme 10), the exocyclic amine of N-9-THP protected idelalisib **123** was alkylated with α -bromoacetonitrile to give a mixture of

protected **126** as well as deprotected **127** nitrile product. The latter was isolated in 15% yield.

Our final task was to synthesize the final alcohol analogue **72**. This would be conducted in a two-step procedure where *tert*-butyl ester would be introduced at exocyclic amine (Scheme 11) and reduced to the corresponding primary alcohol. It was believed that THP might be unsuitable for this two-step reaction, because it proved to be unstable in the desired reaction condition and this led to the side products and accordingly low yields in the previous two reactions (Scheme 10), Thus, the THP group was removed and replaced by a sufficiently stable protecting group. Lebraud *et al*⁹⁶ mentioned that *para*-methoxybenzyl (PMB) group was more stable than THP as a protecting group for N-9 of a purine. To make the final alcohol product **72**. N-9-PMB protected idelalisib analogue **128** underwent reaction with *tert*-butyl bromoacetate in dry DMF at 60°C with K₂CO₃ used as a base (Scheme 11), LC-MS and thin-layer chromatography (TLC) clearly showed the formation of tertiary amine product **129** with no side products observed. However, ester hydrolysis took place during the aqueous work-up, which reduced the yield of the pure product to 15%, while the yield of the resulting carboxylic acid **130** was 26%.

Scheme 11. Synthesis of the ester product **129** and the side product **130**



^aReagents and conditions: (a) K₂CO₃ (3 equiv), DMF, 50 °C, 16 h, after work-up yield of **129** is 15%, yield of **130** is 26%.

3.5.1.2.7 Deprotection of PMB group and formation of the deprotected ester

There were a plethora of reagents that were reported in the literature for deprotection of PMB from N-9 of purine including refluxing trifluoroacetic acid (TFA)²⁹⁷, TFA in DCM-anisole²⁹⁸, TFA/triisopropylsilane²⁹⁹, ceric ammonium nitrate (CAN)^{300,301} and 2,3-dichloro-5,6-dicyano-1,4-benzoquinone (DDQ). In order to investigate the optimum conditions for deprotection of PMB, the simple protected purine (9-PMB-6-chloropurine **110**) was chosen as a model substrate (Table 21). It was found that TFA/triisopropylsilane and CAN were the only methods which achieved complete consumption of the starting material **110**, TFA/triisopropylsilane gave the cleanest reaction, while the CAN reaction resulted in the formation of side products, while other reagents (DDQ, neat TFA and TFA/anisole) resulted in undesirable partial deprotection of the starting material with appearance of side products (Table 21).

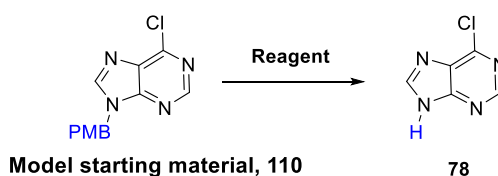


Table 21. PMB-deprotection conditions screening.

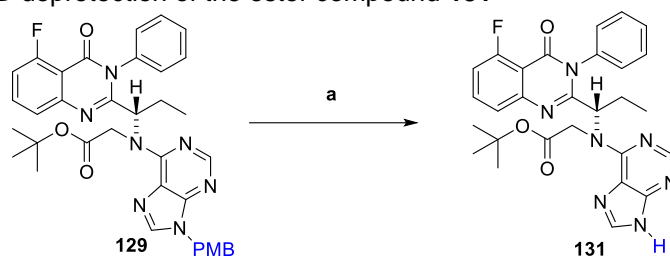
Reagent	Solvent	Temp (°C)	Conv ^b (%)	Purity ^c (%)
TFA	triisopropylsilane	60°	100	100
CAN	CH ₃ CN: H ₂ O	RT	100	70
TFA with anisole	DCM	40	70	60
DDQ	DCM	RT	40	40

^{b,c} Conversion and purity were based on LC/MS analysis.

Based on this, TFA/triisopropylsilane and CAN were selected as PMB-deprotecting reagents in the current synthesis. However, upon exposure of *tert*-butyl ester **129** to TFA/triisopropylsilane, no conversion took place,

changing the reagent to CAN resulted in the *N*-deprotected product **131** with 16% yield (Scheme 12).

Scheme 12. PMB-deprotection of the ester compound **129**



^aReagents and conditions: (a) CAN (3 equiv), CH₃CN: H₂O (1: 1), rt, yield 16%.

3.5.1.2.8 Reduction of ester

The last step of synthesis was to reduce the *tert*-butyl ester **131** to the final alcohol **72**. In this reaction, lithium aluminium hydride could not be used, because of the presence of the tertiary aromatic amide, thus weaker reducing agent was required. Studies have found that lithium borohydride could selectively reduce the ester in the presence of amide under mild condition (0°C)^{302–304}. It was reported that, for the reduction of ester, 2 equivalents of lithium borohydride was required³⁰². Although the reaction led to complete consumption of the starting ester, it gave a mixture of product **72** and side product in a 1:1 ratio. The purification step proved impossible, even in HPLC, since the product and the side product have similar polarity. Surprisingly, the side product was identified by crude¹H NMR and LC-MS analysis as a cyclised compound **133** (Figure 72). A plausible mechanism for the formation of **133** involves intramolecular reductive amination of N-7 of purine with the aldehyde **132** produced as an intermediate during the reduction of ester **129** to alcohol **72** (Scheme 13). In addition to that, the ease of the formation of 6-membered ring could promote the formation of the cyclised side product **133** (Figure 72b)^{305–307}.

Chapter 3

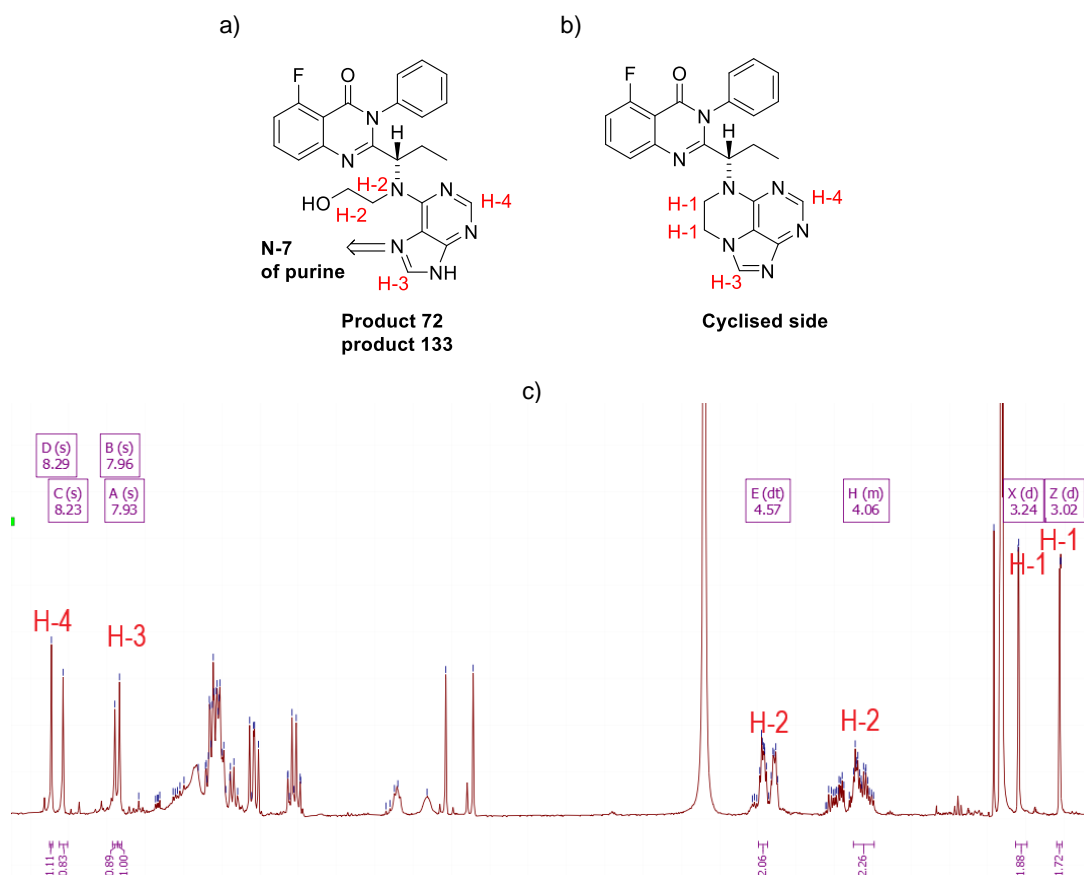
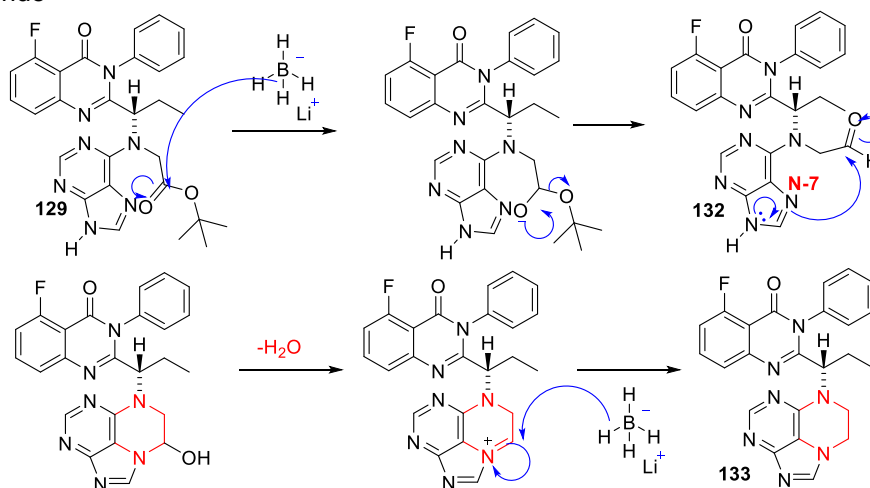


Figure 72. a) The desired product **72**. b) The suggested cyclised side product **133**. c) ¹H NMR spectrum of the crude product (a mixture of compound **72** and **133**). Peaks at 3.02 and 3.24 ppm are assigned to H-1 of the side product **133**. Peaks at 4.06 and 4.57 ppm are assigned to H-2 of the product **72**. Peaks at 7.93 and 7.96 ppm are assigned to the H-3 of the product **72** and side product **133**. Peaks at 8.23 and 8.29 ppm are assigned to the H-4 of the product **72** and the side product **133**.

Scheme 13. Proposed mechanism of intramolecular reductive amination induced by lithium borohydride



Chapter 3

To avoid the generation of the cyclised side product **133**, it was suggested that alkylation at N-7 through NH-tautomerization of the imidazole ring might be avoided by blocking N-9 with a protecting group (Figure 73).

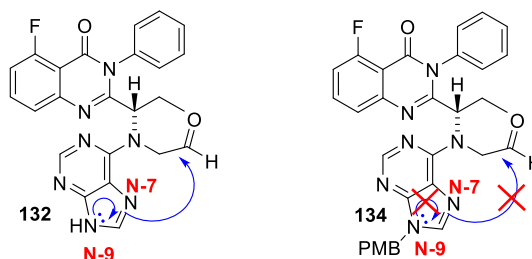
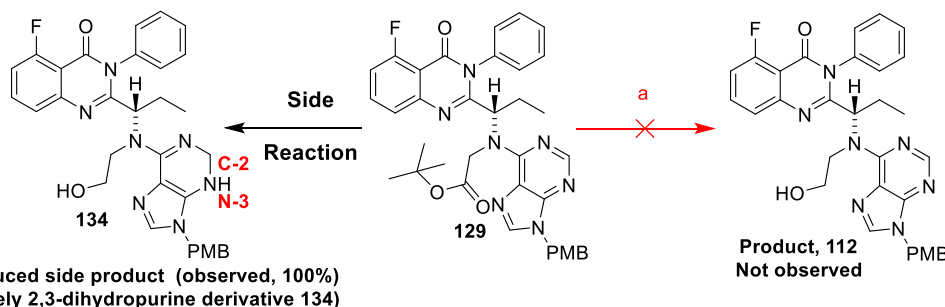


Figure 73. Strategy to prevent the formation of the cyclised side product **133** by blocking N-9 of purine.

Hence, the reduction of the ester was carried out first, followed by the deprotection step, where the *N*-9-PMB-protected ester **129** was treated with LiBH_4 in dry THF at 0°C (Scheme 14). Unfortunately, over-reduced side product was obtained in 100% yield, with partial hydrogenation of one of the aromatic rings which can be observed from ^1H NMR studies. The partial reduction was believed to occur on the pyrimidine ring of purine to afford the 2,3-dihydropurine derivative **134** (Scheme 14), where a new CH_2 proton signal appeared at 5.11 ppm assigned to the 2-methylene hydrogen of 2,3-dihydropurine. This finding is in agreement with a study published by Shadbolt *et al*³⁰⁸, which reported that the reduction of heterocyclic ring systems, usually occurs at an unsubstituted carbon. For example, Shadbolt *et al*³⁰⁸ reported that when 2,4,5-trisubstituted pyrimidines (**135- 137**) were treated with LiBH_4 , partial hydrogenation occurs to generate 1,6-dihydropyrimidines (**138- 140**) (Scheme 15)³⁰⁸.

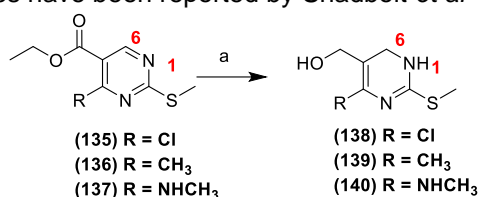
Chapter 3

Scheme 14. Failed attempt to synthesize the final alcohol **112** via ester **129** reduction using LiBH_4



^aReagents and conditions: (a) LiBH_4 (2 equiv), THF, 0 °C, 1 h, (unsuccessful, possible formation of the over-reduced side product **134**, yield 100%).

Scheme 15. Examples of the partial reduction of pyrimidine ester derivatives by LiBH_4 to give 1,6-dihydropyrimidines have been reported by Shadbolt *et al*³⁰⁸

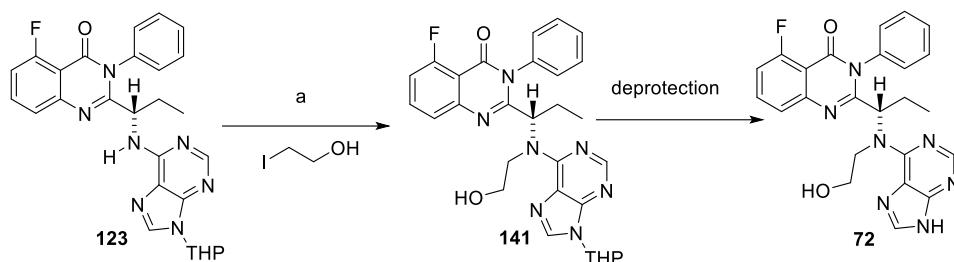


^aReagents and conditions: (a) LiBH_4 (1 equiv), THF, 0 °C, 2 h, yield 23- 92%.

3.5.1.2.9 N-alkylation of exocyclic amine in the presence of Grignard reagent

After an attempt to reduce the ester **129** to alcohol product **112** was unsuccessful. It was suggested to use an efficient alternative method for the direct *N*-alkylation of exocyclic amine with a hydroxyethyl halide, where the exocyclic amino group of compound **54** was subjected to deprotonation with a Grignard reagent in THF, followed by addition of alkylating agent (2-iodoethanol) to the deprotonated substrate to complete the reaction (Scheme 16). The pKa of the Grignard reagent is approximately 30.1³⁰⁹. Hence it should be able to deprotonate the aryl exocyclic amine exhibiting the pKa value of 10.29³¹⁰. The reaction resulted in the formation of the tertiary amine product **141** which on subsequent deprotection of THP gave the final *N*-hydroxyethyl idelalisib analogue **72**.

Scheme 16. Synthesis of the final alcohol product **72** with the Grignard reagent used as the base



^aReagents and conditions: (a) *i*-PrMgCl (1.1 equiv), THF, 70 °C, 16 h, yield 18%. (b) HCl, ethanol, rt, 4 h, yield 90%.

3.5.1.3 Conclusion of Chemistry

The synthesis of the exocyclic *N*-substituted idelalisib was challenging because of the difficulty in the alkylation of the exocyclic amine, it was proposed that the purine ring effectively retards the alkylation of the exocyclic amine due to the two potential factors. Firstly, the purine ring is a bulky group which could exert steric hindrance on the nearby nucleophile. A second reason is that purine is a heteroaromatic system which could reduce the nucleophilicity of the attached amine by a combination of resonance delocalization and inductive effects. Additionally, the two nitrogen atoms of imidazole ring of purine (N-7 and N-9) are reactive and they create unwanted reactions that compete with the desired reaction, for instance N-9 formed the regioisomeric side products (as seen in scheme 9). As a result, two additional protection and deprotection steps were necessary, which increased the number of steps in the synthesis. It must be pointed out that they were two findings which could have implementations in the future synthesis of this series of compounds.

Alkylation and formation of 3ry amine. In general, formation of tertiary amine containing one purine ring on the nitrogen atom. proved difficult, only extremely reactive alkylating reagent like α -haloamide, α -halonitrile and α -

haloester can achieve this task. Additionally, *N*-alkylation could be effectively carried out by deprotonation of the exocyclic amine with the use of strong base such as a Grignard reagent followed by addition of electrophiles.

Protection and deprotection strategies of N-9-purine. In this research, THP has been found to be the best protecting group for N-9 of purine, because it could be installed and removed easily relative to other N-9 protecting groups such as PMB. However, surprisingly, it was found that THP-protecting group was unstable under the basic conditions required for the *N*-alkylation of the exocyclic amine, resulted in the occurrence of the regioisomeric side product.

3.6 Biological section

The ten low molecular weight compounds (fragments, **77- 87**) were tested (Table 22), which were defined as the final products without the purine hinge binder for their activity against the four isoforms of PI3K. These fragments possessed linear side chains ranging from *n*-ethyl to *n*-butyl at the exocyclic amine (Figure 74). The side chains of compounds (**79, 80** and **81**) contained a terminal hydroxyl group which capable of exploring new binding interaction with the affinity pocket, whereas fragments (**82- 84**) had non-polar side chain, provided reference compounds in which hydrogen bonding was not possible. The aim of this SAR study was to identify the fragment-sized affinity pocket binder with optimum linker length which could work as an advantageous chemical starting point for the future project, aiming at growing the fragment into idelalisib analogue after attaching it to the purine hinge binder (Figure 74), which could improve the potency.

Chapter 3

Figure 74. Fragment-based screening to identify the most potent affinity pocket binding fragment.

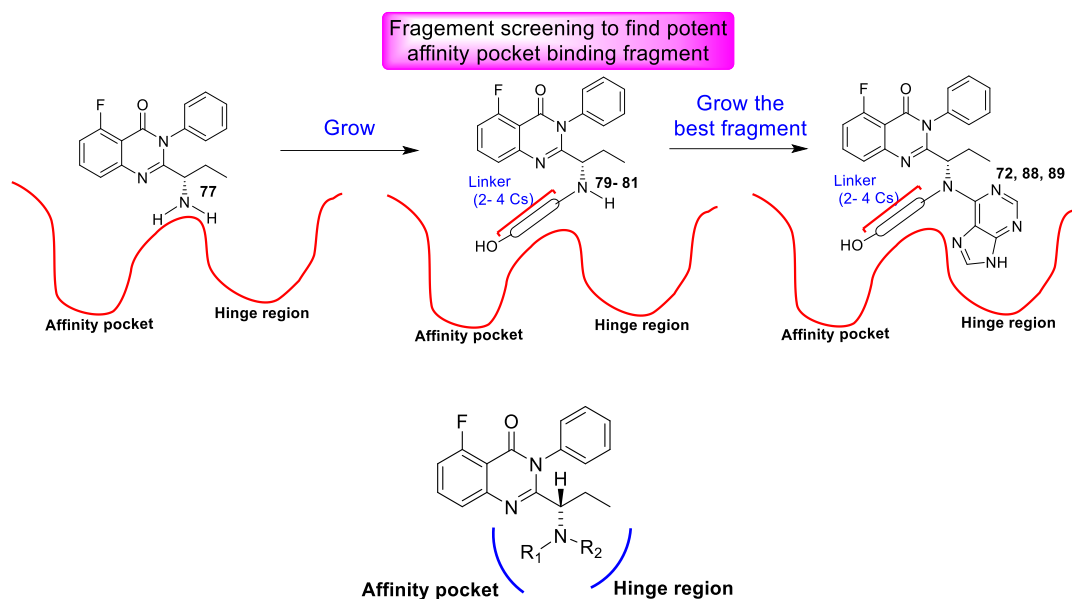


Table 22. Biological evaluation and isoform selectivity for PI3K δ for compounds (**77**, **79-87** and **76**).

Compd	R ₁	R ₂	Isoform potency ^{a,b} IC ₅₀ (μM)			
			PI3K δ	PI3K α	PI3K β	PI3K γ
77	H	H	>28	>28	>28	>28
82		H	>28	>28	>28	>28
79		H	1.4	2.8	>28	5.5
142		H	>28	>28	>28	>28
84		H	>28	>28	>28	17.5
85			3.5	>28	>28	11
81		H	>28	>28	>28	>28
86		H	>28	>28	>28	>28
87			14	>28	14	1.75
81		H	10	>28	>28	>28

^aPotency against the different PI3K isoforms is given as IC₅₀ values (n = 1). ^bThe potency threshold for the PI3K δ assay is ~ IC₅₀ 0.001 μM due to substrate concentration. Compounds with IC₅₀ > 28 μM exhibited no inhibitory activity.

The starting point for the modification was the primary amine intermediate **77**, with no hinge binder (purine ring), which exhibited no activity at all isoforms

of class-I PI3K ($IC_{50} > 28 \mu\text{M}$), this result was consistent with the findings of the previous studies which proved that the purine ring (hinge binder) is the most crucial part of the structure of the propeller-shaped PI3K δ inhibitors^{144,153,244,311}, identifying the key role of the interaction with hinge region in the PI3K δ inhibition.

Monoalkylation of primary amine **77** with ethyl, propyl and butyl produced the secondary amines **82**, **84** and **86**, respectively, which showed no noticeable change in PI3K δ activity compared to the primary amine **77**, such findings were not unexpected, given the fact that the side chains of these compounds did not possess hydrogen bond donor or acceptor, no hydrogen bond was formed with the polar residues in the affinity pocket. The introduction of the second propyl group at the exocyclic amine of compound **84** resulting in *N,N*-dipropyl derivative **85** which demonstrated low micromolar range inhibitory activity against PI3K δ ($IC_{50} = 3.5 \mu\text{M}$) and mid-micromolar range against γ isoform ($IC_{50} = 11 \mu\text{M}$). This significant enhancement of the activity of dipropyl analogue **85** over monopropyl analogue **84** could be attributed to that the additional second propyl group could form a C-H/ π interaction with Trp⁷⁶⁰ in tryptophan shelf. This was supported by docking studies which revealed that one of the propyl group sat at the tryptophan shelf where the distance between this group and the indole ring of the Trp⁷⁶⁰ is located within the optimum distance range of C-H/ π interaction (3.8- 4.4 \AA) (Figure 75b)³¹². If this finding was confirmed by crystal structure, it would be for the first time, as far as known, for any propeller-shaped inhibitor to involve in interaction with tryptophan shelf^{174,313,314}. Dibutyl derivative **87** demonstrated a slight improvement in δ and β activity (IC_{50} value of 14 μM) compared to the

monobutyl analogue **86**, surprisingly, it displayed a great increase in the potency against PI3K γ with IC_{50} equals to 1.7 μ M.

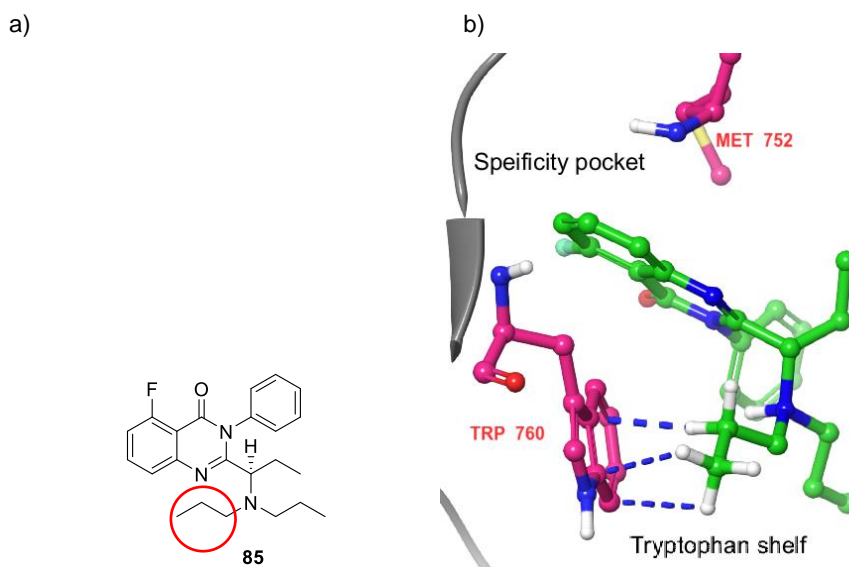


Figure 75. a) Compound **85**, highlights the propyl group that forms a potential C-H/ π interaction with the tryptophan shelf. b) Compound **85** docked into PI3K δ model (generated from PDB code 4XE0). The propyl group makes a C-H/ π interaction with Trp⁷⁶⁰ at the tryptophan shelf. Blue dashed lines represent the proposed C-H/ π interactions.

Introduction of hydroxyethyl group into the primary amine of compound **77** resulted in β -amino alcohol analogue **79**, with considerable activity against PI3K δ (IC_{50} = 1.4 μ M). The higher activity of the compound **78** compared to the non-hydroxylated analogue **82**, may be explained by either formation of hydrogen bond interaction between compound **79** and PI3K δ , where the hydroxy group acted as a hinge binder or directed toward the affinity pocket. The binding mode of compound **79** with PI3K δ was suggested by molecular docking analysis (Figure 76), it was found that the hydroxyethyl group extended into the affinity pocket, where it involved in an enhanced hydrogen bond with the side chain carboxylate of Asp⁹¹¹ (Figure 76b), thereby indicating why this compound had gained activity against PI3K δ . Thus, two-carbon atom was the optimum length of linker to promote the interaction with the affinity pocket. The importance of the hydroxyl group was probed by blocking

it with a benzyl group in compound **142** resulting in a significant deterioration of activity, which proved that the presence of a free hydroxyl group was an important factor behind PI3K δ activity.

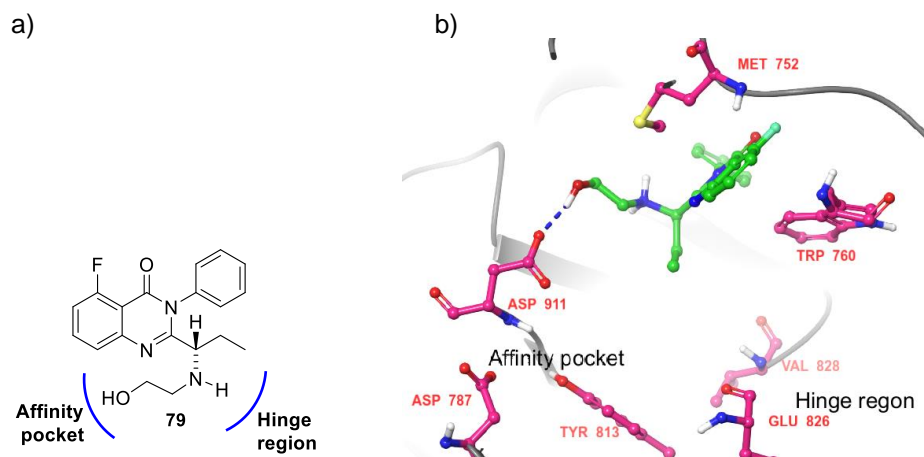


Figure 76. Compound **79**, highlights the hydroxyethyl group. b) Compound **79** docked into the PI3K δ model (generated from PDB code 4XE0) reveals that the hydroxyethyl group extending into the affinity pocket rather than interacting with residues on the hinge region.

Monoalkylation of primary amine with 3-hydroxypropyl, resulted in γ -amino alcohol analogue **80**, which surprisingly showed no activity against all four isoforms of class I PI3K. This indicated that propyl chain was too long which positioned the hydroxyl group at too great a distance to interact with the affinity pocket efficiently. Whereas δ -amino alcohol **81** exhibited modest potency at PI3K δ with IC_{50} value in the mid-micromolar range (IC_{50} = 10 μ M), while it did not exhibit any activity against the other three isoforms.

3.6.1 Conclusion derived from the initial SAR study (Table 22)

In this study, a screening strategy was used to identify affinity pocket binding fragments. Table 22 showed that the PI3K δ inhibitory activity afforded by compounds (**79- 87**) were clearly dependent on linker length, because only compound **79** with an ethylene bridge was active in low micromolar range (IC_{50} = 1.4 μ M) compared to the propyl **80** and butyl **81** analogues. The docking results appeared to be consistent with inhibitory activity of compound

79, which revealed that promising activity displayed by a hydroxyethyl compound **79** could be due to the interaction with Asp⁹¹¹ residue in the affinity pocket, which indicated that ethyl linker exhibited the optimal chain length needed to fit the H.B.D and/or H.B.A into the affinity pocket. Compound **79** with its low molecular weight (MW= 341 Da) could act as an excellent starting point for further optimisation into larger and more potent compounds for example *N*-hydroxyethyl idelalisib **72**, by attaching it with the purine hinge binder (Figure 77). It would be interesting to see whether the final compound **72** will show higher PI3K δ activity and selectivity than the lead compound (idelalisib **8**) and by how much.

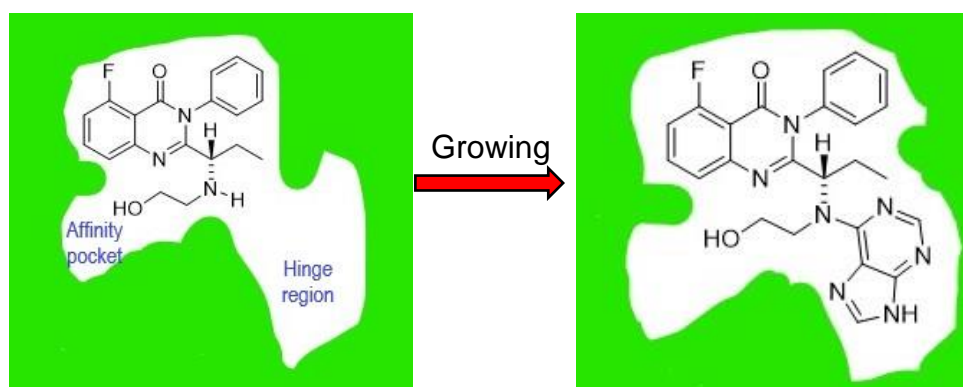


Figure 77. Strategy for fragment optimisation by joining the compound **79** with a purine hinge binder to produce the final compound **72**.

3.6.2 The linking strategy to make the final compounds

Three final products were prepared by using fragment-based extension approaches, by joining the fragment **79** with the purine hinge binder to create the final compound **72** (Figure 77). Whereas the final compound **125** and **127** contain amide and nitrile group, respectively, at the other end of the linker for binding to the affinity pocket. Thus, Linker **72** terminated in a hydroxy group, linker **125** terminated in amide and linker **127** terminated in nitrile.

3.6.3 Screening of the final compounds (Single concentration compound screening) (Table 23)

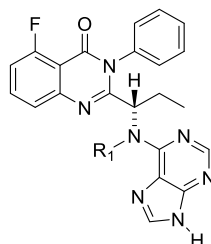


Table 23. % inhibition of PI3K δ activity at 1 μ M and 500 nM of compounds (idelalisib **8**, **72**, **125** and **127**).

		Inhibition of PI3K δ^a	
Compd	R ₁	% Inhibition at 1 μ M	% Inhibition at 500 nM
8	H	76	80
72		42	2
125		18	*
127		44	5

^aPI3K δ % inhibition was determined at 1 μ M and 500 nM compound concentration.
*Compound **125** was not tested at 500 nM final concentration.

Unfortunately, the final compounds (**72**, **125** and **127**) could not be synthesized before the screening deadline, this had been attributed to challenges associated with the formation of these compounds that were mentioned in the Chemistry Section. Consequently, these compounds could not be sent to GSK to have full IC₅₀ measurements. Thus, an internal screening was performed by our group at the University of Nottingham, which would be a single-concentration screen against PI3K δ at 1 μ M and 500 nM final concentration. The details will be discussed in Chapter 7, Section 7.4.1.3.

Compounds **72**, **125**, **127** and idelalisib (**8**) were tested at single concentration (1 μ M) for their inhibitory activity against PI3K δ (Table 23), which would give

preliminary activity data to choose compounds for further more detailed screening (500 nM), the FDA-approved idelalisib (**8**) was included for direct comparison. First a preliminary screening with an inhibitor concentration of 1 μ M showed that PI3K δ was inhibited by 76% at 1 μ M idelalisib (**8**). The alcohol **72** and nitrile **127** analogues were active against PI3K δ , with > 40% inhibition at 1 μ M. By contrast, amide derivative **125** showed a little activity (< 20%). The active compounds from primary screening, alcohol **72** and nitrile **127** were selected to test at 500 nM final compound concentrations against PI3K δ , however, these compounds exhibiting < 10% inhibitory activity at 500 nM concentration (**72**: 2%, **127**: 5%), while the control compound (idelalisib **8**) showed 80% inhibition.

The poor activity of the alcohol **72**, amide **125** and nitrile **127** compounds compared with idelalisib (**8**) was somewhat surprising, because it was thought that these compounds would be higher or at least equipotent to idelalisib (**8**), as they are able to make the same interactions as that of parent compound (idelalisib, **8**). This indicated that the addition of the new functional group to the exocyclic amine can significantly deteriorate the PI3K δ potency. This drastic decrease in the potency could be reasoned by the steric clash that might occur between the additional functional group and the PI3K δ enzyme, where the new substituents could cause undesirable interactions with the so-called gatekeeper residues (Ile⁸²⁵) at the entrance of the affinity pocket in the PI3K δ binding site (Figure 78). This steric clash would orient the hinge binder purine out of the preferred binding conformation, resulted in the loss of a crucial hydrogen bonds with Val⁸²⁸ and Glu⁸²⁶ in the hinge region and deterioration of the activity (Figure 78b). Docking study was used to provide

evidence to support this hypothesis, it revealed that the purine ring of compound **8** did not form any hydrogen bond interactions with Val⁸²⁸ and Glu⁸²⁶ in the hinge region (Figure 79b) as idelalisib (**8**) did. It was hypothesized that this lack of interactions would orient the compound **72** away from the ATP binding site, translated experimentally by a major drop in activity

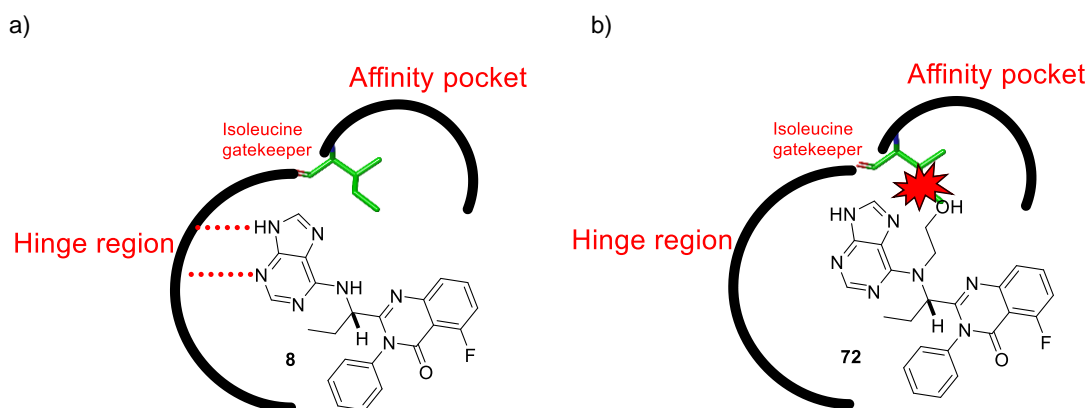


Figure 78. a) Idelalisib-PI3K δ is depicted by a chemical structure, the gatekeeper residue (Ile⁸²⁵) (highlighted in green) controls the accessibility to the affinity pocket. The chemical structure depicts the purine ring that engages in crucial hydrogen bonds to the hinge region. Dashed red lines represent the proposed hydrogen bonds with the hinge region. b) Compound **72**-PI3K δ is depicted by a chemical structure, the steric clash between the hydroxyethyl group and the isoleucine gatekeeper, impedes drug binding through loss of a crucial hydrogen bonding interaction to the hinge region.

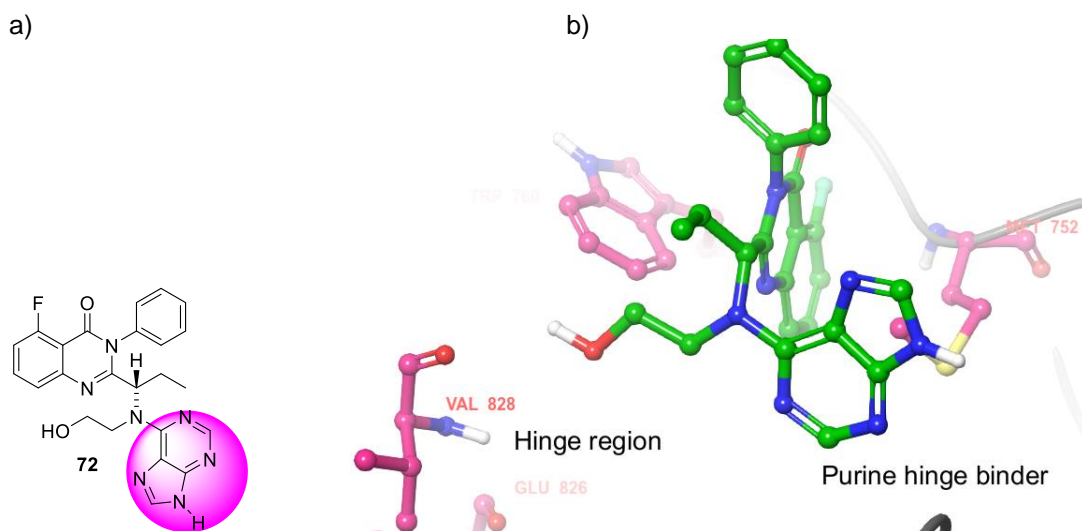


Figure 79. a) Compound **72**, highlights the purine hinge binder b) Compound **72** docked into the PI3K δ model (generated from PDB code 4XE0) reveals that the purine ring does not involve in a critical hinge region hydrogen bond interaction, probably due to the steric clash between the newly introduced substituent (hydroxyethyl) with the isoleucine gatekeeper, which disrupts the overall binding conformation, leading to a loss in the PI3K δ potency.

against PI3K δ . Generally, loss of hydrogen bond interaction with the hinge region was the major reason for the deterioration of activity of a plethora of kinase inhibitors including PI3K δ inhibitors^{315–318}. Before going any further, important details about the gatekeeper need to be covered.

3.6.4 Gatekeeper

Is a single residue that is located at the kinase hinge region and governed access of the inhibitors deep in the affinity pocket^{29,45,317,319–321}, which appeared to take part in affecting the sensitivity of inhibitors in a plethora of PI3Ks. The size of the gatekeeper's side chain determines the size of the kinase inhibitors that can be accommodated³²⁰. Most of kinases possess small threonine residue as a gatekeeper^{29,321,322}. However, the four isoforms of class I PI3K including PI3K δ have a bulky isoleucine at this position, which makes the entrance of the affinity pocket narrow and restricted resulting in a steric clash which prevented compounds **72**, **125** and **127** from binding properly^{45,323}. It was hypothesized that the poor activity of the compounds **72**, **125** and **127** was probably due to loss of the crucial hydrogen bond interaction with the hinge region of PI3K δ , that was caused by the steric clash between the newly introduced functional group with the isoleucine gatekeeper. In Terstiege *et al*²⁰ reported that the compound **143** with a pyrazole ring oriented towards the affinity pocket showed excellent potency against PI3K δ with IC₅₀ of 4 nM (Table 24), however, dimethylation of the pyrazole ring at C-3 and C-5 resulted in compound **144** with a 700-fold drop in potency. The authors explained the lack of potency for dimethylpyrazole analogue **144** by proposing that the two methyl groups would clash with the gatekeeper residue

(Ile⁸²⁵), rendering it incapable of adopting a favourable conformation for establishing two hydrogen bonds with the kinase hinge region.

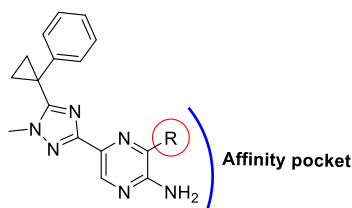


Table 24. Biological evaluation for PI3K δ for compounds **143** and **144** reported by Ina Terstiege *et al*²²⁰.

compd	R ₁	PI3K δ IC ₅₀ (nM)
143 ²²⁰		4
144 ²²⁰		2800

3.6.5 Determination of IC₅₀ (Table 25)

As a part of a collaboration with GSK, idelalisib (**8**) was sent along with other nine compounds to GSK for screening for activity (defined by IC₅₀) against PI3K (Table 25). Among these, compounds **117**, **120** and **146** were *N*-9-regioisomeric side products, although these compounds have emerged as side products during synthesis of the desired product, they would be screened to determine the impact of the lack of the one of the conserved pair of hydrogen bonds to the hinge on PI3K δ activity.

Carboxylic acid **145** produced as a side product during the synthesis of ester **129** and tested against the four isoforms of class I PI3K. The carboxylate group of compound **145** could bind to the affinity pocket as a hydrogen bond acceptor, where it could make an enhanced hydrogen bond with Tyr⁸¹³ residue or a salt bridge with Lys⁷⁷⁹ (Figure 56b). However, unexpectedly, compound **145** was 400-fold less active against PI3K δ than the parent

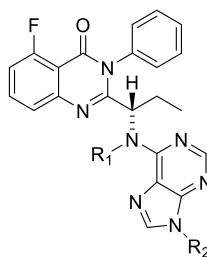


Table 25. Biological evaluation and isoform selectivity for PI3K δ for compounds (**8**, **116**, **117**, **119**, **120**, **145**, **146** and **147**).

Compd	R ₁	R ₂	Isoform potency ^{a,b} IC ₅₀ (nM)			
			PI3K δ	PI3K α	PI3K β	PI3K γ
8	H	H	11	14000	2800	56
145		H	4400	14000	17500	14000
119		H	1750	28000	28000	14000
120	H		3500	28000	28000	28000
146		H	11000	14000	28000	28000
147	H		10000	28000	28000	22000
116		H	14000	28000	28000	14000
117	H		28000	28000	28000	22000

^aPotency against the different PI3K isoforms is given as IC₅₀ values (n = 1). ^bThe potency threshold for the PI3K δ assay is ~ IC₅₀ 1 nM due to substrate concentration.

molecule (idelalisib **8**) (Table 25), which indicated that the carboxymethyl group of compounds **145** group did not occupy the affinity pocket. This finding was consistent with the hypothesis that the bulky isoleucine (gatekeeper) hindered access to the affinity pocket and thus would clash sterically with the additional substituent (carboxymethyl group) of compound **145**, this would influence the positioning of the hinge binder (purine) and its potential for hydrogen bonding with the hinge region.

Insertion of ally group to the exocyclic amine of idelalisib (**8**) led to a 150-fold drop in the activity of compound **119**, while its N-9-regioisomeric derivative

121 was 318-fold less active (IC_{50} value of 3.5 μ M) (Table 25), supporting the role of the NH-9 of purine at the hinge region for PI3K δ inhibition, where it acts as a hydrogen bond donor to the backbone oxygen of Glu^{826 153}. This finding is in agreement with WO 2014/128612 A1 study³²⁴, which mentioned that the loss of a hydrogen bond donor (NH-9 of purine) could have a significant impact on PI3K δ activity, for instance, removal of a hydrogen bond donor of compound **148** via methylation of N-9 of purine resulting in derivative **149** with 17-fold drop in PI3K δ potency (Table 26).

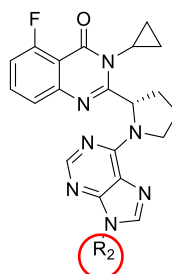


Table 26. Biological evaluation for PI3K δ for compounds **148** and **149** described in the WO 2014/128612 A1 study³²⁴.

compd	R ₂	PI3K δ IC ₅₀ (nM)
148 ³²⁴	-H	85
149 ³²⁴	-CH ₃	1430

N-arylation of idelalisib (**8**) with *p*-nitrophenyl led to the two regioisomeric substitution products **146** and **147** which exhibited similar activity against PI3K δ with mid-micromolar range (IC_{50} = 10 μ M) (Table 25). The *p*-nitrobenzyl derivatives **116** and its regioisomer **117** were the least active compounds in this series, where the former was shown to exhibit activity in mid-micromolar range (IC_{50} value of 14 μ M), while the latter showed no inhibitory activity (Table 25). A general finding obtained from this series of exocyclic *N*-substituted idelalisib derivatives (**8**, **116**, **119**, **145** and **146**) was that as the bulk of the exocyclic amine substituent increases, PI3K δ activity decreases

(*p*-nitrobenzyl < *p*-nitrophenyl < carboxymethyl < allyl < hydrogen) (Table 27), which proved that the steric clash between the exocyclic amine substituent and the gatekeeper (Ile⁸²⁵) was the main reason behind the poor activity of these compounds towards PI3K δ .

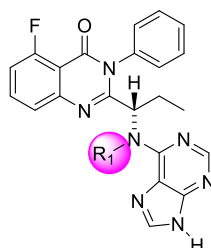


Table 27. The influence of the bulkiness of the exocyclic amine substituent on the PI3K δ activity in compounds (idelalisib **8**, **116**, **119**, **145** and **146**).

Compd	8	119	145	146	116
R ₁	H				
PI3K δ IC ₅₀ (nM)	11	1750	4400	11000	14000
Bulkiness of substituent increases PI3K δ activity decreases					

3.6.6 Conclusion derived from the second structure activity relationship (Table 23 and Table 25)

The conclusion derived from studies of the SAR of compounds (**8**, **116**, **117**, **119**, **120**, **145**, **146** and **147**) was that the exocyclic *N*-alkylation was associated with loss of potency, which was rationalised to steric hindrance between the new substituent with the gatekeeper (Ile⁸²⁵), which controls the access to the affinity pocket, disrupted the binding of inhibitors to the active site of PI3K δ . Similarly, activity was lost when a new functionality was introduced at N-9 of the purine hinge binder of idelalisib (**8**). This large decrease in the activity was attributed to the loss of the strong hydrogen bond interaction with Glu⁸²⁶ in the hinge region. This finding provides additional

support to the key role of the double hydrogen bond interactions at the hinge region in determining PI3K δ inhibitory activity^{144,153,155,244}.

3.6.7 Effect of the ethyl side chain (R_3) on PI3K δ activity

To probe the importance of the α -ethyl side chain (R_3) for the PI3K δ activity of idelalisib (**8**), the biological activity of idelalisib (**8**) was compared to that of its des-ethylated analogue **106** (Table 28).

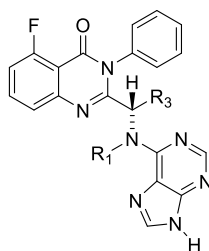


Table 28. Biological evaluation and isoform selectivity for PI3K δ for compounds **1** and **106**.

Compd	R_1	R_3	Isoform potency ^{a,b} IC ₅₀ (nM)			
			PI3K δ	PI3K α	PI3K β	PI3K γ
8	H		11	14000	2800	56
106	H	H	4400	14000	17500	14000

^aPotency against the different PI3K isoforms is given as IC₅₀ values (n = 1). ^bThe potency threshold for the PI3K δ assay is ~ IC₅₀ 1 nM due to substrate concentration.

Des-ethylated analogue **106** showed weak PI3K δ inhibitory activity in micromolar range (IC₅₀ = 4.4 μ M), with 400-fold less activity than idelalisib (**8**) (Table 28). Somoza *et al*¹⁸⁰ who first published the crystal structure of idelalisib (**8**) with PI3K δ reported that the role of the ethyl group in idelalisib (**8**) is to make hydrophobic interactions with Ile⁸²⁵, Met⁹⁰⁰ and Met⁷⁵². However, this could not explain the dramatic loss of potency observed for des-ethylated analogue **106**. It was believed that ethyl group might have additional role beyond making hydrophobic interactions with PI3K δ active site. Cushing *et al*¹⁵⁶ pointed out in his series of propeller-shaped inhibitors, that shared chemical similarity to idelalisib (**8**) (Table 29), that the presence

of the alkyl group at position α to the exocyclic amine, could restrict the free rotation around the bond at the 2-position of quinazolinone core, which resulted in increasing the molecular rigidity in low energy state closer to the binding conformation, where the ethyl group acted as a conformational blocker to fix the purine ring into a desired orientation for effective binding with the hinge region. Cushing *et al*¹⁵⁶ synthesized and compared des-methyl analogue **104**, S-methyl isomer **105** and R-methyl isomer **150** on the basis of their PI3K δ activity. The S-methyl isomer **105** was found to be 5 times more active than des-methyl analogue **104** and about 370 times than the R-methyl isomer **150** (Table 29). The author hypothesized that the steric clash between the R-methyl group and the protein might account for the loss of activity of the R-methyl isomer.

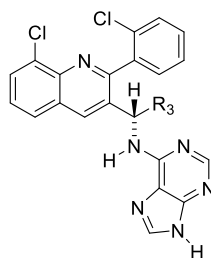


Table 29. Comparison of the PI3K δ activity of S-methyl analogue **105** with des-methyl **104** and R-methyl analogues **150**.

Compd	R ₃	PI3K δ IC ₅₀ (nM)
104	H	39
105	S-methyl	8
150	R-methyl	2960

3.7 Conclusion

In summary, the FDA-approved PI3K δ inhibitor idelalisib (**8**) was used as a starting point for the current study. The aim herein was to increase the inhibitor potency of idelalisib (**8**) by exploring interactions with residues within the unoccupied affinity pocket. The initial step was screening of fragment-like

compounds (without the purine hinge binder) to select the best starting point. Fragment **79** with an ethyl linker between the quinazolinone scaffold and a terminal hydrogen bond donating moiety showed promising activity with low micromolar range (IC_{50} = 1.4 μ M). The molecular docking study revealed a key hydrogen bonding interaction between the hydroxyethyl group of fragment **79** and the unoccupied affinity pocket, which may explain its higher PI3K δ potency. Encouraged by this finding, compound **79** was selected for fragment growing approach, after encountering many challenges experienced during the synthesis of the target compounds **72**, **125** and **127**, unfortunately. They were inactive with dramatic loss of activity in comparison with idelalisib (**8**). It was theorized that the newly introduced substituent would clash with the gatekeeper residue (Ile⁸²⁵), resulted in the loss of hydrogen bonds with the hinge region and reorientation of the ligands which led to a negative impact on PI3K δ activity. Moreover, it was noted that alkylation of NH-9 of purine binding to the hinge region with different substituents resulted in compounds with very weak PI3K δ potency, proved that the double-hydrogen bond interactions with the hinge region to be essential for the inhibitory activity toward PI3K δ . Lastly, it was also found that the PI3K δ activity of idelalisib (**8**) is 440-fold higher than the activity reported for the analogue with deleted ethyl side chain **106**, suggesting that the ethyl side chain plays a key role in reducing the conformational flexibility and locked the inhibitor in the favourable binding conformation.

Chapter 4 Design, Synthesis and Pharmacological Characterization of Novel N-7-substituted purine derivatives as PI3K δ selective Inhibitors (Propeller-shaped inhibitors).

4.1 Aim

A complex of idelalisib (**8**) bound to PI3K δ (see Figure 56 in Chapter 3) indicates that there is unoccupied pocket called the affinity pocket. In this medicinal chemistry project, this unused affinity pocket was explored with a functional group to gain additional binding to improve the binding affinity between the inhibitor class (idelalisib, **8**) and PI3K δ .

A previous study in Chapter 3 has shown that the addition of the extra functional group into the exocyclic amine in order to gain access to the unoccupied affinity pocket resulted in severe loss of PI3K δ potency (Figure 80), this is likely due to steric clash that might occur between the exocyclic *N*-substituent and the bulky side chain of the isoleucine (Ile⁸²⁵) gatekeeper which prevents the compounds from binding. The results suggest that the exocyclic amine may not be the ideal position for the extension of the binding group into the affinity pocket (Figure 80). Therefore, correctly positioning a binding group on the idelalisib structure relative to the affinity pocket may remove this steric contact with the isoleucine gatekeeper (Ile⁸²⁵) and result in increased activity.

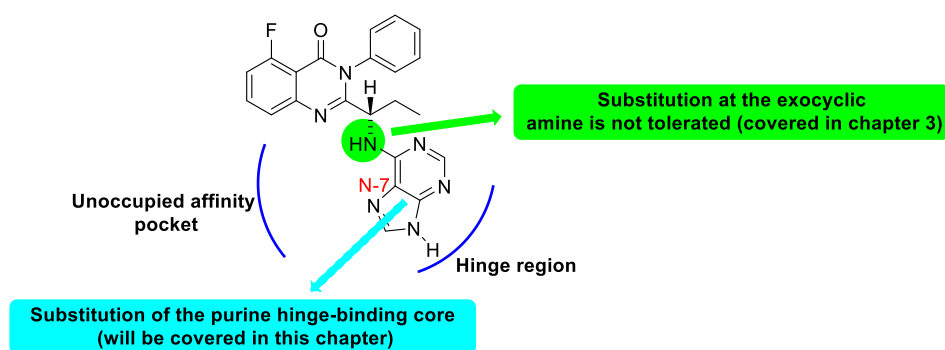


Figure 80. The selective PI3K δ inhibitor idelalisib (**8**), highlights the effect of new substituents in different positions of idelalisib (**8**) towards the PI3K δ inhibitory activity. SAR studies discussed in Chapter 3, reveals that substitution of idelalisib (**8**) on the exocyclic amine results in loss of PI3K δ activity. In Chapter 4, SAR will focus on the substitution of the purine hinge binder of idelalisib (**8**).

Subsequently, the aim of this chapter was to orient the binding group into the affinity pocket by joining it to idelalisib (**8**) using a new point of attachment. After reviewing data from several studies focusing on PI3K δ inhibitors^{144,154,155,173}, it was concluded that the binding group can be directed into the affinity pocket when it is attached to the hinge region binding group (Figure 80). This strategy has led to the identification of highly potent PI3K δ inhibitors. For instance, Brendt *et al*¹⁷³ projected a *m*-fluorophenol group from the hinge binding scaffold (pyrazolopyrimidineamine moiety) of compound **10** into the affinity pocket (see Figure 57b in Chapter 3), where the phenolic hydroxyl group serves as a hydrogen bond acceptor to Tyr⁸¹³ and as a hydrogen bond donor for the side chain of Asp⁷⁸⁷ within the affinity pocket. These novel interactions lead to a 186-fold increase of potency against PI3K δ , compared to the parent compound **9** (see Table 19 in Chapter 3).

In another interesting study, Patel *et al*¹⁵⁵ reported the design of the PI3K δ inhibitor **152** with sub-nanomolar activity (Table 30) *via* substitution of a new binding group (pyrazole) on the hinge-binding core (4-aminopyrimidine) (Figure 81a). The pyrazole group extends into the affinity pocket where it

establishes double hydrogen bond interactions with Lys⁷⁷⁹ and Asp⁷⁸⁷ (Figure 81b) leading to a dramatic 330-fold increase in potency against PI3K δ compared with the unsubstituted derivative **151** (Table 30).

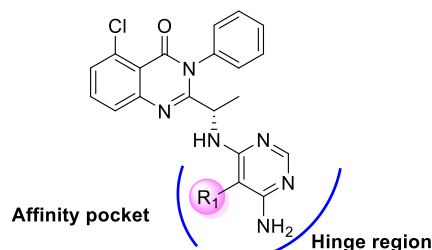
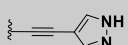
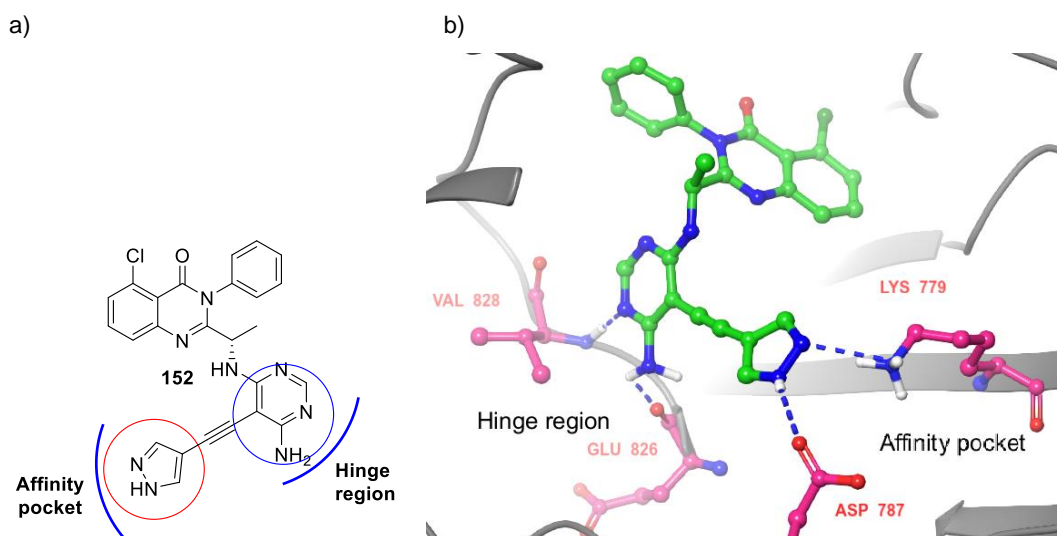


Table 30. Biological evaluation and isoform selectivity for PI3K δ for compounds **151** and **152** reported by Patel *et al*¹⁵⁵, Compound **152** shows improvement in PI3K δ potency compared with the parent compound **151**.

compd	R ₁	PI3K δ IC ₅₀ (nM)	Isoform selectivity		
			δ/α	δ/β	δ/γ
151 ¹⁵⁵	-H	99	1600	120	320
152 ¹⁵⁵		0.3	1500	260	230



Based on the previous findings, the design strategy is to introduce the new functional group to the purine hinge binder of idelalisib (**8**) that could then extend towards the affinity pocket interacting with the polar residues lining the

pocket. Substitution at the N-7 site of purine provides the best conventional extension strategy to position the binding group into the affinity pocket (Figure 82), this can be attributed to three factors. First, based on the crystal structure of idelalisib (**8**) in murine PI3K δ (PDB code 4XE0), the N-7 position of purine is the closest idelalisib atom to the unoccupied affinity pocket, as shown in (Figure 82b). The second factor is that idelalisib (**8**) in complex with PI3K δ adopts a bound conformation that orients the N-7 atom of the purine towards the opening of the affinity pocket (Figure 82b), it is thus apparent that substitution at the N-7 position may extend deep into the affinity pocket. The third factor is that introduction of a binding group onto the N-7 of purine generates a structure which is more synthetically feasible, whereas introduction of the functional group on the carbon skeleton of purine such as the C-8 position demands a more complicated synthesis (Figure 82a).

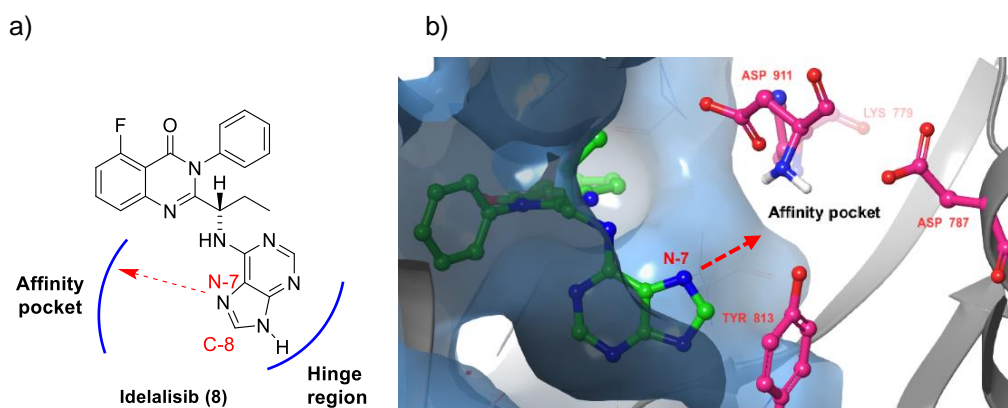


Figure 82. a) The selective PI3K δ inhibitor idelalisib (**8**). b) Crystal structure of murine PI3K δ (PDB code 4XE0) with idelalisib (**8**) bound. It shows that idelalisib (**8**) adopts a conformation allowing the N-7 atom of the purine ring to orient towards the opening of the affinity pocket.

4.2 Drawback associated with the extension of binding group from N-7 of purine

Targeting the affinity pocket with a functional group substituted at N-7 purine of idelalisib (**8**) might be a promising strategy, however, there is a major challenge that may negatively affect the PI3K δ activity, where the N-7

substitution leads to the loss of the tautomeric proton on the N-9 atom of the purine ring (Figure 83). The NH-9 proton acts as a hydrogen bond donor to the backbone oxygen atom of Glu⁸²⁶ in the hinge region (Figure 83a), where the absence of this critical hydrogen bond could lead to a major loss in the PI3K δ activity. Accordingly, idelalisib analogues with N-7-substituted purine can only form a single hydrogen bond with the hinge region through the N-3 of purine as a hydrogen bond acceptor (Figure 83b), whereas the lead compound (idelalisib **8**) makes two hydrogen bonds to the hinge region using the N-3 and NH-9 of the purine ring (Figure 83a)¹⁸⁰.

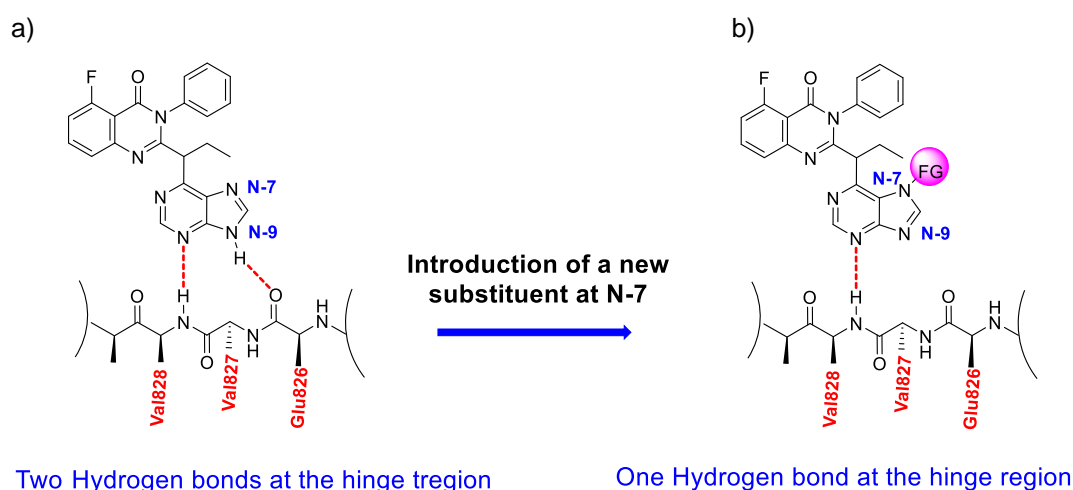


Figure 83. Schematic representation of ligand binding interactions in the hinge region of PI3K δ . a) the purine group of idelalisib (**8**) forms two hydrogen bonds to the hinge backbone. b) Installation of a new substituent at the N-7 of the purine, leads to the loss of the hydrogen bond between NH-9 of purine and the backbone carbonyl of Glu⁸²⁶.

Interestingly, Patel *et al*¹⁵⁵ published a study which focused on the importance of the hydrogen bond donor at the hinge region to the PI3K δ activity. It was found the removal of the amino group (-NH₂) from a pyrimidine hinge binder in compound **153** resulted in a des-amino analogue **154** with a dramatic drop (17-fold) in PI3K δ potency (Table 31), which was caused by loss of important hydrogen bond interaction. However, the addition of the affinity pocket binding moiety (nitrile group) to the compound **154** resulting in compound **155** which

Chapter 4

exhibited 210-fold improvement in potency against PI3K δ (IC_{50} = 8 nM) (Table 31). These interesting findings suggest that the loss of the strong hydrogen bond between the $-NH_2$ of **153** and the hinge region can be compensated by the gain of new binding interactions within the affinity pocket. For comparison, compound **155** which has affinity pocket binding motif (nitrile) but lacking the hydrogen bond donor ($-NH_2$) is 12 times more potent than compound **153** which has the hydrogen bond donor ($-NH_2$) but lacking the affinity pocket binder (nitrile) (Table 31).

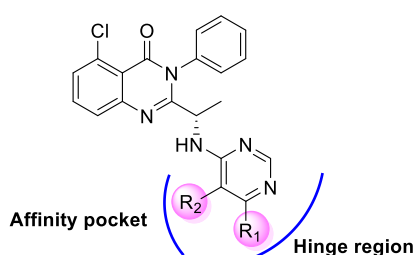


Table 31. Biological evaluation for PI3K δ for compounds (**153-155** reported by Patel *et al*¹⁵⁵), it displays the number of hydrogen bonding interactions between each compound and the hinge region.

Compd	R ₁ (hinge binder)	R ₂ (affinity pocket binder)	PI3K δ IC ₅₀ (nM)	Number of H.B at the hinge region
153 ¹⁵⁵	NH ₂ -	H-	99	dual
154 ¹⁵⁵	H-	H-	1700	single
155 ¹⁵⁵	H-	CN-	8	single

Based on the results obtained from Patel *et al* study¹⁵⁵, one might expect that the proposed N-7-substituted purine derivatives which have affinity pocket binding groups could be more potent than the parent compound (idelalisib **8**) despite the absence of the hydrogen bond donor for the hinge region.

4.3 Medicinal chemistry strategy

The success of the extension strategy to the affinity pocket depends on the careful selection of the linker length and the terminal binding group (Figure 84).

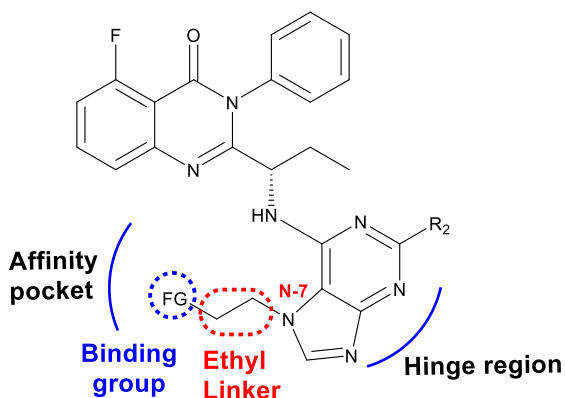


Figure 84. General structure of the series of N-7-substituted purine derivatives, bearing an affinity pocket-binding group (highlighted in blue) connected through an ethyl linker (highlighted in red) to the purine hinge binder.

4.3.1 Length of the linker

The first step is to determine the length of the linker that could effectively connect the N-7 of purine to the affinity pocket binder (polar functional group).

The length of the linker is important in order to arrange the binding group at a distance compatible with the formation of a hydrogen bond with the polar residues lining the affinity pocket. It was proposed to use a flexible alkyl linker to allow better placement of the binding group within the affinity pocket. The ethyl linker was selected based on the observation of the distance between the entrance of the affinity pocket and the N-7 atom of the purine hinge binder (3.70 Å) (Figure 85a), the length of a spacer of two carbon chain will have a distance of 2.52 Å³²⁵, in addition to the bond that links the ethyl chain to the heteroatom functional group (O or N), the projected distance of C-O and C-N are 1.17 and 1.47 Å, respectively³²⁵. Thus, the full linker length is approximately between 3.70- 3.00 Å (Figure 85b). This is in good agreement

to the estimated distance between the N-7 atom of purine and the entrance of the affinity pocket (3.70 Å) (Figure 85a), which indicates that the ethyl linker has the optimum length to place the binding group at the distance permitting the establishment of a hydrogen bond with Asp⁹¹¹ and Tyr⁸¹³.

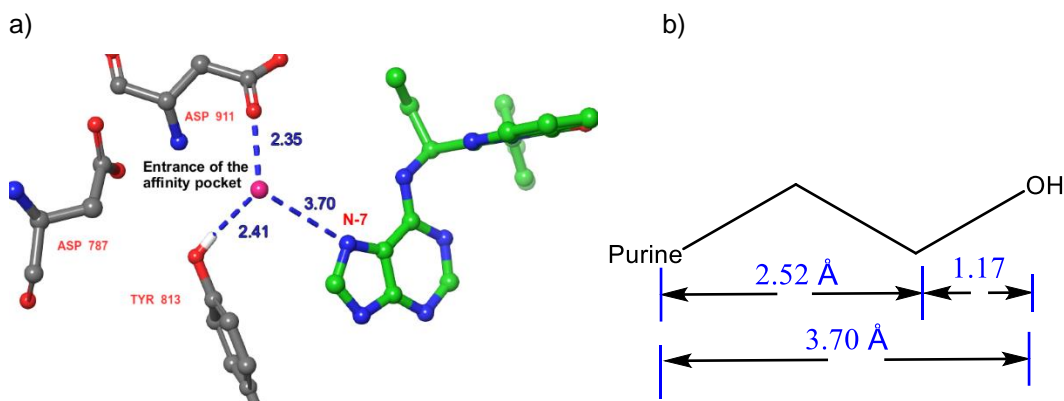


Figure 85. a) Crystal structure of murine PI3K δ (PDB code 4XE0) with idelalisib (**8**) bound, highlights the distance between the N-7 atom of the purine and the entrance of the affinity pocket (represented by a magenta sphere), which is within hydrogen bonding distance to Asp911 and Tyr⁸¹³. b) Maximum bond distance between the purine core and the functional group (hydroxyl) is 3.70Å, when a two-carbon atom linker is employed^{325,326}. This is in good agreement to the estimated distance between the N-7 atom of purine and the centre of the affinity pocket (3.70Å).

4.3.2 Affinity pocket-binding group (binding group)

The affinity pocket binding moieties (Figure 84) used in the current study can be classified into two types.

4.3.2.1 Commonly used polar functional group

The first group include the functional groups that are commonly found in drug molecules and traditionally used to engage in either hydrogen bonding or ionic interactions with polar residues of the target protein, which involves hydroxyl (-OH), amino (-NH₂), amido (-CONH₂) and urea (-NH-CO-NH₂) (Table 32). These groups consist of OH and NH groups that can donate hydrogen bonds or C=O that can accept them. The hydroxyl group has the ability to serve as both hydrogen bond donor and acceptor (Table 32). An amino group can take part in electrostatic interactions with the two negatively

charged aspartates (Asp⁷⁸⁷ and Asp⁹¹¹) lining the affinity pocket. An amide (-CONH₂) can donate and accept three hydrogen bonds (Table 32). Finally, the urea group (-NH-CO-NH₂) could bind within the affinity pocket through a set of four hydrogen bonds, where the oxygen atom acts as a hydrogen bond acceptor and the -NH and -NH₂ protons act as hydrogen bond donors (Table 32)³²⁷. Additionally, a reference compound **160** bearing an ethyl group extending into the affinity pocket would be synthesized. Because the ethyl linker lacks the polar functional group, it cannot form hydrogen bond with the affinity pocket, thus ethyl analogue **160** would be expected to show much less PI3K δ activity than the other analogues (**156-159**).

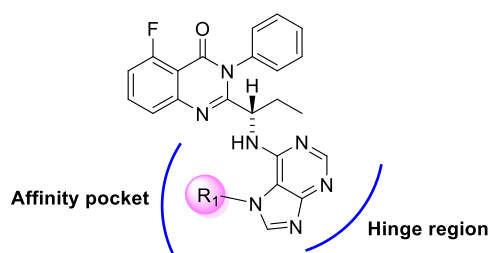


Table 32. Number of hydrogen bond donors and acceptors in the binding groups of compounds (**156-160**), and types of interactions that can make with variable residues of the affinity pocket.

Compd	R ₁	Number of H.B.D	Number of H.B.A	Possible interaction with the affinity pocket
156		1	1	hydrogen bond
157		2	0 (ionized)	1-hydrogen bond 2-salt bridge 3-cation-pi
158		2	1	hydrogen bond
159		3	1	hydrogen bond
160		0	0	Van der Waals interactions

4.3.2.2 Affinity pocket binder from the previously published work

Previous studies proved that there are certain functional groups that preferably bind to the affinity pocket and are able to increase the activity against PI3K δ . For instance, Patel *et al*¹⁵⁵ used the nitrile group to project deep into the affinity pocket, where it forms a new hydrogen bond to Tyr⁸¹³ (Figure 86b). This additional hydrogen bond helps to explain the 245-fold increase in PI3K δ activity with the nitrile-containing compound **161** compared to the parent unsubstituted compound **151** (Table 33). Moreover, Patel *et al*¹⁵⁵ proved that the extension of the acetylene of **162** into the affinity pocket improved the PI3K δ affinity by 990-fold compared to its parent compound **151** (Table 33). Although no explanation was given for the observed activity of compound **162**, it was hypothesized that the hydrogen bond interaction between the relatively acidic proton of the terminal acetylene and the side chain of Asp⁷⁸⁷ or Asp⁹¹¹ lining the affinity pocket could be the reason behind the high activity (IC₅₀ value of 0.1 nM) of the acetylene-containing compound **162**.

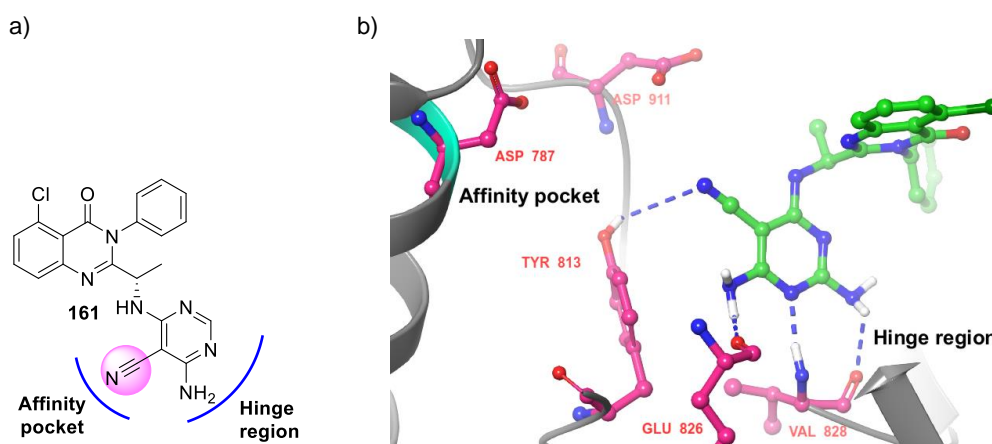


Figure 86. a) The nitrile-containing compound **161**, highlights the nitrile group (in pink) that projects from the hinge binding group (aminopyrimidine) into the affinity pocket. b) Crystal structure of murine PI3K δ (PDB code 5I4U) with compound **161** bound. Nitrile group forms a hydrogen bond with the side chain of Tyr⁸¹³ in the affinity pocket. Blue dashed lines represent the proposed hydrogen bonds with the affinity pocket and hinge region.

Chapter 4

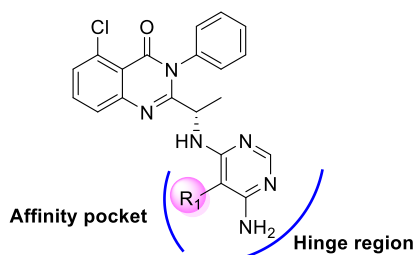


Table 33. Biological evaluation for PI3K δ for the nitrile **161** and acetylene **162** derivatives. The unsubstituted analogue **151** is used as a reference.

compd	R ₁	PI3K δ IC ₅₀ (nM)
151	-H	99
161		0.4
162		0.1

Consequently, the nitrile **163** and acetylene **164** containing analogues would be designed and synthesized (Table 34).

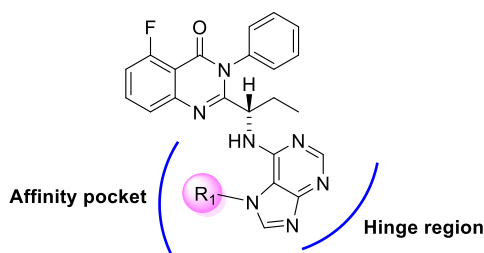


Table 34. Structure of the some proposed compounds belonging to N-7 substituted purine series (**163-166**).

Compd	R ₁
163	
164	
165	
166	

Erra *et al*¹⁵⁴ in his series of pyrrolotriazinone derivatives used the methanesulfonamide (-NH-SO₂-CH₃) group installed at position 3 of the phenyl ring of compound **167**. The NH₂SO₂Me-phenyl ring group extends

towards the affinity pocket and was shown to have a dramatic effect on the PI3K δ inhibition (IC_{50} value of 0.3 nM) (Table 35), where the methanesulfonamide group acts as a hydrogen bond acceptor and forms a hydrogen bond with the side chain of Lys⁷⁷⁹ in the affinity pocket (Figure 87)¹⁵⁴. It was thus recommended to test the effect of methanesulfonamide in this series of N-7-substituted purine derivatives. (Table 34).

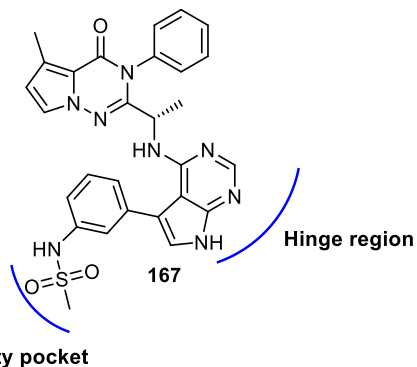


Table 35. Biological evaluation and isoform selectivity for PI3K δ for compound **167** reported by Erra *et al*¹⁵⁴.

Isoform potency ^{a,b} IC_{50} (nM)	Isoform selectivity			
	PI3K δ	δ/α	δ/β	δ/γ
0.3		2433	123	5.6

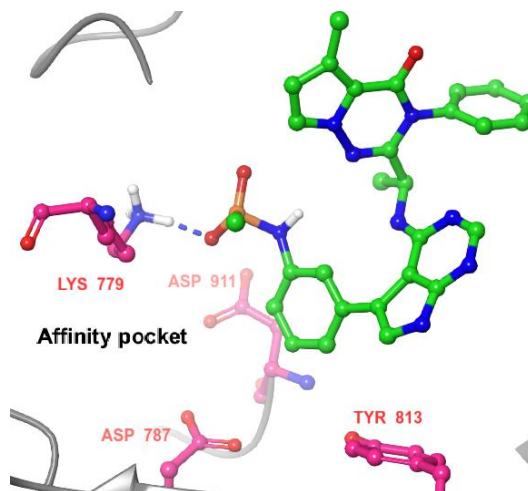


Figure 87. Crystal structure of human PI3K δ (PDB code 6G6W) with compound **167** bound. Blue dashed line represents the proposed hydrogen bond between the methylsulfonamide group and Lys⁷⁷⁹ in the affinity pocket.

Novartis scientists reported the development of leniolisib (**7**) (Figure 88a), which is in a late-stage pipeline for treatment of APDS. They described the

importance of the trifluoromethyl moiety extending towards the affinity pocket for modulating PI3K δ activity, where they found that the replacement of the trifluoromethyl interacting group of **7** with hydrogen **168** reduces the PI3K δ potency by a factor of 5 (Table 36). This indicates that the trifluoromethyl group interacts with the affinity pocket, by making a charge-enhanced hydrogen bond interaction with the side chain of Lys⁷⁷⁹ (Figure 88b).

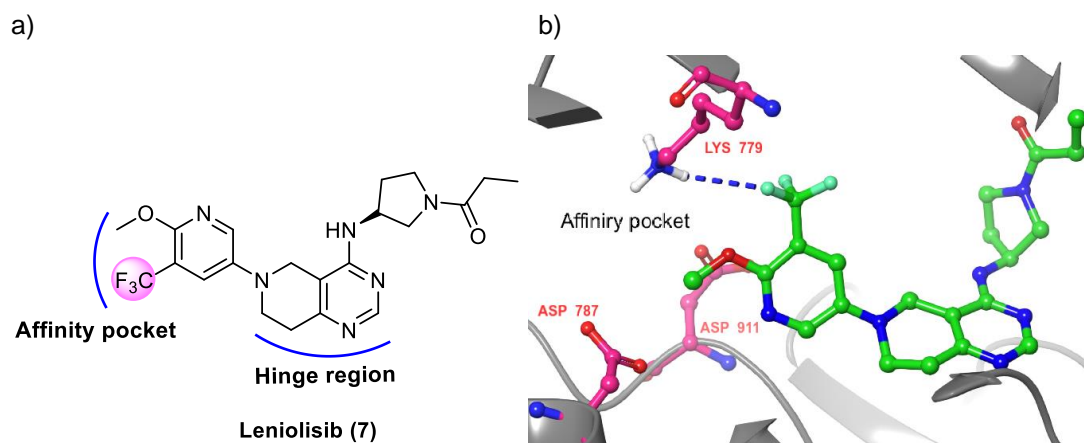


Table 36. Biological evaluation and isoform selectivity for PI3K δ for leniolisib (**7**), highlights the trifluoromethyl group that forms a hydrogen bond interaction with the affinity pocket. The unsubstituted analogue **168** is used as a reference²³⁹.

compd	R ₁	PI3K δ IC ₅₀ (nM)	Isoform selectivity		
			δ/α	δ/β	δ/γ
168 ²³⁹	-H	132	50	68	>70
7 ²³⁹	-CF ₃	27	29	63	>70

4.3.3 Modification of Hinge-binding moiety

As mentioned before, insertion of a functional group to the N-7-purine of idelalisib (**8**) leads to the loss of the hydrogen bond donor NH-9 of purine,

which makes an important interaction with the backbone carbonyl of Glu⁸²⁶ in the hinge region (Figure 89a and 89b). It was thought that this loss can be compensated through the introduction of a new hydrogen bond donor (-NH₂) into the 2-position of purine (Figure 89c), which can make a new hydrogen bond with the hinge region. Patel *et al*¹⁵⁵ showed that the newly added amino group at the 2-position (equivalent to the position 2 of purine) of 2,4-diaminopyrimidine of compound **169** (Figure 90a) can make a novel hydrogen bond with the carbonyl backbone of Val⁸²⁸ at the hinge region (Figure 90b), in addition to the two traditional hydrogen bonds that are made through N-3 and 4-amino group (equivalent to N-3 and NH-9 of purine), thus, compound **169** forms triple hydrogen bonds with the hinge region.

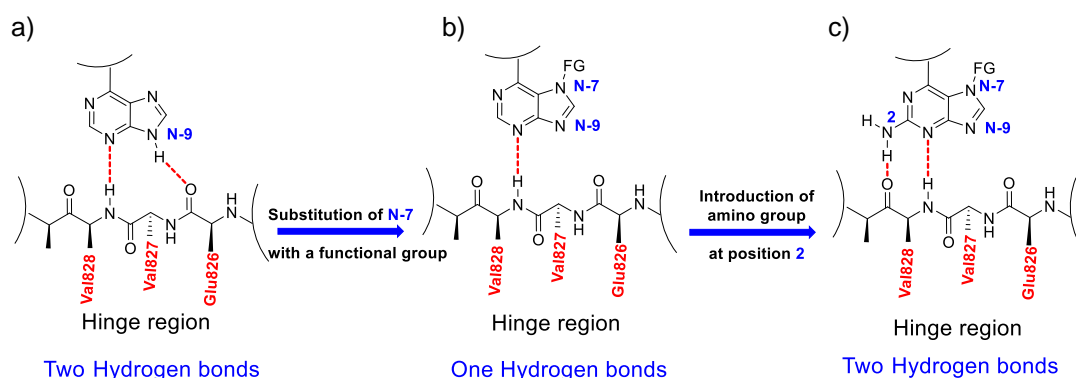


Figure 89. A schematic representation of the hinge binding region depicts the potential number of hydrogen bonds connecting three different purine derivatives with Val⁸²⁸ and Glu⁸²⁶ at the hinge region. a) Unsubstituted purine forms two hydrogen bonding interactions, b) the N-7-substituted purine derivative can only form one hydrogen bond, c) the introduction of amino group at 2-position of purine aimed to restore the double hydrogen bonds, which could rescue any loss of PI3K δ activity.

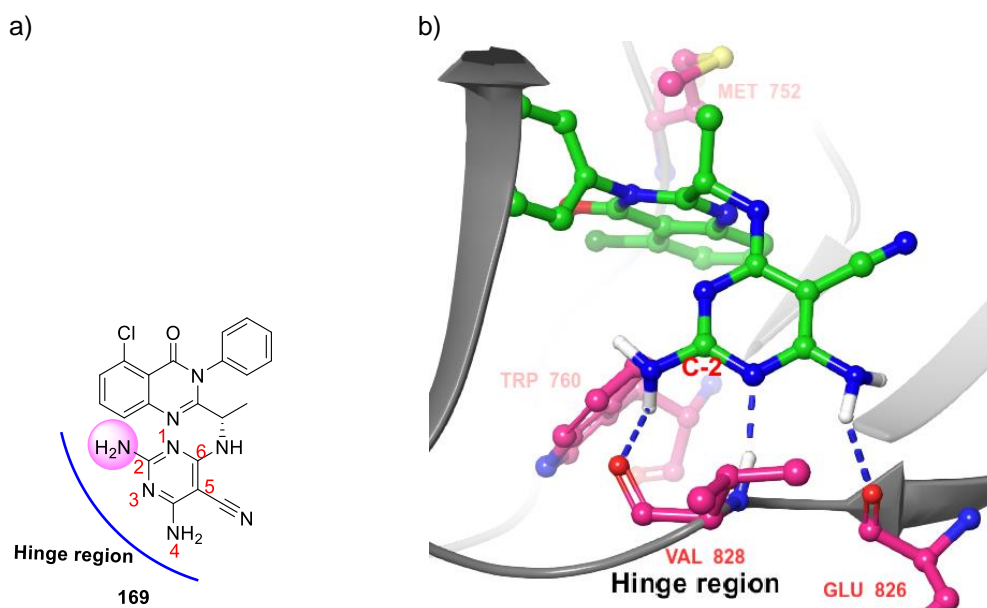


Figure 90. a) Compound **169**, the pyrimidine ring is numbered, highlights the newly introduced amino group (in pink) at the 2-position, which forms a third hydrogen bond with the hinge region b) Crystal structure of murine PI3K δ (PDB code 5I4U) with compound **169** bound. Blue dashed lines represent the triple hydrogen bonds formed between the diaminopyrimidine group with the amide back bone of Glu⁸²⁶ and Val⁸²⁸ at the hinge region.

The 2-aminopyrimidine ring can be regarded as a bioisosteric replacement for the 2,4-diaminopyrimidine hinge binder of compound **169**, due to their high degree of the structural similarity (Figure 91), Hence, a new series of N-7-substituted purine-based compounds (Table 37) would be synthesized with an amino group installed at the 2-position of the purine ring to serve as a hydrogen bond donor and restore the dual hydrogen bonds with the hinge region.

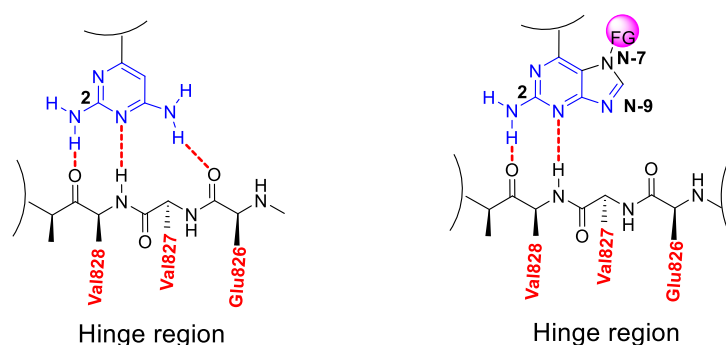


Figure 91. Comparison of the chemical structure between 2,4-diaminopyrimidine hinge binder of compound **169** and the proposed 2-amino-7-substituted purine hinge binder. It reveals striking structural similarity (highlighted in blue) between the two heterocyclic systems, which indicates that the 2-amino group of 2-amino purine may make the same interaction at the hinge region as the 2-amino group of 2,4-diaminopyrimidine hinge binder.

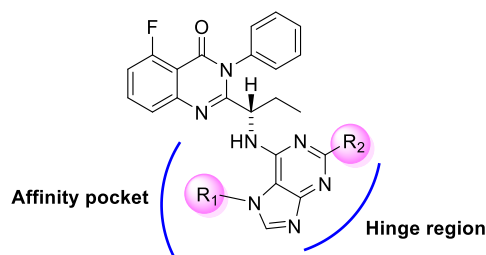


Table 37. Structure of the proposed compounds belonging to 2-amino-N-7-substituted purine series **170** and **171**.

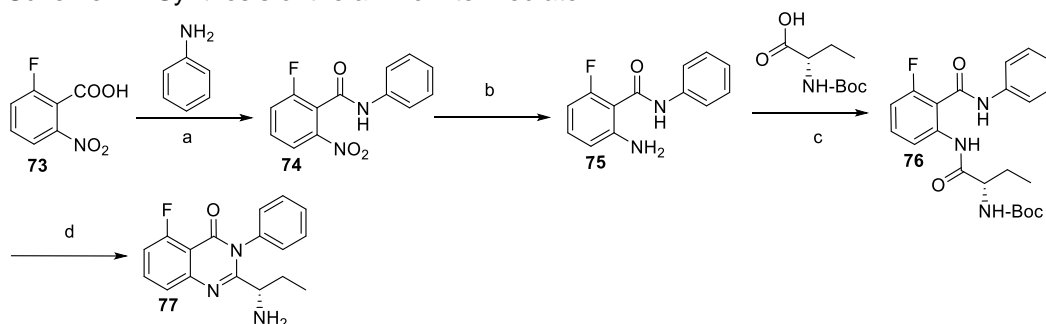
Compd	R ₁	R ₂
170		-NH ₂
171		-NH ₂

4.4 Discussion

4.4.1 Chemistry Section

The synthetic protocol was similar to that used in Chapter 3 for the synthesis of idelalisib (**8**), except for the addition of the extra substituent to the N-7 position of purine. The synthetic plan involves first the formation of the two intermediates, the quinazolinone derivative **77** and N-7-substituted-6-chloropurine. These two intermediates then can react together to form the proposed final products.

Scheme 17. Synthesis of the amino intermediate **77**



^aReagents and conditions: (a) HATU (2.5 equiv), DIPEA (3 equiv), DMF, rt, 24 h, yield 98%; (b) H₂, 10% Pd/C (0.05 equiv), methanol, rt, 12 h, yield 100%; (c) IBCF (3.5 equiv), NMM (3.5 equiv), THF, 60 °C, 24 hr, yield 61%; (d) HMDS (9 equiv), I₂ (3 equiv), DCM, rt, 24 h, yield 56%.

The key intermediate **77** was synthesized according to the general synthetic route shown in Scheme 17. Treatment of the benzoic acid derivative **73** with aniline gave **74** in 98% yield which then underwent catalytic hydrogenation of the nitro group to give the corresponding aniline derivative **75** in 100% yield, followed by IBCF-promoted coupling with (*S*)-2-(Boc-amino)butyric acid to generate the desired diamide product **76**. Finally, the reaction of **76** with HMDS in the presence of the 3 equivalents of iodine resulted in cyclisation to give the key amino intermediate **77** in moderate yield (56%).

The last step involves the nucleophilic displacement of N-7-substituted-6-chlorinepurine with **77**, which was expected to be straightforward. However, synthesis of N-7-substituted-6-chloropurine intermediates was the most challenging step in the entire synthesis, this was due to the fact that N-9 of 6-chloropurine **78** is known to be more reactive than N-7, as the steric hindrance exerted by the 6-chlorine atom disfavors the reaction at N-7 (Figure 92). Thus, the direct alkylation of 6-chloropurine **78** resulted in the formation of two regioisomers N-7 (desired) and N-9 (undesired) the latter always being the major regioisomer.

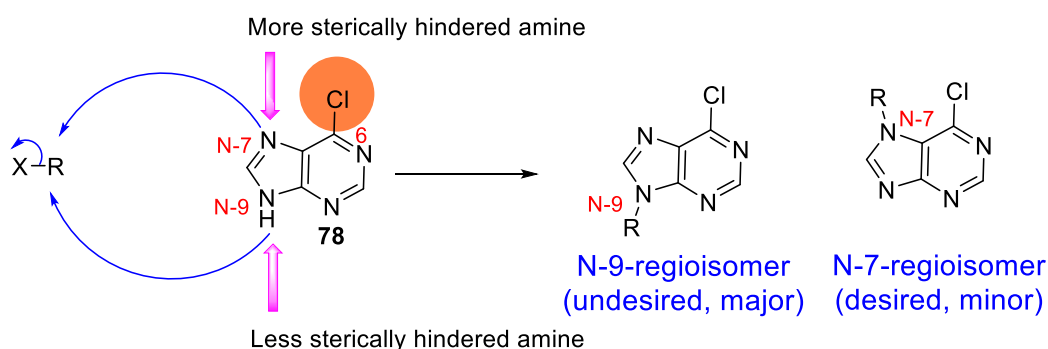
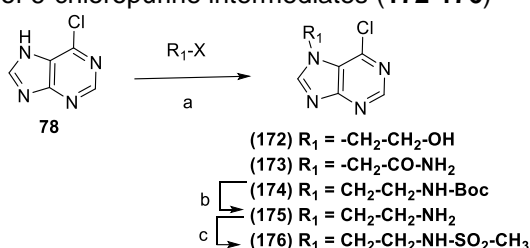


Figure 92. General alkylation of 6-chloropurine **78**, illustrates the steric effect exerted by the 6-chlorine atom on the N-7 of purine, results in a significant decrease in the nucleophilic characteristics of N-7 in contrast to N-9 of purine. Thus, N-9 atom undergoes alkylation faster than the N-7 atom.

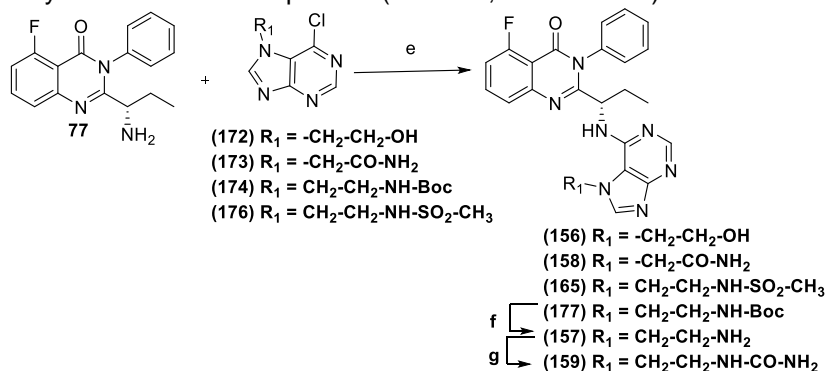
4.4.1.1 Synthesis of N-7-substituted purine derivatives

4.4.1.1.1 Direct alkylation method

Traditional alkylation methodology (Scheme 18) was applied for the incorporation of suitable functional groups at the N-7 atom of purine. This method was based on a direct nucleophilic substitution reaction, where the 6-chloropurine was alkylated with a variety of alkylating reagents, K_2CO_3 was selected as a base to promote the reaction.

Scheme 18. Synthesis of 6-chloropurine intermediates (**172-176**)

^aReagents and conditions: (a) K_2CO_3 (3 equiv), CH_3CN , rt, 24 h, yields 7-16%; (b) 4 N HCl, dioxane, 2 h, yield 97%; (c) methanesulfonyl chloride (1.1 equiv), triethylamine (1.1 equiv), DCM, rt, 16 h, yield 44%.

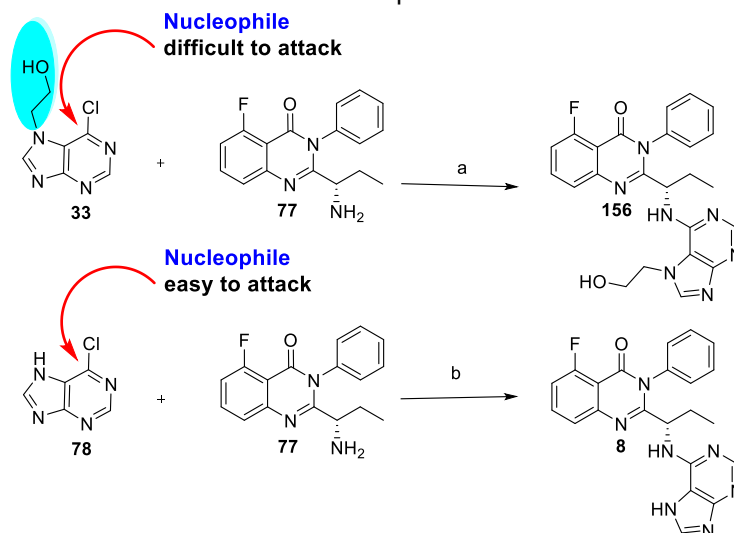
Scheme 19. Synthesis of final compounds (**156-159**, **165** and **177**)

^aReagents and conditions: (e) DIPEA (10 equiv), *tert*-butanol, 100 °C, 72 h, yields 10- 30%; f) 4 N HCl, dioxane; rt, 2 h, yield 95%; g) Trimethylsilyl isocyanate (2 equiv), TEA (2 equiv), DCM, rt, 18 h, yield 68%.

Following a synthetic procedure reported by Zhang *et al*³²⁸, 6-chloropurine **78** and 2-iodoethanol were reacted in a 1: 3 ratio in the presence 3 equivalents of K_2CO_3 in water at RT for 16 h, to give a mixture of the N-7 **172** and N-9 **178** regioisomers in a 1:1.3 ratio with 37% overall yield. The isolated N-7-isomer was treated with the primary amine **77** in the presence of DIPEA

in *tert*-butanol to give the alcohol product **156** (Scheme 19), this reaction required high temperature (100 °C) and prolonged reaction time (3 days) to obtain a low yield (18%), this can best be explained due to significant steric hindrance provided by N-7-hydroxyethyl group (Scheme 20), whereas in comparison, the reaction of the primary amine **77** with 7-unsubstituted 6-chloropurine **78** to generate idelalisib (**8**) required a shorter reaction time and lower temperature to achieve optimum yield of 65% (Scheme 20).

Scheme 20. The effect of the steric hindrance exerted by the N-7-substituent on the reactivity of 6-chloropurine derivative **172** towards nucleophilic aromatic substitution reaction



^aReagents and conditions: a) DIPEA (10 equiv), *tert*-butanol, 100 °C, 72 h, yield 18%. b) DIPEA (10 equiv), *tert*-butanol, 85°C, 16 h, yield 65%.

The synthesis of amide **173**, was carried out starting from 6-chloropurine **78** which was alkylated with 2-bromoacetamide in the presence of K₂CO₃ in acetonitrile at RT for 3 days to afford 47% yield of a mixture of regioisomeric products N-7 **173** and N-9 **179** in a ratio of 1:7. The 7-isomer **173** was isolated from the mixture by flash chromatography in 7% yield (Scheme 18). Treatment of **173** with the primary amine **77** in *tert*-butanol at 100°C, gave the amide product **158** in 10% yield (Scheme 19), with 48% of starting amine **77** and 70% of starting purine **173** being recovered. A low yield (10%) obtained

for the product **158** was probably due to two reasons. First, the steric hindrance applied by N-7-substituent. Second, the lack of solubility of the amide intermediate **173** in *tert*-butanol.

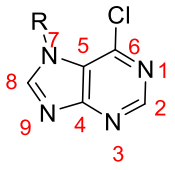
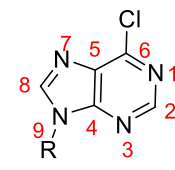
6-Chloropurine **78** was treated with 3 equiv of *N*-*boc*-2-bromoethyl amine and 3 equiv. of K₂CO₃ in acetonitrile at RT for 18 h, to give the N-7 regioisomer **174** in 10% isolated yield, following chromatography (Scheme 18), in addition to 60% of the undesired N-9 regioisomer **180**. The obtained N-7-purine intermediated **174** was used for alkylation of the primary amine **77**, using DIPEA in *tert*-butanol to give compound **177** in an overall yield 30% (Scheme 19). After the deprotection step using 4 N HCl in dioxane, the final amine product **157** was isolated as its hydrochloride salt in 95% yield. Finally, **157** was reacted with trimethylsilyl isocyanate at RT in DCM to yield the urea product **159** in 68% yield.

4.4.1.1.2 Differentiation of N-7 and N-9-substituted purine derivatives using ¹H and ¹³C NMR

1D NMR spectroscopy is an attractive tool for distinguishing between N-7 and N-9 purine isomers³²⁹, due to the high sensitivity of ¹H and ¹³C chemical shifts to the substituent position. Much efforts have been given to evaluate the effect of the substituent site in the purine ring on ¹H and ¹³C chemical shifts^{329,330}. Dracinsky *et al*³²⁹ and Kjellberg *et al*³³⁰ have studied the effect of the substituent site on the chemical shift of protons and carbons in a large range of purines, where they found that N-7 and N-9 regioisomers of the substituted purine precursor showed characteristic differences in their ¹H and ¹³C NMR chemical shifts, that can be utilized to distinguish between the two regioisomers. The authors compared the ¹H and ¹³C chemical shifts of proton

and carbons between the regioisomeric N-7 and N-9 pairs of different purine series (Table 38)^{329,330}. This study illustrates a general rule for ^1H and ^{13}C chemical shift changes. In the N-7-regioisomer, the C-8 signal appeared about 3-6 ppm down field and C-4 appeared 7-10 ppm lower field of their positions in N-9 regioisomer. On the contrary, the signal of C-5 appeared about 8-9 ppm up field and C-6 2-6 ppm up field in N-7-regioisomer than in N-9-regioisomer. While the C-2 signal was the least affected as it is distal to the alkylation site. The general trends for the difference in ^1H and ^{13}C chemical shifts of N-7 and N-9 regioisomers of different 6-substituted purines are summarized in Table 38^{329,330}.

Table 38. The difference of ^1H and ^{13}C Chemical shift between the regioisomeric N-7 and N-9 pairs of substituted purines, which were reported by Dracinsky *et al*³²⁹ and Kjellberg *et al*³³⁰.

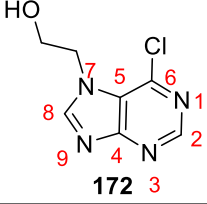
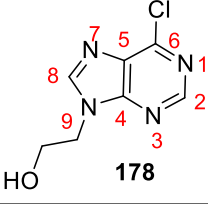
Proton and carbon	 N-7-regioisomer	differences in the chemical shift (ppm)	 N-9-regioisomer
H-8	down field	not reported	up field
C-4	down field	7- 10	up field
C-8	down field	3- 6	up field
C-5	up field	8- 9	down field
C-6	up field	2- 6	down field
C-2	no change	-	no change

Cells highlighted in blue represent more deshielded signals, cells highlighted in red represent more shielded signals.

General rules presented in Table 38 can be applied to distinguish between N-7 and N-9-regioisomers of 6-substituted purines synthesized in this study. The ^1H and ^{13}C chemical shifts of alcohol derivatives **172** and **178** were determined and assigned (Table 39). After straightforward comparison with

Table 38, it was found that the compound **172** is in accord with N-7 substitution and compound **178** with N-9 substitution (the colours of the cells in Table 39 match those of Table 38). Moreover, the differences in the chemical shift values between the same carbons of **172** and **178** are in excellent agreement with those observed in Table 38.

Table 39. Comparison of ^1H and ^{13}C NMR chemical shifts (δ , ppm) between pairs of regioisomers **172** and **178**.

Proton and carbon		differences in the chemical shift values (ppm)	
H-8	8.74	0.09	8.65
C-4	162.20	9.62	152.58
C-8	151.80	3.35	148.45
C-5	122.62	8.7	131.32
C-6	142.51	6.76	149.27
C-2	152.09	0.29	151.80

Cells highlighted in blue represent more deshielded signals, cells highlighted in red represent more shielded signals.

The differentiation of N-7 **173** and N-9 **179** regioisomeric pairs of the amide derivatives and N-7 **174** and N-9 **180** regioisomeric pairs of boc-protected amine derivatives, was achieved in the same way as mentioned for the alcohol regioisomeric derivatives **172** and **178**.

4.4.1.1.3 Challenges encountered in the direct alkylation method

The major synthetic problem associated with the direct alkylation method is that it led to predominant formation of the unwanted N-9-regioisomer, as it is less sterically hindered than the N-7 regioisomer. Accordingly, a large amount of the starting material **78** was required in order to prepare enough quantity

of N-7 substituted purine intermediate for the next reaction step. Moreover, the two regioisomers of 6-chloropurine have the same molecular mass and similar polarity, making purification and characterization processes challenging and time-consuming. In order to avoid this problem, an alternative synthetic route should be pursued to avoid the formation of the undesired N-9-regioisomer and achieve regioselective N-7-alkylation of 6-chloropurine.

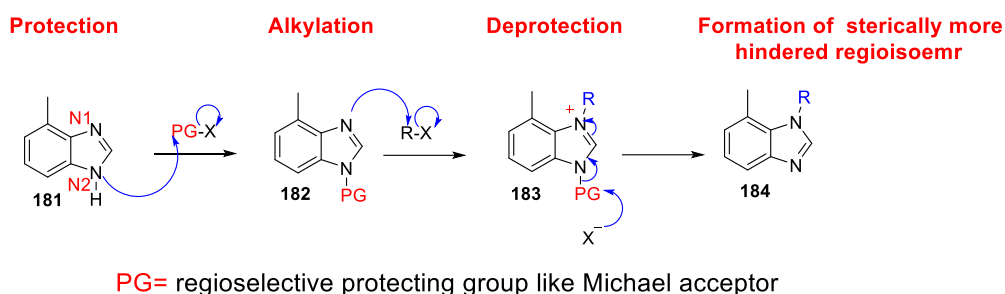
4.4.2 Regiospecific N-7 alkylation of 6-chloropurine derivatives

Chen *et al*³³¹ developed methodology for the regioselective formation of the key intermediates N-7 substituted purine. In this method, 6-chloropurine is treated with an alkylmagnesium reagent, instead of K₂CO₃, prior to the addition of the alkylating reagent, to give N-7 substituted purine as the only regioisomer. The exact mechanism for this reaction is still not fully understood³³¹. However, it was hypothesized that this reaction follows similar mechanistic pathway as the previously reported regioselective *N*-alkylation of the more hindered nitrogen of benzimidazole **181**, shown in Scheme 21^{332,333}, where the less-hindered NH-9 is deprotonated by the Grignard reagent and then coordinates to the magnesium of MgCl gives the complex **186** (Scheme 22), with the less-hindered N-9 of purine is now blocked, the N-7 of purine attacks the alkylating reagent to provide a quaternary imidazolium salt **187**, finally it undergoes in situ deprotection of the protected N-9 to generate N-7-substituted purine **188** as a single regioisomer.

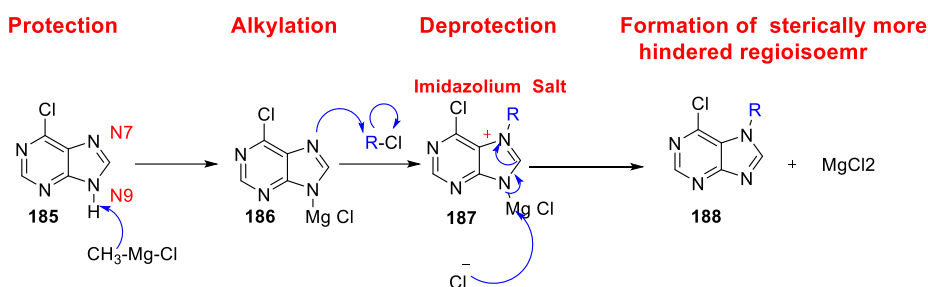
In order to test the applicability of this new method in the present study. 6-chloropurine **32** was treated with isopropylmagnesium chloride, followed by addition of ethyl iodide (Scheme 23), resulted in the formation of one

Chapter 4

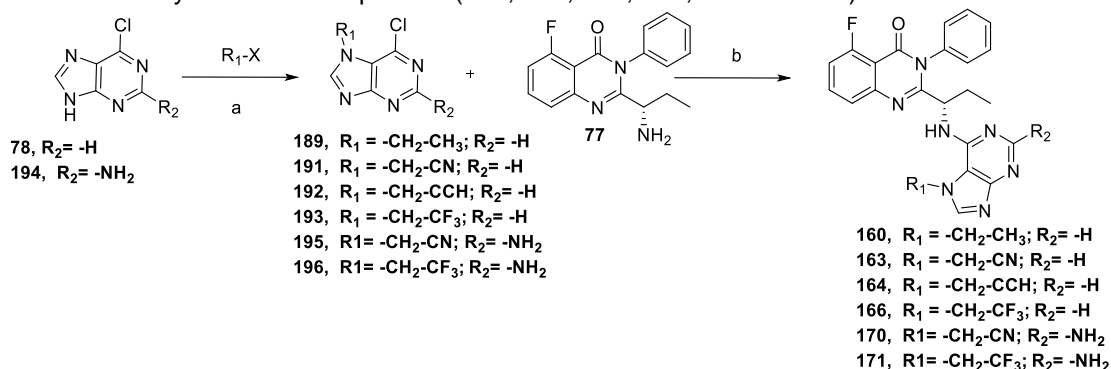
Scheme 21. The mechanism proposed by Van Deg Berge *et al*^{332,333} for regioselective *N*-alkylation of the more sterically hindered nitrogen (N-1) in 6-methylbenzimidazole **181**.



Scheme 22. The proposed mechanism for the regioselective *N*-alkylation of the more hindered N-7 of purine



Scheme 23. Synthesis of compounds (**160**, **163**, **164**, **166**, **170** and **171**)



^aReagents and conditions: (a) *i*-PrMgCl (1.1 equiv), dry THF, 60 °C, 18 h, yields 31- 62%; (b) DIPEA (10 equiv), *tert*-butanol, 100 °C, 72 h, yields 6- 41%.

regioisomer in 37% yield. The identity of the regioisomer was confirmed by comparison its ¹H and ¹³C chemical shifts along with literature data reported for 6-chloro-N-7-ethylpurine **189** and 6-chloro-N-9-ethylpurine **190** (Table 40)³³⁴. The resulting spectra were in good agreement to literature values of N-7 regioisomer **189**. This suggested that this reaction is completely regioselective and gives the desired, more sterically hindered N-7-isomer. On

the other hand, the undesired N-9-regioisomers was not detected by TLC, LCMS and NMR.



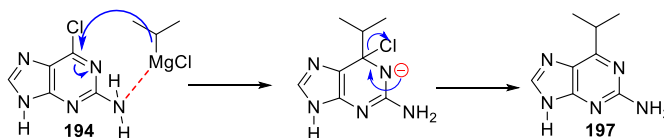
Table 40. Comparison the chemical shifts (ppm) of the carbon atoms in an unidentified regioisomer with literature data reported for 6-chloro-N-7-ethylpurine **189** and 6-chloro-N-9-ethylpurine **190**³³⁴.

Carbon	N-7-regioisomer 189 (literature value)	Unidentified regioisomer	N-9-regioisomer 190 (literature value)
C-11	16.7	17.25	15.20
C-10	41.8	42.30	39.47
C-5	121.8	122.34	131.21
C-6	142.45	141.9	147.40
C-8	150.5	150.97	149.27
C-2	151.5	151.97	151.59
C-4	161.6	162.12	152.02

Encouraged by this excellent result, this regioselective alkylation method has been extended to synthesise a variety of N-7 substituted purine derivatives (Scheme 23). Alkylation of 6-chloropurine with bromoacetonitrile and propargyl bromide provided the desired nitrile **191** and propargyl **192** derivatives in 44% and 31% yields, respectively (Scheme 23). In both cases, exclusively one regioisomer was detected *via* TLC, LC-MS and NMR. Best yield of N-7-substituted purine (62%) was obtained when using 2,2,2-trifluoroethyl trifluoromethanesulfonate as an alkylating reagent to afford the trifluoroethylated intermediate **193**.

In the preparation of the 2-aminopurine final compounds **170** and **171**, 2-amino-6-chloropurine **194** was chosen as a starting material, instead of 6-chloropurine **78**. Accordingly, **194** was treated with a 1.1 equivalent of isopropylmagnesium chloride, followed by addition of bromoacetonitrile and 2,2,2-trifluoroethyl trifluoromethanesulfonate to give **195** and **196** in 14% and 6% yields, respectively (Scheme 23). Low yields of the N-7 substituted purines obtained when 2-amino-6-chloropurine was used as a starting material in contrast to 6-chloropurine, this was attributed to two reasons. First, formation of significant quantity of the side product **197**, resulting from nucleophilic displacement of 2-amino-6-chloropurine **194** with the isopropyl group from the Grignard reagent (Scheme 24). Second, N-7 selectivity was reduced, with a small amount of N-9 substituted regioisomer were detected in these cases, where N-7/N-9 selectivity was reduced from 25:1 to 5:1, when changing the starting material from 6-chloropurine to 2-amino-6-chloropurine. This result is consistent with data reported by Chen *et al*³¹ which demonstrated that the yield and regiochemistry were diminished upon the regioselective alkylation of 2-substituted-6-chloropurine compared to the 6-chloropurine **78**.

Scheme 24. Proposed mechanism for the nucleophilic displacement of 6-chloro group in the 2-amino-6-chloropurine **194** by the Grignard reagent and formation of the 6-isopropylpurine side product **197**



Nucleophilic attack of amine **77** on N-7-substituted purine **195** and **196** in the presence of DIPEA in *tert*-butanol yielded final compounds **170** and **171**, respectively (Scheme 23). The 2-aminopurine-containing compounds **170**

and **171** were obtained in poor yield (9% and 6%, respectively) (Scheme 23), compared to their des-amino analogues **163** and **166** (37% and 23% respectively), which can be attributed to the low solubility of the starting purines **195** and **196** in the *tert*-butanol.

4.4.3 Biology Section

The target compounds were screened by GSK for their *in vitro* inhibitory activity against the four isoforms of class I PI3K (Table 41). In this SAR study, idelalisib (**8**) was used as a reference inhibitor and displayed an IC₅₀ value of 11 nM against PI3K δ .

Disappointingly, all of the compounds in Table 41 showed poor or no inhibitory activities against the four isoforms of class I PI3K. Compared to the control compound (idelalisib **8**), these compounds were much less potent inhibitors of PI3K δ , where most of them were at least 1000-fold less active than idelalisib **8** against PI3K δ . Taken together, this SAR study indicates that the substitution at the N-7 position of the purine ring produced a detrimental effect on the PI3K δ potency. It is noteworthy to mention that the compounds **166** and **171** bearing trifluoroethyl group in the purine hinge binder showed better activity against PI3K δ (IC₅₀ values of 2.80 and 2.22 μ M) compared to the rest of the compounds in this series. The reason for the improvement in PI3K δ potency of the trifluoroethyl analogues is not clear. Moreover, the acetylene-containing compound **164** was also found to display PI3K δ inhibitory potency in the low micromolar range (IC₅₀= 5.5 μ M).

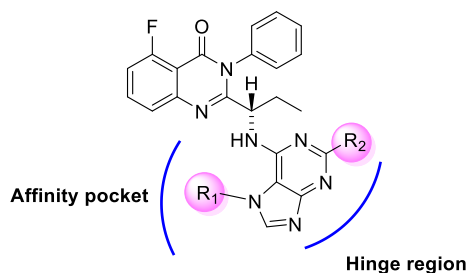


Table 41. Biological evaluation and isoform selectivity for PI3K δ for compounds (**8**, **156-160**, **163-166**, **170** and **171**).

Compd	R ₁	R ₂	Isoform potency ^{a,b} IC ₅₀ (nM)			
			PI3K δ	PI3K α	PI3K β	PI3K γ
8	-H	-H	11	14000	2800	56
156		-H	>28000	>28000	>28000	>28000
157		-H	11000	>28000	>28000	>28000
158		-H	22000	>28000	>28000	>28000
159		-H	22000	>28000	>28000	>28000
160		-H	>28000	>28000	>28000	>28000
163		-H	14000	>28000	>28000	>28000
164		-H	5500	>28000	>28000	17500
165		-H	>28000	>28000	>28000	>28000
166		-H	2800	>28000	>28000	11000
170		-NH ₂	10000	>28000	>28000	22000
171		-NH ₂	2225	>28000	>28000	7000

^aPotency against the different PI3K isoforms is given as IC₅₀ values (n = 2). The standard errors were not provided by GlaxoSmithKline (GSK). ^bThe potency threshold for the PI3K δ assay is \sim IC₅₀ 1 nM due to substrate concentration.

4.4.3.1 Reasons for the poor activity of the series of N-7-substituted purine derivatives

There are two possible reasons for the poor PI3K activity of idelalisib derivatives bearing a new substituent in the N-7 position of the purine ring.

4.4.3.1.1 Loss of hydrogen bond donor (NH-9)

As previously discussed in Section 4.2, NH-9 of idelalisib (**8**) acts as a hinge binder by donating a hydrogen bond to the backbone oxygen atom of Glu⁸²⁶ (Figure 83). However, the N-7-substituted purine derivatives of idelalisib lacks the hydrogen donor necessary to form the second hydrogen bond with the hinge. Thus, one could hypothesize that the absence of this hydrogen bond could explain the sudden loss of activity of this series of N-7 substituted purine derivatives. However, several studies have provided evidence that this hypothesis was unlikely to be true. For example, Novartis³²⁴ have reported a PI3K δ inhibitor **198** with IC₅₀ value of 150 nM (Table 42). The purine ring of **198** forms a bidentate hydrogen bond interaction with the hinge region between the hydrogen bond acceptor purine N-3 and the amide backbone of Val⁸²⁸ and the hydrogen bond donor NH-9 of the purine to carbonyl backbone of Glu⁸²⁶. Surprisingly, removing the hydrogen bond donor by replacing the NH-9 of purine with a sulphur atom **199**, increased potency at PI3K δ by about 20-folds (Table 42), which suggested that that the hydrogen bond made by NH-9 of the purine ring is not crucial for PI3K δ activity.

Taken together, findings from Novartis³³⁵ study suggested that the absence of the hydrogen bond donor (NH-9) of the purine hinge-binding group has absolutely no effect on PI3K δ activity. Moreover, they uncovered that a single hydrogen bond acceptor (N-3) of the purine hinge binder is enough to achieve a satisfactory inhibition of PI3K δ . These examples rule out the lack of the hydrogen bond donor (NH-9) as a main factor in the significant loss of PI3K δ potency of this series of N-7-substituted purine derivatives and suggests that there is alternative reason for the activity loss.

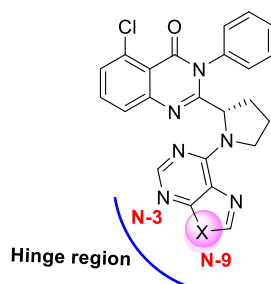


Table 42. Biological evaluation for PI3K δ for compounds **198** and **199** described in WO 2014/128612 A1 study³²⁴.

compd	-X-	PI3K δ IC ₅₀ (nM)
198 ³²⁴	-NH-	150
199 ³²⁴	-S-	7

4.4.3.1.2 Steric clash with the gatekeeper Ile⁸²⁵ side chain

Unfavourable steric clash between the newly added bulky substituent at the N-7 position of purine and the isoleucine (Ile⁸²⁵) gatekeeper, provides a possible explanation for the observed loss in PI3K δ potency³³⁶. As mentioned in the previous chapter, the gatekeeper residue is present in all kinases^{320,337}, which is situated at the entrance of the affinity pocket and plays a role in controlling the sensitivity of a wide range of kinase inhibitors^{323,336}. Kinases that have small residues (Gly, Ala, Thr, Val or Cys) at this position, can be targeted by inhibitors from structurally diverse chemical classes. Whereas, kinases which have a bulky side chain (Ile, Met or Glu) at the gatekeeper position are widely resistant, because of steric hindrance¹⁴². PI3K δ has a bulky isoleucine gatekeeper which limits accessibility to the affinity pocket (Figure 93). It was hypothesized that the steric clash between the N-7 substituent and the gatekeeper Ile⁸²⁵ displaces N-7 substituted purine derivatives from their optimal orientation (Figure 94), where these compounds are oriented in such way that the N-7 substituent escapes the steric clash with the gatekeeper Ile⁸²⁵, which in turn disrupts the hydrogen bonding between

the purine ring and the hinge region^{338,339}, this consequently results in a significant loss in PI3K δ potency (202- to 2500-fold).

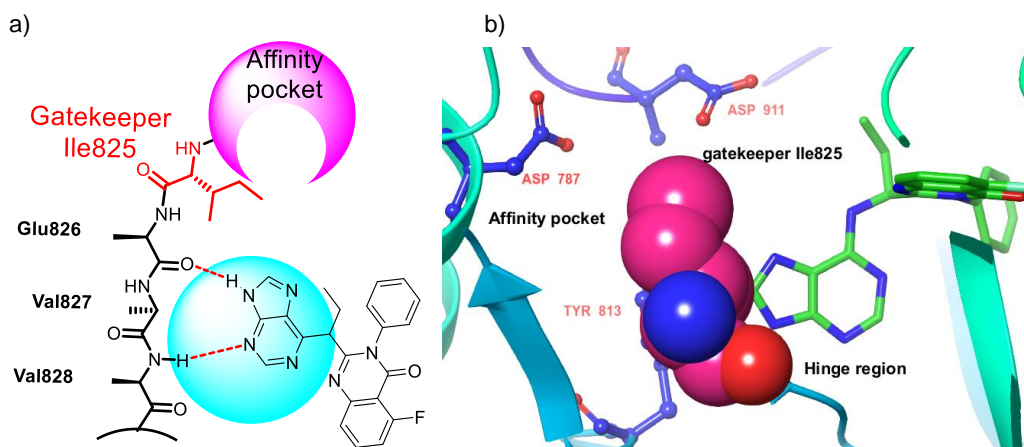


Figure 93. a) Schematic representation of idelalisib (**8**) binding interactions in the binding site of PI3K δ . The gatekeeper residue Ile⁸²⁵ (highlighted in red) limits the accessibility to the affinity pocket. b) Crystal structure of murine PI3K δ (PDB code 4XE0) with idelalisib (**8**) bound, highlights the gatekeeper Ile⁸²⁵ (represented by a space-filling model) that is located between the affinity pocket and the hinge region, where it restricts the access to the affinity pocket.

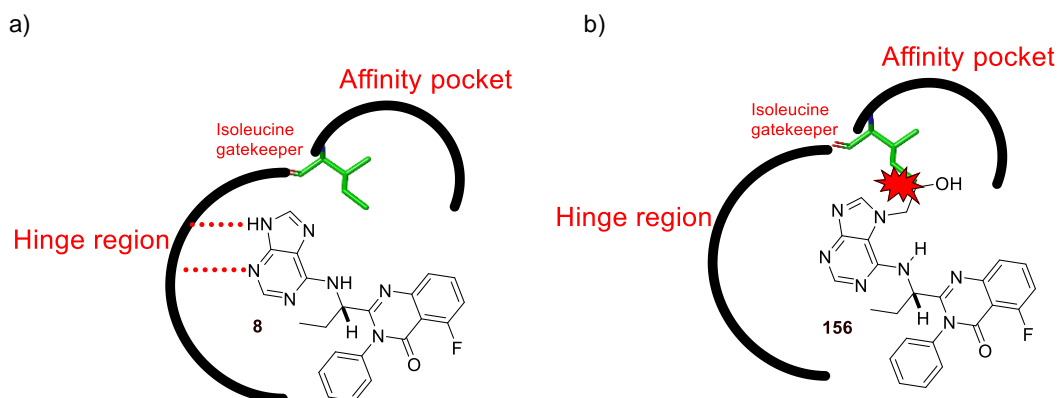


Figure 94. a) Idelalisib-PI3K δ interactions are depicted by a chemical structure, the gatekeeper residue (Ile⁸²⁵) (highlighted in green) controls the accessibility to the affinity pocket. The chemical structure depicts the purine ring that engages in crucial hydrogen bonds to the hinge region. Dashed red lines represent the proposed hydrogen bonds with the hinge region. b) Compound **156**-PI3K δ is depicted by a chemical structure, Ile⁸²⁵ obstructs access to the affinity pocket and results in serious steric clash with the hydroxyethyl group at the N-7 position of the purine ring, therefore hinders crucial hydrogen bond interaction with the hinge region, leads to compound **156** being more than 2500-fold less potent than idelalisib (**8**).

4.4.3.2 Docking study

To verify the hypothesis discussed above and to rationalize the observed PI3K δ activities for all reported compounds, docking analysis were conducted to determine the binding mode of this series of compounds in the

active site of the PI3K δ enzyme, compound **156** was used as an example. (Figure 95b) shows that compound **156** did not dock into the active site of PI3K δ like idelalisib (**8**) (Figure 95a). The introduction of the bulky substituent at N-7 position of the purine ring might make steric clashes with the gatekeeper Ile⁸²⁵ and could be a reason why these compounds were unable to bind into the active site. Therefore, no interaction was observed between the purine ring of compound **156** and the hinge region of PI3K δ (Figure 95b), the absence of this interaction is suggested to be responsible for the loss of activity of these series of compounds as compared to idelalisib (**8**).

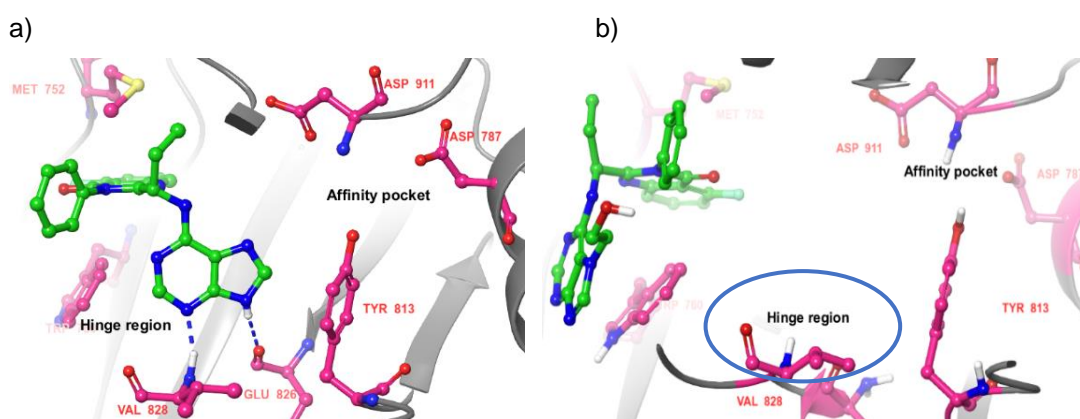


Figure 95. a) Crystal structure of murine PI3K δ (PDB code 4XE0) with idelalisib (**8**) bound. b) compound **156** docked into the PI3K δ -model (generated from PDB 4XE0), it reveals that the purine ring of compound **156** fails to form hydrogen bond with the hinge region of PI3K δ active site as in idelalisib (**8**). The missing hinge region is marked by a blue circle.

4.4.3.3 Clinical example of the gatekeeper influences inhibitor-kinase interaction resulting in significant effect on inhibitory activity

The two tyrosine kinase inhibitors (imatinib **200** and ponatinib **201**) give a relevant example of the significant role played by the gatekeeper residue in influencing the biological activity of kinase inhibitors. Imatinib (**200**) (Figure 96a) is a first generation ATP-competitive inhibitor of BCR-ABL, approved for the treatment of chronic myeloid leukaemia (CML)^{340,341}, imatinib (**200**) has shown sub-micromolar inhibitory activity (IC₅₀ value of 100 nM) against the

wild type of BCR-ABL expressed in Ba/F3 transfected cells (Table 43), which has a threonine (Thr315) in the gatekeeper position (Table 43)^{342,343}. However, it was found to be poorly active (IC_{50} = 13200 nM) against the T315I mutant form of BCR-ABL, in which the Thr315 gatekeeper is replaced by a more bulky isoleucine (Table 43)³⁴²⁻³⁴⁴, this is due to the steric clash created between the side chain of isoleucine with a hydrogen atom of the exocyclic amino group of imatinib (**200**) (Figure 96c), precludes imatinib (**200**) from binding to the active site, results in a significant loss of activity^{345,346}.

Table 43. Biological activity of imatinib (**200**) and ponatinib (**201**) against the wild-type and T315I-mutated BCR-ABL expressed in Ba/F3 transfected cells, highlights chemical nature of the linkers connecting the hinge-binding group to the affinity pocket binder in both compounds³⁴³.

Compd	Wild-type BCR-ABL		BCR-ABL ^{T315I}		Type of linker
	IC ₅₀ (nM)	gatekeeper	IC ₅₀ (nM)	gatekeeper	
Imatinib (200) ³⁴³	100.0	Thr315	13200.	Ile315	amine (tetrahedral and flexible)
Ponatinib (201) ³⁴³	1.1	Thr315	11.0	Ile315	Acetylene (rigid and linear)

To overcome imatinib-resistant BCR-ABL mutation, the third-generation BCR-ABL inhibitor ponatinib (**201**) (Figure 97a) has been developed, which demonstrated excellent inhibitory activity against BCR-ABL^{T315I} (IC_{50} value of 11 nM) with 1200-fold more activity than imatinib (**200**) (Table 43)^{342,343}. Liu *et al*³⁴⁰ suggested that the plausible explanation for the high activity observed for ponatinib (**201**) is the ability of the acetylene linker to escape the steric contact with isoleucine gatekeeper due to its small size (Figure 97b)^{339,340}.

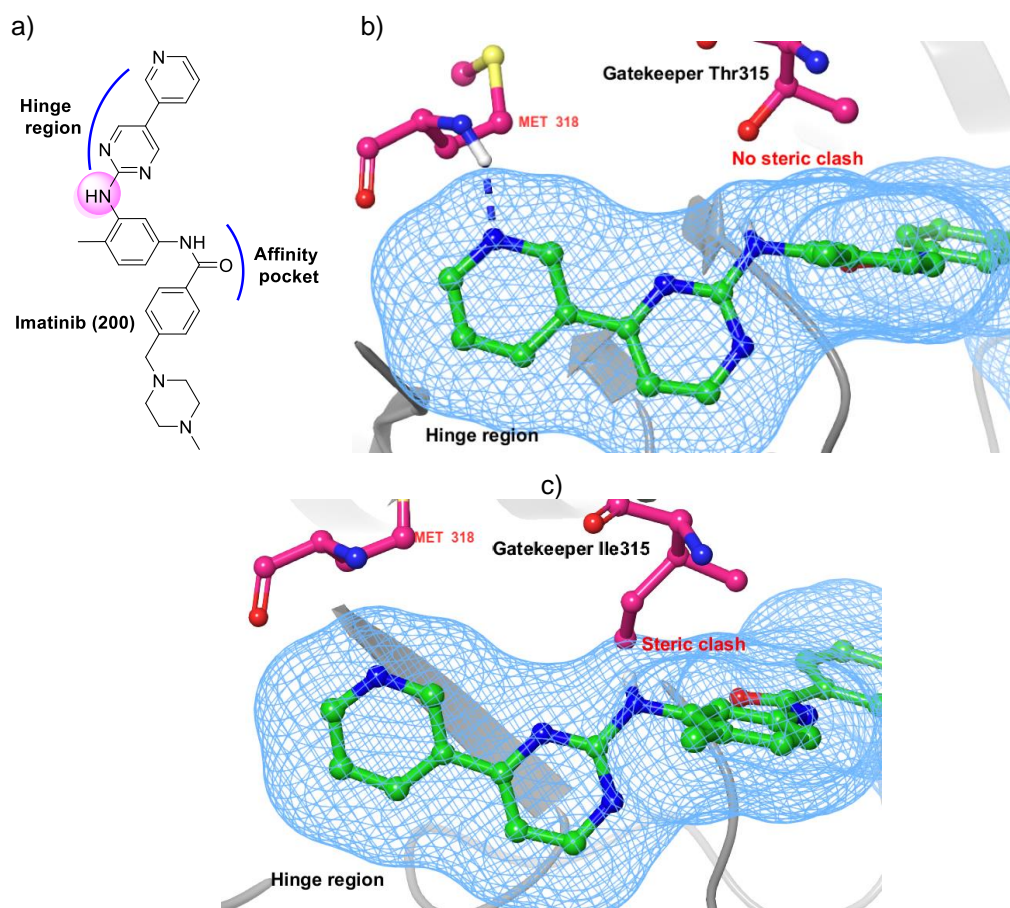


Figure 96. a) The first-generation BCR-ABL inhibitor imatinib (**200**), highlighted the exocyclic amine (in pink). b) Crystal structure of murine wild-type BCR-ABL (PDB code 1IEP) with imatinib (**200**) bound. c) Wild-type BCR-ABL has a small gatekeeper residue (Thr³¹⁵), which does not cause a steric hindrance with the exocyclic amine of imatinib (**200**). c) The mutation of the gatekeeper Thr315 to the bulkier Isoleucine (Ile³¹⁵) leads to steric clash with the exocyclic amine of imatinib (**200**), which explains why imatinib (**200**) is 130-fold less potent against T315I-mutant BCR-ABL compared to the wild-type enzyme. T315I mutation was performed computationally.

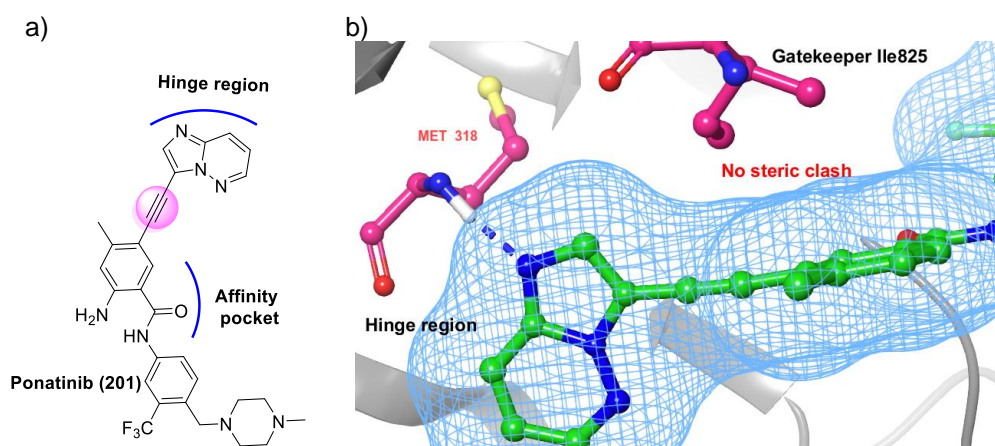


Figure 97. a) The third-generation BCR-ABL inhibitor ponatinib (**201**), highlights the acetylene linkage between the pyrrolopyridazine hinge binder and the diarylamide side chain that occupies the affinity pocket. b) Crystal structure of murine T315I-mutant Bcr-AbL (PDB code 3IK3) with ponatinib (**201**) bound, ponatinib (**201**) avoids the steric clash with the gatekeeper Ile⁸²⁵ residue, due to a lesser sterically demanding acetylene linker, which explains why ponatinib (**201**) is only 10-fold less potent against T315I-mutant BCR-ABL compared to the wild-type enzyme.

4.4.3.4 The reason for the steric clash between the series of N-7-substituted purine derivatives and the gatekeeper Ile⁸²⁵

Based on the example of imatinib (**200**) and ponatinib (**201**), it seems likely that the poor PI3K δ potency of the compounds described in this chapter was due to the steric clash created between the gatekeeper Ile⁸²⁵ and the ethyl linker connecting the purine hinge binder to the terminal functional groups (Figure 98a). The ethyl linker adopted a three-dimensional tetrahedral geometry with high degree of flexibility (Figure 98b)³⁴⁷; thus it could not pass the narrow channel embraced by gatekeeper Ile⁸²⁵ to reach the affinity pocket, resulted in an undesirable steric clash.

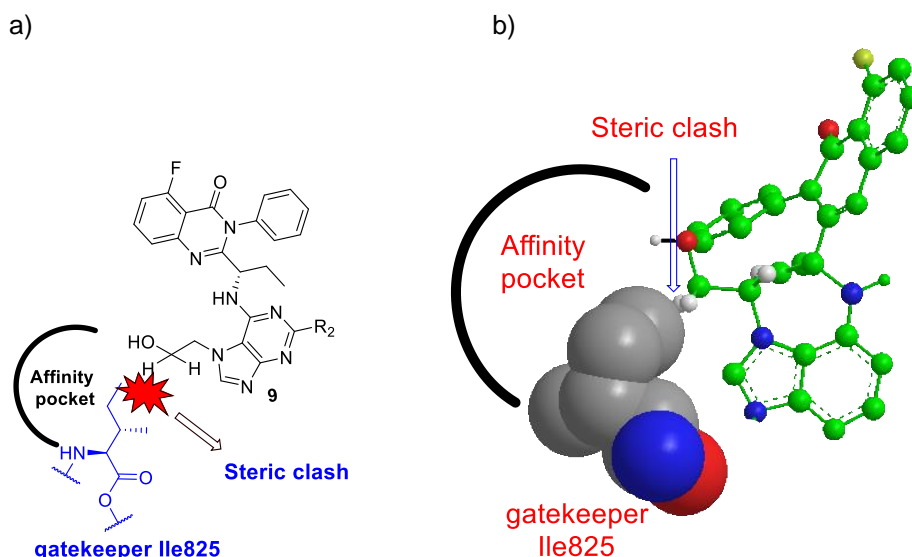


Figure 98. a) 2D-representation of the alcohol compound **156** binding interaction in the active site of PI3K δ . Highlights the proposed steric clash between the gatekeeper Ile⁸²⁵ with the tetrahedral ethyl linker b) 3D-representation of the alcohol compound **156** binding interaction in the active site of PI3K δ . The three-dimensional chemical structures of compound **156** and gatekeeper isoleucine were generated using Chem3D Ultra XML. It highlights the proposed steric clash between the tetrahedral ethyl linker and the gatekeeper Ile⁸²⁵, preventing the optimal fit of compound **156** into the PI3K δ binding site. The gatekeeper Ile⁸²⁵ is represented as a space-filling model to study steric hindrance.

Extensive literature search relating to PI3K δ inhibitors strongly supports the above mentioned hypothesis^{144,145,154,155}, where there have been no reports that tried to use alkyl group as a linker to connect the hinge-binding scaffold with the terminal binding group. Instead of that, a survey of PI3K δ inhibitors

Chapter 4

demonstrates that the linker used to connect between the hinge-binding moiety and the terminal functional group is exclusively linear acetylene or planar aryl group. For example, in a series of highly potent quinazolinone derivatives **152**, **202** and **203** (Table 44), acetylene linker was used to place nitrogen heterocycles within the affinity pocket (Figure 99), which was reflected by a more than 200-fold increase in PI3K δ activity as compared to their parent compound **151** (Table 44).

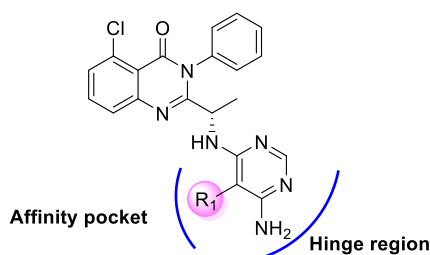


Table 44. Biological evaluation and isoform selectivity for PI3K δ for compounds (**152**, **202** and **203** reported by Patel *et al*¹⁵⁵), highlights the acetylene linker connecting the affinity pocket-binding groups (heteroaryl rings) to the aminopyrimidine hinge binder. The unsubstituted analogue **151** is used as a reference.

compd	R ₁	PI3K δ IC ₅₀ (nM)	Isoform selectivity		
			δ/α	δ/β	δ/γ
151 ¹⁵⁵	-H	99	1600	120	320
152 ¹⁵⁵		0.3	1500	260	230
202 ¹⁵⁵		0.5	620	240	100
203 ¹⁵⁵		0.4	3200	52	512

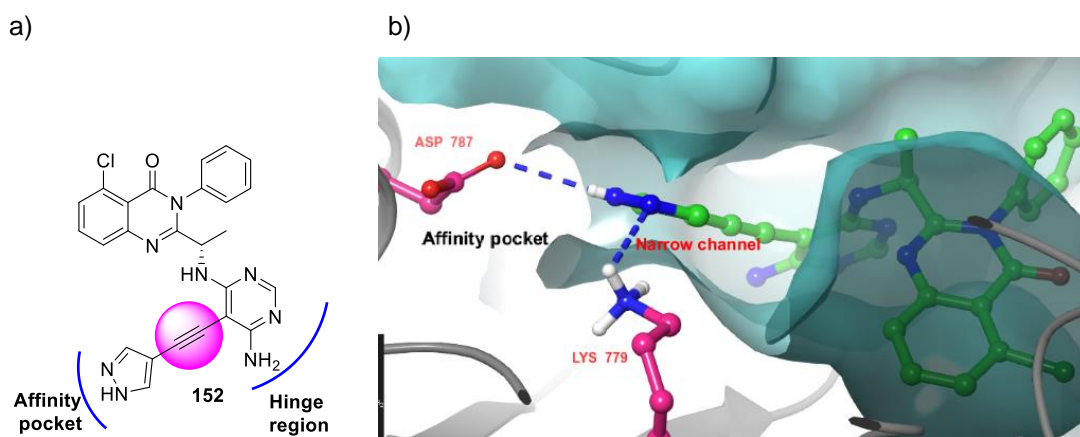


Figure 99. a) Compound **152**, highlights the acetylene linker connecting the affinity pocket-binding group (pyrazole) to the aminopyrimidine hinge-binding core. b) Crystal structure of murine PI3K δ (PDB code 5I6U) with compound **152** bound, acetylene linker can pass the narrow channel embraced by gatekeeper Ile⁸²⁵ and reach the affinity pocket. Blue dashed lines represent the proposed hydrogen bonds that take place between the pyrazole ring with Asp⁷⁸⁷ and Lys⁷⁷⁹ in the affinity pocket.

Furthermore, in the pyrazolopyrimidineamine derivative **10** reported by Berndt *et al*¹⁴⁹. The use of the rigid phenyl linker (Figure 100) directs the functional groups (hydroxyl) into the affinity pocket shows 186-fold improvement in PI3K δ potency compared with the parent compound **9** (Table 45).

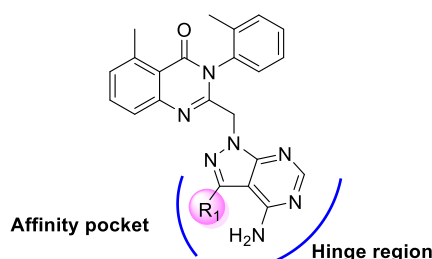
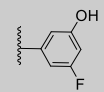


Table 45. Biological evaluation and isoform selectivity for PI3K δ for compound **10**, highlights the phenyl linker connecting the affinity pocket-binding groups (hydroxyl and fluorine) to the pyrazolopyrimidine hinge binder. The unsubstituted analogue **9** is used as a reference.

compd	R ₁	PI3K δ IC ₅₀ (nM)	Isoform selectivity		
			δ/α	δ/β	δ/γ
9 ¹⁴⁹	-H	130	1538	123	469
10 ¹⁴⁹		0.7	1857	314	47

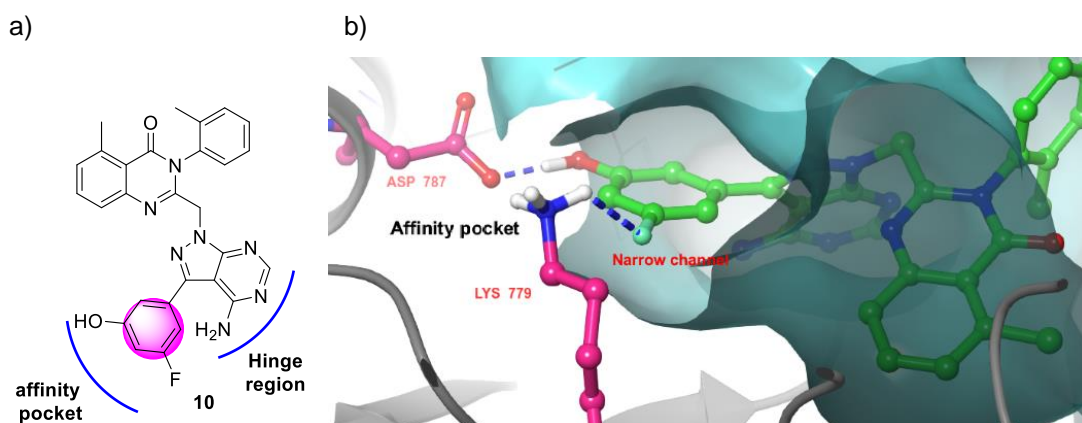


Figure 100. a) Compound **10**, highlights the phenyl linker connecting the affinity pocket-binding groups (hydroxyl) to the pyrazolopyrimidineamine hinge-binding core. b) Crystal structure of murine PI3K δ (PDB code 2WXG) with compound **10** bound. phenyl linker can pass the narrow channel embraced by gatekeeper Ile⁸²⁵ and reach the affinity pocket. Blue dashed lines represent the proposed hydrogen bonds that take place between the phenol group in compound **10** with Asp⁷⁸⁷ and Tyr⁸¹³ in the affinity pocket.

The previous findings clearly highlight the important role of the linker geometry for PI3K δ potency, as both the planar aryl and linear acetylene linkers have the ability to deliver the functional group into the affinity pocket bypass the gatekeeper Ile⁸²⁵. Therefore, it was proposed to use a suitable rigid planar linker, in order to prevent the steric collision with the gatekeeper Ile⁸²⁵ and access the affinity pocket. This will be discussed in more detail in Chapter 5.

4.5 Conclusion

This chapter has the same aim as the previous chapter, which was to attach a new functional group to the idelalisib (**8**) structure to gain access to the nearby unoccupied affinity pocket and achieve additional binding interactions, which may result in increased PI3K δ activity. As seen in Chapter 3, the incorporation of the polar functional groups into the exocyclic amine of idelalisib (**8**) resulted in a dramatic reduction in PI3K δ potency. It was hypothesized that changing the position of the functional group on idelalisib (**8**) structure can bring it into a good position for binding to the affinity pocket.

Thus, in this chapter, substituents containing polar functional groups was added at the N-7 position of the purine ring of idelalisib (**8**). For this purpose, a series of novel N-7-substituted purine derivatives of idelalisib have been designed, synthesized and evaluated for their PI3K δ activity with idelalisib (**8**) as a positive reference. Disappointingly, all compounds exhibited weak or no activity against PI3K δ with almost 200- to 2500-folds less active than idelalisib (**8**). Taken together, the results of Chapter 3 and 4 suggested that substitution of idelalisib (**8**) with a functional group at all possible positions resulted in a loss of activity (Figure 101), which could be attributed to the steric clash created between the gatekeeper Ile⁸²⁵ and the extra functional group, resulted in the loss of the most favourable geometry for hydrogen bond interaction between the purine ring and the hinge region. The cause of the steric clash may be attributable to high flexibility and/or tetrahedral geometry of the alkyl linker connecting the hinge-binding scaffold to the terminal functional group. Hence, replacement of alkyl linker by a more rigid aryl or acetylene linker could avoid any steric overlap with the gatekeeper Ile⁸²⁵ and ultimately improve the PI3K δ activity.

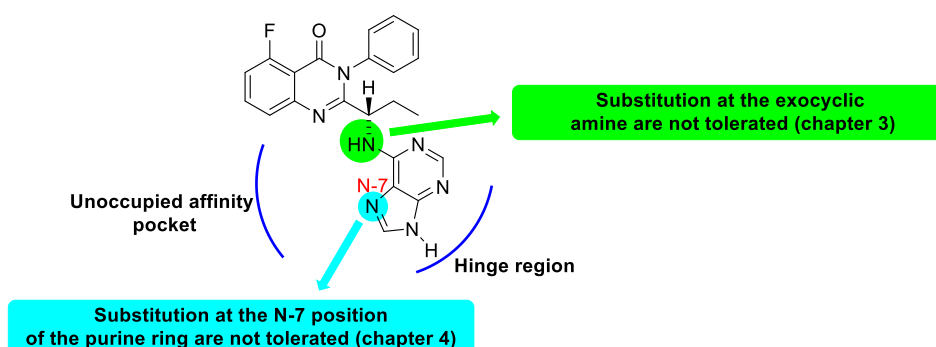


Figure 101. The selective PI3K δ inhibitor idelalisib (**8**), highlights the influence of new substituent in different positions of idelalisib (**8**) on PI3K δ inhibitory activity. SAR studies discussed in Chapter 3, revealed that substitution of idelalisib (**8**) at the exocyclic amine results in loss of PI3K δ activity, whereas SAR studies discussed in Chapter 4, revealed that substitution of idelalisib (**8**) at the N-7 position of purine results in loss of activity.

Chapter 5 Design, Synthesis, biological evaluation and docking studies of pyrimidine derivatives as highly potent and selective PI3K δ inhibitors (propeller-shaped inhibitor)

5.1 Aim

As seen in the previous two chapters, substitution of idelalisib (**8**) on the exocyclic amine or the N-7 position of the purine ring resulted in a dramatic loss of PI3K δ inhibitory activity. This could be reasoned by the steric clash that might occur between the gatekeeper Ile⁸²⁵ and the tetrahedral alkyl linker connecting the affinity pocket-binding group to the purine hinge binding moiety. This may explain why alkyl linkers have not been in PI3K δ inhibitors (Figure 102b). Accordingly, in this chapter, it was proposed to use a planar linker to avoid the steric contact with the gatekeeper Ile⁸²⁵. Furthermore, subtle structural modification of the idelalisib (**8**) structure would be made by replacement of the purine hinge binder with the structurally similar aminopyrimidine.

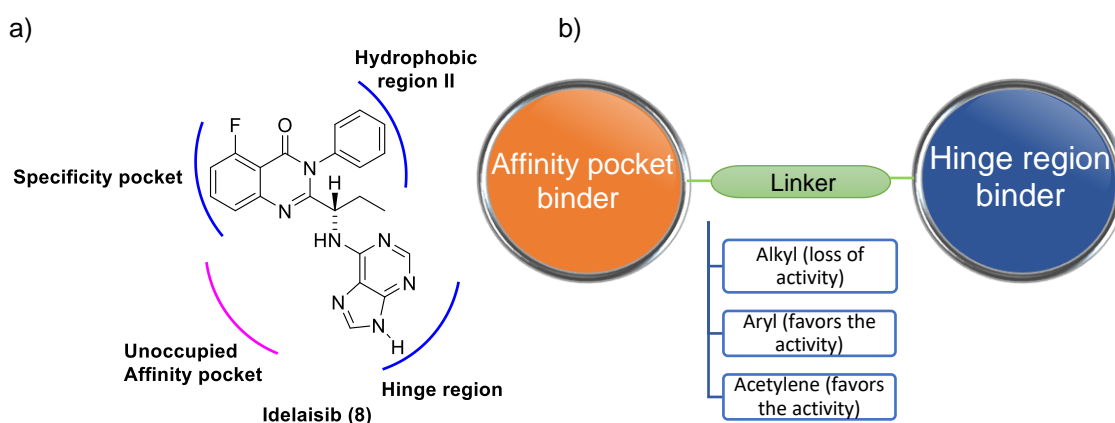


Figure 102. a) The selective PI3K δ inhibitor idelalisib (**8**) and its binding interactions at PI3K δ , highlighting the unoccupied affinity pocket; b) Schematic diagram displaying the three types of linkers (alkyl, aryl and acetylene) connecting the hinge binder to the affinity pocket-binding group in PI3K δ inhibitors, it shows that incorporation of an alkyl linker leads to a major loss of PI3K δ activity, whereas the introduction of aryl and acetylene linkers increased PI3K δ potency.

5.2 Types of the linker used in the previously reported PI3K δ inhibitors

Previous studies on PI3K δ inhibitors revealed that the design of highly potent PI3K δ inhibitors relies on the introduction of a planar aryl or linear acetylene linker between the hinge-binding scaffold and the affinity pocket-binding group.

5.2.1 Planar aryl linker

An interesting study was published by Erra *et al*¹⁵⁴ describing a series of pyrrolotriazinone compounds and their activity as PI3K δ inhibitors. Some of the compounds were reported to be highly potent with IC₅₀ in the sub-nanomolar range (Table 46). These active compounds consist of aromatic or heteroaromatic linkers connecting the affinity pocket-binding groups to the hinge-binding scaffold (pyrrolopyrimidine). For example, compound **204** interacts with the affinity pocket *via* hydroxyl and methanesulfonamido groups, which are linked to the hinge binder through a phenyl spacer (Figure 103). On the other hand, Compounds **205** and **206** consist of pyrazole and indole rings, respectively, which simultaneously act as a linker and affinity pocket binding moiety (Table 46).

5.2.2 Linear acetylene linker

Although the use of acetylene group in medicinal chemistry is not popular; it has been widely exploited as a linker in the development of PI3K δ inhibitors targeting the affinity pocket. Berndt *et al*¹⁷³ reported the design of a novel quinazolinone **11** with acetylene utilized as a linker to connect the hinge binding moiety (pyrazolopyrimidineamine) to the terminal functional group

(hydroxyl) (Figure 104). Compound **11** shows remarkable improvement (19-fold) in PI3K δ potency compared with the parent compound **9** (Table 47).

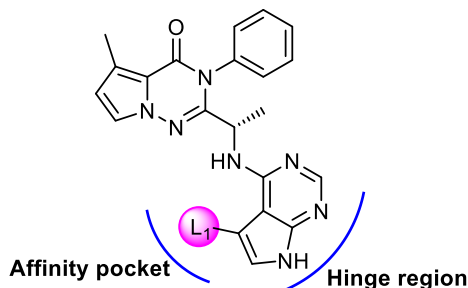
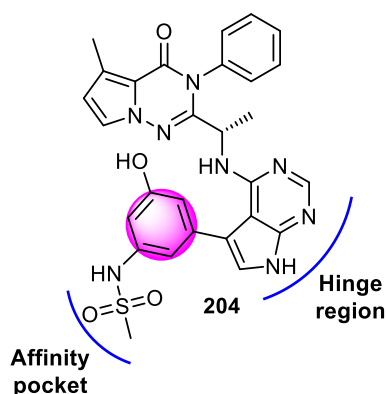


Table 46. Biological evaluation for PI3K δ for compounds (**204-206** reported by Erra *et al*¹⁵⁴), highlights the aryl/heteroaryl linkers and the functional groups that form hydrogen bond interactions with the affinity pocket.

compd	Linker (L ₁)	Functional group	PI3K δ IC ₅₀ (nM)
204 ¹⁵⁴		R ₁ = R ₂ =	0.2
205 ¹⁵⁴			0.4
206 ¹⁵⁴			0.2

a)



b)

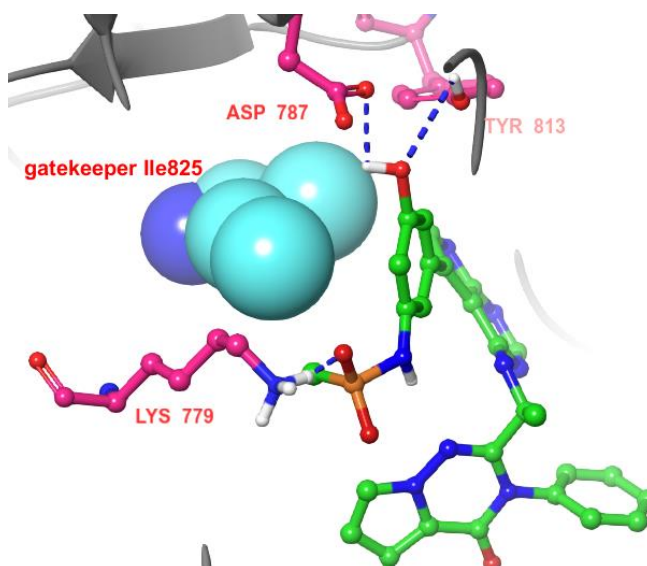


Figure 103. a) Compound **204**, highlights the phenyl linker connecting the affinity pocket-binding groups (hydroxyl and methanesulfonamido) to the pyrrolopyrimidine hinge binder. b) Crystal structure of human PI3K δ (PDB code 6G6W) with compound **204** bound. There is no apparent steric clash between the phenyl linker and the gatekeeper Ile⁸²⁵ (represented by a space-filling model). Blue dashed lines represent the proposed hydrogen bonds.

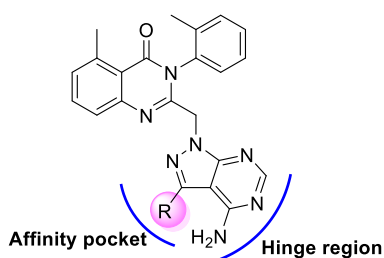
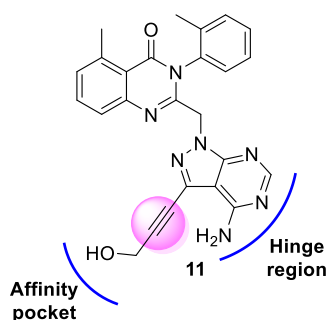


Table 47. Biological evaluation for PI3K δ for the acetylene-containing compound **11**, highlights the acetylene linker and the functional group (hydroxyl group) that forms hydrogen bond interactions with the affinity pocket. The unsubstituted analogue **9** is used as a reference¹⁷³.

compd	Linker (L ₁)	Functional group (R ₁)	PI3K δ IC ₅₀ (nM)
Reference 9 ¹⁷³		-	130
11 ¹⁷³			7

a)



b)

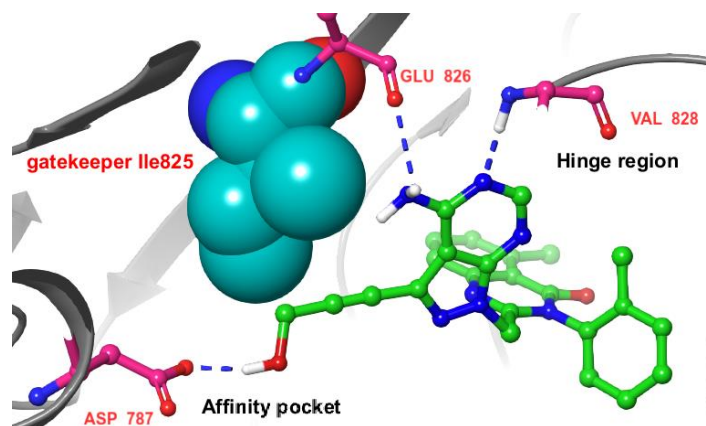


Figure 104. a) Compound **11**, highlights the acetylene linker connecting the affinity pocket-binding group (hydroxyl) to the pyrazolopyrimidine hinge-binding core. b) Crystal structure of murine PI3K δ (PDB code 2WXI) with compound **11** bound. There is no apparent steric clash between the acetylene linker and the gatekeeper Ile⁸²⁵ (represented by a space-filling model). Blue dashed lines represent the proposed hydrogen bonds.

5.3 Reasons for selection of planar aryl and linear ethynyl linkers in PI3K δ inhibitors

Although structurally the affinity pocket has a wide cavity, the entrance to the affinity pocket is narrow due to the presence of the gatekeeper Ile⁸²⁵. Using aryl rings and ethynyl linkers appears to prevent a steric contact with the gatekeeper Ile⁸²⁵. Aromatic rings adopt a planar geometry, whereas the ethynyl linker adopts a linear structure, thus they are able to traverse the gatekeeper Ile⁸²⁵ residue and allows the functional group to extend into the

affinity pocket leading to the increased PI3K δ activity (Figure 103b) (Figure 104b). Whereas the tetrahedral shape of the alkyl linker is more likely to experience a steric clash with the gatekeeper Ile⁸²⁵, that prevents the functional group entering the affinity pocket, resulting in a dramatic loss in PI3K δ potency. The affinity pocket resembles the letter box in that it has a deep bottom but it is only accessible via a narrow entrance (Figure 105). According to this, the linkers of the PI3K δ inhibitors need to be planar similar to a letter in order pass the narrow channel embraced by gatekeeper Ile⁸²⁵ to reach into the affinity pocket.

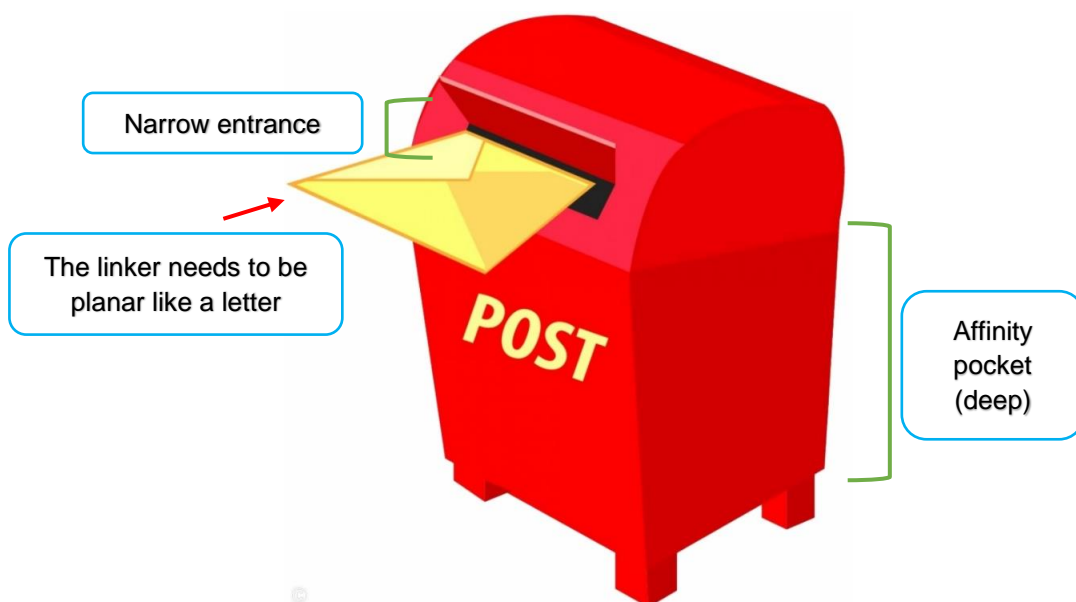


Figure 105. The affinity pocket resembles a letter box, where the access to the large cavity is highly restricted by the gatekeeper Ile⁸²⁵. As a result, the linker should have a planar geometry, just like a letter, to allow the inhibitor to enter the affinity pocket and make additional hydrogen bonds with the protein.

5.4 Medicinal chemistry strategy

In this medicinal chemistry effort, a new strategy was followed for a structural modification of the lead compound (idelalisib **8**), which was achieved by: 1) the replacement of the purine hinge-binding scaffold with a 4-aminopyrimidine ring, 2) decoration of this ring at position 5 with a variety of substituents able to target the affinity pocket.

5.4.1 Modification of the hinge-binding scaffold

The previous chapter has shown that the addition of the new substituent (affinity pocket binder) at the N-7 position of the purine ring in idelalisib (**8**) resulted in a dramatic drop in PI3K δ activity compared to the parent compound (idelalisib **8**), suggesting that the substitution of the purine hinge binder is not tolerated for PI3K δ inhibition. These disappointing results encouraged us to conduct structural optimisation of the hinge binding scaffold by replacing the purine ring with a 4-aminopyrimidine ring, which can be easily decorated with functional groups at the 5-position. This optimisation design strategy is based on the findings from Patel *et al*¹⁵⁵ study (Table 48), which reported that 5-substituted aminopyrimidine series (**151**, **161** and **162**) displayed greater than 250-fold increase in PI3K δ activity versus the unsubstituted compound **151**, suggesting that the 4-aminopyrimidine scaffold orients the 5-substituent into the right position to make new binding interactions within the affinity pocket. For instance, the crystal structure of

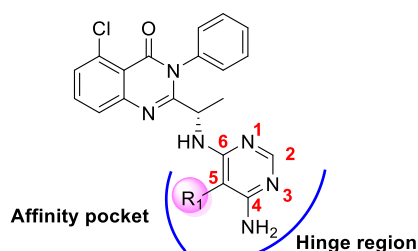


Table 48. Biological evaluation for PI3K δ for compounds (**151**, **161** and **162** reported by Patel *et al*¹⁵⁵), highlights the affinity-pocket binding groups (R₁) projected from the 5-position of 4-aminopyrimidine hinge-binding scaffold. The unsubstituted analogue **151** is used as a reference.

compd	R ₁	PI3K δ IC ₅₀ (nM)
151 ¹⁵⁵		99
161 ¹⁵⁵		0.4
162 ¹⁵⁵		0.1

PI3K δ in complex with compound **161** (Figure 106b) reveals that the nitrile group projected from the 5-position of the 4-aminopyrimidine core into the affinity pocket, where it makes a hydrogen bond interaction with the phenolic side chain of Tyr⁸¹³. Hence, in this chapter, a new series of PI3K δ inhibitors based on the 4-aminopyrimidine hinge binder was synthesized and evaluated for their PI3K δ inhibitory effect.

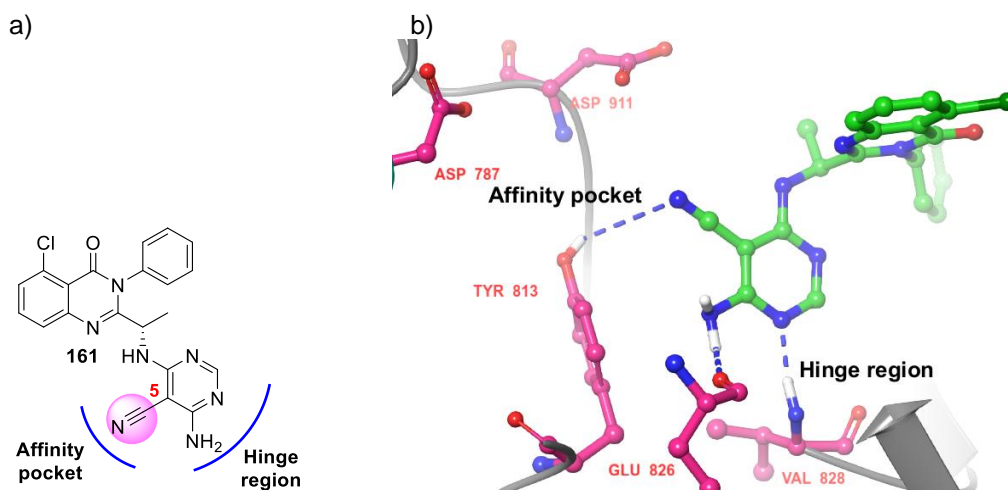


Figure 106. a) The nitrile-containing compound **161**, highlights the 4-aminopyrimidine carrying a nitrile group at position 5. b) Crystal structure of murine PI3K δ (PDB code 5I4U) with compound **161** bound, highlights the nitrile group that projects from the 5-position of the 4-aminopyrimidine core into the affinity pocket, making a hydrogen bond with Tyr⁸¹³. Blue dashed lines represent the proposed hydrogen bonds with the affinity pocket and hinge region.

5.4.2 Linker

As was previously mentioned, all of the reported PI3K δ inhibitors targeting the affinity pocket contained either a planar aryl or linear acetylene group as a linker to connect the hinge-binding scaffold with a terminal binding group (Table 49). A Study of the wide range of functional groups was conducted, with the aim of finding a novel planar linker for developing new potent PI3K δ inhibitors (Table 49). It was found that the amide group adopts a trigonal planar geometry, owing to the resonance between the lone pair on the amide nitrogen and the carbonyl pi orbital, which gives some double-bond character

to the C-N bond (Figure 107)^{348–350}. Consequently, the atoms comprising the amide and also those directly connected to it are forced to lie in the same plane.

Table 49. Examples of planar and linear functional groups, which can be used as linkers in the development of PI3K δ inhibitors.

Planar or linear linker	Use in PI3K δ inhibitors
Aryl group	Widely used
Acetylene group	Widely used
Amide group	Reported only in one PI3K δ inhibitor

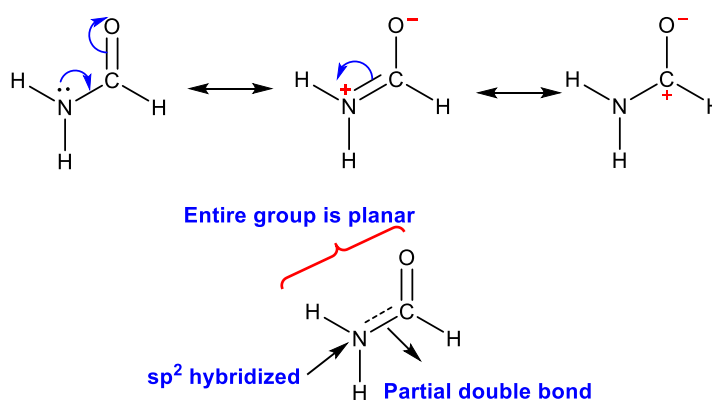


Figure 107. Resonance structures of amide. The delocalisation of the nitrogen lone pair into the pi system of the carbonyl group, results in a partial double bond between the nitrogen atom and the carbonyl carbon of the amide with the nitrogen atom being sp²-hybridized. Thus, the entire amide group tends to be planar.

Based on this idea, the present study reported the synthesis of a new class of PI3K δ inhibitors based on 4-aminopyrimidine scaffold with an amide linker to a terminal functional group that projects into the affinity pocket. To the best of authors' knowledge, compound **208** is the only PI3K δ inhibitor reported to have an amide linker (Figure 108)¹⁵⁴. The excellent PI3K δ activity displayed by compound **208** (IC₅₀ value of 0.2 nM), indicates that the use of an amide group as a linker could represent a promising strategy in the development of highly potent inhibitors of PI3K δ .

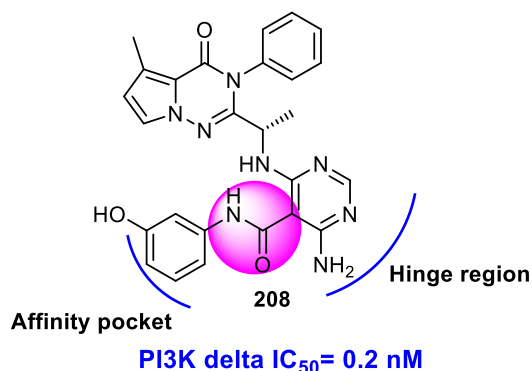


Figure 108. Structure and biological activity of the only PI3K δ inhibitor **208** reported to have an amide linkage between the aminopyrimidine hinge binder and the phenol group that occupies the affinity pocket¹⁵⁴.

5.4.3 Types of functional groups

In this project, a new approach is applied for designing compounds as potent PI3K δ inhibitors by exploring a variety of affinity pocket-binding groups (heteroaromatic, aromatic and aliphatic rings) some of them not commonly seen in the previously discovered PI3K δ inhibitors. The affinity pocket-binding groups used in this SAR study can be classified on the basis of their chemical structure into two groups: 1) five-membered heteroaromatic rings, 2) miscellaneous functional groups.

5.4.3.1 Five-membered heteroaromatic ring

Five-membered heterocycles were selected to explore the affinity pocket, because they successfully served as affinity pocket-binding groups for highly potent PI3K δ inhibitors in the past^{154,220}. In addition, only a small number of PI3K δ inhibitors have been reported with five-membered heterocycles acting as affinity pocket binders. An interesting study published by Erra *et al*¹⁵⁴ showed that extension of the pyrazole ring toward the affinity pocket offered a PI3K δ inhibitor **205** with IC₅₀ as low as 0.4 nM (Table 50). Whereas the change of a pyrazole for a *N*-methylpyrazole ring in the affinity pocket resulted in compound **209** with an IC₅₀ = 0.2 nM.

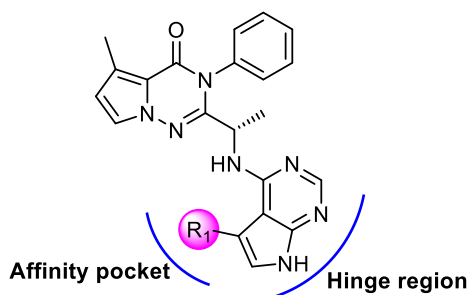


Table 50. Biological evaluation for PI3K δ for compounds **205** and **209** having five-membered heterocycles as the affinity pocket-binding group¹⁵⁴.

compd	Affinity pocket-binding group (R ₁)	PI3K δ IC ₅₀ (nM)
205 ¹⁵⁴		0.4
209 ¹⁵⁴		0.2

Based on the findings of Erra *et al*¹⁵⁴ study, In this research, three regioisomers of *N*-methylpyrazole derivatives (**210-211**) were synthesized with an aim to obtain high PI3K δ potency (Table 51). However, the synthesis of the pyrazole derivative **212** was planned but due to the challenges in the process of synthesis it was not made.

In addition, molecular docking studies have been performed to identify the binding interactions of a plethora of five-membered heterocyclic derivatives in the active site of the PI3K δ enzyme. The docking study results revealed that, among all 25 compounds docked against PI3K δ , 5-methyl-1,3,4-thiadiazole **214** and isoxazole **215** derivatives could form hydrogen bond interactions with the residues located within the affinity pocket. In both cases, the *N*-3 atom of the thiadiazol ring in **214** (Figure 109b) and the oxygen atom of the isoxazole ring in **215** acts as hydrogen bond acceptors to the primary amine of Lys⁷⁷⁹. Whereas the remaining 23 heterocyclic derivatives did not form any key hydrogen bond with the affinity pocket. Hence, based on these

docking results, only compounds **214** and **215** were selected to test for their *in vitro* activity against PI3K δ (Table 51).

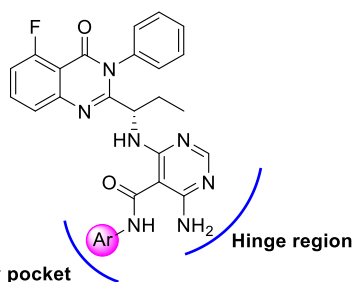
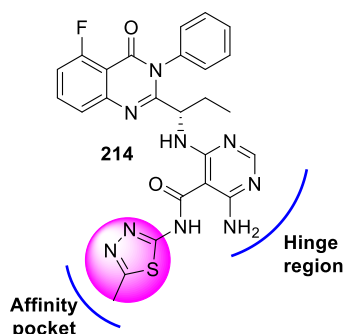


Table 51. Structure of the proposed compounds (**210-215**) having five-membered heterocycles as the affinity pocket-binding group.

compd	R ₁
210	
211	
212	
213 was not synthesized	
214	
215	

a)



b)

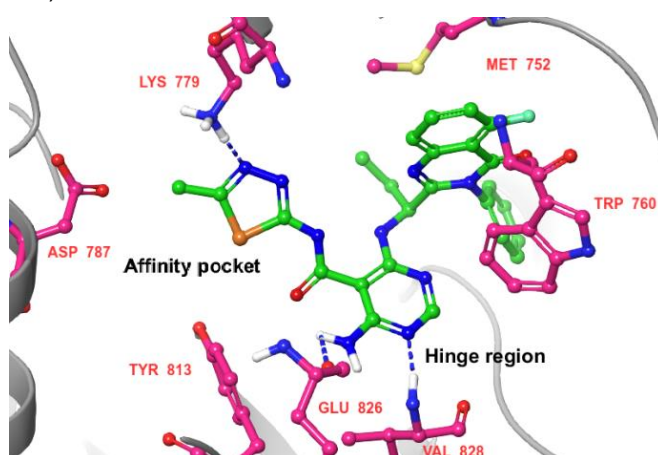


Figure 109. a) Compound **214**, highlights the 5-methyl-1,3,4-thiadiazole ring (in pink) that extends into the affinity pocket. b) Compound **214** docked into the PI3K δ model (generated from PDB code 5I6U). In the affinity pocket, the thiadiazole ring forms a hydrogen bond to the amino group of Lys⁷⁷⁹ through the *N*-4 nitrogen atom. Blue dashed lines represent the proposed hydrogen bonds with the affinity pocket and hinge region.

5.4.3.2 Miscellaneous functional groups

In addition to the heterocyclic derivatives, it was suggested to develop a new approach which consists of exploring the affinity pocket with different functional groups (Table 52), taking into account the size of the pocket as well as the chemical nature of the amino acids comprising it.

5.4.3.2.1 Phenyl group

One of the objectives of this chapter was to identify the amino acids and the type of interactions (hydrogen bond, cation-pi or pi-pi) involved in the binding between the affinity pocket of PI3K δ and the ligands used in this study. Phenyl derivative **216** (Table 52) lacking the heteroatoms has been synthesized to test whether the hydrogen bonding groups has any importance towards the activity of the heterocyclic derivatives (**210-215**) listed in Table 51. As shown in Figure 110, the affinity pocket consists of 5 residues, one of these residues is Tyr⁸¹³ which can form a pi-pi interaction with the phenyl group of **216**. There is also Lys⁷⁷⁹, which may also interact with the phenyl group of **216** *via* a cation-pi interaction. Therefore, if the phenyl analogue **216** exhibited a similar level of activity to the heterocyclic derivatives (**210-215**), then it is very likely that the inhibitors would form a pi-pi interaction with Tyr⁸¹³ or cation-pi interaction with Lys⁷⁷⁹. On the other hand, if the phenyl analogue **216** was much less active than the heterocycles-containing compounds (**210-215**), then this would suggest that the interactions between the heterocyclic derivatives (**210-215**) and the affinity pocket are mediated primarily through hydrogen bond interactions.

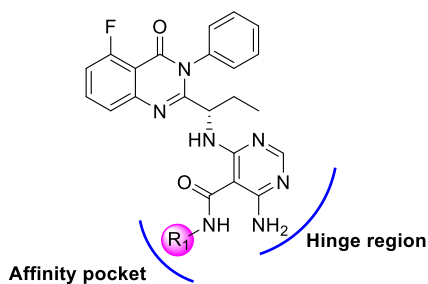


Table 52. Structure of the proposed compounds (**216-220**) having miscellaneous functional groups as the affinity pocket-binding group.

compound	R ₁
216	
217	
218	
219	
220	

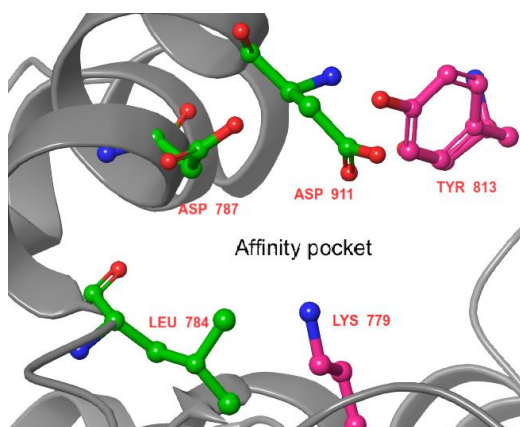


Figure 110. Crystal structure of murine PI3K δ (PDB code 4XE0) displays the 5 residues that line the affinity pocket. Tyr⁸¹³ and Lys⁷⁷⁹ (highlighted in magenta) can make a pi-pi and cation-pi interactions, respectively, with the phenyl group of compound **216**.

5.4.3.2.2 Saturated bioisosters of phenyl ring

Additionally, cyclopropyl and cyclohexyl groups were employed as saturated bioisosters for the heterocycles and phenyl group. To the best of authors' knowledge, this is the first study to target the affinity pocket using saturated groups, where the affinity pocket has always been filled by aryl or heteroaryl groups (Table 46)^{144,145,154,155,159}. Thus, the use of cyclopropyl in **217** and

cyclohexyl in **218** as affinity pocket-binding groups can provide advantages in terms of intellectual property and physical properties (fraction of sp^3 carbon atoms (F_{sp^3}), solubility, lipophilicity and topological polar surface area).

Our idea of introducing a cyclopropane group into the affinity pocket is based on the assumption that this group may interact favourably with Tyr⁸¹³ in the affinity pocket through a pi-pi interaction. The cyclopropyl is considered to be isosteric to the phenyl ring, this is due to the fact that the cyclopropyl ring behaves like the double bonds of alkenes, with a greater p-character (partial aromatic character) than the normal aliphatic C-C bond^{351–354}. The Coulson-Moffitt model for cyclopropane suggests that C-C bond in cyclopropane has about 20% less orbital overlap than the corresponding C-C bond in ethane^{354,355}, thus C-C bond in cyclopropane is neither a sigma nor pi bond, it is intermediate between them (Figure 111)³⁵⁶. This type of bond is named a bent bond or banana bond^{353,354}. Furthermore, in terms of physiochemical properties, cyclopropyl analogue **217** has a smaller molecular weight and greater proportions of sp^3 carbons (higher F_{sp^3}) than the phenyl **216** and heterocyclic (**210-215**) analogues (Table 53). Therefore, the cyclopropyl-containing compound **217** could provide improved physical characteristics, for example solubility³⁵⁷.

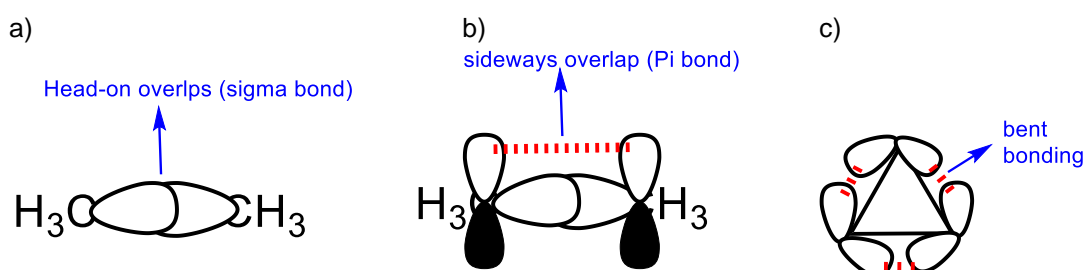


Figure 111. a) The sigma bond in ethane is formed by end-to-end overlap of atomic orbitals. b) The pi bond in ethene is formed by the lateral overlap of atomic orbitals. c) The Coulson-Moffitt model suggests that the C-C bond in cyclopropane is intermediate between sigma (end-on) and pi bond (lateral), which is called a bent bond or banana bond³⁵⁶.

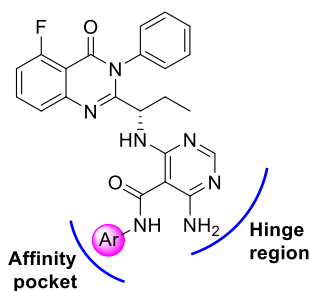
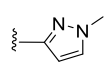


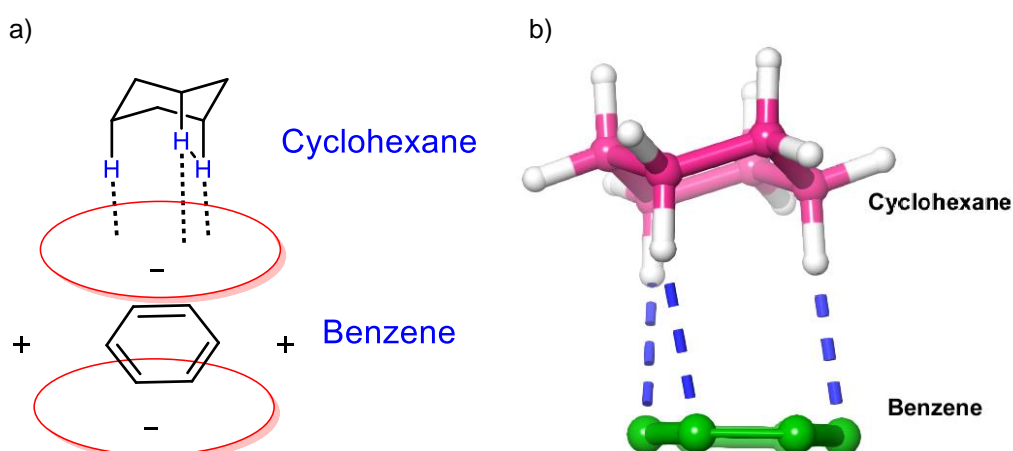
Table 53. Comparison of the physical properties of methylpyrazole **211**, phenyl **216** cyclopropyl **217** analogues^{264,357-359}, the cyclopropyl analogue exhibits improved physical properties when compared to the other analogues.

Physical properties	Compound 211 Ar= 	Compound 216 Ar= 	Compound 217 Ar= 	Optimal range for oral bioavailability
MW	513.54	509.55	473.51	<500
Fsp³	0.11	0.107	0.24	>0.47
tPSA	140.14	124.54	124.54	60-140 Å ²

To identify the type of hydrophobic interactions that may be involved in the binding of phenyl analogue **216** to the affinity pocket, **218** was synthesized, which contained a cyclohexyl ring as an affinity pocket binding moiety. In contrast to the phenyl group, the cyclohexyl group has no possibility to form a pi-pi interaction, however, it can make a C-H/pi interaction with the side chain of Tyr⁸¹³ lining the affinity pocket. Ninkovic *et al*⁶⁰ and Gunaydin *et al*⁶¹ pointed out that the C-H/pi interaction between cyclohexane and benzene ring is stronger than that between two benzene rings (Table 54), Ninkovic *et al*⁶⁰ attributed this to the ability of the cyclohexane ring to make 3 C-H/pi interactions, which work cooperatively (Figure 112). Moreover, it was reasoned that replacing the phenyl group with its saturated counterpart (cyclohexyl) leads to the increase of molecule saturation (Fsp³ value), that would inevitably result in improved physical properties. The comparison between C-H/pi and pi/pi interactions is shown in Table 54.

Table 54. Comparison of the nature and characteristics of the C-H/ π interaction with the π - π interaction, reported by Ninkovic *et al.*⁶⁰.

Characteristic	C-H/ π interaction	π - π stacking interaction
Interacting groups	Cyclohexyl-phenyl	Phenyl-phenyl
Number	3 (C-H/ π) interactions	1 π - π interaction
Strength	-3.27 Kcal/mol	-2.84 Kcal/mol
Geometry	Stacked geometry and T-shaped geometry	Stacked geometry and T-shaped geometry

Figure 112. a) Schematic representation of the cyclohexane-benzene interaction. b) 3D-representation of the cyclohexane-benzene interaction, highlighting the formation of the 3 C-H/ π interactions between the axial hydrogens of cyclohexane and pi cloud of benzene.

5.4.3.2.3 Define the size limit of the affinity pocket

The quinoline analogue **219** (Table 52) was synthesized to examine the effect of extending a bulky bicyclic ring into the affinity pocket, which would provide information regarding the size limitation of the affinity pocket. If the quinoline-containing compound **219** displayed similar or higher activity than that of the other above-mentioned analogues (**210-218**), then this would indicate that the affinity pocket of PI3K δ is large enough to tolerate a wide variety of ring systems, ranging in size from five-membered monocycles to bicyclic ring system.

5.4.3.2.4 Investigate the role of the amide linker in ligand binding

The amide linker has the simple role of connecting the aminopyrimidine hinge-binding scaffold to the terminal functional group. However, oxygen and hydrogen in the amide linker can participate in hydrogen bond interactions with the residues lining the affinity pocket. To explore this possibility, the primary amide derivative **220** was synthesised (Table 52), in which the functional group that interacts with the affinity pocket does not present.

5.4.3.2.5 Reference compound

The next step was to synthesize a reference compound in which the binding interactions with the affinity pocket are not possible, to compare its PI3K δ potency to those of the other analogues in this series, which will help determine the extent to which the potency is enhanced by making additional interactions with the affinity pocket. The original strategy was to synthesize the compound **221**, which has no substitution on the 5-position of the aminopyrimidine hinge binder (Table 55). Unfortunately, compound **221** could

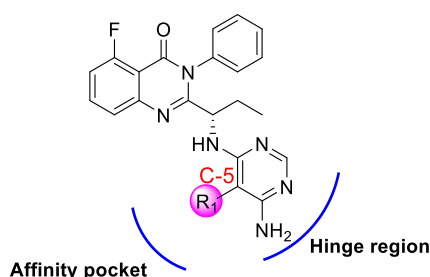


Table 55. Structure of the proposed reference compounds **221** and **222**, lacking the affinity pocket-binding group and amide linker at the 5-position of the 4-aminopyrimidine hinge binder.

compd	R ₁
221 (Cannot be synthesized)	
222	

not be synthesized, this had been attributed to challenges associated with the last step in the synthesis of this compound (more details in the Chemistry Section 5.5.1.3). Consequently, aldehyde derivative **222** was synthesized to be used as an alternative reference (Table 55). Compound **222** is not likely to be involved in interactions with the residues lining the affinity pocket due to lack of affinity pocket-binding group and NH₂ group of the amide linker.

5.4.3.3 Investigate the role of the hydrogen bond donor at the hinge region

Most δ -selective PI3K inhibitors traditionally make two hydrogen bonds to the hinge region *via* the hydrogen bond donor/acceptor pair of the hinge-binding scaffold. However, in one example reported by Novartis³³⁵, Compound **199** does not make the typical hydrogen bond donor interaction with the PI3K δ hinge region, as it lacks the hydrogen bond donor in the hinge binding moiety (thiazolopyrimidine) (Table 56). However, **199** still display 12-times greater activity than the parent compound **198** containing hydrogen bond donor (NH-9 of purine) (Table 56), which can be involved in hydrogen bonding with the

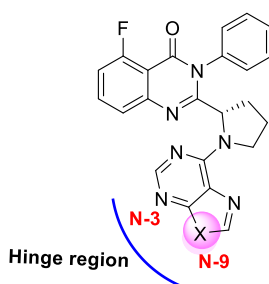


Table 56. Biological evaluation for PI3K δ for compounds (**198**, **199** and **223**)³³⁵. Compound **198** which has no a hydrogen bond donor, shows 12-fold improvement in PI3K δ potency over the parent purine derivative **199**.

compound	-X-	PI3K δ IC ₅₀ (nM)
198 ³³⁵	-NH-	150
199 ³³⁵	-S-	7
223 ³³⁵	-NCH ₃ -	1430

backbone carbonyl of Glu⁸²⁶ in the hinge region. Based on this example, it was hypothesized that the presence of hydrogen bond donor (4-NH₂) at the hinge binding moiety is not necessary to achieve high PI3K δ inhibiting activity.

Quite strikingly, masking the hydrogen bond donor of **198** with *N*-9 methylation of purine resulted in compound **223** which showed 10-fold decrease in activity compared to the parent compound **198** (Table 56). The biological results of **199** and **223** are somewhat contradictory as both compounds lack the hydrogen bond donor, but there is a dramatic difference (205-fold) in the PI3K δ potency between them. These observations suggest that the complete removal of the amino group does not reduce the PI3K δ inhibitory activity. Whereas, substitution of this amino group leads to a significant decrease in the PI3K δ activity, suggesting a low tolerance for the substituent protruding toward the hinge region.

To test this hypothesis in the current study, two compounds **224** and **225** were designed and docked into the active site of the PI3K δ enzyme (Figure 113 and Figure 114). In both compounds, the amino group at the 4-position of the 4-aminopyrimidine hinge binder has been removed. In compound **224** the 4-amino group has been replaced by a chlorine atom (Figure 113a), whereas the 4-amino group of compound **225** has been replaced by a hydrogen atom (Figure 114a). The docking results revealed that the chlorine atom of compound **224** makes steric clashes with Val⁸²⁸, a residue lining the hinge region and thus moves the pyrimidine hinge binder away from the hinge region (Figure 113b). As a consequence, the *N*-3 atom (acceptor) of the pyrimidine cannot make a hydrogen bond with the amide backbone (donor)

of the hinge Val⁸²⁸. This lack of interaction is explained by 3.48 Å separation distance between *N*-3 atom of pyrimidine and the amide backbone of Val⁸²⁸ (Figure 113b). This distance is not consistent with the range for hydrogen bond length (2.5- 3.2 Å)^{362,363}. Thus, the chloride analogue **224** does not make any hydrogen contact with the hinge region. Based on this docking result, compound **224** is expected to have a little or no inhibitory activity against PI3K δ .

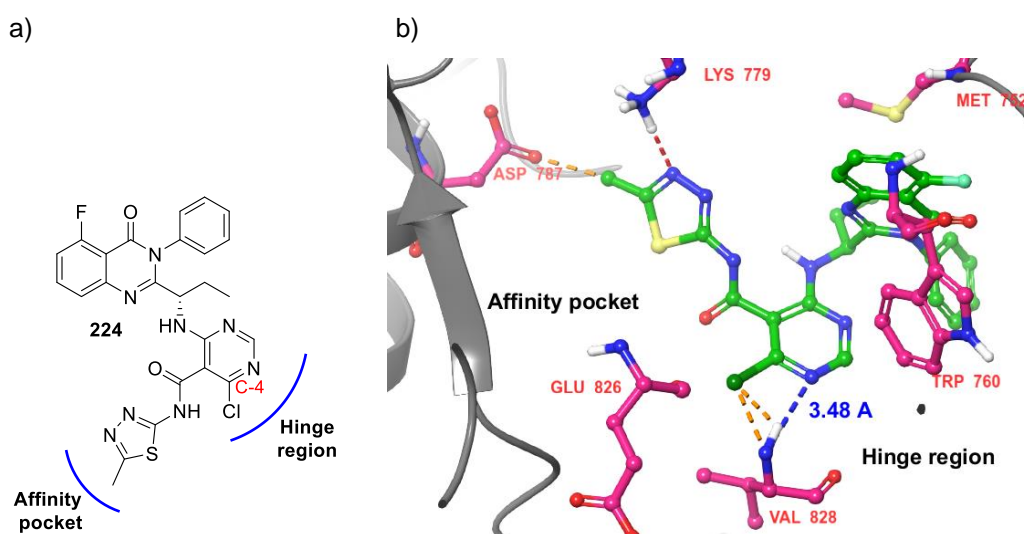


Figure 113. a) The chlorine-containing compound **224**. b) Compound **224** docked into the PI3K δ model (generated from PDB code 5I6U), steric clashes are represented by orange dashed lines and interatomic distance (in Å) is represented by a blue dashed line. It reveals that the steric clash created between the chlorine atom on pyrimidine and Val⁸²⁸ moves the pyrimidine ring away from the hinge region, thus, the *N*-3 atom of pyrimidine cannot form a hydrogen bond with the amide backbone of Val⁸²⁸, this lack of interaction is explained by 3.48 Å separation between *N*-3 atom of pyrimidine and the backbone amide of Val⁸²⁸. As a consequence, compound **224** does not form any hydrogen bonds with the hinge region.

On the other hand, the docking result of compound **225** showed that the hydrogen atom in the 4-position of the pyrimidine hinge binder does not give rise to a steric clash with Val⁸²⁸ (Figure 114b), because of its small size. Thereby, the pyrimidine ring of compound **225** comes close to the hinge region and makes a hydrogen bond with the amide backbone of Val⁸²⁸ through its *N*-3 substituent (Figure 114b), whereas the distance between the

donor and acceptor is 2.82 Å, which falls within the optimal range for hydrogen bonds (2.5 to 3.2 Å)³⁶⁴.

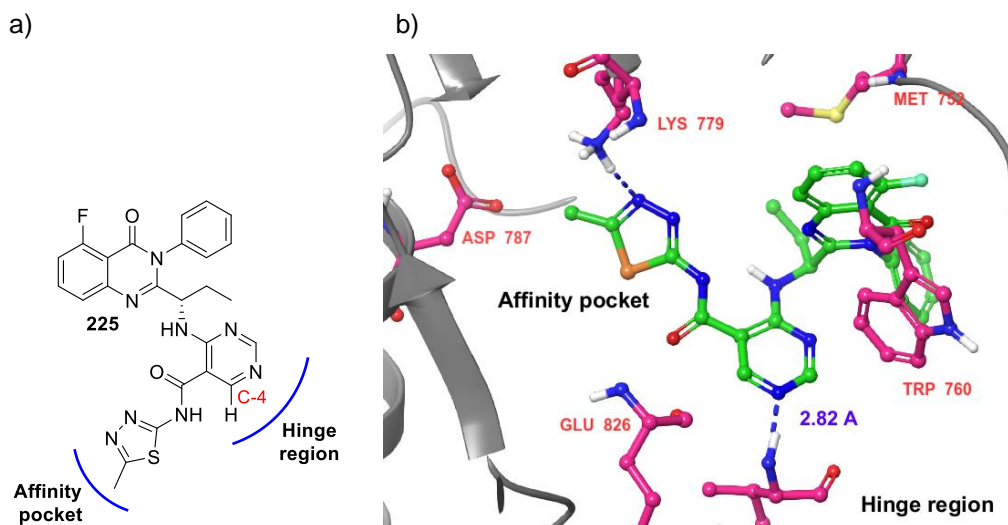


Figure 114. a) Compound **225**, which is unsubstituted at position 4 of the pyrimidine hinge binder. b) Compound **225** docked into the PI3K δ model (generated from PDB code 516U), interatomic distance (in Å) is represented by a blue dashed line. It reveals that the distance between N-3 of pyrimidine and the amide backbone of Val⁸²⁸ is 2.82 Å which is within the optimum range of hydrogen bond formation (2.5 to 3.2 Å), suggesting that compound **225** can form one hydrogen bond with the hinge region.

Taken together, the findings of Novartis³²⁴ and the above mentioned docking studies suggest a hypothesis that the absence of a hydrogen bond donor in the hinge binding motif may result in a slight decrease to no change in PI3K δ inhibitory activity, whereas, the replacement of an amino group by atoms other than hydrogen or groups of atoms leads to a major loss in the PI3K δ activity that may be caused by the steric clash with Val⁸²⁸ at the hinge region. It was decided to test this hypothesis in the current study, by designing compounds **226** and **227** (Table 57) in which the hydrogen bond donor (4-amino group) is removed and replaced with a hydrogen atom, then the IC₅₀ values of **226** and **227** are compared with those of the corresponding 4-aminopyrimidine analogues **210** and **211**, respectively.

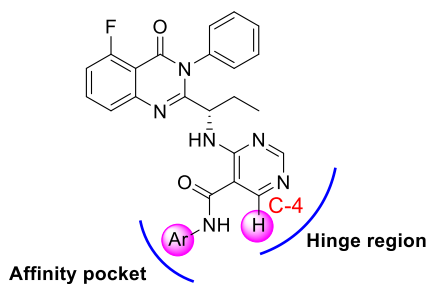


Table 57. Structure of the proposed compounds belonging to 4-desaminopyrimidine derivatives **226** and **227**.

compd	R ₁
226	
227	

5.5 Discussion

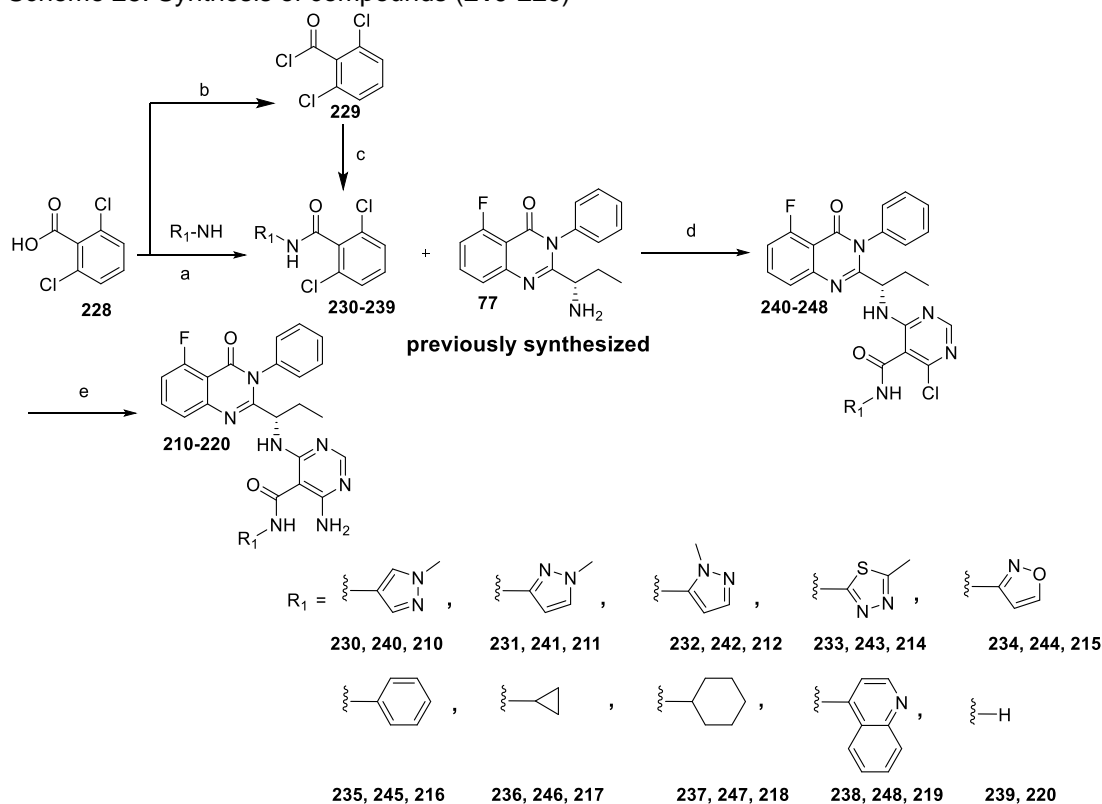
5.5.1 Chemistry Section

The synthetic protocol is almost similar to what was used in Chapters 3 and 4 for the synthesis of idelalisib derivatives. However, the structure of the inhibitors in this study is subtly different from those of idelalisib derivatives in that they utilize 4-aminopyrimidine hinge-binding motif instead of purine.

The synthesis of the quinazolinone intermediate **77** (the upper part of the molecules) has been outlined previously in Chapter 3 and 4 (Scheme 3 and 17). Therefore, this study focused on the synthesis of 4-aminopyrimidine derivatives (the lower part of the molecules) followed by the installation of these groups on the primary amine of quinazolinone intermediate **77**. The synthetic route of each final product (**210-222**) was divided into three steps (Scheme 25): 1. amide coupling of pyrimidine carboxylic acid derivative **228** with various aromatic and aliphatic amines (step a) 2. aromatic nucleophilic substitution (S_NAr) reactions of the resulting amides with primary amine

intermediate **77** (step d) 3. amination of 4-chloropyrimidine derivatives with ammonia (step e).

Scheme 25. Synthesis of compounds (**210-220**)



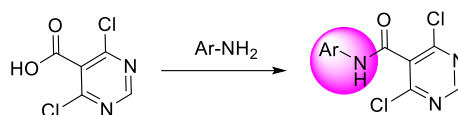
^aReagents and conditions: (a) 2-bromo-1-ethyl pyridinium tetrafluoroborate (BEP) (1.1 equiv), DIPEA (3.2 equiv), DCM, rt, 24 h, yields 10-63%; (b) SOCl_2 , 80°C, 1 h, yields 90%; (c) NH_4OH -dioxane (1:1, v/v), 50°C, 1h, yield 31%; (d) DIPEA (10 equiv), dioxane, 50°C, 30 min, yields 23-74%; (e) Cu_2O (0.01 equiv), NH_4OH -NMP (1:1, v/v), microwave, 50°C, 30 min, yields 9-57%.

5.5.1.1 Amide coupling of pyrimidine carboxylic acid derivatives (step a)

Our synthetic approach to the hinge-binding scaffold starting from 4,6-dichloropyrimidine-5-carboxylic acid **228** (Scheme 25), which can react with several heteroaryl and alicyclic amines to provide the corresponding pyrimidine amides (**230-238**). A wide range of conventional amide coupling reagents (HATU, 1-ethyl-3-(3-dimethylaminopropyl)carbodiimide (EDCI), benzotriazole-1-yloxytripyrrolidinophosphonium hexafluorophosphate (PyBOP), bromotripyrrolidinophosphonium hexafluorophosphate (PyBroP)

and ethylchloroformate) under different conditions were tested but generally no amide product was obtained (Table 58). The failure of this reaction is probably due to a combination of two factors. First, the carboxyl group in 4,6-dichloropyrimidine-5-carboxylic **228** is highly sterically hindered as it is flanked by the two bulky chlorine atoms. Secondly, the heteroaryl amines are poor nucleophiles as the lone pair of electrons on the exocyclic nitrogen takes part in resonance stabilisation with the heterocyclic rings.

Table 58. Screening of coupling reagents and bases for the synthesis of pyrimidine amide intermediates (**230-238**).



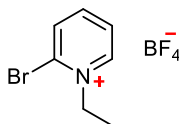
Coupling reagent	Base ^b	Conv ^c (%)
HATU	DIPEA	0
EDCI	DIPEA	0
PyBrop	DIPEA	0
PyBOP	DIPEA	0
Ethylchloroformate	K ₂ CO ₃	0

^bThe reactions were carried out in the presence of 3 equiv of base.

^cConversion was based on LC-MS analysis.

These disappointing results stimulated us to search for more efficient coupling reagents. Li *et al*^{365,366} have reported the utilisation of a novel coupling reagent called 2-bromo-1-ethyl pyridinium tetrafluoroborate (BEP) **249** (Figure 115) which was found to be the most efficient reagent for the preparation of a series of sterically hindered amino acids. Consequently, in this study, BEP was used as a reagent for the coupling of different heteroaryl amines with 4,6-dichloropyrimidine-5-carboxylic acid **228** in CH₂Cl₂ at RT, the corresponding *N*-heteroaryl amides derivatives (**230-234**) were obtained in 10-35% yields (Scheme 25). Using the same reaction condition, the

carboxylic acid **228** was reacted with aniline, cyclopropylamine and cyclohexylamine to afford the corresponding amides **235**, **236** and **237**, respectively in modest yields (25-28%).



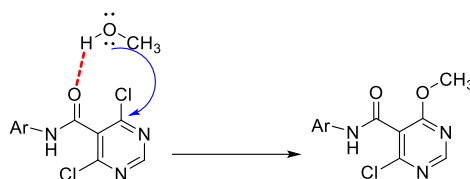
BEP (249)

Figure 115. The powerful coupling reagent 2-bromo-1-ethyl pyridinium tetrafluoroborate **249** (BEP) used in the synthesis of *N*-heteroaryl amides **230-238**^{365,366}.

Finally, the primary amide intermediate **239** was prepared *via* two successive reactions from the commercially available 4,6-dichloropyrimidine-5-carboxylic acid **228** (Scheme 25). First, compound **228** was refluxed in thionyl chloride to generate the corresponding acid chloride **229**. This compound **229** thus obtained was treated with ammonium hydroxide (28% ammonia in water) in dioxane at 0 °C to cleanly afford the corresponding primary amide **239** (63% over two steps). It is noteworthy that the reaction temperature should be kept below 0 °C, to avoid the formation of the side product that results from aromatic nucleophilic substitution (S_NAr) at the easily displaceable chlorine atoms in 4,6-dichloropyrimidine-5-carbonyl chloride **229**.

It should also be noted that in the amide coupling reaction of 4,6-dichloropyrimidine-5-carboxylic acid **228** with different amines (step a), the use of protic solvent, in particular methanol, has to be avoided due to the high reactivity of dichloropyrimidine starting material **228** towards S_NAr displacement, whereas one of the chlorine atoms can be easily replaced by a methoxy group *via* hydrogen bond-catalysed nucleophilic substitution (Scheme 26).

Scheme 26. Hydrogen bond-catalysed nucleophilic substitution of a chlorine atom by a methoxy group typically happens when methanol is used as a reaction solvent or eluent in column chromatography



5.5.1.2 nucleophilic substitution of the chlorine atom in 4,6-dichloropyrimidine (230-239) (step d)

The next step is the nucleophilic displacement of 4-chlorine of 4,6-dichloropyrimidine derivatives (**230-239**) with the primary amine intermediate **77** to provide the late-stage intermediates (**240-248**) (Scheme 25). The reaction was carried out in dioxane using DIPEA as a base at 50 °C to afford the monochloropyrimidine derivatives (**240-248**) in moderate to good yields (23-72%). In most cases, the reaction was finished in less than one hour, with both reactants completely consumed. Two reasons can be suggested for this high reactivity. First, the two chlorine atoms attached to the pyrimidine ring have a negative inductive effect, thus they reduce the electron density in the ring and makes it more susceptible to nucleophilic attack. Consequently, one of the two of the chlorine atoms was quickly displaced by the primary amine **77**. Second, the pyrimidine ring is more reactive towards nucleophilic substitution reaction than the other six-membered nitrogen heterocycles. John *et al*⁶⁷ and Katritzky *et al*⁶⁴ reported that halogen substituents in the 4-position of the pyrimidine ring are more easily displaced than those in the pyrazine, pyridazine and pyridine (Figure 116).

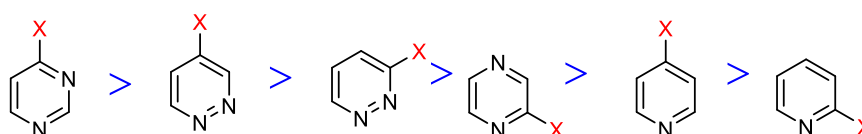
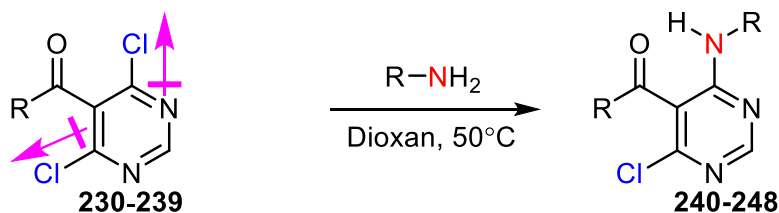


Figure 116. Comparison of the relative reactivity of the halopyrimidine to nucleophilic displacement with the corresponding pyridazine, pyrazine and pyridine³⁶⁷.

5.5.1.3 Amination of the late-stage 4-chloropyrimidine intermediates with ammonia (step e)

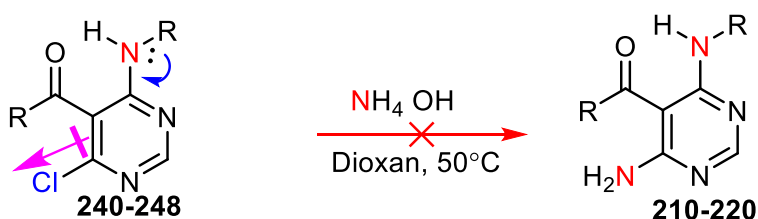
The last step is the amination of the monochloropyrimidine intermediates (240-248) using ammonia to generate the final screening compounds (210-220) (Scheme 25). The monochloropyrimidine-containing intermediates (240-248) proved unreactive under the same conditions used for amination of dichloropyrimidine derivatives (230-239) in the previous step (Figure 117), due to the introduction of the electron-donating primary amine **77** into the pyrimidine ring in step d, which increases the electron density of the pyrimidine ring and makes it more resistant to nucleophilic attack than the 4,6-dichloropyrimidine-containing compounds (Figure 117).

Step d



chlorine atom takes electron density away from the pyrimidine ring makes it susceptible to nucleophilic attack

Step e



Alkylamine group donates electron density to the pyrimidine ring makes it resistant to nucleophilic attack

Figure 117. Explain the difference in reactivity towards amino nucleophiles between dichloropyrimidine derivative (in step d) and monochloropyrimidine derivative (in step e) under the same reaction conditions.

The failure of the monochloropyrimidine derivatives to undergo traditional nucleophilic aromatic substitution reaction prompted us to investigate the transition-metal mediated nucleophilic aromatic substitutions as an alternative approach to incorporate ammonia into monochloropyrimidine

derivatives (**240-248**). Elmkaddem *et al*⁶⁸ and Xu *et al*⁶⁹ have reported the copper-catalysed amination of electron-rich aryl halides using ammonium hydroxide as the ammonia source in NMP. As a starting point, the reaction parameters such as types of copper catalysts, reaction temperature and time were screened. Compounds **241**, **242** and **243** were allowed to react with 5 mol% of copper (II) oxide in a 50:50 NH₃.H₂O:NMP mixture at 80°C for 3 h under microwave condition, to give the corresponding aminopyrimidine products **211**, **212** and **214**, respectively, in moderate yields (20-37%) (Table 59). However, in all the cases, a significant amount of unknown side product was detected and isolated. By combination of LC-MS and ¹H NMR, the side product has been identified as the lactam analogues (**250-252**) (Table 59), resulting from the nucleophilic displacement of chlorine with hydroxyl derived from aqueous ammonium hydroxide.

Although the desired products were obtained, the reaction conditions must be optimized to suppress the formation of the lactam side product, which possess similar polarity to the desired products and thereby making the purification process very challenging and time-consuming.

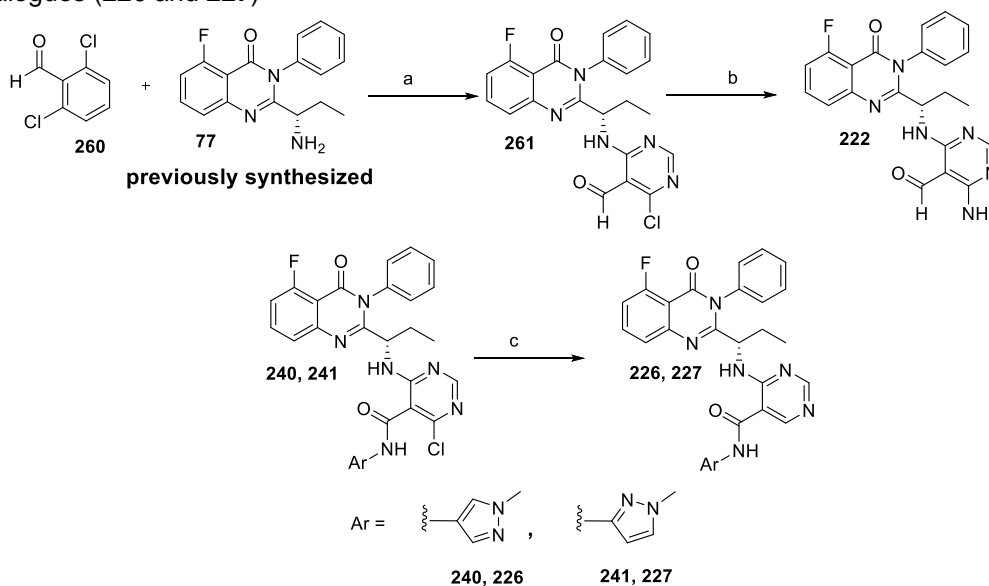
The optimized reaction conditions involved the use of copper (I) oxide as a catalyst instead of copper (II) oxide. Xu *et al*⁶⁹ reported that copper (I) oxide was found to be the most effective catalyst for the amination of aryl halides with ammonia. Accordingly, the reaction of several chloropyrimidine derivatives (**240**, **244- 249**) with ammonium hydroxide was carried out in the presence of copper (I) oxide as a catalyst, at different temperatures (60, 50

is worth noting that the cyclohexyl-containing compound **218** was obtained in poor yield (5%), most likely due to the poor solubility of the substrate **247** in the reaction solvent ($\text{NH}_3 \cdot \text{H}_2\text{O}$: NMP, 1:1), factors such as high lipophilicity of **247** ($\text{cLogP} = 5.42$) may be related to this poor solubility.

5.5.2 Synthesis of aldehyde analogue **220** (reference)

The synthesis of aldehyde-containing compound **220** to be used as a reference, started from 4,6-dichloropyrimidine-5-carboxaldehyde **260** (Scheme 27). In the first step, nucleophilic attack of primary amine **77** on aldehyde **260** in the presence of DIPEA gave intermediate **261** in good yield (64%). Subsequent amination of **261** with Cu_2O in NH_4OH : NMP (1: 1, v/v) at 40°C providing the corresponding arylamine **222** in 18% yield.

Scheme 27. Synthesis of the aldehyde-containing analogue **222** and the two des-aminated analogues (**226** and **227**)



^aReagents and conditions: (a) DIPEA (10 equiv), dioxane, 50°C , 30 min, yield 64%; (b) Cu_2O (0.01 equiv), NH_4OH -NMP (1:1, v/v), microwave, 40°C , 60 min, yield 18%; (c) Zn powder (3 equiv), acetic acid (10 equiv), THF, 70°C , 3 h, yield of **226** is 54%, yield of **227** is 33%.

5.5.3 Synthesis of des-aminated analogues **226** and **227**

The final task was to synthesize the final compounds **226** and **227**, which lack the hydrogen bond donor (NH_2) on the hinge-binding scaffold. In this case,

the late-stage 4-chloropyrimidine intermediates **240** and **241** were employed as substrates which would undergo a hydrodechlorination reaction. Catalytic hydrogenation is frequently selected as a method for the replacement of chlorine with hydrogen. However, treatment of **240** and **241** with hydrogen gas in the presence of a palladium catalyst failed to afford the final products **226** and **227**, probably because the pyrimidine rings of **240** and **241** are electron-rich systems due to the presence of the electron-donating alkylamino substituent, which made the rings resistant to the Pd-catalysed hydrodechlorination (see Section 5.5.1.3 and Figure 117).

Therefore, an alternative synthetic route is required. Xingyong *et al.*⁶⁷⁰ reported a new method for replacing chlorine atoms of chlorinated heterocyclic compounds with hydrogens. In this method, the chlorinated heterocyclic compounds were treated with zinc catalyst and acetic acid in refluxing THF for 3 h to yield the corresponding dechlorinated products (Scheme 27). Under the same reaction conditions, the chloropyrimidine derivatives **240** and **241** were converted to the corresponding dechlorinated analogues **226** and **227** in isolated yields of 54% and 33%, respectively. It is believed that the role of the acetic acid was simply to provide a source of hydrogen (Scheme 28).

Scheme 28. Acetic acid reacts with zinc to produce zinc acetate and hydrogen gas necessary for hydrodehalogenation reaction



5.5.4 Biology Section

Herein, the biological activity of the series of 4-aminopyrimidines (**211-220**) was measured against PI3K δ enzyme. Furthermore, the chloropyrimidine intermediates (**230-239**) and lactam side products (**250-259**) were also tested

for their inhibitory activity against PI3K δ . The chloropyrimidine intermediates (**230-239**) were screened to assess the effect of replacing the hydrogen bond donor (amino group) with a bulky non-hydrogen bonding atom (chlorine) on PI3K δ activity. On the other hand, although the lactam derivatives (**250-259**) have emerged as side products during synthesis of the desired aminopyrimidine products, they still possess a hydrogen bond donor (lactam N-H) and acceptor (lactam carbonyl group) pair at the hinge binding group, which enable them to make a bi-dentate contact to the hinge region. Thus, these compounds have been evaluated for inhibitory activities against PI3K δ .

Key elements of this experimental design including primary screening of all compounds against PI3K δ at 1 μ M and 500 nM final compound concentrations, then the full IC₅₀ of the active compounds would be determined to confirm their inhibitory activity. In each assay, the FDA-approved idelalisib (**8**) was included for direct comparison.

5.5.4.1 Single-concentration screening assay

5.5.4.1.1 Initial screening (1 μ M final concentration)

For this experiment, a set of 8 compounds were tested, including 3 aminopyrimidine derivatives (**211**, **212** and **214**), 3 chloropyrimidine derivatives (**241**, **242** and **243**) and 3 lactam side products (**250**, **251** and **252**) in addition to idelalisib (**8**), which represent compounds that were prepared when this assay was performed. All compounds were tested at a single concentration (1 μ M) for their inhibitory activity against PI3K δ (Table 60). Furthermore, the PI3K δ selectivity of these compounds was assessed by testing against PI3K α , the non-selective PI3K inhibitor (pictilisib **4**, see

Chapter 5

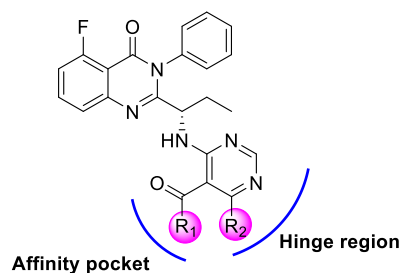


Table 60. % inhibition of PI3K δ activity at 1 μ M and 500 nM of compounds (**8**, **210-212**, **214-220**, **222**, **226**, **227**, **241-243** and **250-252**).

Compd	R ₁	R ₂	Inhibition of PI3K δ^a	
			% Inhibition at 1 μ M	% Inhibition at 500 nM
Idelalisib (8)	-	-	76.2	79.9
210		-NH ₂	n/a	77.3
211		-NH ₂	56.0	1
212		-NH ₂	66.8	53.0
214		-NH ₂	58.5	54.7
215		-NH ₂	n/a	75.1
216		-NH ₂	n/a	69.5
217		-NH ₂	n/a	64
218		-NH ₂	n/a	87.7
219		-NH ₂	n/a	78.1
220	-NH ₂	-NH ₂	n/a	69.4
222	-H	-NH ₂	n/a	81.9
226		-H	n/a	11.7
227		-H	n/a	4.0
241		-Cl	14.1	n/a
242		-Cl	5.73	n/a
243		-Cl	24.4	n/a
250		-OH	12.2	n/a
251		-OH	28.1	n/a

Compd	R ₁	R ₂	Inhibition of PI3K δ^a	
			% Inhibition at 1 μ M	% Inhibition at 500 nM
252		-OH	20.9	n/a

^aPI3K δ % inhibition was determined at 1 μ M and 500 nM compound concentration. n/a means that the compound was not tested in this assay.

Chapter 2) was selected as a reference compound in this selectivity study, since it is a potent inhibitor of PI3K α (IC₅₀ value of 44 nM) (see Section 2.1 in Chapter 2).

Encouragingly, all three aminopyrimidine derivatives (**211**, **212** and **213**) showed significant inhibitory activity against PI3K δ (66.9%, 56.0% and 58.5%, respectively), nearly equipotent to the positive control of idelalisib (**8**) (76.2%) (Table 60). On the other hand, the PI3K δ selectivity of the aminopyrimidine derivatives (**211**, **212** and **213**) over PI3K α was also investigated. Interestingly, the two pyrazole regioisomers **211** and **212** showed weak activity against PI3K α (34.5%, 33.3%, respectively) at 1 μ M concentration, whilst the thiadiazole analogue **213** provided no inhibition (0%). In contrast, the reference compound (pictilisib **4**) at 1 μ M led to 81.9% inhibition of PI3K α activity. These results suggest that the three aminopyrimidine derivatives exhibit a high degree of PI3K δ selectivity.

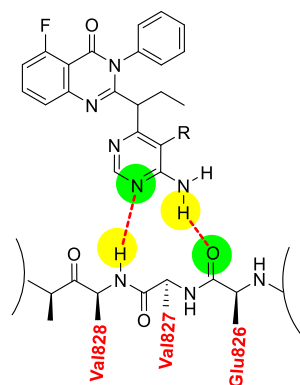
In contrast to aminopyrimidines (**211**, **212** and **213**), their chloropyrimidine analogues **241**, **242** and **243** displayed weak inhibitory activities (5.7%, 14.1% and 24.4%, respectively) against PI3K δ (Table 60). This analysis revealed that substitution of the hydrogen bond donor (amino group) with a bulky atom (chlorine) resulted in a large drop in PI3K δ potency. These findings clearly support the hypothesis (see Section 0) that replacement of an amino group by other groups or atoms other than hydrogen atoms might create a steric

clash with the hinge residues, resulted in significant loss of the PI3K δ inhibitory activity. Docking study of compound **243** was performed to further strengthen this hypothesis (see Figure 113b), it showed that the pyrimidine ring of compound **243** did not form any hydrogen bond with Val⁸²⁸ and Glu⁸²⁶ in the hinge region, which could be reasoned by the steric clash that might occur between the chlorine atom and the backbone amide of Val⁸²⁸.

Furthermore, the three lactam side products (**250**, **251** and **252**) exhibited < 30% inhibitory activity (**250**:12.2%, **251**: 28.1%, and **252**: 20.9%, respectively) (Table 60). Such findings were surprising, given the fact that the hinge binding group of these compounds does contain the hydrogen bonding donor/acceptor pair, typical for kinase inhibitors. It was proposed that the lactam side products failed to hydrogen bond with the hinge region of PI3K δ , This fact was attributed to the inversion of the positions of the hydrogen-bond donor/acceptor in contrast to their aminopyrimidine analogues (Figure 118a), whereas the hydrogen bond donor and acceptor of the lactam side products (**250**, **251** and **252**) are oriented in the opposite direction to the hydrogen bond donor residue (Val⁸²⁸) and acceptor residue (Glu⁸²⁶) in the hinge region (Figure 118b). Furthermore, the lactam carbonyl oxygen of (**250**, **251** and **252**) is oriented towards the backbone carbonyl of Glu⁸²⁶, which might result in the repulsive electrostatic interaction (Figure 118b).

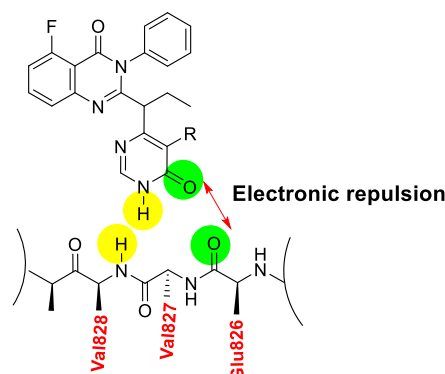
Based on the preliminary results described above, the aminopyrimidine-containing derivatives were the only compounds which showed greater than 50% inhibition against PI3K δ at 1 μ M, coupled with a good target selectivity, thus they were selected for further more detailed screening (500 nM) to confirm their activity.

a) Aminopyrimidine product



Two Hydrogen bonds at the hinge region

b) Lactam side product



No hydrogen bond

Figure 118. a) Schematic representation of the ligand binding interactions in the hinge region of PI3K δ . The hydrogen bond donors and acceptors are highlighted in yellow and green, respectively. a) the aminopyrimidine group forms two hydrogen bonds to the hinge backbone. b) In the pyrimidone ring of lactam side products the positions of hydrogen-bond donor and acceptor are inverted, thus lactam side products do not form hydrogen bonds with the hinge region. Moreover, electronic repulsion may occur between the lactam oxygen and the backbone carbonyl oxygen of Glu⁸²⁶.

5.5.4.1.2 Initial screening (500 nM final concentrations)

In the second preliminary screening, all the aminopyrimidine analogues (**210-212** and **214-220**) and the 2 des-aminated analogues (**226** and **227**) were tested for their inhibitory activity against PI3K δ at a single-concentration (500 nM) (Table 60).

Quite strikingly, the cyclohexyl analogue **218** showed the most inhibitory activity in this series (87.7%), which was slightly higher than that of idelalisib (**8**) (79.9%). Although it is too early to discuss the activity of this compound, to the best of the authors' knowledge, this is the first preliminary study to suggest that extension of saturated group (cyclohexyl) into the affinity pocket resulting in high PI3K δ potency, this is due to the fact that the affinity pocket has been traditionally occupied by aryl or heteroaryl groups.

Furthermore, pyrazole (**210**: 77.3%), isoxazole (**215**: 75.1%) phenyl (**216**: 69.5%) aldehyde (**222**: 81.9%), quinoline (**219**: 78.1%) and amide (**220**: 69.4%) analogues showed comparable inhibitory activity to the control

idelalisib (**8**) (79.9%). In addition, the three compounds, **212** (53.0%), **214** (54.7%) and **217** (64.0%) were found to be slightly less potent than idelalisib (**8**) (79.9%) (Table 60).

On the other hand, replacement of 1-methylpyrazol-4-yl group of **210** with 1-methylpyrazol-3-yl resulted in the regioisomeric analogue **211** (Figure 119). Quite surprisingly, an interesting difference in the PI3K δ inhibitory activity was observed between the two regioisomeric pyrazoles (**210**: 77.3%, **211**: 1%) (Table 60). This result indicates that variation in the position of the pyridine-type nitrogen atom (green circle in Figure 119) in the pyrazole ring affects the PI3K δ activity. It was hypothesized that the unexpected very poor activity (1%) of 1,4-pyrazole regioisomer **211** is attributed to the electrostatic repulsion that might occur between the pyridine-type nitrogen atom of pyrazole ring and the nearby residues in the affinity pocket. This hypothesis was suggested based on a relevant example reported by Patel *et al*¹⁵⁵. In their research for novel and selective PI3K δ inhibitors, Patel *et al*¹⁵⁵ synthesized the quinazolinone derivatives **203** and **262** bearing pyrazine and pyridazine rings, respectively, that extend into the affinity pocket (Figure 120). These two regioisomeric compounds were compared on the basis of their PI3K δ activity. It was found that the pyrazine analogue **203** is 600-fold more potent than the corresponding pyridazine counterpart **262** (Figure 120). The author hypothesized that the electrostatic repulsion between the pyridazine nitrogen atom (green circle in Figure 120) and the nearby residues that line the affinity pocket might account for the loss of PI3K δ activity of **262**.

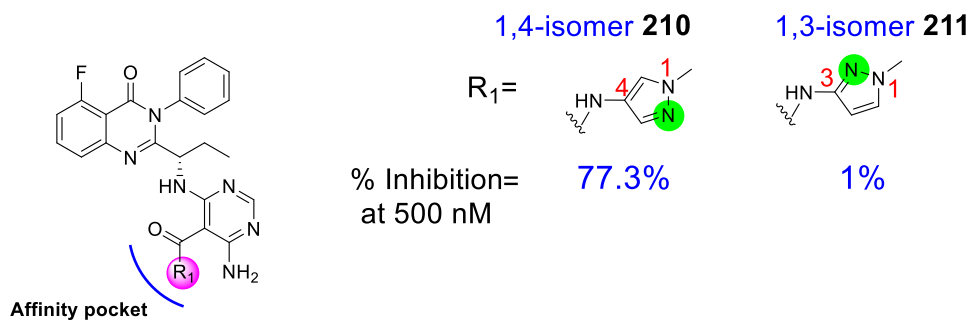


Figure 119. A comparison of the inhibitory activity between 1,4- and 1,3-pyrazole regioisomers (**210** and **211**, respectively) against PI3K δ at a single concentration (500 nM). Only 1,4-isomer **210** has PI3K δ inhibitory activity while 1,3-isomer **211** is inactive.

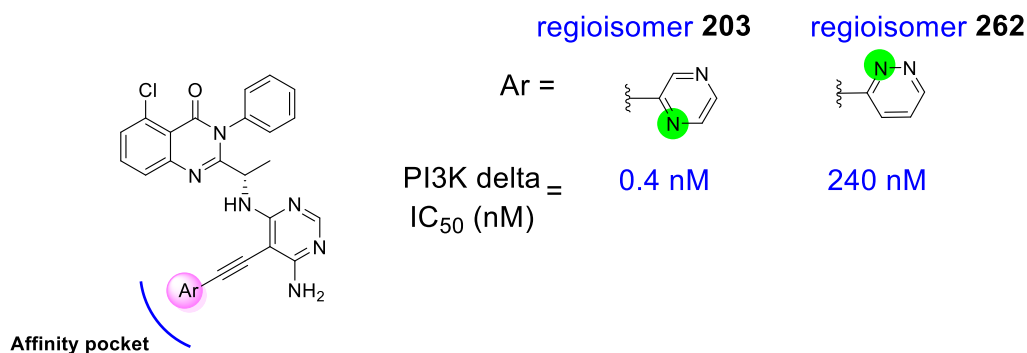


Figure 120. A comparison of the PI3K δ potency between the two regioisomers (**203** and **262** reported by Patel *et al*¹⁵⁵). The pyrazine analogue **203** is 600-fold more potent than the corresponding pyridazine counterpart **262**.

Unexpectedly, compounds **226** and **227** which do not possess a hydrogen bond donor (amino group) at the hinge-binding motif show very weak inhibitory activity at 500 nM (11.7 and 4%, respectively) (Table 60). Such findings are not consistent with the previously mentioned hypothesis (see Section 0) that the presence of hydrogen bond donor (4-NH₂) at the hinge binding moiety is preferred but it is not essential for PI3K δ inhibition and could be replaced with a hydrogen atom, since the inhibitors are still able to form a single hydrogen bond with the hinge region through the *N*-3 position of the pyrimidine ring. Taken together, these results demonstrated that the double hydrogen bonds made by the 4-NH₂ and *N*-3 of 4-aminopyrimidine hinge binder can both contribute to the PI3K δ potency of this series, indicating that the hydrogen bond formed by the 4-NH₂ is indispensable.

To sum up, among the 12 tested compounds, most of compounds displayed considerable PI3K δ inhibitory activity. Especially the cyclohexyl-containing analogue **218** gave the highest level of PI3K δ inhibition with 87.7%.

5.5.4.2 IC₅₀ determination

The eight most active compounds (**210**, **212**, **214-220** and **222**) identified from single-point screening (500 nM), would be tested further in a dose-response assay to determine their IC₅₀ values. However, the inhibitor screening assay which is carried out by researchers at Monash University was delayed due to COVID-19. Thus, the IC₅₀ data for the reported compounds were not included in this thesis. Hopefully, they will be available before the viva.

Chapter 6 General conclusion and recommendations for future work

6.1 General conclusion

This research project focused on PI3K δ enzyme, which is predominately expressed in leukocytes where it plays an important physiological role in the activation, proliferation and survival of immune cells (B- and T-cells). However, dysregulation of PI3K δ pathway leads to the development of different types of haematological malignancies such as CLL, FL and SLL. Furthermore, aberrations in PI3K δ pathway have been implicated in the aetiology of several autoimmune diseases such as rheumatoid arthritis and systemic lupus erythematosus. Hence, inhibition of PI3K δ provides a promising therapeutic opportunity to treat different types of blood cancer and autoimmune diseases. Accordingly, the aim of this research was to discover and develop novel orally active small molecule inhibitors of PI3K δ , it is important for these inhibitors not only to display potent PI3K δ inhibition, but also to exhibit high selectivity toward PI3K δ in order to prevent off-target adverse events resulting from non-selective inhibition of PI3K α , β and γ .

Currently, there is only one FDA-approved selective PI3K δ inhibitor named idelalisib (**8**), which is used for the treatment of three types of haematological malignancies including CLL, relapsed FL and relapsed SLL. However, idelalisib (**8**) tends to cause serious side effects which encompass: diarrhoea, serious hepatotoxicity, colitis, serious pneumonitis and neutropenia, which frequently lead to idelalisib (**8**) dose reduction and treatment discontinuation, indicating a high need for novel, equieffective and less toxic selective PI3K δ inhibitors, which underlying the driving motivation for this PhD research.

Chapter 7

This thesis reports the design and synthesis of 92 novel compounds belong to the two classes of selective PI3K δ inhibitors: 1) flat-shaped inhibitors, 2) propeller-shaped inhibitors. These two classes of inhibitors differ in their binding modes in the binding site of PI3K δ . All the compounds reported in this study were biologically evaluated for their inhibitory activity against PI3K δ . Furthermore, the selectivity of these compounds was tested for inhibition of PI3K δ versus other class I PI3K isoforms (PI3K α , β and γ).

Chapter 2 focused on flat-shaped PI3K δ inhibitors, in which the non-selective PI3K inhibitor pictilisib (**4**) provided a new starting point for a lead optimisation programme, which resulted in the synthesis of 41 novel thienopyrimidine derivatives with potent activity against PI3K δ (IC_{50} values ranging from 1.1 to 44 nM). In addition, upon comparison with the lead compound pictilisib (**4**), all derivatives elicited far superior selectivity profile for PI3K δ over the other class I PI3K isoforms. Two regions of PI3K δ binding site were responsible for conferring high PI3K δ potency and selectivity of the reported inhibitors. First, tryptophan shelf which defines the region of space located between δTrp^{760} and δThr^{750} (Figure 121), this region is exclusively present in PI3K δ , but absent in PI3K α , β and γ . In this project, the tryptophan shelf was targeted using aliphatic heterocycles, which were able to make C-H/ π interactions with Trp^{760} . Secondly, the non-conserved residues that surround the affinity pocket were exploited to aid PI3K δ selectivity. These residues made hydrogen bond networks with the conserved residues lining the affinity pocket. This new hydrogen bond network was only accommodated in PI3K δ , but was not accommodated in the remaining isoforms. The SAR research for the affinity pocket binding moiety displayed that PI3K selectivity improved in

series indole > indazole ≈ phenol, whereas the PI3K potency improved in series phenol > indole ≈ indazole.

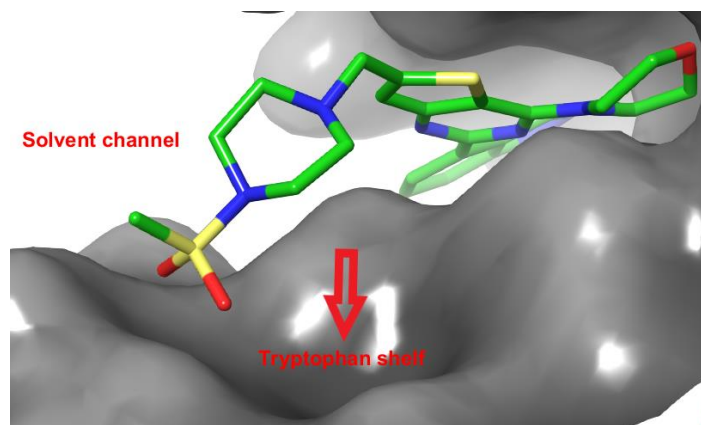


Figure 121. Crystal structure of murine PI3K δ (PDB code 2WXP) with pictilisib (**4**) bound. Highlights the shallow dimple, termed the tryptophan shelf, which is exclusively found in the PI3K δ isoform and not in the other three isoforms¹⁶⁰. The side chain (4-methanesulfonyl-piperazine-ylmethyl group) of pictilisib (**4**) points towards the solvent channel, where it does not play a significant role in the binding¹⁸². Thus, in Chapter 2, structural modifications on pictilisib (**4**) were conducted to develop inhibitors capable of accessing the tryptophan shelf. These modifications resulted in an improved PI3K δ potency and selectivity.

Among this series of 41 PI3K δ inhibitors, the best selective compound was **48**, which bears a 4-fluoropiperidine substituent extending towards the tryptophan shelf and an indole ring occupying the affinity pocket. Additionally, in silico screening for the inhibitors in this chapter was performed to determine the drug-like physiochemical properties, it was found that compound **48** had more optimal physiochemical and ADME properties for oral drugs, than the other analogues and the lead compound pictilisib (**4**). Taking together, indole **48** is a promising potential drug for the treatment of different types of blood cancers (such as leukaemia and lymphoma) and autoimmune diseases (such as rheumatoid arthritis and asthma).

Chapter 3, 4 and 5 focused on propeller-shaped PI3K δ inhibitors, which bind to PI3K δ in a mode different from that of flat-shaped inhibitors. In this study, the only FDA-approved selective PI3K δ inhibitor idelalisib (**8**) was used as a starting point for chemical modifications with the aim of improving PI3K δ

potency. In this study, idelalisib (**8**) was first synthesised and tested in enzymatic assay and found to inhibit the PI3K δ activity with IC_{50} of 11 nM, meaning there was substantial room for improvement of potency to 1 nM or even sub-nanomolar range. The crystal structure (PDB code 4XE0) revealed that idelalisib (**8**) bound to PI3K δ at three interaction points (specificity pocket, hinge region and hydrophobic region II), leaving the fourth region (affinity pocket) unexploited. Thus, a structure-based inhibitor design program was conducted, focused on increasing the size of idelalisib (**8**) by adding a new substituent to access the unoccupied affinity pocket. This strategy is known as drug extension, which may result in a significant improvement in the PI3K δ binding affinity.

Hence, in Chapter 3, structure-based drug design was conducted by introducing hydrogen bond donor or/and acceptor substituent into the exocyclic amine of the lead compound idelalisib (**8**) (Figure 122). After overcoming major synthetic challenges, a series of new exocyclic N-substituted idelalisib derivatives were finally obtained. Unfortunately, all compounds were inactive or far less active than idelalisib (**8**) (Figure 122). According to the results of Chapter 3, it was proposed to use an alternative attachment site to connect the new substituent to idelalisib (**8**). Based on the examples of PI3K δ inhibitors reported in the literature, it was suggested that substitution at the N-7 site of purine provided the best conventional extension strategy to position the binding group into the unoccupied affinity pocket (Figure 122), this was because the N-7 atom of the purine was oriented towards the opening of the unoccupied affinity pocket. Accordingly, in this

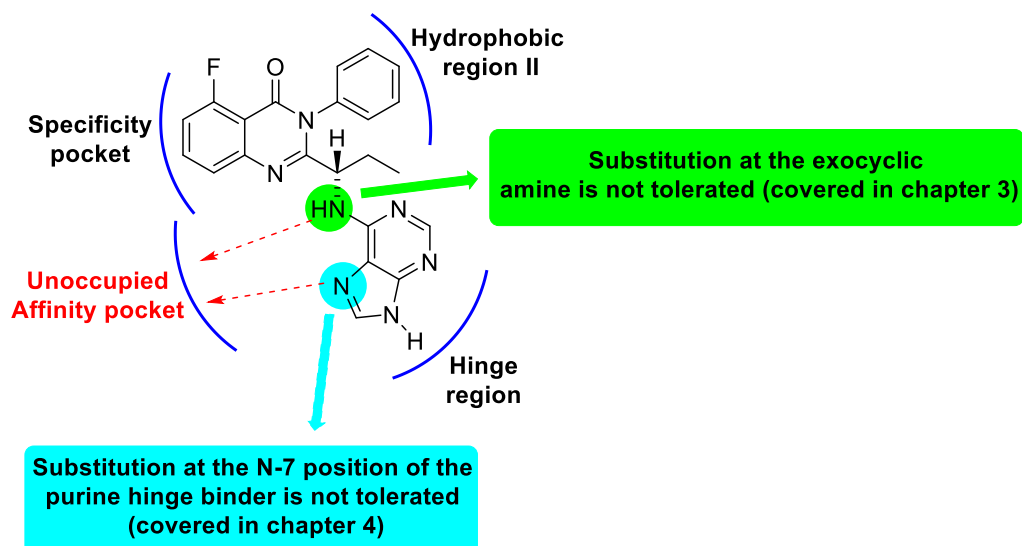


Figure 122. The selective PI3K δ inhibitor idelalisib (**8**), highlighting the positions of idelalisib (**8**) for the extension of the binding group into the unoccupied affinity pocket. SAR studies discussed in Chapter 3, reveal that substitution of idelalisib (**8**) on the exocyclic amine (in green) results in loss of PI3K δ activity. On the other hand, SAR studies discussed in Chapter 4, reveal that the addition of the extra substituent to the N-7 position of purine (in cyan) produces a detrimental effect on the PI3K δ potency.

chapter, series of novel N-7 substituted purines were synthesized and tested for their PI3K δ potency and selectivity. Disappointingly, all compounds exhibited weak or no activity against PI3K δ with almost 200-2500-fold less active than idelalisib (**8**). It was reasoned that the steric clash between the newly added substituent, and the isoleucine (Ile⁸²⁵) gatekeeper (Figure 123) could account for the substantial loss of PI3K δ potency observed across all compounds of Chapter 3 and 4. The cause of the steric clash may be attributable to high flexibility and/or tetrahedral geometry of the alkyl linker connecting the hinge-binding scaffold to the terminal functional group (Figure 123).

In light of the findings in Chapter 3 and 4, it was decided to use a planar or linear linker, to connect between the affinity pocket-binding group and the purine hinge binding moiety (Figure 134), in order to avoid the steric contact with the gatekeeper residue Ile⁸²⁵. All of the reported PI3K δ inhibitors

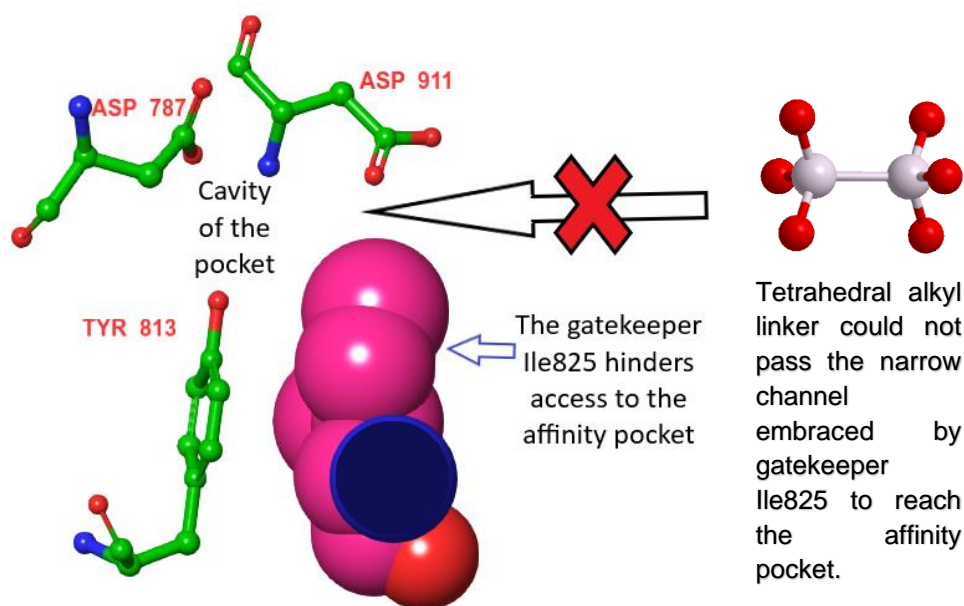


Figure 123. Crystal structure of murine PI3K δ (PDB code 4XE0) shows that the gatekeeper residue Ile⁸²⁵ (represented by a space-filling model) located at the entrance to the affinity pocket, where it limits accessibility to this pocket. Thus, steric clash is highly likely to occur between the gatekeeper Ile⁸²⁵ and compounds covered in Chapter 3 and 4, due to the tetrahedral geometry of the alkyl linkers, connecting the hinge-binding scaffold to the affinity pocket binder.

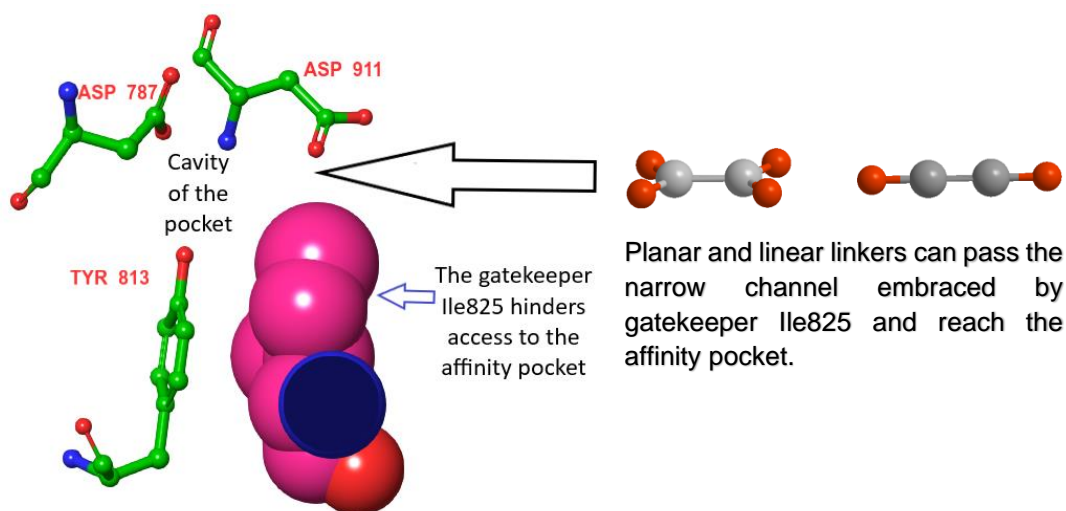


Figure 134. The use of linkers with planar or linear geometry allows the inhibitor to enter into the affinity pocket, as these linkers are able to traverse the gatekeeper Ile⁸²⁵ residue and prevent the steric clash.

targeting the affinity pocket contained either a planar aryl or linear acetylene group as a linker. Thus, a planar amide group was selected as a novel spacer to develop patentable PI3K δ inhibitors (Figure 135). Furthermore, the disappointing results obtained from Chapter 3 and 4 encouraged us to conduct structural optimisation of the hinge binding scaffold by replacing the

purine ring with a 4-aminopyrimidine ring (Figure 135), which can be easily decorated at position 5 with a linker attached to affinity pocket-binding groups (Figure 135).

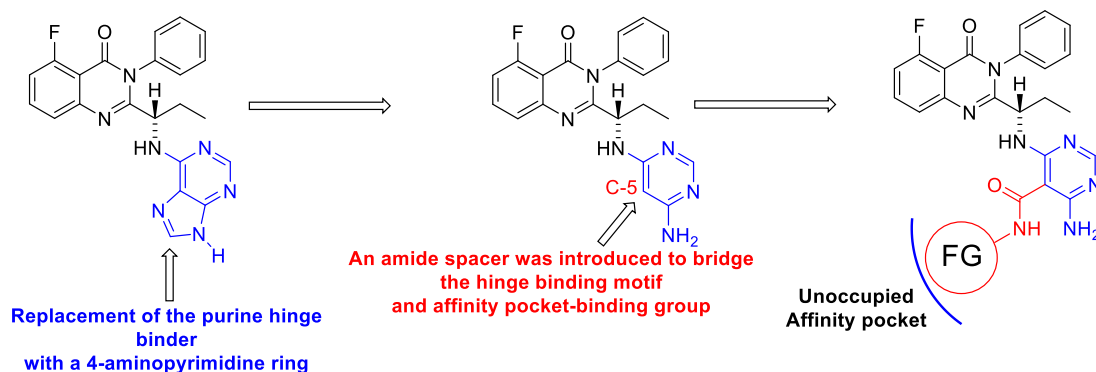


Figure 135. Structural modifications of idelalisib (**8**) were performed in Chapter 5, resulted in the development of new amide containing 4-aminopyrimidine derivatives with potent inhibitory activity against PI3K δ in the primary screening assay (1 μ M and 500 nM single concentration compound screening).

In Chapter 5, three series of pyrimidine derivatives were synthesized and tested for the *in vitro* inhibition of PI3K δ at a concentration of 1 μ M and 500 nM. The three series include 1) 13 compounds belong to 4-chloropyrimidine derivatives, 2) 7 compounds belong to 4-pyrimidinone derivatives, 3) 13 compounds belong to 4-aminopyrimidine derivatives. The former two series did not display any activity versus PI3K δ at concentration as high as 1 μ M. These findings clearly indicate that the presence of a hydrogen bond donor (-NH₂) at position 4 of the pyrimidine ring is required for the inhibition of PI3K δ . While the third series of 4-aminopyrimidine derivatives showed significant inhibitory activity against PI3K δ at a single concentration of 1 μ M and 500 nM. Interestingly, 7 compounds from this series exhibited equal or even superior potency to idelalisib (**8**) towards PI3K δ . For example, cyclohexyl derivative **218**, which was the most potent inhibitor in this series of 4-aminopyrimidines, showed higher PI3K δ inhibitory activity (87.7%) than idelalisib (**8**) (79.9%) at a single concentration of 500 nM. These results

suggested that the use of an amide group as a linker represent a promising and novel strategy in the development of new, highly potent PI3K δ inhibitors, with the potential to treat different types of blood cancers and autoimmune diseases. The second screening step aimed to determine the IC₅₀ of 13 compounds, belonging to this series of amide bearing 4-aminopyrimidines, that exhibited significant inhibition toward PI3K δ at 1 μ M and 500 nM.

6.2 Recommendations for future work

Although many of 92 compounds tested in this thesis potentially inhibited PI3K δ , recommendations for future research have been made to develop more potent and selective PI3K δ inhibitors with improved physiochemical profile. Furthermore, this future study also suggested that PI3K δ could serve as a promising therapeutic target for treatment of COVID-19-associated acute respiratory distress syndrome (ARDS).

6.2.1 Flat-shaped PI3K δ inhibitors (Chapter 2)

Future studies will be aimed at the design and synthesis of more novel flat-shaped PI3K δ inhibitors, focusing on modifications of substituents that extend toward tryptophan shelf and affinity pocket to improve PI3K δ activity and selectivity.

6.2.1.1 Tryptophan shelf

As previously mentioned (see Section 2.5.3 of Chapter 2), it was believed that the introduction of fluorine atom into the piperidine ring enhanced the PI3K δ activity and selectivity (Table 62) potentially by attracting the electron density away from the piperidine ring and made the piperidine hydrogens more acidic and thus strengthening the C-H/ π interaction in the tryptophan shelf, resulting

in the most selective PI3K δ inhibitor **48** among the thienopyrimidine series (see Figure 49 (Plot of PI3K δ activity as a function of PI3K δ isoform selectivity (vs PI3K α) in Chapter 2).

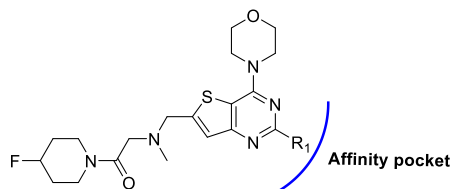


Table 62. Biological evaluation and isoform selectivity for PI3K δ for compounds pictilisib (**4**), idelalisib (**8**) and fluoropiperidine derivatives **48** and **49**.

		Isoform potency ^{a,b} IC ₅₀ (nM)	Isoform selectivity		
Compd	R ₁	PI3K δ	δ/α	δ/β	δ/γ
Pictilisib (4)	-	11	4	20	20
Idelalisib (8)	-	11	14000	56	56
48		4.4	506	636	161
49		1.1	16	505	32

Marvin, C *et al*^{β71} have measured and tabulated the inductive substituent constant for many hundreds of substituent groups, which have higher and lower inductive substituent constants than fluorine atom. Monofluorinated analogue **48** with its excellent activity and selectivity profile will be used as a basis of comparison to measure any increase or decrease in the inhibitory activity that may be brought about by replacement of fluorine with another atom or group. The objective of this future research is to design and synthesize some novel piperidine analogues, which have electron withdrawing substituents that are stronger or weaker than fluorine on their piperidine ring (Table 63). The expectation is that piperidine analogues having

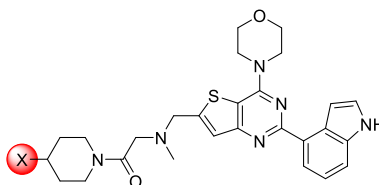


Table 63. Inductive substituent constants for many substituent groups, it also highlighted the biological activity of 4-fluoropiperidine **48** and 4-unsubstitutedpiperidine **37** derivatives.

Compd	X-	Inductive Substituent Constant	PI3K δ potency IC ₅₀ (nM)	Less inductive groups
37	H-	0.00	11	↑
263	CH ₃ -	-0.05		
264	MeO-	0.25		
265	CF ₃ -	0.42		
266	Cl-	0.47		
48	F-	0.52	4.4	
267	CN-	0.58		↓
268	NH ₃ ⁺	0.60		
269	MeNH ₂ ⁺ -	0.60		
270	MeSO ₂ ⁻	0.61		
271	SCN-	0.61		
272	Me ₂ NH ⁺ -	0.70		
273	Me ₃ N ⁺ -	0.93		
274	NO ₂ ⁻	0.76		

electron-withdrawing groups stronger than fluorine will provide higher PI3K δ activity and selectivity than compound **48** (Table 63), while those having electron-withdrawing groups weaker than fluorine will provide less PI3K δ activity and selectivity than compound **48** (Table 63). This study may provide the rationalization for the difference in PI3K δ activity of analogues having different substitution on the piperidine ring.

The second approach is to replace the piperidine ring with the six-membered heteroaryl rings. Brandl, M, *et al*⁵² reported that the protons of sp²-carbons

are in general more acidic than the hydrogens on saturated sp^3 -carbon atoms, thus unsaturated heterocycles, such as pyridine and pyrazine could make stronger C-H/ π interactions than their saturated counterparts piperidine and piperazine. Targeting the tryptophan shelf with an aryl group (phenyl) was not a novel idea and had been done before in this project (compounds **34** and **35** in Chapter 2) as well as by Terstiege *et al*²²⁰ group (compound **67** in Chapter 2)²²⁰, where the phenyl derivatives showed weaker activity in contrast to the saturated heterocycles such as piperidine and morpholine, however, in this study the tryptophan shelf will be targeted with aromatic heterocycles, which are generally more electron deficient compared to phenyl ring (Figure 136)^{372,373}, and thus they have more acidic protons and able to make stronger C-H/ π interactions with Trp⁷⁶⁰ in contrast to the benzene ring. To the best of authors' knowledge, unsaturated heterocycles have not previously been used to explore the tryptophan shelf.

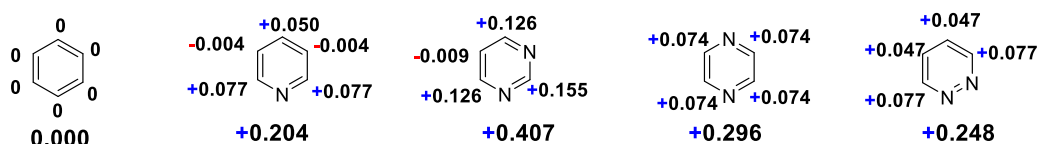


Figure 136. The local and total pi-deficiency of the four six-membered unsaturated heterocycles showed that they are more electron deficient than benzene^{373,374}. The pi-deficiency values of benzene were taken from a study of 'Anion- π interactions: from concept to application' conducted by Xiaonan Kan *et al*³⁷⁴, while the pi-deficiency values of the four six-membered unsaturated heterocycles were taken from a book 'The Chemistry of Heterocycles' written by Vishnu Ji Ram *et al*³⁷⁵.

6.2.1.2 Affinity pocket

6.2.1.2.1 Investigate the role of the hydrogen bond donor (hydrogen at C-2 on indole) in PI3K δ selectivity.

As pointed out in Chapter 2 (see Section 2.5.1 on pages 63 to 66), Sutherlin *et al*¹⁶⁰ hypothesized that the high PI3K δ selectivity of indole analogues was due to the presence of hydrogen bond donor (C-2 proton) which made a

hydrogen bond network with Tyr⁸¹³ and His⁹⁰⁹ that could be only accommodated in PI3K δ (see Figure 34 in Chapter 2). Although Sutherlin's hypothesis was accepted by many researchers¹⁴⁴, there is an element of doubt about its validity. The basis of this doubt is on the evidence presented in the Safina *et al*¹⁶¹ study, which was published two months before Sutherlin *et al* paper¹⁶⁰, as one of the findings to emerge from Safina *et al*¹⁶¹ study was that the 2-methylindole derivative **63**, which did not have a proton (hydrogen bond donor) at position 2 of the indole ring, showed similar PI3K δ selectivity profile to its 2-unsubstituted indole analogue **62** (Table 64), indicating that the absence of the hydrogen bond donor (C-2 proton) did not have impact on the selectivity for PI3K δ over the remaining isoforms, which was not consistent with Sutherlin *et al*¹⁶⁰ theory.

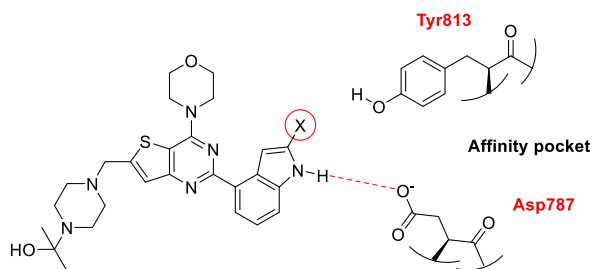


Table 64. Biological evaluation and isoform selectivity for PI3K δ for compounds **62** and **63** reported by Safina *et al*¹⁶¹.

compd	X	PI3K δ IC ₅₀ (nM)	Isoform selectivity		
			δ/α	δ/β	δ/γ
62 ¹⁶¹	H	1.8	129	104	1444
63 ¹⁶¹	CH ₃	1.1	122	101	715

Therefore, it was decided to further test Sutherlin *et al*¹⁶⁰ hypothesis in the best selective compound **48** reported in the thienopyrimidine series by removing the hydrogen bond donor, this can be achieved by the substitution of acidic hydrogen at C-2 position of the indole ring with another atom or group which cannot act as a hydrogen bond donor. Fluorine atom will be the best

Chapter 7

option due to its small Van der Waals radius which is slightly higher than that of hydrogen (1.47 and 1.20 Å, respectively)^{376,377}. The use of small Van der Waals atoms is to eliminate the possibility of steric clash with the binding site that could arise when bulkier atoms or groups are used, if the 2-fluoroindole analogue **275** was more potent or equipotent to the 2-non-substituted indole derivative **48** (Table 65), then the Sutherland *et al*¹⁷² theory about the high PI3K δ selectivity of indole analogues was not true.

The synthesis of 2-fluoroindole derivatives is not widely known, this has been attributed to challenges associated with the synthesis of such compounds, however, Ichikawa *et al*⁷⁸ developed a new two-step method to synthesize 2-fluoroindole-4-boronic acid pinacol ester **278** From *o*-tosylamino- β,β -difluorostyrene derivative **276** (Scheme 29), which can be utilised to synthesize the 2-fluoroindole-containing compound **275** (Scheme 30).

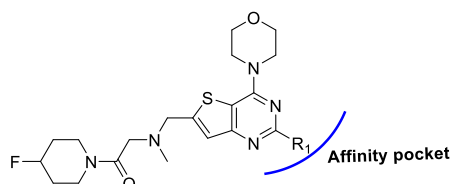
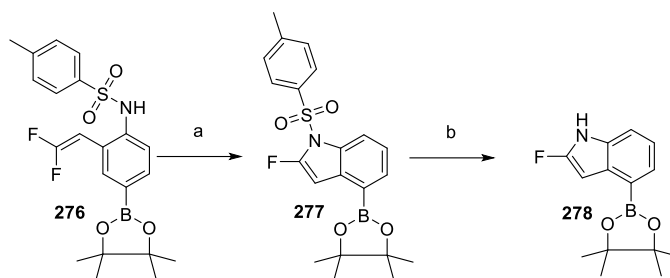
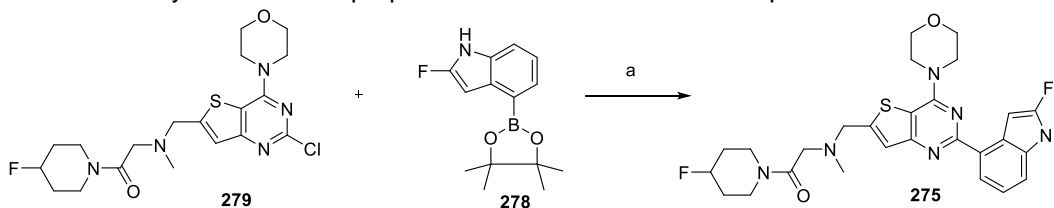


Table 65. Biological evaluation and isoform selectivity for PI3K δ for compound **48** and suggested compound **275**, which is aimed to be synthesised in the future.

compound	R ₁	PI3K δ IC ₅₀ (nM)	Isoform selectivity		
			δ/α	δ/β	δ/γ
48		4.4	506	636	161
275		?	?	?	?

Scheme 29. Synthesis of 2-Fluoroindole -4-boronic acid pinacol ester **278** reported by Ichikawa *et al*⁶⁷⁸

^aReagents and conditions: (a) sodium hydride, DMF, 70°C, 23 h, yields 73%; (b) KOH, THF, ethanol, rt, 2h, yields 53%.

Scheme 30. Synthesis of the proposed 2-fluoroindole based compound **275**

^aReagents and conditions: (a) Na₂CO₃, EtOH, bis(triphenylphosphine) palladium (II) chloride, microwave 125 °C, 3 h.

6.2.1.2 Investigate the correlation between the hydrogen bond donor (phenolic proton) acidity and PI3K δ potency

The next step in the future work will be on the phenol derivative **49**, which was emerged to be the most active compound in the whole series, with 10 times more active than the clinically approved idelalisib (**8**) (Table 62). It has already been mentioned that the high PI3K δ activity of the phenol derivatives in contrast to their indole and indazole counterparts might be due to the formation of stronger hydrogen bond with Lys⁷⁷⁹ and Asp⁷⁸⁷ in the affinity pocket (Figure 137b), because phenol is a stronger hydrogen bond donor. Further research will attempt to modify the strength of hydrogen bond to improve the PI3K δ activity by introducing an electron-withdrawing group into the para-position to the OH group (Table 66). The ortho substitution will be avoided to prevent the formation of intramolecular hydrogen bond which will mask the donor ability of phenolic hydroxyl group resulting in diminishing the

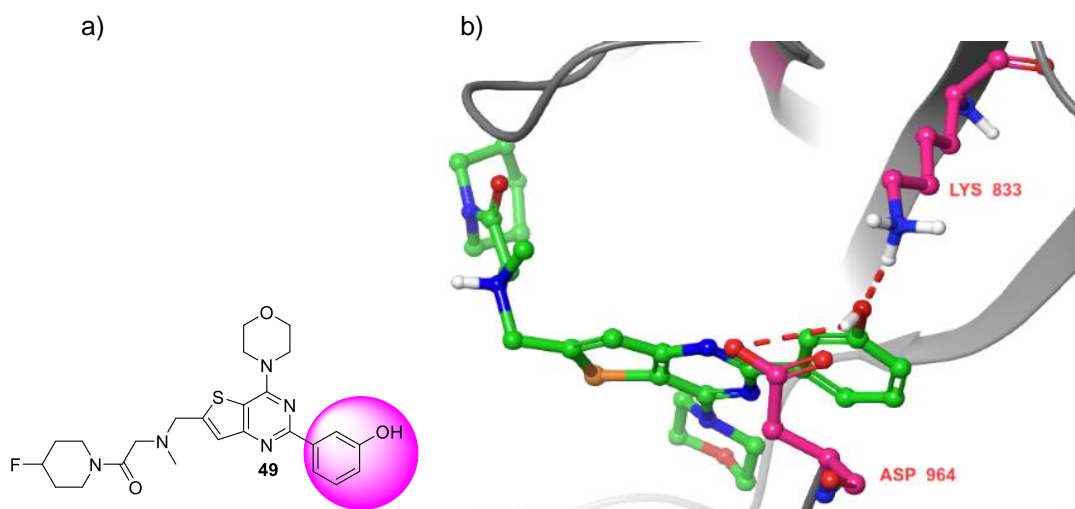


Figure 137. a) Compound **49**, highlights the phenol group that bound to the affinity pocket. b) Compound **49** docked into (K802T) PI3K δ (generated from PDB code 4EZJ). Dashed pink lines represent the proposed charge-enhanced hydrogen bonds.

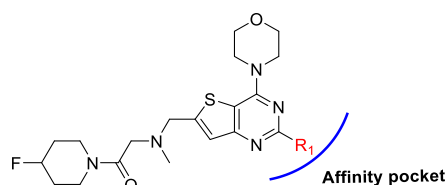
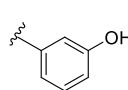
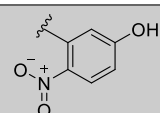
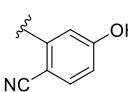
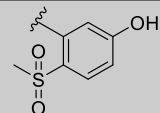
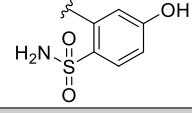
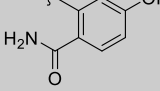


Table 66. Biological evaluation and isoform selectivity for PI3K δ for compound **49** and suggested compounds (**280-284**), which are aimed to be synthesised in the future.

compd	R ₁	PI3K δ IC ₅₀ (nM)	Isoform selectivity			pKa of parent phenols (ChemicalBook database)
			δ/α	δ/β	δ/γ	
49		1.1	16	505	32	9.89
280		?	?	?	?	7.15
281		?	?	?	?	7.97
282		?	?	?	?	7.83
283		?	?	?	?	7.81
284		?	?	?	?	8.60

PI3K δ activity³⁷⁹. The strength of the hydrogen bond depends on the value of pKa, therefore as the acidity of the phenol increases the hydrogen bond donating ability also increases. Accordingly, the aim of this study is to synthesize numerous phenol derivatives with a powerful electron-withdrawing group in para-position to a hydroxy group. (Table 66).

6.2.2 Propeller-shaped PI3K δ inhibitors (Chapter 5)

6.2.2.1 Escape from flatland

To the best of authors' knowledge, the chemical structures of the vast majority of the reported PI3K δ inhibitors contain 4 to 5 aromatic rings^{144,154,155,173}, thus they are more planar and contain less fraction of sp³ carbons in contrast to other drugs³⁸⁰. Ritchie *et al*³⁸¹ mentioned that most of the compounds that contain more than 3 aromatic rings exhibit poor aqueous solubility, resulting in deterioration in compound developability and increased risk of attrition in drug development^{382,383}. By contrast, increase in the Fsp³ content by replacement of aromatic rings with aliphatic rings leads to an increase in the aqueous solubility and reduction in lipophilicity, which positively affects the developability of drug candidates^{357,381,384}. Furthermore, Lovering *et al*³⁵⁷ and Hetal *et al*³⁸⁵ reported that compounds with enriched sp³ carbon content tend to possess out-of-plane substituents, which can lead to additional PI3K δ -ligand interactions^{357,386}.

Consequently, the future study will be focused on the development of PI3K δ inhibitors with desirable drug properties, by limiting the number of aromatic rings and increasing the Fsp³ content, this approach is known as escape from flatland. The suggested compounds comprise a hinge binding scaffold (4-aminopyrimidine) and affinity pocket-binding group connected through a

cyclopropyl linker (Figure 138). The utilisation of the saturated cyclopropyl as a linker represents an alternative approach to the widely used aryl and acetylene groups (see Section 5.2.1 and 5.2.2 in Chapter 5). The cyclopropane group is unique among alicycles for having a planar geometry, like aryl groups³⁸⁷, which enables it to avoid the steric clash with the gatekeeper Ile⁸²⁵ and allows the functional group to access the affinity pocket. As far as is known, this is the first study employing a saturated group as a linker in the design of PI3K δ inhibitors, therefore, it can provide an advantage in term of novel intellectual property. Furthermore, compared with the phenyl linker, which is widely applied for the design of PI3K δ inhibitors, the introduction of cyclopropyl linker leads to the superior physiochemical properties such as a smaller molecular weight, higher Fsp³ carbons, greater aqueous solubility and lower lipophilicity (Figure 138).

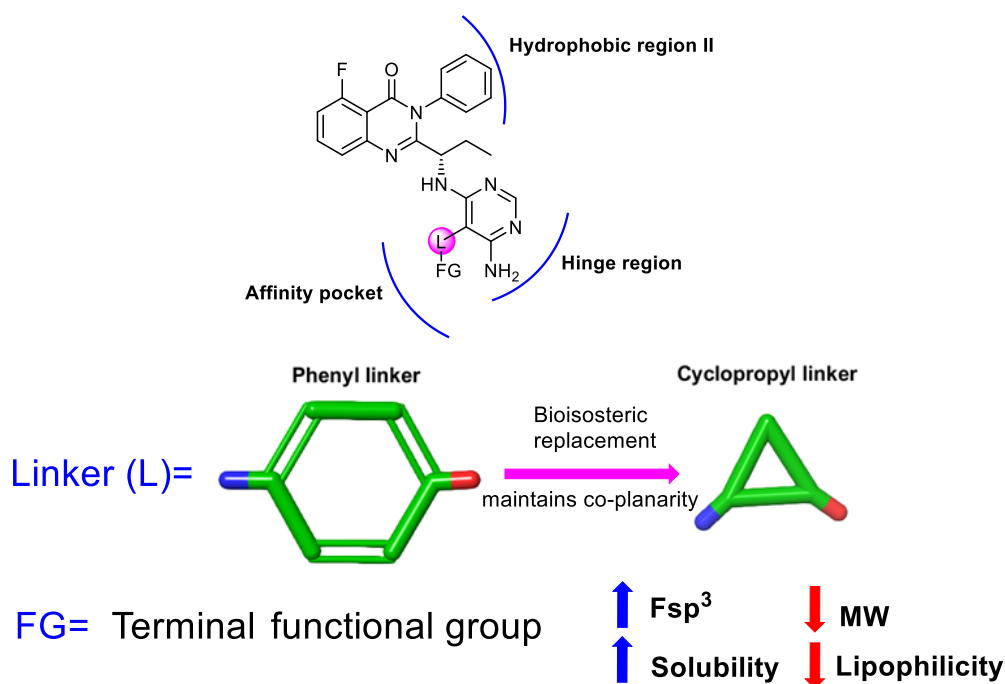


Figure 138. Replacement of the phenyl linker with a bisosteric cyclopropyl group can provide an advantage in terms of physical properties (Fsp³, molecular weight, solubility and lipophilicity).

In addition to cyclopropane group, there are other saturated rings have emerged as bioisosters for phenyl rings due to their rigidity, planarity and size, suggesting that they might be utilized as a spacer between the hinge binder and affinity pocket-binding moiety. These groups include cubane, bicyclopentane and bicyclooctane (Figure 139)³⁸⁸, which might have a beneficial impact on the future design of patent-free PI3K δ inhibitors with high 3-dimensionality.

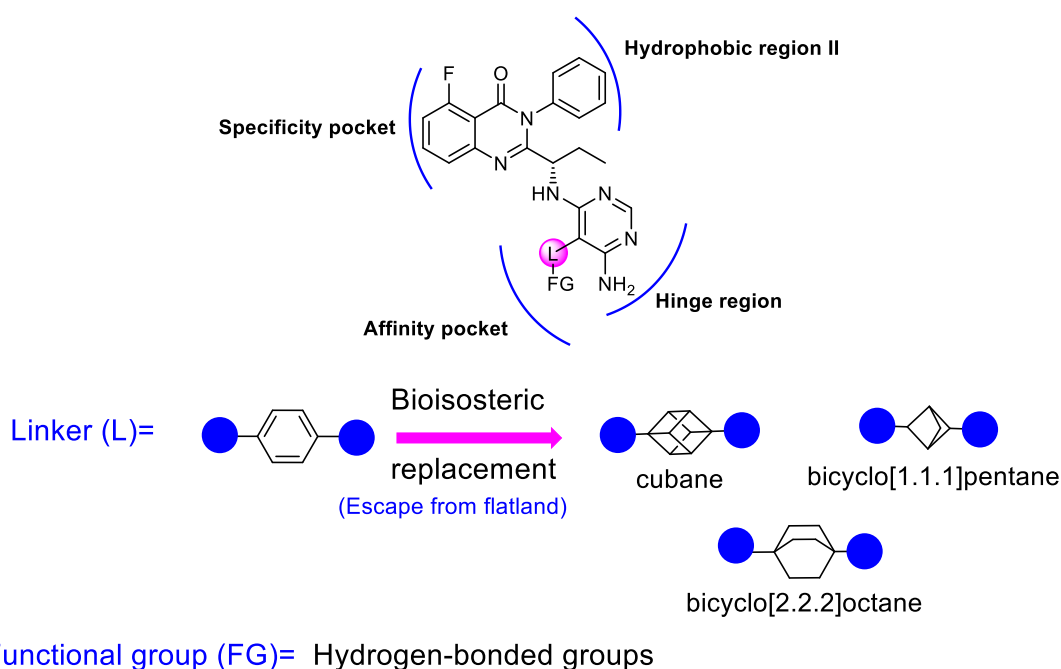


Figure 139. Bioisosteric replacement of benzene ring with three saturated bioisosters (cubane, bicyclo[1,1,1]pentane, bicyclo[2,2,2]octane) to create patent-free molecules with improved physical properties (solubility and permeability)³⁸⁸.

Moreover, the phenyl group, that extends into the hydrophobic region II will also undergo structural modifications by bioisosteric replacement with a saturated group. The objective of this modification is to further improve the physicochemical properties of the new series of PI3K δ inhibitors. Somoza *et al*¹⁸⁰ reported that the phenyl moiety of idelalisib (**8**), that inserts deep into the hydrophobic region II, only engaged in hydrophobic interactions with the side chains of Asp⁸³², Thr⁸³³ and Asn⁸³⁶. This suggests that substitution of the

phenyl ring with a cyclopropyl would maintain potency at PI3K δ , since the latter group, like the former, is also capable of making hydrophobic interactions. This is supported by evidence from Novartis study³³⁵, which showed that compound **286** with a cyclopropyl group oriented towards the hydrophobic region II displayed equipotent activity against PI3K δ , compared with its phenyl counterpart **285** (Table 67)³²⁴. Based on this, the cyclopropyl group is adopted as a hydrophobic region II-binding motif for the design of future inhibitors, which ultimately leads to the development of a novel series of dicyclopropyl-containing PI3K δ inhibitors (Table 68).

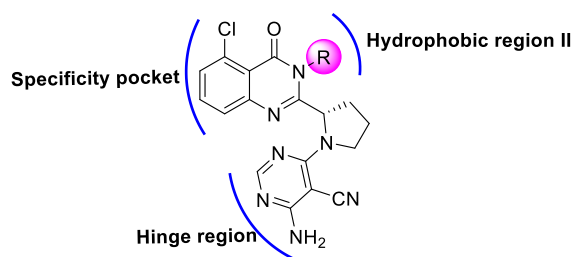


Table 67. SAR exploration of the hydrophobic region II (reported by Novartis)³²⁴.

compd	R	PI3K δ IC ₅₀ (nM)
285 ³²⁴		3
286 ³²⁴		7

The introduction of a cyclopropyl group to replace the phenyl substituent affords compounds with physicochemical properties (molecular weight, tPSA and HBD/ HBA) within a range expected to be optimum for oral bioavailability (Table 69). Furthermore, the Fsp³ values for this series of dicyclopropyl derivatives are 0.64, which is consistent with optimal Fsp³ values (0.47-0.75) for the most FDA-approved small molecules (Table 69)³⁵⁷. Lovering *et al*³⁵⁷ reported that compounds having Fsp³ greater than 0.47 have often favourable aqueous solubility and high selectivity to a given biological target by making

additional protein-ligand interactions not accessible to a planar aromatic ring^{357,385}.

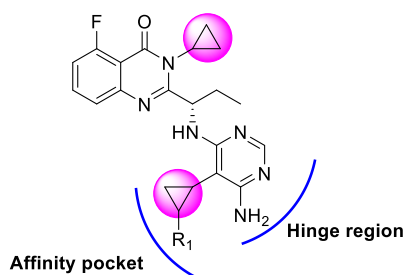


Table 68. Structure of the proposed dicyclopropyl-containing compounds (**287- 291**), the first cyclopropyl group acts as a linker to connect the aminopyrimidine hinge-binding core with a terminal binding group (R_1), whereas the second cyclopropyl group acts as a hydrophobic-region II binding motif.

compd	R_1
287	
288	
289	
290	
291	

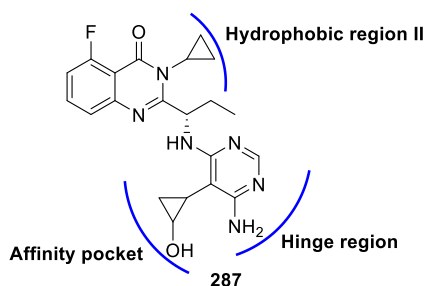
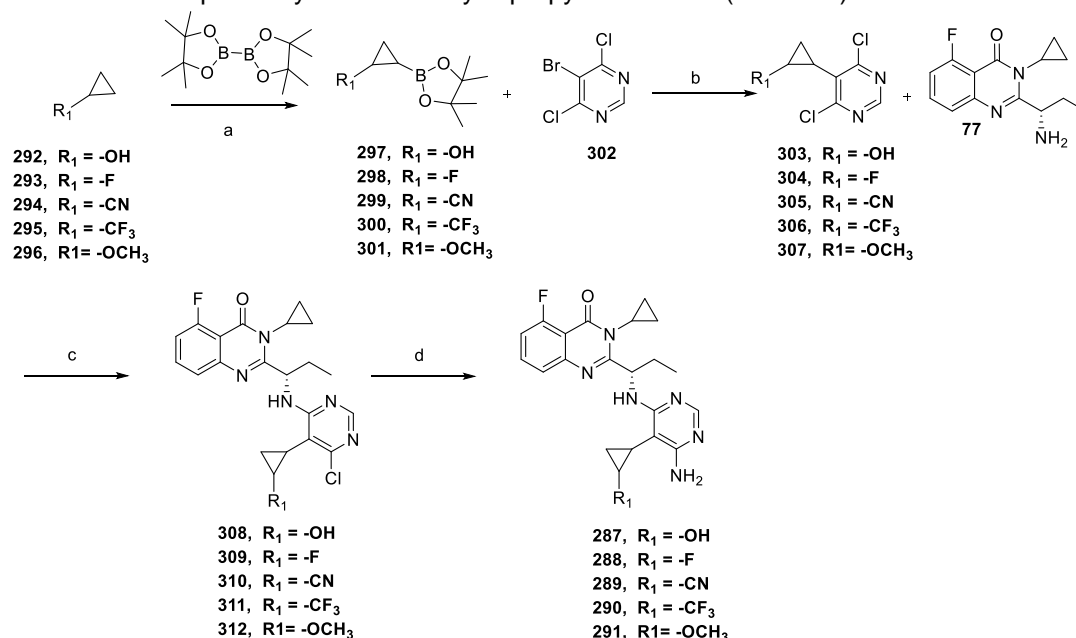


Table 69. Physicochemical properties of dicyclopropyl-containing compound **287**. It displays that compound **287** has the appropriate physicochemical properties required for optimal oral bioavailability^{264,357-359}.

Physical properties	Compound 287	Optimal range for oral bioavailability
Molecular weight	409.47	<500
Fsp³	0.642	0.47-0.75
H.B. D	3	<5
H.B. A	6	<10
tPSA	121.46	60-140 A°
clog P	1.05	2-3
Rotatable bonds	6	<10

Hence, the main objective of future study is to design and synthesize a novel series of dicyclopropyl derivatives as potential PI3K δ inhibitors (**287- 291**) (Table 68). Herein, a synthetic method has been reported for the preparation of these compounds (Scheme 31). The first key step of the synthesis is based on the borylation of mono substituted cyclopropanes (**292- 296**) with pinacolborane in the presence of an iridium catalyst³⁸⁹. Next, the obtained boronate ester (**297- 301**) is subjected to the Suzuki coupling with 4,6-dichloro-5-bromopyrimidine **302** to generate the respective coupling products (**303- 307**), followed by a subsequent substitution with the primary amine intermediate **77** to afford the monochloropyrimidine derivatives (**308- 312**). Finally, the second chloride of compounds (**308- 312**) was substituted by an amino group using ammonium hydroxide in NMP to generate the final screening diaminopyrimidines (**287- 291**).

Scheme 31. Proposed synthesis of dicyclopropyl derivatives (**287- 291**)



^aReagents and conditions: (a) (1,5-cyclooctadiene)(methoxy)iridium(I) dimer (0.03 equiv), 2,9-dimethyl-1,10-phenanthroline (0.06 equiv), THF, 90°C, 18 h; (b) Na₂CO₃ (3 equiv), bis(triphenylphosphine) palladium (II) chloride (0.1 equiv), EtOH, microwave 125 °C, 3 h; (c) DIPEA (10 equiv), dioxane, 50°C, 30 min; (d) Cu₂O (0.01 equiv), NH₄OH-NMP (1:1, v/v), microwave, 50°C, 30 min.

6.2.3 A novel potential role of PI3K δ inhibitors in the treatment of COVID-19 induced acute respiratory distress syndrome (ARDS)

ARDS is a life-threatening condition, characterized by acute severe hypoxemia due to massive alveolar damage, allows fluid from the surrounding small blood vessels to accumulate in alveoli and limiting oxygen intake, makes it difficult for lung to provide enough oxygen to the body's vital organs³⁹⁰. ARDS is the leading source of morbidity in hospitalised COVID-19 patients^{391,392}, where ARDS causes COVID-19 patients to lose their ability to breathe on their own and may require assistance via mechanical ventilation to help the circulation of oxygen³⁹³. Thus, unified ARDS treatment can play an important role in reducing the mortality of COVID-19. It is now widely accepted that ARDS is caused by neutrophils infiltration into the lung, where neutrophils are activated and release of inflammatory mediators resulting in direct alveolar and endothelial injury^{394,395}. neutrophils are recruited to the lung in response to pro-inflammatory mediators (TNF- α , IL-6, IL-8 and IL-10) secreted by alveolar macrophages^{394,395}. It has been reported that Bruton tyrosine kinase (BTK) is a key signalling enzyme controlling the secretion of TNF- α , IL-6, IL-8 and IL-10 from alveolar macrophages (Figure 140)^{394,396}. Thus, pharmacological inhibition of BTK activity would be an effective strategy to treat ARDS. Recently, AstraZeneca has initiated a clinical trial of BTK inhibitor (acalabrutinib, **313**) (Figure 141) in severely ill COVID-19 patients with acute respiratory distress syndrome (ARDS)³⁹⁷. Early data suggest that acalabrutinib (**313**) was able to reduce inflammation and improve survival among hospitalized COVID-19 patients³⁹⁷.

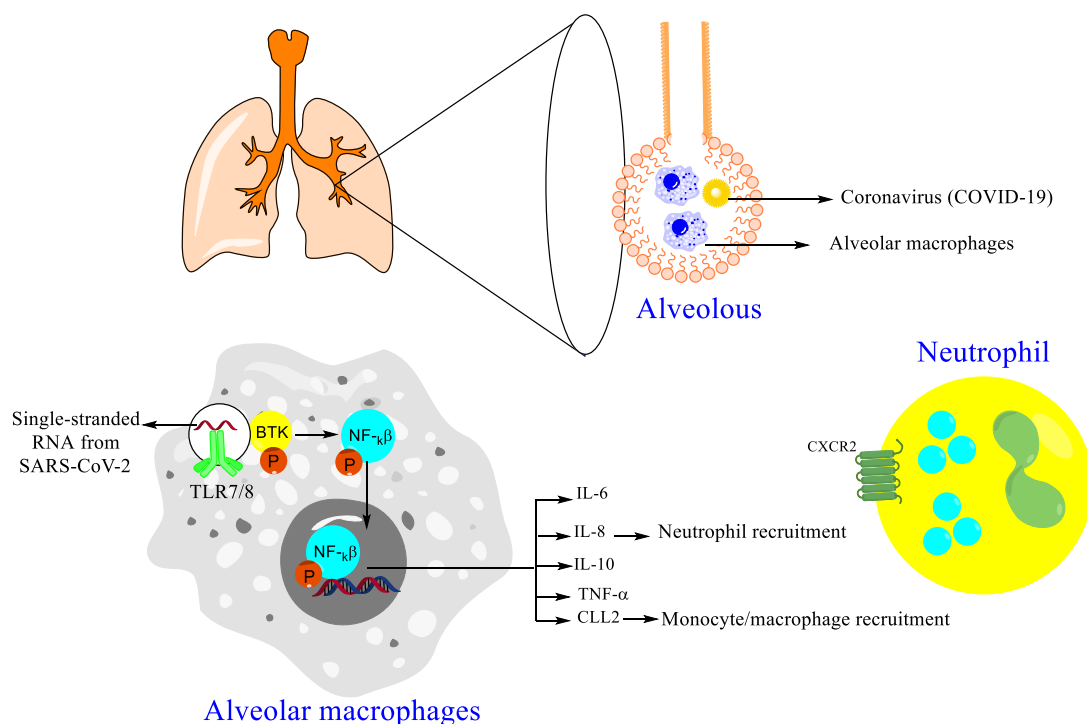


Figure 140. The role of BTK in the pathogenesis of COVID-19-associated acute respiratory distress syndrome (ARDS). Alveolar macrophages recognise the viral particle or cellular debris containing viral single-stranded RNA (ssRNA) and clear them by phagocytosis. In alveolar macrophages, Toll-like receptors (TLRS) directly recognize and bind to the viral single-stranded RNA, resulting in the activation of BTK signalling pathway. BTK then activates the transcription factor NF- κ B and thereby initiates NF- κ B translocation to the nucleus, leading to the transcription and secretion of pro-inflammatory cytokines, which are responsible for the rapid recruitment of neutrophils and monocytes/macrophages to the lung at a later stage of severe COVID-19 infection³⁹⁷.

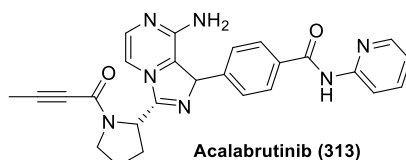


Figure 141. The BTK inhibitor acalabrutinib (**313**), which is currently undergoing phase II clinical trials for the treatment of coronavirus-induced acute respiratory distress syndrome^{398,399}.

Songbo Xie *et al*⁴⁰⁰ and Hawkins *et al*⁴⁰¹ reported that PI3K δ pathway also triggers the production of proinflammatory cytokines/chemokines (TNF- α , IL-6 and IL-10) by alveolar macrophages (Figure 142). Suggesting that PI3K δ signalling, like BTK, may play a key role in the pathogenesis of ARDS. Accordingly, the objective of the future study is to evaluate the therapeutic effect of PI3K δ inhibitor on release of pro-inflammatory mediators from alveolar macrophages to identify whether PI3K δ inhibitors have potential as

a new therapeutic agent for COVID19-associated ARDS. Furthermore, the synergetic inhibition effect of PI3K δ inhibitor and BTK inhibitor (acalabrutinib, **313**) will also be investigated. If the benefit of PI3K δ inhibitors was confirmed in the previous two above-mentioned studies, then the aim of the next project will be to develop novel dual PI3K δ /BTK inhibitors for the treatment of COVID-19-induced ARDS.

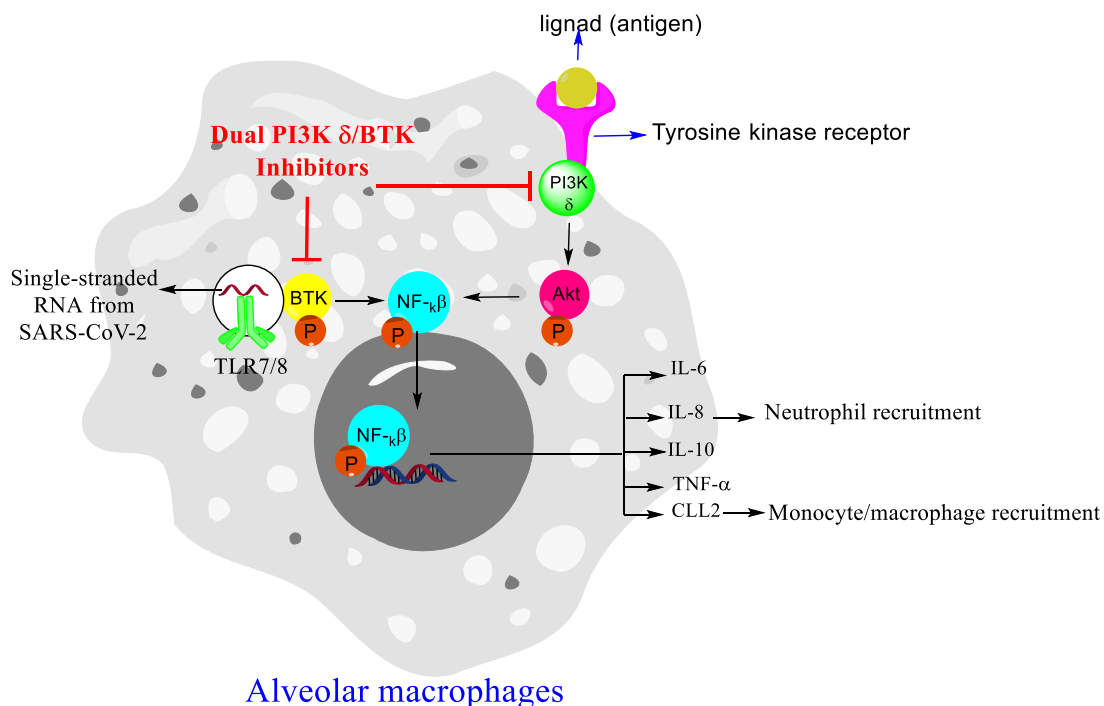


Figure 142. In alveolar macrophages, PI3K δ signalling and BTK signalling share the same transcription factor (NF- κ B), which initiates and regulates the expression of proinflammatory cytokines that trigger ARDS induced by COVID-19 virus. Thus, it was hypothesized that development of dual inhibitors targeting both PI3K δ and BTK can be a promising evolutionary strategy for the treatment of life-threatening acute respiratory syndrome caused by SARS-CoV-2 virus⁴⁰².

Chapter 7 Experimental

7.1 Molecular Docking

All the ligand-protein docking studies were performed using Schrodinger suite 2017 (LLC, New York, NY, USA). The following Maestro 11.7 version packages were used: Protein Preparation Wizard, Grid Generation, LigPrep and Glide ligand docking.

7.1.1 Preparation of protein

The X-ray crystal structure of murine PI3K δ in complex with idelalisib (**8**) (PDB code 4XE0) and compound **66** (PDB code 5IS5) and the crystal structure of human K802T-mutant PI3K γ in complex with compound **60** (PDB code 4EZJ) and compound **61** (PDB code 4EZK) were used as a protein template. All the selected crystal structures were obtained from the PDB, accessible at www.rcsb.org. The 3-D structure of PI3K δ was prepared using the protein preparation wizard (Schrödinger Suite, version 10.7.15), where the non-protein portion, including ligands and water molecules were eliminated and hydrogen atoms were added to the protein structures. In the final step of protein preparation, proteins structure was minimized using OPLS_2005 force field.

7.1.2 Receptor grid generation

Afterwards, receptor grids were generated by defining the active site with a 3D cubic box using "Receptor Grid Generation" panel in the Grid-based Ligand Docking With Energetics (Glide) application. The receptor grid box was created around the binding site residues which include (Thr⁷⁵⁰, Met⁷⁵², Pro⁷⁵⁸, Trp⁷⁶⁰, Ile⁷⁷⁷, Lys⁷⁷⁹, Leu⁷⁸⁴, Asp⁷⁸⁷, Leu⁷⁹¹, Tyr⁸¹⁵, Glu⁸²⁶, Val⁸²⁷, Val⁸²⁸, Leu⁸²⁹, His⁸³⁰, Ser⁸³¹, Asp⁸³², Thr⁸³³, Leu⁸³⁴, Ala⁸³⁵, Asn⁸³⁶ and Asp⁹¹¹). Each grid is set with inner and outer box sizes of 10 and 30 Å, respectively.

7.1.3 Ligand preparation

All studied inhibitors were sketched using Chemdraw Professional 16 (Version 16.0.1.4, PerkinElmer informatic) in SDF file. The LigPrep 2.5 module (Small-molecule drug Discovery Suite 2017-4, Schrödinger, LLC, New York, NY, USA) was used for the final preparation of ligands into their lowest energy 3D conformation. These energy minimized structures were used for Glide docking.

7.1.4 Ligand virtual screening

All compounds were docked into the active site of the PI3K δ protein using the standard-precision mode of Glide docking (Small-Molecule Drug Discovery Suit 2017-4 Schrödinger, LLC, New York, NY, USA). The number of positions per ligand was set to three, after energy minimisation. The best docked structures were chosen based on consistency of binding mode with retention of critical interactions.

7.2 Analysis of drug-likeness

The physicochemical properties of the studied compounds such as molecular weight, lipophilicity (clog P) and topological polar surface area (tPSA) were calculated using Osiris Data Warrior 5.0.0. software.

7.3 Chemistry

7.3.1 Materials and instrumentation

Reagents and solvents which were used in the experiments were purchased from commercial supplier such as Fluorochem, Sigma-Aldrich, Tokyo Chemical Industry UK and Fisher Scientific. Column chromatography was performed with analytical-grade solvents using silica gel 60 Å, 230-400 mesh particle size (Sigma-Aldrich). Reactions were monitored by thin-layer chromatography (TLC). TLC was performed on Fischer Scientific silica gel plates and visualized by ultraviolet lamp with 254 nm wavelength.

NMR spectra were recorded on a Bruker advance II series (9.4T). ^1H NMR spectra were recorded at 400 MHz and ^{13}C NMR spectra at 100 MHz. Chemical shifts δ are given in [ppm] relative to TMS and all coupling constants J are given in [Hz]. The spectra are referenced to the signal of the deuterated solvent: CDCl_3 ($\delta_{\text{H}}= 7.26$, $\delta_{\text{C}}= 77.16$ ppm), DMSO ($\delta_{\text{H}}= 2.50$, $\delta_{\text{C}}= 39.50$ ppm) and MeOD_4 ($\delta_{\text{H}}= 3.31$, $\delta_{\text{C}}= 49.00$ ppm). The following abbreviations were used to explain the multipliciteis: s, singlet; doublet; t, triplet; q, quartet and m, mutiplet. Furthermore, 2D-NMR experiment (HMPC) was used to distinguish between the regioisomers. The spectra NMR data were analyzed and processed with Mnova 14.1.2 software from Mestrela Research S. L.

LCMS spectra were performed on a Shimadzu UFLCXR system coupled to an Applied Biosystemes API2000, and visualized at 220 nm (channel 2) and 254 nm

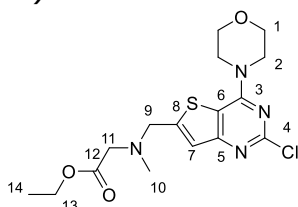
References

(channel 1). LC-MS was carried out using a Phenomenex Gemini-NX C18 110A (50 mm X 2 mm X 3 μ m) at a flow rate 0.5 ml/min over a 5 min period.

All microwave reactions were performed in a Bioteg Initiator Microwave. Sonication were carried out in a Fisher Scientific FS30H Ultrasonic Cleaning Bath.

7.3.2 Experimental for Chapter 2

Ethyl N-((2-chloro-4-morpholinothieno[3,2-d]pyrimidin-6-yl)methyl)-N-methylglycinate (18, 55% yield).



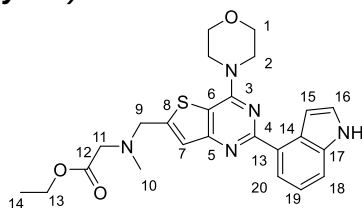
A solution of 2-chloro-4-morpholinothieno [3,2-d]pyrimidine-6-carbaldehyde **17** (10.60 mmol, 1 equiv), sarcosine ethyl ester (10.60 mmol, 1 equiv) and triethylamine (21.2 mmol, 2 equiv) in methanol (30 mL) was stirred for 30 min at RT, followed by the addition of acetic acid (4.8 mL) and the solution was stirred for other 30 min, followed by the addition of picoline borane (21.1 mmol, 2 equiv). The mixture was stirred for 16 h at RT. The solvent was removed and the residue was partitioned between ethyl acetate (100 mL) and saturated sodium hydrogen carbonate (100 mL). The aqueous phase was washed twice with ethyl acetate, then the combined organic phases were dried over (MgSO₄), filtered and concentrated under reduced pressure. The residue was purified by flash column chromatography on silica gel eluting with 3% methanol (containing 0.7N ammonia) in DCM to afford tertiary amine **18** (35.62%) as a white solid. ¹H NMR (400 MHz, DMSO) δ 7.29 (d, J = 1.1 Hz, 1H, H-7), 4.12 (q, J = 7.1 Hz, 2H, H-13), 4.07 (d, J = 1.1 Hz, 2H, H-9), 3.89 (dd, J = 5.8, 4.0 Hz, 4H, H-1), 3.76 (dd, J = 5.7, 3.9 Hz, 4H, H-2), 3.46 (s, H-11), 2.37 (s, 3H, H-10), 1.22 (t, J = 7.1 Hz, 3H, H-14). ¹³C NMR (101 MHz, DMSO-d₆) δ 170.79 (C-12), 163.17 (C-5), 158.44 (C-4), 156.31 (C-3), 154.37 (C-8), 121.92 (C-7), 112.78 (C-6), 66.39 (C-1), 60.50 (C-13), 57.57 (C-11), 55.42 (C-9), 46.47 (C-2), 41.85 (C-10), 14.73 (C-14). LCMS *m/z* calc. for C₁₆H₂₁ClN₄O₃S [M+H]⁺: 385.1, found 384.8 with *t_R* 2.48 min.

General procedure for Suzuki reaction. A mixture of chlorinated pyrimidine **8** (2.6 mmol, 1 equiv), aryl boronic acid (3.9 mmol, 1.5 equiv), aqueous 2 M Na₂CO₃ (7.8 mmol, 3 equiv) and bis(triphenylphosphine) palladium chloride (0.26 mmol, 0.1 equiv) in THF (8 mL) was irradiated under microwave radiation for 3 h at 125 C°. After concentration the residue was purified by flash column chromatography (silica

References

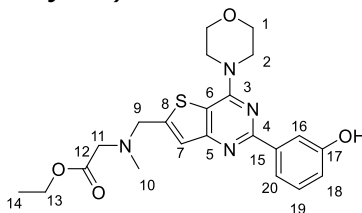
gel), eluting with 0-10% methanol (containing 0.7 N ammonia) in DCM to give the products (**19** and **21**) as solids.

Ethyl-N-((2-(1H-indol-4-yl)-4-morpholinothieno[3,2-d]pyrimidin-6-yl)methyl)-N-methylglycinate (40**, 29% yield).**



^1H NMR (400 MHz, DMSO) δ 11.23 (s, NH), 8.13 (dd, J = 7.5, 1.0 Hz, 1H, H-20), 7.53 (dd, J = 8.0, 0.9 Hz, 1H), 7.47 – 7.43 (m, 2H), 7.43 (s, 1H, H-7), 7.20 (t, J = 7.8 Hz, 1H, H-15), 4.13 (q, J = 7.1 Hz, 2H, H-13), 4.11 – 4.08 (m, 2H, H-9), 4.03 – 3.96 (m, 4H, H-1), 3.83 (dd, J = 5.7, 3.9 Hz, 4H, H-2), 3.47 (s, 2H, H-11), 2.41 (s, 3H, H-10), 1.23 (t, J = 7.1 Hz, 3H, H-14). ^{13}C NMR (101 MHz, DMSO) δ 170.72 (C-12), 162.84 (C-4), 161.70 (C-5), 157.97 (C-3), 151.79 (C-8), 137.47 (C-14), 130.20, 126.80, 126.38, 123.34, 120.90, 120.86, 113.77 (C-6), 112.02 (C-18), 103.84 (C-15), 66.53 (C-1), 60.38 (C-13), 57.44 (C-11), 55.48 (C-9), 46.54 (C-2), 41.77 (C-10), 14.60 (d, J = 7.0 Hz, C-14). LCMS m/z calc. for $\text{C}_{24}\text{H}_{27}\text{N}_5\text{O}_3\text{S}$ $[\text{M}+\text{H}]^+$: 466.2, found 465.8 with t_R 2.48 min (98%).

Ethyl-N-methyl-N-((4-morpholino-2-phenylthieno[3,2-d]pyrimidin-6-yl)methyl)glycinate (41**, 68% yield).**



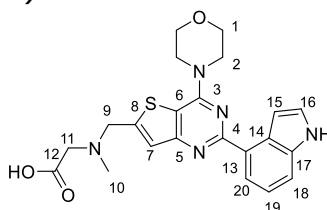
^1H NMR (400 MHz, DMSO- d_6) δ 9.50 (s, OH), 7.89 – 7.68 (m, 2H, H-19/20), 7.38 (s, 1H, H-10), 7.28 (t, J = 8.0 Hz, 1H, H-16), 7.04 – 6.61 (m, 1H, H-18), 4.11 (q, J = 7.1 Hz, 2H, H-13), 3.99 (dd, J = 9.1, 4.4 Hz, 4H, H-1), 3.81 (t, J = 4.7 Hz, 4H, H-2), 3.47 (s, 2H, H-9), 3.35 (s, 2H, H-11), 2.32 (s, 3H, H-10), 1.20 (t, J = 7.1 Hz, 3H, H-14). ^{13}C NMR (101 MHz, DMSO- d_6) δ 170.74 (C-12), 162.83 (C-4), 161.68 (C-5), 157.95 (C-3), 151.76 (C-8), 137.45 (C-14), 130.17, 126.78, 126.36, 123.31, 120.94, 120.82, 113.75 (C-6), 112.05 (C-18), 103.82 (C-15), 66.46 (C-1), 60, 42 (C-13), 59.21 (C-11), 55.91 (C-9), 46.35 (C-2), 42.15 (C-10), 14.53 (C-14). LCMS m/z calc. for $\text{C}_{22}\text{H}_{26}\text{N}_4\text{O}_4\text{S}$ $[\text{M}+\text{H}]^+$: 443.2, found 443.1 with t_R 2.02 min (99%).

General process for ester hydrolysis. To a solution of the ester (**40** and **41**) (2.34 mmol, 1 equiv) in methanol (30 mL), was added KOH (12.38 mmol, 5 equiv). The reaction was then allowed to stir at 50°C for 20 h. The reaction mixture was quenched with 1 M HCl (30 mL) and extracted with ethyl acetate (3*30 mL). The

References

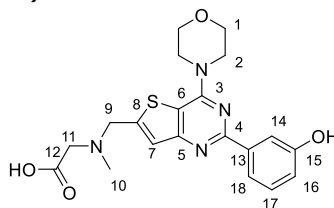
organic layers were combined, dried over anhydrous MgSO_4 , and concentrated under reduced pressure to give the carboxylic acids (**19** and **21**).

***N*-((2-(1*H*-indol-4-yl)-4-morpholinothieno[3,2-*d*]pyrimidin-6-yl)methyl)-*N*-methylglycine (**19**, 95% yield).**



^1H NMR (400 MHz, DMSO) δ 11.56 (s, NH), 8.10 (d, $J = 7.4$ Hz, 1H, H-20), 7.77 (s, OH), 7.62 (d, $J = 7.9$ Hz, 1H), 7.50 (t, $J = 2.8$ Hz, 1H, H-19), 7.30 (s, 1H, H-7), 7.24 (t, $J = 7.8$ Hz, 1H, H-15), 4.47 (s, 2H, H-9), 4.08 (t, $J = 4.5$ Hz, 4H, H-1), 3.85 (t, $J = 4.7$ Hz, 4H, H-2), 3.77 (s, 2H, H-11), 2.65 (s, 3H, H-10). ^{13}C NMR (101 MHz, DMSO) δ 170.43 (C-12), 162.56 (C-4), 161.51 (C-5), 157.60 (C-3), 137.43 (C-17), 127.14, 126.70, 121.27, 120.90 (C-7), 112.74 (C-18), 103.15 (C-15), 66.39 (C-1), 56.28 (C-11), 54.29 (C-9), 46.81 (C-2), 41.38 (C-10). LCMS m/z calc. for $\text{C}_{22}\text{H}_{23}\text{N}_5\text{O}_3\text{S}$ $[\text{M}+\text{H}]^+$: 438.2, found 438.0 with t_R 2.08 min (99%).

***N*-((2-(3-hydroxyphenyl)-4-morpholinothieno[3,2-*d*]pyrimidin-6-yl)methyl)-*N*-methylglycine (**21**, 82% yield).**

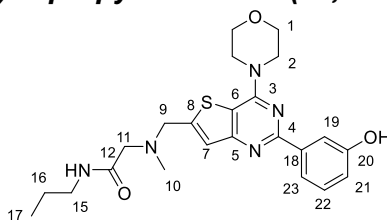


^1H NMR (400 MHz, DMSO- d_6) δ 7.88 – 7.79 (m, 2H, H-14/18), 7.33 (s, 1H, H-7), 7.25 (t, $J = 7.8$ Hz, 1H, H-17), 6.85 (ddd, $J = 7.9, 2.6, 1.1$ Hz, 1H, H-16), 4.10 – 3.90 (m, 6H, H-1/H-9), 3.87 – 3.69 (m, 4H, H-2), 2.35 (s, 3H, H-10). ^{13}C NMR (101 MHz, DMSO- d_6) δ 162.77 (C-12), 159.44 (C-5), 157.82 (C-3), 157.79, 139.96, 129.65 (C-17), 118.95 (C-7), 117.46 (C-16), 114.95 (C-14), 112.57 (C-6), 66.47 (C-1), 55.52 (C-11), 49.06 (C-9), 46.31 (C-2), 42.02 (C-10). LCMS m/z calc. for $\text{C}_{20}\text{H}_{22}\text{N}_4\text{O}_4\text{S}$ $[\text{M}+\text{H}]^+$: 415.1, found 415.0 with t_R 2.01 min (95%).

General procedure for amide coupling. To a solution of carboxylic acid (**19** and **21**) (0.24 mmol, 1 equiv) in DMF (1 mL) was added amine (0.28 mmol, 1.2 equiv), HATU (0.26 mmol, 1.1 equiv) and DIPEA (0.72 mmol, 3 equiv) and the mixture was stirred at RT overnight. The reaction mixture was diluted with ethyl acetate (20 ml) and saturated aqueous NaHCO_3 (20 mL). The water phase was extracted with ethyl acetate (3*20 mL). The combined organic phases were washed with saturated aqueous sodium chloride (20 mL), dried over MgSO_4 , filtered and the crude product was purified by column chromatography on silica gel (DCM/methanol: 10:1) to yield the amides (**22**, **24**, **25**, **27**, **28**, **30**, **31**, **33**, **34**, **36**, **37**, **39** and **42- 55**).

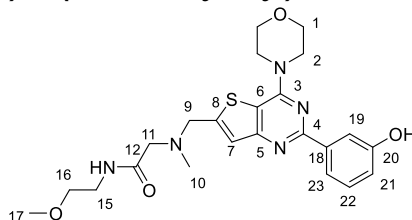
References

2-(((5-(3-hydroxyphenyl)-7-morpholinobenzo[b]thiophen-2-yl)methyl)(methyl)amino)-N-propylacetamide (24, 31.0% yield).



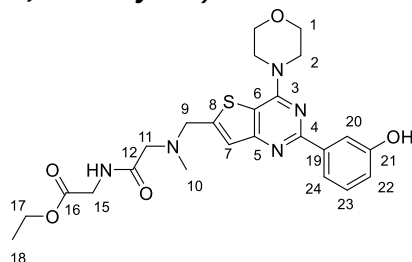
^1H NMR (400 MHz, DMSO) δ 9.49 (s, NH), 7.88 – 7.81 (m, 2H, H-19/H-23), 7.77 (t, J = 6.0 Hz, 1H, H-22), 7.42 (s, 1H, H-7), 7.27 (t, J = 8.2 Hz, OH), 6.88 – 6.82 (m, 1H, H-21), 3.99 (s, 2H, H-9), 3.97 (d, J = 4.8 Hz, 4H, H-1), 3.80 (dd, J = 5.7, 3.9 Hz, 4H, H-2), 3.10 (s, 2H, H-11), 3.09 – 3.05 (m, 2H, H-15), 2.33 (s, 3H, H-10), 1.44 (q, J = 7.2 Hz, 2H, H-16), 0.85 (t, J = 7.4 Hz, 3H, H-17). ^{13}C NMR (101 MHz, DMSO) δ 169.49 (C-12), 162.77 (C-4), 159.54, 157.85 (C-3), 154.28, 151.21, 139.91, 129.72 (C-22), 123.55, 119.03, 117.50 (C-21), 114.92 (C-19), 112.54 (C-5), 66.45 (C-1), 60.14 (C-11), 56.22 (C-9), 46.32 (C-2), 42.76 (C-10), 22.93 (C-16), 11.85 (C-17). LCMS m/z calc. for $\text{C}_{23}\text{H}_{29}\text{N}_5\text{O}_3\text{S}$ $[\text{M}+\text{H}]^+$: 456.2, found 456.1 with t_R 2.21 min (98%).

2-(((5-(3-hydroxyphenyl)-7-morpholinobenzo[b]thiophen-2-yl)methyl)(methyl)amino)-N-(2-methoxyethyl)acetamide (27, 59.5% yield).



^1H NMR (400 MHz, DMSO) δ 9.49 (s, OH), 7.98 – 7.79 (m, 3H, H-19/H-23), 7.42 (s, 1H, H-7), 7.27 (t, J = 7.9 Hz, 1H), 6.91 – 6.81 (m, 1H, H-7), 4.05 – 3.95 (m, 6H, H-1/H-9), 3.81 (t, J = 4.9 Hz, 4H, H-2), 3.39 – 3.28 (m, 4H, H-15/16), 3.25 (s, 3H, H-17), 3.13 (s, 2H, H-11), 2.33 (s, 3H, H-10). ^{13}C NMR (101 MHz, DMSO- d_6) δ 169.68 (C-12), 162.75 (C-4), 159.54, 157.86 (C-3), 139.91, 129.72 (C-22), 119.02 (C-7), 117.50 (C-21), 114.92 (C-18), 112.58 (C-6), 71.04 (C-16), 66.47 (C-1), 60.13 (C-11), 58.35 (C-17), 56.17 (C-9), 46.32 (C-2), 42.68 (C-10), 38.43 (C-15). LCMS m/z calc. for $\text{C}_{23}\text{H}_{29}\text{N}_5\text{O}_4\text{S}$ $[\text{M}+\text{H}]^+$: 472.2, found 472.2 with t_R 2.10 min (94%).

Ethyl-N-(((5-(3-hydroxyphenyl)-7-morpholinobenzo[b]thiophen-2-yl)methyl)-N-methylglycylglycinate (30, 25.5% yield).

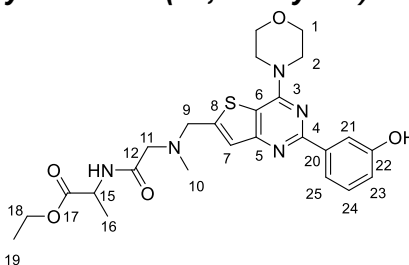


^1H NMR (400 MHz, DMSO) δ 9.50 (s, OH), 8.25 (s, 1H, NH), 7.85 (d, J = 7.3 Hz, 2H, H-20/H-24), 7.47 (s, 1H, H-7), 7.28 (t, J = 7.9 Hz, 1H, H-23), 7.00 – 6.79 (m, 1H, H-

References

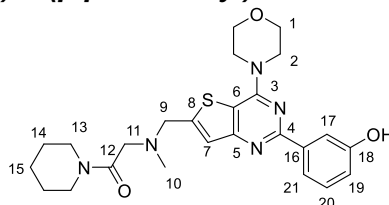
22), 4.04 (s, 2H, H-15), 4.00 (t, $J = 4.7$ Hz, 4H, H-1), 3.93 (d, $J = 6.0$ Hz, 2H, H-9), 3.82 (t, $J = 4.8$ Hz, 4H, H-2), 3.66 (s, 3H, H-17), 3.18 (d, $J = 12.7$ Hz, 2H, H-11), 2.38 (s, 3H, H-10), 1.26 (q, $J = 6.1$ Hz, 3H, H-18). ^{13}C NMR (101 MHz, DMSO- d_6) δ 170.74 (C-16), 162.59 (C-12), 159.42 (C-5), 157.75 (C-3), 139.78, 129.62 (C-23), 121.10, 118.92 (C-7), 117.40 (C-22), 114.82 (C-20), 112.52 (C-6), 66.37 (C-1), 56.02 (C-11), 53.97 (C-9), 52.09 (C-17), 46.21 (C-2), 42.57 (C-10), 42.21 (C-15), 14.6 (C-18). LCMS m/z calc. for $\text{C}_{24}\text{H}_{29}\text{N}_5\text{O}_5\text{S}$ $[\text{M}+\text{H}]^+$: 500.2, found 499.9 with t_R 2.15 min (97%).

EthylN-((2-(3-hydroxyphenyl)-4-morpholinothieno[3,2-d]pyrimidin-6-yl)methyl)-N-methylglycylalaninate (33, 70% yield).



^1H NMR (400 MHz, DMSO) δ 9.50 (s, OH), 8.17 (d, $J = 7.3$ Hz, 1H, H-25), 7.86 (d, $J = 1.8$ Hz, 1H, H-21), 7.42 (s, 1H, H-7), 7.28 (t, $J = 7.8$ Hz, 1H, H-24), 6.95 – 6.60 (m, 1H, H-23), 4.42 – 4.28 (m, 1H, H-15), 4.11 (qp, $J = 7.2, 3.6$ Hz, 2H, H-18), 4.03 (s, 2H, H-9), 3.99 (t, $J = 5.0$ Hz, 4H, H-1), 3.81 (t, $J = 4.8$ Hz, 4H, H-2), 3.62 (dtd, $J = 13.2, 6.6, 3.8$ Hz, 1H), 3.24 – 3.11 (m, 2H, H-11), 2.37 (s, 3H, H-10), 1.26 (t, $J = 6.0$ Hz, 3H, H-16), 1.19 (t, $J = 7.1$ Hz, 3H, H-19). ^{13}C NMR (101 MHz, DMSO- d_6) δ 169.63 (C-17), 162.76 (C-12), 159.54 (C-5), 157.85 (C-3), 139.91, 129.71 (C-24), 123.52, 119.03 (C-7), 117.49 (C-23), 114.93 (C-21), 112.57 (C-6), 66.48 (C-1), 61.05 (C-18), 59.64 (C-11), 56.02 (C-9), 46.32 (C-2), 42.55 (C-10), 17.59 (C-16), 14.49 (C-19). LCMS m/z calc. for $\text{C}_{25}\text{H}_{31}\text{N}_5\text{O}_5\text{S}$ $[\text{M}+\text{H}]^+$: 514.2, found 514.0 with t_R 2.27 min (90%).

2-(((5-(3-hydroxyphenyl)-7-morpholinobenzo[b]thiophen-2-yl)methyl)(methyl)amino)-1-(piperidin-1-yl)ethan-1-one (39, 75.8% yield).

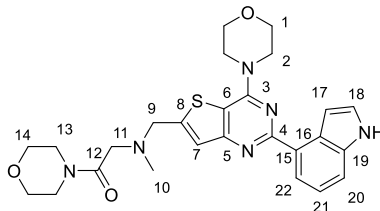


^1H NMR (400 MHz, DMSO) δ 9.50 (s, 1H), 7.85 (d, $J = 8.2$ Hz, 2H, H-17/H-21), 7.38 (s, 1H, H-7), 7.28 (t, $J = 7.8$ Hz, 1H, H-20), 6.96 – 6.78 (m, 1H, H-19), 4.01 (s, 2H, H-9), 3.98 (t, $J = 4.7$ Hz, 4H, H-1), 3.81 (t, $J = 4.8$ Hz, 4H, H-2), 3.45 (d, $J = 4.7$ Hz, 2H, H-11), 3.44 – 3.34 (m, 4H, H-13), 2.32 (s, 3H, H-10), 1.64 – 1.49 (m, 4H, H-14), 1.45 (s, 2H, H-15). ^{13}C NMR (101 MHz, DMSO) δ 167.67 (C-12), 162.75 (C-4), 159.51 (C-5), 157.86 (C-3), 139.93, 129.70 (C-4), 123.35, 119.02 (C-7), 117.48 (C-

References

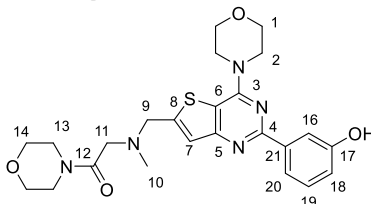
19), 114.92 (C-17), 112.64 (C-6), 66.46 (C-1), 59.17 (C-11), 55.92 (C-9), 46.35 (C-2), 42.12 (C-10), 25.89 (C-14), 24.51 (C-15). LCMS m/z calc. for $C_{25}H_{31}N_5O_3S$ $[M+H]^+$: 482.2, found 482.0 with t_R 2.13 min (95%).

2-(((2-(1H-indol-4-yl)-4-morpholinthieno[3,2-d]pyrimidin-6-yl)methyl)(methyl)amino)-1-morpholinoethan-1-one (42, 69% yield).



1H NMR (400 MHz, DMSO) δ 11.23 (t, J = 2.3 Hz, NH), 8.13 (dd, J = 7.5, 1.0 Hz, 1H, H-22), 7.53 (dt, J = 8.0, 1.0 Hz, 1H, H-20), 7.48 – 7.40 (m, 3H, H-7/H-18/H-20), 7.21 (t, J = 7.8 Hz, 1H, H-17), 4.03 (s, 2H, H-9), 4.00 (dd, J = 5.7, 3.9 Hz, 4H, H-1), 3.84 (dd, J = 5.8, 3.8 Hz, 4H, H-2), 3.62 (d, J = 4.5 Hz, 4H, H-14), 3.57 (ddq, J = 8.8, 5.3, 3.3, 2.8 Hz, 4H, H-13), 3.45 (s, 2H, H-11), 2.34 (s, 3H, H-10). ^{13}C NMR (101 MHz, DMSO) δ 168.35 (C-12), 162.83 (C-4), 161.71 (C-5), 157.95 (C-3), 137.48 (C-19), 130.16, 126.60 (d, J = 39.7 Hz), 123.58, 120.90, 120.88 (C-7), 113.79 (C-20), 112.02 (C-6), 103.83 (C-17), 66.69 (C-14), 66.52 (C-1), 58.93 (C-11), 55.90 (C-9), 46.56 (C-2), 45.95 (C-13), 42.11 (C-10). LCMS m/z calc. for $C_{26}H_{30}N_6O_3S$ $[M+H]^+$: 507.2, found 507.3 with t_R 2.06 min (99%).

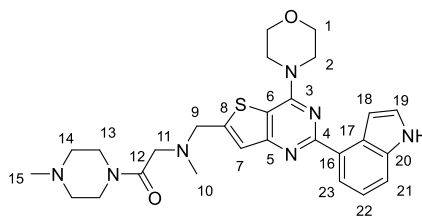
2-(((2-(3-hydroxyphenyl)-4-morpholinthieno[3,2-d]pyrimidin-6-yl)methyl)(methyl)amino)-1-morpholinoethan-1-one (43, 45% yield).



1H NMR (400 MHz, DMSO) δ 9.49 (s, OH), 7.90 – 7.80 (m, 2H, H-16/H-20), 7.38 (d, J = 1.0 Hz, 1H, H-7), 7.31 – 7.24 (m, 1H, H-19), 6.88 – 6.84 (m, 1H, H-18), 4.00 (s, 2H, H-9), 3.98 (dd, J = 5.8, 3.9 Hz, 4H, H-1), 3.88 – 3.78 (m, 4H, H-2), 3.67 – 3.44 (m, 8H, H-13/H-14), 3.43 (s, 2H, H-11), 2.32 (s, 3H, H-10). ^{13}C NMR (101 MHz, DMSO) δ 168.40 (C-12), 162.77 (C-4), 159.51 (C-5), 157.85 (C-3), 151.86, 139.92, 131.95 (d, J = 9.9 Hz), 129.72, 129.23 (d, J = 11.7 Hz), 123.24, 119.02 (C-7), 117.48 (C-18), 114.91 (C-16), 112.58 (C-6), 66.68 (C-14), 66.47 (C-1), 58.94 (C-11), 55.87 (C-9), 46.35 (C-2), 45.94 (C-13), 42.10 (C-10). LCMS m/z calc. for $C_{24}H_{29}N_5O_4S$ $[M+H]^+$: 484.2, found 483.9 with t_R 2.12 min (95%).

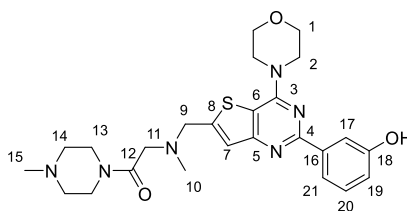
2-(((2-(1H-indol-4-yl)-4-morpholinthieno[3,2-d]pyrimidin-6-yl)methyl)(methyl)amino)-1-(4-methylpiperazin-1-yl)ethan-1-one (44, 67% yield).

References



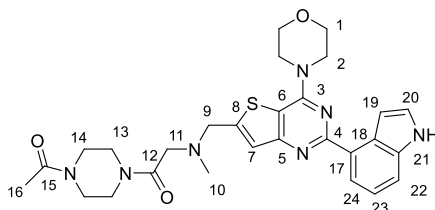
^1H NMR (400 MHz, DMSO) δ 11.23 (t, J = 2.4 Hz, NH), 8.13 (d, J = 7.5 Hz, 1H, H-23), 7.53 (d, J = 8.0 Hz, 1H, H-22), 7.46 – 7.43 (m, 2H, H-19/H-21), 7.43 (s, 1H, H-7), 7.20 (t, J = 7.7 Hz, 1H, H-18), 4.00 (d, J = 4.2 Hz, 6H, H-1/H-9), 3.84 (t, J = 4.8 Hz, 4H, H-2), 3.55 (t, J = 5.0 Hz, 2H, H-13), 3.48 (dd, J = 9.2, 4.2 Hz, 2H, H-13), 3.41 (s, 2H, H-11), 2.40 (d, J = 34.9 Hz, 4H, H-14), 2.32 (s, 3H, H-10), 2.22 (s, 3H, H-15). ^{13}C NMR (101 MHz, DMSO) δ 168.18 (C-12), 162.88 (C-4), 161.72 (C-5), 157.96 (C-3), 151.57, 137.48 (C-20), 130.18, 126.80, 126.40, 123.42, 120.89 (d, J = 3.0 Hz, C-7), 113.79 (C-21), 111.98 (C-6), 103.84 (C-18), 66.52 (C-1), 59.30 (C-11), 55.97 (C-9), 55.37 (C-14), 46.56 (C-2), 46.05 (C-13), 45.19 (C-15), 42.14 (C-10). LCMS m/z calc. for $\text{C}_{27}\text{H}_{33}\text{N}_7\text{O}_2\text{S}$ $[\text{M}+\text{H}]^+$: 520.2, found 520.5 with t_R 1.85 min (95%).

2-(((2-(3-hydroxyphenyl)-4-morpholinothieno[3,2-d]pyrimidin-6-yl)methyl)(methyl)amino)-1-(4-methylpiperazin-1-yl)ethan-1-one (45, 43% yield).



^1H NMR (400 MHz, DMSO) δ 9.51 (s, OH), 7.93 – 7.73 (m, 2H, H-17/H-21), 7.37 (s, 1H, H-7), 7.28 (t, J = 8.0 Hz, 1H, H-20), 6.98 – 6.79 (m, 1H, H-19), 3.98 (d, J = 6.1 Hz, 6H, H-1/H-9), 3.82 (t, J = 4.7 Hz, 4H, H-2), 3.52 (d, J = 28.3 Hz, 4H, H-13), 3.41 (s, 2H, H-11), 2.41 (d, J = 34.9 Hz, 4H, H-14), 2.31 (s, 3H, H-10), 2.27 (s, 3H, H-15). ^{13}C NMR (101 MHz, DMSO) δ 168.20 (C-12), 162.79 (C-4), 159.51 (C-5), 157.85, 151.94, 139.92, 129.72, 123.18, 119.02 (C-7), 117.49 (C-19), 114.91 (C-17), 112.56 (C-6), 66.47 (C-1), 59.23 (C-11), 55.91 (C-9), 55.16 (C-14), 54.66, 46.35 (C-2), 45.77 (C-13), 44.95 (C-15), 42.12 (C-10). LCMS m/z calc. for $\text{C}_{25}\text{H}_{32}\text{N}_6\text{O}_3\text{S}$ $[\text{M}+\text{H}]^+$: 497.2, found 497.1 with t_R 1.86 min (99%).

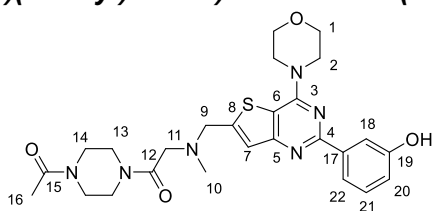
2-(((2-(1H-indol-4-yl)-4-morpholinothieno[3,2-d]pyrimidin-6-yl)methyl)(methyl)amino)-1-(4-acetylpiperazin-1-yl)ethan-1-one (46, 64% yield).



References

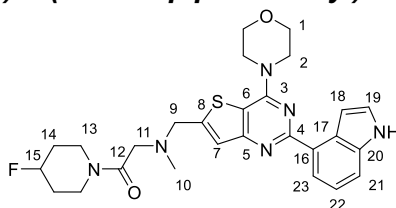
^1H NMR (400 MHz, DMSO) δ 11.24 (s, NH), 8.13 (d, $J = 7.5$ Hz, 1H, H-24), 7.53 (d, $J = 8.0$ Hz, 1H, H-23), 7.45 (d, $J = 3.0$ Hz, 2H, H-20/H-22), 7.33 (s, 1H, H-7), 7.21 (t, $J = 7.8$ Hz, 1H, H-19), 4.04 (s, 2H, H-9), 4.00 (d, $J = 3.7$ Hz, 4H, H-1), 3.89 (t, $J = 4.7$ Hz, 3H, H-14), 3.84 (t, $J = 4.8$ Hz, 4H, H-2), 3.76 (t, $J = 4.7$ Hz, 4H, H-13), 3.45 (s, 2H, H-11), 2.35 (s, 3H, H-10), 2.04 (s, 3H, H-16). ^{13}C NMR (101 MHz, DMSO) δ 169.05 (C-15), 168.35 (C-12), 162.82 (C-4), 161.72 (C-5), 157.95 (C-3), 154.25, 137.48 (C-21), 130.14, 126.80, 126.41, 120.89 (C-7), 113.80 (C-22), 112.01 (C-6), 103.83 (C-19), 66.52 (C-1), 66.43 (C-14), 59.18 (C-11), 55.38 (C-9), 54.08, 46.56 (C-2), 46.35 (C-13), 42.11 (C-10), 21.72 (C-16). LCMS m/z calc. for $\text{C}_{28}\text{H}_{33}\text{N}_7\text{O}_3\text{S}$ $[\text{M}+\text{H}]^+$: 548.2, found 548.3 with t_R 2.02 min (95%).

1-(4-acetylpiperazin-1-yl)-2-(((2-(3-hydroxyphenyl)-4-morpholinothieno[3,2-d]pyrimidin-6-yl)methyl)(methyl)amino)ethan-1-one (47, 68% yield).



^1H NMR (400 MHz, DMSO) δ 8.96 (s, OH), 7.75 (m, 2H, H-7/H-21), 7.41 – 7.31 (m, 2H, H-7/H-21), 6.84 (d, $J = 8.8$ Hz, 1H, H-20), 4.14 – 4.00 (m, 2H, H-9), 3.97 – 3.85 (m, 4H, H-1), 3.85 – 3.76 (m, 8H, H-2/H-14), 3.70 (dt, $J = 9.0, 4.4$ Hz, 4H, H-13), 3.53 (s, 3H, H-11), 2.33 (s, 3H, H-10), 1.87 (s, 3H, H-16). ^{13}C NMR (101 MHz, DMSO) δ 169.13 (C-15), 168.60 (C-12), 162.77 (C-4), 159.42 (C-5), 157.32 (C-3), 156.34, 139.84, 132.62, 132.11, 131.90, 129.83 (C-21), 129.28, 129.17, 122.96, 119.02 (C-7), 116.20 (C-20), 114.91 (C-18), 112.59 (C-6), 66.92 (C-1), 66.84 (C-14), 60.01 (C-11), 55.31 (C-9), 46.50 (C-2), 46.24 (C-13), 42.45 (C-10), 21.74 (C-16). LCMS m/z calc. for $\text{C}_{26}\text{H}_{32}\text{N}_6\text{O}_4\text{S}$ $[\text{M}+\text{H}]^+$: 525.2, found 525.2 with t_R 2.04 min (93%).

2-(((2-(1H-indol-4-yl)-4-morpholinothieno[3,2-d]pyrimidin-6-yl)methyl)(methyl)amino)-1-(4-fluoropiperidin-1-yl)ethan-1-one (48, 66% yield).

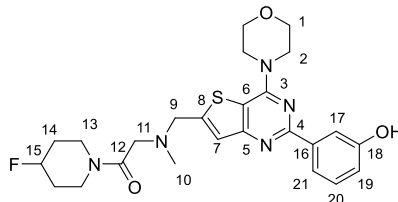


^1H NMR (400 MHz, DMSO) δ 11.23 (t, $J = 2.4$ Hz, NH), 8.13 (dd, $J = 7.5, 1.0$ Hz, 1H, H-23), 7.53 (dt, $J = 8.0, 1.0$ Hz, 1H, H-22), 7.48 – 7.40 (m, 3H, H-7/H-19/H-21), 7.21 (t, $J = 7.8$ Hz, 1H, H-18), 4.90 (ddt, $J = 48.4, 7.1, 3.6$ Hz, 1H, H-15), 4.01 (s, 2H, H-9), 4.01 – 3.98 (m, 4H, H-1), 3.89 – 3.76 (m, 4H, H-2), 3.71 – 3.45 (m, 4H, H-13), 3.44 (s, 2H, H-11), 2.33 (s, 3H, H-10), 2.05 – 1.64 (m, 2H, H-14). ^{13}C NMR (101 MHz, DMSO) δ 168.17 (C-12), 162.86 (C-4), 161.72 (C-5), 157.95 (C-3), 137.48 (C-20), 130.18, 126.80, 126.40, 123.54, 120.89 (d, $J = 2.4$ Hz), 113.79 (C-20), 112.01

References

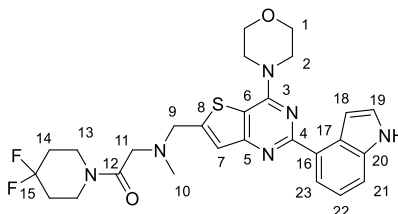
(C-6), 103.84 (C-18), 88.81 (d, $J = 169.4$ Hz, C-15), 66.51 (C-1), 59.32 (C-11), 56.00, 55.38 (C-9), 46.56 (C-2), 42.15 (C-10), 41.77 (C-13), 31.17 (C-14). LCMS m/z calc. for $C_{27}H_{31}FN_6O_2S$ $[M+H]^+$: 523.2, found 523.1 with t_R 2.22 min (97%).

1-(4-fluoropiperidin-1-yl)-2-(((2-(3-hydroxyphenyl)-4-morpholinothieno[3,2-d]pyrimidin-6-yl)methyl)(methyl)amino)ethan-1-one (49, 44% yield).



1H NMR (400 MHz, DMSO) δ 9.50 (s, OH), 7.85 (dd, $J = 7.0, 1.5$ Hz, 2H, H-17/21), 7.38 (d, $J = 1.1$ Hz, 1H, H-7), 7.28 (t, $J = 7.9$ Hz, 1H, H-20), 7.04 – 6.67 (m, 1H, H-19), 4.99 – 4.78 (m, 1H, H-15), 4.00 (s, 3H, H-9), 3.98 (d, $J = 4.7$ Hz, 4H, H-1), 3.81 (t, $J = 4.7$ Hz, 4H, H-2), 3.46 (s, 4H, H-13), 3.43 (s, 2H, H-11), 2.31 (s, 3H, H-10), 2.07 – 1.54 (m, 4H, H-14). ^{13}C NMR (101 MHz, DMSO) δ 168.18 (C-12), 162.79 (C-4), 159.52 (C-5), 157.85 (C-3), 151.82, 139.92, 129.72 (C-20), 123.25, 119.02 (C-7), 117.49 (C-19), 114.91 (C-17), 112.57 (C-6), 88.81 (d, $J = 169.4$ Hz, C-15), 66.46 (C-1), 59.28 (C-12), 55.96 (C-9), 46.35 (C-2), 42.14 (C-10), 41.74 (C-13), 38.01 (C-14). LCMS m/z calc. for $C_{25}H_{30}FN_5O_3S$ $[M+H]^+$: 500.2, found 500.1 with t_R 2.13 min (94%).

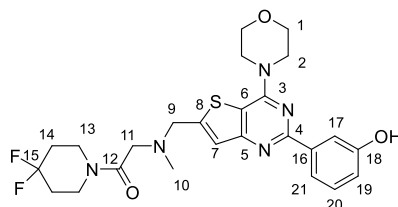
2-(((2-(1H-indol-4-yl)-4-morpholinothieno[3,2-d]pyrimidin-6-yl)methyl)(methyl)amino)-1-(4,4-difluoropiperidin-1-yl)ethan-1-one (50, 88% yield).



1H NMR (400 MHz, DMSO) δ 11.23 (t, $J = 2.3$ Hz, NH), 8.13 (dd, $J = 7.5, 1.0$ Hz, 1H, H-23), 7.53 (dt, $J = 8.1, 1.0$ Hz, 1H, H-22), 7.47 – 7.43 (m, 3H, H-7/H-19/H-21), 7.21 (t, $J = 7.7$ Hz, 1H, H-18), 4.02 (s, 2H, H-9), 4.01 – 3.97 (m, 4H, H-1), 3.83 (dd, $J = 5.7, 3.9$ Hz, 4H, H-2), 3.61 (dd, $J = 15.4, 9.4$ Hz, 4H, H-13), 3.47 (s, 2H, H-11), 2.33 (s, 3H, H-10), 2.09 (q, $J = 13.1$ Hz, 4H, H-14). ^{13}C NMR (101 MHz, DMSO) δ 168.45 (C-12), 165.05, 162.82 (d, $J = 10.3$ Hz, C-4), 161.74 (C-5), 157.95 (C-3), 151.27, 137.48 (C-20), 130.17 (C-19), 126.80, 126.39, 125.62, 123.59, 123.22, 120.89 (d, $J = 2.2$ Hz), 113.79 (C-21), 111.99 (C-6), 103.84 (C-18), 66.51 (C-1), 59.28 (C-11), 55.98 (C-9), 46.56 (C-2), 42.16 (C-10), 38.71 (C-13), 31.24 (C-14). LCMS m/z calc. for $C_{27}H_{30}F_2N_6O_2S$ $[M+H]^+$: 541.2, found 541.1 with t_R 2.20 min (95%).

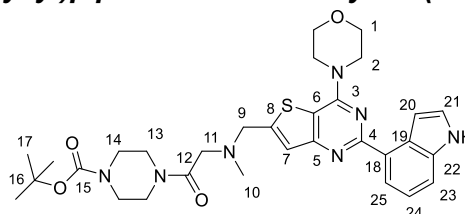
1-(4,4-difluoropiperidin-1-yl)-2-(((2-(3-hydroxyphenyl)-4-morpholinothieno[3,2-d]pyrimidin-6-yl)methyl)(methyl)amino)ethan-1-one (51, 52% yield).

References



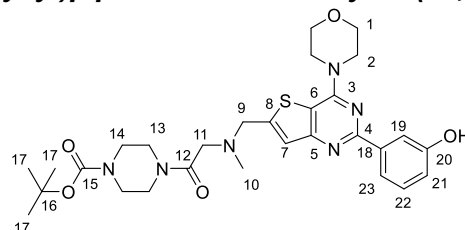
^1H NMR (400 MHz, DMSO) δ 9.50 (s, OH), 7.89 – 7.81 (m, 2H, H-17/H-21), 7.38 (s, 1H, H-7), 7.28 (t, J = 8.0 Hz, 1H, H-20), 6.94 – 6.80 (m, 1H, H-19), 4.00 (s, 2H, H-9), 4.00 – 3.97 (m, 4H, H-1), 3.81 (t, J = 4.7 Hz, 4H, H-2), 3.61 (dd, J = 17.1, 5.9 Hz, 4H, H-13), 3.47 (s, 2H, H-11), 2.32 (s, 3H, H-10), 2.01 (d, J = 52.1 Hz, 4H, H-14). ^{13}C NMR (101 MHz, DMSO) δ 168.43 (C-12), 162.78 (C-4), 159.53 (C-5), 157.85 (C-3), 151.68, 139.91, 129.72 (C-20), 123.34, 119.02 (C-7), 117.49 (C-19), 114.91 (C-17), 112.57 (C-6), 66.46 (C-1), 59.21 (C-11), 55.91 (C-9), 46.35 (C-2), 42.15 (C-10), 38.65 (C-14). LCMS m/z calc. for $\text{C}_{25}\text{H}_{29}\text{F}_2\text{N}_5\text{O}_3\text{S}$ $[\text{M}+\text{H}]^+$: 518.2, found 517.9 with t_R 2.21 min (99%).

tert-butyl 4-(N-((2-(1H-indol-4-yl)-4-morpholinothieno[3,2-d]pyrimidin-6-yl)methyl)-N-methylglycyl)piperazine-1-carboxylate (52, 56% yield).



^1H NMR (400 MHz, DMSO) δ 11.23 (d, J = 2.4 Hz, NH), 8.13 (d, J = 7.4 Hz, 1H, H-25), 7.53 (d, J = 8.0 Hz, 1H, H-24), 7.44 (t, J = 2.4 Hz, 2H, H-21/H-23), 7.43 (s, 1H, H-7), 7.20 (t, J = 7.8 Hz, 1H, H-20), 4.00 (d, J = 5.7 Hz, 6H, H-1/H-9), 3.83 (t, J = 4.7 Hz, 4H, H-2), 3.54 (t, J = 5.2 Hz, 4H, H-13), 3.43 (s, 2H, H-11), 3.32 (t, J = 5.2 Hz, 4H, H-14), 2.32 (s, 3H, H-10), 1.43 (s, 9H, H-17). ^{13}C NMR (101 MHz, DMSO) δ 168.42 (C-15), 162.89 (C-4), 161.73 (C-5), 157.94 (C-3), 154.33, 151.46, 137.48 (C-22), 130.18 (C-21), 126.80, 126.39, 123.45, 120.88 (d, J = 2.0 Hz, C-7), 113.78 (C-23), 111.97 (C-6), 103.84 (C-20), 78.64 (C-16), 66.53 (C-1), 59.33 (C-11), 55.99 (C-9), 47.94 (C-14), 46.57 (C-2), 44.95 (C-13), 42.13 (C-10), 28.51 (C-17). LCMS m/z calc. for $\text{C}_{31}\text{H}_{39}\text{N}_7\text{O}_4\text{S}$ $[\text{M}+\text{H}]^+$: 606.3, found 606.2 with t_R 2.27 min (97%).

tert-butyl 4-(N-((2-(3-Hydroxyphenyl)-4-morpholinothieno[3,2-d]pyrimidin-6-yl)methyl)-N-methylglycyl)piperazine-1-carboxylate(53,64% yield).

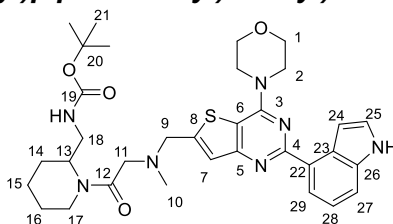


^1H NMR (400 MHz, DMSO) δ 9.49 (s, OH), 7.95 – 7.79 (m, 2H, H-19/23), 7.38 (d, J = 1.0 Hz, 1H, H-7), 7.27 (t, J = 8.1 Hz, 1H, H-22), 6.92 – 6.81 (m, 1H, H-21), 4.00 (s,

References

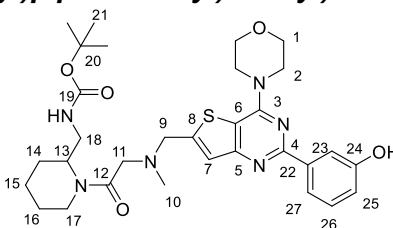
2H, H-9), 3.99 – 3.95 (m, 4H, H-1), 3.81 (dd, $J = 5.7, 3.9$ Hz, 4H, H-2), 3.52 (d, $J = 5.8$ Hz, 4H, H-13), 3.44 (d, $J = 10.3$ Hz, 4H, H-14), 2.31 (s, 3H, H-10), 1.43 (s, 9H, H-17). ^{13}C NMR (101 MHz, DMSO) δ 168.41 (C-15), 162.81 (C-4), 159.52 (C-5), 157.85 (C-3), 154.32, 151.87, 139.92, 129.72 (C-22), 123.20, 119.02 (C-7), 117.49 (C-21), 114.91 (C-19), 112.55 (C-6), 79.64 (C-16), 66.49 (C-1), 59.28 (C-11), 55.94 (C-9), 46.36 (C-2), 45.15 (C-14), 42.12 (C-10), 41.37 (C-13), 28.51 (C-17). LCMS m/z calc. for $\text{C}_{29}\text{H}_{38}\text{N}_6\text{O}_5\text{S}$ $[\text{M}+\text{H}]^+$: 583.3, found 583.0 with t_R 2.34 min (98%).

tert-butyl ((1-(N-((2-(1H-indol-4-yl)-4-morpholinothieno[3,2-d]pyrimidin-6-yl)methyl)-N-methylglycyl)piperidin-2-yl)methyl)carbamate(54, 34% yield).



^1H NMR (400 MHz, DMSO) δ 11.23 (s, 1H), 8.13 (d, $J = 7.5$ Hz, 1H), 7.53 (d, $J = 8.0$ Hz, 1H), 7.44 (p, $J = 3.0$ Hz, 2H), 7.42 (s, 1H), 7.21 (t, $J = 7.7$ Hz, 1H), 4.44 – 4.17 (m, 1H, H-13), 4.02 (s, 2H, H-11), 4.00 (d, $J = 4.4$ Hz, 4H, H-1), 3.84 (t, $J = 4.7$ Hz, 4H, H-2), 3.65 (d, $J = 13.8$ Hz, 2H, H-17), 3.32 – 3.05 (m, 2H, H-18), 2.33 (s, 3H, H-10), 1.67 – 1.55 (m, 6H, H-14/H-15/H-16), 1.34 (s, 9H, H-21). ^{13}C NMR (101 MHz, DMSO) δ 168.60 (C-12), 162.89 (C-4), 161.73 (C-5), 157.93 (C-3), 137.48 (C-26), 126.78, 126.44, 120.86, 113.89 (C-27), 103.74 (C-24), 66.55 (C-1), 59.28 (C-11), 55.98 (C-9), 49.03 (C-13), 46.58 (C-2), 42.35, (C-18) 42.06 (C-10), 38.31, 28.25 (C-14), 27.56 (C-21), 22.73 (C-15), 22.65 (C-16). LCMS m/z calc. for $\text{C}_{33}\text{H}_{43}\text{N}_7\text{O}_4\text{S}$ $[\text{M}+\text{H}]^+$: 634.3, found 634.2 with t_R 2.31 min (97%).

tert-butyl ((1-(N-((2-(3-Hydroxyphenyl)-4-morpholinothieno[3,2-d]pyrimidin-6-yl)methyl)-N-methylglycyl)piperidin-2-yl)methyl)carbamate (55, 97% yield).



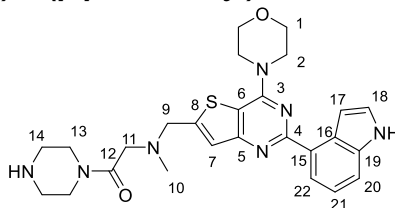
^1H NMR (400 MHz, DMSO) δ 9.50 (s, OH), 7.89 – 7.81 (m, 2H, H-23/H-27), 7.36 (s, 1H, H-7), 7.27 (t, $J = 8.1$ Hz, 1H, H-26), 6.92 – 6.82 (m, 1H, H-25), 4.36 – 4.12 (m, 1H, H-13), 3.99 (s, 2H, H-9), 3.98 (d, $J = 5.0$ Hz, 4H, H-1), 3.81 (t, $J = 4.8$ Hz, 4H, H-2), 3.28 – 2.95 (m, 4H, H-17/H-18), 2.31 (d, $J = 1.8$ Hz, 3H, H-10), 1.79 – 1.48 (m, 6H, H-14/H-15/H-16), 1.40 (s, 9H, H-21). ^{13}C NMR (101 MHz, DMSO) δ 168.60 (C-12), 162.77 (C-4), 159.50 (C-5), 157.85 (C-3), 156.24, 139.94, 132.52, 132.00, 131.90, 129.71 (C-26), 129.28, 129.17, 122.96, 119.02 (C-7), 117.47 (C-25), 114.91 (C-23), 112.59 (C-6), 78.26 (C-20), 66.47 (C-1), 59.35 (C-11), 55.90 (C-9), 51.64,

References

46.37 (C-2), 41.88 (C-10), 38.72 (C-17), 36.25 (C-16), 31.24 (C-21), 28.68 (C-16), 28.63 (C-15). LCMS m/z calc. for $C_{31}H_{42}N_6O_5S$ $[M+H]^+$: 611.3, found 611.2 with t_R 2.35 min (90%).

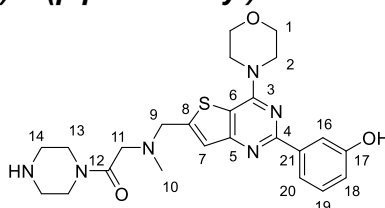
General procedure for boc-deprotection. To the above amides (**52- 55**) (0.16 mmol, 1 equiv) was added 4 N HCl in 1, 4-Dioxane (2 mL) and the reaction mixture was stirred at RT for 1 h. The excess hydrogen chloride solution was evaporated to yield the hydrochloride salt of the amines (**56-59**) as oils.

2-(((2-(1H-Indol-4-yl)-4-morpholinothieno[3,2-d]pyrimidin-6-yl)methyl)(methyl)amino)-1-(piperazin-1-yl)ethan-1-one (56**, 98 % yield).**



1H NMR (400 MHz, DMSO) δ 11.37 (s, NH), 9.87 (s, 1H, NH), 8.12 (d, $J = 7.4$ Hz, 1H, H-22), 7.59 – 7.50 (m, 1H, H-21), 7.45 (t, $J = 2.8$ Hz, 2H, H-18/H-20), 7.44 – 7.38 (m, 1H, H-7), 7.38 – 7.28 (m, 3H), 7.20 (t, $J = 7.7$ Hz, 1H, H-17), 4.17 (s, 2H, H-9), 4.01 (t, $J = 4.7$ Hz, 4H, H-1), 3.85 (t, $J = 4.8$ Hz, 4H, H-2), 3.74 (d, $J = 5.1$ Hz, 4H, H-13), 3.38 (s, 2H, H-11), 3.17 (s, 2H, H-), 3.14 (d, $J = 5.8$ Hz, 2H, H-14), 3.06 (d, $J = 5.4$ Hz, 2H, H-14), 2.35 (s, 3H, H-10). ^{13}C NMR (101 MHz, DMSO) δ 168.85 (C-12), 164.97 (C-4), 157.13 (C-3), 137.36 (C-19), 126.63, 121.01 (C-7), 116.33, 113.90 (C-20), 112.07 (C-6), 102.38 (C-17), 66.25 (C-1), 56.20 (C-2), 50.59 (C-13), 47.35 (C-14), 46.91 (C-2), 41.94 (C-10). LCMS m/z calc. for $C_{26}H_{31}N_7O_2S$ $[M+H]^+$: 506.2, found 506.5 with t_R 1.85 min (99%).

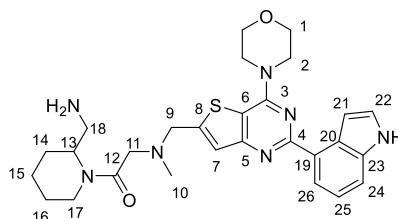
2-(((2-(3-Hydroxyphenyl)-4-morpholinothieno[3,2-d]pyrimidin-6-yl)methyl)(methyl)amino)-1-(piperazin-1-yl)ethan-1-one (57**, 99% yield).**



1H NMR (400 MHz, DMSO) δ 9.77 (s, OH), 7.92 (dd, $J = 7.9, 1.4$ Hz, 1H, H-20), 7.87 (t, $J = 2.1$ Hz, 1H, H-16), 7.68 – 7.53 (m, 1H, H-19), 7.03 (dd, $J = 8.0, 2.5$ Hz, 1H, H-18), 4.42 (s, 2H, H-9), 4.12 (t, $J = 4.6$ Hz, 4H, H-1), 3.86 (t, $J = 4.9$ Hz, 4H, H-2), 3.74 – 3.62 (m, 4H, H-13), 3.35 (s, 2H, H-11), 3.24 – 3.03 (m, 4H, H-14). ^{13}C NMR (101 MHz, DMSO) δ 168.40 (C-18), 158.20 (C-5), 157.21 (C-3), 131.89, 130.20, 129.24 (d, $J = 11.7$ Hz, C-19), 119.52 (C-7), 115.53 (C-18), 114.49 (C-16), 66.32 (C-1), 59.35 (C-11), 55.88 (C-9), 46.92 (C-2), 42.64 (C-14), 41.88 (C-10). LCMS m/z calc. for $C_{24}H_{30}N_6O_5S$ $[M+H]^+$: 483.2, found 483.2 with t_R 1.87 min (97%).

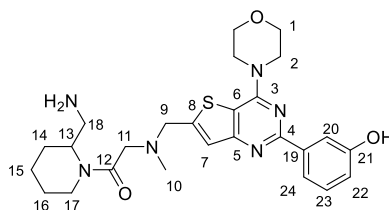
References

2-(((2-(1H-Indol-4-yl)-4-morpholinothieno[3,2-d]pyrimidin-6-yl)methyl)(methyl)amino)-1-(2-(aminomethyl)piperazin-1-yl)ethan-1-one (58, 97% yield).



^1H NMR (400 MHz, DMSO) δ 11.70 (s, NH), 8.27 (s, NH_2), 8.19 (d, $J = 4.7$ Hz, 1H, H-26), 8.07 (t, $J = 7.7$ Hz, 1H, H-25), 7.73 (dd, $J = 8.1, 2.6$ Hz, 1H, H-24), 7.60 (d, $J = 2.8$ Hz, 1H, H-22), 7.30 (td, $J = 7.8, 2.5$ Hz, 1H, H-7), 7.13 (s, 1H, H-21), 4.51 (t, $J = 18.2$ Hz, 2H, H-9), 4.25 – 4.16 (m, 4H, H-1), 3.90 (t, $J = 4.7$ Hz, 4H, H-2), 3.62 (d, $J = 30.9$ Hz, 2H, H-17), 3.44 (d, $J = 3.0$ Hz, 2H, H-11), 2.94 (s, 2H, H-18), 2.34 (s, 3H, H-10), 1.65 (dd, $J = 45.9, 32.7$ Hz, 6H, H-14/H-15/H-16). ^{13}C NMR (101 MHz, DMSO) δ 168.43 (C-12), 162.77 (C-4), 157.10 (C-3), 137.36 (C-23), 126.63, 121.92, 121.01 (C-7), 113.90 (C-24), 102.39 (C-21), 66.25 (C-1), 59.43 (C-11), 56.03 (C-9), 46.91 (C-2), 34.48, 25.51 (C-14), 22.40 (C-16), 18.88 (C-15). LCMS m/z calc. for $\text{C}_{28}\text{H}_{35}\text{N}_7\text{O}_2\text{S}$ $[\text{M}+\text{H}]^+$: 534.3, found 534.3 with t_R 1.95 min (97%).

1-(2-(aminomethyl)piperidin-1-yl)-2-(((2-(3-hydroxyphenyl)-4-morpholinothieno[3,2-d]pyrimidin-6-yl)methyl)(methyl)amino)ethan-1-one (59, 98% yield).

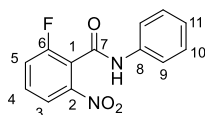


^1H NMR (400 MHz, DMSO) δ 8.56 (s, OH), 8.00 – 7.84 (m, 2H, H-20/H-24), 7.72 – 7.49 (m, 1H, H-23), 7.48 – 7.21 (m, 1H, H-7), 7.09 – 7.00 (m, 1H, H-22), 4.48 (s, 2H, H-9), 4.13 (d, $J = 4.7$ Hz, 4H, H-1), 3.86 (t, $J = 4.8$ Hz, 6H, H-2/H-17), 3.49 (d, $J = 16.0$ Hz, OH), 3.40 (s, 1H, H-11), 3.30 (s, OH), 2.91 (d, $J = 9.2$ Hz, 2H, H-17), 2.70 (s, 2H, H-18), 1.94 – 1.20 (m, 6H, H-14/H-15/H-16). ^{13}C NMR (101 MHz, DMSO) δ 168.17 (C-12), 158.22 (C-5), 157.22 (C-3), 131.95 (d, $J = 9.2$ Hz), 130.21, 129.30 (C-28), 119.55 (C-7), 115.59 (C-22), 114.55 (C-20), 66.31 (C-1), 60.57 (C-11), 53.90 (C-9), 46.95 (C-2), 43.93 (C-18), 41.81 (C-10), 40.94 (C-17), 34.52, 26.04 (C-14), 21.71 (d, $J = 7.0$ Hz, C-16), 18.87 (C-15). LCMS m/z calc. for $\text{C}_{26}\text{H}_{34}\text{N}_6\text{O}_3\text{S}$ $[\text{M}+\text{H}]^+$: 511.2, found 511.2 with t_R 1.94 min (96%).

7.3.3 Experimental for Chapter 3

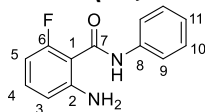
2-fluoro-6-nitro-N-phenylbenzamide (74, 98% yield).

References



To a solution of 2-fluoro-6-nitrobenzoic acid **73** (5.40 mmol, 1 equiv) in DMF (10 mL) was added aniline (6.48 mmol, 1.2 equiv), HATU (5.94 mmol, 1.1 equiv) and DIPEA (16.20 mmol, 3 equiv). The reaction mixture was stirred at RT for 18 h, at which time it was diluted with ethyl acetate (50 mL) and washed with saturated sodium bicarbonate (2* 40 mL), water (40 mL) and brine (40 mL). The organic layer was then dried over MgSO₄ and concentrated under reduced pressure. The crude product was purified by flash column chromatography (DCM/methanol: 10:1) to yield amide **74** (98%) as a yellow solid. ¹H NMR (400 MHz, DMSO-d₆) δ 10.83 (s, NH), 8.12 (dt, J = 8.1, 1.0 Hz, 1H, H-3), 7.92 – 7.76 (m, 1H, H-4), 7.70 – 7.60 (m, 1H, H-5), 7.39 (dd, J = 8.5, 7.4 Hz, 2H, H-9), 7.24 – 7.09 (m, 2H, H-10), 7.07 – 6.91 (m, 1H, H-11). ¹³C NMR (101 MHz, DMSO-d₆) δ 160.16 (C-7), 159.42 (C-6), 146.73 (d, J = 5.2 Hz) (C-2), 138.92 (C-8), 132.37 (d, J = 9.0 Hz) (C-4), 129.46 (C-10), 124.69 (C-11), 121.13 (C-5), 121.10 (C-13), 119.93 (C-3), 114.31 (C-1). LCMS *m/z* calc. for C₁₃H₉FN₂O₃ [M+H]⁺: 261.1, found 261.2 with *t_R* 2.66 min.

2-amino-6-fluoro-N-phenylbenzamide (75, 100% yield).



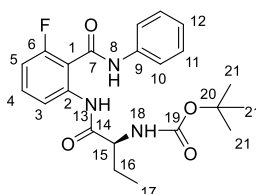
To a solution of nitro compound **74** (3.84 mmol, 1 equivalent) in methanol (15 mL) was added 10% Pd/C (0.096 mmol, 0.025 equiv) and the reaction was stirred under hydrogen atmosphere for 16 h. The crude product was filtered through Celite and filtrate was concentrated in vacuum to give amine **75** (100%) as a brown solid. ¹H NMR (400 MHz, DMSO-d₆) δ 10.28 (s, NH), 7.73 (d, J = 7.9 Hz, 2H, H-9), 7.34 (t, J = 7.7 Hz, 2H, H-10), 7.12 (dt, J = 19.7, 7.6 Hz, 2H, H-4/11), 6.57 (d, J = 8.3 Hz, 1H, H-5), 6.40 (t, J = 9.2 Hz, 1H, H-3), 5.77 (s, NH₂). ¹³C NMR (101 MHz, DMSO) δ 163.50 (C-7), 160.66 (d, J = 243.1 Hz, C-6), 149.78 (d, J = 6.2 Hz, C-2), 139.44 (C-8), 131.81 (d, J = 11.1 Hz, C-4), 129.13 (C-10), 124.14 (C-11), 120.26 (C-9), 111.86 (d, J = 2.3 Hz, C-3), 109.07 (d, J = 19.2 Hz, C-1), 102.40 (d, J = 22.7 Hz, C-5). LCMS *m/z* calc. for C₁₃H₁₁FN₂O [M+H]⁺: 231.1, found 231.2 with *t_R* 2.70 min.

General procedure for amide coupling. To a solution of α-N-Boc-amino acid (13.02 mmole, 3 equiv) in dry THF (15 mL) at -15 °C was slowly added N-methylmorpholine (15.19 mmol, 3.5 equiv) dropwise followed by isobutylchloroformate (15.19 mmole, 3.5 equiv). The reaction mixture was stirred at -10 °C under N₂ for 2 h. Compound **75** (4.34 mmol, 1 equiv) was then added to the above reaction mixture over 0.5 h. The resulting solution was stirred for 18 h at 60

References

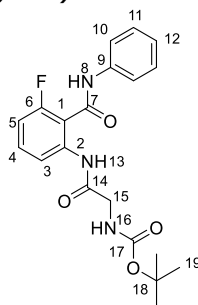
°C at which time it was concentrated under reduced pressure. The residue was dissolved in ethyl acetate (50 mL) and the organic phase was washed with water (3 * 40 mL) and brine (1* 40 mL). The organic layer was then dried over MgSO₄ and concentrated under reduced pressure. The crude product was purified by flash column chromatography (10-15% ethyl acetate in petroleum ether) to yield the diamides (**76** and **108**) as solids.

tert-butyl (1-((3-fluoro-2-(phenylcarbamoyl)phenyl)amino)-1-oxobutan-2-yl)carbamate (76, 61% yield).



¹H NMR (400 MHz, DMSO) δ 10.62 (s, NH-13), 10.03 (s, NH-8), 8.03 (d, *J* = 8.3 Hz, 1H, H-4), 7.76 (d, *J* = 8.0 Hz, 2H, H-10), 7.52 (q, *J* = 7.8 Hz, 1H, H-5), 7.35 (q, *J* = 7.5 Hz, 3H, H-11, NH-18), 7.13 (q, *J* = 9.2, 8.1 Hz, 2H, H-5/H-12), 3.93 (dt, *J* = 8.4, 4.3 Hz, 1H, H-15), 1.92 – 1.72 (m, 1H, H-16), 1.59 (dq, *J* = 14.7, 7.6 Hz, 1H, H-16), 1.32 (s, 9H, H-21), 0.91 – 0.86 (m, 3H, H-17). ¹³C NMR (101 MHz, DMSO) δ 171.96 (C-14), 161.90 (C-7), 160.76 (C-6), 158.32 (C-6), 156.17 (C-19), 139.07, 138.21, 132.24 (d, *J* = 9.9 Hz, C-4), 129.10 (C-11), 124.53 (C-12), 120.45 (C-9), 118.01 (C-3), 116.17 (d, *J* = 18.6 Hz, C-5), 111.57 (d, *J* = 22.4 Hz, C-1), 78.80 (C-20), 57.48 (C-15), 28.47 (C-21), 24.85 (C-16), 11.00 (C-17). LCMS *m/z* calc. for C₂₂H₂₆FN₃O₄ [M+H]⁺: 416.2, found 416.4 with *t_R* 2.91 min.

tert-butyl (2-((3-fluoro-2-(phenylcarbamoyl)phenyl)amino)-2-oxoethyl)carbamate (108, 20% yield).



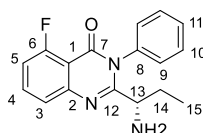
¹H NMR (400 MHz, DMSO) δ 10.62 (s, 1H, NH-13), 10.03 (s, 1H, NH-8), 8.03 (d, *J* = 8.3 Hz, 1H, H-3), 7.76 (d, *J* = 8.0 Hz, 2H, H-10), 7.52 (q, *J* = 7.8 Hz, 1H, H-4), 7.35 (q, *J* = 7.5 Hz, 3H, H-11), 7.13 (q, *J* = 9.2, 8.1 Hz, 2H, H-5/H-12), 3.93 (dt, *J* = 8.4, 4.3 Hz, 1H, NH-16), 3.36 (s, H-15), 2.51 (t, *J* = 2.1 Hz, 1H, H-15), 1.32 (s, 9H, H-19). ¹³C NMR (101 MHz, DMSO) δ 171.96 (14), 161.90 (C-7), 160.76 (C-6), 158.32 (C-6), 156.17 (C-17), 139.07, 138.21, 132.24 (d, *J* = 9.9 Hz, C-4), 129.10 (C-11), 124.53 (C-12), 120.45 (C-10), 118.01 (C-3), 116.17 (d, *J* = 18.6 Hz, C-5), 111.57 (d, *J* = 22.4

References

Hz, C-1), 78.80 (C-18), 57.48 (C-15), 28.47 (C-19). LCMS m/z calc. for $C_{20}H_{22}FN_3O_4$ $[M+H]^+$: 388.2, found 388.3 with t_R 2.87 min.

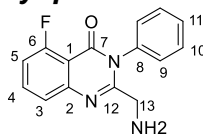
General procedure for the synthesis of quinazolinone derivatives. To a suspension of the diamide (**76** and **108**) (4.44 mmol, 1 equiv) and iodine (12.43 mmol, 2.8 equiv) in DCM (60 mL) at RT was slowly added HMDS (35.52 mmol, 8 equiv) over 1 h. The reaction mixture was stirred at RT for 18 h. The reaction was quenched with 5% sodium thiosulfate solution (30 mL), diluted with DCM (50 mL) and stirred for a further 50 min at 25 °C. The organic layer was separated and washed with 5% sodium thiosulfate solution (2 * 40 mL), water (1 * 40 mL) and brine (1 * 40 mL). The organic layer was dried over anhydrous sodium sulfate, filtered and evaporated. The residue was purified by silica gel chromatography eluting with 2% methanol in DCM to yield the quinazolinone derivatives (**77** and **109**) as yellow solids.

2-((S)-1-aminopropyl)-5-fluoro-3-phenyl-2,3-dihydroquinazolin-4(1H)-one (77**, 56% yield).**



1H NMR (400 MHz, Chloroform- d) δ 7.69 (td, J = 8.2, 5.4 Hz, 1H), 7.55 (dddd, J = 13.4, 11.8, 6.5, 3.3 Hz, 4H), 7.28 (ddd, J = 7.5, 4.1, 2.0 Hz, 2H), 7.16 – 7.04 (m, 1H), 3.43 (dd, J = 7.5, 5.2 Hz, 1H, H-13), 1.87 – 1.70 (m, 2H, H-14), 0.81 (t, J = 7.4 Hz, 3H, H-15). ^{13}C NMR (101 MHz, Chloroform- d) δ 162.78 (C-7), 161.23 (C-6), 160.13, 159.42 (d, J = 4.4 Hz), 149.50, 136.20, 134.81 (d, J = 10.5 Hz, C-4), 130.03, 129.73, 129.43, 129.00, 128.27, 123.16 (d, J = 4.3 Hz, C-3), 113.25 (d, J = 20.7 Hz, C-5), 54.30 (C-13), 30.25 (C-14), 10.53 (C-15). LCMS m/z calc. for $C_{17}H_{16}FN_3O$ $[M+H]^+$: 298.1, found 298.3 with t_R 1.96 min (99%).

2-(aminomethyl)-5-fluoro-3-phenylquinazolin-4(3H)-one (109**, 20 %yield).**

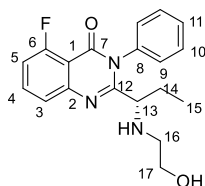


1H NMR (400 MHz, Chloroform- d) δ 7.73 (td, J = 8.2, 5.4 Hz, 1H), 7.64 – 7.50 (m, 4H), 7.32 – 7.22 (m, 2H), 7.15 (ddd, J = 10.5, 8.1, 1.0 Hz, 1H, H-5), 5.30 (s, 2H, H-13), 3.49 (s, NH2). ^{13}C NMR (101 MHz, $CDCl_3$) δ 162.78 (C-7), 160.14 (C-6), 159.16 (d, J = 4.4 Hz), 157.51, 149.19, 135.46, 134.90 (C-4), 130.06, 129.65, 128.23, 123.10 (d, J = 4.2 Hz, C-3), 113.52 (d, J = 20.8 Hz, C-5), 110.66 (d, J = 5.9 Hz, C-1), 45.03 (C-13). LCMS m/z calc. for $C_{15}H_{12}FN_3O$ $[M+H]^+$: 270.1, found 270.2 with t_R 0.74 min.

References

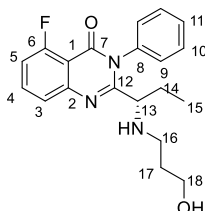
General procedure for nucleophilic substitution of alkyl halides. Alkyl halide derivative was added to a solution of primary amine **77** (0.39 mmol, 1 equiv) in acetonitrile (20 mL) followed by K_2CO_3 (2.34 mmol, 6 equiv). The reaction mixture was stirred at reflux for 24 h. Upon cooling to RT, insoluble solid was filtered off. The solvent was then removed under reduced pressure and the resulting residue was purified by flash chromatography (1.5% methanol in DCM) to yield the products (**79-87**) as white solids.

(S)-5-fluoro-2-(1-((2-hydroxyethyl)amino)propyl)-3-phenylquinazolin-4(3H)-one (79, 30% yield).



1H NMR (400 MHz, Chloroform- d) δ 7.71 (td, $J = 8.2, 5.3$ Hz, 1H), 7.62 – 7.49 (m, 4H), 7.28 (t, $J = 4.5$ Hz, 1H), 7.23 – 7.18 (m, 1H), 7.13 (dd, $J = 10.5, 8.1$ Hz, 1H, H-5), 3.53 (t, $J = 5.2$ Hz, 2H, H-17), 3.21 (dd, $J = 7.9, 4.6$ Hz, 1H, H-13), 2.80 (dt, $J = 12.2, 4.9$ Hz, 1H, H-16), 2.53 (dt, $J = 11.7, 5.3$ Hz, 1H, H-16), 1.71 (dq, $J = 14.6, 7.3, 4.5$ Hz, 1H, H-14), 1.54 (dp, $J = 14.6, 7.4$ Hz, 1H, H-14), 0.83 (t, $J = 7.3$ Hz, 3H, H-15). ^{13}C NMR (101 MHz, Chloroform- d) δ 162.83 (C-7), 160.74 (C-6), 160.17 (C-6), 159.36 (d, $J = 4.3$ Hz), 149.38 (C-12), 135.99, 134.94 (d, $J = 10.5$ Hz, C-4), 130.08, 129.86, 129.59, 128.95, 128.27, 123.09 (d, $J = 4.3$ Hz, C-3), 113.37 (d, $J = 20.8$ Hz, C-5), 60.95 (C-13), 60.53 (C-17), 49.37 (C-16), 28.84 (C-14), 10.80 (C-15). LCMS m/z calc. for $C_{19}H_{20}FN_3O_2$ $[M+H]^+$: 341.2, found 342.3 with t_R 1.87 min (99%).

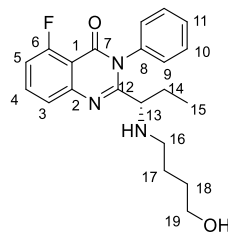
(S)-5-fluoro-2-(1-((3-hydroxypropyl)amino)propyl)-3-phenylquinazolin-4(3H)-one (80, 51% yield).



1H NMR (400 MHz, Chloroform- d) δ 7.86 – 7.64 (m, 1H), 7.58 (m, 4H), 7.28 (td, $J = 4.2, 2.1$ Hz, 2H), 7.21 (dt, $J = 8.4, 1.7$ Hz, 1H), 7.18 – 7.03 (m, 1H, H-5), 3.86 – 3.65 (m, 2H, H-18), 3.27 (dd, $J = 8.0, 4.5$ Hz, 1H, H-13), 2.95 (ddd, $J = 10.8, 6.2, 4.0$ Hz, 2H, H-16), 2.52 (ddd, $J = 11.8, 7.8, 4.2$ Hz, 2H, H-17), 1.74 – 1.59 (m, 2H, H-14), 0.82 (t, $J = 7.4$ Hz, 3H, H-15). ^{13}C NMR (101 MHz, Chloroform- d) δ 162.83 (C-7), 160.29 (C-6), 149.37 (C-12), 135.92, 134.96 (d, $J = 10.4$ Hz, C-4), 130.11, 129.93, 129.66, 128.94, 128.28, 123.10 (d, $J = 4.3$ Hz, C-3), 113.40 (d, $J = 20.6$ Hz, C-5), 64.26 (C-18), 60.75 (C-13), 48.24 (C-16), 30.69 (C-14), 28.85 (C-17), 10.74 (C-15). LCMS m/z calc. for $C_{20}H_{22}FN_3O_2$ $[M+H]^+$: 356.2, found 356.3 with t_R 1.92 min (99%).

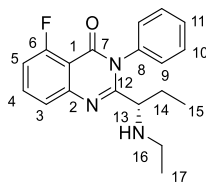
References

S)-5-fluoro-2-(1-((4-hydroxybutyl)amino)propyl)-3-phenylquinazolin-4(3H)-one (81, 34% yield).



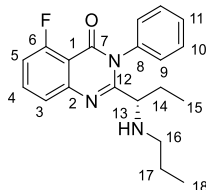
^1H NMR (400 MHz, Chloroform- d) δ 7.72 (q, J = 7.4 Hz, 1H), 7.56 (dq, J = 13.2, 7.6 Hz, 4H), 7.35 – 7.21 (m, 1H), 7.22 – 7.07 (m, 2H), 3.58 (tt, J = 14.4, 11.2, 4.9 Hz, 2H, H-19), 3.24 (t, J = 6.1 Hz, 1H, H-13), 2.75 (dd, J = 11.5, 5.9 Hz, 2H, H-16), 2.42 – 2.16 (m, 2H, H-18), 1.72 (tt, J = 13.5, 7.3 Hz, 2H, H-14), 1.49 – 1.23 (m, 2H, H-17), 0.83 (t, J = 7.4 Hz, 3H, H-15). ^{13}C NMR (101 MHz, Chloroform- d) δ 162.83 (C-7), 160.18 (C-6), 159.31 (d, J = 4.3 Hz), 149.39 (C-12), 135.87, 134.93 (d, J = 10.4 Hz, C-4), 130.09, 129.90, 129.65, 128.96, 128.32, 123.14 (d, J = 4.3 Hz, C-3), 113.38 (d, J = 20.7 Hz, C-5), 62.58 (C-19), 60.51 (C-13), 48.00 (C-16), 32.27 (C-18), 28.84 (C-17), 28.67 (C-14), 10.58 (C-15). LCMS m/z calc. for $\text{C}_{21}\text{H}_{24}\text{FN}_3\text{O}_2$ $[\text{M}+\text{H}]^+$: 370.2, found 370.3 with t_R 1.95 min (98%).

(S)-2-(1-(ethylamino)propyl)-5-fluoro-3-phenylquinazolin-4(3H)-one (82, 26% yield).



^1H NMR (400 MHz, CDCl_3) δ 7.71 (td, J = 8.2, 5.4 Hz, 1H), 7.64 – 7.50 (m, 4H), 7.28 (d, J = 1.6 Hz, 1H), 7.27 – 7.19 (m, 1H), 7.12 (ddd, J = 10.4, 8.2, 1.1 Hz, 1H, H-5), 3.23 (dd, J = 7.1, 5.4 Hz, 1H, H-13), 2.58 (dq, J = 10.9, 7.1 Hz, 1H, H-16), 2.41 (dq, J = 10.9, 7.1 Hz, 1H, H-16), 1.70 (dq, J = 14.8, 7.4, 5.4 Hz, 1H, H-14), 1.57 (dp, J = 14.4, 7.3 Hz, 1H, H-14), 1.05 (t, J = 7.1 Hz, 3H, H-17), 0.83 (t, J = 7.4 Hz, 3H, H-15). ^{13}C NMR (101 MHz, CDCl_3) δ 162.85 (C-7), 161.20 (C-6), 160.20, 159.51 (d, J = 4.5 Hz), 149.66, 136.22, 134.78 (d, J = 10.4 Hz, C-4), 129.84 (d, J = 17.1 Hz), 129.44, 129.01, 128.52, 123.20 (d, J = 4.2 Hz, C-3), 113.14 (d, J = 20.7 Hz, C-5), 110.65 (C-1), 60.49 (C-13), 42.28 (C-16), 28.68 (C-14), 15.46 (C-17), 10.65 (C-15). LCMS m/z calc. for $\text{C}_{19}\text{H}_{20}\text{FN}_3\text{O}$ $[\text{M}+\text{H}]^+$: 326.2, found 326.0 with t_R 1.93 min (95%).

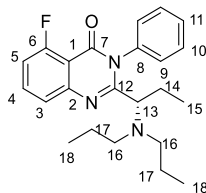
(S)-5-fluoro-3-phenyl-2-(1-(propylamino)propyl)quinazolin-4(3H)-one (84, 45% yield).



References

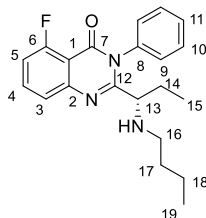
^1H NMR (400 MHz, Chloroform-d) δ 7.71 (td, J = 8.2, 5.4 Hz, 1H), 7.57 (dddd, J = 11.8, 10.1, 5.5, 3.2 Hz, 4H), 7.38 – 7.19 (m, 2H), 7.12 (ddd, J = 10.4, 8.1, 1.0 Hz, 1H, H-5), 3.21 (dd, J = 7.3, 5.3 Hz, 1H, H-13), 2.47 (ddd, J = 10.9, 7.8, 6.7 Hz, 1H, H-16), 2.35 (ddd, J = 10.9, 7.9, 5.9 Hz, 1H, H-16), 1.70 (ddd, J = 13.2, 7.3, 5.4 Hz, 1H, H-14), 1.56 (dt, J = 14.1, 7.2 Hz, 1H, H-14), 1.49 – 1.34 (m, 2H, H-17), 0.90 (t, J = 7.4 Hz, 3H, H-18), 0.82 (t, J = 7.4 Hz, 3H, H-15). ^{13}C NMR (101 MHz, Chloroform-d) δ 162.83 (C-7), 161.16 (C-6), 160.19, 159.50 (d, J = 4.3 Hz), 149.64 (C-12), 136.19, 134.77 (d, J = 10.4 Hz, C-4), 129.90, 129.73, 129.42, 128.99, 128.49, 123.18 (d, J = 4.3 Hz, C-3), 113.12 (d, J = 20.7 Hz, C-5), 60.69 (C-13), 50.02 (C-16), 28.65 (C-14), 23.38 (C-17), 11.74 (C-18), 10.69 (C-15). LCMS m/z calc. for $\text{C}_{20}\text{H}_{22}\text{FN}_3\text{O}$ $[\text{M}+\text{H}]^+$: 340.2, found 340.4 with t_R 2.04 min (98%).

(S)-2-(1-(dipropylamino)propyl)-5-fluoro-3-phenylquinazolin-4(3H)-one (84, side product).



^1H NMR (400 MHz, Chloroform-d) δ 7.70 (td, J = 8.2, 5.4 Hz, 1H), 7.59 – 7.38 (m, 5H), 7.21 – 7.07 (m, 2H), 3.41 (dd, J = 9.6, 4.5 Hz, 1H, H-13), 2.54 (ddd, J = 13.2, 9.2, 6.1 Hz, 2H, H-16), 2.25 (ddd, J = 13.1, 9.3, 5.4 Hz, 2H, H-16), 2.15 (ddt, J = 14.2, 9.6, 7.1 Hz, 1H, H-14), 1.65 (dtt, J = 14.7, 7.5, 3.5 Hz, 1H, H-14), 1.22- 0.90 (m, 4H, H-17), 0.83 (t, J = 7.3 Hz, 3H, H-15), 0.68 (t, J = 7.3 Hz, 6H, H-18). ^{13}C NMR (101 MHz, Chloroform-d) δ 161.18 (C-6), 149.66 (C-12), 136.21, 134.84, 134.74, 129.91, 129.74, 129.44, 129.00, 128.50, 123.22, 123.17 (C-3), 113.24 (C-5), 113.03, 60.69 (C-13), 50.03 (C-16), 28.65 (C-14), 23.39 (C-17), 11.73 (C-18), 10.69 (C-15). LCMS m/z calc. for $\text{C}_{23}\text{H}_{28}\text{FN}_3\text{O}$ $[\text{M}+\text{H}]^+$: 382.2, found 382.3 with t_R 2.22 min (99%).

(S)-2-(1-(butylamino)propyl)-5-fluoro-3-phenylquinazolin-4(3H)-one (86, 34 % yield).

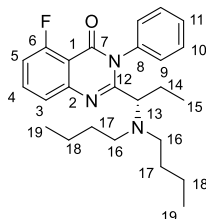


^1H NMR (400 MHz, Chloroform-d) δ 7.71 (td, J = 8.2, 5.4 Hz, 1H), 7.61 – 7.48 (m, 4H), 7.30 – 7.22 (m, 2H), 7.12 (ddd, J = 10.5, 8.2, 1.1 Hz, 1H, H-5), 3.21 (dd, J = 7.2, 5.3 Hz, 1H, H-13), 2.51 (dt, J = 11.1, 6.9 Hz, 1H, H-16), 2.37 (dt, J = 11.0, 6.6 Hz, 1H, H-16), 1.76 – 1.64 (m, 1H, H-14), 1.56 (dp, J = 14.5, 7.3 Hz, 1H, H-14), 1.45 – 1.25 (m, 4H, H-17/18), 0.89 (t, J = 7.1 Hz, 3H, H-15), 0.82 (t, J = 7.4 Hz, 3H, H-19). ^{13}C NMR (101 MHz, Chloroform-d) δ 162.84 (C-7), 161.23 (C-6), 160.19, 159.51 (d,

References

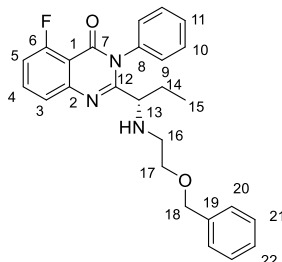
J = 4.4 Hz), 149.66 (C-12), 136.21, 134.76 (d, J = 10.5 Hz, C-4), 129.88, 129.72, 129.41, 128.99, 128.50, 123.17 (d, J = 4.3 Hz, C-3), 113.11 (d, J = 20.7 Hz, C-5), 60.73 (C-13), 47.76 (C-16), 32.37 (C-17), 28.67 (C-14), 20.32 (C-18), 13.92 (C-19), 10.70 (C-15). LCMS *m/z* calc. for C₂₁H₂₄FN₃O [M+H]⁺: 354.2, found 354.3 with *t_R* 2.12 min (99%).

(S)-2-(1-(dibutylamino)propyl)-5-fluoro-3-phenylquinazolin-4(3H)-one (87, side product).



¹H NMR (400 MHz, Chloroform-d) δ 7.69 (d, J = 5.4 Hz, 1H), 7.58 – 7.41 (m, 5H), 7.18 – 7.08 (m, 2H, H-5), 3.43 (dd, J = 9.9, 4.2 Hz, 1H, H-13), 2.57 (ddd, J = 14.2, 8.6, 5.6 Hz, 2H, H-16), 2.18 (m, 2H, H-16), 1.78 – 1.55 (m, 1H, H-14), 1.48 – 1.21 (m, 1H, H-14), 1.20 – 0.90 (m, 8H, H-16/17), 0.84 (t, J = 7.3 Hz, 3H, H-15), 0.77 (t, J = 6.9 Hz, 6H, H-19). ¹³C NMR (101 MHz, Chloroform-d) δ 162.75 (C-7), 161.14 (C-6), 156.95, 149.19 (C-12), 136.56, 134.46 (d, J = 10.3 Hz, C-4), 130.62, 129.19 (d, J = 1.9 Hz), 128.86, 128.13, 123.55 (d, J = 4.3 Hz, C-3), 113.19 (d, J = 20.7 Hz, C-5), 63.95 (C-13), 50.51 (C-16), 30.97 (C-17), 20.45 (C-14), 18.55 (C-18), 13.96 (C-19), 11.37 (C-15). LCMS *m/z* calc. for C₂₅H₃₂FN₃O [M+H]⁺: 410.3, found 410.4 with *t_R* 2.38 min (99%).

(S)-2-(1-((2-(benzyloxy)ethyl)amino)propyl)-5-fluoro-3-phenylquinazolin-4(3H)-one (142, 47% yield).

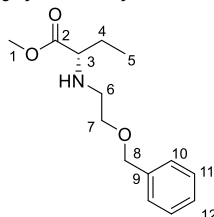


¹H NMR (400 MHz, Chloroform-d) δ 7.70 (td, J = 8.2, 5.4 Hz, 1H), 7.64 – 7.44 (m, 5H), 7.41 – 7.29 (m, 5H), 7.22 (dt, J = 6.7, 2.3 Hz, 1H), 7.13 (ddd, J = 10.4, 8.2, 1.0 Hz, 1H, H-3), 4.50 (d, J = 2.1 Hz, 2H, H-18), 4.08 – 3.69 (m, 1H, H-17), 3.55 (dt, J = 9.7, 4.9 Hz, 1H, H-17), 3.35 (s, NH), 2.82 (ddt, J = 11.9, 8.6, 4.5 Hz, 1H, H-16), 2.65 (d, J = 11.3 Hz, 1H, H-16), 1.77 (dt, J = 13.6, 6.7 Hz, 1H, H-14), 1.62 (dq, J = 14.1, 7.1 Hz, 1H, H-14), 0.84 (t, J = 7.4 Hz, 3H, H-15). ¹³C NMR (101 MHz, Chloroform-d) δ 162.81 (C-7), 160.16 (C-6), 138.17, 135.95, 134.85 (d, J = 10.4 Hz, C-4), 129.96, 129.74, 129.03, 128.48, 128.37, 127.66, 123.28 (d, J = 4.3 Hz, C-3), 123.23, 113.44 (d, J = 20.7 Hz, C-5), 72.98 (C-18), 60.69 (C-17), 47.42 (C-16), 29.71 (C-14), 10.47

References

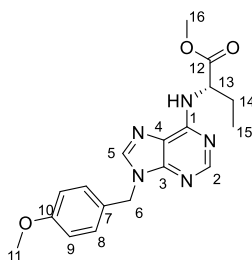
(C-15). LCMS m/z calc. for $C_{26}H_{26}FN_3O_2$ $[M+H]^+$: 432.2, found 432.1 with t_R 2.29 min (90%).

methyl (S)-2-((2-(benzyloxy)ethyl)amino)butanoate (100, 28% yield).



To a magnetically stirred solution of methyl (S)-2-aminobutanoate (8.53 mmol, 1 equiv) in CH_3CN (10 mL) was added ((2-bromoethoxy)methyl)benzene **99** (10.23 mmol, 1.2 equiv) and K_2CO_3 (51.18 mmol, 6 equiv). The reaction mixture was stirred at reflux for 18 h. The solvent was then removed under reduced pressure and the resulting residue was purified by flash chromatography (ethyl acetate/ petroleum ether, 1:1) to give secondary amine **100** as a yellowish green oil. 1H NMR (400 MHz, Chloroform- d) δ 7.37 (s, 2H), 7.35 (s, 2H), 7.34 – 7.26 (m, 1H, H-12), 4.55 (d, J = 2.4 Hz, 2H, H-8), 3.73 (s, 3H, H-1), 3.64 – 3.51 (m, 2H, H-7), 3.26 (t, J = 6.5 Hz, 1H, H-3), 2.87 (ddd, J = 11.7, 6.7, 4.7 Hz, 1H, H-6), 2.70 (ddd, J = 12.2, 5.4, 4.5 Hz, 1H, H-6), 1.90 (s, NH), 1.71 (dtd, J = 13.7, 7.4, 1.5 Hz, 2H, H-4), 0.95 (t, J = 7.4 Hz, 3H, H-5). ^{13}C NMR (101 MHz, Chloroform- d) δ 175.57 (C-2), 138.33 (C-9), 128.38 (C-11), 127.69 (C-10), 127.60 (C-12), 73.00 (C-8), 69.77 (C-1), 62.88 (C-7), 51.62 (C-3), 47.57 (C-6), 26.48 (C-4), 10.11 (C-5). LCMS m/z calc. for $C_{14}H_{21}NO_3$ $[M+H]^+$: 252.2, found 252.2 with t_R 1.94 min.

methyl (S)-2-((9-(4-methoxybenzyl)-9H-purin-6-yl)amino)butanoate (101, 34% yield).



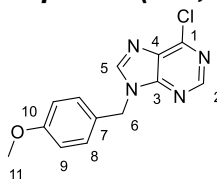
n -butanol (2 mL) was added to methyl (S)-2-aminobutanoate (1.822 mmol, 2.5 equiv), and the resulting solution was transferred to a microwave vial containing 6-chloro-9-(4-methoxybenzyl)-9H-purine **110** (0.728 mmol, 1 equiv). DIPEA (5.832 mmol, 8 equiv) was added and the reaction mixture was heated to 120°C for 4 h in the microwave. Upon cooling to RT, the reaction mixture was concentrated to dryness under reduced pressure. The crude residue was purified by flash chromatography (ethyl acetate/ petrol ether, 1:1) to give arylamine **101** (34% yield) as a yellowish green oil. 1H NMR (400 MHz, $CDCl_3$) δ 8.42 (s, 1H, H-2), 7.73 (s, 1H, H-5), 7.30 – 7.22 (m, 2H, H-8), 6.89 (d, J = 8.6 Hz, 2H, H-9), 6.28 (s, NH), 5.31 (s,

References

2H, H-6), 4.96 (s, 1H, H-13), 4.18 (t, $J = 6.6$ Hz, 3H, H-16), 3.81 (s, 3H, H-11), 2.18 – 2.02 (m, 1H, H-14), 1.93 (dp, $J = 14.5, 7.3$ Hz, 1H, H-14), 0.93 (t, $J = 6.6$ Hz, 3H, H-15). ^{13}C NMR (101 MHz, CDCl_3) δ 173.18 (C-12), 159.62 (C-10), 154.15, 153.04 (C-2), 139.86 (C-5), 129.34 (C-8), 127.61, 114.38 (C-9), 60.38 (C-13), 55.30 (C-11), 52.26 (C-16), 46.73 (C-6), 25.78 (C-14), 9.82 (C-15). LCMS m/z calc. for $\text{C}_{18}\text{H}_{21}\text{N}_5\text{O}_3$ $[\text{M}+\text{H}]^+$: 356.2, found 356.3 with t_R 2.65 min.

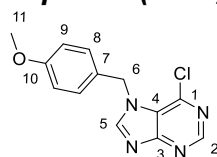
General procedure for the N-9-alkylation of 6-chloropurine. A stirred suspension of potassium carbonate (19.41 mmol, 3 equiv) in DMF (10 mL) was treated with 6-chloro-9H-purine **78** (6.47 mmol, 1 equiv) under N_2 atmosphere at RT for 1 h. *p*-methoxybenzyl bromide (5.55 mmol, 0.85 equiv) was added to the reaction mixture, and the resulting solution was stirred at RT for 12 h. The solvent was then removed via rotary evaporation and the residue dissolved in ethyl acetate (100 mL) and washed with water (2* 100 mL) and brine (1* 100 mL), the organic layer was dried over MgSO_4 , filtered and evaporated. The crude product was purified by silica gel chromatography (30- 40% ethyl acetate in petroleum ether) to yield N-9-alkylated-6-chloropurine **110** with N-7-regioisomer **110b** as white solids.

6-chloro-9-(4-methoxybenzyl)-9H-purine (110, 52% yield).



^1H NMR (400 MHz, DMSO-d_6) δ 8.82 (s, 1H, H-2), 8.80 (s, 1H, H-5), 7.45 – 7.21 (m, 2H, H-8), 6.96 – 6.83 (m, 2H, H-9), 5.45 (s, 2H, H-6), 3.71 (s, 3H, H-11). ^{13}C NMR (101 MHz, DMSO-d_6) δ 159.50 (C-10), 152.04 (C-1), 149.60 (C-3), 147.67 (C-5), 131.32 (C-4), 129.84 (C-8), 128.35 (C-7), 114.54 (C-9), 55.53 (C-11), 47.07 (C-6). LCMS m/z calc. for $\text{C}_{13}\text{H}_{11}\text{ClN}_4\text{O}$ $[\text{M}+\text{H}]^+$: 275.1, found 275.1 with t_R 2.55 min.

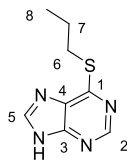
6-chloro-7-(4-methoxybenzyl)-7H-purine (110b, 28%).



^1H NMR (400 MHz, Chloroform- d) δ 8.88 (s, 1H, H-2), 8.21 (s, 1H, H-5), 7.17 (d, $J = 8.7$ Hz, 2H, H-8), 6.92 (d, $J = 8.7$ Hz, 2H, H-9), 5.63 (s, 2H, H-6), 3.82 (s, 3H, H-11). ^{13}C NMR (101 MHz, Chloroform- d) δ 162.09 (C-10), 160.03, 152.52 (C-2), 148.93 (C-5), 143.17, 128.89 (C-8), 126.25, 114.75 (C-9), 55.38 (C-11), 50.43 (C-6). LCMS m/z calc. for $\text{C}_{13}\text{H}_{11}\text{ClN}_4\text{O}$ $[\text{M}+\text{H}]^+$: 275.1, found 275.1 with t_R 2.49 min.

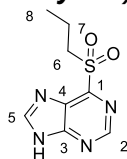
6-(propylthio)-9H-purine (97, 13% yield).

References



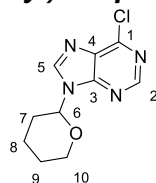
1-propanethiol (25 mmol, 4 equiv) was added to a solution of 6-chloropurine **78** (6.46 mmol, 1 equiv) and DBU (12.92 mmol, 2 equiv) in DMF (10 mL). The reaction mixture was stirred for 18 h at RT at which time it was concentrated under reduced pressure. The residue was rediluted in ethyl acetate, and the organic phase was washed with water (3* 50 mL) and brine (1* 50 mL). The organic layer was then dried over Na₂SO₄, filtered and concentrated. The resulting residue was purified by flash chromatography on silica gel eluting with 2.5% MeOH containing 0.7N ammonia in DCM to give thioether **97** (168 mg, 13%) as a white solid. ¹H NMR (400 MHz, Chloroform-d) δ 13.55 (s, NH), 8.79 (s, 1H, H-2), 8.31 (s, 1H, H-5), 3.41 (t, J = 7.2 Hz, 2H, H-6), 1.85 (q, J = 7.3 Hz, 2H, H-7), 1.10 (t, J = 7.3 Hz, 3H, H-8). ¹³C NMR (101 MHz, Chloroform-d) δ 165.44 (C-1), 151.42 (C-2), 141.21 (C-5), 129.72 (C-4), 30.82 (C-6), 22.87 (C-7), 13.46 (C-8). LCMS *m/z* calc. for C₈H₁₀N₄S [M+H]⁺: 195.1, found 195.2 with *t_R* 2.31 min.

6-(propylsulfonyl)-9H-purine (98, 36% yield).



To a solution of thioether **97** (2.573 mmol, 1 equiv) in DCM (10 mL) was added oxone (24.45 mmol, 9.5 equiv). The solution was stirred for 18 h at RT. The solvent was removed in vacuum and the crude residue was dissolved in ethyl acetate (30 mL). The insoluble solid was filtered off, then the filtrate was concentrated in vacuum to yield sulfone **98** (36% yield) as a yellowish green solid. ¹H NMR (400 MHz, DMSO-d₆) δ 9.15 (s, 1H, H-2), 8.90 (s, 1H, H-5), 3.50–3.33 (t, 2H, H-6), 1.71 (hept, J = 7.6 Hz, 2H, H-7), 0.97 (t, J = 7.4 Hz, 3H, H-8). ¹³C NMR (101 MHz, DMSO-d₆) δ 165.44 (C-1), 155.73 (C-3), 151.74 (C-2), 143.89 (C-5), 134.13 (C-4), 60.00 (C-6), 16.02 (C-7), 13.13 (C-8). LCMS *m/z* calc. for C₈H₁₀N₄O₂S [M+H]⁺: 227.1, found 227.3 with *t_R* 1.90 min.

6-chloro-9-(tetrahydro-2H-pyran-2-yl)-9H-purine (122, 90% yield).



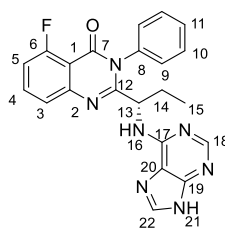
To a magnetically stirred suspension of 6-chloro-9H-purine **78** (6.512 mmol, 1 equiv) and 4-methylbenzenesulfonic acid (13.025 mmol, 2 equiv) in ethyl acetate (15 mL)

References

was added 3,4-dihydro-2H-pyran (19.536 mmol, 3 equiv). The reaction mixture was stirred at 90°C and the solid slowly dissolved over 1 h. The cloudy yellow solution was filtered and concentrated in vacuo. The pale-yellow residue was purified via column chromatography (1:1 ethyl acetate: hexane) to afford 6-chloro-9-(tetrahydro-2H-pyran-2-yl)-9H-purine **122** (90% yield) as a colorless oil which slowly crystallized. ¹H NMR (400 MHz, DMSO) δ 8.92 (s, 1H, H-2), 8.81 (s, 1H, H-5), 5.79 (dd, J = 10.8, 2.3 Hz, 1H, H-6), 4.03 (ddt, J = 11.6, 4.2, 2.4 Hz, 1H, H-10), 3.85 – 3.61 (m, 1H, H-10), 2.34 (tdd, J = 13.4, 10.8, 4.4 Hz, 2H, H-7), 2.01 (ddq, J = 18.3, 13.1, 3.3 Hz, 2H, H-8), 1.61 (td, J = 9.9, 9.1, 4.6 Hz, 2H, H-9). ¹³C NMR (101 MHz, DMSO) δ 152.27 (C-2), 151.77 (C-1), 149.76 (C-3), 146.03 (C-5), 131.42 (C-4), 82.15 (C-6), 68.23 (C-10), 30.14 (C-7), 24.90 (C-9), 22.67 (C-8). LCMS *m/z* calc. for C₁₀H₁₁ClN₄O [M+H]⁺: 239.1, found 238.7 with *t_R* 2.33 min.

General procedure for nucleophilic aromatic substitution of 6-chloropurine. *tert*-butanol (5 mL) was added to the starting amine (**77** and **109**) (1.68 mmol, 1 equiv) and the resulting solution was transferred to a microwave tube containing 6-chloropurine derivative (**78**, **110** and **122**) (2.184 mmol, 1.3 equiv). DIPEA (16.80 mmol, 10 equiv) was added and the reaction mixture was heated to 130 °C for 16 h in the microwave. The solvent was then removed under reduced pressure and the resulting residue was diluted with DCM (50 mL) and washed with water (1 * 50 mL) and brine (1 * 50 mL). The organic layer was dried over anhydrous sodium sulfate, filtered and evaporated under reduced pressure. The resulting residue was purified by flash chromatography (silica gel), eluting with 5% methanol (containing 0.7 N ammonia) in DCM to give arylamines (**8**, **128**, **106**, **111** and **123**) as white solids.

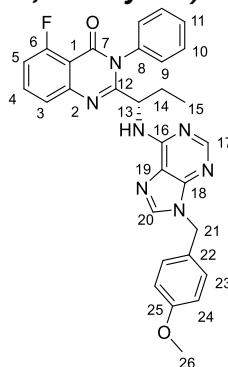
(S)-2-(1-((9H-purin-6-yl)amino)propyl)-5-fluoro-3-phenylquinazolin-4(3H)-one (8**, 75% yield).**



¹H NMR (400 MHz, DMSO-d₆) δ 12.56 (s, 1H, N-21), 8.16 (s, 1H, H-18), 7.79 (td, J = 8.2, 5.3 Hz, 2H), 7.66 – 7.41 (m, 6H), 7.27 (dd, J = 10.9, 8.1 Hz, 1H, H-3), 4.69 (s, 1H, N-16), 2.04 – 1.73 (m, 2H, H-14), 0.76 (t, J = 7.3 Hz, 3H, H-15). ¹³C NMR (101 MHz, DMSO-d₆) δ 162.32 (C-7), 159.70 (C-6), 158.91, 152.39, 149.55, 136.52, 135.77 (d, J = 10.5 Hz, C-4), 131.35 – 126.05 (m), 123.53 (C-3), 113.58 (d, J = 20.3 Hz, C-5), 110.79 (d, J = 5.6 Hz, C-1), 55.38 (C-13), 26.28 (C-14), 11.37 (C-15). LCMS *m/z* calc. for C₂₂H₁₈FN₇O [M+H]⁺: 416.2, found 416.2 with *t_R* 2.43 min (95%).

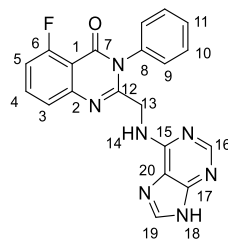
References

(S)-5-fluoro-2-(1-((9-(4-methoxybenzyl)-9H-purin-6-yl)amino)propyl)-3-phenylquinazolin-4(3H)-one (128, 65 % yield).



^1H NMR (400 MHz, CDCl_3) δ 8.32 (s, 1H, H-17), 7.85 – 7.44 (m, 7H), 7.40 – 7.31 (m, 1H), 7.28 (s, 1H, H-20), 7.26 (d, $J = 8.6$ Hz, 2H), 7.16 – 7.09 (m, 1H), 6.89 (d, $J = 8.6$ Hz, 2H, H-24), 5.30 (s, 2H, H-21), 3.81 (s, 3H, H-26), 2.05 – 1.89 (m, 1H, H-14), 1.80 (dp, $J = 14.9, 7.5$ Hz, 1H, H-14), 0.87 (t, $J = 7.4$ Hz, 3H, H-15). ^{13}C NMR (101 MHz, CDCl_3) δ 171.14 (C-22), 159.51 (d, $J = 35.1$ Hz), 135.66, 134.75 (C-4), 129.94, 129.60, 129.46 (d, $J = 9.4$ Hz), 128.94, 114.42, 113.39 (C-5), 60.40 (C-26), 55.32 (C-13), 46.82 (C-21), 27.80 (C-14), 10.15 (C-15). LCMS m/z calc. for $\text{C}_{30}\text{H}_{26}\text{FN}_7\text{O}_2$ $[\text{M}+\text{H}]^+$: 536.2, found 536.3 with t_R 2.89 min (96%).

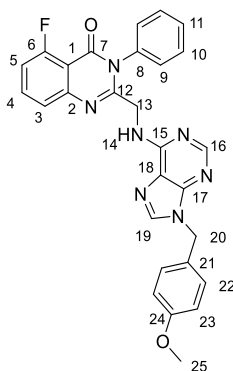
2-(((9H-purin-6-yl)amino)methyl)-5-fluoro-3-phenylquinazolin-4(3H)-one (106, 18% yield).



^1H NMR (400 MHz, DMSO-d_6) δ 13.01 (s, 1H, NH-18), 8.15 (s, 1H, H-16), 7.91 – 7.75 (m, 1H, H-19), 7.70 – 7.44 (m, 7H), 7.31 (dd, $J = 11.0, 8.2$ Hz, 1H, H-5), 4.27 (s, 2H, H-13). ^{13}C NMR (101 MHz, DMSO) δ 162.33 (C-7), 159.71 (C-6), 158.67, 152.59 (C-16), 149.30 (C-19), 136.22, 135.94 (d, $J = 10.8$ Hz, C-4), 130.17, 129.86, 129.17, 123.51 (C-3), 113.76 (d, $J = 20.4$ Hz, C-5), 110.74 (C-1), 55.37 (C-13). LCMS m/z calc. for $\text{C}_{20}\text{H}_{14}\text{FN}_7\text{O}$ $[\text{M}+\text{H}]^+$: 388.1, found 388.1 with t_R 2.27 min (99%).

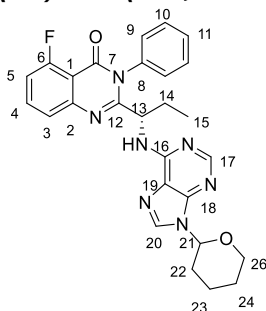
5-fluoro-2-(((9-(4-methoxybenzyl)-9H-purin-6-yl)amino)methyl)-3-phenylquinazolin-4(3H)-one (111, 39% yield).

References



^1H NMR (400 MHz, CDCl_3) δ 8.35 (s, 1H, H-16), 7.76 (s, 1H, H-19), 7.71 (dd, $J = 8.2, 5.3$ Hz, 1H), 7.61 (dd, $J = 6.2, 4.5$ Hz, 4H), 7.44 – 7.32 (m, 2H), 7.31 – 7.21 (m, 2H, H-22), 7.16 (dd, $J = 10.3, 8.4$ Hz, 1H, H-5), 6.95 – 6.84 (m, 2H, H-23), 5.30 (s, 2H, H-20), 4.47 (s, 2H, H-13), 3.80 (s, 3H, H-25). ^{13}C NMR (101 MHz, CDCl_3) δ 162.78 (C-7), 160.13 (C-6), 159.64, 158.99 (d, $J = 4.5$ Hz), 153.88, 153.34, 153.03 (C-16), 148.65 (C-19), 139.95, 135.10 (d, $J = 10.6$ Hz, C-4), 130.34, 130.01, 129.34, 128.29, 127.59, 123.30 (d, $J = 4.2$ Hz, C-3), 119.97, 114.40, 113.89 (d, $J = 20.8$ Hz, C-5), 110.81 (d, $J = 6.0$ Hz, C-1), 55.32 (C-25), 46.76 (C-30), 29.71 (C-13). LCMS m/z calc. for $\text{C}_{28}\text{H}_{22}\text{FN}_7\text{O}_2$ $[\text{M}+\text{H}]^+$: 508.2, found 508.2 with t_R 2.77 min (98%).

5-fluoro-3-phenyl-2-((1S)-1-((9-(tetrahydro-2H-pyran-2-yl)-9H-purin-6-yl)amino)propyl)quinazolin-4(3H)-one (123, 60% yield).



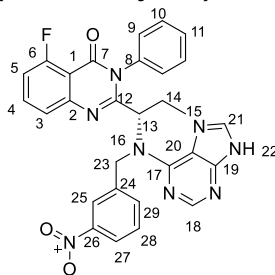
^1H NMR (400 MHz, CDCl_3) δ 8.29 (s, 1H, H-17), 8.02 (s, 1H, H-20), 7.75 – 7.43 (m, 6H), 7.40 – 7.32 (m, 1H), 7.26 (d, $J = 7.7$ Hz, 1H), 7.18 – 7.02 (m, 1H, H-3), 5.71 (dd, $J = 10.2, 2.5$ Hz, 1H, H-21), 4.22 – 4.13 (m, 1H, H-26), 3.84 – 3.72 (m, 1H, H-26), 2.22 – 1.91 (m, 3H, H-14/H-22), 1.78 (qdd, $J = 11.1, 6.8, 3.3$ Hz, 3H, H-14/H-24), 1.70 – 1.58 (m, 1H, H-24), 0.87 (dq, $J = 8.4, 3.5, 2.8$ Hz, 3H, H-15). ^{13}C NMR (101 MHz, CDCl_3) δ 162.78 (C-7), 160.12, 159.35, 158.19, 154.03, 152.88 (C-17), 149.22 (C-2), 137.84, 135.71, 134.80 (d, $J = 10.4$ Hz, C-4), 129.98, 129.62, 129.51 (d, $J = 1.7$ Hz), 128.94 (d, $J = 4.8$ Hz), 123.40 (d, $J = 4.2$ Hz, C-2), 113.46 (d, $J = 20.6$ Hz, C-5), 110.82 (d, $J = 5.9$ Hz, C-1), 81.79 (C-21), 68.82 (C-26), 31.95 (d, $J = 1.5$ Hz, C-22), 24.92 (C-24), 23.94 (C-14), 22.86 (C-23), 10.16 (C-15). LCMS m/z calc. for $\text{C}_{27}\text{H}_{26}\text{FN}_7\text{O}_2$ $[\text{M}+\text{H}]^+$: 500.2, found 499.9 with t_R 2.86 min.

General procedure for nucleophilic substitution of allyl, benzyl and phenyl halides. 2-propanol (3 mL) was added to idelalisib (**8**) (0.134 mmol, 1 equiv) and the

References

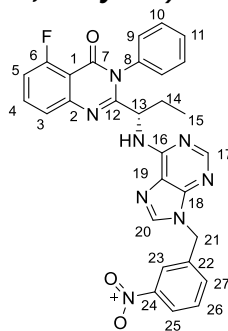
resulting solution was transformed to a microwave vial containing allyl, benzyl or phenyl halide (0.202 mmol, 1.5 equiv). DIPEA (0.804 mmol, 6 equiv) was added and the reaction mixture was heated to 130 °C for 2 h in the microwave. The solvent was evaporated and the crude residue was purified by column chromatography, eluting with 2-3% methanol in DCM to yield the tertiary amines (**116-121**, **146** and **147**) as oils.

(S)-5-fluoro-2-(1-((4-nitrobenzyl)(9H-purin-6-yl)amino)propyl)-3-phenylquinazolin-4(3H)-one (116, 40% yield).



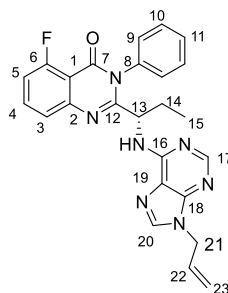
¹H NMR (400 MHz, CDCl₃) δ 8.26 (d, *J* = 2.0 Hz, 1H, H-18), 8.20 (dt, *J* = 8.2, 1.5 Hz, 1H, H-25), 8.10 (s, 1H, H-21), 8.05 (s, 1H, H-21), 7.81 (d, *J* = 7.8 Hz, 1H), 7.70 (dt, *J* = 8.3, 4.2 Hz, 1H), 7.64 – 7.46 (m, 5H), 7.43 – 7.32 (m, 2H), 7.17 – 7.07 (m, 1H, H-5), 5.71 – 5.57 (m, 2H, H-23), 5.17 (dd, *J* = 8.4, 4.3 Hz, 1H, H-13), 1.97 (ddd, *J* = 14.3, 7.4, 4.5 Hz, 1H, H-14), 1.83 (dp, *J* = 14.8, 7.4 Hz, 1H, H-14), 0.84 (t, *J* = 7.4 Hz, 3H, H-15). ¹³C NMR (101 MHz, CDCl₃) δ 162.68 (C-7), 160.03 (C-6), 159.20, 157.07, 154.32, 152.47 (C-18), 149.86, 148.95, 148.50, 141.46, 136.38, 135.66, 135.06 (d, *J* = 10.3 Hz, C-4), 134.36, 130.30, 129.87, 129.76, 129.67, 129.06, 128.65, 123.88, 123.52 (C-3), 122.96, 113.75 (d, *J* = 20.6 Hz, C-5), 110.73 (d, *J* = 5.8 Hz, C-1), 53.24 (C-13), 52.49 (C-23), 27.80 (C-14), 10.19 (C-15). LCMS *m/z* calc. for C₂₉H₂₃FN₈O₃ [M+H]⁺: 551.2, found 551.1 with *t*_R 2.34 min (90%).

(S)-5-fluoro-2-(1-((9-(3-nitrobenzyl)-9H-purin-6-yl)amino)propyl)-3-phenylquinazolin-4(3H)-one (117, 7% yield).



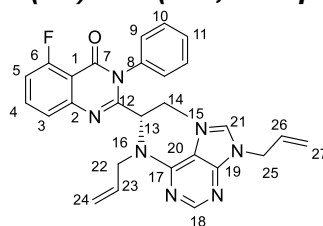
¹H NMR (400 MHz, CDCl₃) δ 8.32 (s, 1H, H-17), 8.21 (s, 1H, H-23), 8.18 (s, 1H, H-20), 7.85 (s, 1H), 7.76 – 7.43 (m, 8H), 7.36 (d, *J* = 7.5 Hz, 1H), 7.12 (t, *J* = 9.3 Hz, 1H, H-5), 5.48 (s, 2H, H-21), 5.23 (s, NH), 2.12 – 1.92 (m, 1H, H-14), 1.87 – 1.59 (m, 1H, H-14), 0.88 (t, *J* = 7.5 Hz, 3H, H-15). ¹³C NMR (101 MHz, Chloroform-*d*) δ 153.32 (C-17), 137.82 (C-20), 135.65 (C-4), 134.79, 133.62, 130.16, 129.98, 129.66,

References



^1H NMR (400 MHz, Chloroform- d) δ 8.21 (s, 1H, H-17), 7.71 (s, 1H, H-20), 7.62 – 7.56 (m, 1H), 7.55 – 7.35 (m, 4H), 7.31 – 7.21 (m, 1H), 7.03 (ddd, J = 10.4, 8.1, 1.1 Hz, 1H, H-5), 5.96 (ddt, J = 17.0, 10.2, 5.7 Hz, 1H, H-22), 5.28 – 5.18 (m, 2H, H-23), 4.72 (dt, J = 5.7, 1.6 Hz, 2H, H-21), 1.87 (dtd, J = 14.8, 7.3, 4.7 Hz, 1H, H-14), 1.71 (dp, J = 14.8, 7.3 Hz, 1H, H-14), 0.79 (t, J = 7.4 Hz, 3H, H-15). ^{13}C NMR (101 MHz, Chloroform- d) δ 162.63 (C-7), 158.29 (C-6), 154.04, 152.92 (C-17), 149.22 (C-20), 139.88, 135.69, 134.87 (C-4), 134.76, 131.91 (C-22), 129.99, 129.64, 129.52, 128.96, 123.37, 123.33 (C-3), 118.92 (C-23), 113.48 (d, J = 20.7 Hz, C-5), 45.72 (C-21), 29.71 (C-14), 10.14 (C-15). LCMS m/z calc. for $\text{C}_{25}\text{H}_{22}\text{FN}_7\text{O}$ $[\text{M}+\text{H}]^+$: 456.2, found 456.1 with t_R 2.76 min (99%).

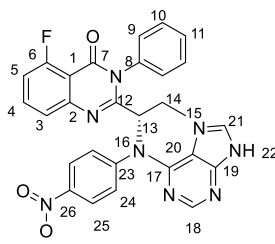
(S)-5-fluoro-3-phenyl-2-(1-(vinyl(9-vinyl-9H-purin-6-yl)amino)propyl)quinazolin-4(3H)-one (121, side product).



^1H NMR (400 MHz, DMSO- d_6) δ 9.14 (s, 1H, H-18), 8.88 (d, J = 49.1 Hz, 3H), 8.27 (d, J = 8.3 Hz, 2H), 8.08 (s, 1H, H-21), 7.80 (dd, J = 27.8, 7.6 Hz, 2H), 7.56 (s, 2H), 7.49 – 7.01 (m, 6H), 6.13 (ddt, J = 16.5, 10.0, 6.1 Hz, 1H, H-23), 5.93 (ddt, J = 17.0, 10.2, 5.7 Hz, 1H, H-23/H-26), 5.28 – 5.18 (m, 4H, H-24/H-27), 4.75 (dt, J = 5.7, 1.6 Hz, 2H, H-25), 2.12 – 1.92 (m, 1H, H-14), 1.87 – 1.59 (m, 1H, H-14),, 0.81 (m, 3H, H-15). ^{13}C NMR (101 MHz, DMSO) δ 162.78 (C-7), 160.12 (C-6), 159.35, 158.19, 154.03, 152.88 (C-17), 149.19 (C-2), 137.84, 135.71, 134.76 (d, J = 10.4 Hz, C-4), 129.98, 129.62, 129.51 (d, J = 1.7 Hz), 128.94 (d, J = 4.8 Hz), 123.40 (d, J = 4.2 Hz, C-2), 113.42 (d, J = 20.6 Hz, C-5), 110.62 (d, J = 5.9 Hz, C-1) 39.38 (C-14), 66.80 (C-13) 48.93 (C-22), 44.57 (C-25), 23.74 (C-14), 12.80 (C-15). LCMS m/z calc. for $\text{C}_{28}\text{H}_{26}\text{FN}_7\text{O}$ $[\text{M}+\text{H}]^+$: 496.2, found 496.2 with t_R 2.26 min (99%).

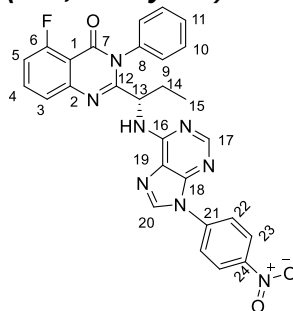
(S)-5-fluoro-2-(1-((4-nitrobenzyl)(9H-purin-6-yl)amino)propyl)-3-phenylquinazolin-4(3H)-one (146, 27% yield).

References



^1H NMR (400 MHz, Chloroform-*d*) δ 8.66 – 8.56 (m, 2H, H-25), 8.54 (s, 1H, H-18), 8.17 (s, 1H, H-21), 7.94 – 7.79 (m, 2H), 7.75 – 7.56 (m, 4H), 7.50 – 7.40 (m, 1H), 7.33 (dt, $J = 6.8, 2.3$ Hz, 1H), 7.16 – 7.09 (m, 1H, H-3), 7.05 (d, $J = 8.2$ Hz, 1H), 5.54 (d, $J = 8.1$ Hz, 1H, H-13), 1.85 (dt, $J = 7.4, 3.7$ Hz, 1H, H-14), 1.54 (dt, $J = 14.5, 7.3$ Hz, 1H, H-14), 0.72 (t, $J = 7.4$ Hz, 3H, H-15). ^{13}C NMR (101 MHz, Chloroform-*d*) δ 162.88 (C-7), 160.78 (C-6), 160.22, 158.87 (d, $J = 4.3$ Hz), 157.97, 153.94 (C-18), 149.27, 148.44, 147.81, 144.29 (C-21), 140.63, 135.26 (d, $J = 1.8$ Hz, C-4), 130.23, 129.97, 129.66, 129.06, 128.42, 126.05 (C-25), 125.94 (C-24), 122.40 (d, $J = 4.2$ Hz, C-3), 113.91 (d, $J = 20.7$ Hz, C-5), 110.83 (C-1), 52.52 (C-13), 27.02 (C-14), 9.55 (C-15). LCMS m/z calc. for $\text{C}_{28}\text{H}_{21}\text{FN}_8\text{O}_3^-$ $[\text{M}+\text{H}]^+$: 537.2, found 537.1 with t_R 2.78 min (95%).

(S)-5-fluoro-2-(1-((9-(4-nitrophenyl)-9H-purin-6-yl)amino)propyl)-3-phenylquinazolin-4(3H)-one (147, 57% yield).



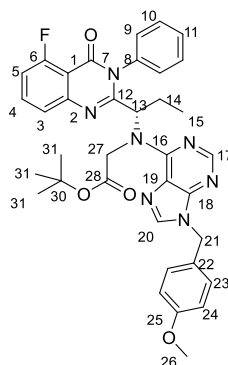
^1H NMR (400 MHz, Chloroform-*d*) δ 8.45 (dd, $J = 9.1, 2.6$ Hz, 2H), 8.37 (s, 1H, H-17), 8.21 (s, 1H, H-20), 8.06 (d, $J = 9.0$ Hz, 2H), 7.78 – 7.46 (m, 5H), 7.42 – 7.31 (m, 1H), 7.13 (dd, $J = 10.4, 8.2$ Hz, 1H), 6.75 (s, 1H), 5.24 (s, NH), 2.00 (ddt, $J = 14.7, 12.0, 7.4$ Hz, 1H, H-14), 1.83 (dp, $J = 15.0, 7.5$ Hz, 1H, H-14), 0.90 (t, $J = 7.3$ Hz, 3H, H-15). ^{13}C NMR (101 MHz, Chloroform-*d*) δ 162.78 (C-24), 162.55 (C-7), 160.12 (C-6), 159.25 (d, $J = 4.5$ Hz), 154.38, 153.89 (C-17), 149.06, 146.47 (C-20), 140.17, 137.99, 135.60 (C-4), 134.88, 130.03, 129.63, 128.82, 125.45, 123.11 (d, $J = 36.6$ Hz, C-23), 113.64 (d, $J = 20.8$ Hz, C-5), 110.85 (C-1), 52.48 (C-13), 27.73 (C-14), 10.15 (C-15). LCMS m/z calc. for $\text{C}_{28}\text{H}_{21}\text{FN}_8\text{O}_3^-$ $[\text{M}+\text{H}]^+$: 537.2, found 537.1 with t_R 2.96 min (98%).

General procedure for nucleophilic substitution of α -haloesters, α -haloamide and α -halonitrile. Alkylating agent (0.500 mmol, 2.5 equiv) was added dropwise to a stirred solution of secondary amine (**123** and **128**) (0.200 mmol, 1 equiv) and

References

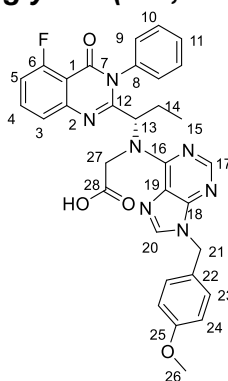
K₂CO₃ (0.80 mmol, 4 equiv) in DMF (1 mL). The reaction mixture was stirred for 18 h at 60°C under nitrogen atmosphere, the solvent was removed and the residue was purified by flash column chromatography (30-40% ethyl acetate in petroleum ether) to yield the tertiary amines (**129**, **126** and **124**). Carboxylic acid **130** produced as a side product during the synthesis of ester **129**.

tert-butyl (S)-N-(1-(5-fluoro-4-oxo-3-phenyl-3,4-dihydroquinazolin-2-yl)propyl)-N-(9-(4-methoxybenzyl)-9H-purin-6-yl)glycinate (129, 27% yield).



¹H NMR (400 MHz, Chloroform-d) δ 8.18 (s, 1H, H-17), 7.68 (td, J = 8.1, 5.0 Hz, 1H), 7.61 (d, J = 4.7 Hz, 3H), 7.52 – 7.38 (m, 1H), 7.19 (d, J = 8.3 Hz, 2H), 7.08 (dd, J = 10.2, 8.1 Hz, 1H), 7.00 – 6.90 (m, 2H, H-23), 6.87 – 6.76 (m, 2H, H-24), 6.70 (t, J = 7.5 Hz, 1H), 5.20 (d, J = 14.9 Hz, 1H, H-27), 5.04 (d, J = 5.5 Hz, 1H, H-27), 4.91 – 4.70 (m, 1H, H-13), 4.64 (d, J = 16.3 Hz, 1H, H-27), 4.29 (d, J = 16.3 Hz, 1H, H-27), 3.85 (s, 3H, H-26), 1.86 (dt, J = 13.8, 7.3 Hz, 1H, H-14), 1.55 (dd, J = 7.9, 3.6 Hz, 1H, H-14), 1.26 (s, 9H, H-31), 0.88 (t, J = 7.4 Hz, 3H, H-15). ¹³C NMR (101 MHz, Chloroform-d) δ 168.65 (C-28), 163.24 (C-7), 161.95 (C-6), 159.10 (C-22), 155.78, 151.61 (C-17), 142.15 (C-30), 137.25 (C-8), 135.17 (d, J = 10.4 Hz, C-4), 129.38, 129.28, 114.34 (C-24), 113.71 (d, J = 20.8 Hz, C-5), 110.25 (C-1), 80.78 (C-30), 66.42 (C-13), 55.40 (C-26), 46.52 (C-27), 27.72 (C-31), 23.83 (C-4), 10.28 (C-15). LCMS *m/z* calc. for C₃₆H₃₆FN₇O₄ [M+H]⁺: 650.3, found 650.1 with *t_R* 2.53 min.

(S)-N-(1-(5-fluoro-4-oxo-3-phenyl-3,4-dihydroquinazolin-2-yl)propyl)-N-(9-(4-methoxybenzyl)-9H-purin-6-yl)glycine (130, side product, 26% yield).

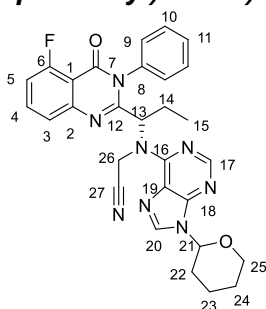


¹H NMR (400 MHz, Chloroform-d) δ 8.79 (s, H-17), 8.25 (s, 1H, H-20), 7.76 – 7.43 (m, 6H), 7.44 – 7.32 (m, 4H), 7.20 – 7.01 (m, 2H), 6.86 – 6.70 (m, 2H, H-24), 6.17

References

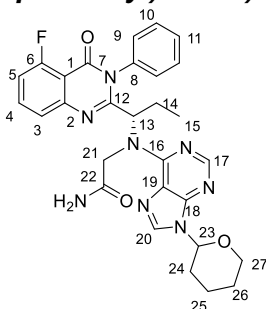
(d, $J = 7.0$ Hz, 1H, H-27) 5.22 (s, 2H, H-21), 4.75 – 4.60 (m, 1H, H-27), 4.48 (q, $J = 16.1$ Hz, 1H, H-27), 3.77 (s, 3H, H-26), 2.34 – 1.77 (m, 1H, H-14), 1.85 – 1.56 (m, 1H, H-14), 0.87 (t, $J = 7.4$ Hz, 3H, H-15). ^{13}C NMR (101 MHz, CDCl_3) δ 171.18 (C-28), 165.64, 162.82 (C-7), 160.36 (C-6), 160.16, 156.93, 150.48 (C-17), 148.24, 148.23, 143.54 (C-20), 135.39, 135.29 (C-4), 135.18, 130.14, 129.96, 129.78, 129.20, 128.38, 124.69, 123.02 (C-3) 114.15 (d, $J = 20.8$ Hz, C-5), 110.85 (C-1), 110.69, 55.31 (C-13), 53.38 (C-26), 51.41 (C-27), 49.21 (C-21), 26.50 (C-14), 9.62 (C-15). LCMS m/z calc. for $\text{C}_{32}\text{H}_{28}\text{FN}_7\text{O}_4$ $[\text{M}+\text{H}]^+$: 594.2, found 594.0 with t_R 2.60 min.

2-(((S)-1-(5-fluoro-4-oxo-3-phenyl-3,4-dihydroquinazolin-2-yl)propyl)(9-(tetrahydro-2H-pyran-2-yl)-9H-purin-6-yl)amino)acetonitrile (126, 7% yield).



^1H NMR (400 MHz, MeOD) δ 8.30 (s, 1H, H-17), 7.99 (s, 1H, H-20), 7.80 (td, $J = 8.2$, 5.4 Hz, 1H), 7.69 – 7.62 (m, 1H), 7.63 – 7.48 (m, 5H), 7.25 (ddd, $J = 11.0$, 8.2, 1.0 Hz, 1H, H-3), 5.48 (d, $J = 5.0$ Hz, 1H, H-21), 5.40 (d, $J = 5.0$ Hz, 1H, H-26), 4.27 – 4.18 (m, 1H, H-25), 3.88 – 3.76 (m, 1H, H-25), 2.37 (tdd, $J = 13.4$, 10.8, 4.4 Hz, 2H, H-22), 2.25 – 1.94 (m, 3H, H-14/H-23), 1.80 (m, 2H, H-14/H-24), 1.67– 1.55 (m, 1H, H-24), 0.90 (t, $J = 7.4$ Hz, 3H, H-15). ^{13}C NMR (101 MHz, MeOD) δ 163.17 (C-7), 160.74, 159.31, 157.27, 153.09, 152.25 (C-17), 149.28, 148.32, 143.78 (C-20), 135.88, 135.63 (d, $J = 10.7$ Hz, C-4), 129.46, 129.36, 128.92 (d, $J = 15.6$ Hz), 123.52 (d, $J = 4.4$ Hz, C-3), 119.93, 113.40 (d, $J = 20.8$ Hz, C-5), 110.87 (d, $J = 5.9$ Hz, C-1), 53.76 (C-13), 36.78 (C-26), 30.20 (C-22), 26.51 (C-14), 24.87 (C-24), 22.70 (23), 9.38 (C-15). LCMS m/z calc. for $\text{C}_{29}\text{H}_{27}\text{FN}_8\text{O}_2$ $[\text{M}+\text{H}]^+$: 539.2, found 538.9 with t_R 2.25 min.

2-(((S)-1-(5-fluoro-4-oxo-3-phenyl-3,4-dihydroquinazolin-2-yl)propyl)(9-(tetrahydro-2H-pyran-2-yl)-9H-purin-6-yl)amino)acetamide (124, 8 % yield).

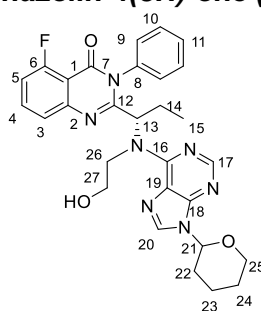


^1H NMR (500 MHz, Chloroform- d) δ 8.20 (s, 1H, H-17), 8.01 (s, 1H, H-20), 7.73 – 7.41 (m, 6H), 7.43– 7.31 (m, 1H), 7.22 (d, $J = 7.7$ Hz, 1H), 7.09– 6.94 (m, 1H, H-3),

References

5.79 (dd, $J = 10.2, 2.5$ Hz, 1H, H-21), 4.18 – 4.10 (m, 1H, H-25), 4.20 – 4.06 (m, 1H, H-25), 3.82 – 3.70 (m, 3H, H-22/H-26), 2.15 – 1.84 (m, 3H, H-22/H-23), 2.04 – 1.73 (qdd, $J = 11.1, 6.8, 3.3$ Hz, 3H, H-14/H-24), 1.63 – 1.51 (m, 1H, H-24), 0.89 (t, $J = 7.3$ Hz, 3H, H-15). ^{13}C NMR (101 MHz, MeOD) δ 167.87 (C-22), 162.53 (C-7), 160.74, 159.31, 157.27, 153.09, 152.25 (C-17), 149.28, 146.19 (C-20), 143.78, 135.68 (C-8), 135.47 (d, $J = 10.7$ Hz, C-4), 129.46, 129.36, 128.92 (d, $J = 15.6$ Hz), 122.39 (d, $J = 4.4$ Hz, C-3), 119.93, 113.71 (d, $J = 20.8$ Hz, C-5), 110.87 (d, $J = 5.9$ Hz, C-1), 81.92 (C-21), 68.20 (C-25), 55.60 (C-13), 41.06 (C-26), 36.78 (C-26), 30.15 (C-22), 25.64 (C-14), 24.87 (C-24), 22.67 (23), 10.05 (C-15). LCMS m/z calc. for $\text{C}_{24}\text{H}_{21}\text{FN}_8\text{O}_2$ $[\text{M}+\text{H}]^+$: 473.2, found 472.8 with t_R 2.49 min

5-fluoro-2-((1S)-1-(2-hydroxyethyl)(9-(tetrahydro-2H-pyran-2-yl)-9H-purin-6-yl)amino)propyl)-3-phenylquinazolin-4(3H)-one (141, 18% yield).

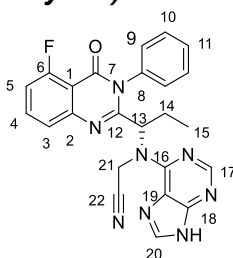


To a cooled (0°C) solution of compound **123** (0.20 mmol, 1 equiv) in THF (2 mL) under N_2 was added isopropylmagnesium chloride (2M/THF, 0.22 mmol, 1.1 equiv). The mixture was allowed to stir at 0°C under nitrogen atmosphere for 30 min. 2-iodoethanol (0.40 mmol, 2 equiv) was then added to the reaction mixture. After stirring for 16 h at 70°C , the solution was evaporated until dryness. The resultant solid was purified by flash column chromatography (100% ethyl acetate) to yield alcohol **141** as a white solid. ^1H NMR (500 MHz, Chloroform- d) δ 8.27 (s, 1H, H-17), 8.01 (s, 1H, H-20), 7.73 – 7.41 (m, 6H), 7.43– 7.31 (m, 1H), 7.22 (d, $J = 7.7$ Hz, 1H), 7.16– 7.00 (m, 1H, H-3), 5.72 dd, $J = 10.2, 2.5$ Hz, 1H, H-21), 4.66 – 4.34 (m, 2H, H-27), 4.22 – 4.14 (m, 1H, H-25), 4.20 – 4.06 (m, 1H, H-25), 3.82 – 3.70 (m, 3H, H-22/H-26), 2.20 – 1.89 (m, 3H, H-22/H-23), 1.75 (qdd, $J = 11.1, 6.8, 3.3$ Hz, 3H, H-14/H-24), 1.69 – 1.57 (m, 1H, H-24), 0.90 (dq, $J = 8.4, 3.5, 2.8$ Hz, 3H, H-15). ^{13}C NMR (101 MHz, CDCl_3) δ 162.81 (C-7), 160.15, 159.38, 158.21, 154.06, 152.91 (C-17), 149.25 (C-2), 137.87, 135.74, 134.84 (d, $J = 10.4$ Hz, C-4), 129.99, 129.66, 129.54 (d, $J = 1.7$ Hz), 128.96 (d, $J = 4.8$ Hz), 123.43 (d, $J = 4.2$ Hz, C-2), 113.49 (d, $J = 20.6$ Hz, C-5), 110.86 (d, $J = 5.9$ Hz, C-1), 82.14 (C-21), 68.25 (C-25), 61.58 (C-26), 54.34 (C-25) 30.14 (d, $J = 1.5$ Hz, C-22), 25.51 (C-14), 24.92 (C-24), 22.67 (C-23), 9.38 (C-15). LCMS m/z calc. for $\text{C}_{29}\text{H}_{30}\text{FN}_7\text{O}_3$ $[\text{M}+\text{H}]^+$: 544.2, found 543.9 with t_R 2.74 min.

References

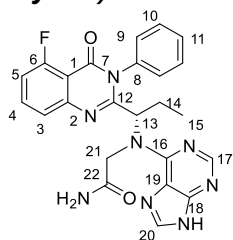
General method for THP-deprotection. Hydrochloric acid (1 M, 1 mL) was added dropwise to a solution of THP-protected amines (**126**, **124**, and **141**) (0.092 mmol, 1 equiv) in a mixture of ethanol (3 mL) and water (3 mL). The reaction mixture was stirred for 5 h at RT at which time it was concentrated under reduced pressure. The residue was then dissolved in ethyl acetate (30 mL), and the organic phase was washed with water (2* 20 mL) and brine (2* 20 mL). The organic solution was dried over anhydrous Na₂SO₄, filtered and the filtrate was concentrated under pressure to yield the unprotected amines (**127**, **125** and **72**).

(S)-2-((1-(5-fluoro-4-oxo-3-phenyl-3,4-dihydroquinazolin-2-yl)propyl)(9H-purin-6-yl)amino)acetonitrile (127**, 16% yield).**



¹H NMR (400 MHz, MeOD) δ 8.37 (s, 1H, H-17), 7.99 (s, 1H, H-20), 7.80 (td, *J* = 8.2, 5.4 Hz, 1H), 7.69 – 7.62 (m, 1H), 7.59 – 7.44 (m, 5H), 7.22 (ddd, *J* = 11.0, 8.2, 1.0 Hz, 1H, H-3), 5.45 (d, *J* = 5.0 Hz, 1H, H-21), 5.11 (dd, *J* = 8.9, 4.3 Hz, 1H, H-21), 2.41 – 1.97 (m, 2H, H-14), 0.92 (t, *J* = 7.4 Hz, 3H, H-15). ¹³C NMR (101 MHz, MeOD) δ 162.77 (C-7), 160.12, 159.33, 157.26, 153.08, 152.00 (C-17), 149.28, 148.18, 143.72 (C-20), 135.88, 135.23 (d, *J* = 10.7 Hz, C-4), 129.46, 129.36, 128.92 (d, *J* = 15.6 Hz), 123.18 (d, *J* = 4.4 Hz, C-3), 119.95, 113.29 (d, *J* = 20.8 Hz, C-5), 110.80 (d, *J* = 5.9 Hz, C-1), 54.03 (C-13), 36.44 (C-21), 26.51 (C-14), 9.38 (C-15). LCMS *m/z* calc. for C₂₄H₁₉FN₈O [M+H]⁺: 455.2, found 454.9 with *t_R* 2.15 min (90%).

(S)-2-((1-(5-fluoro-4-oxo-3-phenyl-3,4-dihydroquinazolin-2-yl)propyl)(9H-purin-6-yl)amino)acetamide (125**, 12% yield).**

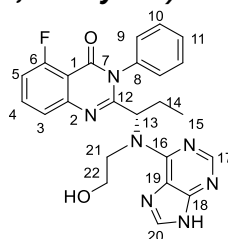


¹H NMR (400 MHz, MeOD) δ 8.64 (s, 1H, H-17), 8.46 (s, 1H, H-20), 7.82 (td, *J* = 8.2, 5.3 Hz, 1H), 7.75 – 7.43 (m, 6H), 7.30 – 7.19 (m, 1H, H-3), 5.26 (s, NH₂), 5.23 – 5.05 (m, 1H, H-13), 3.93 (s, 2H, H-21), 2.06 – 1.93 (m, 2H, H-14), 0.93 (t, *J* = 7.4 Hz, 3H, H-15). ¹³C NMR (101 MHz, MeOD) δ 167.89 (C-22), 162.56 (C-7), 152.04 (C-17), 149.22 (C-2), 148.66, 143.50 (C-20), 135.73, 135.40 (C-4), 129.69 (d, *J* = 12.4 Hz), 128.84 (d, *J* = 5.7 Hz), 123.11 (C-3), 110.79 (d, *J* = 5.6 Hz, C-1), 54.61 (C-13), 41.06

References

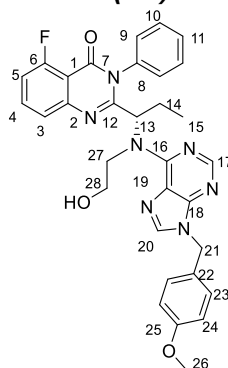
(C-21), 26.58 (C-14), 9.50 (C-15). LCMS m/z calc. for $C_{24}H_{21}FN_8O_2$ $[M+H]^+$: 473.2, found 472.8 with t_R 2.06 min (95%).

(S)-5-fluoro-2-(1-((2-hydroxyethyl)(9H-purin-6-yl)amino)propyl)-3-phenylquinazolin-4(3H)-one (72, 90% yield).



1H NMR (400 MHz, MeOD) δ 8.16 (d, $J = 1.0$ Hz, 1H, H-17), 7.70 – 7.58 (m, 2H), 7.54 (ddd, $J = 7.7, 6.0, 3.3$ Hz, 1H), 7.51 – 7.45 (m, 2H), 7.44 – 7.35 (m, 2H), 7.08 (ddd, $J = 11.0, 8.2, 1.0$ Hz, 1H, H-3), 4.68 – 4.36 (m, 2H, H-22), 3.93 (t, $J = 4.6$ Hz, 1H, H-21), 3.41 (qdd, $J = 9.7, 5.7, 3.7$ Hz, 1H, H-21), 1.93 (dtt, $J = 15.0, 7.5, 3.4$ Hz, 1H, H-14), 1.76 (ddq, $J = 14.5, 9.0, 7.2$ Hz, 1H, H-14), 0.79 (t, $J = 7.4$ Hz, 3H, H-15). ^{13}C NMR (101 MHz, MeOD) δ 162.65 (C-7), 159.16, 158.03, 153.95, 151.61 (C-17), 149.01 (C-2), 135.55 (d, $J = 94.4$ Hz, C-4), 129.41, 129.28 (d, $J = 7.4$ Hz), 129.06, 128.79, 122.99 (C-3), 113.09 (C-1), 110.79 ((d, $J = 5.9$ Hz, C-1), 61.55 (C-22), 54.30 (C-13), 49.47 (C-21), 26.27 (C-14), 9.77 (C-15). LCMS m/z calc. for $C_{24}H_{22}FN_7O_2$ $[M+H]^+$: 460.2, found 459.7 with t_R 2.31 min (96%).

(S)-5-fluoro-2-(1-((2-hydroxyethyl)(9-(4-methoxybenzyl)-9H-purin-6-yl)amino)propyl)-3-phenylquinazolin-4(3H)-one (112, 31% yield).



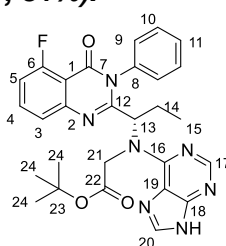
$LiBH_4$ (1M/THF; 0.169 mmol, 2 equiv) was added to a solution of ester **129** (0.0847 mmol, 1 equiv) in dry THF (3 mL) at 0 °C. After 2 h, the reaction mixture was quenched with methanol (3 mL) and the solution was evaporated to dryness under reduced pressure. The resulting residue purified via flash column chromatography (100% ethyl acetate) to afford alcohol **112** as a white solid. 1H NMR (400 MHz, Chloroform- d) δ 7.69 (s, 1H, H-17), 7.68 – 7.60 (m, 2H), 7.43 – 7.36 (m, 2H), 7.34 (s, 1H), 7.26 – 7.04 (m, 5H), 6.95 – 6.89 (m, 2H, H-24), 5.19 – 5.05 (m, 2H, H-21), 4.58 – 4.44 (m, 1H, H-27), 4.08 – 3.96 (m, 2H, H-27), 3.97 – 3.88 (m, 1H, H-28), 3.83 (s, 3H, H-26), 3.74 (m, H-28), 2.13 – 1.96 (m, 1H, H-14), 1.85 – 1.68 (m, 1H, H-14), 0.83 (t, $J = 7.3$ Hz, 3H, H-15). ^{13}C NMR (101 MHz, Chloroform- d) δ 159.77 (C-

References

6), 149.66, 148.63, 147.65 (C-17), 143.99, 136.23 (d, $J = 12.1$ Hz, C-4), 134.48, 129.27, 129.03, 128.62, 128.36 127.65, 123.51 (C-3), 121.94, 114.38 (C-24), 113.00 (d, $J = 20.9$ Hz, C-5), 63.66 (C-13), 59.31 (C-28), 55.36 (C-26), 53.31 (C-27), 46.65 (C-21), 28.44 (C-14), 10.36 (C-15). LCMS m/z calc. for $C_{32}H_{30}FN_7O_3$ $[M+H]^+$: 580.2, found 580.0 with t_R 2.33 min.

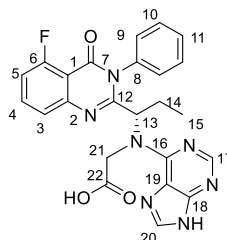
General method for PMB-deprotection. To a solution of protected amines (**129** and **130**) (0.0675 mmol, 1 equiv) in CH_3CN/H_2O (1/1, 2 mL), was added CAN (0.337 mmol, 5 equiv). The reaction mixture was stirred at RT for 18 h, at which time it was concentrated under reduced pressure. The resulting residue was purified by flash chromatography (100% ethyl acetate) to yield the free amines (**131** and **145**).

tert-butyl (S)-N-(1-(5-fluoro-4-oxo-3-phenyl-3,4-dihydroquinazolin-2-yl)propyl)-N-(9H-purin-6-yl)glycinate (131**, 31%).**



1H NMR (400 MHz, $CDCl_3$) δ 7.67 (tdd, $J = 7.7, 5.3, 1.7$ Hz, 1H), 7.60 (s, 1H, H-20), 7.45 (s, 1H), 7.35 (t, $J = 7.6$ Hz, 1H), 7.28 (s, 1H), 7.26 – 7.14 (m, 2H), 7.11 – 7.03 (m, 1H), 7.02 – 6.88 (m, 1H, H-3), 5.49 (ddd, $J = 9.3, 6.7, 2.8$ Hz, 1H, H-13), 4.59 (dd, $J = 28.6, 16.3$ Hz, 1H, H-21), 4.34 (dd, $J = 32.6, 16.3$ Hz, 1H, H-21), 2.23 – 2.09 (m, 1H, H-14), 2.04 – 1.96 (m, 1H, H-14), 1.23 (s, 9H, H-24), 0.92 – 0.86 (m, 3H, H-15). ^{13}C NMR (101 MHz, $CDCl_3$) δ 167.29 (C-22), 162.71 (C-7), 160.05 (d, $J = 4.6$ Hz, C-6), 159.72, 150.16 (C-17), 148.00, 146.26 (C-20), 136.41 (d, $J = 23.1$ Hz), 134.23 (d, $J = 9.9$ Hz, C-4), 133.43, 129.55, 129.01 (d, $J = 3.4$ Hz), 128.36, 128.11, 123.53 (d, $J = 4.2$ Hz, C-3), 122.24, 112.77 (d, $J = 20.6$ Hz, C-5), 110.95 (C-1), 81.51 (C-23), 68.72 (C-13), 50.11 (C-21), 40.88 (C-24), 24.88 (C-14), 10.21 (C-15). LCMS m/z calc. for $C_{28}H_{28}FN_7O_3$ $[M+H]^+$: 530.2, found 530.1 with t_R 2.31 min.

(S)-N-(1-(5-fluoro-4-oxo-3-phenyl-3,4-dihydroquinazolin-2-yl)propyl)-N-(9H-purin-6-yl)glycine (145**, 50%).**



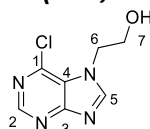
1H NMR (400 MHz, Methanol- d_4) δ 8.27 (s, 1H, H-17), 7.99 – 7.74 (s, 1H, H-20), 7.66 (dt, $J = 8.2, 4.0$ Hz, 1H), 7.61 – 7.45 (m, 3H), 7.24 (dd, $J = 10.9, 8.1$ Hz, 1H, H-5), 5.65 – 5.22 (m, 2H, H-21), 1.16 (dd, $J = 6.1, 2.6$ Hz, 1H, H-14), 1.04 (d, $J = 7.1$

Hz, 1H, H-14), 0.90 – 0.84 (m, 3H, H-15). ^{13}C NMR (101 MHz, MeOD) δ 171.58 (C-22), 162.43 (C-7), 161.95 (C-6), 151.54 (C-17), 141.96 (C-20), 129.24, 128.08, 127.30, 119.99, 119.82, 111.09, 56.40 (C-13), 52.58 (C-21), 26.43 (C-14), 9.00 (C-15). LCMS m/z calc. for $\text{C}_{24}\text{H}_{20}\text{FN}_7\text{O}_3$ $[\text{M}+\text{H}]^+$: 474.2, found 474.1 with t_R 2.80 min, (96%).

7.3.4 Experimental for Chapter 4

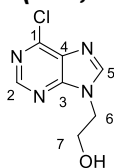
General procedure for the N-7-alkylation of 6-chloropurine. To a stirred solution of 6-chloropurine **78** (19.04 mmol, 1 equiv) in acetonitrile (15 mL) was added K_2CO_3 (58.20 mmol, 3 equiv). The reaction mixture was allowed to stir at RT for 30 min. Alkylating agent (38.08 mmol, 2 equiv) was then added and the resulting mixture was stirred for 18 h. The solvent was removed and the residue was purified by column chromatography (2% methanol in ethyl acetate) to yield the N-7-substituted-6-chloropurines (**172**, **173** and **174**) as well as the N-9-regioisomers (**178**, **179** and **180**) as white solids.

2-(6-chloro-7H-purin-7-yl)ethan-1-ol (**172**, 16% yield).



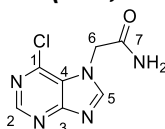
^1H NMR (400 MHz, DMSO) δ 8.80 (s, 1H, H-2), 8.74 (s, 1H, H-5), 4.87 (d, $J = 50.2$ Hz, OH), 4.54 (t, $J = 5.3$ Hz, 2H, H-6), 3.79 (t, $J = 5.3$ Hz, 2H, H-7). ^{13}C NMR (101 MHz, DMSO) δ 162.20 (C-3), 152.09 (C-2), 151.83 (C-5), 142.51 (C-1), 122.62 (C-4), 60.56 (C-7), 49.62 (C-6). LCMS m/z calc. for $\text{C}_7\text{H}_7\text{ClN}_4\text{O}$ $[\text{M}+\text{H}]^+$: 199.0, found 198.9 with t_R 1.04 min.

2-(6-chloro-9H-purin-9-yl)ethan-1-ol (**178**, 21 % yield).



^1H NMR (400 MHz, DMSO) δ 8.78 (s, 1H, H-2), 8.65 (s, 1H, H-5), 5.01 (t, $J = 5.5$ Hz, OH), 4.35 (t, $J = 5.4$ Hz, 2H, H-6), 3.80 (q, $J = 5.2$ Hz, 2H, H-7). ^{13}C NMR (101 MHz, DMSO) δ 152.58 (C-4), 151.81 (C-2), 149.27 (C-1), 148.45 (C-5), 131.32 (C-4), 59.34 (C-7), 47.08 (C-6). LCMS m/z calc. for $\text{C}_7\text{H}_7\text{ClN}_4\text{O}$ $[\text{M}+\text{H}]^+$: 199.0, found 198.9 with t_R 1.07 min.

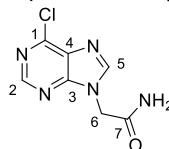
2-(6-chloro-7H-purin-7-yl)acetamide (**173**, 7% yield).



References

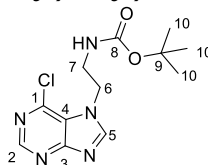
^1H NMR (400 MHz, DMSO- d_6) δ 8.81 (s, 1H, H-2), 8.75 (s, 1H, H-5), 7.83 (s, 1H, NH), 7.45 (s, 1H, NH), 5.17 (s, 2H, H-6). ^{13}C NMR (101 MHz, DMSO- d_6) δ 168.69 (C-7), 161.95 (C-3), 152.25 (C-2), 152.02 (C-5), 142.83 (C-1), 123.21 (C-4), 49.08 (C-6). LCMS m/z calc. for $\text{C}_7\text{H}_6\text{ClN}_5\text{O}$ $[\text{M}+\text{H}]^+$: 212.0, found 211.9 with t_R 0.65 min.

2-(6-chloro-9H-purin-9-yl)acetamide (179, 42% yield).



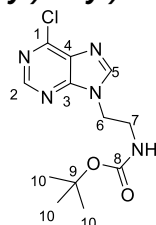
^1H NMR (400 MHz, DMSO- d_6) δ 8.77 (s, 1H, H-5), 8.64 (s, 1H, H-2), 7.83 (s, 1H, NH), 7.43 (s, 1H, NH), 4.99 (s, 2H, H-6). ^{13}C NMR (101 MHz, DMSO- d_6) δ 168.00 (C-7), 152.70 (C-1), 152.02 (C-2), 149.32 (C-3), 148.91 (C-5), 130.99 (C-4), 45.98 (C-6). LCMS m/z calc. for $\text{C}_7\text{H}_6\text{ClN}_5\text{O}$ $[\text{M}+\text{H}]^+$: 212.0, found 211.9 with t_R 0.65 min.

tert-butyl (2-(6-chloro-7H-purin-7-yl)ethyl)carbamate (174, 10% yield).



^1H NMR (400 MHz, Chloroform- d) δ 8.68 (s, 1H), 8.11 (s, 1H), 5.88 (t, $J = 6.1$ Hz, NH), 4.63 (t, $J = 5.4$ Hz, 2H), 3.64 (q, $J = 5.9$ Hz, 2H), 1.41 (s, 9H). ^{13}C NMR (101 MHz, Chloroform- d) δ 161.55 (C-3), 156.14 (C-8), 152.05 (C-2), 149.62 (C-5), 142.91 (C-1), 122.17 (C-4), 80.01 (C-8), 46.97 (C-6), 41.42 (C-7), 28.31 (C-10). LCMS m/z calc. for $\text{C}_{12}\text{H}_{16}\text{ClN}_5\text{O}_2$ $[\text{M}+\text{H}]^+$: 298.1, found 298.0 with t_R 2.33 min.

tert-butyl (2-(6-chloro-9H-purin-9-yl)ethyl)carbamate (180, 60% yield).



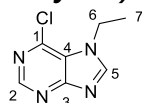
^1H NMR (400 MHz, Chloroform- d) δ 8.72 (s, 1H, H-2), 8.09 (s, 1H, H-5), 5.14 (d, $J = 6.3$ Hz, NH), 4.47 (t, $J = 5.7$ Hz, 2H, H-6), 3.61 (q, $J = 5.9$ Hz, 2H, H-7), 1.39 (s, 9H, H-10). ^{13}C NMR (101 MHz, Chloroform- d) δ 155.88 (C-8), 151.91 (C-5), 151.84 (C-3), 150.92 (C-1), 145.66 (C-2), 131.55 (C-4), 80.14 (C-9), 44.19 (C-6), 40.11 (C-7), 28.24 (C-10). LCMS m/z calc. for $\text{C}_{12}\text{H}_{16}\text{ClN}_5\text{O}_2$ $[\text{M}+\text{H}]^+$: 298.1, found 298.0 with t_R 2.40 min.

General method for regiospecific N-7-alkylation of 6-chloropurine. To a solution of 6-chloro-9H-purine (6.46 mmol, 1 equiv) in dry THF (10 mL) was added isopropylmagnesium chloride (2M/THF, 7.10 mmol, 1.1 equiv) and the reaction was stirred at RT under N_2 for 30 minutes. The alkylating reagent (19.38 mmol, 3 equiv) was then added and the reaction mixture was stirred at 70°C for 16 h at which time

References

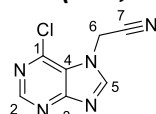
it was concentrated under reduced pressure. The resulting residue was purified by silica gel chromatography, eluting with 5% methanol in DCM to yield exclusively the N-7-alkylated-6-chloropurines (**189**, **191**, **192**, **193**, **195** and **196**) as white solids.

6-chloro-7-ethyl-7H-purine (189, 37% yield).



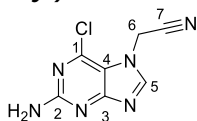
^1H NMR (400 MHz, DMSO) δ 8.84 (s, 1H, H-2), 8.79 (s, 1H, H-5), 4.51 (q, $J = 7.2$ Hz, 2H, H-6), 1.48 (t, $J = 7.2$ Hz, 3H, H-7). ^{13}C NMR (101 MHz, DMSO- d_6) δ 162.12 (C-3), 151.97 (C-2), 150.97 (C-5), 142.45 (C-1), 122.34 (C-4), 42.30 (C-6), 17.25 (C-7). LCMS m/z calc. for $\text{C}_7\text{H}_7\text{ClN}_4$ $[\text{M}+\text{H}]^+$: 183.0, found 182.7 with t_R 1.88 min.

2-(6-chloro-7H-purin-7-yl)acetonitrile (191, 44% yield).



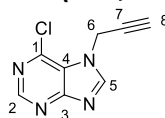
^1H NMR (400 MHz, DMSO) δ 8.89 (s, 1H, H-2), 8.87 (s, 1H, H-5), H-2, 5.78 (s, 2H, H-6). ^{13}C NMR (101 MHz, DMSO) δ 161.99 (C-3), 152.95 (C-2), 151.31 (C-3), 142.78 (C-1), 122.37 (C-4), 116.26 (C-7), 35.43 (C-6). LCMS m/z calc. for $\text{C}_7\text{H}_4\text{ClN}_5$ $[\text{M}+\text{H}]^+$: 194.0, found 193.9 with t_R 1.03 min.

2-(2-amino-6-chloro-7H-purin-7-yl)acetonitrile (195, 14% yield).



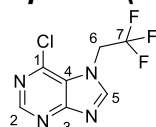
^1H NMR (400 MHz, DMSO) δ 8.44 (s, 1H, H-5), 6.82 (s, NH_2), 5.59 (s, 2H, H-6). ^{13}C NMR (101 MHz, DMSO) δ 164.65 (C-3), 160.95 (C-1), 149.98 (C-5), 142.77 (C-2), 116.48 (C-4), 114.83 (C-7), 35.13 (C-6). LCMS m/z calc. for $\text{C}_7\text{H}_5\text{ClN}_6$ $[\text{M}+\text{H}]^+$: 209.0, found 208.9 with t_R 0.75 min.

6-chloro-7-(prop-2-yn-1-yl)-7H-purine (192, 31% yield).



^1H NMR (400 MHz, DMSO) δ 8.89 (s, 1H, H-2), 8.84 (s, 1H, H-5), 5.40 (d, $J = 2.5$ Hz, 2H, H-6), 3.66 (t, $J = 2.5$ Hz, 1H, H-8). ^{13}C NMR (101 MHz, DMSO) δ 162.08 (C-3), 152.54 (C-2), 150.83 (C-5), 142.93 (C-1), 122.30 (C-4), 78.41 (C-7), 78.25 (C-8), 36.97 (C-6). LCMS m/z calc. for $\text{C}_8\text{H}_5\text{ClN}_4$ $[\text{M}+\text{H}]^+$: 193.0, found 192.9 with t_R 2.03 min.

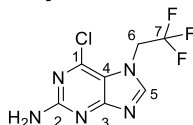
6-chloro-7-(2,2,2-trifluoroethyl)-7H-purine (193, 62% yield).



References

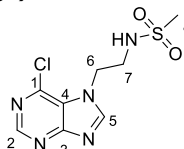
^1H NMR (400 MHz, DMSO) δ 8.94 (s, 1H, H-2), 8.90 (s, 1H, H-5), 5.54 (q, J = 8.8 Hz, 3H, H-6). ^{13}C NMR (101 MHz, DMSO) δ 161.93 (C-3), 152.84 (C-2), 152.01 (C-5), 142.88 (C-1), 124.98 (C-7), 122.58 (C-4), 46.79 (q, J = 34.4 Hz, C-6). LCMS m/z calc. for $\text{C}_7\text{H}_4\text{ClF}_3\text{N}_4$ $[\text{M}+\text{H}]^+$: 237.0, found 236.7 with t_R 2.23 min.

6-chloro-7-(2,2,2-trifluoroethyl)-7H-purin-2-amine (196, 6% yield).



^1H NMR (400 MHz, DMSO) δ 8.49 (s, 1H, H-5), 6.81 (s, NH_2), 3.34 (s, 2H, H-6). ^{13}C NMR (101 MHz, DMSO) δ 164.52 (C-3), 160.77 (C-1), 150.72 (C-5), 142.88 (C-2), 123.74 (d, J = 279.8 Hz, C-7), 115.13 (C-4), 46.55 (d, J = 34.1 Hz, C-6). LCMS m/z calc. for $\text{C}_7\text{H}_5\text{ClF}_3\text{N}_5$ $[\text{M}+\text{H}]^+$: 252.0, found 251.2 with t_R 1.73 min.

N-(2-(6-chloro-7H-purin-7-yl)ethyl)methanesulfonamide (176, 62 % yield).

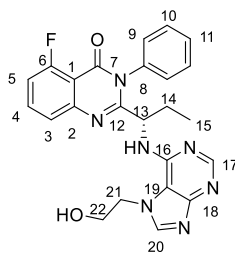


To a 0°C solution of amine **175** (1.01 mmol, 1 equiv) and triethylamine (1.113 mmol, 1.1 equiv) in DCM (3 mL) was added methanesulfonyl chloride (1.11 mmol, 1.1 equiv). The reaction mixture was stirred at ambient temperature for 16 h. The solvent was then removed under reduced pressure and the resulting residue was purified by flash chromatography (silica gel), eluting with 5% methanol (containing 0.7 N ammonia) in DCM to yield sulfonamide **176** (23% yield) as a white solid. ^1H NMR (400 MHz, D_2O) δ 8.72 (s, 1H, H-2), 8.60 (s, 1H, H-5), 3.83 – 3.69 (m, 2H, H-6), 3.43 – 3.35 (m, 2H, H-7), 2.89 (s, 3H, H-8). ^{13}C NMR (101 MHz, D_2O) δ 151.84 (C-2), 151.61 (C-5), 143.93 (C-1), 58.43 (C-6), 41.03 (C-8), 39.15 (C-7). LCMS m/z calc. for $\text{C}_8\text{H}_{10}\text{ClN}_5\text{O}_2\text{S}$ $[\text{M}+\text{H}]^+$: 276.0, found 275.9 with t_R 0.82 min.

General procedure for nucleophilic aromatic substitution of N-7-substituted-6-chloropurine derivatives. To a stirred solution of primary amine **77** (0.33 mmol, 1 equiv) in *tert*-butanol (3 mL) was added N-7-substituted-6-chloropurines (**172-174**, **176**, **189**, **191-193**, **195** and **196**) (0.43 mmol, 1.3 equiv) and DIPEA (3.3 mmol, 10 equiv). The reaction mixture was stirred at 110°C for 48 h at which time the solution was evaporated in vacuo to dryness. The resulting residue was purified by flash chromatography (silica gel), eluting with 5% methanol (containing 0.7 N ammonia) in ethylacetate to afford the arylamines (**156**, **157-160**, **163-166**, **170**, **171** and **177**) as white solids.

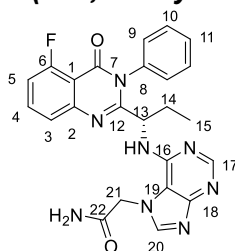
(S)-5-fluoro-2-(1-((7-(2-hydroxyethyl)-7H-purin-6-yl)amino)propyl)-3-phenylquinazolin-4(3H)-one (156, 18% yield).

References



^1H NMR (400 MHz, MeOD) δ 8.27 (s, 1H, H-17), 8.25 (s, 1H, H-20), 7.74 (dt, J = 13.4, 3.8 Hz, 2H, H-3), 7.65 (dt, J = 7.9, 4.5 Hz, 1H), 7.62 – 7.56 (m, 2H), 7.56 – 7.43 (m, 2H), 7.18 (dd, J = 10.9, 8.2 Hz, 1H, H-3), 4.69 (dt, J = 15.4, 4.3 Hz, 1H, H-21), 4.64 – 4.50 (m, 1H, H-21), 4.04 (t, J = 4.6 Hz, 2H, H-22), 2.03 (dtd, J = 20.0, 12.6, 10.0, 5.9 Hz, 1H, H-14), 1.88 (dq, J = 14.7, 7.3 Hz, 1H, H-14), 0.91 (t, J = 7.3 Hz, 3H, H-15). ^{13}C NMR (101 MHz, MeOD) δ 162.51 (C-7), 159.88, 159.85, 159.20 (C-18), 158.11, 151.70 (C-17), 151.16 (C-16), 149.40 (C-2), 145.90 (C-20), 136.04 (C-8), 135.11 (d, J = 10.5 Hz, C-4), 122.97 (d, J = 4.1 Hz, C-3), 113.08 (C-5), 112.87 (C-19), 110.18 (d, J = 6.0 Hz, C-1), 61.55 (C-22), 54.28 (C-13), 49.45 (C-21), 26.27 (C-14), 9.77 (C-15). LCMS m/z calc. for $\text{C}_{24}\text{H}_{22}\text{FN}_7\text{O}_2$ $[\text{M}+\text{H}]^+$: 460.2, found 459.9 with t_R 2.32 min (95%).

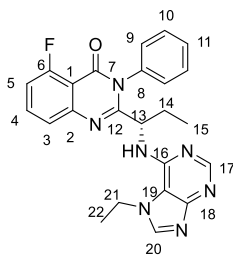
(S)-2-(6-((1-(5-fluoro-4-oxo-3-phenyl-3,4-dihydroquinazolin-2-yl)propyl)amino)-7H-purin-7-yl)acetamide (158, 10% yield).



^1H NMR (400 MHz, Methanol- d_4) δ 8.28 (s, 1H, H-17), 8.22 (s, 1H, H-20), 7.79 (dt, J = 8.4, 4.2 Hz, 1H), 7.66 (qd, J = 8.2, 7.3, 2.5 Hz, 2H), 7.62 – 7.46 (m, 4H), 7.21 (dd, J = 10.9, 8.2 Hz, 1H, H-3), 5.32-5.14(m, 2H, H-21), 2.06 (dtd, J = 14.9, 7.4, 4.5 Hz, 1H, H-14), 1.87 (dp, J = 14.8, 7.2 Hz, 1H, H-14), 0.90 (t, J = 7.4 Hz, 3H, H-15). ^{13}C NMR (101 MHz, Methanol- d_4) δ 170.21 (C-22), 162.53 (C-7), 159.90 (C-18), 159.77 (d, J = 4.3, C-6) 158.96 (C-12), 151.99 (C-17), 149.21 (C-2), 135.92 (C-20), 135.19 (d, J = 10.3 Hz, C-4), 129.33 (C-10), 129.01 (C-9), 128.79 (C-11), 122.82 (d, J = 4.3 Hz, C-3), 113.20 (C-5), 112.99 (C-1), 110.22 (C-19), 54.13 (C-13), 49.03 (C-21), 26.23 (C-14), 9.52 (C-15). LCMS m/z calc. for $\text{C}_{24}\text{H}_{21}\text{FN}_8\text{O}_2$ $[\text{M}+\text{H}]^+$: 473.2, found 472.9 with t_R 2.28 min (96%).

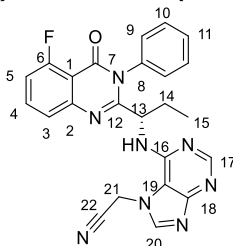
(S)-2-(1-((7-ethyl-7H-purin-6-yl)amino)propyl)-5-fluoro-3-phenylquinazolin-4(3H)-one (160, 37% yield).

References



^1H NMR (400 MHz, MeOD) δ 8.31 (s, 1H, H-17), 8.28 (s, 1H, H-20), 7.77 (td, J = 8.2, 5.4 Hz, 1H), 7.72 – 7.56 (m, 4H), 7.56 – 7.50 (m, 1H), 7.46 (d, J = 8.2 Hz, 1H), 7.18 (ddd, J = 10.9, 8.2, 1.0 Hz, 1H, H-3), 5.05 (dd, J = 9.2, 3.7 Hz, 1H, H-13), 4.65 (ddt, J = 21.8, 14.6, 7.3 Hz, 2H, H-21), 2.05 (ddp, J = 15.0, 7.5, 3.8 Hz, 1H, H-14), 1.93 (ddt, J = 14.3, 9.2, 7.3 Hz, 1H, H-14), 1.63 (t, J = 7.2 Hz, 3H, H-22), 0.89 (t, J = 7.3 Hz, 3H, H-15). ^{13}C NMR (101 MHz, MeOD) δ 162.55 (C-7), 159.88, 159.85, 159.42 (C-18), 158.11, 151.78 (C-17), 151.08 (C-16), 150.03 (C-2), 145.87 (C-20), 136.30 (C-8), 135.17 (d, J = 10.5 Hz, C-4), 122.46 (d, J = 4.1 Hz, C-3), 113.10 (C-5), 112.89 (C-19), 110.20 (d, J = 6.0 Hz, C-1), 54.30 (C-13), 41.97 (C-21), 26.22 (C-14), 16.08 (C-22), 9.77 (C-15). LCMS m/z calc. for $\text{C}_{24}\text{H}_{22}\text{FN}_7\text{O}$ $[\text{M}+\text{H}]^+$: 444.2, found 443.9 with t_R 2.51 min (96%).

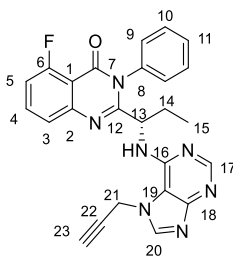
(S)-2-(6-((1-(5-fluoro-4-oxo-3-phenyl-3,4-dihydroquinazolin-2-yl)propyl)amino)-7H-purin-7-yl)acetonitrile (163, 37% yield).



^1H NMR (400 MHz, Methanol- d_4) δ 8.33 (s, 2H, H-17/20), 7.77 – 7.67 (m, 2H), 7.63 (ddt, J = 8.7, 7.6, 3.0 Hz, 1H), 7.57 – 7.49 (m, 3H), 7.47 (d, J = 8.2 Hz, 1H), 7.14 (ddd, J = 10.8, 8.2, 1.0 Hz, 1H, H-3), 5.99 – 5.76 (m, NH), 3.89 (pd, J = 6.3, 4.9 Hz, 1H, H-21), 3.53 (qd, J = 7.0, 2.0 Hz, 1H, H-21), 2.19 – 1.88 (m, 2H, H-14), 0.92 (t, J = 7.3 Hz, 3H, H-15). ^{13}C NMR (101 MHz, Methanol- d_4) δ 162.46 (C-7), 159.83 (C-18), 159.73 (d, J = 4.2 Hz, C-6), 159.10 (d, J = 13.4 Hz, C-12), 152.59 (C-17), 150.24 (C-16), 149.16 (C-2), 145.95 (d, J = 2.4 Hz, C-20), 135.86 (C-8), 135.16 (d, J = 10.6 Hz, C-4), 129.35 (d, J = 4.7 Hz, C-10), 129.08 (C-9), 128.78 (C-11), 122.74 (d, J = 4.2 Hz, C-8), 114.69 (d, J = 1.5 Hz, CN), 113.09 (d, J = 20.9 Hz, C-5), 111.48 (C-19), 110.21 (d, J = 6.1 Hz, C-5), 20.01 (C-21), 54.57 (C-13), 25.95 (C-14), 9.98 (C-15). LCMS m/z calc. for $\text{C}_{24}\text{H}_{19}\text{FN}_8\text{O}$ $[\text{M}+\text{H}]^+$: 455.2, found 454.8 with t_R 2.55 min (99%).

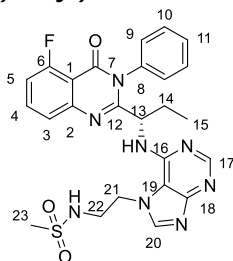
(S)-5-fluoro-3-phenyl-2-(1-((7-(prop-2-yn-1-yl)-7H-purin-6-yl)amino)propyl)quinazolin-4(3H)-one (164, 41% yield).

References



^1H NMR (400 MHz, MeOD) δ 8.31 (s, 2H, H-17/20), 7.77 (td, J = 8.2, 5.4 Hz, 1H), 7.71 – 7.61 (m, 1H), 7.61 – 7.57 (m, 2H), 7.54 – 7.44 (m, 1H), 7.18 (ddd, J = 10.9, 8.2, 1.1 Hz, 1H, H-3), 5.48 (qd, J = 18.3, 2.6 Hz, 2H, H-21), 5.00 (dd, J = 8.9, 3.9 Hz, 1H, H-13), 3.63 – 3.39 (m, 1H, H-23), 2.07 (dtd, J = 15.0, 7.5, 4.0 Hz, 1H, H-14), 1.91 (ddt, J = 14.3, 8.9, 7.2 Hz, 1H, H-14), 0.92 (t, J = 7.4 Hz, 3H, H-15). ^{13}C NMR (101 MHz, MeOD) δ 162.53 (C-7), 159.90, 159.68 (d, J = 4.3 Hz, C-18), 158.89, 152.32, 150.27, 149.13 (C-2), 145.21 (C-20), 135.87 (C-8), 135.26 (d, J = 10.6 Hz, C-4), 129.70 – 129.20 (m), 128.92 (d, J = 7.7 Hz), 122.78 (d, J = 4.2 Hz, C-3), 113.16 (d, J = 20.9 Hz, C-5), 111.73, 110.22 (d, J = 6.1 Hz, C-1), 77.19 (C-23), 77.05 (C-22), 54.14 (C-13), 36.34 (C-21), 26.23 (C-14), 9.61 (C-15). LCMS m/z calc. for $\text{C}_{25}\text{H}_{20}\text{FN}_7\text{O}$ $[\text{M}+\text{H}]^+$: 454.2, found 453.9 with t_R 2.57 min (99%).

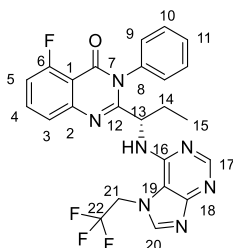
(S)-N-(2-(6-((1-(5-fluoro-4-oxo-3-phenyl-3,4-dihydroquinazolin-2-yl)propyl)amino)-7H-purin-7-yl)ethyl)methanesulfonamide (165, 3% yield).



^1H NMR (400 MHz, MeOD) δ 8.33 (s, 1H, H-17), 8.27 (s, 1H, H-20), 7.82 – 7.70 (m, 2H), 7.63 (dd, J = 12.1, 6.0 Hz, 3H), 7.51 (d, J = 8.2 Hz, 2H), 7.30 – 7.14 (m, 1H, H-3), 5.00 (dd, J = 8.9, 4.4 Hz, 1H, H-13), 4.78 – 4.41 (m, 2H, H-21), 3.85 – 3.41 (m, 2H, H-22), 2.89 (s, 3H, H-23), 2.01 (dd, J = 15.4, 8.2 Hz, 2H, H-14), 0.89 (t, J = 7.4 Hz, 3H, H-15). ^{13}C NMR (101 MHz, MeOD) δ 162.53 (C-7), 159.90 (C-18), 159.11 (d, J = 32.4 Hz), 152.31, 150.12 (C-16), 149.13 (C-2), 147.51 (C-20), 135.87 (C-8), 135.25 (d, J = 10.6 Hz, C-4), 129.40 (d, J = 3.9 Hz), 129.26, 129.03, 128.78, 122.78 (d, J = 4.2 Hz, C-3), 113.11 (d, J = 20.9 Hz, C-5), 111.75, 110.26 (d, J = 6.1 Hz, C-1), 58.11 (C-21), 54.58 (C-13), 38.54 (C-22), 25.86 (C-14), 23.39 (C-23), 10.08 (C-15). LCMS m/z calc. for $\text{C}_{25}\text{H}_{25}\text{FN}_8\text{O}_3\text{S}$ $[\text{M}+\text{H}]^+$: 537.2, found 536.9 with t_R 2.40 min (90%).

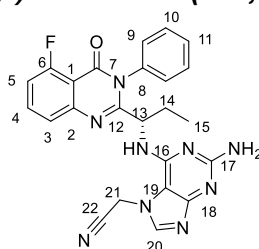
(S)-5-fluoro-3-phenyl-2-(1-((7-(2,2,2-trifluoroethyl)-7H-purin-6-yl)amino)propyl)quinazolin-4(3H)-one (166, 23% yield).

References



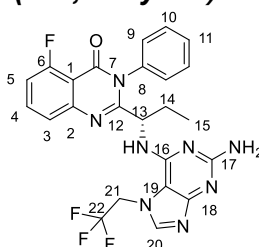
^1H NMR (400 MHz, MeOD) δ 8.38 (s, 1H, H-17), 8.35 (s, 1H, H-20), 7.77 (td, J = 8.2, 5.4 Hz, 1H), 7.73 – 7.55 (m, 3H), 7.51 (dd, J = 7.5, 2.0 Hz, 1H), 7.45 (d, J = 8.3 Hz, 1H), 7.19 (dd, J = 10.9, 8.2 Hz, 1H, H-19), 5.68 (dq, J = 16.7, 8.4 Hz, 1H, H-21), 5.45 (dq, J = 17.1, 8.7 Hz, 1H, H-21), 4.99 (dd, J = 9.6, 3.7 Hz, 1H, H-13), 2.40 – 1.80 (m, 1H, H14), 0.86 (t, J = 7.3 Hz, 3H, H-15). ^{13}C NMR (101 MHz, MeOD) δ 162.56 (C-7), 159.93, 159.70 (C-18), 159.11 (d, J = 32.4 Hz), 152.31, 150.12 (C-16), 149.22 (C-2), 147.09 (C-20), 135.87 (C-8), 135.22 (d, J = 10.6 Hz, C-4), 129.40 (d, J = 3.9 Hz), 129.26, 129.03, 128.78, 122.61 (d, J = 4.2 Hz, C-3), 113.11 (d, J = 20.9 Hz, C-5), 111.75, 110.26 (C-1), 66.00 (C-21), 54.54 (C-13), 25.88 (C-14), 9.76 (C-16). LCMS m/z calc. for $\text{C}_{24}\text{H}_{19}\text{F}_4\text{N}_7\text{O}$ $[\text{M}+\text{H}]^+$: 498.2, found 497.8 with t_R 2.70 min (90%).

(S)-2-(2-amino-6-((1-(5-fluoro-4-oxo-3-phenyl-3,4-dihydroquinazolin-2-yl)propyl)amino)-7H-purin-7-yl)acetonitrile (170, 9% yield).



^1H NMR (400 MHz, MeOD) δ 8.04 (s, 1H, H-20), 7.80 (td, J = 8.3, 5.5 Hz, 1H), 7.69 – 7.55 (m, 4H), 7.55 – 7.47 (m, 1H), 7.22 (ddd, J = 10.9, 8.2, 1.0 Hz, 1H, H-3), 5.85 – 5.55 (m, 1H, H-21), 5.06 (dd, J = 8.9, 4.1 Hz, 1H, H-21), 2.14 – 2.02 (m, 1H, H-14), 1.98 – 1.78 (m, 1H, H-14), 0.89 (t, J = 7.4 Hz, 3H, H-15). ^{13}C NMR (101 MHz, MeOD) δ 162.56 (C-7), 160.05, 159.93, 159.85, 158.48, 150.75 (C-16), 149.17, 144.75 (C-20), 135.78 (C-8), 135.21 (d, J = 10.6 Hz, C-4), 129.38 (d, J = 3.7 Hz), 129.31, 128.94 (d, J = 3.2 Hz), 122.93 (C-3), 114.73, 113.31, 113.10 (C-5), 110.26 (C-1), 105.64, 53.59 (C-13), 26.04 (C-14), 19.68 (C-21), 9.67 (C-15). LCMS m/z calc. for $\text{C}_{24}\text{H}_{20}\text{FN}_9\text{O}$ $[\text{M}+\text{H}]^+$: 470.2, found 469.9 with t_R 2.19 min (96%).

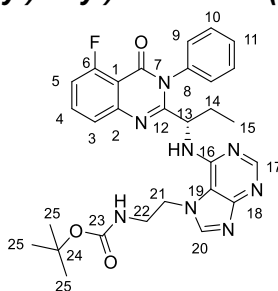
(S)-2-(1-((2-amino-7-(2,2,2-trifluoroethyl)-7H-purin-6-yl)amino)propyl)-5-fluoro-3-phenylquinazolin-4(3H)-one (171, 6% yield).



References

^1H NMR (400 MHz, MeOD) δ 8.08 (s, 1H, H-20), 7.81 (td, J = 8.3, 5.4 Hz, 1H), 7.66 (ddd, J = 7.7, 6.1, 2.2 Hz, 1H), 7.59 (t, J = 2.6 Hz, 3H), 7.51 (dd, J = 8.6, 6.1 Hz, 2H), 7.23 (dd, J = 10.9, 8.2 Hz, 2H), 5.47 (dt, J = 16.6, 8.3 Hz, 1H, H-21), 5.37 (dq, J = 17.1, 8.7 Hz, 1H, H-21), 5.08 (dd, J = 9.1, 3.9 Hz, 1H, H-13), 2.09 – 1.98 (m, 1H, H-14), 1.86 (ddd, J = 14.0, 8.9, 7.0 Hz, 1H, H-14), 0.83 (t, J = 7.3 Hz, 3H, H-15). ^{13}C NMR (101 MHz, MeOD) δ 162.53 (C-7), 159.90, 159.68 (C-18), 150.54 (C-16), 149.15 (C-2), 147.09 (C-20), 135.79 (C-8), 135.21 (d, J = 10.6 Hz, C-4), (129.41 (d, J = 5.3 Hz), 129.29, 128.91 (d, J = 10.8 Hz), 122.67 (C-3), 113.16 (d, J = 20.9 Hz, C-5), 111.73, 110.26 (C-1), 53.40 (C-13), 26.09 (C-14), 9.44 (C-15). LCMS m/z calc. for $\text{C}_{24}\text{H}_{20}\text{F}_4\text{N}_8\text{O}$ $[\text{M}+\text{H}]^+$: 513.2, found 512.8 with t_R 2.31 min (96%).

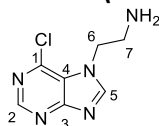
***tert*-butyl (S)-2-(6-((1-(5-fluoro-4-oxo-3-phenyl-3,4-dihydroquinazolin-2-yl)propyl)amino)-7H-purin-7-yl)ethyl)carbamate (177, 30% yield).**



^1H NMR (400 MHz, Methanol- d_4) δ 8.31 (s, 1H, H-17), 8.20 (s, 1H, H-20), 7.78 – 7.71 (m, 3H), 7.58 (ddd, J = 34.9, 15.9, 7.9 Hz, 4H), 7.44 (d, J = 8.2 Hz, 1H), 7.17 (t, J = 9.3 Hz, 1H), 5.05 (d, J = 9.5 Hz, NH), 4.61 (t, J = 7.4 Hz, 2H, H-21), 3.76 – 3.44 (m, 2H, H-22), 2.18 (dt, J = 21.3, 10.3 Hz, 1H, H-14), 1.74 (s, 1H, H-14), 1.33 (s, 9H, H-25), 0.91 (t, J = 7.7 Hz, 3H, H-15). ^{13}C NMR (101 MHz, Methanol- d_4) δ 162.52 (C-7), 159.89 (C-18), 159.53 (C-6), 158.59 (C-16), 157.27 (C-12), 151.81 (C-17), 150.35 (C-), 149.35 (C-2), 145.63 (C-20), 135.96 (C-8), 135.13 (d, J = 10.7 Hz, C-4), 129.31 (C-10), 129.09 (C-9), 128.75 (C-11), 122.87 (C-8), 112.99 (d, J = 20.4 Hz, C-5), 111.75, 110.22 (d, J = 6.0 Hz, C-1), 79.23 (C-24), 54.89 (C-13), 45.49 (C-21), 41.16 (C-22), 27.19 (C-25), 25.51 (C-14), 10.42 (C-15). LCMS m/z calc. for $\text{C}_{29}\text{H}_{31}\text{FN}_8\text{O}_3$ $[\text{M}+\text{H}]^+$: 559.3, found 558.8 with t_R 2.64 min.

General method for *N*-Boc deprotection. To the Boc-protected amines (**174** and **177**) (0.143 mmol, 1 equiv) was added 4 N HCl in 1,4-dioxane (3 mL) and the solution was stirred at ambient temperature for 2 h. The solvent was removed in vacuo and the resulting yellow solid was triturated with diethyl ether to yield the hydrochloride salt of the amines (**175** and **157**).

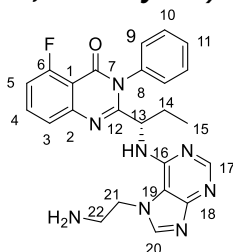
2-(6-chloro-7H-purin-7-yl)ethan-1-amine (175, 100 % yield).



References

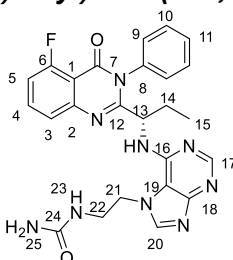
^1H NMR (500 MHz, Chloroform- d) δ 8.68 (s, 1H, H-2), 8.11 (s, 1H, H-5), 4.42 (t, J = 3.4 Hz, 2H, H-6), 3.10 (tt, J = 6.3, 3.3 Hz, 2H, H-7). ^{13}C NMR (101 MHz, Chloroform- d) δ 161.23 (C-3), 156.22 (C-2), 149.53 (C-5), 142.75 (C-1), 122.66 (C-4), 46.69 (C-6), 41.72 (C-7). LCMS m/z calc. for $\text{C}_7\text{H}_8\text{ClN}_5$ $[\text{M}+\text{H}]^+$: 198.1, found 197.9 with t_R 1.40 min.

(S)-2-(1-((7-(2-aminoethyl)-7H-purin-6-yl)amino)propyl)-5-fluoro-3-phenylquinazolin-4(3H)-one (157, 100 % yield).



^1H NMR (400 MHz, Methanol- d_4) δ 8.74 (s, 1H, H-17), 8.65 (s, 1H, H-20), 7.85 (td, J = 8.2, 5.4 Hz, 1H), 7.75 – 7.55 (m, 6H), 7.26 (dd, J = 10.8, 8.2 Hz, 1H, H-3), 5.24 (dddd, J = 27.8, 15.6, 8.3, 4.2 Hz, 2H, H-21), 3.68 (tq, J = 13.4, 8.0, 6.7 Hz, 2H, H-22), 2.32 – 2.02 (m, 2H, H-14), 0.89 (t, J = 7.3 Hz, 3H, H-15). ^{13}C NMR (101 MHz, Methanol- d_4) δ 162.53 (C-7), 159.90 (C-18), 159.18 (d, J = 4.4 Hz, C-6), 158.05 (C-12), 152.02 (C-16), 149.85 (C-2), 148.49 (C-17), 146.19 (C-20), 135.68 (d, J = 10.6 Hz, C-4), 135.47 (C-8), 129.72 (d, J = 3.9 Hz, C-10), 129.52 (C-9), 128.92 (d, J = 8.8 Hz, C-11), 122.39 (C-3), 113.71 (d, J = 20.7 Hz, C-5), 112.07 (C-19), 110.31 (C-10), 55.60 (C-13), 44.77 (C-21), 39.78 (C-22), 25.64 (C-14), 10.05 (C-15). LCMS m/z calc. for $\text{C}_{24}\text{H}_{23}\text{FN}_8\text{O}$ $[\text{M}+\text{H}]^+$: 459.2, found 459.0 with t_R 2.06 min (95%).

(S)-1-(2-(6-((1-(5-fluoro-4-oxo-3-phenyl-3,4-dihydroquinazolin-2-yl)propyl)amino)-7H-purin-7-yl)ethyl)urea (159, 68% yield).



To a stirred solution of amine hydrochloride salt **157** (0.079 mmol, 1 equiv) and triethylamine (0.238 mmol, 3 equiv) in DCM (2 mL) was added trimethylsilyl isocyanate (0.086 mmol, 2 equiv). The reaction mixture was stirred for 18 h at RT under a nitrogen atmosphere. The solvent was then removed under reduced pressure and the resulting residue was purified by flash chromatography (silica gel), eluting with 7.5% methanol (containing 0.7 N ammonia) in DCM to afford urea **159** (68% yield) as a white solid. ^1H NMR (400 MHz, Methanol- d_4) δ 8.34 (s, 1H, H-17), 8.26 (s, 1H, H-20), 7.96 – 7.31 (m, 6H), 7.17 (s, 1H, H-3), 5.41 (s, 1H, H-25), 4.69 (s, 2H, H-21), 3.74 (t, J = 51.7 Hz, 2H, H-22), 2.07 (d, J = 40.1 Hz, 2H, H-14), 0.88

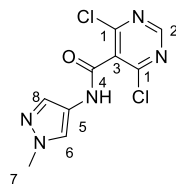
References

(s, 3H, H-15). ^{13}C NMR (101 MHz, MeOD) δ 162.50 (C-6), 160.70 (C-24), 159.87 (C-18), 159.41, 151.32 (C-17), 150.66 (C-16), 149.33 (C-2), 145.97 (C-20), 135.94, 135.21 (d, $J = 10.9$ Hz, C-4), 129.41 (d, $J = 8.3$ Hz), 129.25, 128.95 (d, $J = 3.9$ Hz), 122.87, 113.01 (d, $J = 20.9$ Hz, C-5), 111.81, 110.19 (C-1), 55.07 (C-13), 46.36 (C-21), 40.86 (C-22), 25.58 (C-14), 10.33 (C-15). LCMS m/z calc. for $\text{C}_{25}\text{H}_{24}\text{FN}_9\text{O}_2$ $[\text{M}+\text{H}]^+$: 502.2, found 501.9 with t_R 2.31 min (97%).

7.3.5 Experimental for Chapter 5

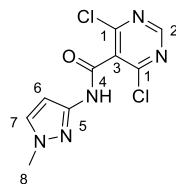
General procedure for amide coupling. To a cooled (0°C) solution of 4,6-dichloropyrimidine-5-carboxylic acid **228** (5.18 mmol, 1 equiv) and BEP (5.70 mmol, 1.1 equiv) in DCM (15 mL) was added DIPEA (18.13 mmol, 3.5 equiv). The resulting mixture was stirred at RT for 1 h. Amine (5.18 mmol, 1 equiv) was then added. After stirring for 18 h at RT, the solvent was evaporated under reduced pressure. The resulting residue was purified using silica gel chromatography (DCM/ ethyl acetate: 70: 30) to yield the amides (**230-238**).

4,6-dichloro-N-(1-methyl-1H-pyrazol-4-yl)pyrimidine-5-carboxamide (230, 21% yield).



^1H NMR (400 MHz, Methanol- d_4) δ 8.92 (s, 1H, H-2), 8.05 (s, 1H, H-8), 7.59 (s, 1H, H-6), 3.93 (s, 3H, H-7). ^{13}C NMR (101 MHz, Methanol- d_4) δ 163.20 (C-4), 158.60 (C-2), 158.15 (C-1), 138.05 (C-5), 130.09 (C-8), 129.87 (C-3), 122.48 (C-6), 37.91 (C-7). LCMS m/z calc. for $\text{C}_9\text{H}_7\text{Cl}_2\text{N}_5\text{O}$ $[\text{M}+\text{H}]^+$: 272.0, found 272.1 with t_R 2.15 min.

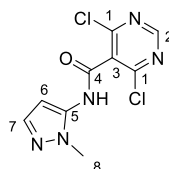
4,6-dichloro-N-(1-methyl-1H-pyrazol-3-yl)pyrimidine-5-carboxamide (231, 33% yield).



^1H NMR (400 MHz, Chloroform- d) δ 9.23 (s, NH), 8.85 (s, 1H, H-2), 7.33 (d, $J = 2.3$ Hz, 1H, H-7), 6.82 (d, $J = 2.4$ Hz, 1H, H-6), 3.74 (s, 3H, H-8). ^{13}C NMR (101 MHz, Chloroform- d) δ 159.13 (C-4), 158.32 (C-1), 158.16 (C-2), 145.78 (C-5), 131.41 (C-7), 129.77 (C-3), 98.21 (C-6), 38.74 (C-8). LCMS m/z calc. for $\text{C}_9\text{H}_7\text{Cl}_2\text{N}_5\text{O}$ $[\text{M}+\text{H}]^+$: 272.0, found 271.8 with t_R 2.22 min.

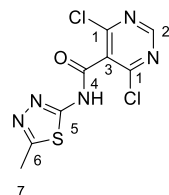
4,6-dichloro-N-(1-methyl-1H-pyrazol-4-yl)pyrimidine-5-carboxamide. (232, 18% yield).

References



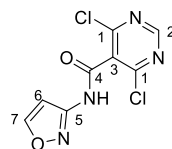
^1H NMR (400 MHz, Chloroform- d) δ 8.86 (s, 1H, H-2), 7.45 (d, J = 2.0 Hz, 1H, H-7), 6.35 (d, J = 2.0 Hz, 1H, H-6), 3.84 (s, 3H, H-8). ^{13}C NMR (101 MHz, Chloroform- d) δ 159.91 (C-4), 158.86 (C-2), 158.49 (C-1), 138.60 (C-7), 133.45 (C-5), 129.30 (C-3), 101.28 (C-6), 36.13 (C-8). LCMS m/z calc. for $\text{C}_9\text{H}_7\text{Cl}_2\text{N}_5\text{O}$ $[\text{M}+\text{H}]^+$: 272.0, found 271.8 with t_R 2.21 min.

4,6-dichloro-N-(5-methylthiazol-2-yl)pyrimidine-5-carboxamide (233, 10% yield).



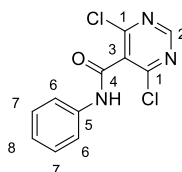
^1H NMR (400 MHz, Methanol- d_4) δ 8.98 (s, 1H, H-2), 2.76 (s, 3H, H-7). ^{13}C NMR (101 MHz, Methanol- d_4) δ 162.15 (C-4), 158.75 (C-2), 158.44 (C-1), 147.30 (C-5), 145.70 (C-6), 128.77 (d, J = 26.3 Hz, C-3), 13.67 (C-7). LCMS m/z calc. for $\text{C}_8\text{H}_5\text{Cl}_2\text{N}_5\text{OS}$ $[\text{M}+\text{H}]^+$: 290.0, found 289.8 with t_R 2.41 min.

4,6-dichloro-N-(isoxazol-3-yl)pyrimidine-5-carboxamide (234, 11% yield).



^1H NMR (400 MHz, Methanol- d_4) δ 8.94 (s, 1H, H-2), 8.67 (d, J = 1.8 Hz, 1H, H-7), 7.09 (d, J = 1.7 Hz, 1H, H-6). ^{13}C NMR (101 MHz, Methanol- d_4) δ 162.96 (C-4), 160.03 (C-1), 158.37 (C-2), 158.28 (C-7), 156.76 (C-5), 104.04 (C-6). LCMS m/z calc. for $\text{C}_8\text{H}_4\text{Cl}_2\text{N}_4\text{O}_2$ $[\text{M}+\text{H}]^+$: 259.0, found 261.9 with t_R 2.67 min.

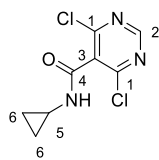
4,6-dichloro-N-phenylpyrimidine-5-carboxamide (235, 25% yield).



^1H NMR (400 MHz, Methanol- d_4) δ 8.92 (s, 1H, H-2), 7.73 – 7.61 (m, 2H, H-6), 7.41 (dd, J = 8.6, 7.4 Hz, 2H, H-7), 7.27 – 7.18 (m, 1H, H-8). ^{13}C NMR (101 MHz, Methanol- d_4) δ 160.13 (C-4), 158.40 (C-1), 158.01 (C-2), 137.58 (C-5), 130.25 (C-3), 128.76 (C-7), 124.97 (C-8), 119.88 (C-6). LCMS m/z calc. for $\text{C}_{11}\text{H}_7\text{Cl}_2\text{N}_3\text{O}$ $[\text{M}+\text{H}]^+$: 268.0, found 269.1 with t_R 2.60 min.

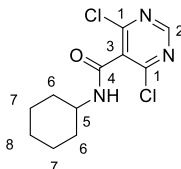
4,6-dichloro-N-cyclopropylpyrimidine-5-carboxamide (236, 25% yield).

References



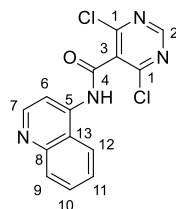
^1H NMR (400 MHz, Methanol- d_4) δ 8.87 (s, 1H, H-2), 2.91 (tt, J = 7.4, 3.9 Hz, 1H, H-5), 0.94 – 0.80 (m, 2H, H-6), 0.75 – 0.55 (m, 2H, H-6). ^{13}C NMR (101 MHz, Methanol- d_4) δ 163.66 (C-4), 158.36 (C-1), 157.91 (C-2), 129.99 (C-3), 22.27 (C-5), 4.96 (C-6). LCMS m/z calc. for $\text{C}_8\text{H}_7\text{Cl}_2\text{N}_3\text{O}$ $[\text{M}+\text{H}]^+$: 232.0, found 233.9 with t_R 1.44 min.

4,6-dichloro-N-cyclohexylpyrimidine-5-carboxamide (237, 28% yield).



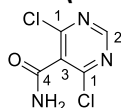
^1H NMR (400 MHz, Methanol- d_4) δ 8.86 (s, 1H, H-2), 3.89 (tt, J = 10.2, 3.9 Hz, 1H, H-5), 2.24 – 1.94 (m, 2H, H-6), 1.82 (dp, J = 10.9, 3.6, 3.0 Hz, 2H, H-6), 1.68 (dq, J = 12.1, 3.8 Hz, 1H, H-8), 1.53 – 1.09 (m, 4H, H-7). ^{13}C NMR (101 MHz, Methanol- d_4) δ 161.36 (C-4), 158.31 (C-2), 157.73 (C-1), 130.28 (C-3), 48.96 (C-5), 31.81 (C-6), 25.19 (C-8), 24.43 (C-7). LCMS m/z calc. for $\text{C}_{11}\text{H}_{13}\text{Cl}_2\text{N}_3\text{O}$ $[\text{M}+\text{H}]^+$: 274.0, found 274.2 with t_R 2.68 min.

4,6-dichloro-N-(quinolin-4-yl)pyrimidine-5-carboxamide (238, 31% yield).



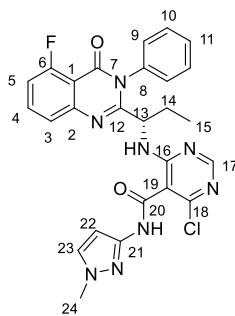
^1H NMR (400 MHz, Methanol- d_4) δ 8.98 (s, 1H, H-2), 8.89 (d, J = 5.1 Hz, 1H, H-7), 8.29 (d, J = 5.1 Hz, 1H), 8.24 (dd, J = 8.5, 1.2 Hz, 1H), 8.10 (dd, J = 8.6, 1.1 Hz, 1H), 7.84 (ddd, J = 8.4, 6.9, 1.3 Hz, 1H), 7.68 (ddd, J = 8.3, 6.9, 1.2 Hz, 1H), 6.63 – 6.34 (m, 1H, H-6). ^{13}C NMR (101 MHz, Methanol- d_4) δ 163.20 (C-4), 161.26, 158.30 (C-2), 150.25 (C-2), 148.29, 141.26, 140.62, 130.05 (d, J = 5.4 Hz), 128.44, 126.90, 121.31, 121.16, 119.32, 113.06, 107.47 (C-6). LCMS m/z calc. for $\text{C}_{14}\text{H}_8\text{Cl}_2\text{N}_4\text{O}$ $[\text{M}+\text{H}]^+$: 319.0, found 321.2 with t_R 2.08 min.

4,6-dichloropyrimidine-5-carboxamide (239, 63% yield).



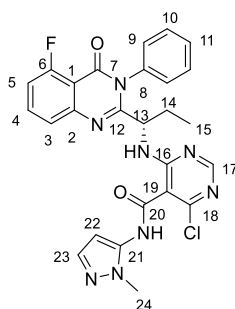
A solution of 4,6-dichloropyrimidine-5-carboxylic acid **228** (5.18 mmol, 1 equiv) in thionyl chloride (5 mL) was refluxed for 1 h. After cooling at ambient temperature, the solvent was removed under reduced pressure. THF (5 mL) and 25% aqueous ammonia (5 mL) were then added to the residue, and the mixture was stirred at 0°C for 2 h. The solvent was evaporated under reduced pressure and the resulting

References



^1H NMR (400 MHz, Methanol- d_4) δ 8.25 (s, 1H, H-17), 7.79 (td, J = 8.2, 5.5 Hz, 1H), 7.69 – 7.53 (m, 5H), 7.48 (dd, J = 8.5, 5.7 Hz, 2H), 7.26 – 7.17 (m, 1H), 6.70 (d, J = 2.3 Hz, 1H, H-22), 4.92 (dd, J = 8.8, 4.2 Hz, NH), 2.06 – 1.91 (m, 1H, H-14), 1.79 (ddt, J = 16.0, 14.4, 7.3 Hz, 1H, H-14), 0.82 (t, J = 7.4 Hz, 3H, H-15). ^{13}C NMR (101 MHz, Methanol- d_4) δ 162.49, 161.78, 159.91, 157.69, 157.34 (C-17), 154.96, 149.12, 146.05, 135.76, 135.13 (d, J = 10.4 Hz, C-4), 131.24, 129.49, 129.32 (d, J = 2.5 Hz), 128.96, 128.86, 123.09 (d, J = 4.2 Hz), 113.20 (d, J = 20.4 Hz, C-3), 112.14, 110.28 (d, J = 6.1 Hz, C-5), 97.60 (C-22), 53.95 (C-13), 37.51 (C-24), 26.09 (C-14), 9.30 (C-15). LCMS m/z calc. for $\text{C}_{26}\text{H}_{22}\text{ClFN}_8\text{O}_2$ $[\text{M}+\text{H}]^+$: 533.2, found 532.8 with t_R 2.80 min (96%).

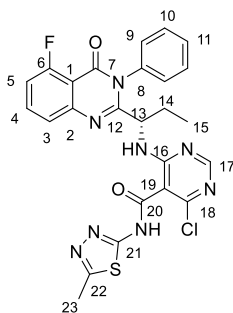
(S)-4-chloro-6-((1-(5-fluoro-4-oxo-3-phenyl-3,4-dihydroquinazolin-2-yl)propyl)amino)-N-(1-methyl-1H-pyrazol-5-yl)pyrimidine-5-carboxamide (242, 59% yield).



^1H NMR (400 MHz, Methanol- d_4) δ 8.29 (s, 1H, H-17), 7.79 (td, J = 8.2, 5.4 Hz, 1H), 7.66 – 7.55 (m, 4H), 7.51 – 7.45 (m, 3H), 7.21 (ddd, J = 10.9, 8.2, 1.0 Hz, 1H), 6.52 (d, J = 2.1 Hz, 1H, H-22), 4.93 (dd, J = 8.8, 4.1 Hz, NH), 3.85 (s, 3H, H-24), 2.01 – 1.91 (m, 1H, H-14), 1.86 – 1.71 (m, 1H, H-14), 0.83 (t, J = 7.4 Hz, 4H, H-15). ^{13}C NMR (101 MHz, Methanol- d_4) δ 171.57 (C-16), 162.63 (C-20), 162.51 (C-16), 159.92, 159.62 (d, J = 4.2 Hz), 157.79, 157.66 (C-17), 155.37, 149.07, 137.96, 135.75, 135.26 (d, J = 10.7 Hz, C-4), 129.52, 129.36 (d, J = 5.1 Hz), 128.91 (d, J = 5.8 Hz), 122.92 (d, J = 4.3 Hz), 113.27 (d, J = 20.8 Hz, C-3), 111.24, 110.25 (d, J = 6.1 Hz, C-5), 99.65 (C-22), 53.96 (C-13), 34.87 (C-24), 26.10 (C-14), 9.29 (C-15). LCMS m/z calc. for $\text{C}_{26}\text{H}_{22}\text{ClFN}_8\text{O}_2$ $[\text{M}+\text{H}]^+$: 533.2, found 532.7 with t_R 2.78 min (97%).

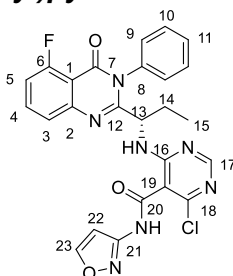
References

4-chloro-6-((1-(5-fluoro-4-oxo-3-phenyl-3,4-dihydroquinazolin-2-yl)propyl)amino)-N-(5-methyl-1,3,4-thiadiazol-2-yl)pyrimidine-5-carboxamide (243, 29% yield).



^1H NMR (400 MHz, Methanol- d_4) δ 8.27 (s, 1H, H-17), 7.77 (td, J = 8.2, 5.4 Hz, 1H), 7.62 (ddd, J = 7.8, 5.0, 3.2 Hz, 1H), 7.56 (dq, J = 3.4, 1.8, 1.3 Hz, 3H) 7.51 – 7.44 (m, 2H), 7.25 – 7.14 (m, 1H), 5.11 – 4.99 (m, NH), 2.73 (s, 3H, H-23), 2.02 – 1.94 (m, 1H, H-14), 1.82 (ddt, J = 17.0, 15.1, 7.8 Hz, 1H, H-14), 0.82 (t, J = 7.3 Hz, 3H, H-15). ^{13}C NMR (101 MHz, Methanol- d_4) δ 171.57 (C-16), 162.47 (C-20), 161.63, 159.83, 159.68 (d, J = 2.3 Hz), 159.39 (C-17), 157.86, 157.65, 157.15, 155.64, 149.13, 135.75, 135.17 (d, J = 10.6 Hz, C-4), 129.41, 129.28 (d, J = 5.7 Hz), 129.12, 128.78, 123.07, 113.22 (d, J = 21.0 Hz, C-3), 110.67, 110.23 (d, J = 6.2 Hz, C-5), 54.34 (C-13), 25.78 (C-14), 13.62 (C-23), 9.58 (C-15). LCMS m/z calc. for $\text{C}_{25}\text{H}_{20}\text{ClFN}_8\text{O}_2\text{S}$ $[\text{M}+\text{H}]^+$: 551.1, found 550.8 with t_R 2.82 min (96%).

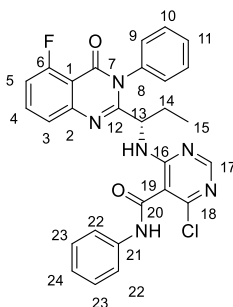
(S)-4-chloro-6-((1-(5-fluoro-4-oxo-3-phenyl-3,4-dihydroquinazolin-2-yl)propyl)amino)-N-(isoxazol-3-yl)pyrimidine-5-carboxamide (244, 37% yield).



^1H NMR (400 MHz, Methanol- d_4) δ 8.62 (d, J = 1.8 Hz, 1H), 8.25 (s, 1H, H-17), 7.75 (td, J = 8.2, 5.4 Hz, 1H), 7.61 (ddd, J = 7.6, 4.5, 3.3 Hz, 1H), 7.55 (dd, J = 4.6, 1.8 Hz, 3H), 7.50 – 7.40 (m, 2H), 7.17 (ddd, J = 10.9, 8.2, 1.0 Hz, 1H), 7.11 (d, J = 1.8 Hz, 1H, H-22), 4.90 (dd, J = 8.9, 4.2 Hz, NH), 3.78 – 3.44 (m, 1H, H-13), 1.97 (qd, J = 7.2, 4.3 Hz, 1H, H-14), 1.80 (ddt, J = 16.1, 14.4, 7.4 Hz, 1H, H-14), 0.82 (t, J = 7.3 Hz, 3H, H-15). ^{13}C NMR (101 MHz, Methanol- d_4) δ 162.45 (d, J = 3.3 Hz), 159.80, 159.72, 159.63 (d, J = 4.3 Hz), 159.56 (C-23), 157.68, 157.61 (C-17), 157.22, 155.17, 149.10, 135.75, 135.14 (d, J = 10.6 Hz, C-4), 129.45, 129.29 (d, J = 2.7 Hz), 129.08, 128.83, 123.05 (d, J = 4.1 Hz), 113.21 (d, J = 20.8 Hz, C-3), 111.67, 110.22 (d, J = 6.0 Hz, C-5), 99.09 (C-99), 54.16 (C-13), 25.93 (C-14), 9.51 (C-15). LCMS m/z calc. for $\text{C}_{25}\text{H}_{19}\text{ClFN}_7\text{O}_3$ $[\text{M}+\text{H}]^+$: 520.1, found 520.1 with t_R 3.05 min (98%).

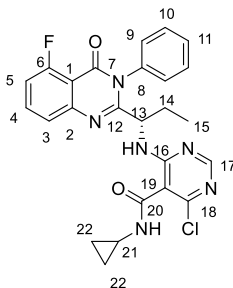
References

(S)-4-chloro-6-((1-(5-fluoro-4-oxo-3-phenyl-3,4-dihydroquinazolin-2-yl)propyl)amino)-N-phenylpyrimidine-5-carboxamide (245, 47% yield).



^1H NMR (400 MHz, Methanol- d_4) δ 8.26 (s, 1H, H-17), 7.73 (t, J = 6.3 Hz, 3H), 7.66 – 7.49 (m, 4H), 7.47 (dd, J = 7.7, 2.0 Hz, 1H), 7.43 – 7.35 (m, 3H), 7.19 (q, J = 10.8, 9.0 Hz, 2H), 4.91 (dd, J = 8.7, 4.1 Hz, 1H, NH), 1.98 (dq, J = 14.8, 8.8, 7.5, 3.5 Hz, 1H, H-14), 1.83 – 1.69 (m, 1H, H-14), 0.81 (t, J = 7.4 Hz, 3H, H-15). ^{13}C NMR (101 MHz, Methanol- d_4) δ 162.42 (C-20), 159.82, 159.62, 157.77, 157.32 (C-17), 154.92, 149.05, 138.01, 135.74, 135.16 (d, J = 10.6 Hz, C-4), 129.52, 129.33 (d, J = 4.8 Hz), 128.91 (d, J = 5.5 Hz), 128.60 (C-23), 124.65, 122.99 (d, J = 4.2 Hz), 120.01 (C-22), 113.21 (d, J = 20.9 Hz, C-3), 112.70, 110.21 (d, J = 6.0 Hz, C-5), 53.92 (C-13), 26.11 (C-14), 9.30 (C-15). LCMS m/z calc. for $\text{C}_{28}\text{H}_{22}\text{ClFN}_6\text{O}_2$ $[\text{M}+\text{H}]^+$: 529.2, found 529.1 with t_R 3.36 min (98%).

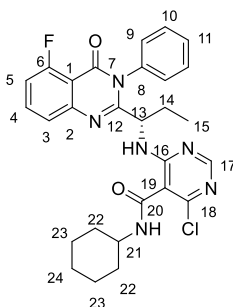
(S)-4-chloro-N-cyclopropyl-6-((1-(5-fluoro-4-oxo-3-phenyl-3,4-dihydroquinazolin-2-yl)propyl)amino)pyrimidine-5-carboxamide (246, 51% yield).



^1H NMR (400 MHz, Methanol- d_4) δ 8.19 (s, 1H, H-17), 7.75 (td, J = 8.2, 5.4 Hz, 1H), 7.63 – 7.42 (m, 6H), 7.13 (ddd, J = 10.9, 8.2, 1.0 Hz, 1H), 4.92 (dd, J = 8.5, 4.2 Hz, 1H), 2.97 (dt, J = 7.3, 3.5 Hz, 1H, H-21), 1.97 (dtt, J = 14.8, 7.4, 3.6 Hz, 1H, H-14), 1.81 – 1.59 (m, 1H, H-14), 0.85 (dd, J = 7.3, 2.0 Hz, 2H, H-22), 0.81 (t, J = 7.4 Hz, 3H, H-15), 0.68 (td, J = 3.6, 1.8 Hz, 2H, H-22). ^{13}C NMR (101 MHz, Methanol- d_4) δ 165.69 (C-20), 162.39, 159.81, 159.46 (d, J = 4.2 Hz), 157.69, 157.27 (C-17), 154.83, 149.03, 135.75, 135.21 (d, J = 10.7 Hz, C-4), 129.57, 129.37 (d, J = 2.0 Hz), 128.98 (d, J = 3.8 Hz), 123.02 (d, J = 4.2 Hz), 113.28 (d, J = 20.7 Hz, C-3), 111.88, 110.20 (d, J = 6.0 Hz, C-5), 53.64 (C-13), 26.31 (C-14), 22.56 (C-21), 9.30 (C-15), 5.19 (C-22). LCMS m/z calc. for $\text{C}_{25}\text{H}_{22}\text{ClFN}_6\text{O}_2$ $[\text{M}+\text{H}]^+$: 493.2, found 493.1 with t_R 2.99 min (98%).

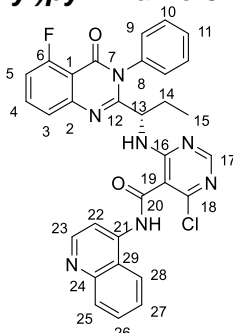
References

(S)-4-chloro-N-cyclohexyl-6-((1-(5-fluoro-4-oxo-3-phenyl-3,4-dihydroquinazolin-2-yl)propyl)amino)pyrimidine-5-carboxamide (247, 72% yield).



^1H NMR (400 MHz, Methanol- d_4) δ 8.21 (s, 1H, H-17), 7.82 (td, J = 8.2, 5.4 Hz, 1H), 7.70 – 7.45 (m, 6H), 7.22 (ddd, J = 10.8, 8.3, 1.0 Hz, 1H), 4.93 (dd, J = 8.5, 4.2 Hz, NH), 3.95 (m, 1 H, H-21), 2.09 – 1.92 (m, 4H, H-22), 1.79 – 1.71 (m, 2H, H-24), 1.59 – 1.34 (m, 4H, H-14/23), 0.81 (t, J = 7.4 Hz, 3H, H-15). ^{13}C NMR (101 MHz, Methanol- d_4) δ 163.26, 162.51, 159.88, 159.70, 159.57, 157.71, 157.11 (C-17), 154.58, 149.08, 135.74, 135.23 (d, J = 10.6 Hz, C-4), 129.57, 129.37 (d, J = 7.7 Hz), 128.88 (d, J = 8.4 Hz), 123.00 (d, J = 4.2 Hz), 113.27 (d, J = 20.9 Hz, C-3), 112.50, 110.21 (d, J = 6.1 Hz, C-5), 53.48 (C-13), 49.09 (C-21), 31.96 (d, J = 5.0 Hz, C-22), 26.32 (C-14), 24.63 (C-24), 23.02 (C-23), 9.05 (C-15). LCMS m/z calc. for $\text{C}_{28}\text{H}_{28}\text{ClFN}_6\text{O}_2$ $[\text{M}+\text{H}]^+$: 535.2, found 536.3 with t_R 3.08 min (94%).

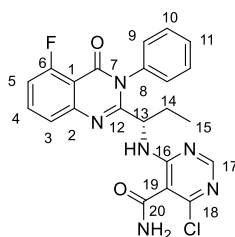
(S)-4-chloro-6-((1-(5-fluoro-4-oxo-3-phenyl-3,4-dihydroquinazolin-2-yl)propyl)amino)-N-(quinolin-4-yl)pyrimidine-5-carboxamide (248, 69% yield).



^1H NMR (400 MHz, Methanol- d_4) δ 8.82 (s, 1H, H-17), 8.33 (d, J = 34.3 Hz, 3H), 8.14 – 7.96 (m, 1H), 7.91 – 7.25 (m, 8H), 7.10 (s, 1H), 6.44 (d, J = 59.5 Hz, 1H, H-22), 1.87 (d, J = 66.2 Hz, 2H, H-14), 0.80 (t, J = 7.4 Hz, 3H, H-15). ^{13}C NMR (101 MHz, Methanol- d_4) δ 163.69 (C-20), 159.80, 157.87, 157.60 (C-17), 155.29, 150.21 (C-23), 148.98, 148.22, 141.69, 140.55, 137.99, 135.74, 135.07 (d, J = 10.5 Hz, C-4), 129.80, 129.49, 129.32 (d, J = 1.8 Hz), 129.05, 128.89, 128.39, 126.53, 122.88, 121.54, 121.18, 119.32, 113.16 (d, J = 21.0 Hz, C-3), 112.64, 112.27, 110.17 (d, J = 5.7 Hz, C-5), 107.42 (C-22), 54.23 (C-13), 26.03 (C-14), 9.61 (C-15). LCMS m/z calc. for $\text{C}_{31}\text{H}_{23}\text{ClFN}_7\text{O}_2$ $[\text{M}+\text{H}]^+$: 580.2, found 579.4 with t_R 2.71 min (99%).

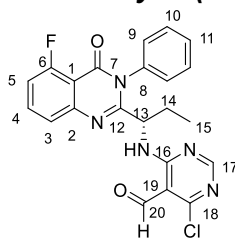
(S)-4-chloro-6-((1-(5-fluoro-4-oxo-3-phenyl-3,4-dihydroquinazolin-2-yl)propyl)amino)pyrimidine-5-carboxamide (249, 74% yield).

References



^1H NMR (400 MHz, Methanol- d_4) δ 8.20 (s, 1H, H-17), 7.75 (td, J = 8.2, 5.4 Hz, 1H), 7.65 – 7.44 (m, 5H), 7.15 (ddd, J = 10.8, 8.2, 1.1 Hz, 1H), 4.90 (dd, J = 8.7, 4.2 Hz, NH), 1.98 (dq, J = 14.8, 7.4, 4.2 Hz, 1H, H-14), 1.77 (ddd, J = 14.0, 8.5, 7.1 Hz, 1H, H-14), 0.82 (t, J = 7.4 Hz, 3H, H-15). ^{13}C NMR (101 MHz, Methanol- d_4) δ 166.78 (C-20), 162.41, 159.99, 159.78, 159.58 (d, J = 4.2 Hz), 157.80, 157.18 (C-17), 154.71, 149.09, 135.78, 135.17 (d, J = 10.5 Hz, C-4), 129.54, 129.34 (d, J = 1.9 Hz), 128.93 (d, J = 4.1 Hz), 123.01 (d, J = 4.2 Hz), 113.23 (d, J = 20.8 Hz, C-3), 111.37, 110.20 (d, J = 6.0 Hz, C-5), 53.86 (C-13), 26.26 (C-14), 9.32 (C-15). LCMS m/z calc. for $\text{C}_{22}\text{H}_{18}\text{ClFN}_6\text{O}_2$ $[\text{M}+\text{H}]^+$: 453.1, found 453.1 with t_R 2.65 min (96%).

(S)-4-chloro-6-((1-(5-fluoro-4-oxo-3-phenyl-3,4-dihydroquinazolin-2-yl)propyl)amino)pyrimidine-5-carbaldehyde (261, 64% yield).



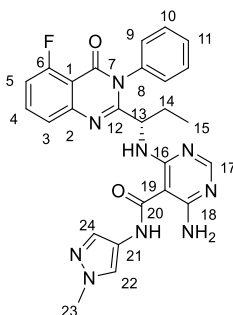
^1H NMR (400 MHz, Methanol- d_4) δ 10.47 – 10.15 (m, 1H, H-20), 8.30 (d, J = 3.2 Hz, 1H, H-17), 7.74 (q, J = 7.0 Hz, 1H), 7.67 – 7.55 (m, 3H), 7.51 (d, J = 9.4 Hz, 3H), 7.15 (d, J = 10.5 Hz, 1H), 5.06 (dd, J = 8.4, 4.3 Hz, NH), 1.56 – 1.41 (m, 1H, H-14), 1.40 – 1.29 (m, 1H, H-14), 0.81 (t, J = 7.4 Hz, 3H, H-15). ^{13}C NMR (101 MHz, Methanol- d_4) δ 191.00 (C-20), 164.65, 162.46, 160.22 (C-17), 157.10, 149.01, 135.55 (d, J = 42.5 Hz, C-4), 129.68, 129.45 (d, J = 7.7 Hz), 129.01, 128.72, 123.09, 113.36 (d, J = 20.7 Hz, C-3), 110.25 (d, J = 6.1 Hz, C-5), 108.09, 53.43 (C-13), 26.66 (C-14), 8.96 (C-15). LCMS m/z calc. for $\text{C}_{22}\text{H}_{17}\text{ClFN}_5\text{O}_2$ $[\text{M}+\text{H}]^+$: 438.1, found 438.3 with t_R 3.01 min (96%).

General procedure for the Cu-catalyzed amination of monochloro pyrimidine derivatives. To a solution of the monochloropyrimidine derivatives (**240- 249** and **261**) (0.187 mmol, 1 equiv) in N-methylpyrrolidinone (0.4 mL) was added Cu_2O (0.0187 mmol, 0.1 equiv) and ammonium hydroxide solution (29% NH_3 , 0.4 mL). The reaction mixture was placed in a microwave oven and heated to 40°C for 30 minutes. The solvent was evaporated and the crude residue was purified using silica gel chromatography (DCM/ ethyl acetate: 10: 90) to yield the aminopyrimidines (**210-**

References

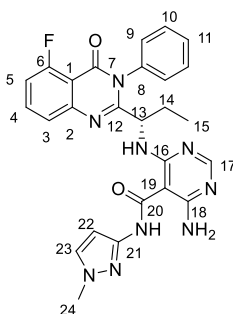
220 and **222**). Lactam side products (**250- 255** and **258**) were formed as side products during the synthesis of the desired aminopyrimidine products.

(S)-4-amino-6-((1-(5-fluoro-4-oxo-3-phenyl-3,4-dihydroquinazolin-2-yl)propyl)amino)-N-(1-methyl-1H-pyrazol-4-yl)pyrimidine-5-carboxamide (210, 39% yield).



^1H NMR (400 MHz, DMSO- d_6) δ 10.14 (s, NH), 7.97 (s, 1H, H-17), 7.88 (s, 1H, H-24), 7.80 (td, $J = 8.1, 5.4$ Hz, 1H), 7.65 – 7.51 (m, 6H), 7.47 (s, 1H, H-22), 7.39 (d, $J = 8.2$ Hz, 1H), 7.28 (dd, $J = 11.0, 8.1$ Hz, 1H), 6.64 (s, NH₂), 4.61 (ddd, $J = 16.5, 7.1, 4.4$ Hz, NH), 3.83 (s, 3H, H-23), 1.93 – 1.79 (m, 1H, H-14), 1.60 (dt, $J = 14.6, 7.5$ Hz, 1H, H-14), 0.72 (t, $J = 7.3$ Hz, 3H, H-15). ^{13}C NMR (101 MHz, DMSO- d_6) δ 163.90, 162.32, 161.07, 159.99, 159.85, 158.80, 158.00, 149.44, 136.52, 135.90, 130.85, 129.87, 129.69, 129.58, 123.44, 122.08 (d, $J = 39.9$ Hz), 113.45, 110.73, 91.74, 53.72 (C-13), 39.10 (C-23), 26.83 (C-14), 10.82 (C-15). LCMS m/z calc. for C₂₆H₂₄FN₉O₂ [M+H]⁺: 514.2, found 514.4 with t_R 2.50 min (95%).

(S)-4-amino-6-((1-(5-fluoro-4-oxo-3-phenyl-3,4-dihydroquinazolin-2-yl)propyl)amino)-N-(1-methyl-1H-pyrazol-3-yl)pyrimidine-5-carboxamide (211, 31 % yield).

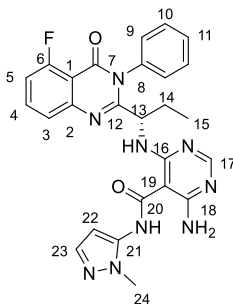


^1H NMR (400 MHz, Methanol- d_4) δ 7.93 (s, 1H, H-17), 7.75 (td, $J = 8.2, 5.4$ Hz, 1H), 7.67 – 7.58 (m, 4H), 7.55 (s, 1H), 7.53 (d, $J = 2.4$ Hz, 1H), 7.49 – 7.44 (m, 1H), 7.18 (ddd, $J = 10.9, 8.2, 1.0$ Hz, 1H), 6.67 (d, $J = 2.3$ Hz, 1H, H-22), 1.92 (ddq, $J = 15.0, 7.6, 3.8$ Hz, 1H, H-14), 1.72 (ddd, $J = 14.3, 8.8, 7.2$ Hz, 1H, H-14), 0.82 (t, $J = 7.4$ Hz, 3H, H-15). ^{13}C NMR (101 MHz, Methanol- d_4) δ 165.09, 162.47, 161.24, 160.27, 159.84, 159.68 (d, $J = 4.2$ Hz), 159.49, 157.68 (C-17), 149.18, 146.50, 135.86, 135.08 (d, $J = 10.5$ Hz, C-4), 131.14, 129.54, 129.26 (d, $J = 15.7$ Hz), 128.85 (d, $J = 15.3$ Hz), 122.94 (d, $J = 4.2$ Hz), 113.03 (d, $J = 21.0$ Hz, C-3), 110.12 (d, $J = 6.1$ Hz,

References

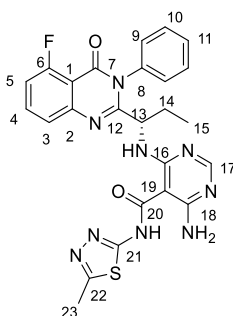
C-5), 97.91, 54.20 (C-13), 37.48 (C-24), 26.38 (C-14), 9.44 (C-15). LCMS m/z calc. for $C_{26}H_{24}FN_9O_2$ $[M+H]^+$: 514.2, found 513.8 with t_R 2.40 min (97%).

(S)-4-amino-6-((1-(5-fluoro-4-oxo-3-phenyl-3,4-dihydroquinazolin-2-yl)propyl)amino)-N-(1-methyl-1H-pyrazol-5-yl)pyrimidine-5-carboxamide. (212, 20% yield).



1H NMR (400 MHz, Methanol- d_4) δ 7.98 (d, J = 16.9 Hz, 1H, H-23), 7.68 – 7.52 (m, 5H), 7.50 – 7.35 (m, 3H), 7.21 (dd, J = 10.8, 8.2 Hz, 1H), 6.46 (d, J = 1.8 Hz, 1H, H-22), 3.82 (s, 3H, H-24), 2.05 – 1.90 (m, 1H, H-14), 1.74 (dt, J = 14.6, 7.5 Hz, 1H, H-14), 0.84 (t, J = 7.4 Hz, 3H, H-15). ^{13}C NMR (101 MHz, Methanol- d_4) δ 135.89, 129.51, 129.21, 128.82, 53.85 (C-13), 26.56 (C-14), 9.32 (C-15). LCMS m/z calc. for $C_{26}H_{24}FN_9O_2$ $[M+H]^+$: 514.2, found 513.8 with t_R 2.45 min (94%).

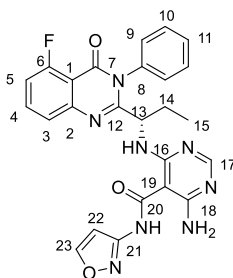
(S)-4-amino-6-((1-(5-fluoro-4-oxo-3-phenyl-3,4-dihydroquinazolin-2-yl)propyl)amino)-N-(5-methyl-1,3,4-thiadiazol-2-yl)pyrimidine-5-carboxamide (214, 37 % yield).



1H NMR (400 MHz, Methanol- d_4) δ 7.84 (s, 1H, H-17), 7.78 (td, J = 8.3, 5.4 Hz, 1H), 7.60 (td, J = 13.4, 11.6, 5.2 Hz, 5H), 7.50 – 7.41 (m, 1H), 7.20 (dd, J = 10.9, 8.2 Hz, 1H), 4.83 (dd, J = 9.0, 4.2 Hz, NH), 2.59 (s, 3H, H-23), 2.03 (ddd, J = 14.3, 7.4, 4.3 Hz, 1H, H-14), 1.88 (ddd, J = 14.1, 8.9, 7.2 Hz, 1H, H-14), 0.89 (t, J = 7.3 Hz, 3H, H-15). ^{13}C NMR (101 MHz, Methanol- d_4) δ 161.93 (C-20), 159.89, 159.50, 157.10, 149.43, 136.06, 135.16 (d, J = 10.3 Hz, C-4), 129.36, 129.19 (d, J = 5.2 Hz), 129.06, 128.67, 122.84 (d, J = 4.2 Hz), 112.97 (d, J = 20.7 Hz, C-3), 110.15 (d, J = 6.2 Hz, C-5), 89.99 (C-19), 54.38 (C-13), 26.57 (C-14), 14.46 (C-23), 9.79 (C-15). LCMS m/z calc. for $C_{25}H_{22}FN_9O_2S$ $[M+H]^+$: 532.2, found 531.8 with t_R 2.40 min (99%).

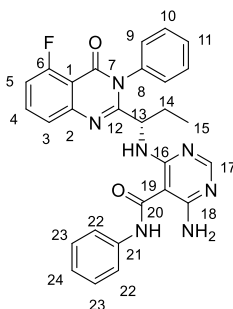
(S)-4-amino-6-((1-(5-fluoro-4-oxo-3-phenyl-3,4-dihydroquinazolin-2-yl)propyl)amino)-N-(isoxazol-3-yl)pyrimidine-5-carboxamide (215, 12% yield).

References



^1H NMR (400 MHz, Methanol- d_4) δ 7.85 – 7.75 (m, 1H), 7.73 (s, 1H, H-17), 7.60 (d, J = 10.6 Hz, 1H), 7.56 (d, J = 2.9 Hz, 5H), 7.43 (d, J = 7.8 Hz, 1H), 7.21 (dd, J = 11.0, 8.0 Hz, 2H), 6.85 (s, NH₂), 2.04 (dt, J = 13.6, 6.8 Hz, 1H, H-14), 1.87 (dt, J = 13.9, 7.5 Hz, 1H, H-14), 0.91 (t, J = 7.3 Hz, 3H, H-15). ^{13}C NMR (101 MHz, Methanol- d_4) δ 167.92, 161.22, 160.41, 157.59, 149.24, 135.89, 135.26, 132.18, 130.99, 129.50, 129.30, 129.19, 128.83, 128.45, 122.76, 113.17, 53.86 (C-13), 26.52 (C-14), 10.01 (C-15). LCMS m/z calc. for $\text{C}_{25}\text{H}_{21}\text{FN}_8\text{O}_3$ $[\text{M}+\text{H}]^+$: 501.2, found 500.1 with t_R 1.85 min (92%).

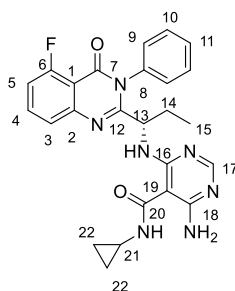
(S)-4-amino-6-((1-(5-fluoro-4-oxo-3-phenyl-3,4-dihydroquinazolin-2-yl)propyl)amino)-N-phenylpyrimidine-5-carboxamide (216, 57% yield).



^1H NMR (400 MHz, Methanol- d_4) δ 7.68 (d, J = 7.9 Hz, 3H), 7.61 (q, J = 9.4, 8.2 Hz, 4H), 7.46 (d, J = 7.3 Hz, 1H), 7.34 (q, J = 8.8, 8.2 Hz, 3H), 7.15 (q, J = 7.5 Hz, 2H), 4.85 (d, J = 3.7 Hz, 1H), 1.92 (ddq, J = 12.0, 8.4, 4.7, 4.2 Hz, 1H, H-14), 1.71 (dq, J = 14.7, 7.4 Hz, 1H, H-14), 0.82 (t, J = 7.3 Hz, 3H, H-15). ^{13}C NMR (101 MHz, Methanol- d_4) δ 162.47 (C-20), 159.97, 159.84, 159.62 (d, J = 4.2 Hz), 159.38, 149.06 (C-17), 138.36, 135.87, 135.14 (d, J = 10.4 Hz, C-4), 129.55, 129.35, 129.20, 128.95, 128.81, 128.47 (C-23), 124.04 (C-24), 122.70 (d, J = 3.9 Hz), 120.29 (C-22), 113.05 (d, J = 20.7 Hz, C-3), 110.12 (d, J = 5.7 Hz, C-5), 53.96 (C-13), 26.50 (C-14), 9.35 (C-15). LCMS m/z calc. for $\text{C}_{28}\text{H}_{24}\text{FN}_7\text{O}_2$ $[\text{M}+\text{H}]^+$: 510.2, found 510.1 with t_R 2.83 min (99%).

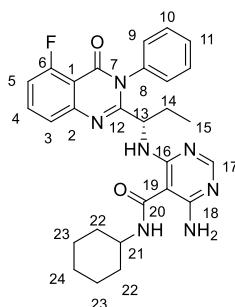
(S)-4-amino-N-cyclopropyl-6-((1-(5-fluoro-4-oxo-3-phenyl-3,4-dihydroquinazolin-2-yl)propyl)amino)pyrimidine-5-carboxamide (217, 23% yield).

References



^1H NMR (400 MHz, Methanol- d_4) δ 7.90 (s, 1H, H-17), 7.81 (td, $J = 8.2, 5.4$ Hz, 1H), 7.68 – 7.52 (m, 6H), 7.45 (dt, $J = 7.4, 1.7$ Hz, 1H), 7.25 – 7.16 (m, 1H), 4.82 (dd, $J = 8.5, 4.1$ Hz, 1H), 2.89 (tt, $J = 7.4, 3.9$ Hz, 1H, H-21), 1.93 (dq, $J = 14.8, 7.5, 4.2$ Hz, 1H, H-14), 1.82 – 1.56 (m, 1H, H-14), 0.89 – 0.74 (m, 5H, H-15/22), 0.72 – 0.65 (m, 2H, H-22). ^{13}C NMR (101 MHz, Methanol- d_4) δ 176.26, 169.28, 162.52, 160.78, 159.85, 159.64 (d, $J = 4.3$ Hz), 159.30, 157.37, 149.20 (C-17), 135.90, 135.23 (d, $J = 10.6$ Hz, C-4), 129.51, 129.27 (d, $J = 12.0$ Hz), 128.85 (d, $J = 2.2$ Hz), 122.72 (d, $J = 4.1$ Hz), 113.09 (d, $J = 20.7$ Hz, C-3), 110.15 (d, $J = 6.1$ Hz, C-5), 53.63 (C-13), 26.59 (C-14), 22.35 (C-21), 9.22 (C-15), 5.31 (d, $J = 11.1$ Hz, C-22). LCMS m/z calc. for $\text{C}_{25}\text{H}_{24}\text{FN}_7\text{O}_2$ $[\text{M}+\text{H}]^+$: 474.2, found 474.1 with t_R 2.34 min (96%).

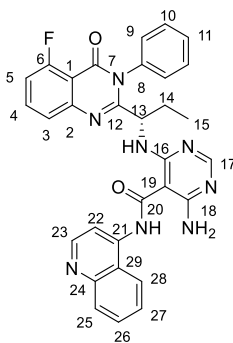
(S)-4-amino-N-cyclohexyl-6-((1-(5-fluoro-4-oxo-3-phenyl-3,4-dihydroquinazolin-2-yl)propyl)amino)pyrimidine-5-carboxamide (218, 18% yield).



^1H NMR (400 MHz, Methanol- d_4) δ 7.82 (d, $J = 5.8$ Hz, 1H, H-17), 7.61 (s, 4H), 7.53 (d, $J = 8.1$ Hz, 1H), 7.46 (d, $J = 7.5$ Hz, 1H), 7.22 (dd, $J = 10.7, 8.1$ Hz, 1H), 3.88 (s, 1H, H-21), 1.82 (d, $J = 12.4$ Hz, 2H, H-14/22), 1.70 (d, $J = 9.6$ Hz, 2H, H-14/22), 1.58 – 1.08 (m, 3H, H-23/24), 0.84 (t, $J = 7.2$ Hz, 3H, H-15). ^{13}C NMR (101 MHz, Methanol- d_4) δ 135.94, 135.20 (d, $J = 10.4$ Hz, C-4), 129.52, 129.34, 129.21, 128.87, 122.73, 113.05 (d, $J = 20.7$ Hz, C-3), 110.20 (d, $J = 6.0$ Hz, C-5), 53.73 (C-13), 48.95 (C-21), 32.36 (C-22), 26.66 (C-14), 25.28 (C-24), 24.85 (C-23), 9.24 (C-15). LCMS m/z calc. for $\text{C}_{28}\text{H}_{30}\text{FN}_7\text{O}_2$ $[\text{M}+\text{H}]^+$: 516.2, found 516.6 with t_R 2.60 min (97%).

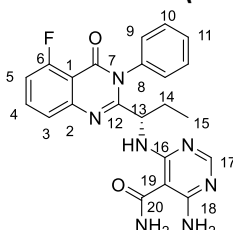
(S)-4-amino-6-((1-(5-fluoro-4-oxo-3-phenyl-3,4-dihydroquinazolin-2-yl)propyl)amino)-N-(quinolin-4-yl)pyrimidine-5-carboxamide (219, 38% yield).

References



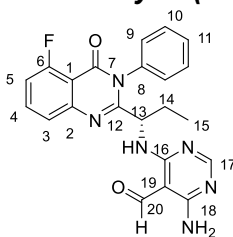
^1H NMR (400 MHz, Methanol- d_4) δ 8.48 – 8.34 (m, 1H), 8.30 (s, 1H, H-17), 7.93 (d, J = 8.7 Hz, 2H), 7.73 (ddd, J = 8.3, 6.8, 1.3 Hz, 1H), 7.68 – 7.51 (m, 4H), 7.51 – 7.35 (m, 3H), 7.23 (d, J = 8.2 Hz, 1H), 7.16 – 7.06 (m, 1H), 2.03 – 1.92 (m, 1H, H-14), 1.88 – 1.66 (m, 1H, H-14), 0.81 (t, J = 7.4 Hz, 3H, H-15). ^{13}C NMR (101 MHz, Methanol- d_4) δ 162.41 (C-20), 159.12 (C-17), 157.88 (d, J = 20.1 Hz), 149.17 (C-23), 148.95, 135.93, 135.68, 135.02 (d, J = 10.4 Hz, C-4), 129.47, 129.28, 129.21, 128.92, 128.82, 126.08 (d, J = 25.7 Hz), 122.68 (d, J = 4.1 Hz), 112.95 (d, J = 20.9 Hz, C-3), 110.08 (d, J = 6.0 Hz, C-5), 54.06 (C-13), 26.54 (C-14), 9.52 (C-15). LCMS m/z calc. for $\text{C}_{31}\text{H}_{25}\text{FN}_8\text{O}_2$ $[\text{M}+\text{H}]^+$: 561.2, found 562.5 with t_R 2.31 min (95%).

(S)-4-amino-6-((1-(5-fluoro-4-oxo-3-phenyl-3,4-dihydroquinazolin-2-yl)propyl)amino)pyrimidine-5-carboxamide (220, 9% yield).



^1H NMR (400 MHz, Methanol- d_4) δ 7.87 – 7.72 (m, 2H), 7.71 – 7.50 (m, 7H), 7.47 (t, J = 10.7 Hz, 1H), 7.22 (dd, J = 10.9, 8.0 Hz, 2H), 2.03 – 1.85 (m, 1H, H-14), 1.72 (dt, J = 14.5, 7.7 Hz, 1H, H-14), 0.83 (t, J = 7.4 Hz, 3H, H-15). ^{13}C NMR (101 MHz, DMSO- d_6) δ 162.32 (C-20), 160.26, 159.73 (d, J = 6.1 Hz), 158.80, 149.43 (C-17), 136.50, 136.40, 135.84 (d, J = 10.8 Hz, C-4), 129.91, 129.70, 129.62 (d, J = 3.8 Hz), 129.46, 123.47, 113.60 (d, J = 20.6 Hz, C-3), 110.75, 53.55 (C-13), 26.92 (C-14), 10.72 (C-15). LCMS m/z calc. for $\text{C}_{22}\text{H}_{20}\text{FN}_7\text{O}_2$ $[\text{M}+\text{H}]^+$: 434.2, found 434.4 with t_R 2.22 min (99%).

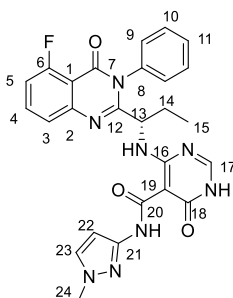
(S)-4-amino-6-((1-(5-fluoro-4-oxo-3-phenyl-3,4-dihydroquinazolin-2-yl)propyl)amino)pyrimidine-5-carbaldehyde (222, 18% yield).



References

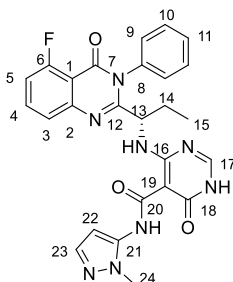
¹H NMR (400 MHz, Methanol-d₄) δ 10.18 (s, 1H, H-20), 7.92 – 7.71 (m, 1H), 7.71 – 7.49 (m, 6H), 7.46 (d, J = 7.3 Hz, 1H), 7.21 (t, J = 9.0 Hz, 1H), 4.97 – 4.91 (m, NH), 1.80 (dt, J = 14.8, 7.4 Hz, 1H, H-14), 1.40 – 1.20 (m, 1H, H-14), 0.84 (t, J = 7.2 Hz, 3H, H-15). ¹³C NMR (101 MHz, Methanol-d₄) δ 158.30, 149.31 (C-17), 135.90, 135.25 (d, J = 10.7 Hz, C-4), 129.49, 129.29 (d, J = 5.2 Hz), 128.87 (d, J = 9.7 Hz), 123.02, 113.12 (d, J = 20.1 Hz, C-3), 110.21 (d, J = 6.1 Hz, C-5), 53.59 (C-13), 26.50 (C-14), 9.32 (C-15). LCMS *m/z* calc. for C₂₂H₁₉FN₆O₂ [M+H]⁺: 419.2, found 419.3 with *t_R* 2.49 min (97%).

(S)-4-((1-(5-fluoro-4-oxo-3-phenyl-3,4-dihydroquinazolin-2-yl)propyl)amino)-N-(1-methyl-1H-pyrazol-3-yl)-6-oxo-1,6-dihydropyrimidine-5-carboxamide (250, 14% yield).



¹H NMR (400 MHz, Methanol-d₄) δ 12.29 (s, NH), 10.84 (d, J = 7.4 Hz, NH), 7.89 (s, 1H, H-17), 7.80 (td, J = 8.2, 5.4 Hz, 1H), 7.67 – 7.61 (m, 2H), 7.60 – 7.56 (m, 2H), 7.55 – 7.50 (m, 1H), 7.47 (dd, J = 7.6, 1.9 Hz, 3H), 7.26 – 7.17 (m, 1H), 6.65 (d, J = 2.3 Hz, 1H, H-22), 4.95 (dq, J = 7.5, 3.9, 3.4 Hz, NH), 2.02 (dd, J = 7.3, 4.3 Hz, 1H, H-14), 1.84 (ddd, J = 14.2, 8.6, 7.1 Hz, 1H, H-14), 0.91 – 0.86 (m, 3H, H-15). ¹³C NMR (101 MHz, Methanol-d₄) δ 165.83, 163.28, 162.64, 162.47, 159.84, 159.78, 158.00, 149.82 (C-17), 149.38, 146.70, 135.98, 135.20 (d, J = 10.6 Hz, C-4), 131.21, 129.49, 129.32 (d, J = 2.8 Hz), 128.84 (d, J = 8.8 Hz), 123.22 (d, J = 4.3 Hz), 113.13 (d, J = 20.7 Hz, C-3), 110.16 (d, J = 6.1 Hz, C-5), 97.25 (C-22), 54.22 (C-13), 37.25 (C-24), 26.89 (C-14), 9.36 (C-15). LCMS *m/z* calc. for C₂₆H₂₃FN₈O₃ [M+H]⁺: 515.2, found 514.9 with *t_R* 2.75 min (93%).

(S)-4-((1-(5-fluoro-4-oxo-3-phenyl-3,4-dihydroquinazolin-2-yl)propyl)amino)-N-(1-methyl-1H-pyrazol-5-yl)-6-oxo-1,6-dihydropyrimidine-5-carboxamide (251, 26% yield).

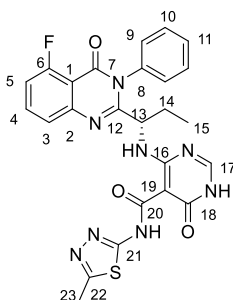


¹H NMR (400 MHz, Methanol-d₄) δ 10.72 (d, J = 7.4 Hz, NH), 7.94 (s, 1H, H-17), 7.81 (td, J = 8.2, 5.4 Hz, 1H, H-23), 7.67 – 7.58 (m, 4H), 7.55 – 7.45 (m, 2H), 7.41

References

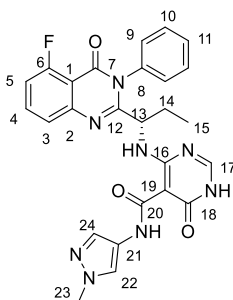
(d, $J = 2.0$ Hz, 1H), 7.22 (dd, $J = 10.9, 8.2$ Hz, 1H), 6.53 (d, $J = 2.0$ Hz, 1H, H-22), 4.97 (dq, $J = 7.5, 3.9, 3.4$ Hz, NH), 3.81 (s, 3H, H-24), 2.04 (ddq, $J = 14.0, 10.8, 7.1, 6.6$ Hz, 1H, H-14), 1.83 (dp, $J = 15.2, 7.5$ Hz, 1H, H-14), 0.88 (t, $J = 7.3$ Hz, 3H, H-15). ^{13}C NMR (101 MHz, Methanol- d_4) δ 163.10, 150.16, 149.33, 137.90, 135.96, 135.28 (d, $J = 10.7$ Hz, C-4), 129.53, 129.35, 128.84, 123.17, 113.28 (d, $J = 20.8$ Hz, C-3), 97.00 (C-19), 89.54 (C-22), 54.20 (C-13), 34.03 (C-24), 26.91 (C-14), 9.26 (C-15). LCMS m/z calc. for $\text{C}_{26}\text{H}_{23}\text{FN}_8\text{O}_3$ $[\text{M}+\text{H}]^+$: 515.2, found 513.8 with t_R 2.45 min (98%).

(S)-4-((1-(5-fluoro-4-oxo-3-phenyl-3,4-dihydroquinazolin-2-yl)propyl)amino)-N-(5-methyl-1,3,4-thiadiazol-2-yl)-6-oxo-1,6-dihydropyrimidine-5-carboxamide (252, 14% yield).



^1H NMR (400 MHz, Methanol- d_4) δ 7.97 (s, 1H, H-17), 7.87 – 7.71 (m, 2H), 7.70 – 7.57 (m, 5H), 7.56 – 7.38 (m, 4H), 7.27 – 7.16 (m, 2H), 5.00 (dd, $J = 8.6, 4.2$ Hz, NH), 2.71 (s, 3H, H-23), 2.05 (ddd, $J = 14.4, 7.4, 4.1$ Hz, 1H, H-14), 1.89 – 1.76 (m, 1H, H-14), 0.88 (t, $J = 7.4$ Hz, 3H, H-15). ^{13}C NMR (101 MHz, Methanol- d_4) δ 163.10, 150.16, 149.33, 137.90, 135.96, , 135.28 (d, $J = 10.3$ Hz, C-4) 129.53, 129.35, 128.84, 123.17, 113.28 (d, $J = 20.7$ Hz, C-3), 97.00, 89.54, 54.20 (C-13), 26.91 (C-14), 17.15 (C-23), 9.26 (C-15). LCMS m/z calc. for $\text{C}_{25}\text{H}_{21}\text{FN}_8\text{O}_3\text{S}$ $[\text{M}+\text{H}]^+$: 533.1, found 532.8 with t_R 2.79 min (94%).

(S)-4-((1-(5-fluoro-4-oxo-3-phenyl-3,4-dihydroquinazolin-2-yl)propyl)amino)-N-(1-methyl-1H-pyrazol-4-yl)-6-oxo-1,6-dihydropyrimidine-5-carboxamide (253, 8% yield).

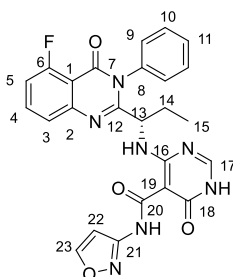


^1H NMR (400 MHz, Methanol- d_4) δ 10.85 (d, $J = 7.3$ Hz, NH), 7.99 (s, 1H, H-17), 7.89 (s, 1H, H-24), 7.81 (td, $J = 8.2, 5.4$ Hz, 1H), 7.66 – 7.56 (m, 5H), 7.50 (ddt, $J = 17.5, 7.7, 1.8$ Hz, 2H), 7.27 – 7.12 (m, 1H), 4.94 (dd, $J = 8.7, 4.3$ Hz, NH), 2.04 (dq, $J = 14.7, 7.4, 4.3$ Hz, 1H, H-14), 1.91 – 1.76 (m, 1H, H-14), 0.89 (t, $J = 7.4$ Hz, 3H, H-15). ^{13}C NMR (101 MHz, Methanol- d_4) δ 165.46 (C-18), 163.12 (C-20), 162.61,

References

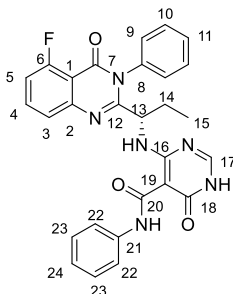
162.48, 159.85, 159.74, 158.04, 149.64, 149.39, 135.99, 135.20 (d, $J = 10.6$ Hz, C-4), 130.43, 129.48, 129.32 (d, $J = 3.6$ Hz), 128.84 (d, $J = 8.6$ Hz), 123.21 (d, $J = 4.3$ Hz), 122.35, 121.09, 113.14 (d, $J = 20.9$ Hz, C-3), 110.21 (d, $J = 6.1$ Hz, C-5), 89.75 (C-19), 54.20 (C-13), 37.69 (C-23), 26.87 (C-14), 9.35 (C-15). LCMS m/z calc. for $C_{26}H_{23}FN_8O_3$ $[M+H]^+$: 515.2, found 515.1 with t_R 2.80 min (96%).

(S)-4-((1-(5-fluoro-4-oxo-3-phenyl-3,4-dihydroquinazolin-2-yl)propyl)amino)-N-(isoxazol-3-yl)-6-oxo-1,6-dihydropyrimidine-5-carboxamide (254, 7% yield, NMR purity 97%).



1H NMR (400 MHz, Methanol- d_4) δ 10.71 (d, $J = 7.4$ Hz, NH), 8.55 (d, $J = 1.7$ Hz, 1H, H-23), 7.93 (s, 1H, H-17), 7.81 (td, $J = 8.3, 5.4$ Hz, 1H), 7.70 – 7.56 (m, 5H), 7.55 – 7.43 (m, 2H), 7.23 (dd, $J = 10.9, 8.2$ Hz, 1H), 7.10 (d, $J = 1.7$ Hz, 1H, H-22), 4.98 (dq, $J = 7.3, 4.1$ Hz, NH), 2.12 – 1.97 (m, 1H, H-14), 1.95 – 1.75 (m, 1H, H-14), 0.88 (t, $J = 7.4$ Hz, 3H, H-15). LCMS m/z calc. for $C_{25}H_{20}FN_7O_4$ $[M+H]^+$: 502.2, found 502.1 with t_R 3.04 min (97%).

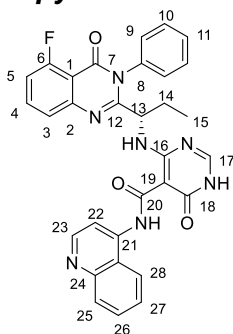
(S)-4-((1-(5-fluoro-4-oxo-3-phenyl-3,4-dihydroquinazolin-2-yl)propyl)amino)-6-oxo-N-phenyl-1,6-dihydropyrimidine-5-carboxamide (255, 6% yield).



1H NMR (400 MHz, Methanol- d_4) δ 7.89 (s, 1H, H-17), 7.80 (td, $J = 8.0, 5.2$ Hz, 1H), 7.62 (p, $J = 8.3, 7.6$ Hz, 6H), 7.53 (d, $J = 7.1$ Hz, 1H), 7.47 (dd, $J = 7.3, 1.9$ Hz, 1H), 7.34 (t, $J = 7.6$ Hz, 2H), 7.21 (dd, $J = 10.8, 8.1$ Hz, 1H), 7.10 (t, $J = 7.2$ Hz, 1H), 4.94 (dd, $J = 8.7, 4.1$ Hz, NH), 2.03 (ddq, $J = 12.0, 8.4, 4.7, 4.2$ Hz, 1H, H-14), 1.84 (dp, $J = 14.4, 7.1$ Hz, 1H, H-14), 0.89 (t, $J = 7.3$ Hz, 3H, H-15). ^{13}C NMR (101 MHz, Methanol- d_4) δ 166.57 (C-18), 163.29, 162.78, 162.47, 158.07, 149.39, 138.29, 136.00, 135.20 (d, $J = 10.4$ Hz), 129.50, 129.32 (d, $J = 2.2$ Hz), 128.85 (d, $J = 7.3$ Hz), 128.52 (C-23), 123.53 (C-24), 123.21, 120.16 (C-22), 113.12 (d, $J = 21.0$ Hz), 110.12 (d, $J = 5.7$ Hz, C-5), 54.28 (C-13), 26.89 (C-14), 9.36 (C-15). LCMS m/z calc. for $C_{28}H_{23}FN_6O_3$ $[M+H]^+$: 511.2, found 511.1 with t_R 3.36 min (99%).

References

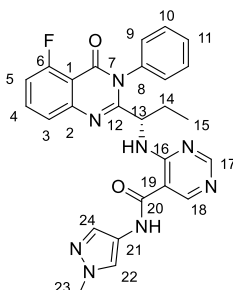
(S)-4-((1-(5-fluoro-4-oxo-3-phenyl-3,4-dihydroquinazolin-2-yl)propyl)amino)-6-oxo-N-(quinolin-4-yl)-1,6-dihydropyrimidine-5-carboxamide (258, 12% yield).



^1H NMR (400 MHz, DMSO- d_6) δ 12.60 (s, NH), 10.80 (d, J = 7.5 Hz, NH), 8.54 (s, 1H), 8.21 (d, J = 8.3 Hz, 1H, H-23), 8.15 (s, 1H, H-17), 8.05 (s, NH), 7.93 – 7.76 (m, 2H), 7.74 – 7.64 (m, 1H), 7.59 (td, J = 8.6, 7.1, 3.8 Hz, 6H), 7.43 – 7.29 (m, 1H), 2.08 – 1.83 (m, 1H, H-14), 1.73 (dt, J = 14.6, 7.5 Hz, 1H, H-14), 0.80 (t, J = 7.3 Hz, 3H, H-15). ^{13}C NMR (101 MHz, DMSO- d_6) δ 167.54 (C-18), 163.50 (C-20), 163.26, 162.31, 161.66, 159.69, 158.74 (d, J = 4.2 Hz), 158.09 (C-17), 151.67, 149.33, 140.16, 139.09, 136.45, 135.95 (d, J = 10.7 Hz, C-4), 130.09, 129.83 (d, J = 4.8 Hz), 129.67, 129.55, 127.07, 123.80, 120.94, 120.02, 113.87 (d, J = 20.3 Hz, C-3), 110.85 (d, J = 5.6 Hz, C-5), 105.75 (C-22), 54.02 (C-13), 27.31 (C-14), 10.45 (C-15). LCMS m/z calc. for $\text{C}_{31}\text{H}_{24}\text{FN}_7\text{O}_3$ $[\text{M}+\text{H}]^+$: 562.2, found 563.1 with t_R 2.37 min (90%).

General procedure for Zn-catalyzed hydrodechlorination of monochloropyrimidine derivatives. To a solution of the monochloropyrimidine derivatives (**240** and **241**) (0.170 mmol, 1 equiv) in THF (1 mL) was added zinc dust (1.70 mmol, 10 equiv) and acetic acid (1.70 mmol, 10 equiv). The reaction mixture was stirred at reflux for 3 h at which time it was concentrated under reduced pressure. The crude residue was purified by flash chromatography (DCM/ methanol (containing 0.7 N ammonia: 99/1) to afford the dechlorinated products (**226** and **227**) as a white solid.

(S)-4-((1-(5-fluoro-4-oxo-3-phenyl-3,4-dihydroquinazolin-2-yl)propyl)amino)-N-(1-methyl-1H-pyrazol-4-yl)pyrimidine-5-carboxamide (226, 54% yield).

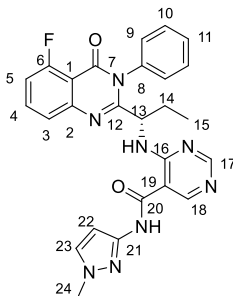


^1H NMR (400 MHz, Methanol- d_4) δ 8.68 (s, 1H, H-17), 8.45 (s, 1H, H-18), 8.07 (s, 1H, H-24), 7.79 (td, J = 8.2, 5.4 Hz, 1H), 7.72 – 7.53 (m, 6H), 7.48 (dd, J = 7.7, 1.9 Hz, 1H), 7.20 (ddd, J = 10.9, 8.2, 1.0 Hz, 1H), 4.94 (dd, J = 8.6, 4.3 Hz, NH), 3.77 – 3.49 (m, 1H, H-13), 2.13 – 2.02 (m, 1H, H-14), 1.83 (ddd, J = 14.1, 8.5, 7.1 Hz, 1H,

References

H-14), 0.88 (t, $J = 7.4$ Hz, 3H, H-15) ^{13}C NMR (101 MHz, Methanol- d_4) δ 163.57, 162.49, 160.00, 159.71 (d, $J = 4.2$ Hz), 158.87 (C-18), 158.10, 153.15 (C-17), 149.27, 135.95, 135.19 (d, $J = 10.6$ Hz, C-4), 130.49, 129.51, 129.33 (d, $J = 2.2$ Hz), 128.86 (d, $J = 9.5$ Hz), 123.04 (d, $J = 4.2$ Hz), 122.63, 121.21, 113.16 (d, $J = 20.8$ Hz, C-3), 110.21 (d, $J = 6.1$ Hz, C-5), 108.80 (C-22), 53.34 (C-13), 37.77 (C-23), 26.54 (C-14), 9.31 (C-15). LCMS m/z calc. for $\text{C}_{26}\text{H}_{23}\text{FN}_8\text{O}_2$ $[\text{M}+\text{H}]^+$: 499.2, found 499.1 with t_R 2.70 min (99%).

(S)-4-((1-(5-fluoro-4-oxo-3-phenyl-3,4-dihydroquinazolin-2-yl)propyl)amino)-N-(1-methyl-1H-pyrazol-3-yl)pyrimidine-5-carboxamide (227, 33% yield).



^1H NMR (400 MHz, Methanol- d_4) δ 8.71 (s, 1H, H-17), 8.45 (s, 1H, H-18), 7.78 (td, $J = 8.2, 5.4$ Hz, 1H), 7.67 – 7.54 (m, 5H), 7.52 (d, $J = 2.3$ Hz, 1H), 7.48 (dd, $J = 7.7, 1.9$ Hz, 1H), 7.20 (ddd, $J = 11.0, 8.2, 1.0$ Hz, 1H), 6.62 (d, $J = 2.3$ Hz, 1H, H-22), 4.95 (dd, $J = 8.6, 4.3$ Hz, NH), 2.10 – 2.02 (m, 1H, H-14), 1.90 – 1.73 (m, 1H, H-14), 0.87 (t, $J = 7.4$ Hz, 3H, H-15). ^{13}C NMR (101 MHz, Methanol- d_4) δ 164.57, 162.48 (C-20), 160.04, 160.00 – 159.58 (m), 159.00 (C-17), 158.03, 153.72 (C-18), 149.26, 146.26, 135.94, 135.18 (d, $J = 10.4$ Hz, C-4), 131.10, 129.53, 129.33 (d, $J = 2.8$ Hz), 128.86 (d, $J = 7.5$ Hz), 123.06 (d, $J = 4.2$ Hz), 113.15 (d, $J = 20.8$ Hz, C-3), 110.22 (d, $J = 6.0$ Hz, C-5), 108.81, 98.03 (C-22), 53.31 (C-13), 37.50 (C-24), 26.54 (C-14), 9.29 (C-15). LCMS m/z calc. for $\text{C}_{26}\text{H}_{23}\text{FN}_8\text{O}_2$ $[\text{M}+\text{H}]^+$: 499.2, found 499.1 with t_R 2.74 min (97%).

7.4 Pharmacology

A total of 92 compounds were screened in this thesis and of these, a total 70 compounds were screened by GSK using a homogenous time-resolved fluorescence (HTRF) assay. The remaining 22 compounds were tested by our group (1 μM final assay concentration) and Monash university (500 nM final assay concentration and IC_{50} determination) using ADP-Glo kinase assay. This chapter will discuss the two above-mentioned assays, with ADP-Glo kinase assay described in more details since it was developed by our group.

7.4.1 ADP-Glo assay

7.4.1.1 Principle

As it was mentioned in Chapter 1, PI3Ks catalyses the transfer of phosphate group from ATP to the 3 position hydroxyl group of the inositol ring of PI(4,5)P₂ to generate PI(3,4,5)P₃ which plays a central role in the regulation of various physiological process including cell growth, proliferation and motility (Figure 1 in Chapter 1)^{403–405}.

The principle of ADP-Glo assay relies on the formation of adenosine diphosphate (ADP) by transferring a phosphate group from adenosine triphosphate (ATP) to PI(4,5)P₂ (Figure 143), which is mediated by PI3K. Then, the ADP-Glo reagent is added to stop the kinase reaction and deplete the residual ATP, leaving only ADP. Finally, the kinase detection reagent is added to convert ADP to ATP (Figure 143), which is in a coupled reaction with luciferase/luciferin, is converted into light (Scheme 32), where the amount of light generated is directly proportional to the ADP produced and the activity of kinase^{406,407}.

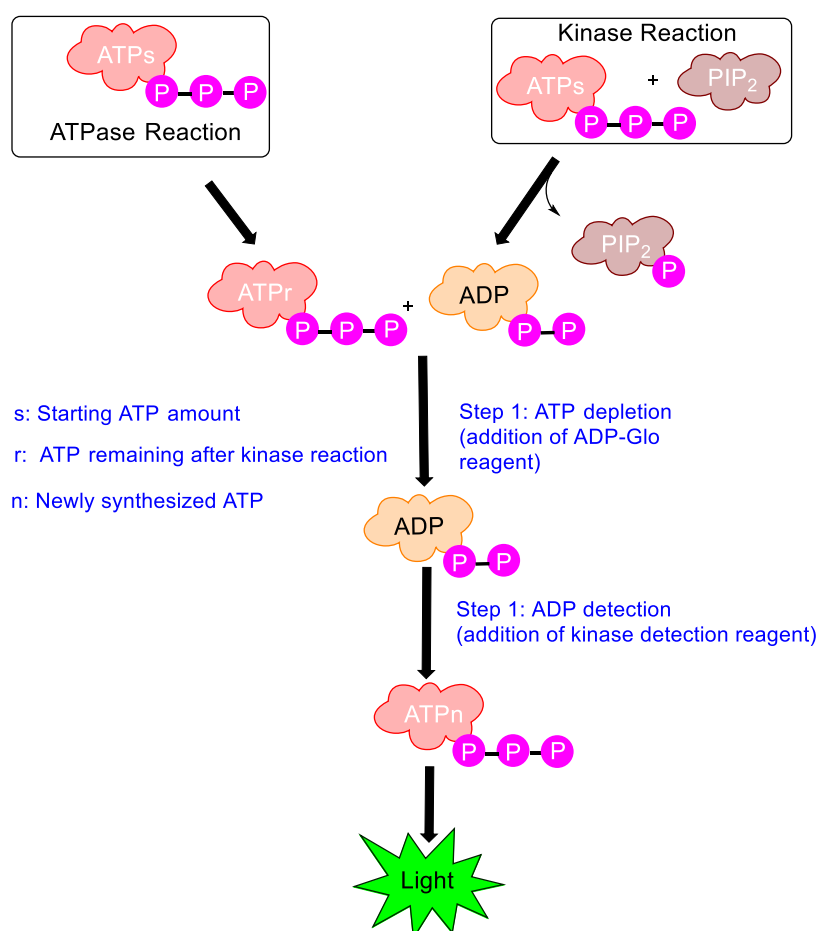
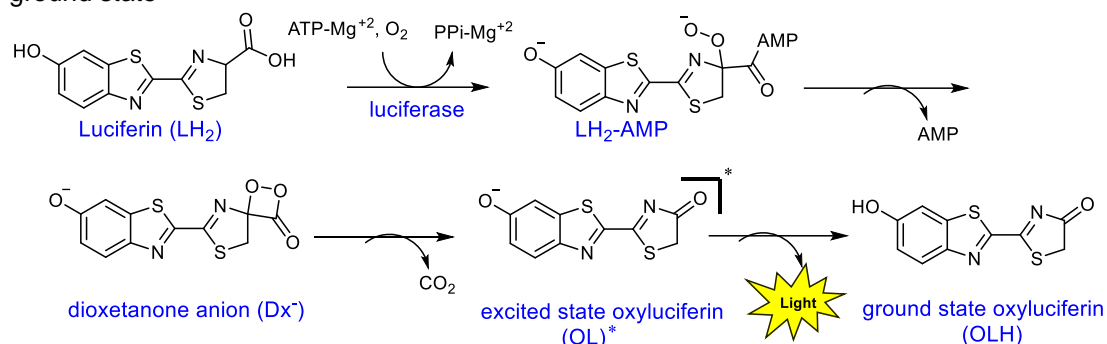


Figure 143. Principle of ADP-Glo assay. The assay is composed of 2 steps: after the kinase or ATPase reaction. In the first step, the ADP-Glo reagent that terminates the kinase reaction and depletes the remaining ATP is added. Then, kinase detection reagent is added to convert ADP to ATP and simultaneously converts the generated ATP into light with the help of a luciferase/luciferin reaction⁴⁰⁶.

References

Scheme 32. Mechanism of bioluminescence in ADP-Glo kinase assay. Luciferase catalyses the oxidation of luciferin to electronically excited oxyluciferin in the presence of ATP and oxygen. The excited oxyluciferin then releases energy in the form of light, as it returns to the ground state



7.4.1.2 Comparison of ADP-Glo to other lipid kinase assays

ADP-Glo assay offers many advantages compared to other 3 kinase assays: radiometric antibody-based ADP detection assay, HTRF assay and antibody-based ADP detection assay^{407,408}.

Robust: it remains unaffected by small variations in method parameters and environmental factors⁴⁰⁶⁻⁴⁰⁸.

Highly sensitive: very low amount of enzymes are needed^{406,409}.

Cost effective and safe: antibodies or radioactive nucleotides are not required; thus, it can be performed by person with no radiation training or license in any research lab and with no concern about the quality of the antibodies⁴¹⁰.

Universal: it is applicable for all classes of kinases⁴¹¹.

Flexible: the assay can be conducted over a wide range of ATP concentration (up to 1 mM), thus AD-Glo assay can distinguish between ATP competitive and non-competitive inhibitors of PI3Ks^{406,407}.

7.4.1.3 Single-concentration screening

Using the ADP-Glo luminescent assay, the compounds in Chapter 5 were tested for inhibition of PI3K δ at 1 μ M and 500 nM final compound concentrations. Screening at 1 μ M single-concentration was carried out by our group, whereas the assay at 500 nM was performed by the Monash university.

7.4.1.3.1 Primary screening (1 μ M)

14 Compounds (**4**, **8**, **72**, **125** and **127** in Chapter 3) and (**211**, **212**, **214**, **241-243** and **250-252** in Chapter 5) were initially tested at a single concentration (1 μ M) for their PI3K δ inhibitory activity and idelalisib (**8**) was used as the positive control. In this assay, all reactions were conducted at RT. Inhibitor (in DMSO), lipid substrate

References

PI(4,5)P₂ (in water and lipid dilution buffer) and enzyme (in PI3K reaction buffer) were pre-incubated for 10 minutes, to allow inhibitor binding to kinase. The kinase reaction was initiated by addition of ATP, following incubation of 40 min, the reaction was stopped by adding (12.5 μ L) of ADP-Glo reagent and the plate was incubated for 40 min followed by addition of (25 μ L) of kinase detection reagent to convert ADP to ATP and the newly synthesised ATP was converted into light using luciferase/luciferin. After an incubation time of 40 min, luminescence was recorded using a plate-reading luminometer.

7.4.1.3.2 Primary screening (500 nM)

18 compounds (**8**, **72** and **127** in Chapter 3) and (**210-212**, **214-220**, **222**, **226** **227**, **240** and **241** in Chapter 5) were tested in a second screen at a single concentration of 500 nM for their inhibitory activity against PI3K δ , these compounds were screened by Monash university using ADP-Glo kinase lipid assay. The experiment was carried out in the same manner as described above at 1 μ M single concentration (see Section 7.4.1.3.1).

7.4.2 Homogenous Time Resolved Fluorescence assay (HTRF)

Potencies for PI3K isoforms (α , β , γ and δ) of 70 compounds in this thesis were measured using a HTRF assay. In contrast to the radioactive assay, the HTRF assay does not require radioisotopes and it can accommodate high ATP concentration, which allows the assay to be carried out under conditions mimicking the physiological environment⁴¹²⁻⁴¹⁴. In addition to that, HTRF assay is easy-to-use with an excellent level of reproducibility^{414,415}. The principle of HTRF assay is based on the unique property of certain pleckstrin homology (PH) domains to interact specifically with PI(3,4,5)P₃⁴¹⁵, where it is believed that the PH domains in modular signalling proteins are the primary intracellular targets of PI(3,4 and 5)P₃. In the HTRF assay, a stable complex is formed between the GST-tagged PH domain and biotinylated short chain PI(3,4,5)P₃ (Figure 144)⁴¹³. The GST-tagged PH domain and biotinylated PI(3,4,5)P₃ recruit fluorophores (Europium-labelled anti-GST monoclonal antibody and Streptavidin-Allophycocyanin, respectively) generating a time-resolved fluorescence resonance energy transfer (TR-FRET). Excitation, at 330 nM, of Europium in the complex leads to a transfer of energy to the Streptavidin-Allophycocyanin, which emits at 665 nM (Figure 144)⁴¹⁶. Non-biotinylated PI(3,4,5)P₃ formed by PI3K activity was detected by displacement of biotinylated PI(3,4,5)P₃ from the signal-generating complex, resulting in a loss of energy transfer and sever drop in signal⁴¹³.

References

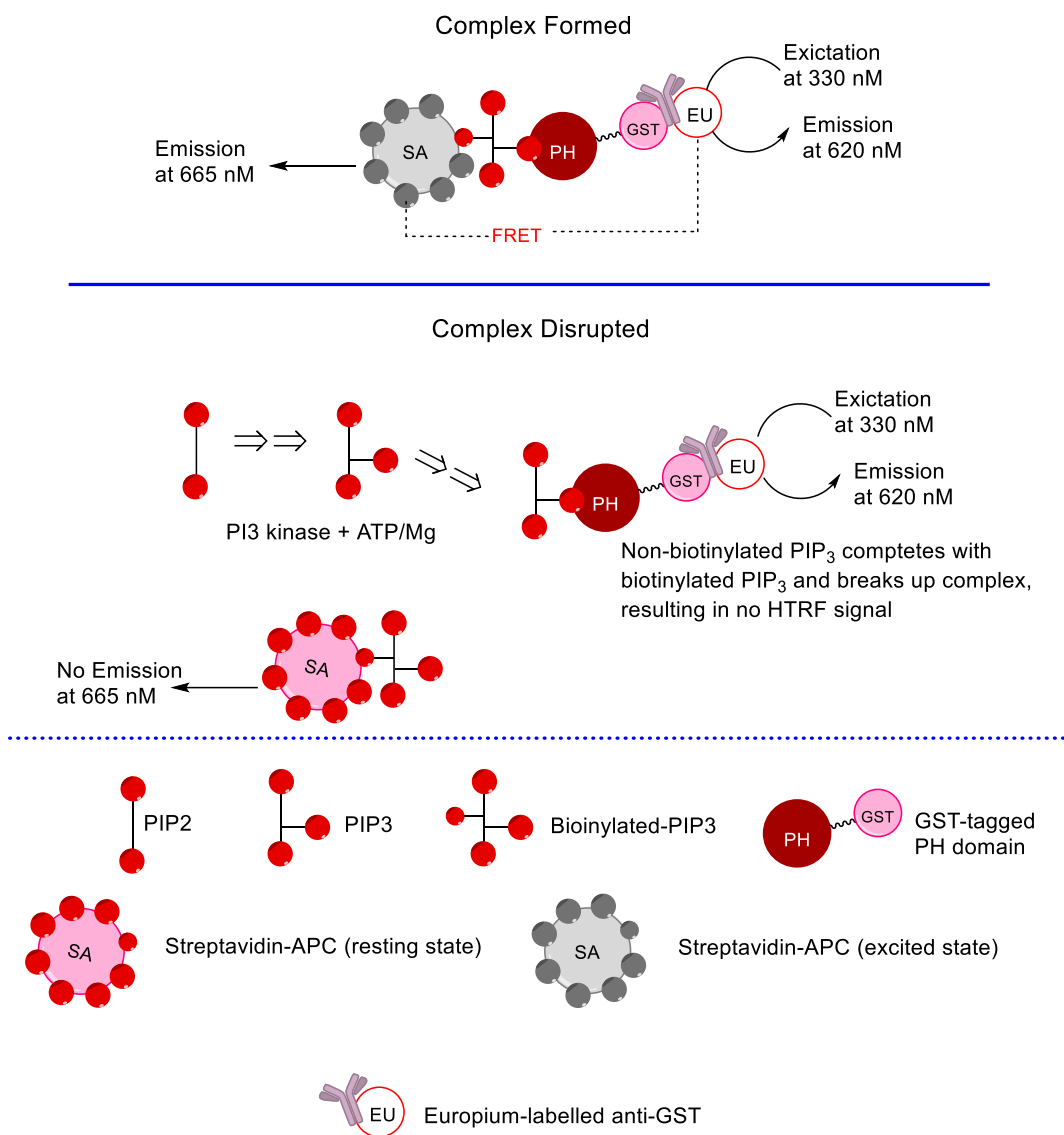


Figure 144. PI3 kinase HTRF Assay principle. The assay is composed of three steps: In the first step, inhibitor is incubated in assay buffer containing PI3-kinase, PI(4,5)P₂ substrate and ATP at RT for 30 minutes. In the second step, the reaction is terminated by the addition of a stop solution containing biotinylated PI(3,4,5)P₃ and ethylenediaminetetraacetic acid (EDTA). The last step involves the addition of detection buffer, containing GST-tagged GRP1 pleckstrin homology (PH) domain, Europium-labelled anti-glutathione S-transferase (GST) antibody and streptavidine-allophycocyanin (APC). After incubation at RT for 14 h, the plate is then read in time-resolved fluorescence mode and the HTRF signal is recorded.

References

- (1) Matte, A. et al. *Structure* **1989**, 6, 413–419.
- (2) Zhang, T. et al. *J. Exp. Bot.* **2016**, 67, 607–618.
- (3) Edelman, A. M. et al. *Ann. Rev. Biochem.* **1987**, 56, 567–613.
- (4) Minor, L. *Handbook of Assay Development in Drug Discovery*, 1st ed.; Taylor & Francis: Broken Raton, 2006.
- (5) Pauls, S. D. et al. *Front. Immunol.* **2012**, 3, 1–20.
- (6) Stankewicz, C. et al. *J. Biomol. Screen.* **2006**, 11, 413–422.
- (7) Mantamadiotis, T. *Cancers (Basel)*. **2017**, 9, 1–13.
- (8) News, T. *Biotechniques*.
- (9) Liu, P. et al. *Nat. Rev. Drug Discov.* **2009**, 8, 627–644.
- (10) Saxton, R. A. et al. *Cell* **2017**, 169, 361–371.
- (11) Magnuson, B. et al. *Biochem. J.* **2012**, 441, 1–21.
- (12) Carpenter, C. et al. *Curr. Opin. Cell Biol.* **1996**, 8, 153–158.
- (13) Hervieu, A. et al. *Front. Mol. Biosci.* **2018**, 5, 1–11.
- (14) Monsalves, E. et al. *Endocr. Relat. Cancer* **2014**, 21, 331–344.
- (15) Vitiello, P. P. et al. *J. Exp. Clin. Cancer Res.* **2019**, 38, 1–12.
- (16) Wang, W. et al. *Int J Cardiol.* **2015**, 181, 180–184.
- (17) Insall, R. H. et al. *Oncogene* **2001**, 1, 743–747.
- (18) Franke, T. F. *Oncogene* **2008**, 27, 6473–6488.
- (19) Lee, H. *Dis. Markers* **2017**, 2017.
- (20) Tyler, W. A. et al. *J. Neurosci.* **2009**, 29, 6367–6378.
- (21) Dan, H. C. et al. *J. Biol. Chem.* **2014**, 289, 25227–25240.
- (22) Hemmings, B. A. et al. *Cold Spring Harb. Perspect. Biol.* **2016**, 4, 1–3.
- (23) Porta, C. et al. *Front. Oncol.* **2014**, 4 APR, 1–11.
- (24) Sridharan, S. et al. *Int. J. Mol. Sci.* **2020**, 21, 1–17.
- (25) Sanchez, V. E. et al. *Int. J. Mol. Sci.* **2019**, 20.
- (26) Teleman, A. A. et al. *Genes Dev.* **2005**, 19, 1844–1848.
- (27) Conche, C. et al. *Mol. Cell. Biol.* **2014**, 34, 3356–3358.
- (28) Keppler-Noreuil, K. M. et al. *Am. J. Med. Genet.* **2016**, 172, 402–421.
- (29) Bunney, P. E. et al. *Physiol. Behav.* **2017**, 176, 139–148.
- (30) Fruman, D. A. and C. R. *Nat. Rev. Drug Discov.* **2014**, 13, 140–156.
- (31) Jung, S. et al. *Front. Immunol.* **2018**, 9, 1–14.
- (32) Fruman, D. A. et al. *Cell* **2017**, 170, 605–635.
- (33) Jean, S. et al. *J. Cell Sci.* **2014**, 127, 923–928.
- (34) Mavrommati, I. et al. *Sci. Rep.* **2016**, 6, 23277.
- (35) Mountford, S. J. et al. *ACS Med. Chem. Lett.* **2015**, 6, 3–6.
- (36) Falasca, M. et al. *J. Biol. Chem.* **2007**, 282, 28226–28236.
- (37) Vanhaesebroeck, B. et al. *Trends Biochem. Sci.* **1997**, 22, 267–272.
- (38) Rao, L. et al. *Mol. Cell. Oncol.* **2020**, 7, 10–12.
- (39) MacDougall, L. K. et al. *Curr. Biol.* **1995**, 5, 1404–1415.
- (40) Zhao, L. *Oncogene* **2008**, 27, 5486–5496.
- (41) Backer, J. M. *Curr Top Microbiol Immunol* **2010**, 346, 87–114.
- (42) Falasca, M. et al. *Biochem. J.* **2012**, 443, 587–601.
- (43) Okkenhaug, K. et al. *Biochem. Soc. Trans.* **2004**, 32, 332–335.
- (44) Wymann, M. P. et al. *Trends Pharmacol. Sci.* **2003**, 24, 366–376.
- (45) Vogt, P. K. *Cancer Cell* **2008**, 14, 107–108.
- (46) Kriplani, N. et al. *Adv. Biol. Regul.* **2015**, 59, 53–64.
- (47) Mazza, S. et al. *Int. J. Biochem. Mol. Biol.* **2011**, 2, 168–182.
- (48) Arcaro, A. et al. *J. Biol. Chem.* **1998**, 273, 33082–33090.
- (49) Thorpe, L. et al. *Nat. Rev. Cancer* **2014**, 15, 7–24.
- (50) Leibiger, B. et al. *FASEB J.* **2010**, 24, 1824–1837.
- (51) Domin, J. et al. **2000**, 275, 11943–11950.
- (52) Srivastava, S. et al. *Mol. Biol. Cell* **2009**, 20, 3783–3791.

References

- (53) Bridges, D. et al. *Mol. Biol. Cell* **2012**, 23, 2955–2962.
- (54) Lindmo, K. *J. Cell Sci.* **2006**, 119, 605–614.
- (55) Van Meir, E. G. *CNS Cancer: Models, Markers, Prognostic Factors, Targets, and Therapeutic Approaches*, 1st ed.; Humana Press: New York, 2009.
- (56) Backer, J. M. *Biochem. J.* **2008**, 410, 1–17.
- (57) Jaber, N. et al. *Ann. N. Y. Acad. Sci.* **2013**, 1280, 48–51.
- (58) Yang, G. et al. *Cell Death Dis.* **2020**, 11, 10–11.
- (59) Metcalf, D. et al. *Exp. Neurol.* **2012**, 238, 22–28.
- (60) Cintas, C. et al. *Front. Oncol.* **2018**, 7, 1–4.
- (61) Shidong, J. Roberts, T. *Curr Opin Cell Biol* **2009**, 21, 199–208.
- (62) Foukas, L. C. et al. *Nature* **2006**, 441, 366–370.
- (63) Sopasakis, V. R. et al. *Cell Metab.* **2011**, 11, 220–230.
- (64) Khamzina, L. et al. *Gastroenterology* **2003**, 125, 572–585.
- (65) Edgerton, D. S. et al. *JCI insight* **2017**, 2, e91863.
- (66) Smith, G. C. et al. *Endocrinology* **2017**, 158, 2436–2438.
- (67) Huang, X. et al. *Int. J. Biol. Sci.* **2018**, 14, 1483–1496.
- (68) Benistant, C. et al. *Oncogene* **2000**, 19, 5083–5090.
- (69) Lindkvist-Petersson, K. et al. *Glucose Transport: Methods and Protocols*, 1st ed.; Humana Press: New York, 2018.
- (70) Okkenhaug, K. et al. *Cancer Discov.* **2016**, 6, 1090–1105.
- (71) U.S. Food and Drug Administration. *Full Prescribing Information for Piqray® (Alpelisib)*; 2019.
- (72) André, F. et al. *N. Engl. J. Med.* **2019**, 380, 1929–1940.
- (73) Markham, A. *Drugs* **2014**, 74, 1555–1558.
- (74) Beeton, C. A. et al. **2000**, 350, 353–359.
- (75) Houslay, D. et al. *Sci Signal* **2017**, 9, 1–27.
- (76) Lynch, J. T. et al. *Mol. Cancer Ther.* **2018**, 17, 2309–2319.
- (77) Chalhoub, N. et al. *Annu Rev Pathol* **2009**, 4, 127–150.
- (78) Durrant, T. N. et al. *Clin. Transl. Med.* **2020**, 9.
- (79) Schmit, F. et al. *Proc. Natl. Acad. Sci. U. S. A.* **2014**, 111, 6395–6400.
- (80) Battram, A. M. et al. *J. Biol. Chem.* **2017**, 292, 1691–1704.
- (81) Gilio, K. et al. *J. Biol. Chem.* **2009**, 284, 33750–33762.
- (82) Kim, S. et al. *J. Biol. Chem.* **2009**, 284, 33763–33772.
- (83) Jackson, S. P. et al. *Nat. Med.* **2005**, 11, 507–514.
- (84) Majithia, A. et al. *Arterioscler. Thromb. Vasc. Biol.* **2019**, 39, 546–557.
- (85) Vanhaesebroeck, B. et al. *J. Mol. Med.* **2016**, 94, 5–11.
- (86) Salamon, R. S. et al. *BioEssays* **2013**, 35, 602–611.
- (87) Andrew, S. et al. *Sci. STKE* **2007**, 2007.
- (88) Takeda, A. J. et al. *Nat. Commun.* **2019**, 10.
- (89) Nürnberg, B. et al. *Biomolecules* **2019**, 9.
- (90) Hirsch, E. et al. **2000**, 287, 1049–1053.
- (91) Ferrandi, C. et al. *J. Pharmacol. Exp. Ther* **2007**, 322, 923–930.
- (92) Banham-Hall, E. et al. *Open Rheumatol. J.* **2012**, 6, 245–258.
- (93) Aksoy, E. et al. *Front. Immunol.* **2018**, 9, 1–7.
- (94) Venable, J. et al. *Recent Pat. Inflamm. Allergy Drug Discov.* **2010**, 4, 1–15.
- (95) Camps, M. et al. *Nat. Med.* **2005**, 11, 936–943.
- (96) Schmid, M. et al. *Cancer Cell* **2011**, 19, 715–727.
- (97) Zhu, J. et al. *RSC Adv.* **2019**, 9, 20207–20215.
- (98) Evans, C. A. et al. *ACS Med. Chem. Lett.* **2016**, 7, 862–867.
- (99) Nichole Tucker. *FDA Grants Fast Track Designation to Eganelisib Combination in TNBC*; 2020.
- (100) Tzenaki, N. et al. *Front. Oncol.* **2013**, 3, 1–16.
- (101) Sepulveda, J. et al. *Hematology - Latest Research and Clinical Advances*; BoD – Books on Demand: London, 2018.
- (102) Fung-Leung, W. P. *Cell. Signal.* **2011**, 23, 603–608.

References

- (103) Choi, M. et al. *Cancer J.* **2011**, *18*, 404–410.
- (104) Kaiko, G. E. et al. *Immunology* **2008**, *123*, 326–338.
- (105) P., K. *Altern. Med. Rev.* **2003**, *8*, 223–246.
- (106) Society, B. et al. **2007**, 6–8.
- (107) Moss, R. B. et al. *Expert Opin. Biol. Ther.* **2004**, *4*, 1887–1896.
- (108) Sakaguchi, S. *Annu. Rev. Immunol.* **2004**, *22*, 531–562.
- (109) Romano, M. et al. *Front. Immunol.* **2019**, *10*.
- (110) Soond, D. R. et al. *Front. Immunol.* **2012**, *3*, 1–8.
- (111) Herman, S. E. M. et al. *Clin. Cancer Res.* **2012**, *18*, 4013–4018.
- (112) Rosato, E. et al. *J Biol Regul Homeost Agents.* **2008**, *22*, 217–224.
- (113) Stark, A. K. et al. *Curr. Opin. Pharmacol.* **2015**, *23*, 82–91.
- (114) Kipps, T. J. et al. *Nat. Rev. Dis. Prim.* **2017**, *3*, 17008.
- (115) Kaur, M. P. et al. **2015**, *3*, 27–33.
- (116) Herman, S. *Blood* **2010**, *116*, 2078–2088.
- (117) Ringshausen, I. *Blood* **2002**, *100*, 3741–3748.
- (118) Carter, M. J. et al. **2016**, *31*, 1423–1433.
- (119) Bose, P. et al. *Oncotarget* **2012**, *3*, 1499–1500.
- (120) Jin, Z. et al. *Cancer Biol. Ther.* **2005**, *4*, 147–171.
- (121) Lampson, B. L. et al. *Expert Opin. Investig. Drugs* **2017**, *26*, 1267–1279.
- (122) Hallek, M. et al. *Blood* **2008**, *111*, 5446–5456.
- (123) *NCCN Clinical Practice Guidelines in Oncology. Chronic Lymphocytic Leukemia/Small Lymphocytic Lymphoma, Version 2.2019.*; 2018.
- (124) Blunt, M. D. et al. *Leuk. Res. Reports* **2015**, *4*, 60–63.
- (125) Ali, K. et al. *Nature* **2014**, No. 3.
- (126) Yang, Q. et al. *Clin. Cancer Res.* **2015**, *21*, 1537–1542.
- (127) Chiu, B. et al. *Cancer Treat Res* **2015**, *165*, 1–25.
- (128) Serrat, N. et al. *Blood Adv.* **2020**, *4*, 4217–4231.
- (129) Yahiaoui, O. I. et al. *BMC Cancer* **2014**, *14*, 1–9.
- (130) Yanaba, K. et al. *Immunol. Rev.* **2008**, *223*, 284–299.
- (131) Hampe, C. *Scientifica (Cairo)*. **2012**, 1–18.
- (132) Fillatreau, S. *Eur. J. Immunol.* **2015**, *45*, 966–970.
- (133) Kaplan, C. D. et al. *J. Immunol.* **2002**, *169*, 5851–5859.
- (134) So, L. et al. *Biochem J* **2012**, *442*, 465–481.
- (135) Burrack, A. L. et al. *Front. Endocrinol. (Lausanne)*. **2017**, *8*, 1–15.
- (136) Soond, D. R. et al. *Blood* **2010**, *115*, 2203–2213.
- (137) Zenobia, C. et al. **2016**, *69*, 142–159.
- (138) Stark, A. et al. **2015**, 82–91.
- (139) Williams, R. et al. *Biochem. Soc. Trans.* **2009**, *37*, 615–626.
- (140) Walker, E. H. et al. *Mol. Cell* **2000**, *6*, 909–919.
- (141) Ward, R. and G. *Kinase Drug Discovery, Illustrate.*; Royal Society of Chemistry: Weinheim, 2012.
- (142) Romano, V. et al. *BMC Res. Notes* **2017**, *10*, 1–12.
- (143) Li, Y. et al. *Int. J. Mol. Sci.* **2015**, *16*, 9314–9340.
- (144) Miller, M. S. et al. *Biomolecules* **2019**, *9*.
- (145) Berndt, A. et al. *Nat Chem Biol* **2010**, *6*, 117–124.
- (146) Workman, P. et al. *Nat. Chem. Biol.* **2010**, *6*, 82–83.
- (147) Fabbro, D. et al. *Br. J. Pharmacol.* **2015**, *172*, 2675–2700.
- (148) Xing, L. et al. *Bioorganic Med. Chem.* **2015**, *23*, 6520–6527.
- (149) Berndt, A. et al. *Nat. Chem. Biol.* **2010**, *6*, 117–124.
- (150) Ghose, A. K. et al. *J. Med. Chem.* **2008**, *51*, 5149–5171.
- (151) Perry, M. W. D. et al. *J. Med. Chem.* **2017**, *60*, 5057–5071.
- (152) Knight, Z. A. et al. *Cell* **2006**, *125*, 733–747.
- (153) Somoza, J. R. et al. *J. Biol. Chem.* **2015**, *290*, 8439–8446.
- (154) Erra, M. et al. *J. Med. Chem.* **2018**, *61*, 9551–9567.
- (155) Patel, L. *J. Med. Chem.* **2016**, *59*, 3532–3548.

References

- (156) Cushing, T. *J. Med. Chem.* **2014**, *58*, 480–511.
- (157) Murray, J. M. et al. *J. Med. Chem.* **2012**, *55*, 7686–7695.
- (158) Perry, M. W. D. et al. *J. Med. Chem.* **2017**, *60*, 5057–5071.
- (159) Schwehm, C. et al. *J. Med. Chem.* **2017**, *60*, 1534–1554.
- (160) Sutherland, D. P. et al. *Bioorganic Med. Chem. Lett.* **2012**, *22*, 4296–4302.
- (161) Safina, B. S. et al. *J. Med. Chem.* **2012**, *55*, 5887–5900.
- (162) Hashemzadeh, K. et al. *Middle East J. Dig. Dis.* **2018**, *11*, 5–16.
- (163) Li, X. et al. *PLoS One* **2018**, *13*, 1–18.
- (164) Fruman, D. **2014**, *13*, 140–156.
- (165) Nunnery, S. E. et al. *Ann. Oncol.* **2019**, *30*, 1–6.
- (166) Buchanan, C. M. et al. *Biomolecules* **2019**, *9*, 1–26.
- (167) Rodon, J. et al. *Cancer Discov.* **2017**, *7*, 666–669.
- (168) Niswender, K. D. et al. *Diabetes* **2003**, *52*, 227–231.
- (169) Flinn, I. W. *Blood* **2018**, *132*, 240–241.
- (170) Rafii, S. et al. *Clin. Cancer Res.* **2015**, *21*, 1869–1876.
- (171) Brammer, J. E. *Blood* **2018**, *131*, 839–840.
- (172) Sutherland, D. P. et al. *J. Med. Chem.* **2011**, *54*, 7579–7587.
- (173) Berndt, A. et al. *Nat. Chem. Biol.* **2010**, *6*, 117–124.
- (174) Workman, P. et al. *Nat. Chem. Biol.* **2010**, *6*, 82–83.
- (175) Aledo, J. C. *BMC Evol. Biol.* **2017**, *17*, 1–13.
- (176) Dienstmann, R. et al. *Mol. Cancer Ther.* **2014**, *13*, 1021–1031.
- (177) Wang, X. et al. *Acta Pharmacol. Sin.* **2015**, *36*, 1170–1176.
- (178) Vangapandu, H. V. et al. *Expert Opin. Investig. Drugs* **2017**, *26*, 625–632.
- (179) Scott, W. J. et al. *ChemMedChem* **2016**, 1517–1530.
- (180) Somoza, J. R. et al. *J. Biol. Chem.* **2015**, *290*, 8439–8446.
- (181) Raynaud, F. I. et al. *Mol. Cancer Ther.* **2009**, *8*, 1725–1738.
- (182) Folkes, A. J. et al. *J. Med. Chem.* **2008**, *51*, 5522–5532.
- (183) Sarker, D. et al. *Clin Cancer Res* **2015**, *21*, 77–86.
- (184) Samuels, Y. *Curr Top Microbiol Immunol.* **2010**, *347*, 21–41.
- (185) Shapiro, G. I. et al. *Invest. New Drugs* **2020**, *38*, 419–432.
- (186) Schöffski, P. et al. *Breast Cancer Res.* **2018**, *20*, 1–12.
- (187) Krop, I. E. et al. *Lancet Oncol.* **2016**, *17*, 811–821.
- (188) Vuylsteke, P. et al. *Ann. Oncol.* **2016**, *27*, 2059–2066.
- (189) Rodrigues, D. A. et al. *Pharmaceuticals* **2019**, *12*, 69.
- (190) Qiu, X. et al. *Future Med. Chem.* **2019**, *11*, 2151–2169.
- (191) Burger, J. A. et al. *Blood* **2009**, *114*, 3367–3375.
- (192) Göckeritz, E. et al. *Int. J. Cancer* **2015**, *137*, 2234–2242.
- (193) Williams, O. et al. *Chem. Biol.* **2010**, *17*, 123–134.
- (194) Hoellenriegel, J. et al. *Blood* **2011**, *118*, 3603–3612.
- (195) Burger, J. A. et al. *Trends Immunol.* **2013**, *34*, 592–601.
- (196) Kaneda, M. M. et al. *Nature* **2016**, *539*, 437–442.
- (197) DiLlino, D. et al. *Leukemia* **2013**, *27*, 170–180.
- (198) Van Attekum, M. H. A. et al. *Haematologica* **2017**, *102*, 1469–1476.
- (199) Balakrishnan, K. et al. *Leukemia* **2015**, *29*, 1811–1822.
- (200) Patel, V. et al. *Leukaemia* **2016**, *31*, 1872–1881.
- (201) Horwitz, S. M. et al. *Blood* **2018**, *131*, 888–898.
- (202) O'Brien, S. et al. *Am. J. Hematol.* **2018**, *93*, 1318–1326.
- (203) Lim, E. L. et al. *Immunology* **2019**, *157*, 210–218.
- (204) Corthay, A. *Scand. J. Immunol.* **2009**, *70*, 326–336.
- (205) Bethesda. *LiverTox: Clinical and Research Information on Drug-Induced Liver Injury*, 2012.
- (206) Yang, J. et al. *Mol. Cancer* **2019**, *18*, 1–28.
- (207) Markham, A. *Drugs* **2017**, *77*, 2057–2062.
- (208) Chauhan, A. et al. *Cancer Manag. Res.* **2021**, *13*, 677–692.
- (209) Krause, G. et al. *Drug Des. Devel. Ther.* **2018**, *12*, 2577–2590.

References

- (210) Klebe, G. In *Drug Design*; Springer Berlin Heidelberg: Berlin, 2013; pp 493–532.
- (211) Hentemann, M. F. WO 2008/070150, 2017.
- (212) Yu, D. et al. *Acta Biochim. Biophys. Sin. (Shanghai)*. **2018**, *50*, 782–792.
- (213) Tarantelli, C. et al. *Blood Adv.* **2020**, *4*, 819–829.
- (214) Dreyling, M. et al. *J. Clin. Oncol.* **2017**, *35*, 3898–3905.
- (215) Cheson, B. D. et al. *Clin Lymphoma Myeloma Leuk* **2018**, *19*, 135–141.
- (216) Patnaik, A. et al. *Ann. Oncol.* **2016**, *27*, 1928–1940.
- (217) Luxenburger, A. et al. *Molecules* **2019**, *24*.
- (218) Hoegenauer, K. et al. *ACS Med. Chem. Lett.* **2016**, *7*, 762–767.
- (219) Wolf, R. M. et al. *ACS Med. Chem. Lett.* **2017**, *173*, 975–980.
- (220) Terstiege, I. et al. *Bioorganic Med. Chem. Lett.* **2017**, *27*, 679–687.
- (221) Feng, Y. et al. *Expert Opin. Ther. Pat.* **2019**, *29*, 925–941.
- (222) Jamee, M. et al. *Clin. Rev. Allergy Immunol.* **2019**.
- (223) Durandy, A. et al. *Blood* **2020**, *135*, 638–643.
- (224) Price, E. J. et al. *Rheumatology* **2017**, *56*, 24–48.
- (225) Roberts, M. *Arthritis Rheumatol* **2014**, *66*, 2558–2569.
- (226) Rao, V. K. et al. *Blood* **2017**, *130*, 2307–2316.
- (227) Taylor, N. *Novartis Sells Phase 3 Rare Disease Drug to Pharming*; 2019.
- (228) Dörner, T. et al. **2018**, 174.1-174.
- (229) Hoegenauer, K. et al. *ACS Med. Chem. Lett.* **2017**, *173*, 975–980.
- (230) Reading, E. *Oncol. Times* *36*, 57.
- (231) Xin, M. et al. *Bioorganic Med. Chem. Lett.* **2017**, *27*, 1972–1977.
- (232) Brown, J. R. *Semin. Oncol.* **2016**, *43*, 260–264.
- (233) Furman, R. R. et al. *N. Engl. J. Med.* **2014**, *370*, 997–1007.
- (234) Staben, S. In *Cancer II*; Waring, M. ., Ed.; Springer International Publishing, 2017; pp 333–370.
- (235) Garces, A. E. et al. *J. Med. Chem.* **2019**, *62*, 4815–4850.
- (236) Miller, B. W. et al. *Clin. Cancer Res.* **2015**, *21*, 1525–1529.
- (237) Gilead Sciences. *Extension Study of Idelalisib in Participants With Chronic Lymphocytic Leukemia (CLL) Who Participated in GS-US-312-0116 (NCT01539512)*; 2019.
- (238) Coutré, S. E. et al. *Leuk. Lymphoma* **2015**, *56*, 2779–2786.
- (239) Forero-Torres, A. et al. *Blood* **2019**, *133*, 1742–1752.
- (240) Mato, A. R. et al. *Cancer Biol. Ther.* **2018**, *19*, 636–643.
- (241) Williams, O. et al. *Chem. Biol.* **2010**, *17*, 123–134.
- (242) Berndt, A. et al. *Nat Chem Biol* **2010**, *6*, 117–124.
- (243) Sutherlin, D. P. et al. *J. Med. Chem.* **2011**, *54*, 7579–7587.
- (244) Andrs, M. et al. *J. Med. Chem.* **2015**, *58*, 41–71.
- (245) Jackson, S. P. et al. WO 2004/016607 B1, 2004.
- (246) Degorce, S. L. et al. *J. Med. Chem.* **2018**, *61*, 8934–8943.
- (247) Littke, A. F. et al. *Angew. Chemie - Int. Ed.* **2002**, *41*, 4176–4211.
- (248) Kotha, S. et al. *Tetrahedron* **2002**, *58*, 9633–9695.
- (249) Abraham, M. H. et al. *J. Chem. Soc., Perkin Trans. 2* **1989**, *25*, 1355–1375.
- (250) Abraham, M. H. *J. Phys. Org. Chem.* **1993**, *6*, 660–684.
- (251) Bauer, C. A. et al. *J. Cheminform.* **2019**, *11*, 1–16.
- (252) Brandl, M. et al. *J. Mol. Biol.* **2001**, *307*, 357–377.
- (253) Nishio, M. *Phys. Chem. Chem. Phys.* **2011**, *13*, 13873–13900.
- (254) Ran, J. et al. *J. Phys. Chem. A* **2006**, *110*, 9702–9709.
- (255) Kozmon, S. et al. *Chem. - A Eur. J.* **2011**, *17*, 5680–5690.
- (256) Vorobyov, I. et al. *J. Chem. Theory Comput.* **2007**, *3*, 1120–1133.
- (257) Zhao, C. et al. *Org. Lett.* **2014**, *16*, 3520–3523.
- (258) Ciunik, Z. et al. *J. Mol. Struct.* **1998**, *442*, 125–134.
- (259) Nishio, M. et al. *Phys. Chem. Chem. Phys.* **2014**, *16*, 12648–12683.
- (260) Gillis, E. P. et al. *J. Med. Chem.* **2015**, *58*, 8315–8359.

References

- (261) Baek, J. Y. et al. *Tetrahedron* **2015**, *71*, 5315–5320.
- (262) M.Trost, B. et al. *Comprehensive Organic Synthesis, Additions to CX π -Bonds*, 1st ed.; Elsevier: Amsterdam, 1991.
- (263) Hann, M. M. et al. *Nat. Rev. Drug Discov.* **2012**, *11*, 355–365.
- (264) Taylor, John. Triggle, D. *Comprehensive Medicinal Chemistry II*, 2nd ed.; Elsevier Science, 2007.
- (265) Saunders, R. A. et al. *New. J. Chem* **2004**, *28*, 166–172.
- (266) Brito, M. A. de. *Brazilian J. Pharm. Sci.* **2011**, *47*, 797–805.
- (267) Zakeri-Milani, P. et al. *DARU* **2006**, *14*, 164–171.
- (268) Fleming, F. F. et al. **1947**, *53*, 7902–7917.
- (269) Liu, J. et al. *Org. Prep. Proced. Int.* **2016**, *48*, 337–341.
- (270) Montalbetti, C. A. G. N. et al. *Tetrahedron* **2005**, *61*, 10827–10852.
- (271) Tong, X. et al. *Res. Chem. Intermed.* **2012**, *38*, 1961–1968.
- (272) Mekala, N. et al. *RSC Adv.* **2018**, *8*, 15863–15869.
- (273) Guangyong, L. et al. CN104130261A, 2014.
- (274) XiaLong, W. et al. CN 201510313025, 2017.
- (275) Kolarski, D. et al. *Org. Lett.* **2017**, *19*, 5090–5093.
- (276) Chang, Y. et al. *Chem. Biol.* **1999**, *6*, 361–375.
- (277) Liu, S. *J Phys Chem* **2011**, *114*, 5913–5918.
- (278) Knipe, A, C. *Organic Reaction Mechanisms 2005: An Annual Survey Covering the Literature Dated January to December 2005 (Organic Reaction Mechanisms Series) 1st Edition*, 1 st editi.; John Wiley & Sons, 2005.
- (279) Liu, J. et al. *J. Am. Chem. Soc.* **2007**, *129*, 5962–5968.
- (280) Legraverend, M. *Tetrahedron* **2008**, *64*, 8585–8603.
- (281) Ferrer, G. et al. WO/2014/060431, 2014.
- (282) Lin, X. et al. *Org. Lett.* **2000**, *2*, 3497–3499.
- (283) Bach, R. D. et al. *J. Org. Chem.* **1986**, *51*, 1030–1033.
- (284) Rablen, P. R. et al. *J. Org. Chem* **2014**, *79*, 867–879.
- (285) Wu, C. et al. *J. AM. CHEM. SOC* **2013**, *136*, 3118–3126.
- (286) Kalsi, P. *Organic Reactions And Their Mechanisms*, 3 rd ed.; New Academic Science: London, 2010.
- (287) Vollhardt, Peter; Schore, N. *Organic Chemistry: Structure and Function*, 7th ed.; WH Freeman: New York, 2014.
- (288) Erden, I. et al. *J. Org. Chem.* **2014**, *79*, 6410–6418.
- (289) Thorpe, J. W. et al. *Can. J. Chem.* **1973**, *51*, 927–935.
- (290) Uggerud, E. *Pure Appl. Chem.* **2009**, *81*, 709–717.
- (291) Vinayak, G. et al. WO/2016/147206, 2016.
- (292) Sharma, A. et al. *ChemistryOpen* **2017**, *6*, 168–177.
- (293) Clayden, J. et al. *Organic Chemistry*, 1 st ed.; OUP Oxford: USA, 2000.
- (294) Clayden, J. et al. *Organic Chemistry*, 2 nd ed.; OUP Oxford: New York, 2012.
- (295) Hajipour, A. R. et al. *Synth. Commun.* **2009**, *39*, 1084–1091.
- (296) Lebraud, H. et al. *Org. Biomol. Chem.* **2013**, *11*, 1874–1878.
- (297) Coxon, C. R. et al. *J. Med. Chem.* **2017**, *60*, 1746–1767.
- (298) De Medeiros, E. F. et al. *Tetrahedron Lett.* **1990**, *31*, 5843–5844.
- (299) Chou-Hsiung, C. University of Nottingham, 2013.
- (300) Annadi, K. et al. *Arkivoc* **2014**, *6*, 108–126.
- (301) Gu, W. et al. *J. Org. Chem.* **2011**, *76*, 8287–8293.
- (302) Soai, K. et al. *J. Chem. Soc. Chem. Commun.* **1983**, No. 12, 668–669.
- (303) Walker, E. H. *Chem. Soc. Rev.* **1976**, *5*, 23–50.
- (304) Katritzky, A. et al. *Comprehensive Organic Functional Group Transformations*; Elsevier Science: New York, 1995.
- (305) Kelleher, F. et al. *Tetrahedron Lett.* **2006**, *47*, 3005–3008.
- (306) Kingsbury, C. *Ring Closures and the Hammond Postulate*; Lincoln, 2016.
- (307) Tewari, N. *Organic Chemistry: A Modern Approach, Volume-III*, 3th ed.; McGraw-Hill Education: Ghennai, 2019.

References

- (308) Shadbolt, R. S. et al. *J. Chem. Soc.* . **1968**, 4, 733–740.
- (309) Silverman, Gary; Rakita, P. *Handbook of Grignard Reagents*, 1st ed.; Taylor & Francis: Boca Roca, U.S, 1996.
- (310) Gilead Sciences. *Product Information, ZYDELIG® (100 Mg and 150 Mg Idelalisib) Tablet*; London, 2017.
- (311) Liu, Y. et al. *Oncotarget* **2017**, 8, 7181–7200.
- (312) Bissantz, C. et al. *J. Med. Chem.* **2010**, 53, 5061–5084.
- (313) Knight, Z. a et al. *Cell* **2006**, 125, 733–747.
- (314) Piks, P. **2010**, 9, 2010.
- (315) Mérour, J. Y. et al. *Molecules* **2014**, 19, 19935–19979.
- (316) Pierre, F. et al. *J. Med. Chem.* **2011**, 54, 635–654.
- (317) Dai, S. et al. *Cells* **2019**, 8, 614.
- (318) Zhou, Y. et al. *Molecules* **2017**, 22.
- (319) Wu, D. et al. *Chem. Commun.* **2018**, 54, 12089–12092.
- (320) Alaimo, P. J. et al. *Bioorganic Med. Chem.* **2005**, 13, 2825–2836.
- (321) Azam, M. et al. *Nat. Struct. Mol. Biol.* **2008**, 15, 1109–1118.
- (322) Schnabel, J. et al. *J. Biol. Chem.* **2018**, 293, 5613–5623.
- (323) Wu, T. J. et al. *Cell Rep.* **2015**, 11, 446–459.
- (324) Guibourdenche, C. et al. WO2014128612A1, 2014.
- (325) Wong, S. S. et al. *Chemistry of Protein and Nucleic Acid Cross-Linking and Conjugation*, 2nd ed.; Taylor & Francis: New York, 2012.
- (326) Locke, G. M. et al. *Chem. Eur. J.* **2019**, 25, 4590–4647.
- (327) Patrick, G. *An Introduction to Medicinal Chemistry*, 6th ed.; Oxford University Press: US, 2017.
- (328) Zhang, Q. et al. *Tetrahedron* **2012**, 68, 7822–7826.
- (329) Dracinsky, M. et al. *Annual Reports on NMR Spectroscopy*, 1st ed.; Webb, G., Ed.; Academic Press, 2014.
- (330) Kjellberg, J. et al. *Tetrahedron* **1986**, 42, 6541–6544.
- (331) Chen, S. et al. *Org. Lett.* **2016**, 18, 16–19.
- (332) Van Den Berge, E. et al. *J. Org. Chem.* **2013**, 78, 12220–12223.
- (333) Emilie Van Den Berge. Catholique De Louvain, 2013.
- (334) Dilek Celik, G. et al. *Med. Chem. Res.* **2013**, 22, 1470–1479.
- (335) Guibourdenche, C. et al. PCT/IB2014/059071, 2014.
- (336) Methot, J. L. et al. *J. Med. Chem.* **2019**, 62, 4370–4382.
- (337) Bhattacharya, A. et al. *Biochemistry* **2019**, 58, 2419–2431.
- (338) Waldmann, H. et al. *Concepts and Case Studies in Chemical Biology*, 1st ed.; Wiley.VCH, 2014.
- (339) Renaud, J.-P. *Structural Biology in Drug Discovery: Methods, Techniques, and Practices*, 1st ed.; John Wiley & Sons, 2020: Hoboken, 2020.
- (340) Liu, J. et al. *RSC Adv.* **2019**, 9, 2092–2101.
- (341) Wojcik, J. et al. *J. Biol. Chem.* **2016**, 291, 8836–8847.
- (342) Redaelli, S. et al. *Am. J. Hematol.* **2012**, 87, 125–128.
- (343) Rossari, F. et al. *J. Hematol. Oncol.* **2018**, 11, 1–14.
- (344) Young, M. A. et al. *Cancer Res.* **2006**, 66, 1007–1014.
- (345) Weinberg, R. A. *The Biology of Cancer*, 2nd ed.; Garland Science: New York, 2013.
- (346) Peter, J.-U. *Polypharmacology in Drug Discovery*, illustrate.; John Wiley & Sons: New Jersey, 2012.
- (347) Motkuri, R. K. et al. *Chem. Commun.* **2011**, 47, 7077–7079.
- (348) Mujika, J. I. et al. *Chem. - A Eur. J.* **2006**, 12, 7215–7224.
- (349) Kotz, J. et al. *Chemistry and Chemical Reactivity, Enhanced Edition*, 7th ed.; Cengage Learning: Belmont, 2009.
- (350) Dewick, P. M. *Essentials of Organic Chemistry: For Students of Pharmacy, Medicinal Chemistry and Biological Chemistry*; John Wiley & Sons: Chichester, 2013.

References

- (351) Shanmugasundararaj, S. et al. *Biophys. J.* **2012**, *103*, 2331–2340.
- (352) Wu, W. et al. *Chem. - A Eur. J.* **2009**, *15*, 9730–9736.
- (353) Kulinkovich, O. G. *Cyclopropanes in Organic Synthesis*; John Wiley & Sons: New Jersey, 2015.
- (354) M.Trost, B. et al. *Comprehensive Organic Synthesis: Selectivity, Strategy, and Efficiency*, 1st ed.; Elsevier Ltd: Oxford, 1991.
- (355) Greenberg, A. et al. *Strained Organic Molecules*; Academic Press: London, 2013.
- (356) Rohit Manglik. *IIT JEE Chemistry | Practice Kit of 20 Topic Wise Mock Test*, 1st ed.; EduGorilla Community Pvt. Ltd: Lucknow, 2020.
- (357) Lovering, F. et al. **2009**, 6752–6756.
- (358) Palm, K. et al. *J. Pharm. Sci.* **1996**, *85*, 32–39.
- (359) Lipinski, C. A. et al. *Adv. Drug Deliv. Rev.* **2012**, *64*, 4–17.
- (360) Ninković, D. B. et al. *Phys. Chem. Chem. Phys.* **2016**, *18*, 25791–25795.
- (361) Gunaydin, H. et al. *ACS Med. Chem. Lett.* **2016**, *7*, 341–344.
- (362) Jeffrey, G. A. *An Introduction to Hydrogen Bonding*, 1st ed.; Oxford University Press: New York, 1997.
- (363) Harris, T. K. et al. *Proteins Struct. Funct. Genet.* **1999**, *35*, 275–282.
- (364) Tansey, J. T. *Biochemistry: An Integrative Approach*, 1st ed.; John Wiley & Sons, 2020: Hoboken, 2020.
- (365) Li, P. et al. *Chem. Lett.* **2000**, No. 3, 204–205.
- (366) Li, P. et al. *J. Org. Chem.* **2000**, *65*, 2951–2958.
- (367) Joule, J. A. et al. *Heterocyclic Chemistry*, 5th ed.; John Wiley & Sons: Chichester, 2013.
- (368) Elmkkaddem, M. K. et al. *Chem. Commun.* **2010**, *46*, 925–927.
- (369) Xu, H. et al. *Chem. Commun.* **2009**, 3035–3037.
- (370) Xingyong, Z. et al. CN105859726 (A), 2016.
- (371) Charton, M. *J. Org. Chem.* **1964**, *29*, 1222–1227.
- (372) Alvares-Builla, Julio. Vaquero, J. Barluenga, J. *Modern Heterocyclic Chemistry*, 4th ed.; Wiley.VCH: Weinheim, 2011.
- (373) Katritzky, Alan. Taylor, R. *Advances in Heterocyclic Chemistry*, 1st ed.; Academic Press, 1990.
- (374) Kan, X. et al. *Chinese Chem. Lett.* **2018**, *29*, 261–266.
- (375) Vishnu Ji Ram et al. *The Chemistry of Heterocycles: Chemistry of Six to Eight Membered N, O, S, P and Se Heterocycles*, 1st ed.; Elsevier, 2019.
- (376) Mahajan, S. *Encyclopedia of Materials: Science and Technology*, 1st ed.; Elsevier Ltd, 2001.
- (377) Loudon, M. *Organic Chemistry*, 5th ed.; Brooks/Cole Gengage: Belmont, 2009.
- (378) Ichikawa, J. et al. *Synthesis (Stuttg.)* **2002**, No. 13, 1917–1936.
- (379) Huque, F. T. T. et al. *Org. Biomol. Chem.* **2003**, *1*, 1419–1424.
- (380) Carles, F. et al. *Molecules* **2018**, *23*, 1–18.
- (381) Ritchie, T. J. et al. *Drug Discov. Today* **2009**, *14*, 1011–1020.
- (382) Aldeghi, M. et al. *Chem. Biol. Drug Des.* **2014**, *83*, 450–461.
- (383) Tajabadi, F. M. et al. *Springer Sci. Rev.* **2013**, *1*, 141–151.
- (384) Méndez-Lucio, O. et al. *Drug Discov. Today* **2017**, *22*, 120–126.
- (385) Thakkar, H. et al. *Int. J. Pharm. Sci. Rev. Res.* **2010**, *4*, 203–223.
- (386) Rafferty, R. J. et al. *Angew. Chemie* **2014**, *126*, 224–228.
- (387) Talele, T. T. *J. Med. Chem.* **2016**, *59*, 8712–8756.
- (388) Mykhailiuk, P. K. *Org. Biomol. Chem.* **2019**, *17*, 2839–2849.
- (389) Hartwig, J. et al. US 2012/0226041, 2012.
- (390) Horie, S. et al. *Intensive Care Med.* **2020**.
- (391) Mondrinos, M. J. et al. *Shock* **2013**, *39*, 467–479.
- (392) Kickbusch, I. et al. *BMJ* **2020**, *368*, 1–2.
- (393) Li, X. et al. *Crit. Care* **2020**, *24*, 1–5.

References

- (394) Swaroopa, D. et al. *Indian J. Crit. Care Med.* **2016**, *20*, 518–525.
- (395) Bhatia, M. et al. *Am. J. Respir. Cell Mol. Biol.* **2012**, *46*, 566–572.
- (396) de Porto, A. P. et al. *Mol. Med.* **2019**, *25*, 3.
- (397) Roschewski, M. et al. *Sci. Immunol.* **2020**, *5*, 1–19.
- (398) Qing, Y. et al. *J. Infect.* **2020**, *80*, 607–613.
- (399) Virgil, H. Acalabrutinib May Be Beneficial for Patients With Advanced COVID-19, Early Data Says <https://www.oncnursingnews.com/view/acalabrutinib-may-be-beneficial-for-patients-with-advanced-covid19-early-data-says>.
- (400) Xie, S. et al. *PLoS One* **2014**, *9*.
- (401) Hawkins, P. T. et al. *Biochim. Biophys. Acta* **2015**, *1851*, 882–897.
- (402) Bi, J. et al. *Clin. Transl. Med.* **2020**, *9*.
- (403) Panayotou, G. et al. *Trends Cell Biol.* **1992**, *2*, 358–360.
- (404) Cantley, L. *Sci.* **2002**, *296*, 1655–1657.
- (405) Okkenhaug, K. et al. *Science (80-)*. **2002**, *297*, 1031–1034.
- (406) Zegzouti, H. et al. *Assay Drug Dev. Technol.* **2009**, *7*, 560–572.
- (407) Tanega, C. et al. *Assay Drug Dev. Technol.* **2009**, *7*, 606–614.
- (408) Vidugiriene, J. et al. *Assay Drug Dev. Technol.* **2009**, *7*, 585–597.
- (409) Jain, R. et al. *MethodsX* **2019**, *6*, 162–168.
- (410) Li, H. et al. *Assay Drug Dev. Technol.* **2009**, *7*, 598–605.
- (411) Zegzouti, H. et al. *ADP-Glo™: A Luminescent ADP Detection Assay for Kinases, and Other ADP-Generating Enzymes*; Madison, 2009.
- (412) Sugita, H. et al. *Biochem. Biophys. Res. Commun.* **2008**, *377*, 941–945.
- (413) Gray, A. et al. *Anal. Biochem.* **2003**, *313*, 234–245.
- (414) Jia, Y. *Expert Opin. Drug Discov.* **2008**, *3*, 1461–1474.
- (415) Huang, W. *Anal Bioanal Chem* **2011**, *6*, 1881–1888.
- (416) Larson, B. et al. *Enzyme* **2009**, 3–6.